TECHNICAL REPORT

No. 3/83

Volume 1

The Advanced Sodium Receiver
(ASR)

- Topic Reports -

prepared by the Contracting Companies

Agip Nucleare, Milano
and
Franco Tosi Industriale, Legnano

IEA-OPERATING AGENT
DEUTSCHE FORSCHUNGS- UND VERSUCHSANSTALT
FÜR LUFT- UND RAUMFAHRT e.V.

OPERATING AGENT

Deutsche Forschungs- und Versuchsanstalt für Luft- und Raumfahrt e.V. (DFVLR)
Linder Höhe, D - 5000 Köln 90; Tel.: D - 2203-6011; Tx: D - 8 874 433 (dfv d) (Dr. W. von Kries)
Apartado 649, Almeria, Spain; Tel.: E - 51-36.51.89; Tx: E - 78 893 (dfv e) (W. Grasse, Project Manager)

INTERNATIONAL TEST AND EVALUATION TEAM

Apartado 649, Almeria, Spain; Tel.: E - 51-36.51.89; Tx: E - 78 893 (dfv e) (C. S. Selvage)

PLANT OPERATION AUTHORITY

Cia. Sevillana de Electricidad S. A.
Apartado 21, Tabernas, Prov. Almeria, Spain; Tel.: E - 51-36.51.89; Tx: E - 78 893 (dfv e) (F. Ruiz Munoz)

SSPS TECHNICAL REPORT No. 3/83

The Advanced Sodium Receiver

(ASR)

- Topic Reports -

Volume 1

by

the Contracting Companies

Agip Nucleare, Milano

and

Franco Tosi Industriale, Legnano

Italy

Prepared for

IEA - OPERATING AGENT DFVLR, Köln

Introduction of the Project Manager

In September 1980, a contract has been signed between the Operating Agent of the SSPS Project on the one hand and a consortium of Italian companies on the other hand, providing the delivery of an "Advanced Sodium-Cooled Receiver (ASR)" to the SSPS CRS Solar Power Plant as an in-kind contribution of the Italian Contracting Party.

The design of this receiver is different from the one used with the original equipment of the plant (cavity receiver). The ASR is an open receiver, having five flat panels in the aperture plane, and is designed for flux densities roughly twice the values of the cavity receiver.

The experiences gained with the ASR will lead to a concept of open receivers that can be part of a commercial solar power plant using the same design principles as used in the ASR. Therefore, it is a step forward into a commercial use of solar power for high temperature applications.

The ASR will be installed on Site during the first half of 1983 to be tested and investigated during the second half of this year.

Careful preparations and calculations have been done during design and construction of the ASR, highlights of this process have been documented in a series of so-called topic reports. These papers are published to give a comprehensive overview of the main features and characteristics of the Advanced Sodium Receiver.

- W. Grasse -

IEA ALMERIA PROJECT

ADVANCED SODIUM RECEIVER (ASR)

TOPIC REPORTS

C O N T E N T S

VOLUME 1

Topic Report Nr. 1 Incident Flux Distribution

Topic Report Nr. 2 Absorber Thermal Analysis

Topic Report Nr. 3 Tube Panel Stress Analysis

Topic Report Nr. 4 Dynamic Model

Topic Report Nr. 5 Final Design of ASR Temperature Control System

VOLUME 2

Topic Report Nr. 6 Operating Conditions to be considered in the Lifetime Analysis

Topic Report Nr. 7 Tube Panel Final Stress Analysis

Topic Report Nr. 8 Final Evaluation of Receiver Thermal State

Topic Report Nr. 9 Receiver Piping System Stress Analysis

Topic Report Nr. 10 Receiver Structure Analysis

Topic Report Nr. 11 DDC Final Configeration

Topic Report Nr. 12 Receiver Headers Stress Analysis

Topic Report Nr. 13 Tube-stirrup Supporting Plate Connection Analysis

Topic Report Nr. 14 Final Workshop Acceptance Procedure

I E A ALMERIA PROJECT

ADVANCED SODIUM RECEIVER

A S R

INCIDENT FLUX DISTRIBUTION

PROGRESS REPORT No. 8 = Revision of TOPIC REPORT Nr. 1

REVISION 0

SEPTEMBER, 1981

PREPARED BY: ENEL

FRANCO TOSI

SNAMPROGETTI

CONTENTS

0. FOREWORD

1. INCIDENT FLUX MAP ON TARGET

2. CLOUD PASSAGE SIMULATION

APPENDIX

FOREWORD

This report is a compilation of the work accomplished by the Italian Consortium SNAMPROGETTI/F.TOSI/ENEL for the Operating Agent (Deutsche Forshungs und Versuchsaustalt fuer Luft und Raumfahrt) of the International Energy Agency (IEA) from april to september, 1981.

The aim is to present the CRS heliostat field output in connection with the use of the Advanced Sodium-Cooled Receiver (ASR). The subject was already discussed in the Topic Report n. 1 (March 1981), but, after the change of the heliostat total error (beam quality and tracking) from the "expected" value 2.6 mrad to the "in field" value 3.1 mrad, updated and revised results are required, in order to go on with the detailed design of the receiver. In fact a deeper approach to problems like stress analysis and life evaluation is heavily conditioned by the accuracy of the thermal input. In consequence of the reduced heliostat precision, aiming points should be shifted towords the target center, in order to control the spillage, but the flux peak increase has to be kept as small as possible. As the margin is not so wide and the adjustment is critical, it becomes necessary a new and exhaustive evaluation of the flux distribution on the target. Taking

into consideration the OA's information deriving from the direct experience in Almeria, the assumption of a total error of 3.5 mrad is checked too and the result presented.

A full treatment of the flux distribution transient, resulting from a cloud passage, taking into account the suggestion of OA/Interatom, is also included and detailed result shown. In order to maintain the consistency with the already presented analysis, the total error is maintained at the previous reference value (2.6 mrad).

1. INCIDENT FLUX MAPS ON TARGET

The task comprises estensive computer-aided analysis to establish the new interface between the Heliostat Field Subsystem and the ASR. Starting from the adopted field layout and focal zones, the updated total error value of 3.1 mrad is adopted. The center target point is heightened (from 43 to 44 m.) in order to take into account the receiver piping and connection arrangements. Mirror reflectivity is .915.
The last release of Helios program (March 1981), checked and modified by SP, is used in this computation. The program outputs (nodal point fluxes at target plane, door plane and protection refractory plane, 11x11 matrix) are graphically presented in order to make easier the evaluation. The cross aiming strategy (see fig. n. 1.1) is maintained, but the B1 and B2 aiming points are shifted to the center (10 cm both in x and z direction). This value is choosen according to the need of containing spillage and flux peak increase within acceptable bounds. The target dimension is 3 x 3 m, whereas the present dimensions of ASR is 2.75 x 2.85 m. The reason is to compute the flux values also on the refractory wall frame and not only at the boundary. Consequently the ASR incident flux interception is over-estimated and the spillage value under-estimated.

Flux patterns at target plane are computed on the basis of the corrected aiming point positions. The consistency of the preliminary results with the basiline specification of Report n. 3 (May, 1980) is verified and the results presented for the instants below indicated:

- Day 80 (spring equinox), noon (design point) (fig. 1.2÷1.7)
- Day 80, 10.30 a.m. (fig. 1.8÷1.10)
- Day 80, 7.15 a.m. (fig. 1.11÷1.13)
- Day 172 (summer solstice), noon (fig. 1.14÷1.16)
- Day 172, 9.30 a.m. (fig. 1.17÷1.19)
- Day 172, 6.15 a.m. (fig. 1.20÷1.22)
- Day 355 (winter solstice), noon (fig. 1.23÷1.25)
- Day 355, 9.30 (fig. 1.26÷1.28)
- Day 355, 8.15 (fig. 1.29÷1.31)

In all the calculations the direct insolation is read on the reference graph (SSPS Report dated 3,1978). The facet curvature is the nominal one (144, 202, 164, 324 m. of radius) as the effect of ambient temperature on curvature radius and consequently on flux distributions has been already analized in Progress Report n. 6 (December, 1980). As shown, the differences caused

in peak flux and spillage are small.
Fig. n. 1.33, 1.34, 1.35 shown the flux peak value, the incident thermal power and the spillage vs time for summer and winter solstice and equinox.
The starting time in the morning must be selected considering the thermal balance of the receiver and the operational constraints. In the present analysis, the assumption "sun at 10 degree above the horizon" is adopted, linking the sun elevation through the local time, with the direct beam (fig. n. 1.32).
This hypothesis corresponds to a direct beam in the range 250 - 300 W/cm^2 and to incident power on the target spreaded from 400 to 600 KW, in consequence on the different working points and efficiency of mirror field.
Fig. 1.36 through 1.38 show respectively the minimum and the maximum spillage, the flux peak on the target and on the frame and the maximum power incident on the target in the day vs the day in the year.
At design point (Day 80, noon) and at a maximum spillage condition (Day 172, h. 6.15), in order to analyze the system reply to subsequent total error adjustment, flux distributions on target are computed again with the same aiming point position but with an error of 3.5 mrad.(fig. 1.39 to 1.46).
Fig. 1.41, 1.42, 1.43 allow the comparison with the previous error hypotheses; 3.5 mrad error results are reported on the previously shown figures too (▲).

Computations at door plane (5x5 m target, 3.1 mrad error, Day 172, noon and 6.15 a.m.) are accomplished, in order to evaluate the thermal flux impinging on door limb and structure (fig. 1.47 to 1.58).
Likewise for a 45 deg. angled lateral bord of refractory protection, incident fluxes are computed at max. spillage condition (3.1 mrad error, Day 172, noon and 6.15 a.m.; 3.5 mrad, Day 172, noon) (fig. 1.59 to 1.73).
Fig. 1.74 to 1.81 show the thermal flux impinging on the receiver casing, 30 cm. before the absorber plane.
The result can be summarized (3.5 mrad value in parenthesis):

	Ø max (W/cm^2)		Incident power (KW)	
	21/6, noon	21/6, 6.15	21/6, noon	21/6, 6.15
Door frame	1.5	2.0 (2.1)		
Receiver contour (right side, 45°)	7.1	4.6 (7.75)	23	34 (47)
Receiver casing	4.5	4.75		

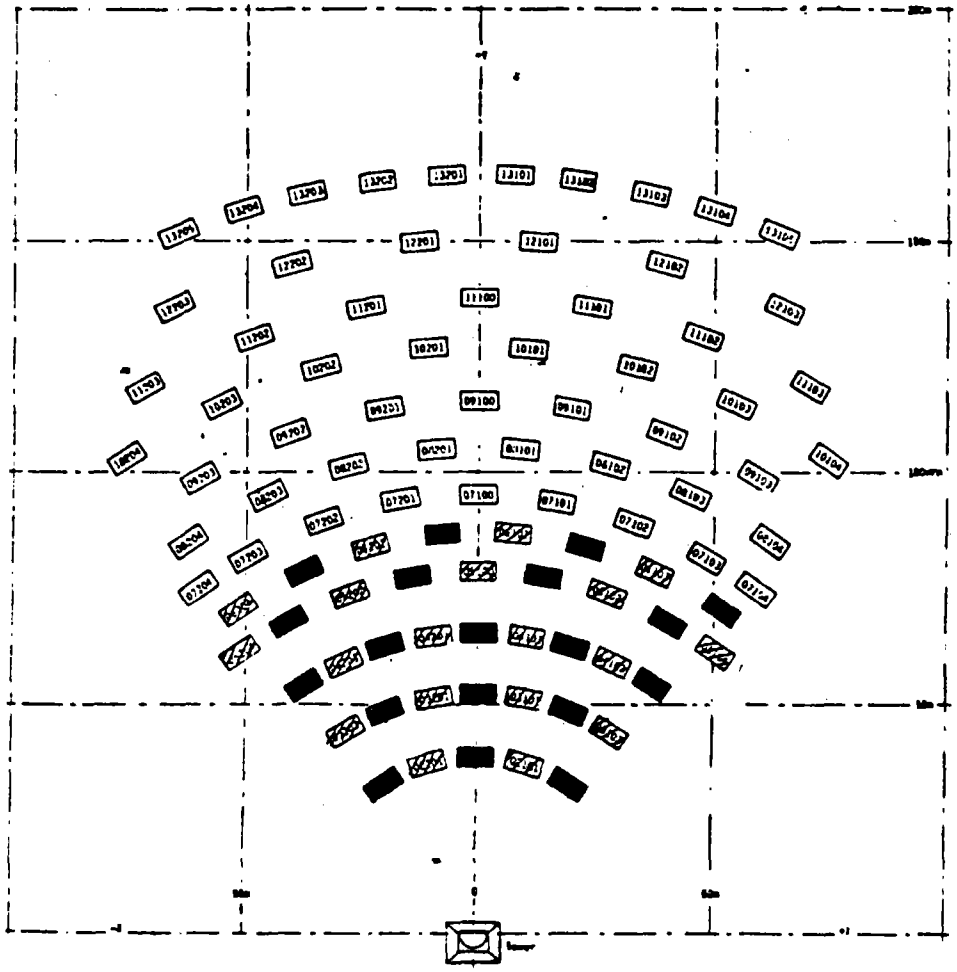

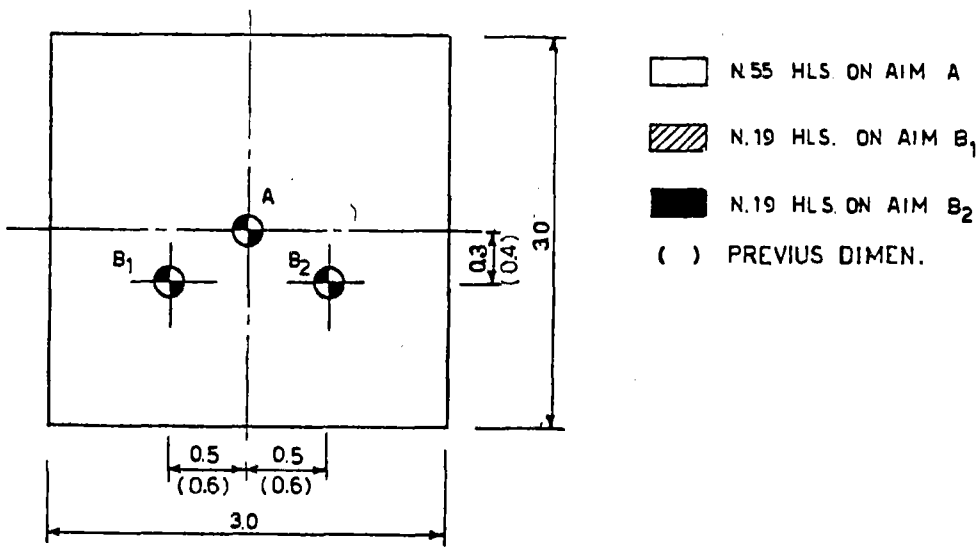

FIG. 1.1 HELIOSTAT FIELD AND AIMING STRATEGY
(STD. DEV. 3.1 AND 3.5 mrad)

ASR-ALMERIA 3.1MRAD ERROR 21/3 NOON

	.08	.27	.65	1,20	1,75	1,98	1,74	1,20	.64	.26	.08
	.30	.93	2,26	4,30	6,38	7,28	6,36	4,28	2,25	.93	.29
	.77	2,48	6,22	12,2	18,6	21,4	18,6	12,2	6,20	2,49	.79
	1,58	5,41	14,3	28,5	43,3	49,7	43,2	28,5	14,3	5,47	1,65
	2,63	10,2	29,3	58,1	82,3	90,7	82,1	57,9	29,2	10,3	2,76
E.	3,45	15,5	50,4	99,3	126,	129,	125,	98,4	49,9	15,6	3,64 W.
	3,46	17,1	59,7	117,	138,	132,	136,	115,	59,1	17,3	3,68
	2,62	12,7	42,7	81,6	94,4	89,6	93,5	80,7	42,3	12,9	2,63
	1,43	6,06	17,8	32,2	38,7	38,6	38,5	32,1	17,8	6,24	1,60
	.53	1,67	4,62	8,00	10,4	11,1	10,4	8,04	4,71	1,98	.62
	.13	.40	.91	1,60	2,22	2,48	2,22	1,60	.94	.43	.15

BOT.

HELST. NO. 93,
INSOL. KW/M2 ,920
DAY NO. 80,
TIME HR. 12,
TOWER HEIGHT M 44,
TARGET DIM. M 3,0X3,0

AIM. NO. 3,
STD.DEV. MRAD. 3,10
INC.POW. KW 2870,
AVERG./PEAK ,23
SPILLAGE % ,12

FIG. 1.2 INCIDENT FLUX ON FLAT TARGET (W/CM2)

ASR-ALMERIA 3.1MRAD ERROR 21/3 NOON

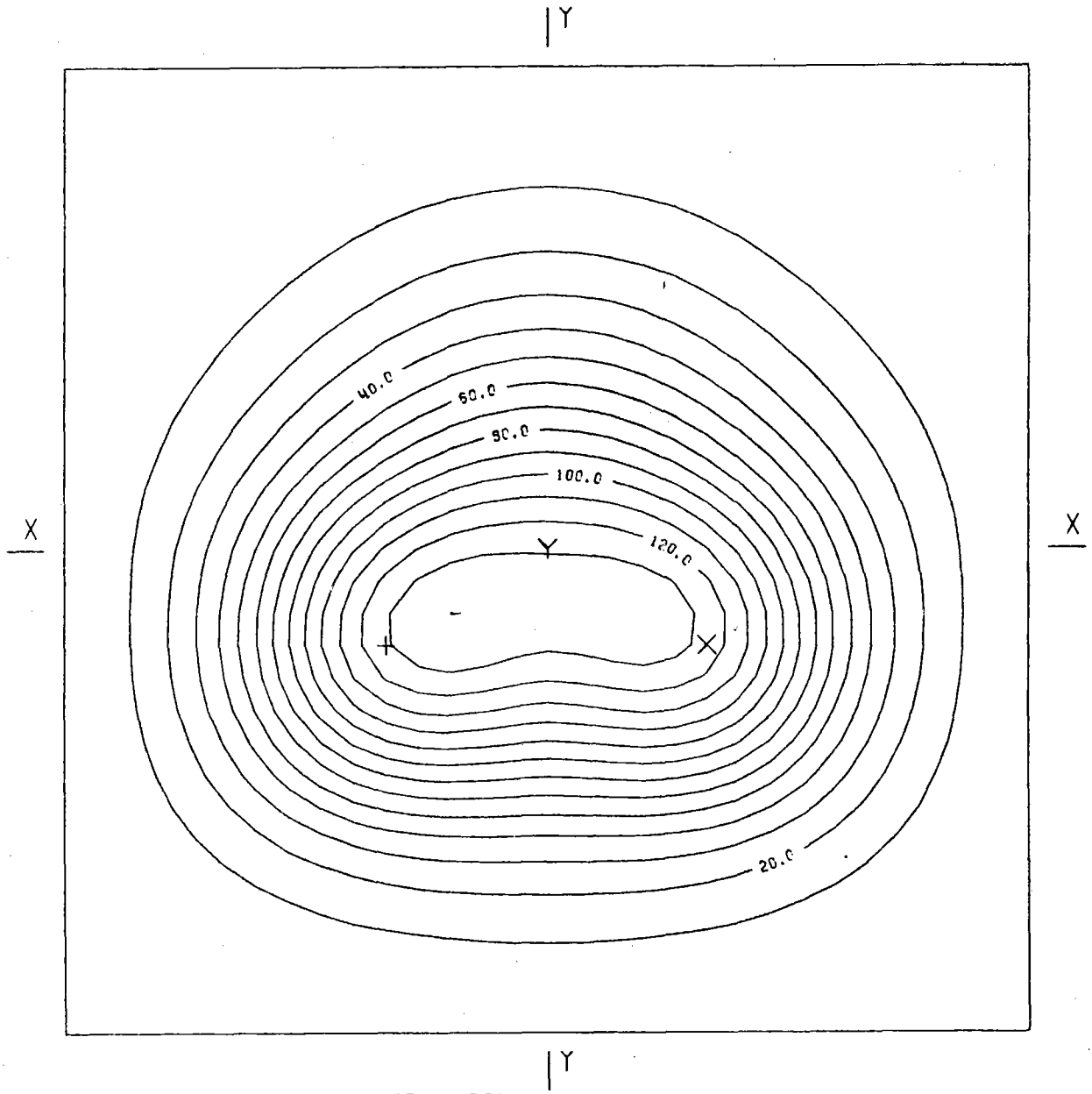

AIMING POINT: + (-,50;-,30)

× (,50;-,30)

Y (,00;,00)

FIG.1.3 EQUIFLUX LINES, SPACING (W/CM2) 10,0

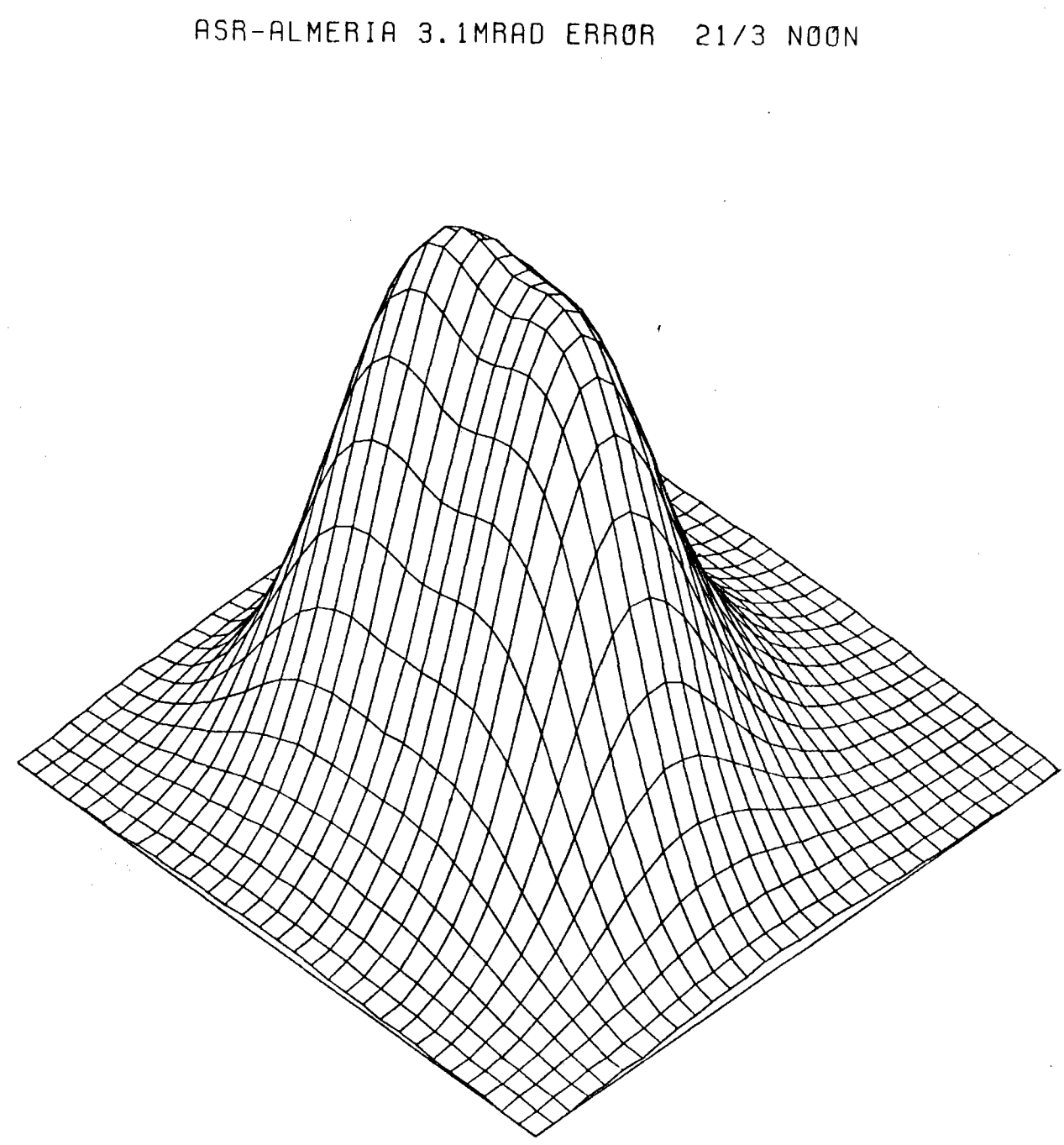

FIG.1.4 THREE-DIM. VIEW ØF INCIDENT FLUX ØN TARGET

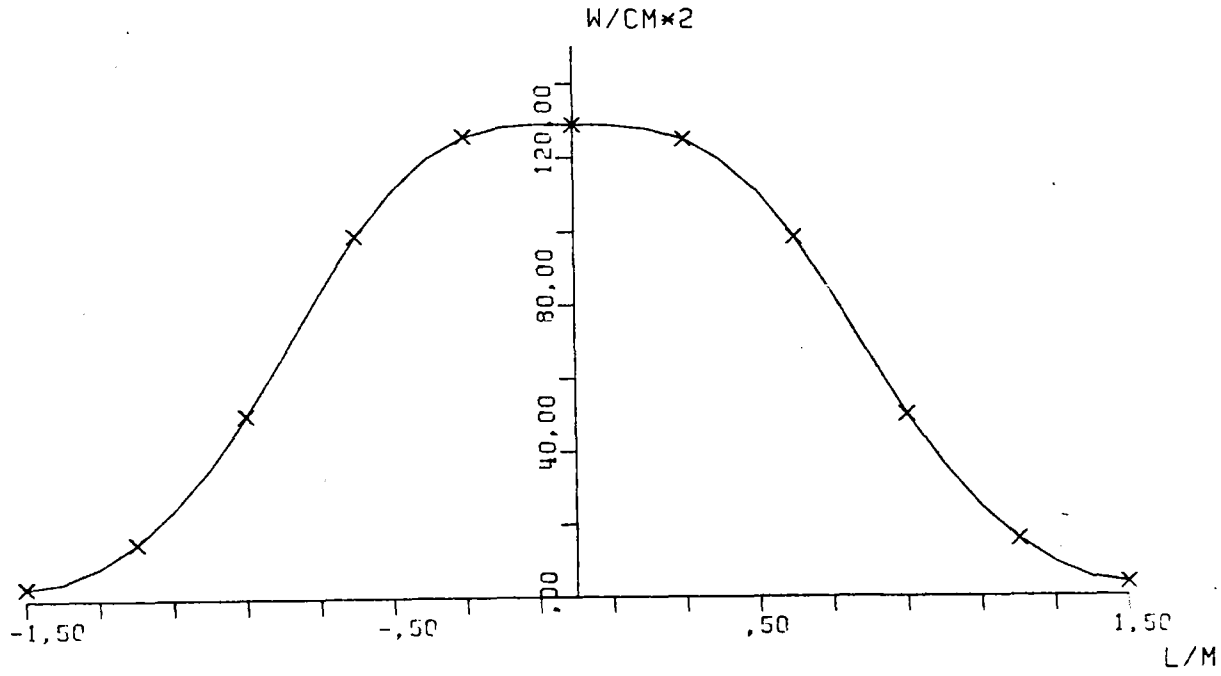

FIG.1.5 SØLAR FLUX ØN TARGET SEC X-X

ASR-ALMERIA 3.1MRAD ERROR 21/3 NOON

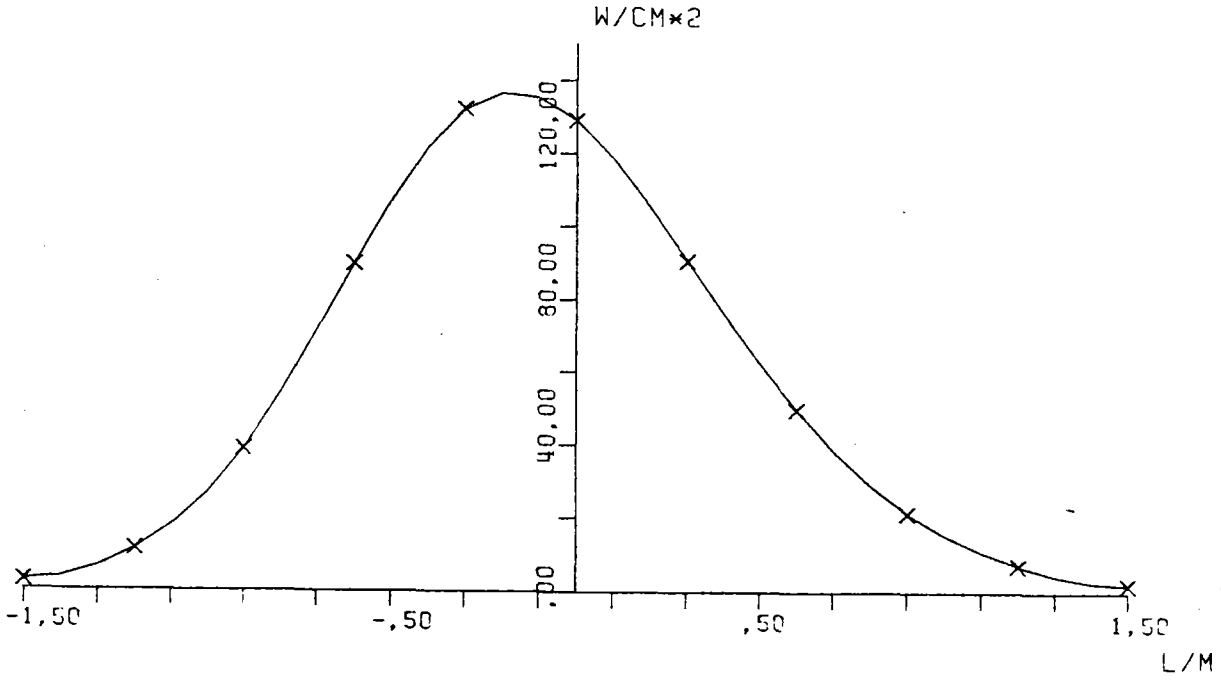

FIG.1.6 SOLAR FLUX ON TARGET SEC Y-Y

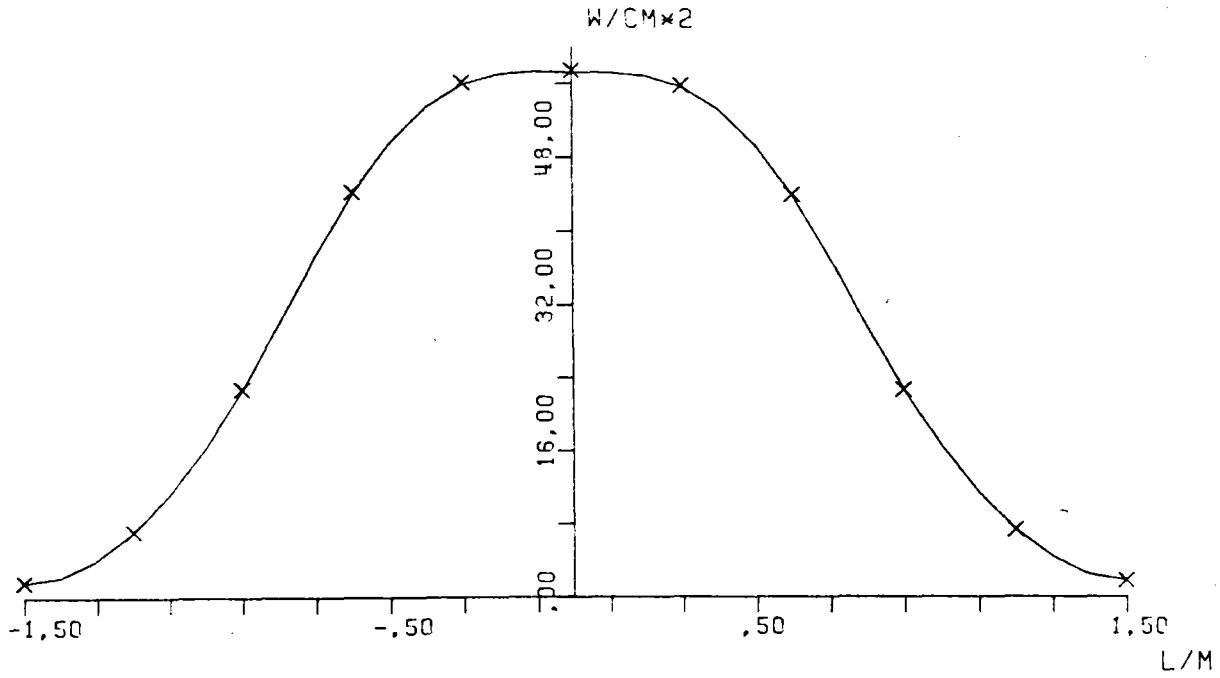

FIG.1.7 AVERAGE SOLAR FLUX ON VERTICAL STRIP

ASR-ALMERIA 3.1 MRD 21/3 H10.30

	,08	,27	,67	1,25	1,64	2,12	1,92	1,38	,60	,36	,13
	,30	,94	2,30	4,39	6,51	7,47	6,62	4,60	2,56	1,15	,42
	,77	2,49	6,26	12,3	18,5	21,1	18,3	12,3	6,64	2,59	1,02
	1,57	5,39	14,2	28,2	41,9	47,3	41,2	27,9	14,6	6,04	2,02
	2,58	9,96	28,6	55,6	77,2	84,3	77,2	55,5	28,7	10,8	3,29
E.	3,38	14,6	46,7	91,4	115.	118.	116.	92,2	47,5	16,2	4,31	W.
	3,44	15,5	52,4	104.	125.	120.	125.	107.	57,3	18,3	4,37	
	2,73	11,5	37,1	73,5	88,1	83,3	86,2	77,1	42,7	13,9	3,27	
	1,67	6,12	17,0	31,5	36,4	37,8	37,7	32,5	18,5	6,62	1,71	
	,76	2,39	5,50	9,04	11,2	11,8	11,2	8,68	4,93	1,98	,58	
	,25	,68	1,35	2,07	2,62	2,65	2,55	1,78	,97	,41	,13	

BØT.

HELST. NØ.	93,	AIM. NØ.	3,
INSOL. KW/M2	,690	STD.DEV. MRAD.	3,10
DAY NØ.	80,	INC.PØW. KW	2720,
TIME HR.	10,30	AVERG./PEAK	,24
TØWER HEIGHT M	44,	SPILLAGE %	1,41
TARGET DIM. M	3,0X3,0		

FIG.1.8 INCIDENT FLUX ØN FLAT TARGET (W/CM2)

ASR-ALMERIA 3.1 MRD 21/3 H10.30

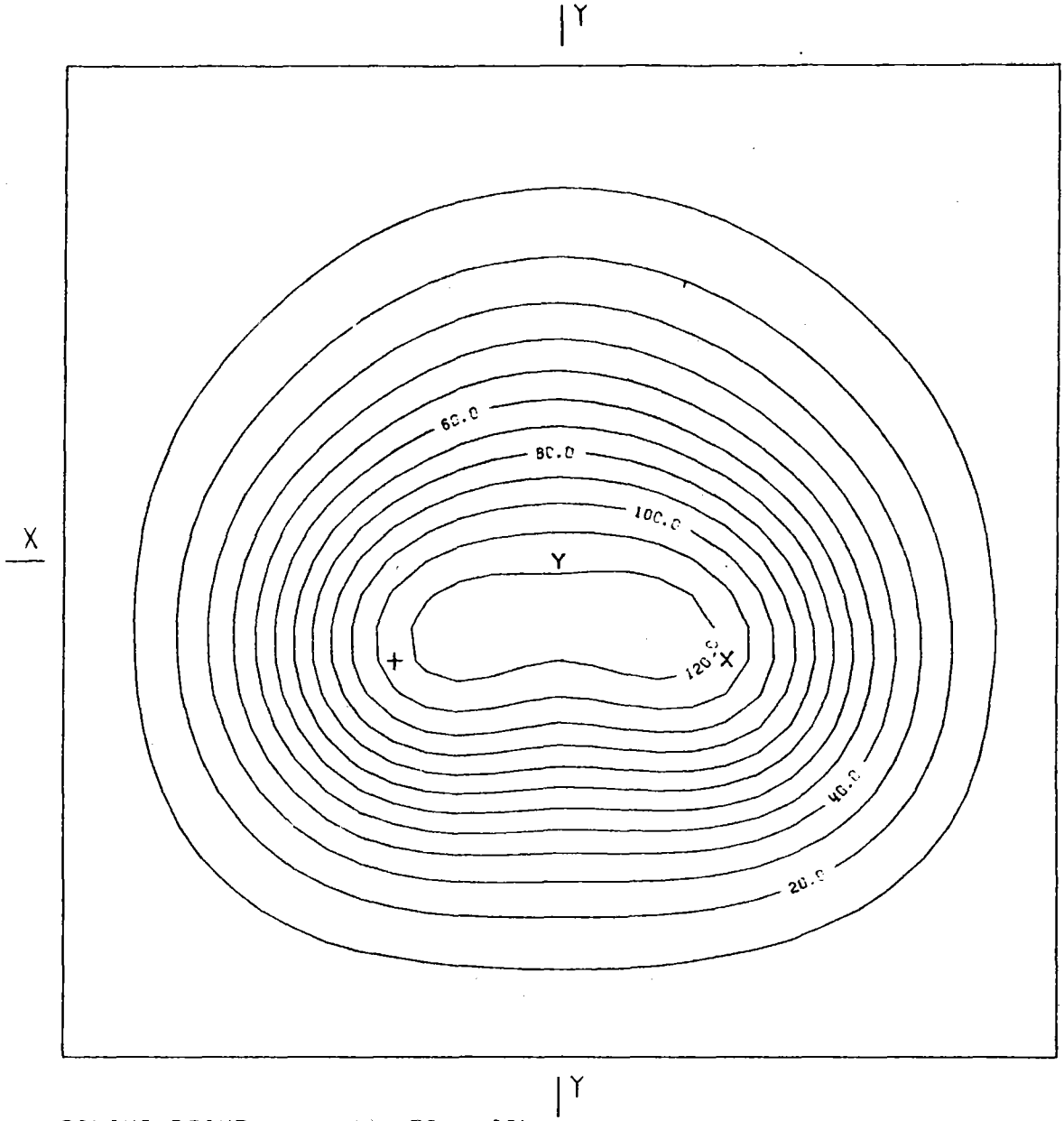

AIMING POINT: + (-,50;-,30)

× (-,50;-,30)

Y (,00;,00)

FIG.1.9 EQUIFLUX LINES, SPACING (W/CM2) 10,0

ASR-ALMERIA 3.1 MRD 21/3 H10.30

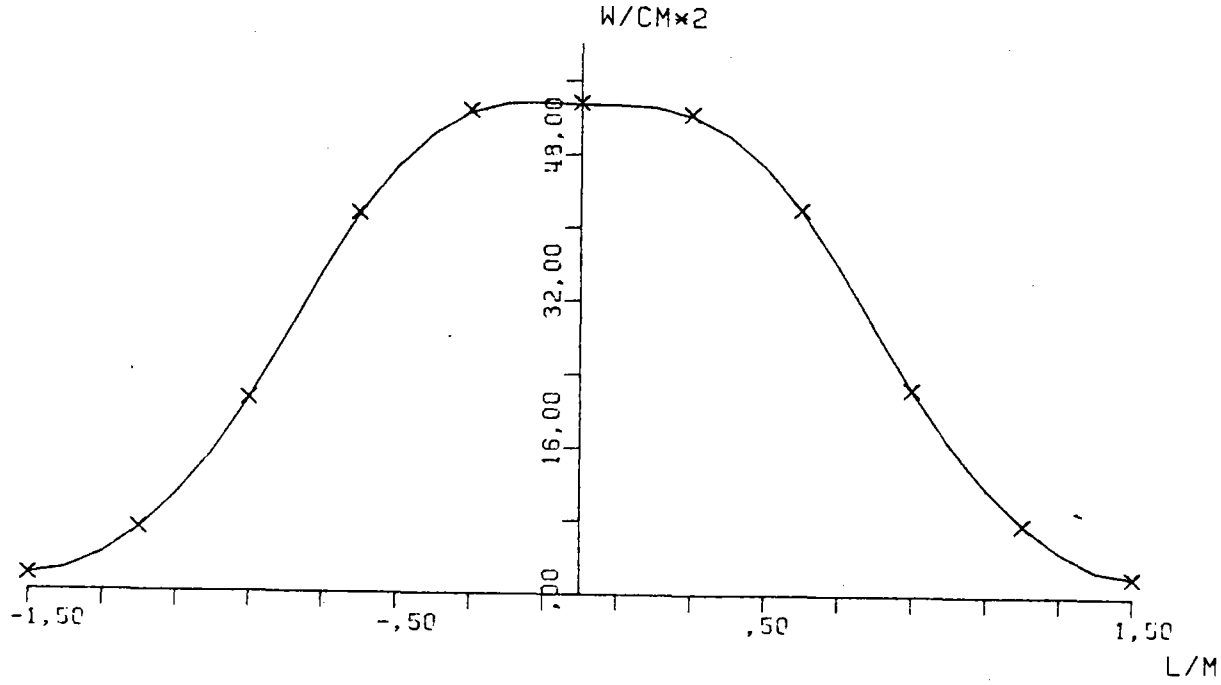

FIG. 1.10 AVERAGE SOLAR FLUX ON VERTICAL STRIP

ASR-ALMERIA 3.1 MRD 21/3 H7.15

	,30	,70	1,26	1,78	2,10	2,19	1,98	1,55	1,18	,90	,66	
	,65	1,55	2,79	3,93	4,75	5,09	4,57	3,51	2,64	1,93	1,33	
	1,22	2,96	5,36	7,54	9,33	10,1	8,99	6,67	4,98	3,39	2,14	
	1,95	4,91	8,98	12,7	15,6	17,2	15,5	11,6	8,19	5,08	2,69	
	2,67	6,94	13,0	18,6	23,0	25,2	23,0	17,8	12,0	6,77	3,43	
E.	3,10	8,08	15,6	22,6	27,9	30,6	28,5	22,7	15,3	8,19	3,71	W.
	3,09	7,70	15,0	22,1	27,4	30,1	28,6	23,4	16,3	8,79	3,69	
	2,77	6,22	11,6	17,2	21,6	23,6	22,9	19,1	14,0	7,90	3,27	
	2,30	4,53	7,64	11,0	13,7	15,3	14,6	12,4	9,36	5,68	2,45	
	1,74	3,06	4,51	5,95	7,33	8,22	7,92	6,55	5,02	3,25	1,51	
	1,17	1,89	2,44	2,67	3,43	3,62	3,61	2,93	2,26	1,54	,77	

BØT.

HELST. NØ.	93,	AIM. NØ.	3,
INSØL. KW/M2	,490	STD.DEV. MRAD.	3,10
DAY NØ.	80,	INC.PØW. KW	930,
TIME HR.	7,15	AVERG./PEAK	,34
TOWER HEIGHT M	44,	SPILLAGE %	8,31
TARGET DIM. M	3,0X3,0		

FIG.1.11 INCIDENT FLUX ØN FLAT TARGET (W/CM2)

ASR-ALMERIA 3.1 MRD 21/3 H7.15

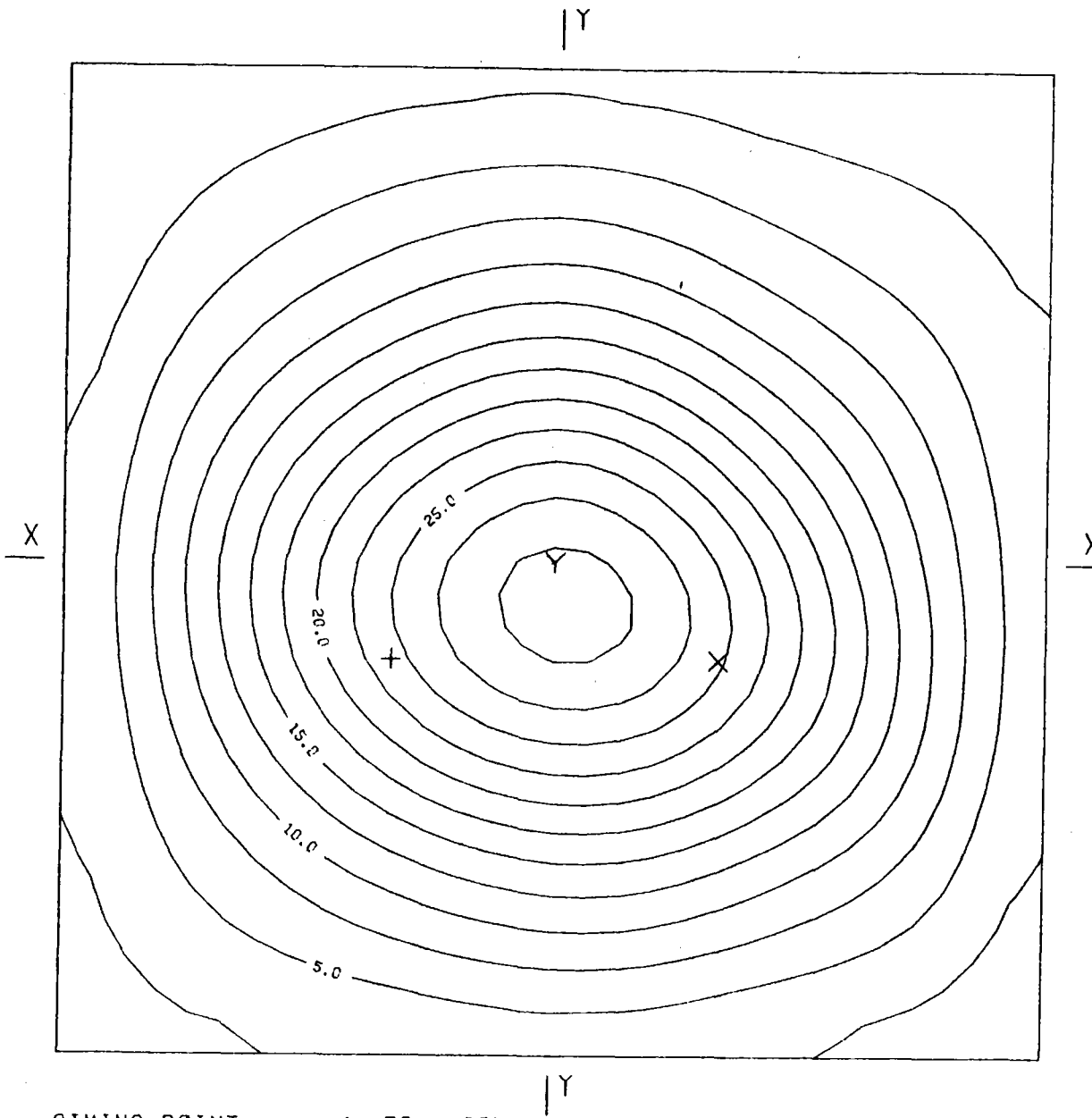

AIMING POINT: + (-,50;-,30)
× (,50;-,30)
Y (,00;,00)

FIG.1.12 EQUIFLUX LINES, SPACING (W/CM2) 2,5

ASR-ALMERIA 3.1 MRD 21/3 H7.15

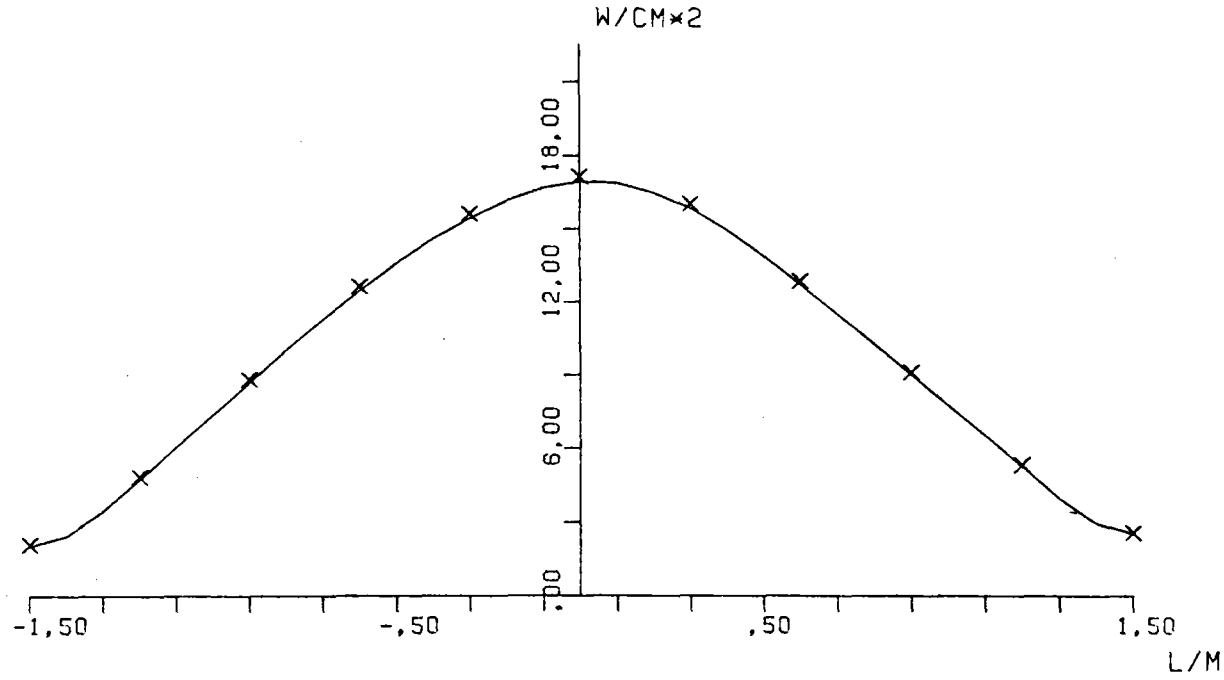

FIG.1.13 AVERAGE SOLAR FLUX ON VERTICAL STRIP

ASR-ALMERIA 3.1 MRD 21/6 NØØN

	,20	,53	1,09	1,82	2,45	2,70	2,44	1,81	1,09	,53	,20	
	,57	1,52	3,23	5,54	7,64	8,50	7,63	5,52	3,22	1,52	,58	
	1,30	3,58	7,65	13,5	19,4	21,5	19,4	13,5	7,55	3,60	1,33	
	2,49	7,27	16,5	29,1	40,6	45,4	40,6	29,0	16,5	7,33	2,57	
	4,00	12,9	31,0	54,0	71,9	78,2	71,7	53,5	30,6	12,9	4,15	
E.	5,29	18,6	49,0	84,5	105,	109,	105,	84,0	48,5	18,9	5,51	W.
	5,60	21,0	57,0	97,5	116,	116,	114,	96,3	56,3	21,2	5,65	
	4,59	16,9	44,0	73,6	86,3	86,2	85,3	72,6	43,4	16,9	4,63	
	2,78	9,24	21,7	35,0	42,2	43,5	42,0	34,5	21,6	9,28	2,96	
	1,18	3,44	7,23	11,4	14,3	15,4	14,3	11,4	7,26	3,51	1,29	
	,35	,93	1,65	2,91	3,60	4,15	3,79	2,91	1,67	,97	,40	

BØT.

HELST. NØ.	93,	AIM. NØ.	3,
INSOL. KW/M2	,955	STD.DEV. MRAD.	3,10
DAY NØ.	172,	INC.PØW. KW	2750,
TIME HR.	12,	AVERG./PEAK	,26
TØWER HEIGHT M	44,	SPILLAGE %	2,06
TARGET DIM. M	3,0X3,0		

FIG.1.14 INCIDENT FLUX ØN FLAT TARGET (W/CM2)

ASR-ALMERIA 3.1 MRD 21/6 NOON

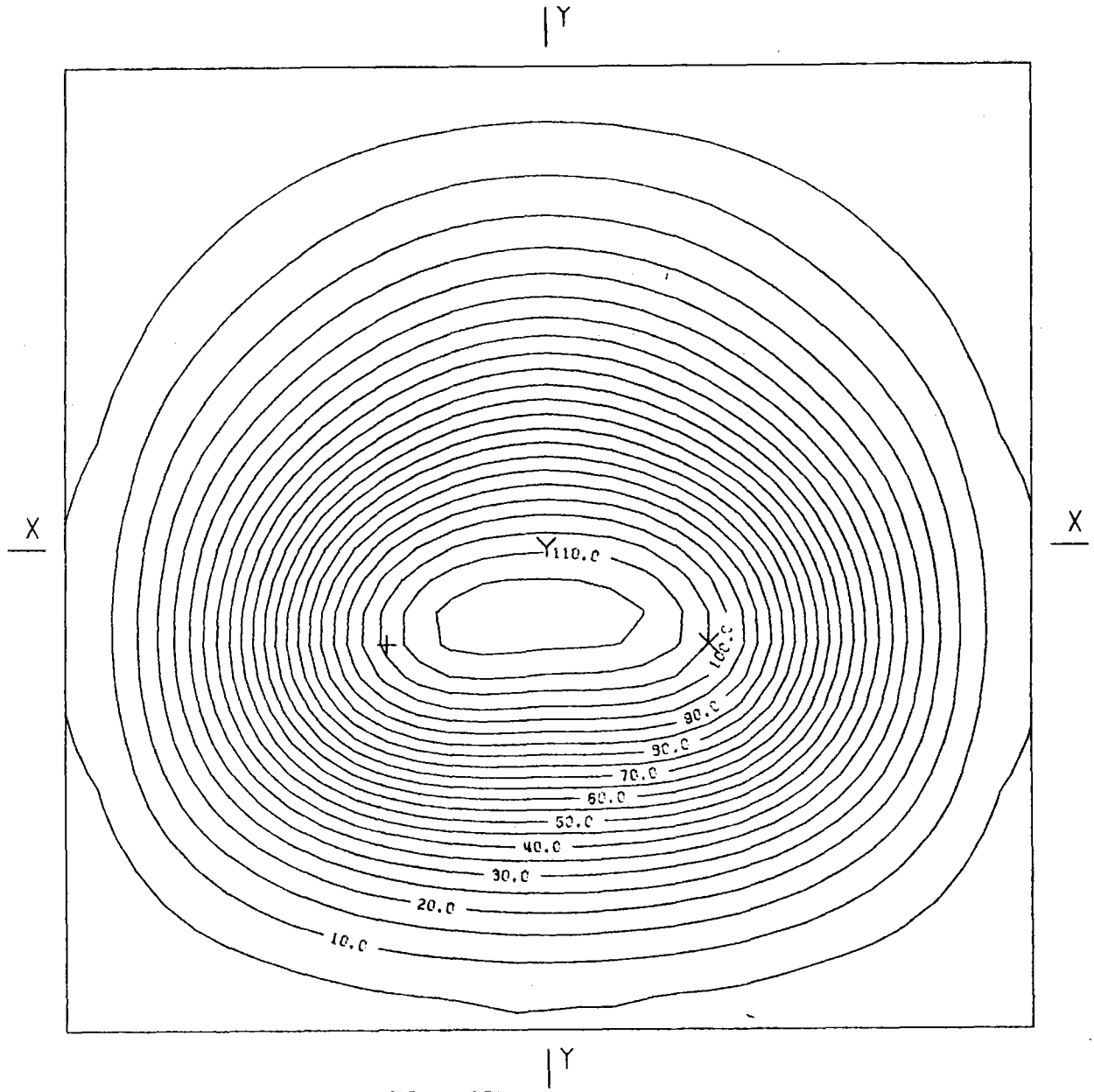

AIMING POINT: + (-,50;-,30)

× (,50;-,30)

Y (,00;,00)

FIG.1.15 EQUIFLUX LINES, SPACING (W/CM2) 5,0

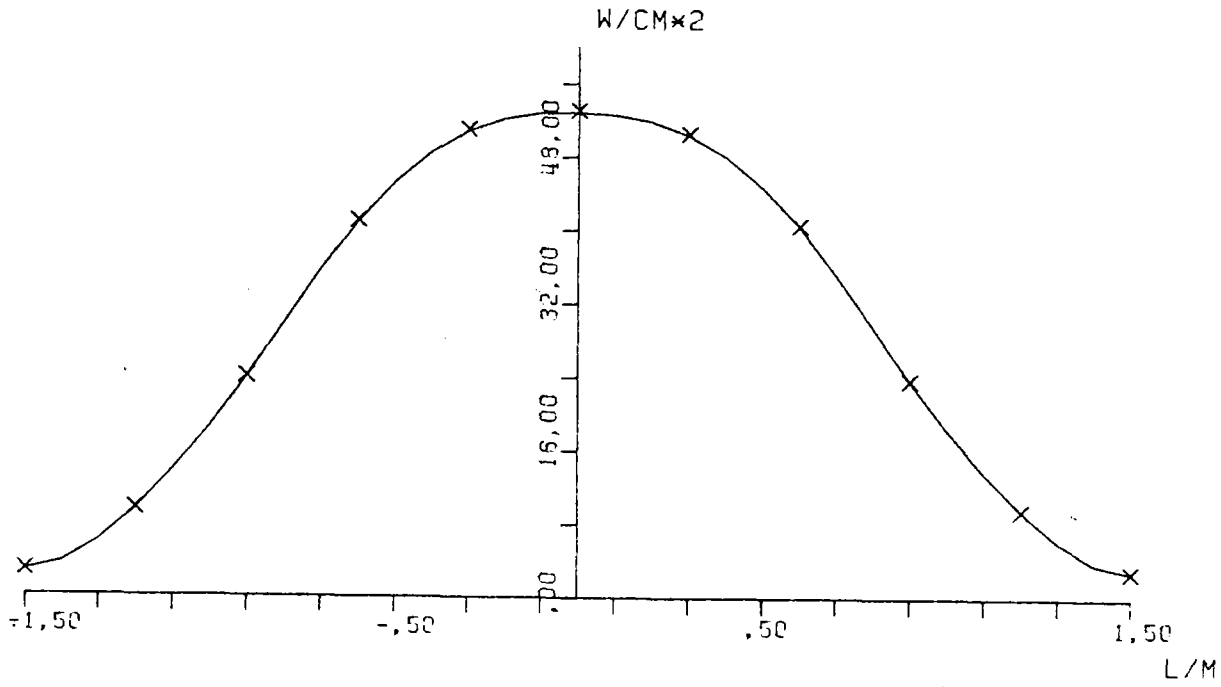

FIG. 1.16 AVERAGE SØLAR FLUX ØN VERTICAL STRIP

ASR-ALMERIA 3.1 MRD 21/6 H9.30

	,29	,74	1,49	2,42	3,23	3,59	3,39	2,77	1,96	1,20	,63	
	,77	1,96	4,02	6,64	8,68	9,77	8,99	7,04	4,77	2,62	1,44	
	1,63	4,29	9,01	15,1	20,3	22,1	19,9	15,1	9,99	5,66	2,69	
	2,92	8,10	17,5	29,3	39,0	42,0	37,7	28,6	18,5	9,66	4,13	
	4,47	13,3	30,3	49,9	62,5	66,5	62,2	48,7	29,7	14,0	5,39	
E.	5,70	17,5	42,5	69,5	83,0	88,6	84,5	68,6	41,1	18,3	6,54	W.
	5,92	18,2	44,0	73,4	88,0	90,0	89,2	76,0	47,5	21,1	7,26	
	5,13	14,7	33,9	57,6	70,9	71,4	70,2	62,5	41,1	18,7	6,41	
	3,91	10,00	21,1	33,5	41,1	42,0	41,2	36,1	23,9	11,4	4,08	
	2,66	5,99	10,7	14,9	17,5	18,6	17,6	14,4	9,40	4,72	1,63	
	1,46	2,79	4,16	5,14	5,97	6,34	5,70	4,33	2,79	1,47	,60	

BØT.

HELST. NØ. 93,
INSOL. KW/M2 ,925
DAY NØ. 172,
TIME HR. 9,30
TOWER HEIGHT M 44,
TARGET DIM. M 3,0X3,0

AIM. NØ. 3,
STD.DEV. MRAD. 3,10
INC.POW. KW 2460,
AVERG./PEAK ,30
SPILLAGE % 3,99

FIG.1.17 INCIDENT FLUX ØN FLAT TARGET (W/CM2)

ASR-ALMERIA 3.1 MRD 21/6 H9.30

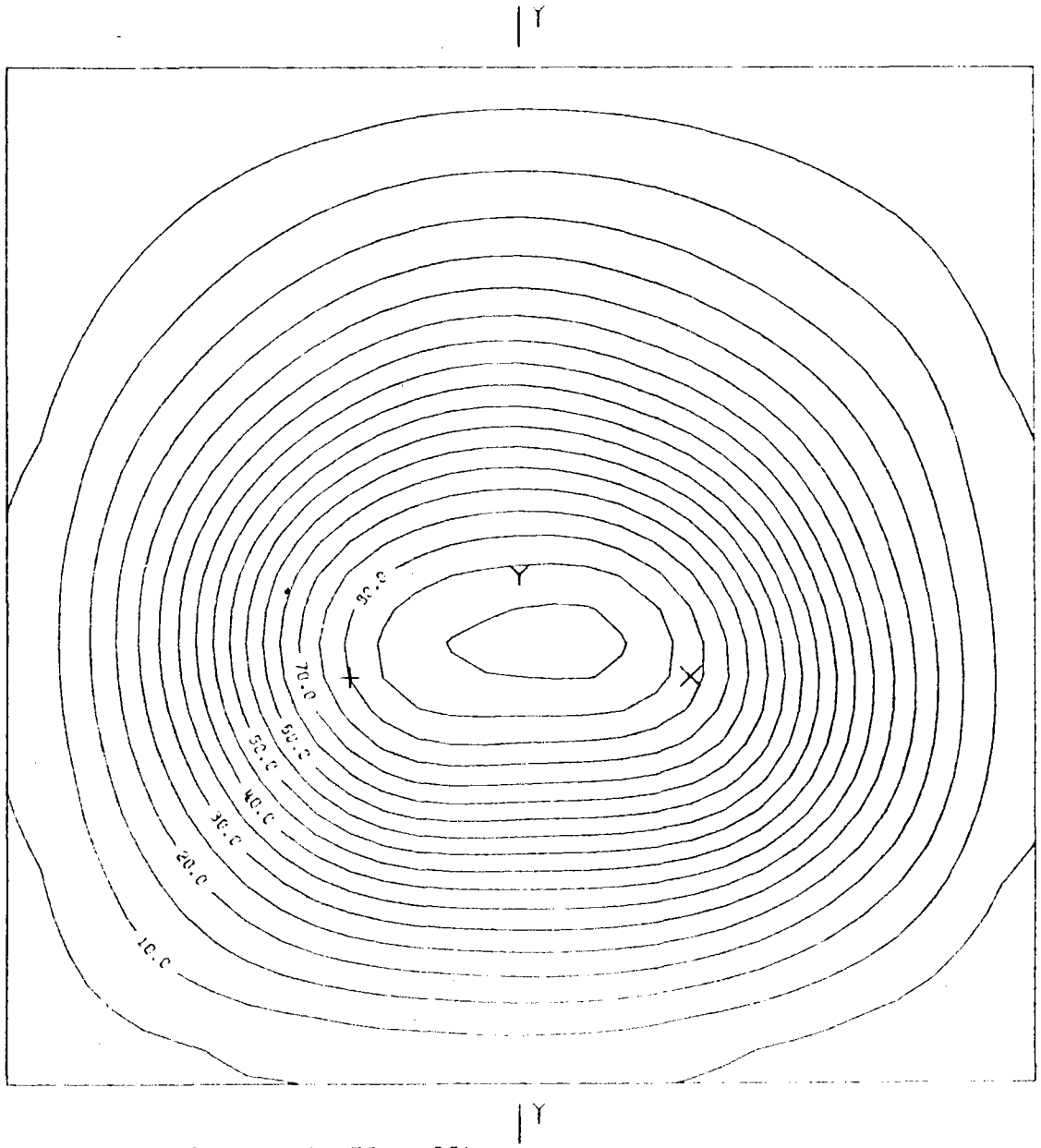

AIMING POINT: + (-,50;-,30)

× (,50;-,30)

Y (,00;,00)

FIG.1.18 EQUIFLUX LINES, SPACING (W/CM2) 5,0

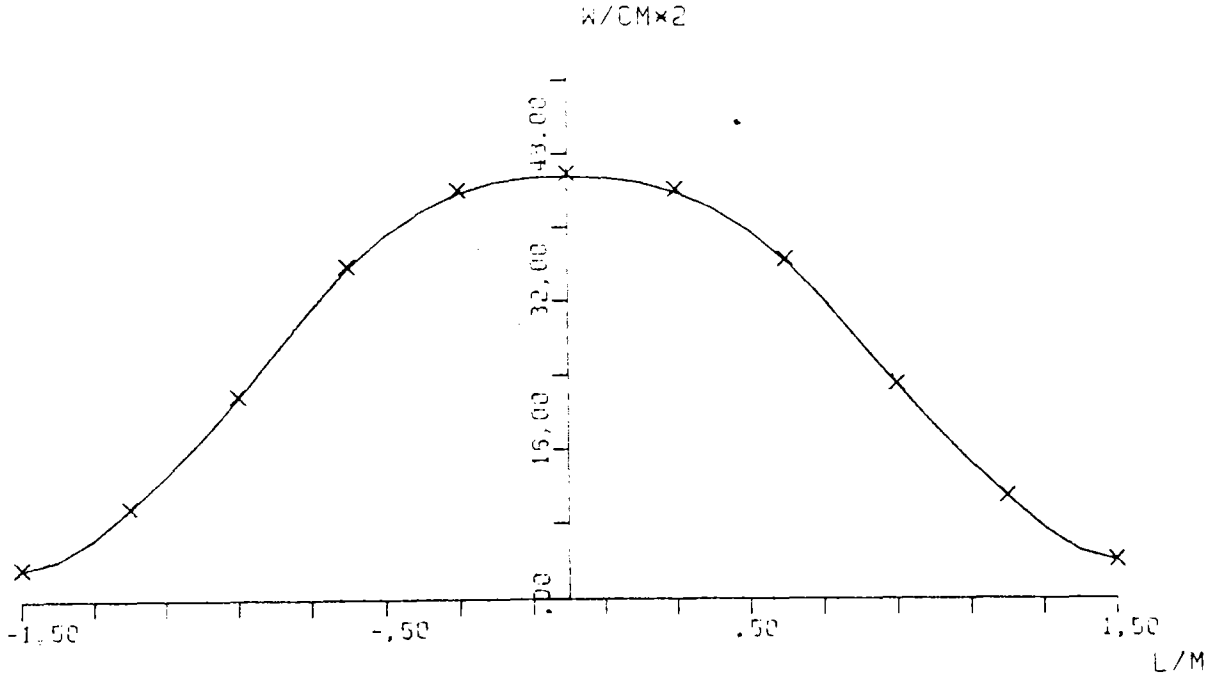

FIG.1.19 AVERAGE SOLAR FLUX ON VERTICAL STRIP

ASR-ALMERIA 3.1MRAD ERROR 21/6 H6.15

	.80	1,76	2,96	3,80	3,70	3,85	3,19	2,48	1,83	1,32	1,01
	1,43	3,05	4,87	5,66	5,93	6,09	5,33	4,16	3,17	2,43	1,91
	2,28	4,73	7,16	8,12	8,81	9,35	8,28	6,52	5,08	4,00	3,04
	3,22	6,46	9,40	10,6	11,9	13,0	11,6	9,24	7,42	5,77	4,14
	4,03	7,80	10,9	12,3	14,4	16,0	14,5	11,6	9,67	7,42	4,95
E.	4,55	8,33	11,3	12,9	15,3	17,5	16,1	13,3	11,1	8,38	5,26	W.
	4,69	8,01	10,6	12,1	14,7	17,1	16,0	13,4	11,3	8,60	5,09	
	4,42	7,00	9,03	10,4	12,9	15,2	14,4	12,1	10,5	8,01	4,52	
	3,78	5,55	6,94	8,12	10,2	12,2	11,7	9,93	8,81	6,78	3,70	
	2,91	3,94	4,78	5,71	7,32	8,86	8,54	7,28	6,62	5,15	2,73	
	1,99	2,49	2,95	3,61	4,81	5,77	5,55	4,80	4,46	3,46	1,77	

BOT.

HELST. NO.	93,	AIM. NO.	3,
INSOL. KW/M2	,51C	STD.DEV. MRAD.	3,10
DAY NO.	172,	INC.POW. KW	748,
TIME HR.	6,15	AVERAG./PEAK	,25
TOWER HEIGHT M	44,	SPILLAGE %	20,72
TARGET DIM. M	3,CX3,0		

FIG.1.20 INCIDENT FLUX ON FLAT TARGET (W/CM2)

ASR-ALMERIA 3.1MRAD ERROR 21/6 H6.15

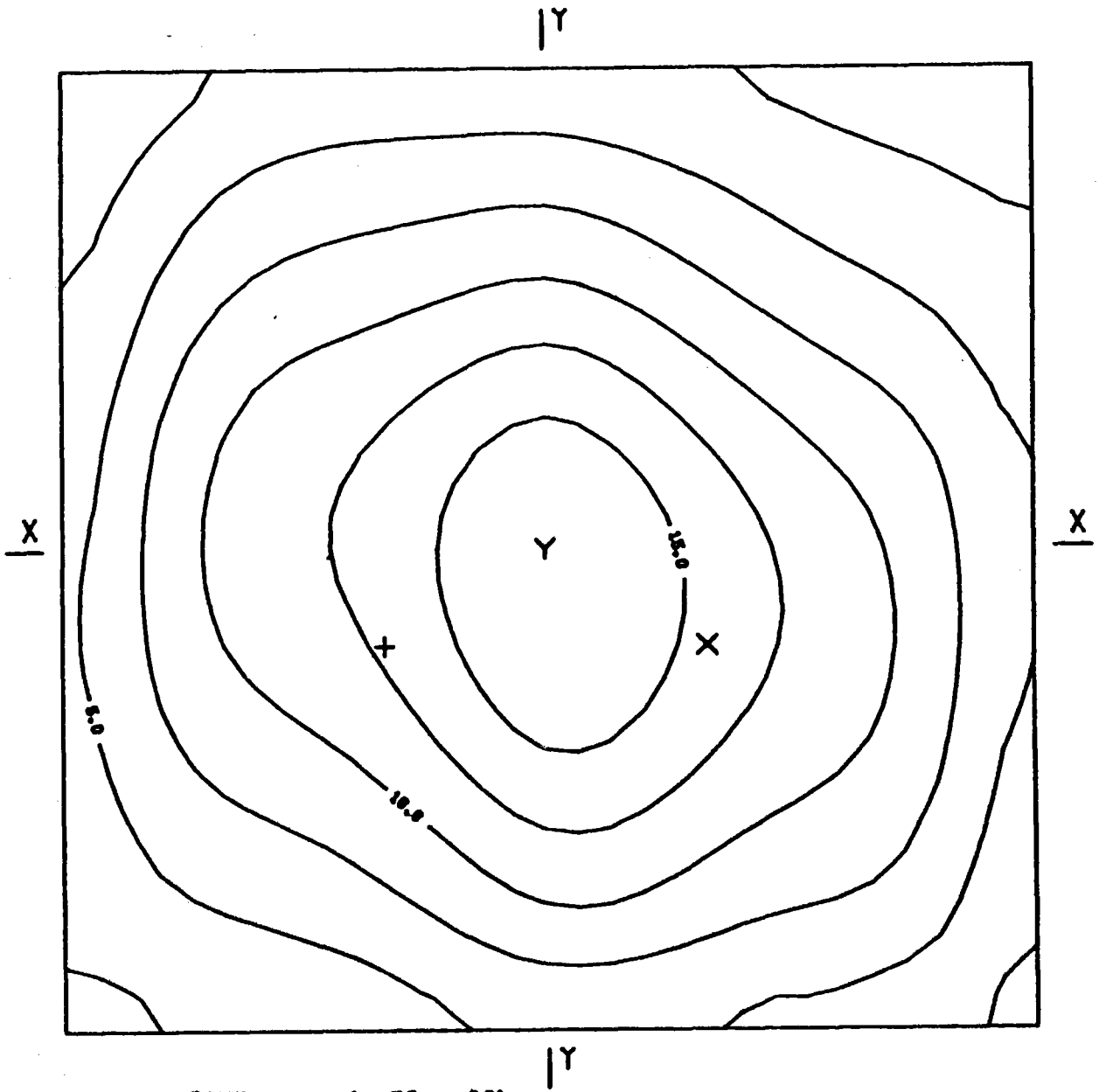

AIMING POINT: + (-,50;-,30)
× (,50;-,30)
Y (,00;,00)

FIG.1.21 EQUIFLUX LINES, SPACING (W/CM2) 2,5

ASR-ALMERIA 3.1MRAD ERROR 21/6 H6.15

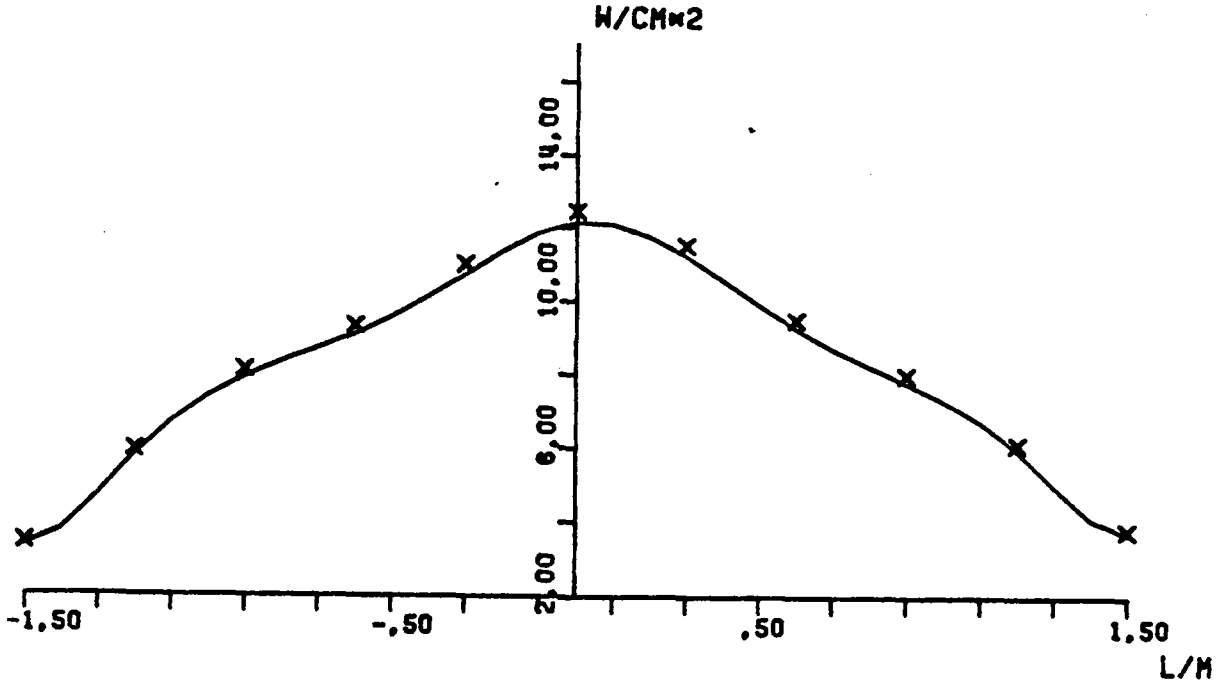

FIG.1.22 AVERAGE SOLAR FLUX ON VERTICAL STRIP

ASR-ALMERIA 3.1 MRD 21/12 NOON

	,05	,19	,49	,93	1,35	1,55	1,35	,92	,48	,19	,05	
	,22	,72	1,79	3,47	5,21	5,97	5,20	3,45	1,78	,71	,22	
	,60	2,01	5,16	10,2	15,7	18,2	15,7	10,2	5,10	1,98	,60	
	1,25	4,50	12,2	24,5	37,5	43,2	37,6	25,1	12,1	4,46	1,29	
	2,04	8,18	24,3	49,1	70,5	78,0	72,2	52,0	24,6	8,23	2,16	
E.	2,58	11,5	37,4	76,9	101.	105.	106.	64,2	39,9	12,0	2,74	W.
	2,45	11,7	40,2	83,1	102.	101.	110.	92,6	44,0	12,4	2,61	
	1,72	8,28	29,2	57,0	68,1	66,7	73,6	63,9	30,6	8,74	1,66	
	,66	3,58	12,3	23,7	28,6	28,6	30,7	26,2	12,9	4,08	,96	
	,29	1,18	3,38	6,16	7,94	8,32	8,13	6,47	3,39	1,25	,34	
	,06	,24	,64	1,16	1,62	1,78	1,60	1,16	,63	,26	,07	

BOT.

HELST. NO. 93,
INSOL. KW/M2 ,750
DAY NO. 355,
TIME HR. 12,
TOWER HEIGHT M 44,
TARGET DIM. M 3,0X3,0

AIM. NO. 3,
STD.DEV. MRAD. 3,10
INC.POW. KW 2270,
AVERG./PEAK ,23
SPILLAGE % ,77

FIG.1.23 INCIDENT FLUX ON FLAT TARGET (W/CM2)

ASR-ALMERIA 3.1 MRD 21/12 NOON

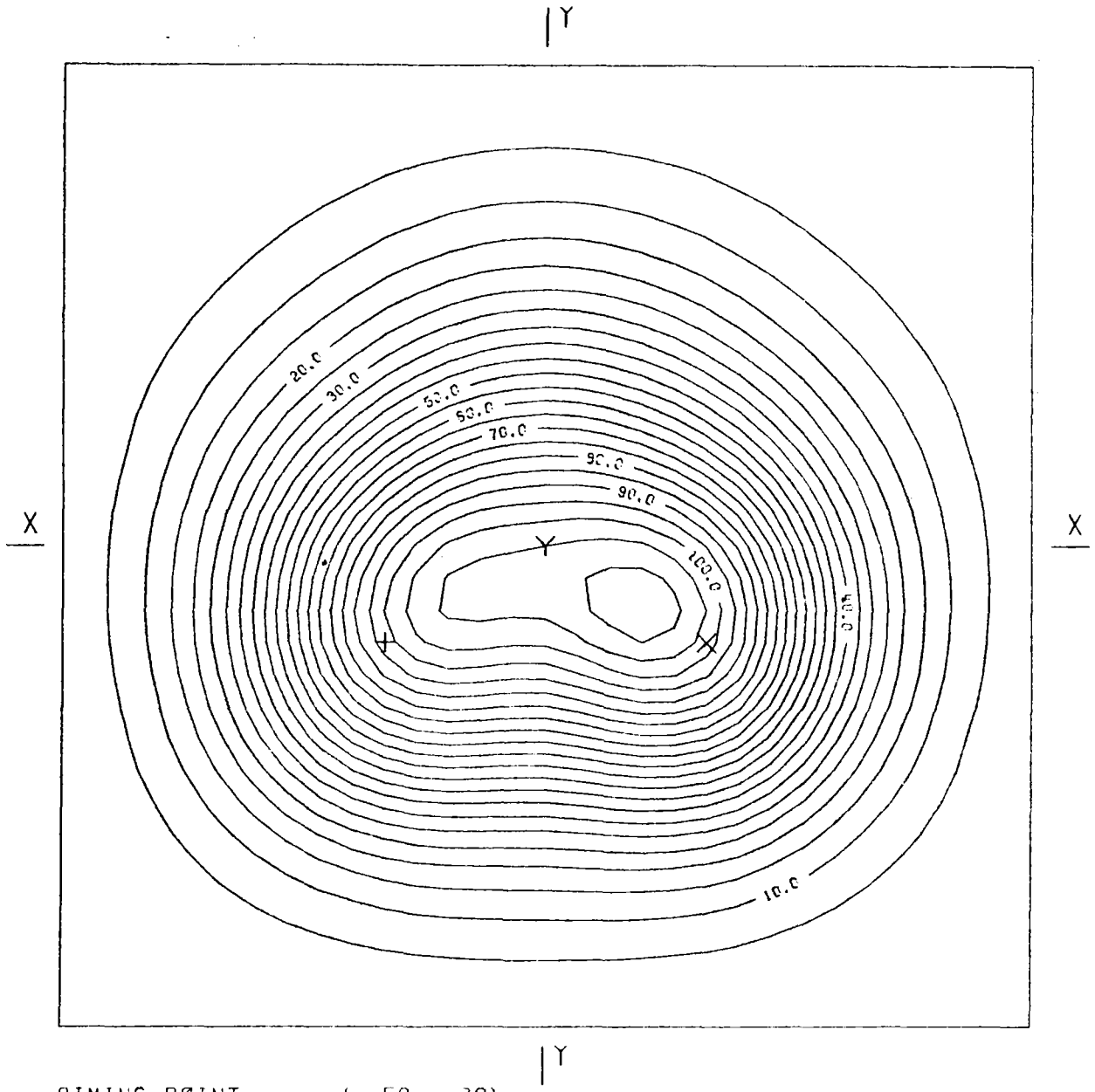

AIMING POINT: + (-,50;-,30)

× (,50;-,30)

Y (,00;,00)

FIG.1.24 EQUIFLUX LINES, SPACING (W/CM2) 5,0

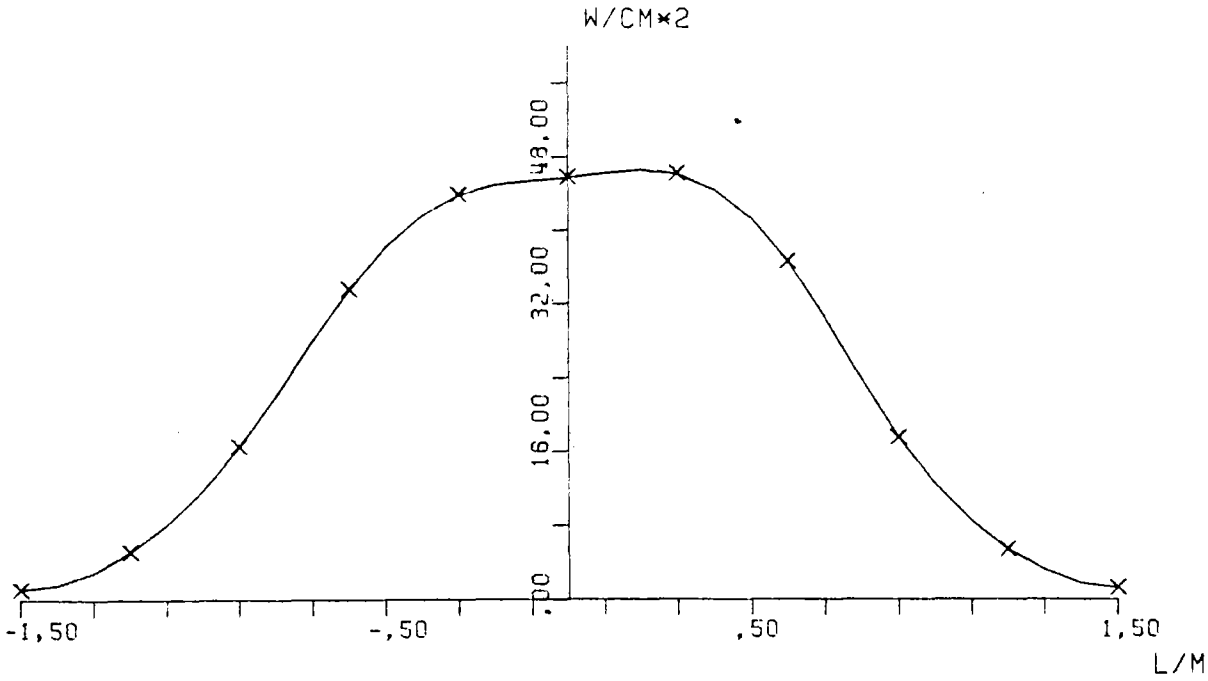

FIG.1.25 AVERAGE SOLAR FLUX ON VERTICAL STRIP

ASR-ALMERIA 3.1 MRD 21/12 H9.30

	,05	,18	,44	,63	1,21	1,38	1,24	,69	,53	,26	,11	
	,20	,63	1,54	2,91	4,28	4,66	4,29	3,02	1,74	,65	,36	
	,51	1,68	4,21	8,13	12,1	13,6	11,9	8,21	4,64	2,20	,69	
	1,04	3,62	9,61	18,6	27,3	30,2	26,7	18,6	10,3	4,53	1,69	
	1,68	6,34	18,4	36,3	49,0	52,1	48,4	36,1	19,2	7,71	2,53	
E.	2,15	8,68	27,3	54,4	68,1	68,7	67,7	54,1	28,3	10,3	3,00	W.
	2,15	8,65	28,3	57,2	69,4	66,9	68,1	57,6	30,3	10,4	2,75	
	1,68	6,61	20,2	40,3	48,9	46,2	47,1	41,0	21,9	7,36	1,68	
	1,05	3,69	10,1	19,0	23,1	22,3	22,1	19,0	10,2	3,51	,91	
	,51	1,58	3,75	6,29	7,46	7,57	7,27	5,78	3,09	1,11	,30	
	,18	,50	1,05	1,56	1,60	1,91	1,75	1,24	,64	,24	,07	

BOT.

HELST. NO. 93,
INSOL. KW/M2 ,610
DAY NO. 355,
TIME HR. 9,30
TOWER HEIGHT M 44,
TARGET DIM. M 3,0X3,0

AIM. NO. 3,
STD.DEV. MRAD. 3,10
INC.POW. KW 1600,
AVERG./PEAK ,26
SPILLAGE % 1,76

FIG.1.26 INCIDENT FLUX ON FLAT TARGET (W/CM2)

ASR-ALMERIA 3.1 MRD 21/12 H9.30

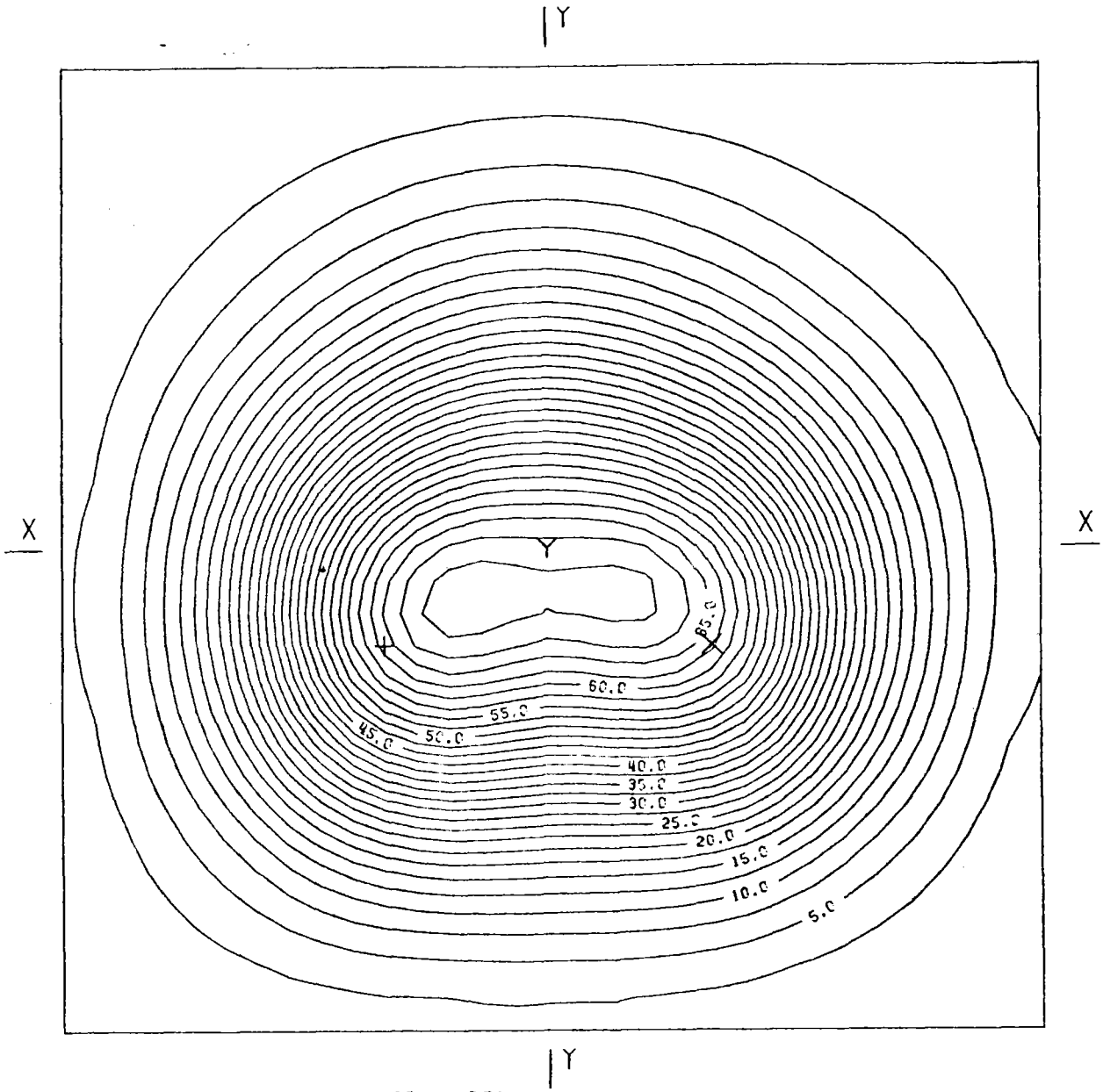

AIMING POINT: + (-,50;-,30)

× (,50;-,30)

Y (,00;,00)

FIG.1.27 EQUIFLUX LINES, SPACING (W/CM2) 2,5

ASR-ALMERIA 3.1 MRD 21/12 H9.30

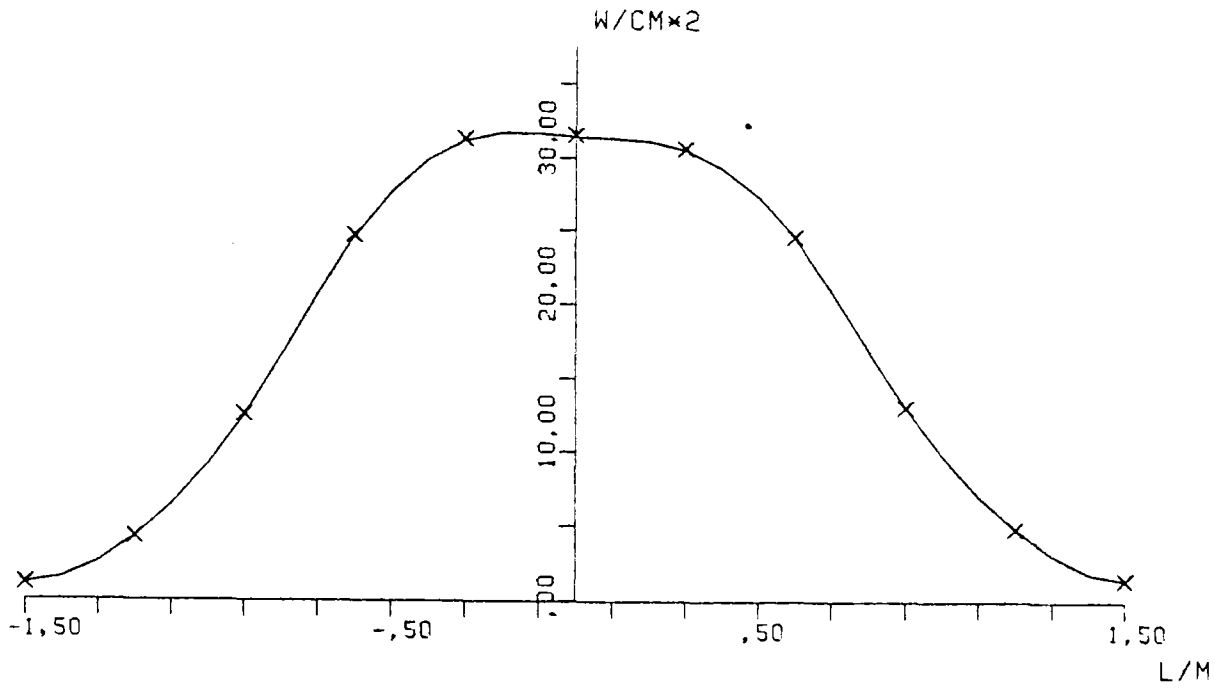

FIG.1.28 AVERAGE SOLAR FLUX ON VERTICAL STRIP

ASR-ALMERIA 3.1 MRD 21/12 H8.15

	,04	,11	,25	,45	,63	,72	,69	,56	,40	,25	,14	
	,13	,36	,80	1,40	1,98	2,21	2,03	1,60	1,11	,66	,34	
	,32	,90	2,01	3,58	4,97	5.40	4,67	3,76	2,47	1,38	,66	
	,63	1,62	4,22	7,40	9.92	10,7	9.75	7,44	4,62	2,38	1,05	
	,99	2,37	7,14	12,3	15,6	17,1	16,1	12,3	7,36	3,53	1,43	
E.	1,22	3,79	9.30	16,0	20,0	21,4	20,9	16,6	9,79	4,49	1,71	W.
	1,20	3,73	9.08	15,6	19,6	20,6	20,6	17,0	10,3	4,66	1,71	
	,97	2,68	6,76	11,7	14,6	15,1	15,0	12,3	8,05	3,65	1,33	
	,67	1,65	4,04	6,70	8,32	8,40	8,17	7,07	4,47	2,05	,75	
	,41	1,02	2,04	3,11	3,66	3,66	3,46	2,68	1,76	,79	,30	
	,21	,47	,66	1,20	1,28	1,26	1,17	,69	,49	,21	,08	

BØT.

HELST. NØ.	93,	AIM. NØ.	3,
INSOL. KW/M2	,300	STD.DEV. MRAD.	3,10
DAY NØ.	355,	INC.POW. KW	557,
TIME HR.	8,15	AVERG./PEAK	,29
TOWER HEIGHT M	44,	SPILLAGE %	3,30
TARGET DIM. M	3,0X3,0		

FIG.1.29 INCIDENT FLUX ØN FLAT TARGET (W/CM2)

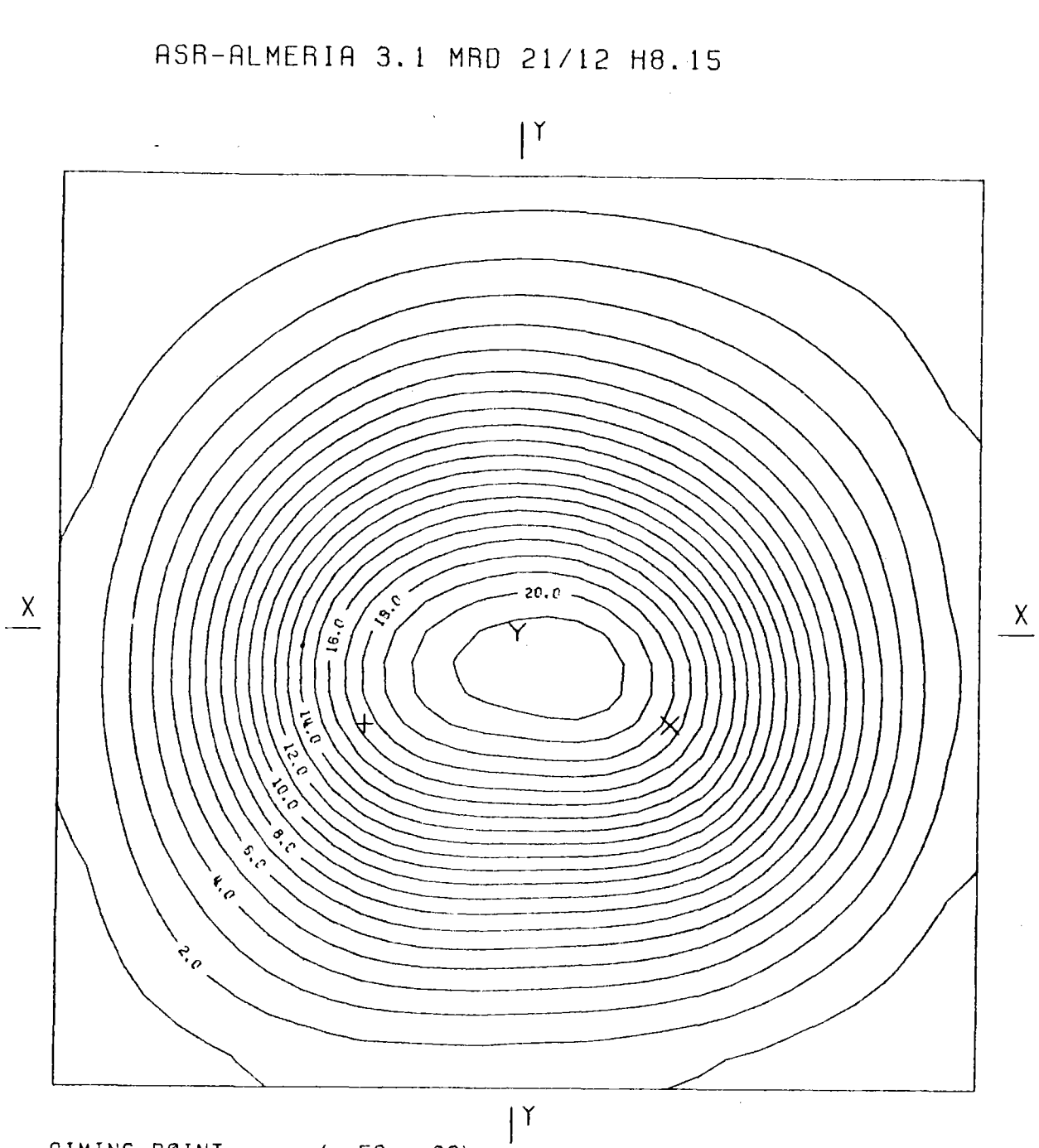

FIG.1.30 EQUIFLUX LINES, SPACING (W/CM2) 1,0

ASR-ALMERIA 3.1 MRD 21/12 H8.15

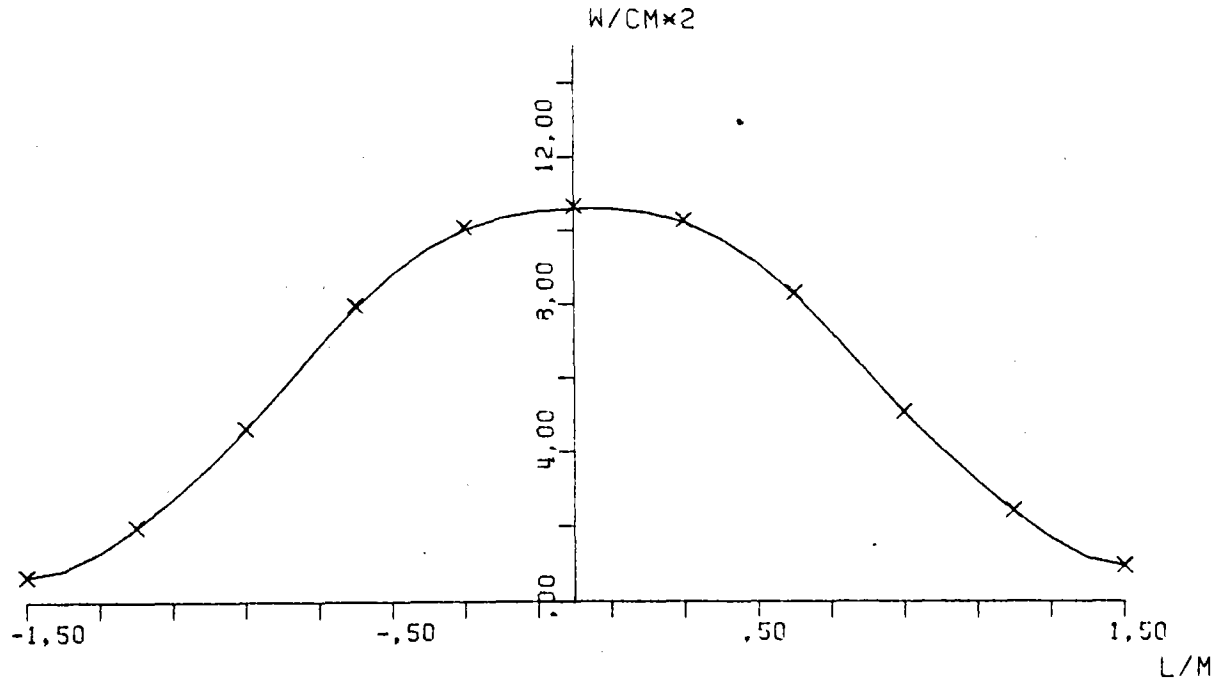

FIG.1.31 AVERAGE SOLAR FLUX ON VERTICAL STRIP

ALMERIA SITE

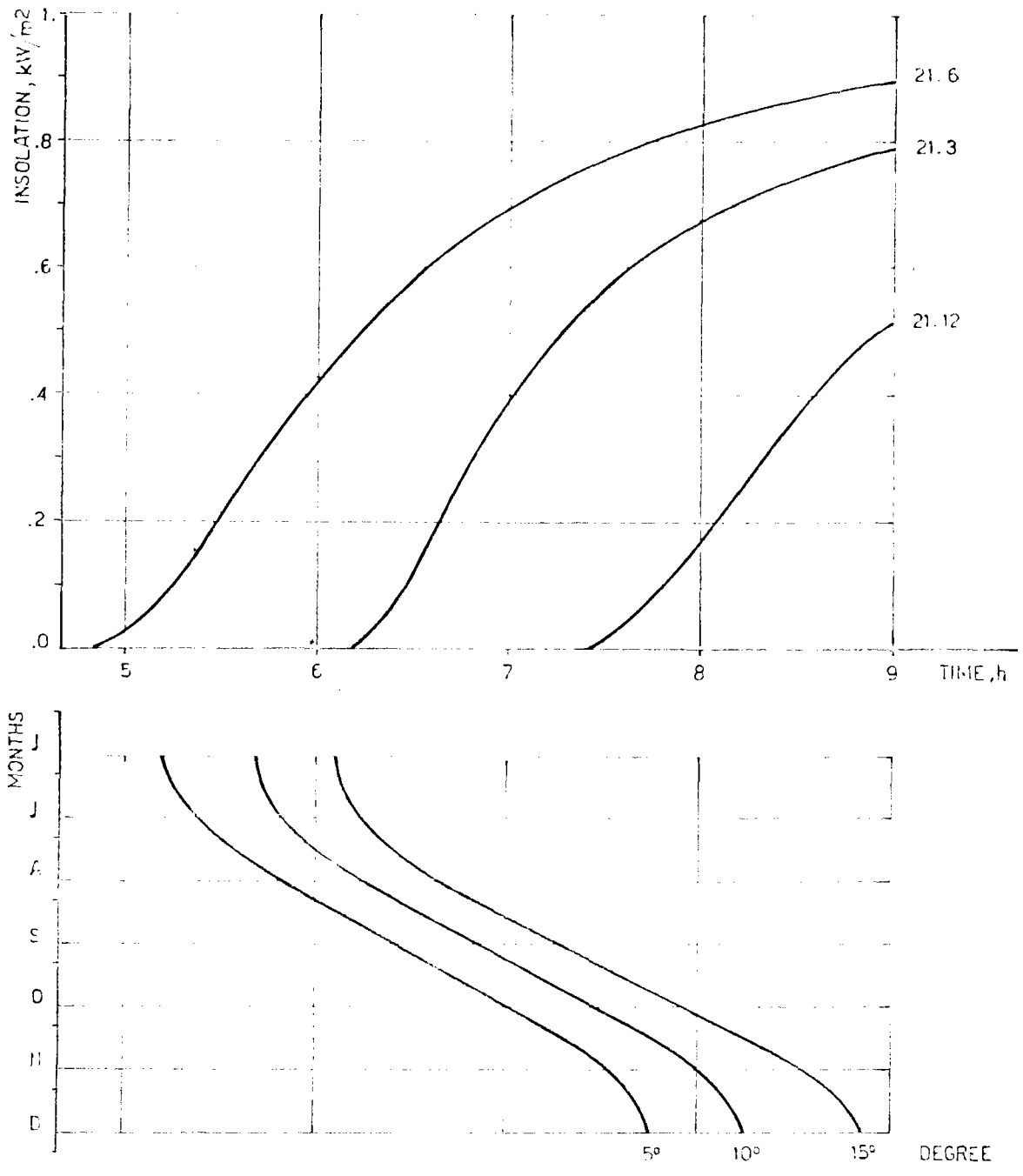

INSOLATION, kW/m2	0.2	0.25	0.3	0.35
SUN ELEVATION, DEG.	7°30'	9°	11°	13°

FIG.1.32 INSOLATION VS SUN ELEVATION

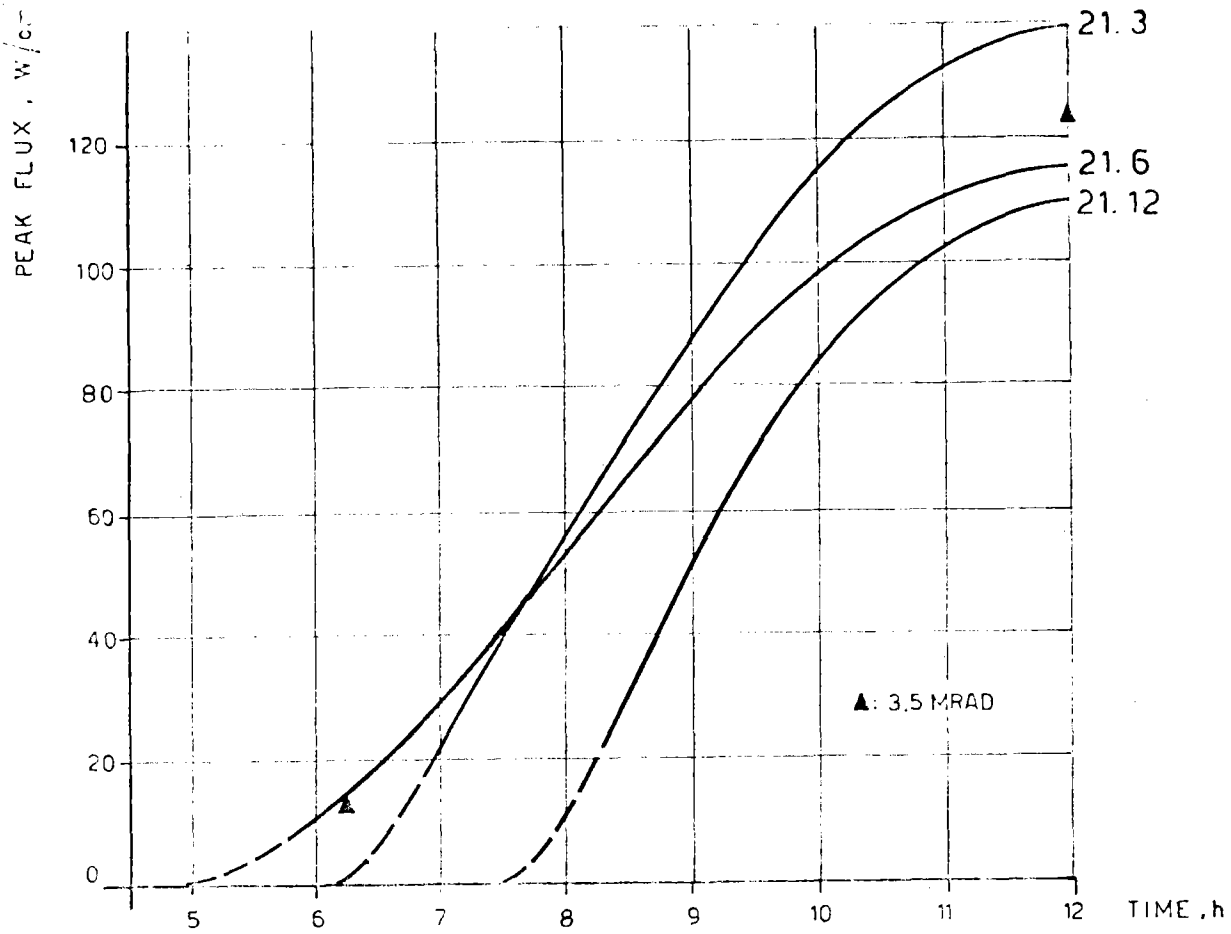

FIG.1.33 INCIDENT PEAK VS TIME

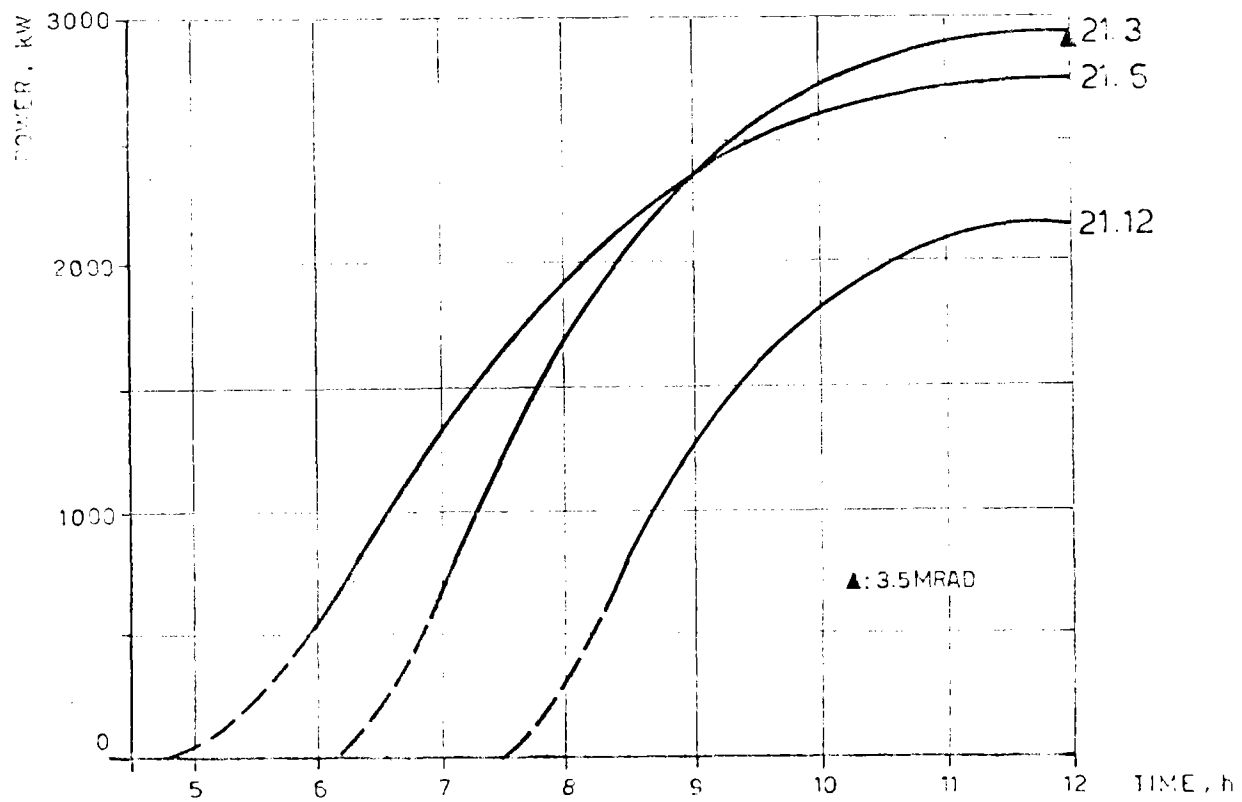

FIG.1.34 INCIDENT POWER VS TIME

ALMERIA - ASR PERFORMANCE

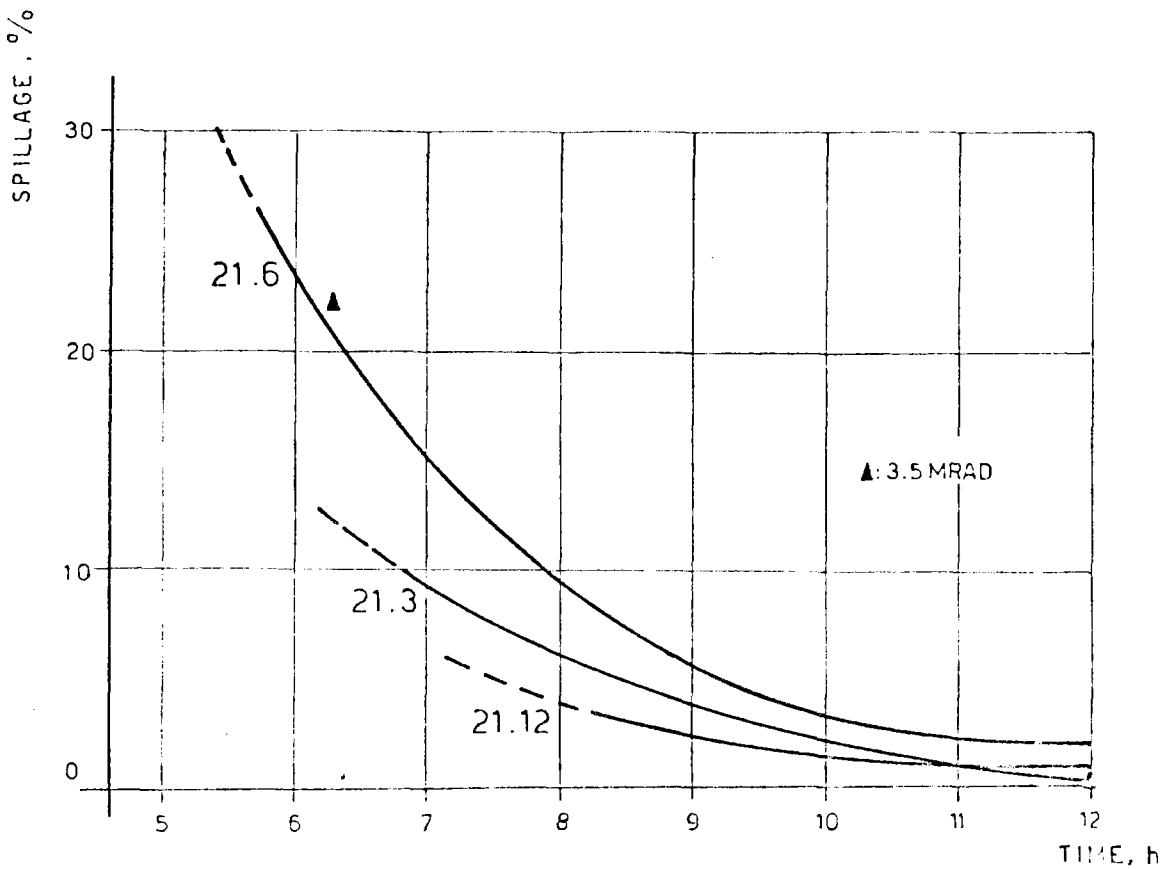

FIG.1.35 SPILLAGE VS TIME ON 3x3 m TARGET

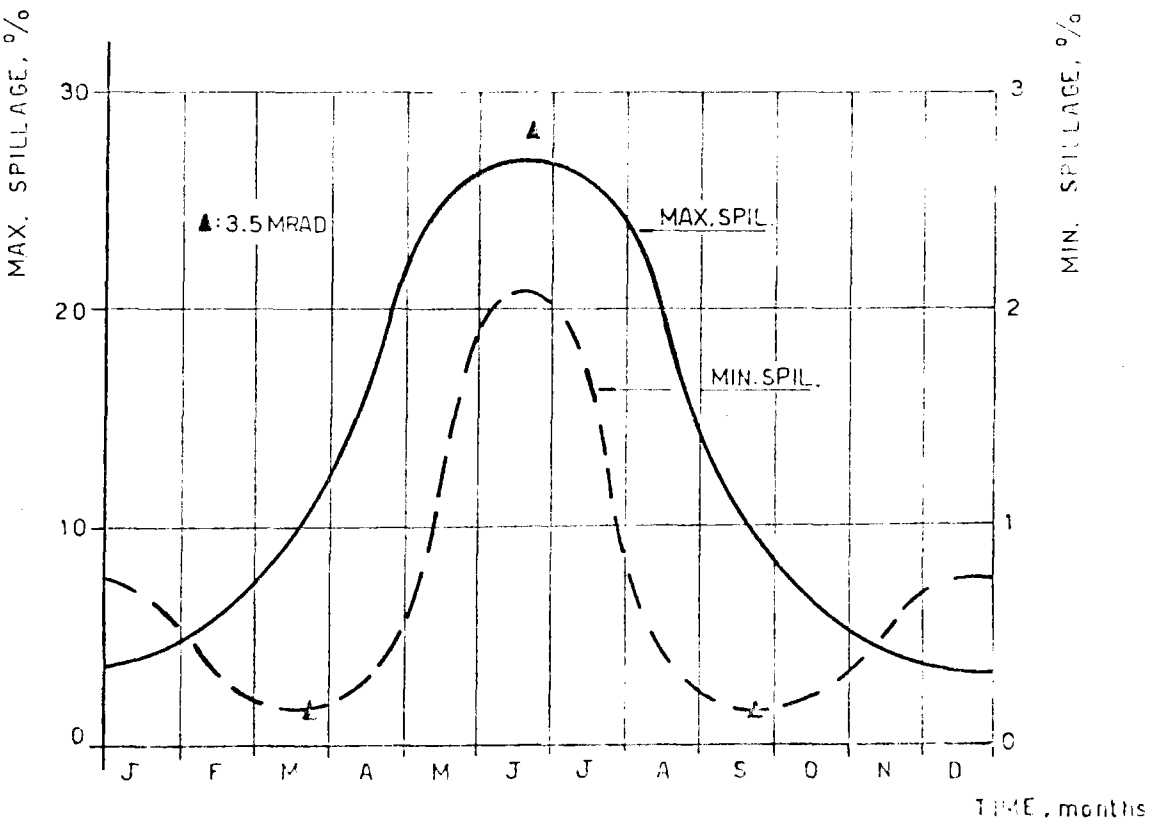

FIG.1.36 MAX. AND MIM. SPILLAGE ON 3x3 m TARGET

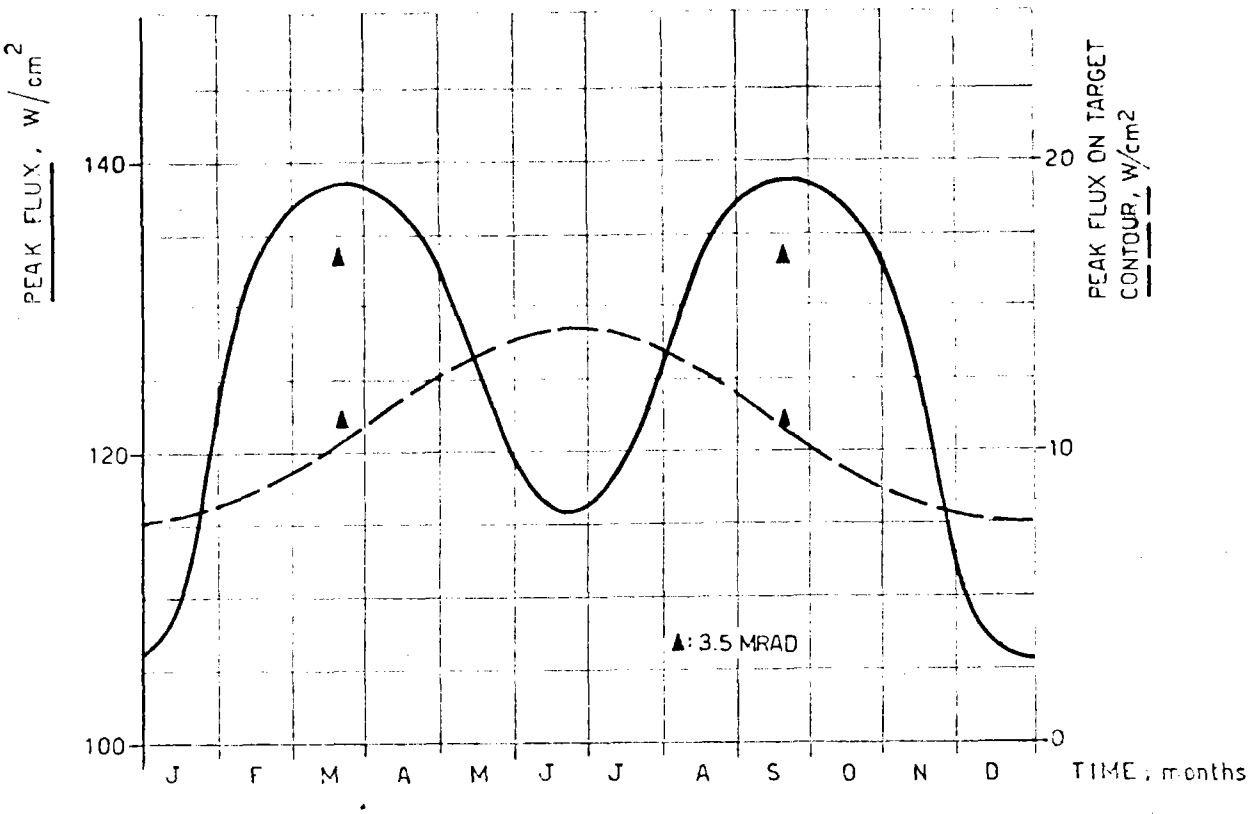

FIG.1.37 MAX INCIDENT FLUX ON 3 x 3 m TARGET

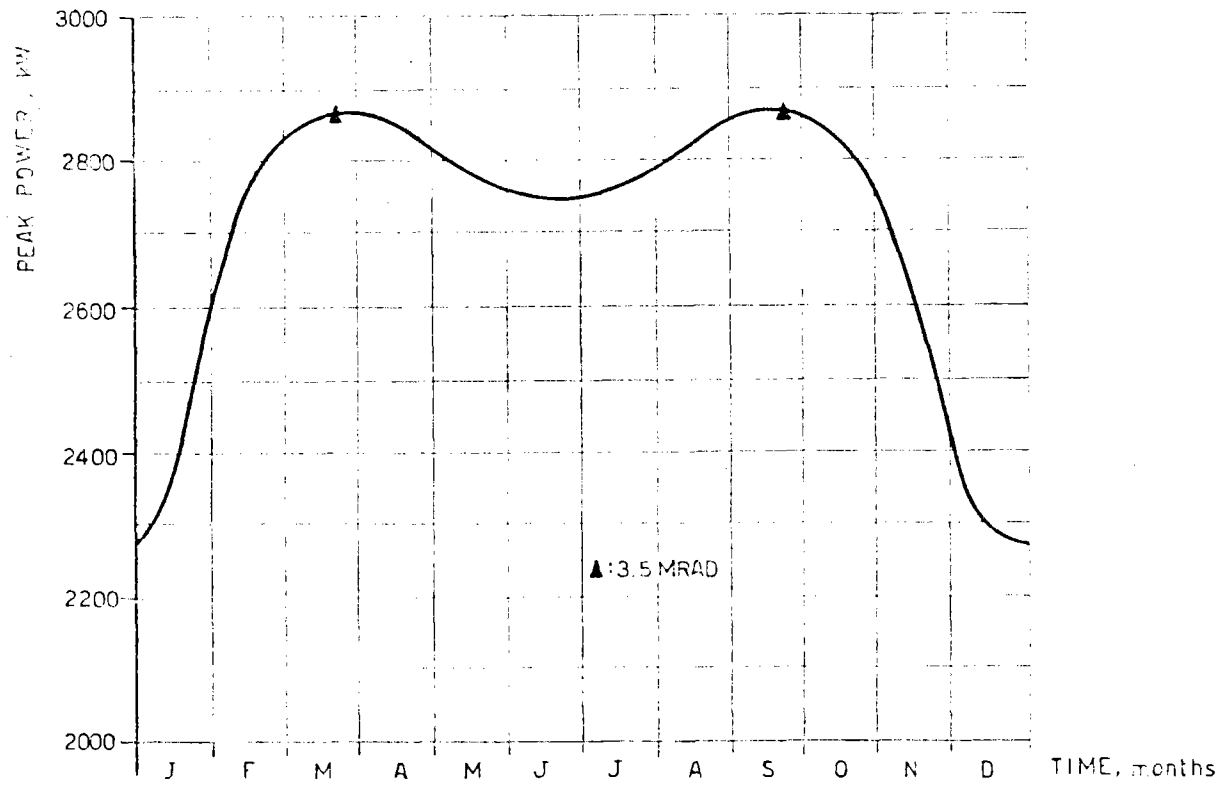

FIG.1.38 MAX INCIDENT POWER ON 3 x 3 m TARGET

ASR-ALMERIA 3.5MRAD ERROR 21/3 NOON

	,14	,42	,95	1,68	2,36	2,64	2,35	1,67	,94	,42	,14	
	,46	1,33	2,98	5,35	7,66	8,64	7,65	5,34	2,97	1,32	,46	
	1,12	3,25	7,51	13,5	20,0	22,7	20,0	13,5	7,50	3,26	1,14	
	2,18	6,75	16,3	30,1	43,1	48,5	43,1	30,1	16,3	6,50	2,25	
	3,52	12,2	31,6	58,2	75,5	85,0	78,3	58,0	31,5	12,2	3,65	
E.	4,54	17,9	51,1	93,5	117,	119,	116,	92,9	50,7	18,0	4,74	W.
	4,57	19,5	58,9	108,	127,	123,	125,	106,	58,3	19,6	4,60	
	3,52	14,6	43,7	78,4	90,9	88,1	90,0	77,5	43,3	14,9	3,74	
	2,00	7,55	20,2	34,9	41,6	41,8	41,4	34,7	20,2	7,70	2,17	
	,79	2,58	6,05	10,1	12,8	13,6	12,5	10,1	6,13	2,69	,69	
	,21	,62	1,35	2,26	3,04	3,35	3,04	2,27	1,38	,66	,24	

BOT.

HELST. NO. 93,
INSOL. KW/M2 ,920
DAY NO. 80,
TIME HR. 12,
TOWER HEIGHT M 44,
TARGET DIM. M 3,0X3,0

AIM. NO. 3,
STD.DEV. MRAD. 3,50
INC.POW. KW 2860,
AVERG./PEAK ,25
SPILLAGE % ,12

FIG.1.39 INCIDENT FLUX ON FLAT TARGET (W/CM2)

ASR-ALMERIA 3.5MRAD ERROR 21/3 NOON

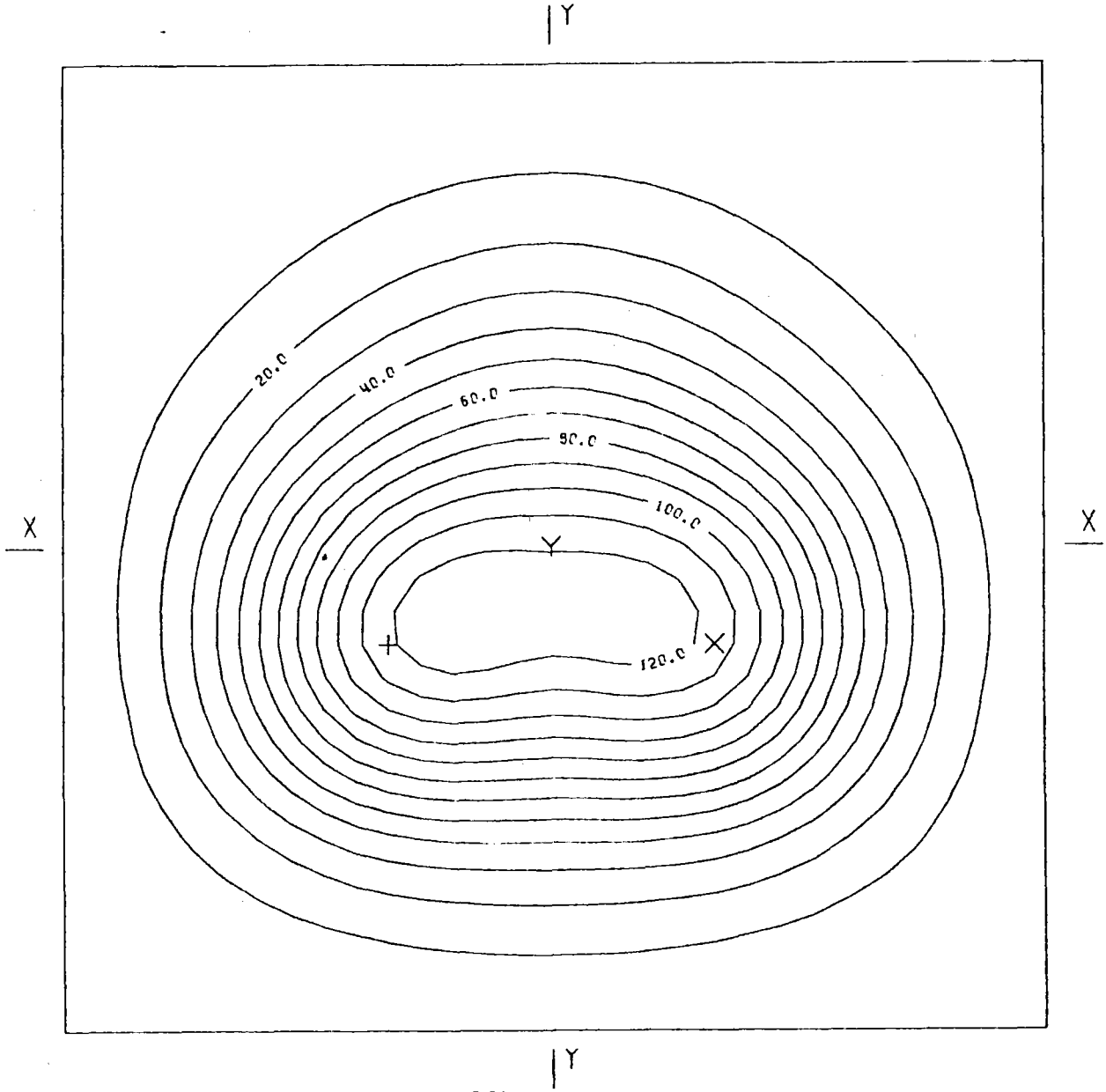

AIMING POINT: + (-,50;-,30)

× (,50;-,30)

Y (,00;,00)

FIG.1.40 EQUIFLUX LINES, SPACING (W/CM2) 10,0

ASR-ALMERIA 3.5MRAD ERROR 21/3 NOON

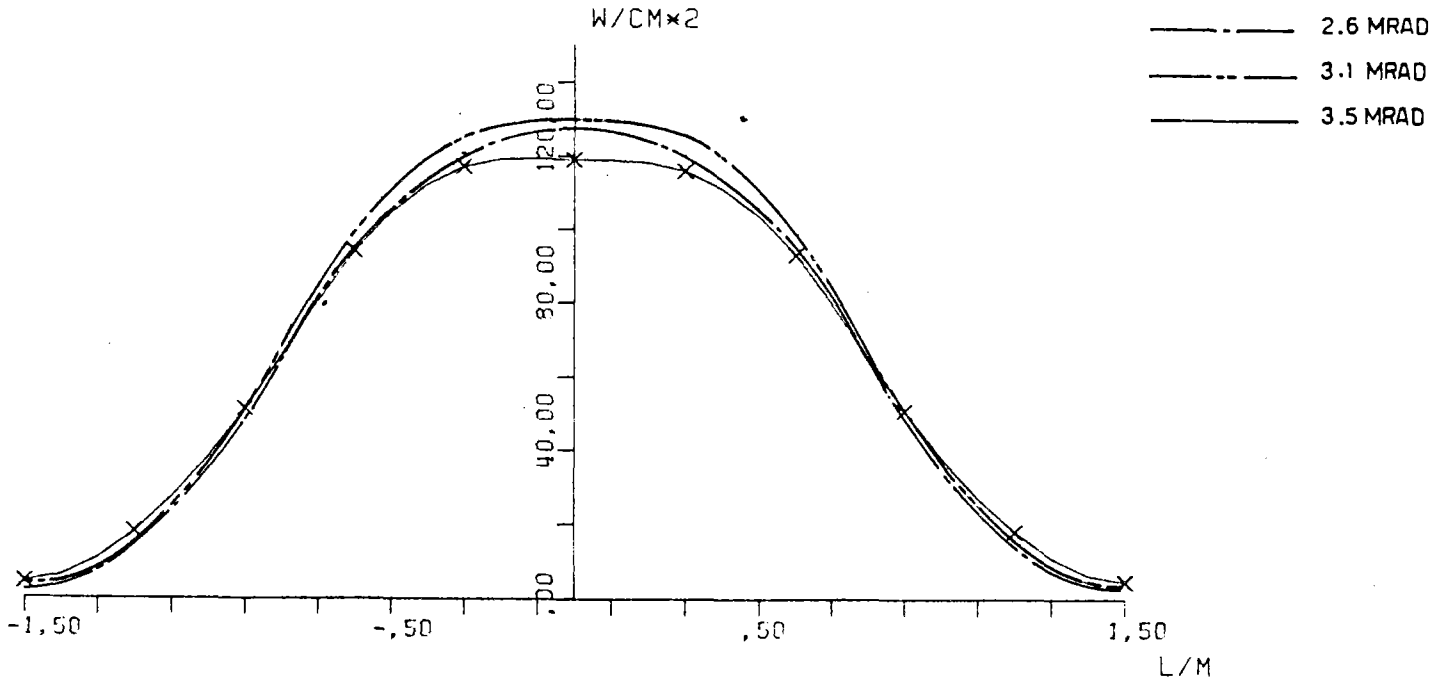

FIG.1.41 SOLAR FLUX ON TARGET SEC X-X

ASR-ALMERIA 3.5MRAD ERROR 21/3 NOON

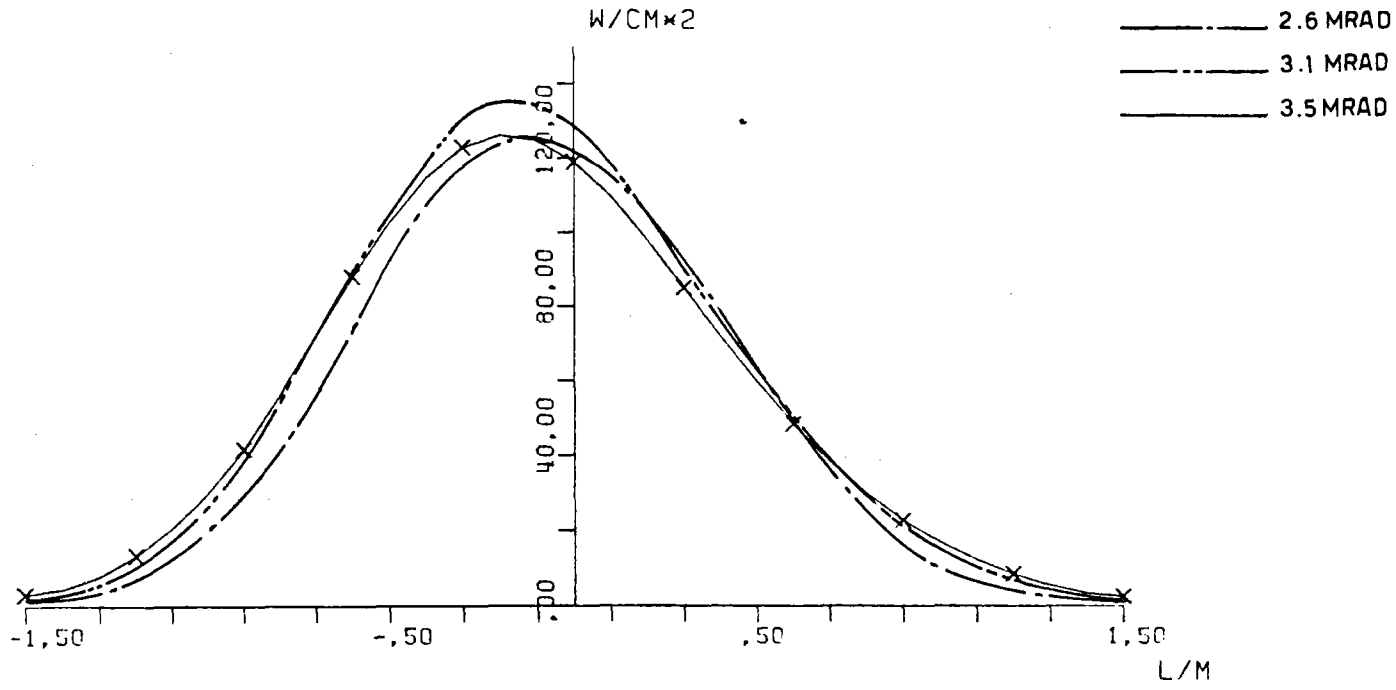

FIG.1.42 SOLAR FLUX ON TARGET SEC Y-Y

ASR-ALMERIA 3.5MRAD ERRØR 21/3 NØØN

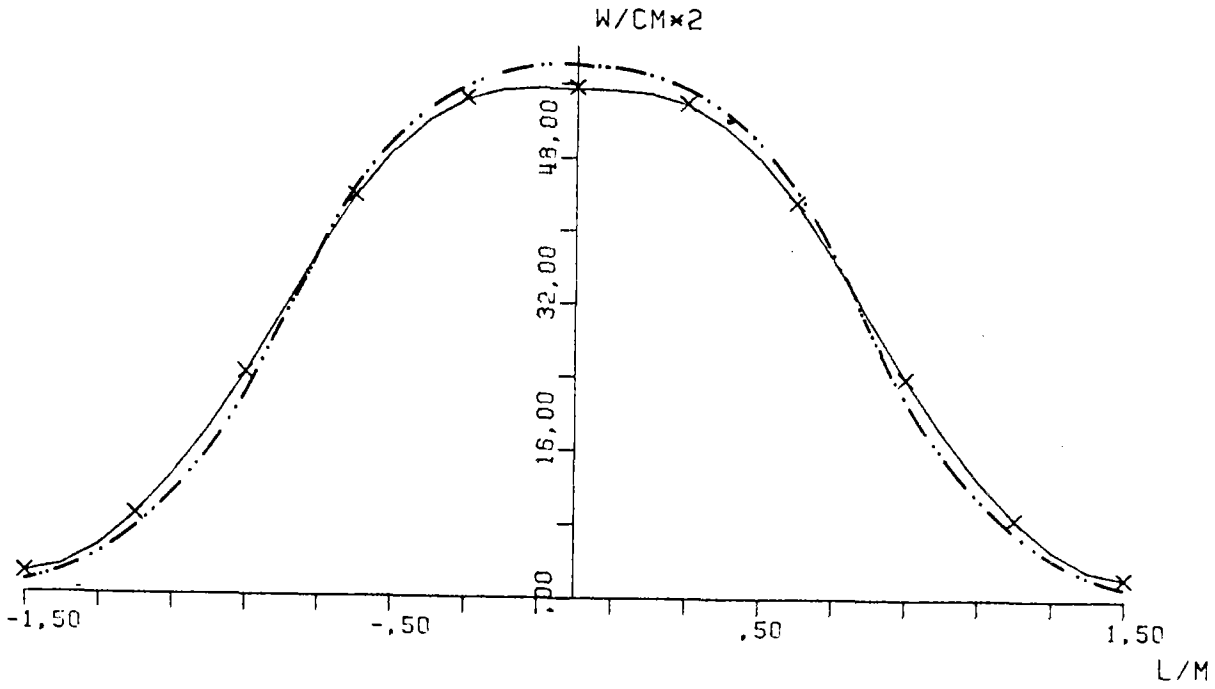

FIG.1.43 AVERAGE SØLAR FLUX ØN VERTICAL STRIP

ASR-ALMERIA 3.5MRAD ERROR 21/6 H6.15

	.81	1.87	2.89	3.60	3.73	3.70	3.27	2.59	1.93	1.42	1.08
	1.59	3.17	4.84	5.61	5.93	6.09	5.38	4.26	3.26	2.52	1.85
	2.47	4.82	7.05	8.01	8.70	9.19	8.22	6.57	5.14	4.03	3.04
	3.41	6.46	9.13	10.4	11.6	12.6	11.4	9.19	7.37	5.71	4.12
	4.20	7.69	10.6	12.1	14.0	15.4	14.1	11.5	8.45	7.26	4.82
E.	4.67	8.17	11.0	12.8	15.0	16.8	15.8	13.0	10.8	8.22	5.90 W.
	4.74	7.85	10.3	12.0	14.4	16.5	15.5	13.1	11.1	8.44	5.18
	4.43	6.69	8.86	10.3	12.7	14.7	14.0	11.9	10.3	7.90	4.67
	3.76	5.50	6.82	8.12	10.1	11.9	11.5	9.83	8.65	6.75	3.86
	2.82	3.96	4.84	5.82	7.37	8.76	8.44	7.26	6.57	5.14	2.66
	2.02	2.56	3.06	3.75	4.80	5.82	5.61	4.86	4.47	3.48	1.81

BOT.

HELST. NO.	93.	AIR. NO.	3.
INSOL. KW/M2	.955	STD.DEV. MRAD.	3.50
DAY NO.	172.	INC.POW. KW	1380.
TIME HR.	6.15	AVERG./PEAK	.49
TOWER HEIGHT M	44.	SPILLAGE %	.30
TARGET DIM. M	3.0X3.0		

FIG.1.44 INCIDENT FLUX ON FLAT TARGET (W/CM2)

ASR-ALMERIA 3.5MRAD ERROR 21/6 H6.15

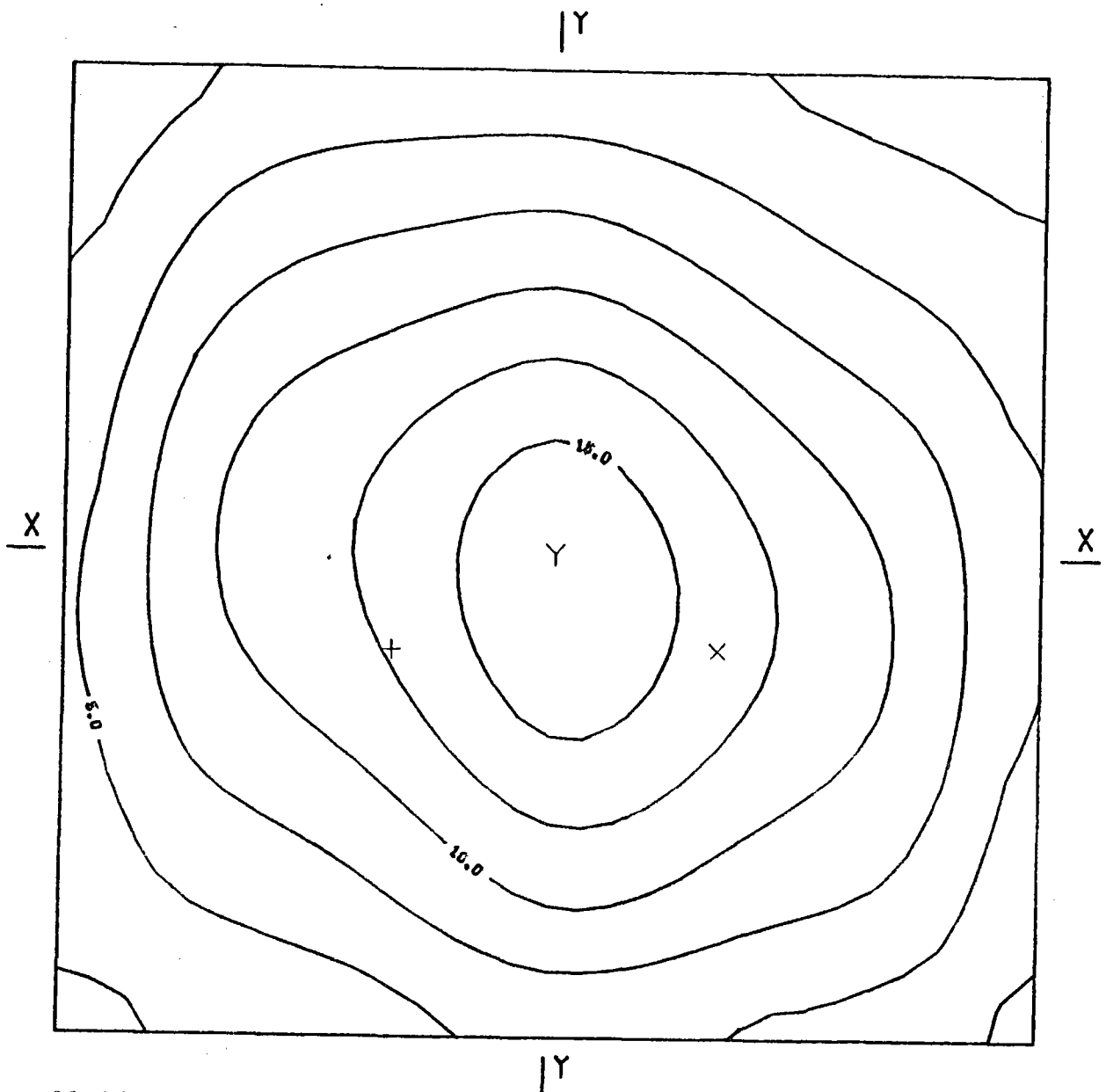

AIMING POINT: + (-.50;-.30)
× (.50;-.30)
Y (.00;.00)

FIG.1.45 EQUIFLUX LINES, SPACING (W/CM2) 2,5

ASR-ALMERIA 3.5MRAD ERROR 21/6 H6.15

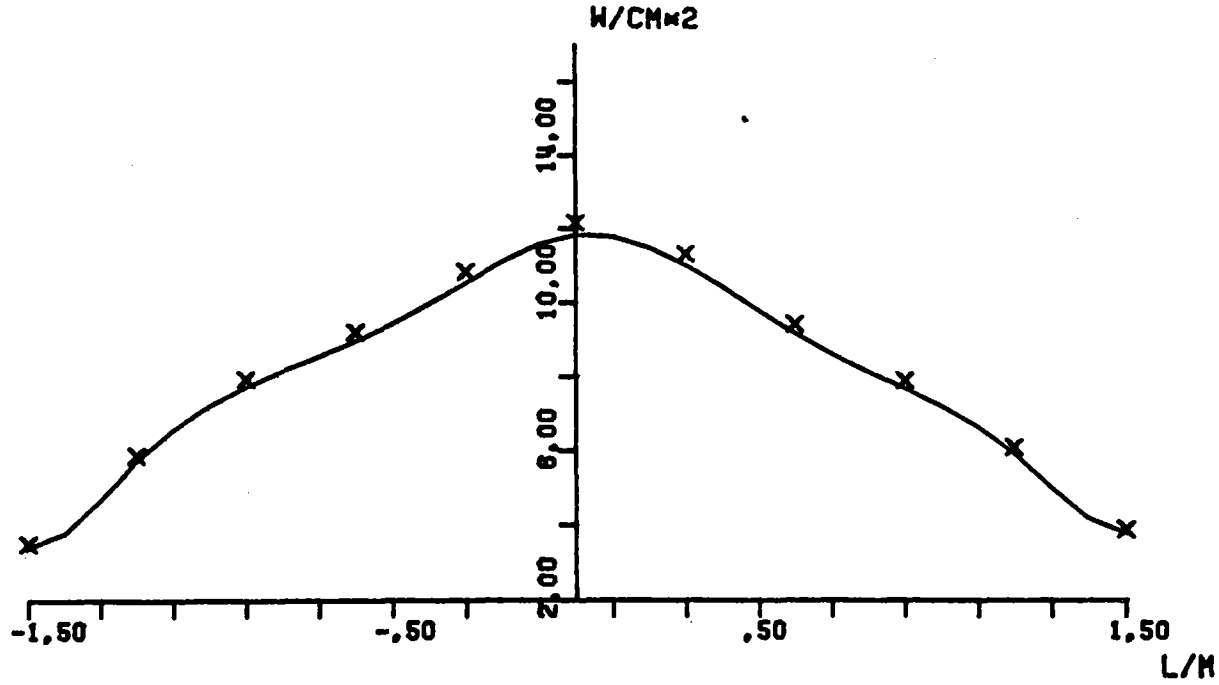

FIG.1.46 AVERAGE SOLAR FLUX ON VERTICAL STRIP

ASR-ALMERIA 3.1 MRD 21/6 NOON DOOR PLAN

	.01	.01	.01	.01	.01	.01	.01	.01	.01	.01	.01	
	.01	.01	.01	.03	.08	.10	.08	.03	.01	.01	.01	
	.01	.01	.08	.38	.95	1.27	.94	.38	.08	.01	.01	
	.01	.06	.54	2.45	6.24	8.59	6.23	2.45	.54	.06	.01	
	.02	.26	2.05	9.39	24.3	33.4	24.3	9.39	2.04	.26	.02	
E.	.05	.66	5.08	23.9	57.9	78.9	58.1	24.0	5.13	.65	.05	W.
	.08	1.15	8.78	41.3	91.0	102.	90.3	41.3	8.93	1.25	.09	
	.03	1.21	8.62	34.3	64.3	72.6	62.9	33.5	8.76	1.49	.15	
	.03	.49	3.19	7.54	11.4	14.7	11.6	7.05	2.97	.70	.10	
	.01	.04	.23	.42	.66	.79	.68	.33	.22	.08	.01	
	.01	.01	.01	.01	.03	.03	.03	.01	.01	.01	.01	

BOT.

HELST. NO.	93.	AIM. NO.	3.
INSOL. KW/M2	.955	STD.DEV. MRAD.	3.10
DAY NO.	172.	INC.POW. KW	2810.
TIME HR.	12.	AVERG./PEAK	.11
TOWER HEIGHT M	44.	SPILLAGE %	-.08
TARGET DIM. M	5.0X5.0	▨ DOOR APERTURE	

FIG.1.47 INCIDENT FLUX ON FLAT TARGET (W/CM2)

ASR-ALMERIA 3.1 MRD 21/6 NOON DOOR PLAN

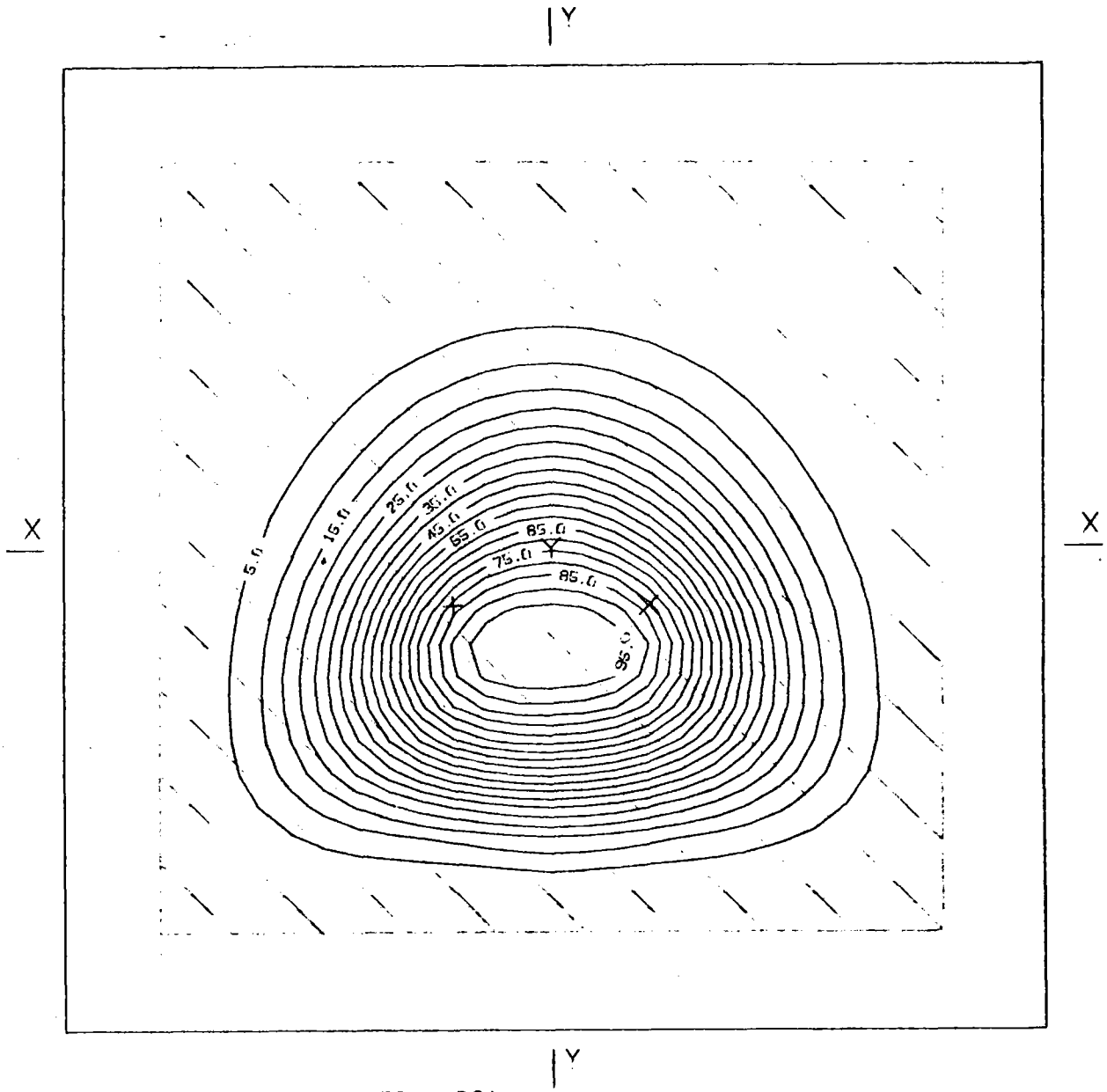

AIMING POINT: + (-.50;-.30)
× (.50;-.30)
Y (.00;.00)

FIG.1.48 EQUIFLUX LINES, SPACING (W/CM2) 5.0

ASR-ALMERIA 3.1 MRD 21/6 NOON DOOR PLAN

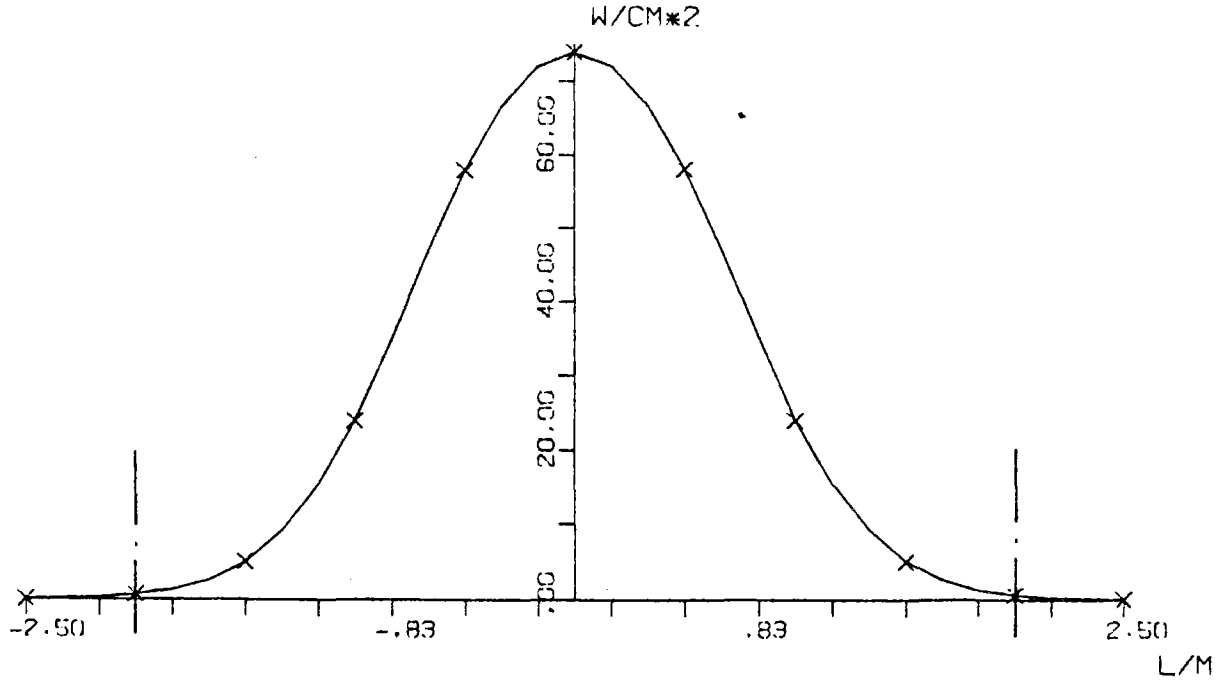

FIG.1.49 SOLAR FLUX ON TARGET SEC X-X

ASR-ALMERIA 3.1 MRD 21/6 NOON DOOR PLAN

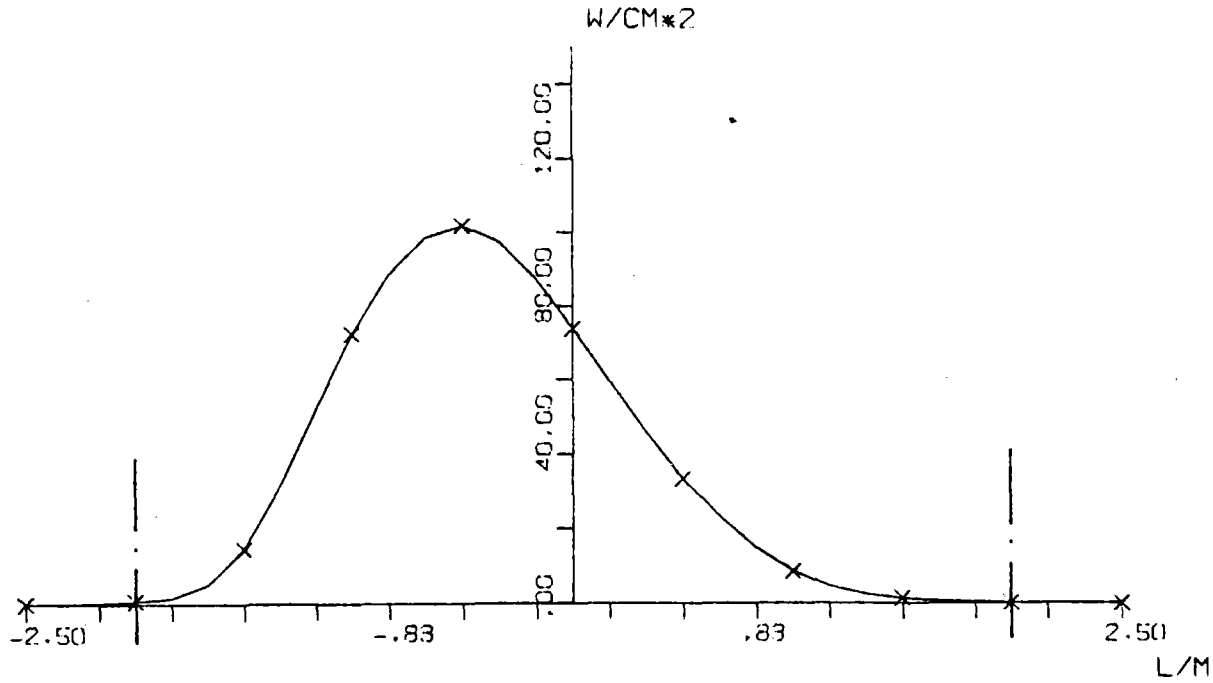

FIG.1.50 SOLAR FLUX ON TARGET SEC Y-Y

ASR-ALMERIA 3.1MRD 21/6 H6.15 DOOR PLAN

	.01	.01	.05	.15	.23	.19	.11	.04	.01	.01	.01	
	.01	.05	.22	.62	.88	.78	.47	.22	.10	.04	.02	
	.03	.15	.66	1.73	2.43	2.36	1.58	.90	.51	.25	.09	
	.08	.39	1.46	3.73	5.13	5.66	4.42	2.84	1.77	.81	.28	
	.22	.79	2.50	6.17	8.44	10.6	9.30	6.69	4.04	1.58	.49	
E.	.43	1.27	3.51	7.77	11.0	15.0	14.2	11.1	6.20	1.99	.47	W.
	.67	1.67	4.05	7.64	11.1	15.6	15.4	12.6	6.81	1.82	.30	
	.80	1.77	3.70	6.07	8.89	12.5	12.5	10.4	5.46	1.28	.15	
	.69	1.47	2.60	3.89	5.77	7.94	7.65	6.30	3.09	.64	.06	
	.43	.92	1.38	2.01	3.12	3.91	3.50	2.74	1.06	.17	.01	
	.19	.53	.57	.82	1.46	1.47	1.24	.85	.20	.02	.01	

BOT.

HELST. NO.	93.	AIM. NO.	3.
INSOL. KW/M2	.510	STD.DEV. MRAD.	3.10
DAY NO.	172.	INC.POW. KW	924.
TIME HR.	6.15	AVERG./PEAK	.24
TOWER HEIGHT M	44.	SPILLAGE %	2.07
TARGET DIM. M	5.0X5.0	▨ DOOR APERTURE	

FIG.1.51 INCIDENT FLUX ON FLAT TARGET (W/CM2)

ASR-ALMERIA 3.1MRD 21/6 H6.15 DOOR PLAN

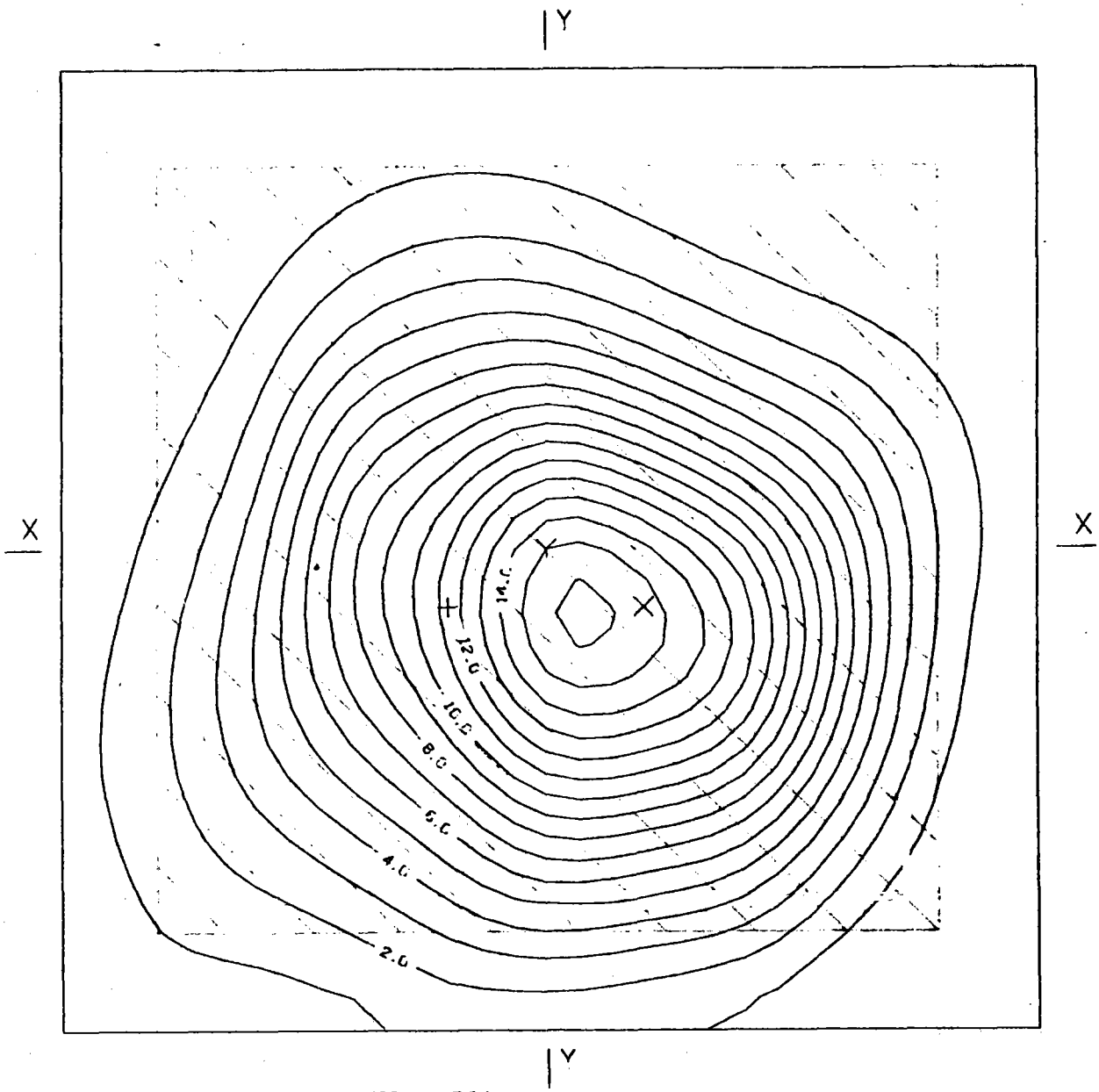

AIMING POINT: + (-.50;-.30)
× (.50;-.30)
Y (.00;.00)

FIG.1.52 EQUIFLUX LINES.SPACING (W/CM2) 1.0

SNAMPROGE.TTI

ASR-ALMERIA 3.1MRD 21/6 H6.15 DOOR PLAN

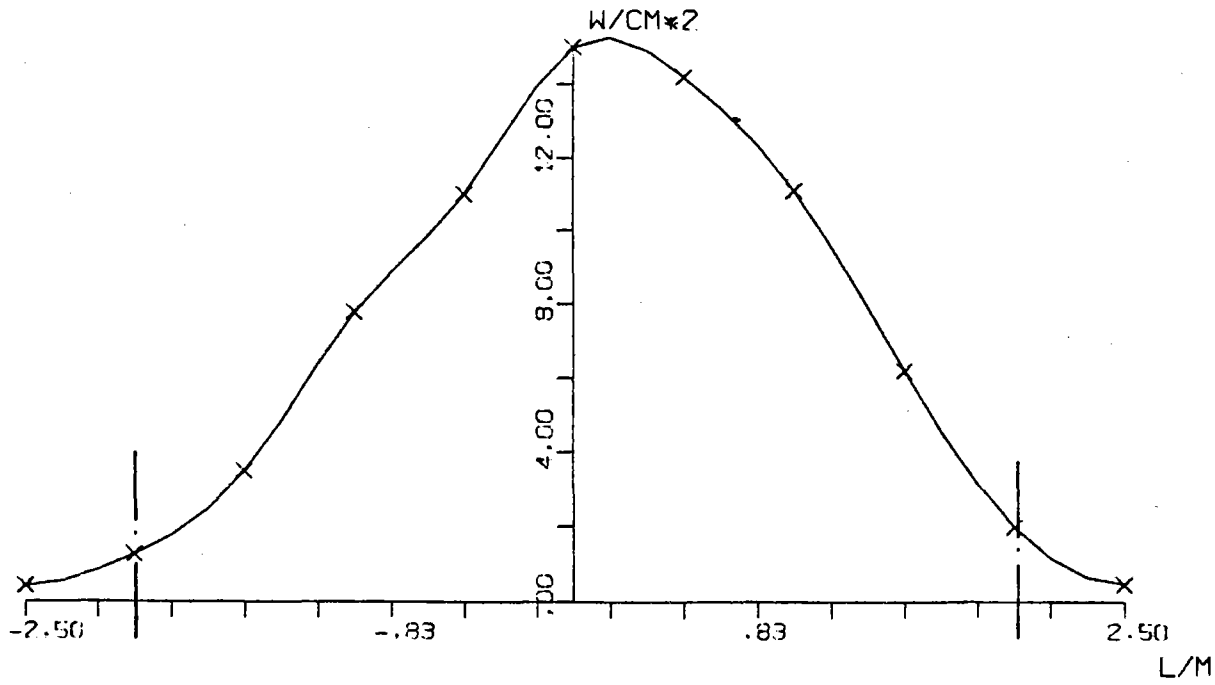

FIG.1.53 SOLAR FLUX ON TARGET SEC X-X

ASR-ALMERIA 3.1MRD 21/6 H6.15 DOOR PLAN

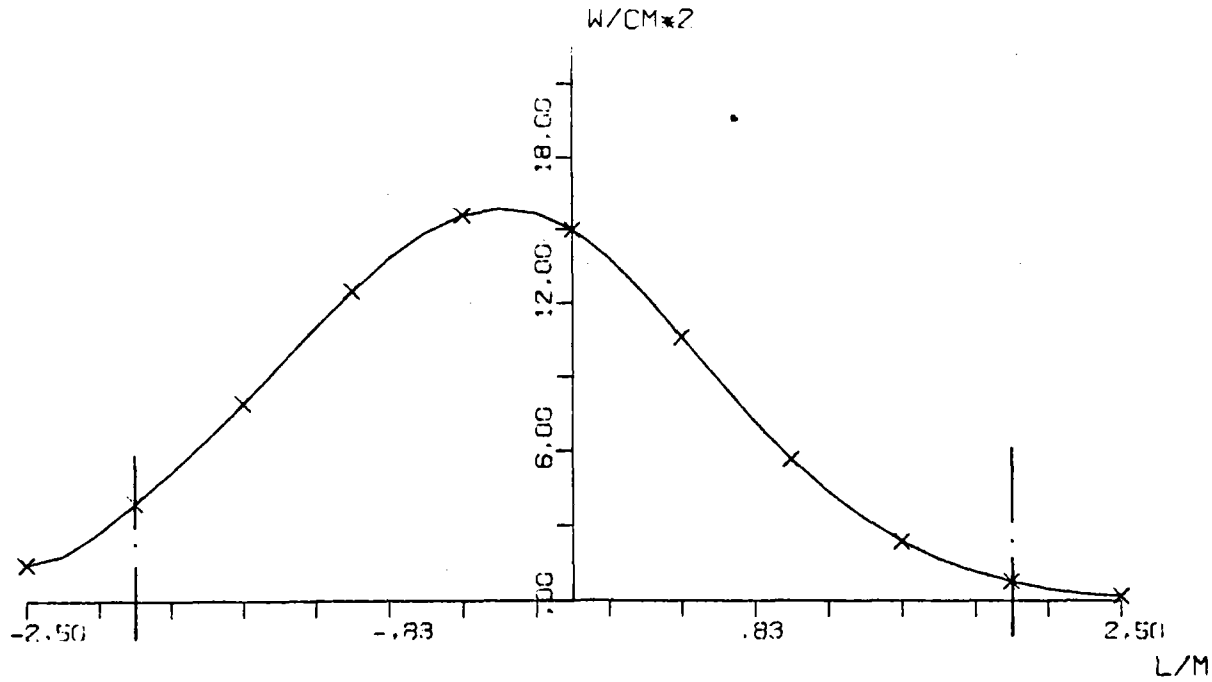

FIG.1.54 SOLAR FLUX ON TARGET SEC Y-Y

ASR-ALMERIA 3.5MRD 21/6 H6.15 DOOR PLAN

	.01	.01	.06	.17	.25	.22	.13	.06	.02	.01	.01
	.01	.06	.25	.65	.91	.83	.53	.27	.13	.06	.02
	.03	.18	.73	1.77	2.44	2.41	1.70	1.00	.57	.29	.11
	.10	.45	1.56	3.74	5.09	5.64	4.51	2.95	1.84	.86	.31
	.24	.85	2.63	6.13	8.34	10.4	9.17	6.63	4.03	1.64	.52
E.	.46	1.33	3.61	7.69	10.8	14.6	13.7	10.7	6.15	2.10	.52	W.
	.69	1.70	4.07	7.56	10.9	15.2	14.9	12.2	6.80	2.00	.37	
	.80	1.78	3.69	6.04	8.85	12.3	12.2	10.1	5.53	1.47	.21	
	.70	1.49	2.62	3.93	5.82	7.90	7.62	6.28	3.22	.77	.09	
	.44	.99	1.43	2.07	3.17	3.96	3.59	2.81	1.19	.23	.02	
	.20	.54	.61	.87	1.48	1.52	1.30	.90	.25	.03	.01	

BOT.

HELST. NO.	93.	AIM. NO.	3.
INSOL. KW/M2	.510	STD.DEV. MRAD.	3.50
DAY NO.	172.	INC.POW. KW	922.
TIME HR.	6.25	AVERG./PEAK	.24
TOWER HEIGHT M	44.	SPILLAGE %	2.28
TARGET DIM. M	5.0X5.0	▨ DOOR APERTURE	

FIG.1.55 INCIDENT FLUX ON FLAT TARGET (W/CM2)

ASR-ALMERIA 3.5MRD 21/6 H6.15 DOOR PLAN

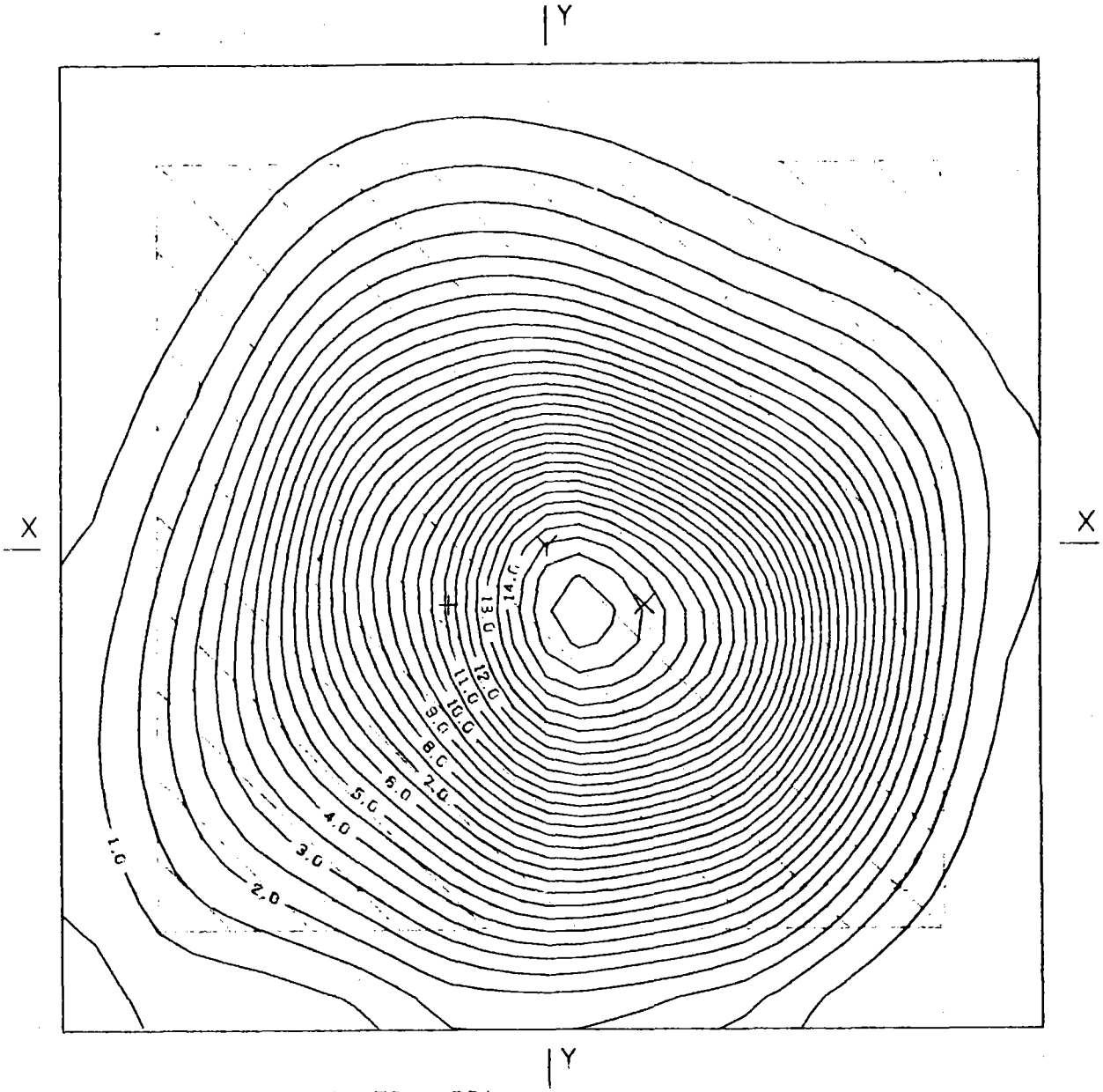

AIMING POINT: + (-.50;-.30)
× (.50,-.30)
Y (.00;.00)

FIG.1.56 EQUIFLUX LINES.SPACING (W/CM2) .5

ASR-ALMERIA 3.5MRD 21/6 H6.15 DOOR PLAN

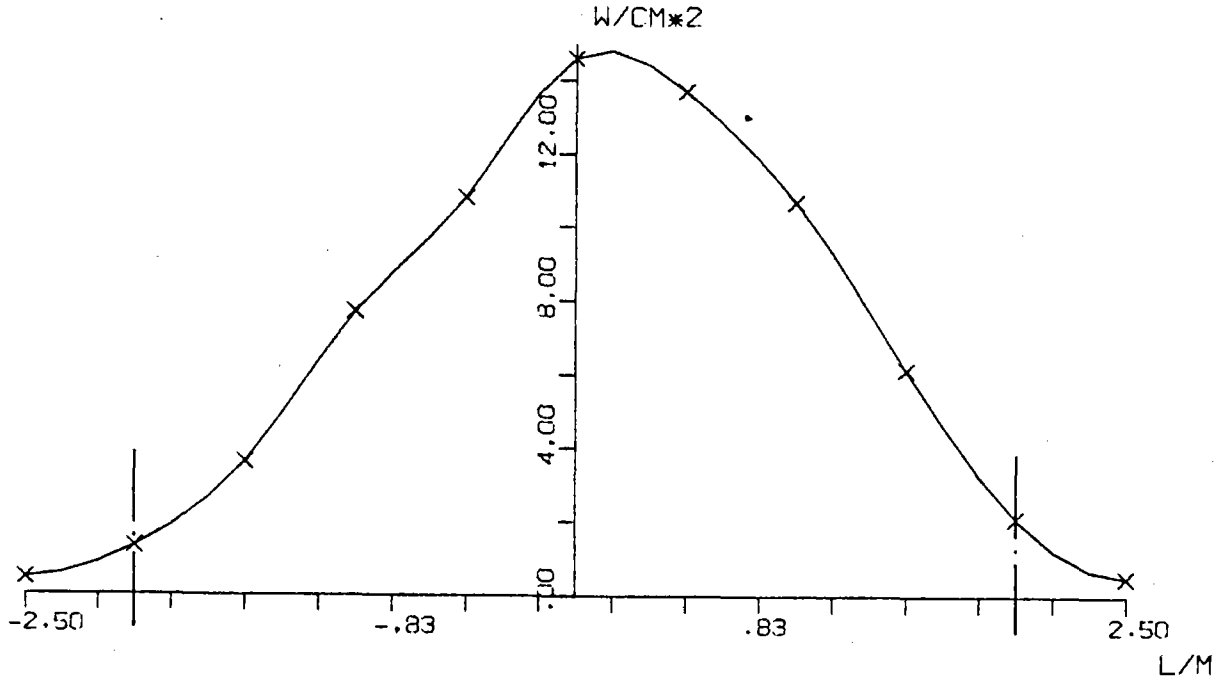

FIG.1.57 SOLAR FLUX ON TARGET SEC X-X

ASR-ALMERIA 3.5MRD 21/6 H6.15 DOOR PLAN

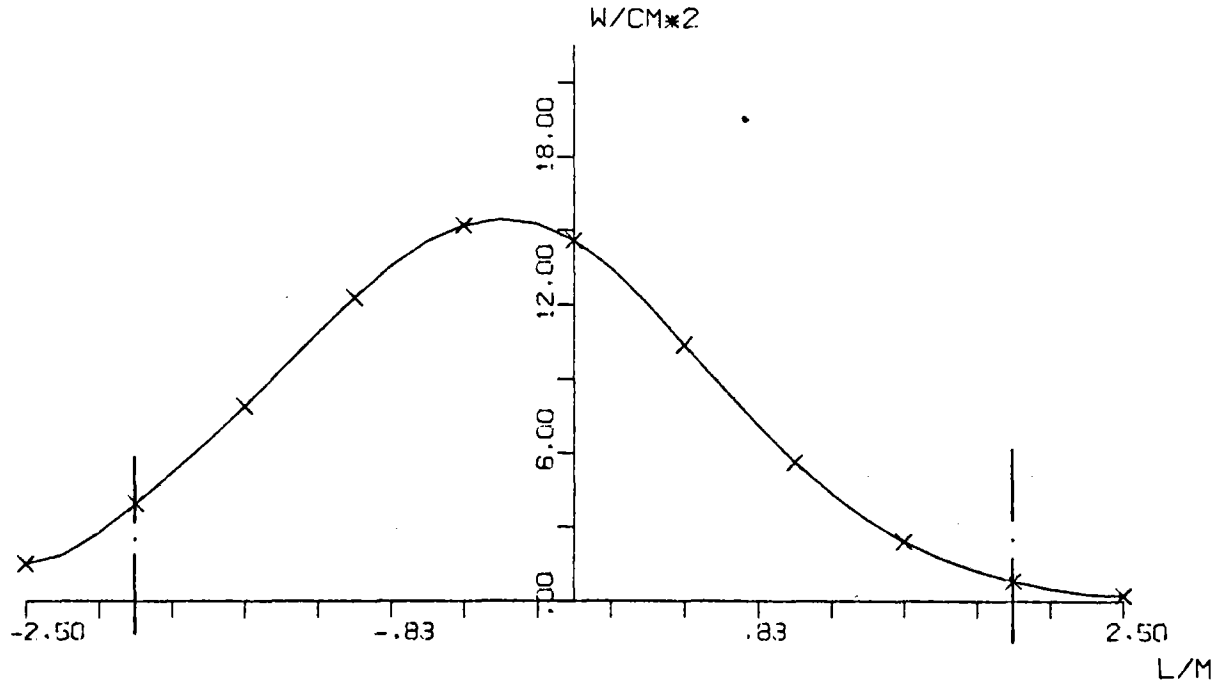

FIG.1.58 SOLAR FLUX ON TARGET SEC Y-Y

ASR-ALMERIA 3.1 MRD 21/6 NOON REC.CONT.

	.26	.22	.19	.16	.13	.11	.09	.09	.07	.05	.04
	.75	.64	.55	.46	.39	.33	.28	.23	.20	.16	.14
	1.75	1.49	1.27	1.08	.91	.77	.65	.55	.46	.39	.33
	3.40	2.89	2.45	2.08	1.76	1.48	1.25	1.06	.89	.75	.63
	5.50	4.66	3.94	3.33	2.81	2.37	2.00	1.69	1.42	1.20	1.02
E.	7.09	6.02	5.10	4.32	3.65	3.09	2.62	2.21	1.88	1.59	1.35 W.
	6.83	5.92	5.08	4.35	3.72	3.19	2.73	2.34	2.01	1.72	1.48
	4.88	4.30	3.77	3.31	2.90	2.54	2.22	1.95	1.71	1.50	1.32
	2.49	2.26	2.05	1.85	1.68	1.51	1.37	1.24	1.12	1.01	.92
	.93	.87	.81	.75	.70	.66	.61	.58	.54	.51	.48
	.27	.25	.24	.23	.22	.21	.20	.19	.18	.18	.17

BOT.

HELST. NO.	93.	AIM. NO.	3.
INSOL. KW/M2	.955	STD.DEV. MRAD.	3.10
DAY NO.	172.	INC.POW. KW	23.
TIME HR.	12.	AVERG./PEAK	.25
TOWER HEIGHT M	44.	SPILLAGE %	99.20
TARGET DIM. M	.4X3.0		

FIG.1.59 INCIDENT FLUX ON FLAT TARGET (W/CM2)
(RIGHT SIDE)

ASR-ALMERIA 3.1 MRD 21/6 NOON REC.CONT.

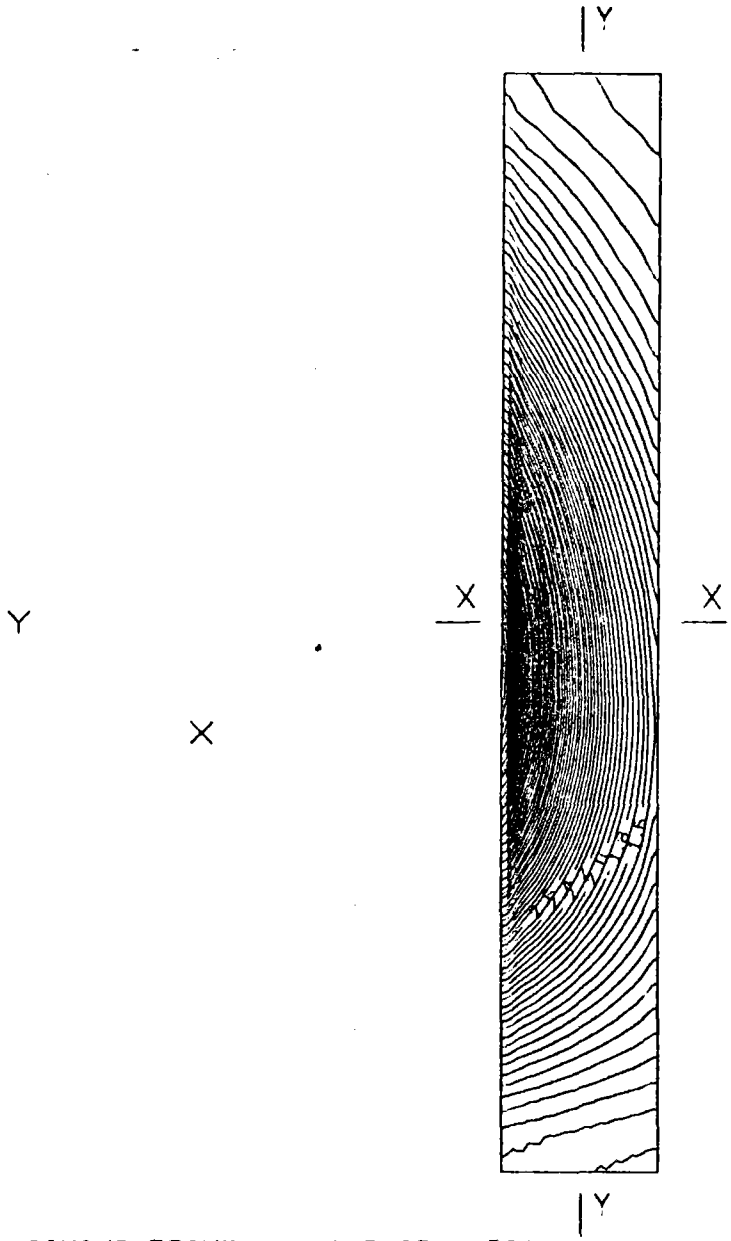

AIMING POINT: + (-2.03;-,30)
× (-1.03;-,30)
Y (-1.53;.00)

FIG.1.60 EQUIFLUX LINES,SPACING (W/CM2) ,1
(RIGHT SIDE)

ASR-ALMERIA 3.1 MRD 21/6 NOON REC.CONT.

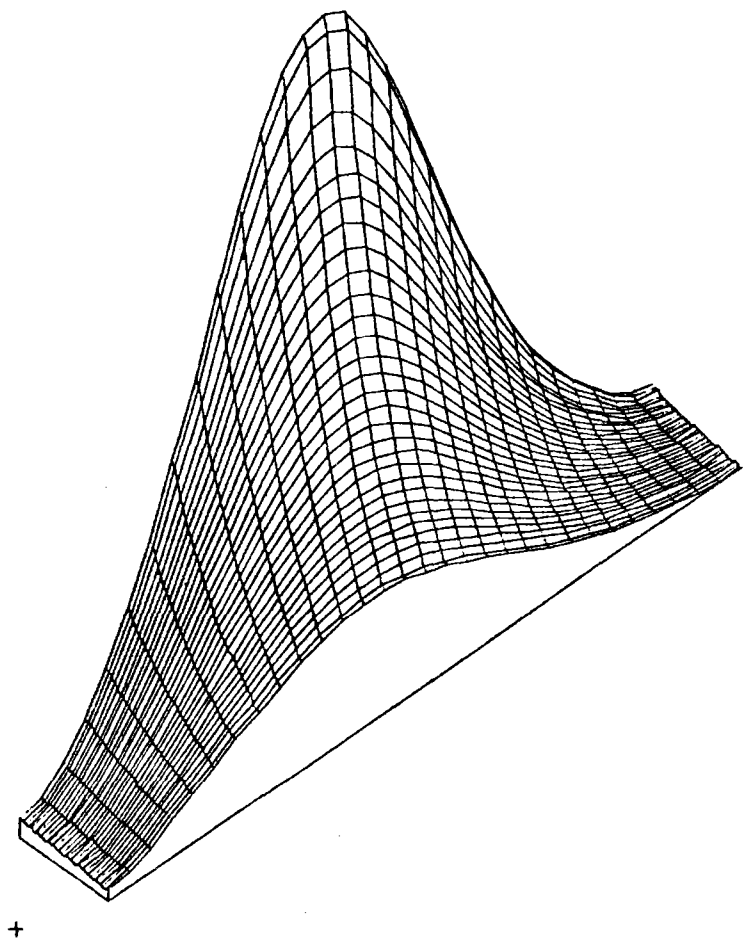

FIG.1.61 THREE-DIM. VIEW OF INCIDENT FLUX ON TARGET (RIGHT SIDE)

ASR-ALMERIA 3.1 MRD 21/6 NOON REC.CONT.

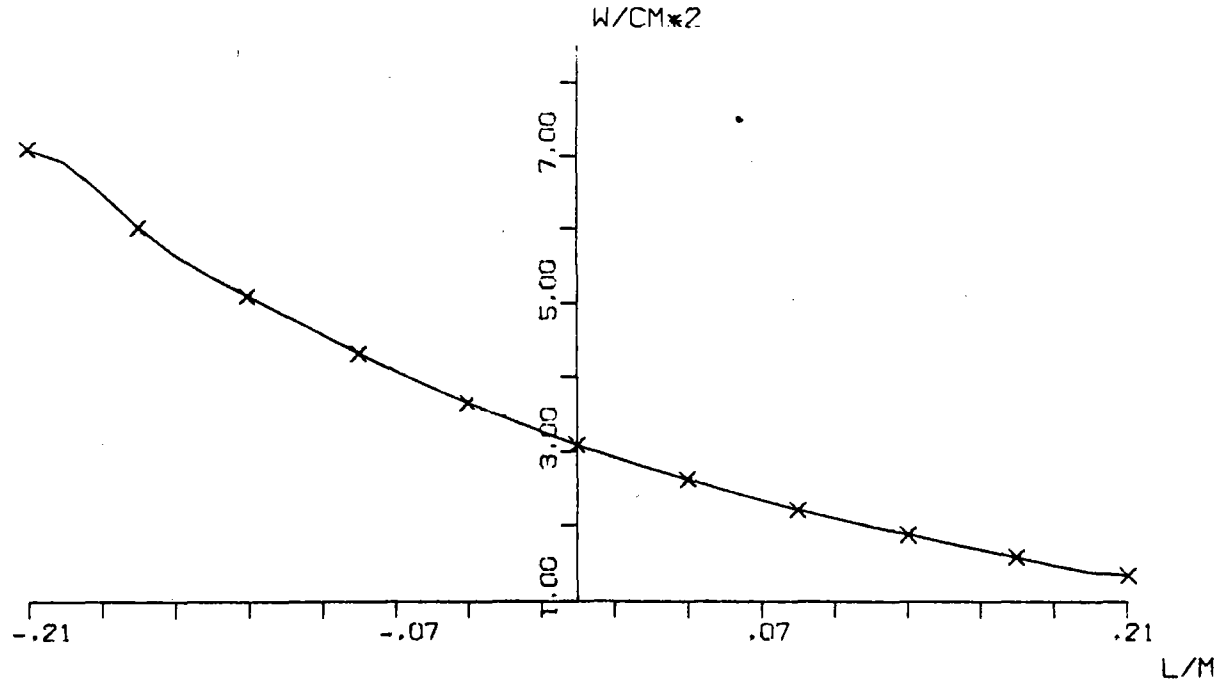

FIG.1.62 SOLAR FLUX ON TARGET SEC X-X
(RIGHT SIDE)

ASR-ALMERIA 3.1 MRD 21/6 NOON REC.CONT.

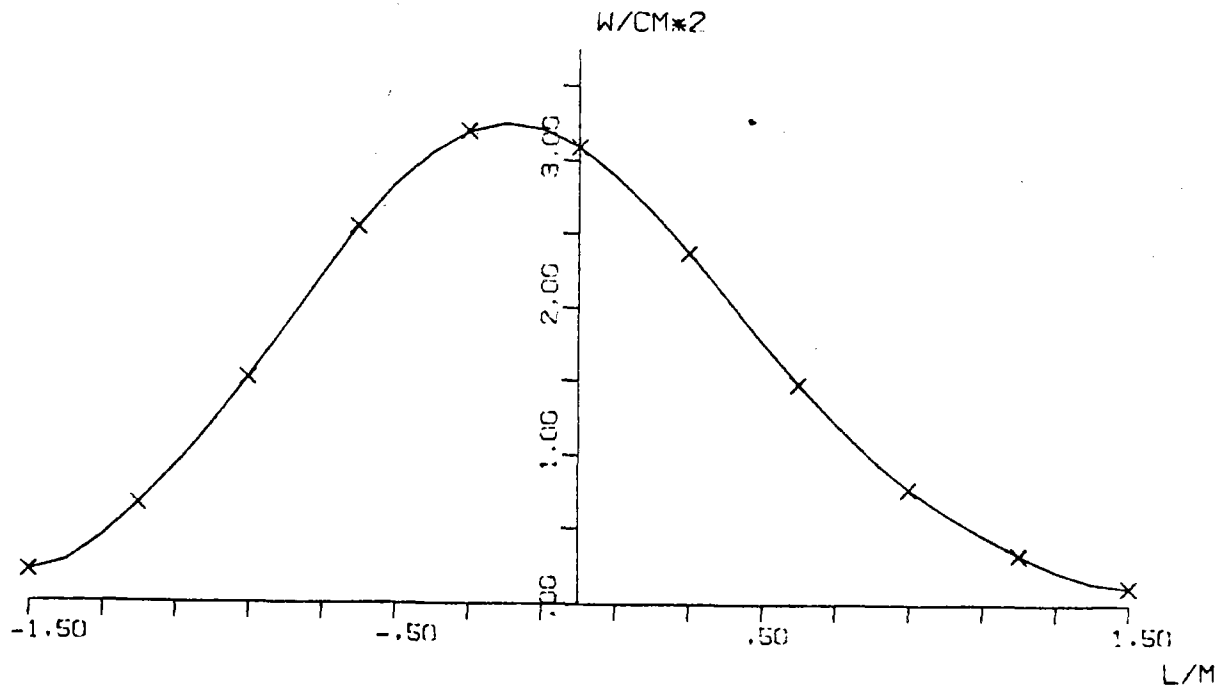

FIG.1.63 SOLAR FLUX ON TARGET SEC Y-Y
(RIGHT SIDE)

ASR-ALMERIA 3.1MRD 21/6 H6.15 REC.CONT.

	1.04	.98	.93	.88	.82	.78	.73	.68	.64	.60	.56
	1.83	1.76	1.69	1.61	1.53	1.46	1.38	1.31	1.24	1.17	1.10
	2.82	2.72	2.63	2.53	2.43	2.33	2.22	2.12	2.01	1.91	1.81
	3.73	3.62	3.51	3.39	3.27	3.14	3.01	2.88	2.75	2.62	2.49
	4.34	4.21	4.08	3.94	3.80	3.66	3.51	3.36	3.21	3.06	2.92
E.	4.54	4.40	4.25	4.10	3.94	3.78	3.62	3.46	3.30	3.14	2.99 W.
	4.39	4.23	4.07	3.90	3.74	3.57	3.40	3.24	3.08	2.92	2.76
	3.97	3.81	3.64	3.47	3.31	3.14	2.97	2.82	2.66	2.51	2.36
	3.38	3.22	3.06	2.90	2.74	2.59	2.44	2.29	2.15	2.01	1.88
	2.67	2.53	2.39	2.25	2.11	1.97	1.84	1.72	1.60	1.49	1.38
	1.91	1.80	1.69	1.57	1.46	1.36	1.26	1.16	1.07	.98	.90

BOT.

HELST. NO.	93.	AIM. NO.	3.
INSOL. KW/M2	.510	STD.DEV. MRAD.	3.10
DAY NO.	172.	INC.POW. KW	34.
TIME HR.	6.15	AVERG./PEAK	.59
TOWER HEIGHT M	44.	SPILLAGE %	96.38
TARGET DIM. M	.4X3.0		

FIG.1.64 INCIDENT FLUX ON FLAT TARGET (W/CM2)
(RIGHT SIDE)

ASR-ALMERIA 3.1MRD 21/6 H6.15 REC.CONT.

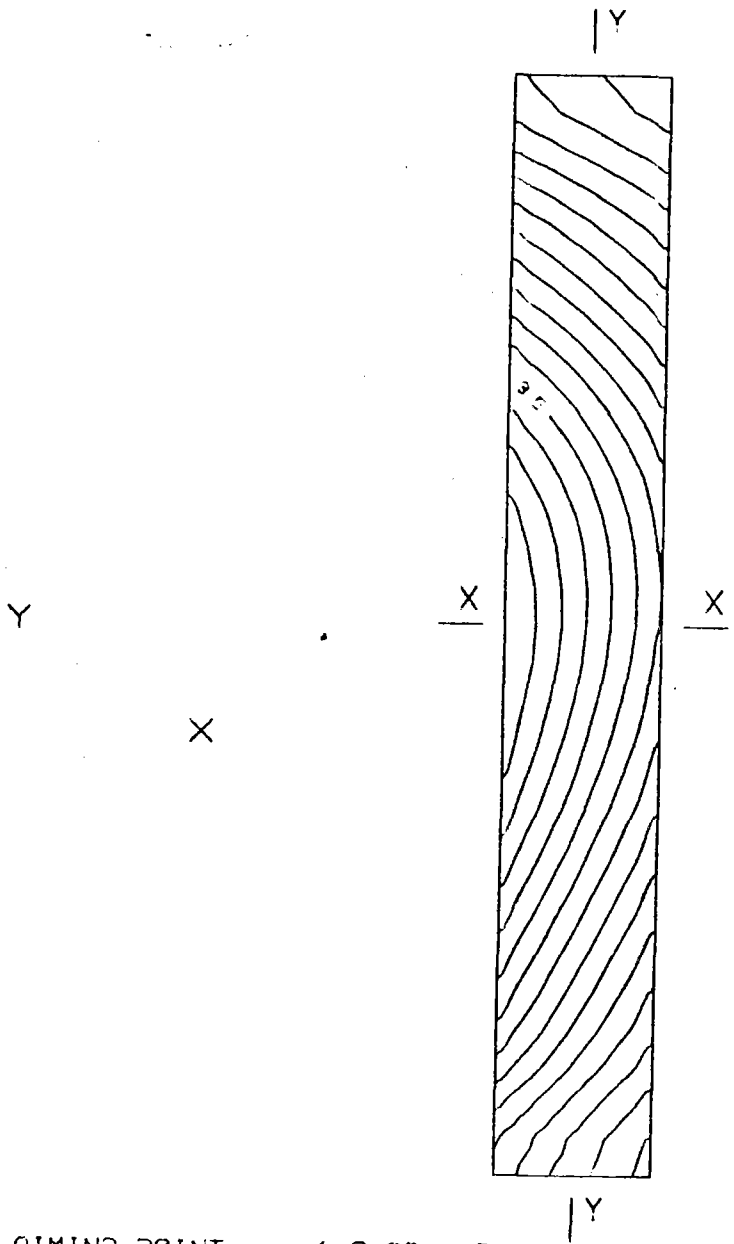

AIMING POINT: + (-2.03;-.30)
× (-1.03;-.30)
Y (-1.53;.00)

FIG.1.65 EQUIFLUX LINES.SPACING (W/CM2) .3
(RIGHT SIDE)

ASR-ALMERIA 3.1MRD 21/6 H6.15 REC.CONT.

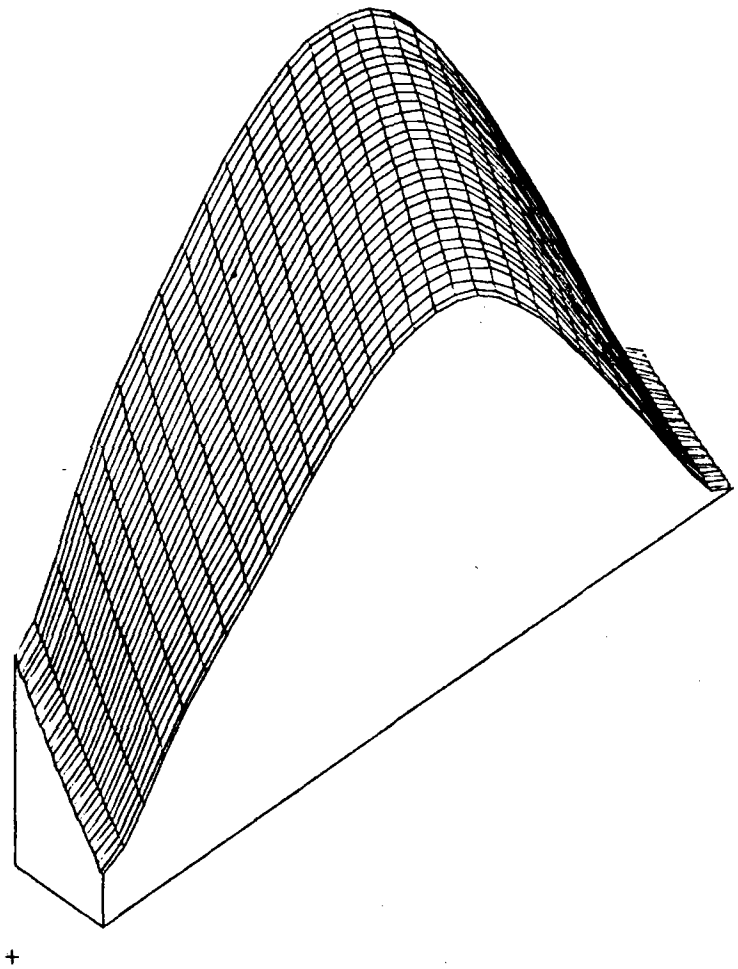

FIG.1.66 THREE-DIM. VIEW OF INCIDENT FLUX ON TARGET (RIGHT SIDE)

ASR-ALMERIA 3.1MRD 21/6 H6.15 REC.CONT.

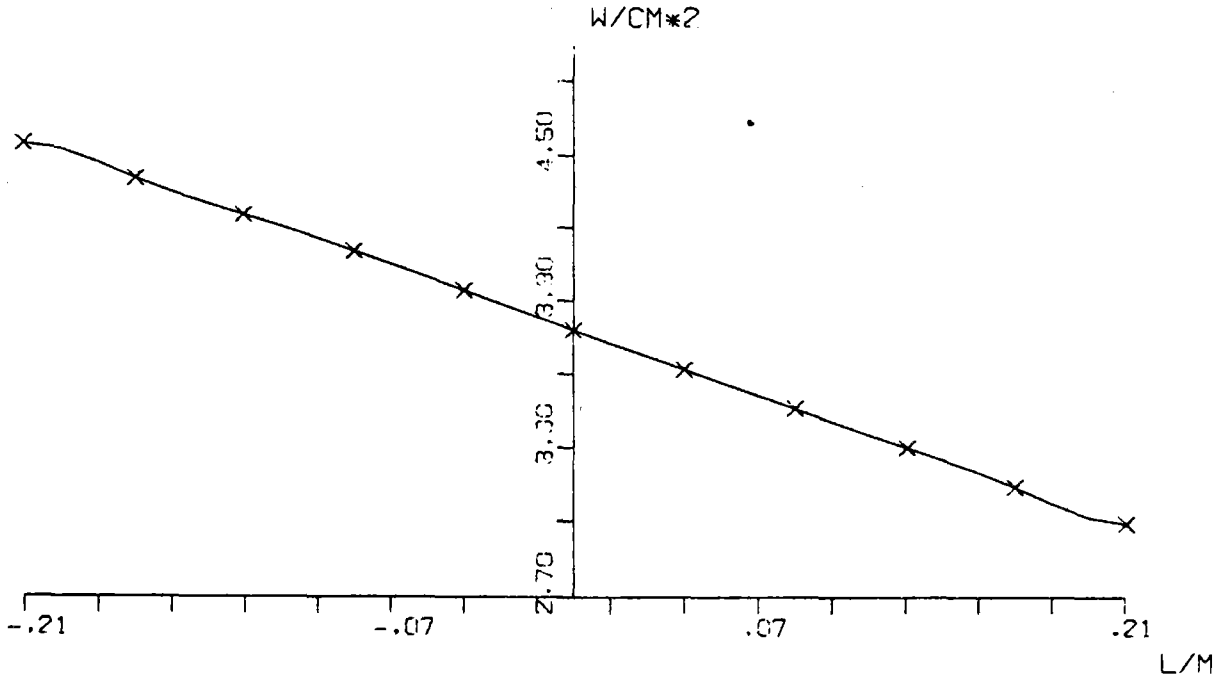

FIG.1.67 SOLAR FLUX ON TARGET SEC X-X
(RIGHT SIDE)

ASR-ALMERIA 3.1MRD 21/6 H6.15 REC.CONT.

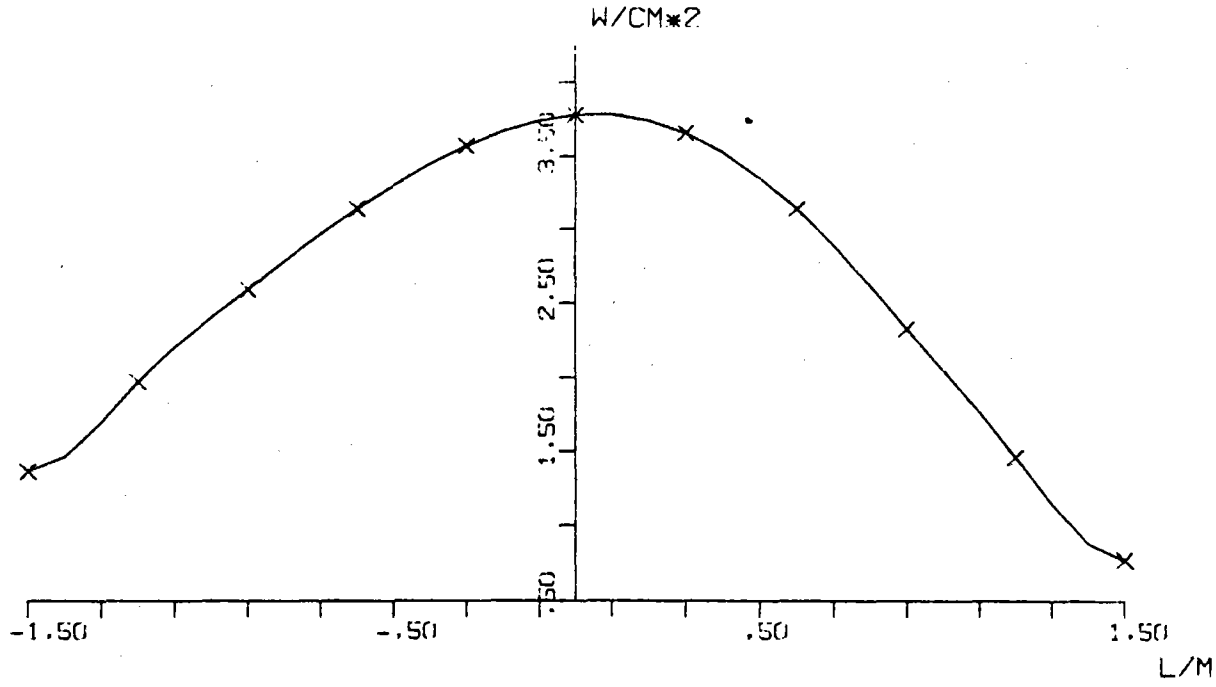

FIG.1.68 SOLAR FLUX ON TARGET SEC Y-Y
(RIGHT SIDE)

ASR-ALMERIA 3.5MRD 21/6 H6.15 REC.CONT.

	1.31	1.26	1.21	1.16	1.12	1.07	1.02	.98	.93	.89	.84	
	2.32	2.24	2.15	2.07	1.98	1.90	1.81	1.72	1.63	1.55	1.47	
	3.68	3.54	3.39	3.24	3.09	2.94	2.79	2.64	2.49	2.34	2.20	
	5.20	4.96	4.72	4.48	4.24	4.00	3.76	3.53	3.31	3.10	2.89	
	6.57	6.22	5.87	5.52	5.18	4.85	4.52	4.21	3.91	3.62	3.35	
E.	7.48	7.04	6.59	6.16	5.73	5.31	4.91	4.53	4.17	3.82	3.50	W.
	7.75	7.25	6.76	6.27	5.79	5.32	4.88	4.46	4.07	3.70	3.36	
	7.36	6.86	6.35	5.86	5.38	4.91	4.47	4.06	3.67	3.31	2.97	
	6.41	5.95	5.49	5.04	4.60	4.18	3.78	3.40	3.05	2.73	2.43	
	5.09	4.71	4.33	3.95	3.59	3.24	2.92	2.61	2.32	2.06	1.82	
	3.61	3.33	3.05	2.78	2.51	2.25	2.01	1.79	1.58	1.39	1.22	

BOT.

HELST. NO.	93.	AIM. NO.	3.
INSOL. KW/M2	.510	STD.DEV. MRAD.	3.50
DAY NO.	172.	INC.POW. KW	47.
TIME HR.	6.25	AVERG./PEAK	.50
TOWER HEIGHT M	44.	SPILLAGE %	95.01
TARGET DIM. M	.4X2.9		

FIG.1.69 INCIDENT FLUX ON FLAT TARGET (W/CM2)
(RIGHT SIDE)

ASR-ALMERIA 3.5MRD 21/6 H6.15 REC.CONT.

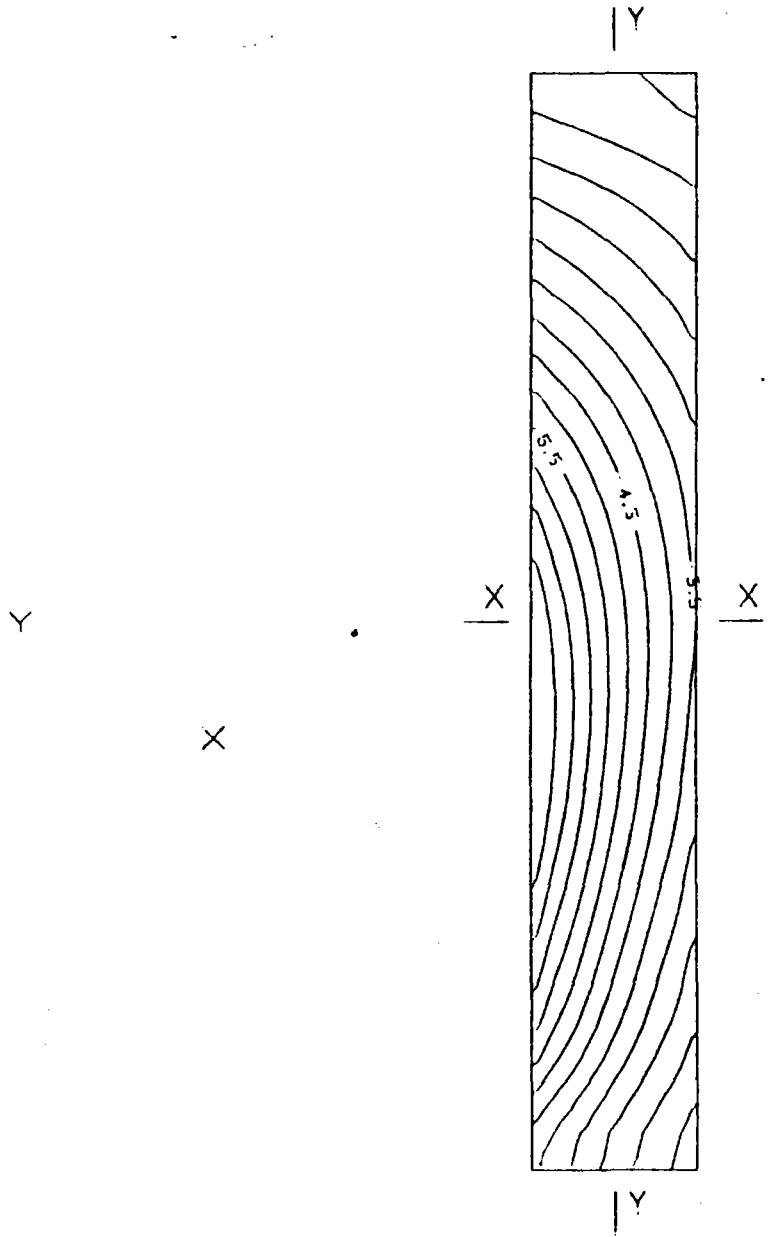

AIMING POINT: + (-2.03;-.30)
× (-1.03;-.30)
Y (-1.53;.00)

FIG.1.70 EQUIFLUX LINES,SPACING (W/CM2) .5
(RIGHT SIDE)

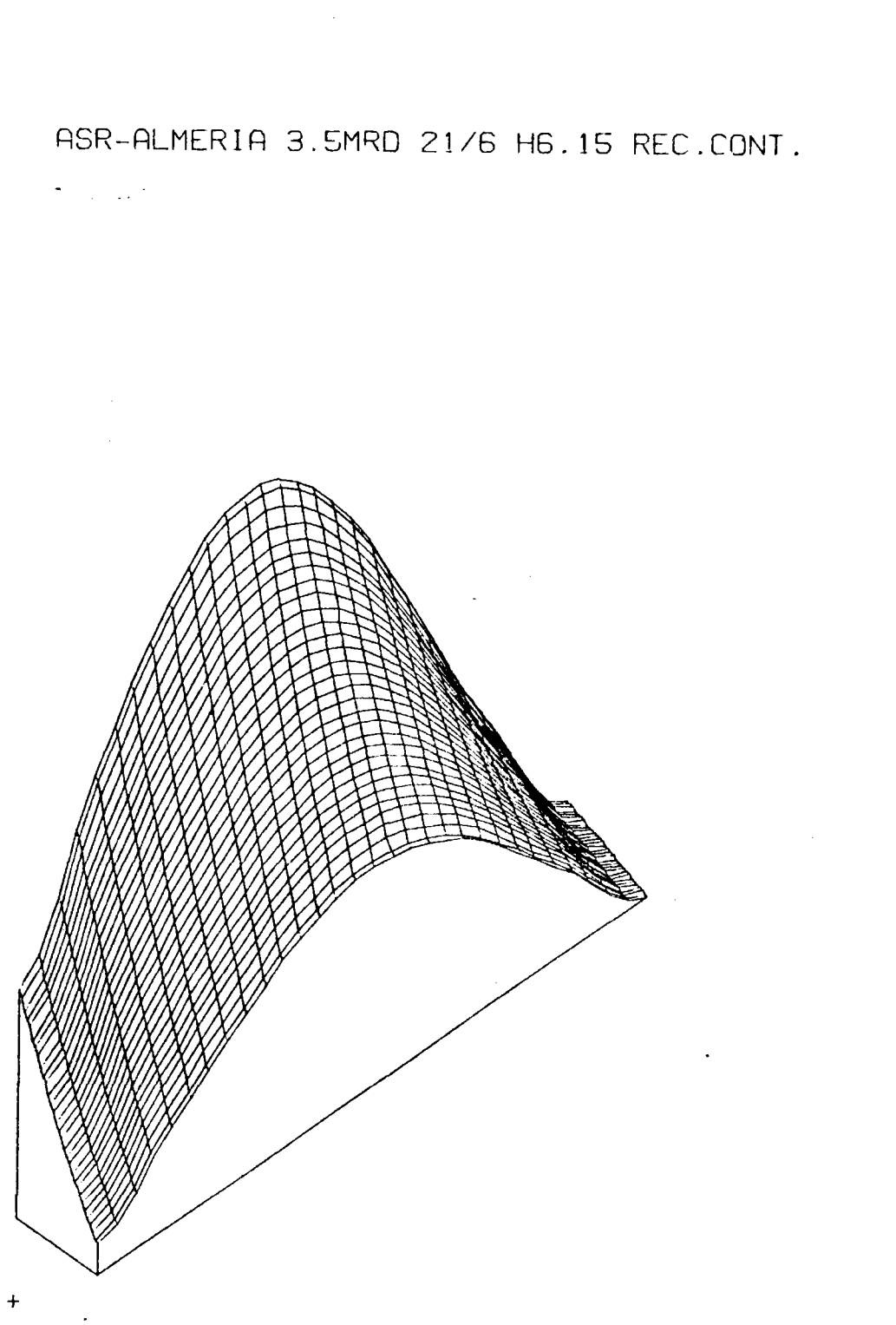

FIG.1.71 THREE-DIM. VIEW OF INCIDENT FLUX ON TARGET (RIGHT SIDE)

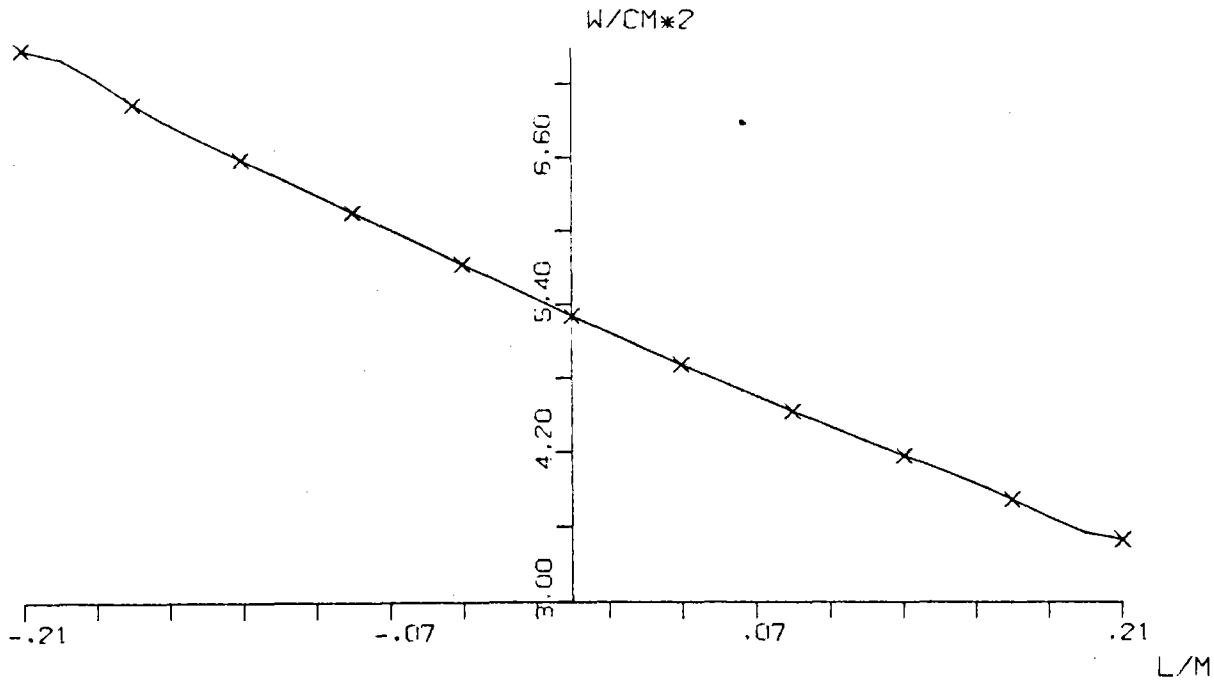

FIG.1.72 SOLAR FLUX ON TARGET SEC X-X
(RIGHT SIDE)

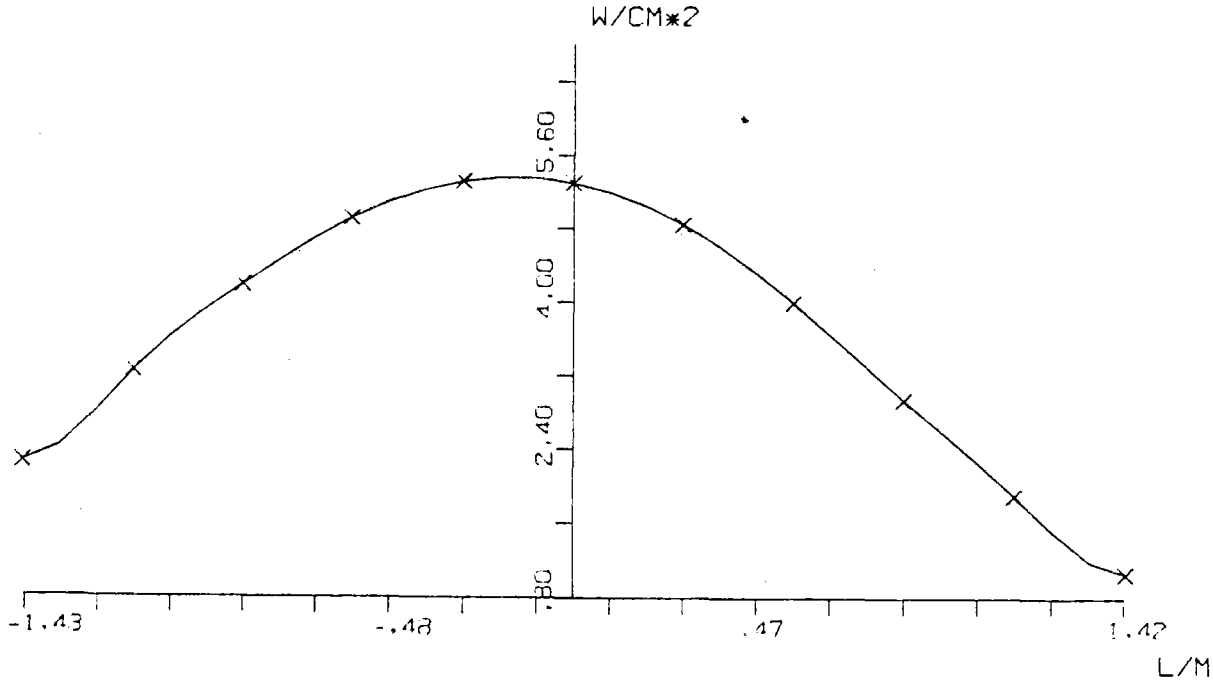

FIG.1.73 SOLAR FLUX ON TARGET SEC Y-Y
(RIGHT SIDE)

ASR-ALMERIA 3.1MRD 21/6 NOON RECEIV.CAS.

	.01	.01	.03	.08	.14	.16	.14	.08	.03	.01	.01	
	.01	.05	.22	.57	1.01	1.21	1.00	.57	.22	.05	.01	
	.04	.25	1.02	2.74	4.99	6.10	4.99	2.73	1.02	.25	.04	
	.13	.80	3.29	9.25	17.4	21.6	17.4	9.25	3.30	.81	.13	
	.29	1.83	7.39	23.3	43.1	52.4	43.2	23.4	8.07	1.85	.30	
E.	.49	3.19	15.4	47.4	80.7	90.9	80.6	47.4	15.6	3.28	.50	W.
	.63	4.27	21.9	69.1	108.	112.	107.	68.4	22.1	4.46	.69	
	.59	3.99	18.8	52.2	77.6	80.1	75.7	51.1	18.7	4.16	.73	
	.32	1.99	7.68	16.4	23.8	27.6	23.7	16.1	7.44	2.16	.46	
	.08	.45	1.34	2.47	3.69	4.36	3.69	2.44	1.33	.31	.13	
	.01	.04	.14	.28	.43	.49	.42	.27	14	.05	.01	

BOT.

HELST. NO.	93.	AIM. NO.	3.
INSOL. KW/M2	.955	STD.DEV. MRAD.	3.10
DAY NO.	172.	INC.POW. KW	2800.
TIME HR.	12.	AVERG./PEAK	.16
TOWER HEIGHT M	44.	SPILLAGE %	.27
TARGET DIM. M	4.0X4.0	▨ CASING APERT.	

FIG.1.74 INCIDENT FLUX ON FLAT TARGET (W/CM2)

ASR-ALMERIA 3.1MRD 21/6 NOON RECEIV.CAS.

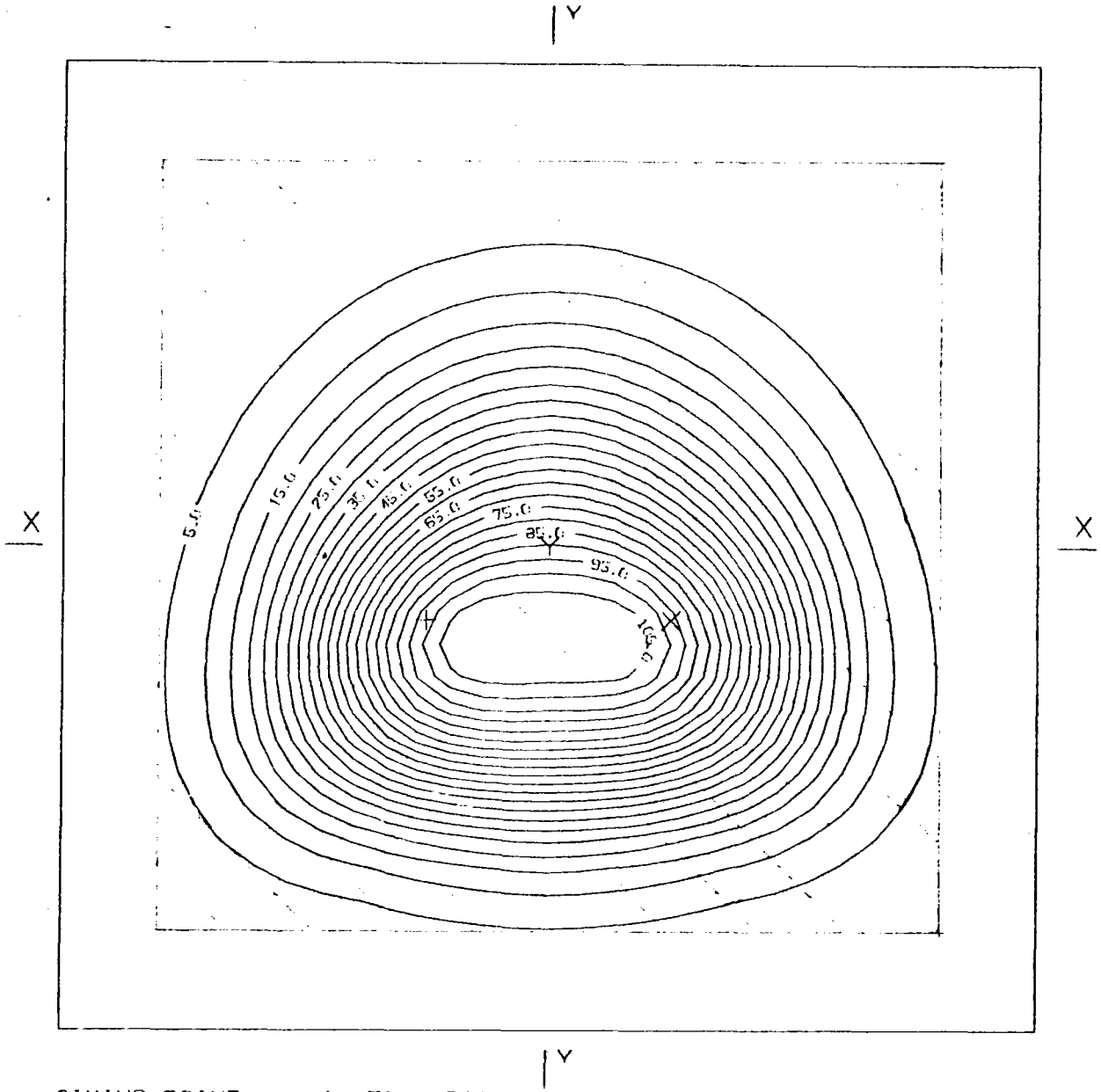

AIMING POINT: + (-.50,-.30)

× (.50,-.30)

Y (.00,.00)

FIG.1.75 EQUIFLUX LINES, SPACING (W/CM2) 5.0

ASR-ALMERIA 3.1MRD 21/6 NOON RECEIV.CAS.

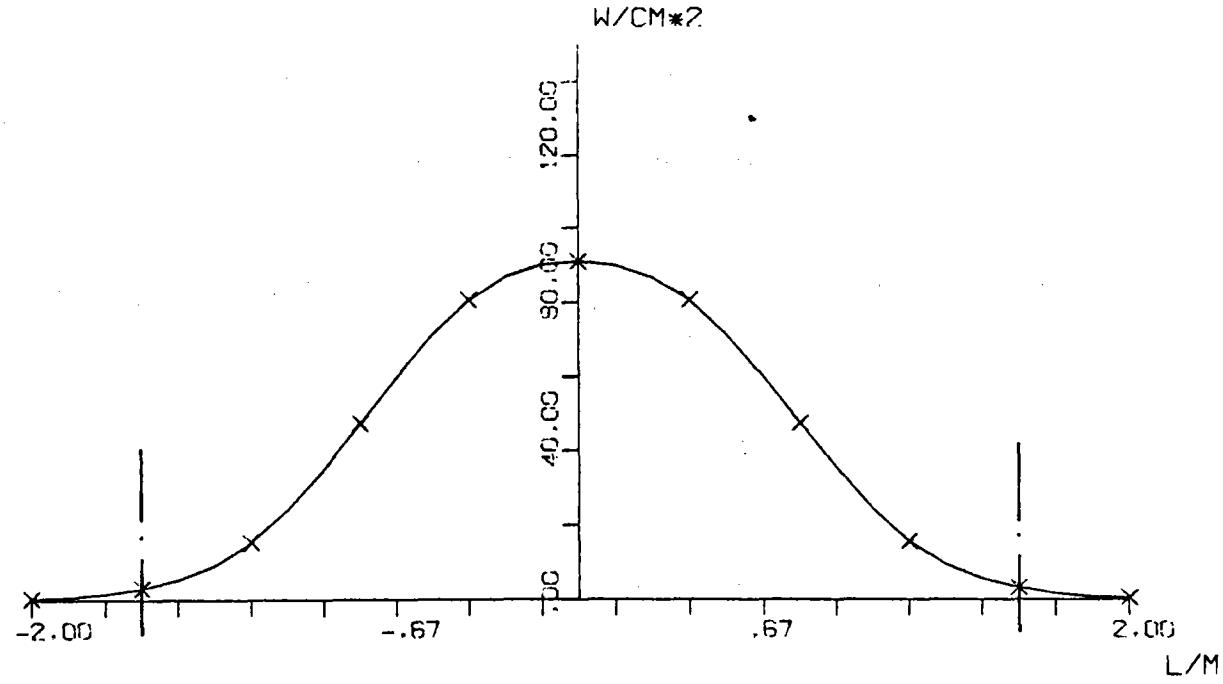

FIG.1.76 SOLAR FLUX ON TARGET SEC X-X

ASR-ALMERIA 3.1MRD 21/6 NOON RECEIV.CAS.

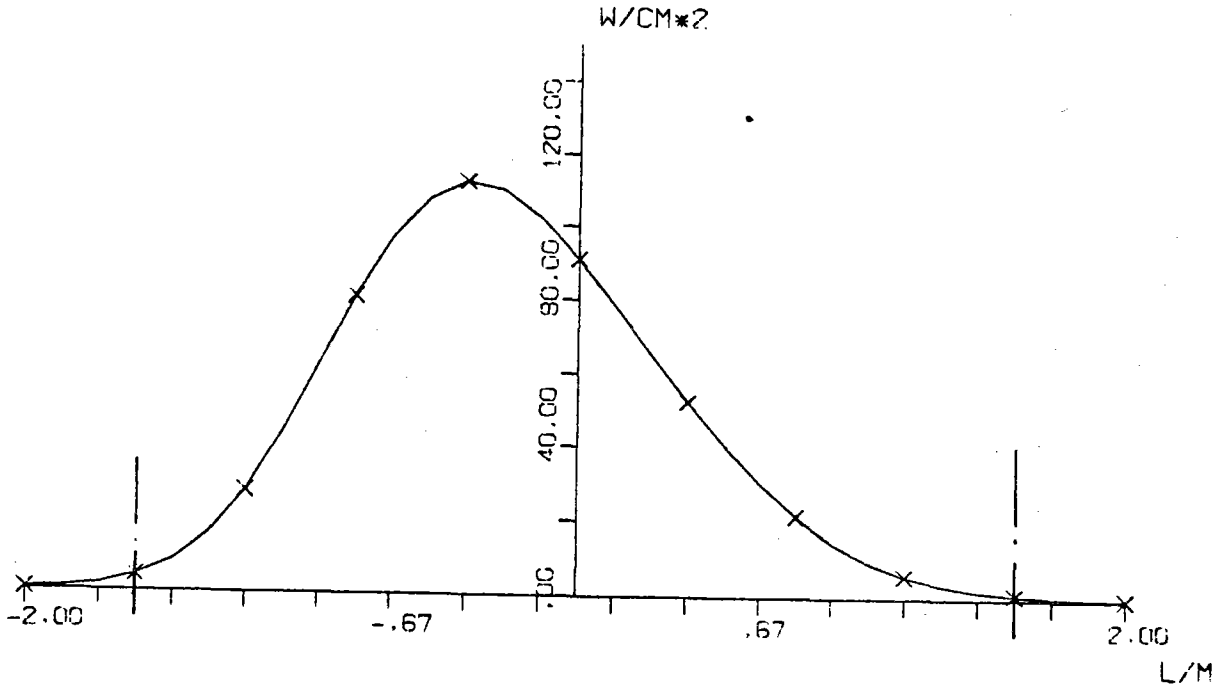

FIG.1.77 SOLAR FLUX ON TARGET SEC Y-Y

ASR-ALMERIA 3.1MRD 21/6 6.15 RECEIV.CAS.

	.04	.16	.49	.93	1.13	1.04	.77	.46	.26	.14	.08
	.11	.43	1.21	2.19	2.54	2.44	1.88	1.22	.76	.49	.30
	.27	.91	2.47	4.23	4.87	5.08	4.10	2.83	1.95	1.32	.77
	.53	1.62	4.23	6.90	7.98	8.99	7.73	5.59	4.13	2.66	1.40
	.88	2.43	6.01	9.43	11.2	13.5	12.1	9.22	6.92	4.60	1.87
E.	1.26	3.14	7.05	10.7	13.1	16.5	15.4	12.2	9.17	4.75	1.91
	1.57	3.54	6.99	10.1	12.7	16.6	15.8	12.9	9.78	4.67	1.60
	1.67	3.44	5.91	8.24	10.6	14.0	13.5	11.3	8.63	3.87	1.15
	1.50	2.82	4.24	5.68	7.65	10.09	9.65	8.18	6.29	2.66	.69
	1.11	1.91	2.58	3.32	4.73	6.05	5.68	4.87	3.66	1.42	.32
	.69	1.06	1.30	1.67	2.60	3.10	2.73	2.46	1.66	.54	.10

W.

BOT.

HELST. NO.	93.	AIM. NO.	3.
INSOL. KW/M2	.510	STD.DEV. MRAD.	3.10
DAY NO.	172.	INC.POW. KW	874.
TIME HR.	6.	AVERG./PEAK	.33
TOWER HEIGHT M	44.	SPILLAGE %	7.37
TARGET DIM. M	4.0X4.0	▨ CASING APERT.	

FIG.1.78 INCIDENT FLUX ON FLAT TARGET (W/CM2)

ASR-ALMERIA 3.1MRD 21/6 6.15 RECEIV.CAS.

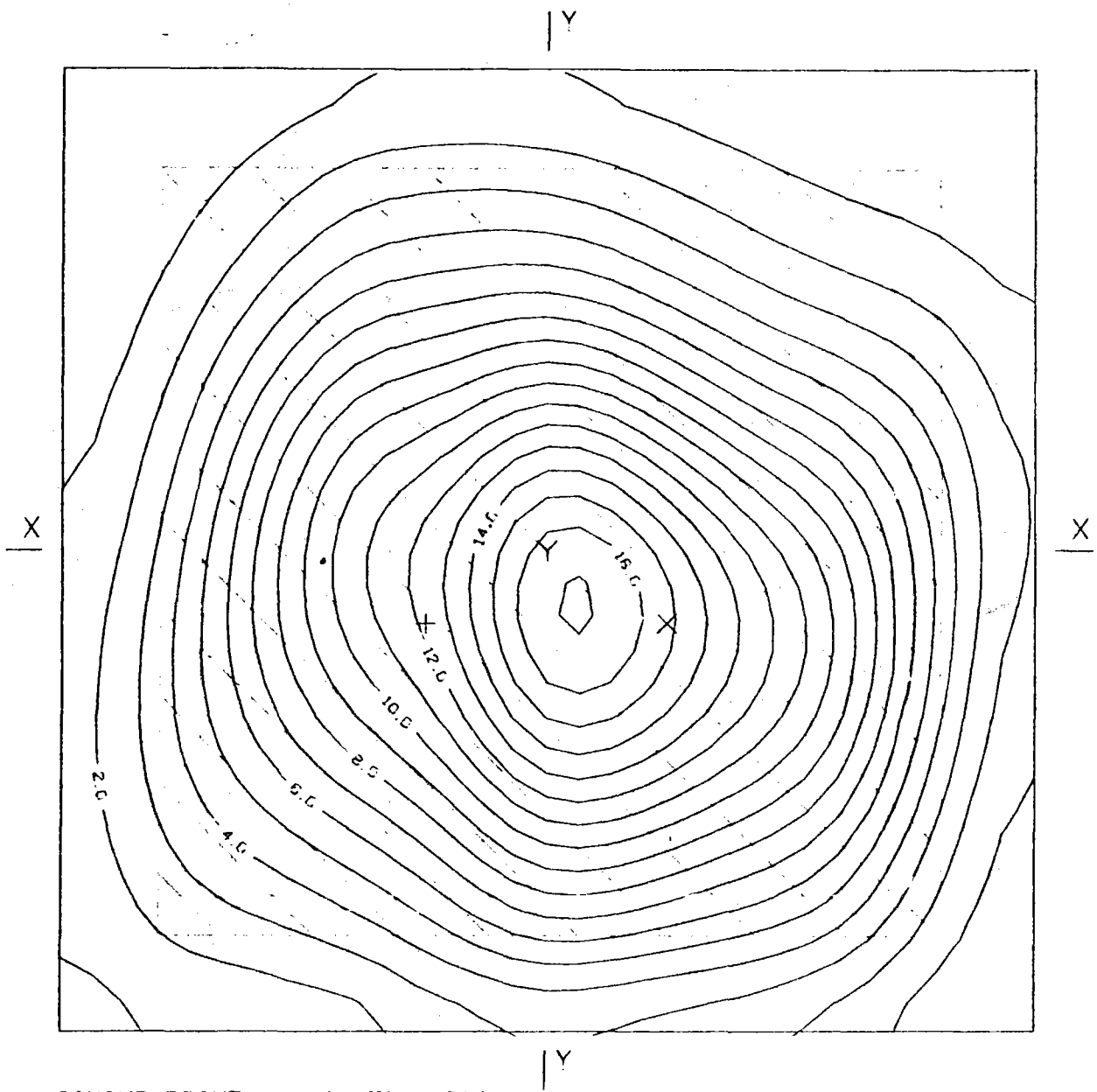

AIMING POINT: + (-.50;-.30)
× (.50;-.30)
Y (.00;.00)

FIG.1.79 EQUIFLUX LINES.SPACING (W/CM2) 1.0

ASR-ALMERIA 3.1MRD 21/6 6.15 RECFIV.CAS.

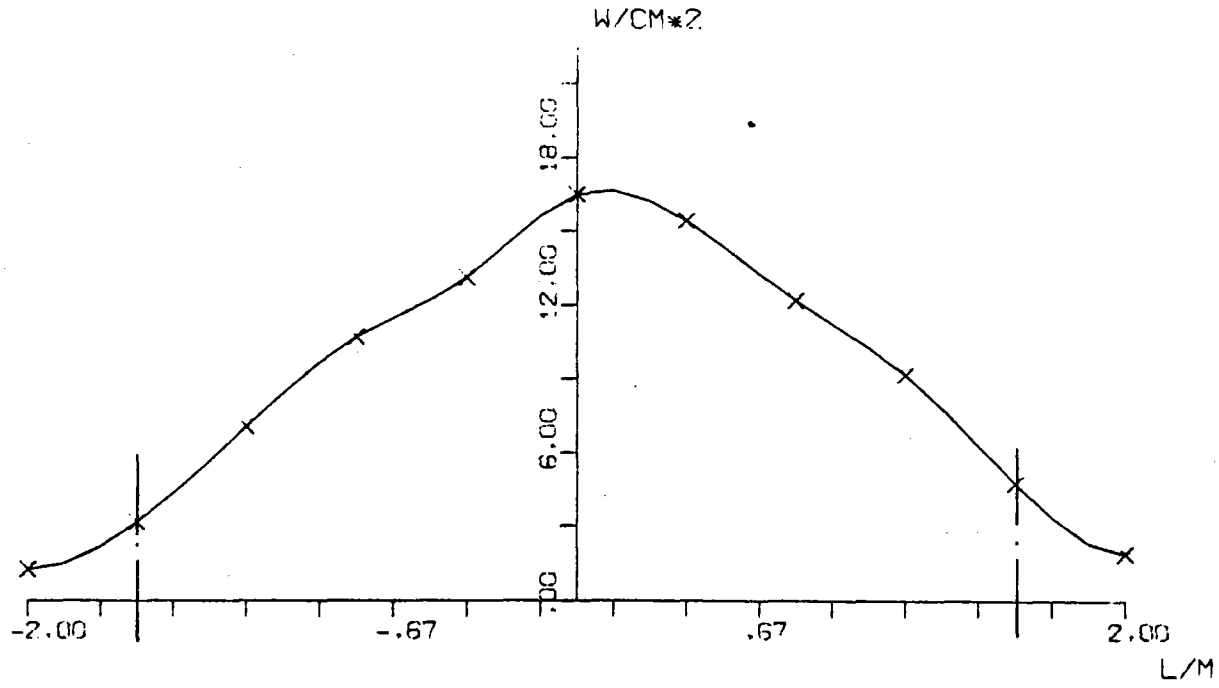

FIG.1.80 SOLAR FLUX ON TARGET SEC X-X

ASR-ALMERIA 3.1MRD 21/6 6.15 RECEIV.CAS.

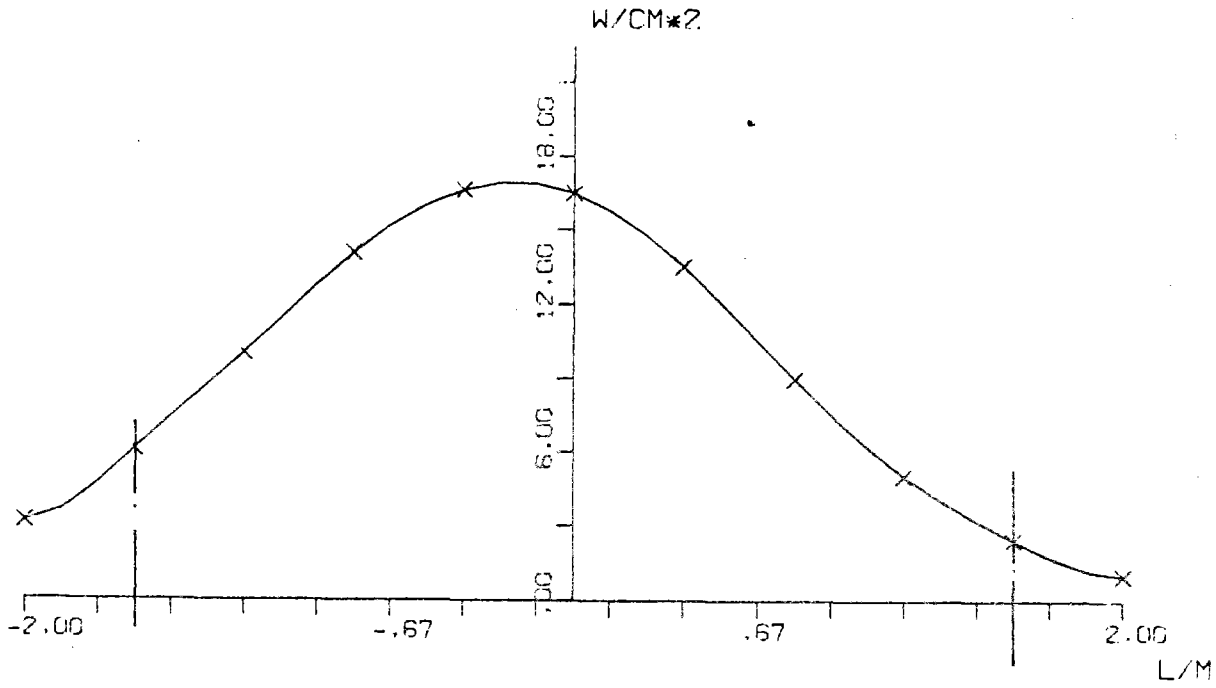

FIG.1.81 SOLAR FLUX ON TARGET SEC Y-Y

2. CLOUD PASSAGE SIMULATION

The effect of a cloud passage over the heliostat field and the consequent flux distribution and power transients are computed and analyzed, simulating a progressive strip by strip heliostat darkening. The thermal flux behaviour at each target point (the velocity of change) during the transient and the flux profile distorsion depend on the direction of cloud and on time. Owing to the adopted cross aiming strategy, the vertical flux distribution simmetry is roughtly maintained when the heliostat field is shaded, as is quite unlikely that clouds darken in average more B1 aimed heliostats than B2 or viceversa.

Further the darkening of the last row heliostats, projecting on the target the largest images, produces a more uniform flux decrease than the one caused by the front row.

To show this effect the North-South cloud passage (and viceversa) is analyzed. The heliostat field is subdivided in five parallel strips, normal to the North-South axis, with different heliostat number but equal N-S width ($\Delta x = 25m$) (see fig. n. 2.1).

Taking into account the Operating Agent's indication and the Tabernas Meteo Data Analysis Results (SSPS Technical Report n. 1/81 by Belgo Nucleaire), the East-West

cloud direction is considered too. In fact the probability of E-W (or W-E) wind is greater than 60% (fig. 2.2) at Tabernas site and clouds are supposed to have the same direction of wind at ground level.
This is an assumption that has to be verified, since at altitude wind direction and velocity generally differ from the same values at ground, depending on the local orography. In order to simulate the E-W cloud passage, the five strips are parallel to N-S axis and 29.5 m. wide (fig. 2.3) ($\Delta y = 29.5$).
For each field strip and reference time, the incident flux distributions are computed using Helios program; then the zone maps are overlapped, following the step by step heliostat field shading (or lighting), each time step (Δt) depending on cloud velocity V and strip width (Δx or Δy).
Using the simple relation $\Delta t = \frac{\Delta x}{V}$ (or $= \frac{\Delta y}{V}$) the time step Δt and the whole transient time $\Delta WT = 5.\Delta t$ can be computed, once a wind velocity is settled (Table I).
Disregarding the mutual interference between contiguous zones is the only approximation as far as incident flux evaluation by means of overlapping is concerned. In fact, as each zone is considered alone, shading and blocking effect between different strips are not included. The resulting error depends on time (minimum at noon in summer) and on field partition (E-W or N-S).
Undoubtedly the grater approximation in the described

model consists in the cloud simulation. In fact we assumed the cloud as sketched by a black sheet fully opaque and without thickness, covering the heliostat field and passing exactly either in North-South (fig. 2.4) or in East-West direction (fig. 2.5). The straight and step limb, together with the lack of thickness, is a poor approximation of a cloud, but it is required in order to semplify the cloud shape. These assumptions steep the flux transient, decreasing the time length. As a possible vertical component of motion is disregarded, the velocity of the cloud is equal to the velocity of its shadow on the ground (sun rays are parallel) and indipendent of sun position. Vertical motion effect can be included, adding however the functional dependance on sun elevation angle θ.
($V = V_{or} + V_{ver}/tg\ \theta$), i.e. on time.
At low sun height the shadow velocity on the ground can be largely increased by vertical motions; luckily the direct beam at the same time is low.
Six different transients are computed and presented
N-S/S-N passage at design point (Day 80, noon)
E-W/W-E passage at design point (Day 80, noon)
E-W/W-E passage at equinox, 9.30 a.m.

This last condition is considered as it shows a marked dissimetry in the heliostat field together with a high direct beam value.

Result analysis

The flux distribution transients, resulting from a N-S or S-N cloud passage, is evaluated at design point (Day 80, noon).

The time step interval Δt can be obtained from fig. 2.6, once the wind velocity is fixed. Fig. 2.7 shows the comparison of the behaviour of the center target incident flux caused by a N-S vs S-N cloud passage; fig. 2.8 and 2.9 display the behaviour of peak flux and power incident on the target. The complete set of flux values on the target during the transients are presented in Progress Report n. 6 (March 81).

The step by step shading of E-W parallel strip maintains the flux distribution symmetry relatively to the vertical target axis, but the flux profile distortion is quite unlike.

This different behaviour between North-South and South-North transient can be estimated comparing fig. 2.10, 2.11 with 2.12, 2.13 (the profiles are presented at subsequent Δt). The largest flux variation occurs at the third time step, and, for both cloud passage directions, is roughly 48 $N/cm^2/\Delta t$ (at center target). As Δt depends on wind velocity, the maximum time gradient vs wind velocity at different positions on the target in plotted herewith, see fig. 2.14. Table II presents an overall review of N-S/S-N results.

Flux distribution transients in consequence of E-W or W-E cloud passage are evaluated at design point (Day 80, noon) and at Day 80, 9.30 a.m.
Fig. n. 2.15 show the time step values vs wind velocity; fig. 2.16 ÷ 2.20 display the incident flux (peak or central target) and the incident power vs time step during a cloud passage at noon and at 9.30 a.m.
The complete flux distributions are collected in Appendix; the overall results are summarized in fig. 2.21 ÷ 2.28. Some general aspects can be pointed out:

- At noon E-W and W-E transients are quite similar but not the same, because although the heliostat working conditions are symmetrical relatively to N-S axis, the images on the target of symmetrical strips are not equal but specular (see fig.A.26,A.50).

- At time different from noon, the mirror field unsymetry relatively to N-S axis (the heliostats facing sun and tower work better) increases the flux unsymetry between the E-W and W-E cloud passage (also the power reflected by equal but N-S symmetrical strips is different; See fig. A.79, A.104).

- When the E-W passage at 9.30 a.m. is compared with a W-E one at 14.30 p.m., the unsymetry again appears, owing to the deforming heliostat image interception by the target plane.

Table III, IV show the main results and evidentiate that the maximum flux variation in a time step occurs at noon (27 $W/cm^2/\Delta t$ at center target point, 45 $W/cm^2/\Delta t$ for peak value). Again the maximum flux time gradient can be expressed as a function of wind velocity, using the definition $\Delta t = \Delta y/V = 29.5$ m/V. The results are summarized in fig. n. 2.29. Fig. 2.30 shows the normalized power incident to the target vs time step, the normalized peak and center target flux behaviour are shown in Fig. 2.31, 2.32 (compare with fig. 2.33 for N-S/S-N cloud passage).

TABLE I

Whole transient time ΔWT vs cloud velocity V

Cloud velocity (Km/h)	N-S/S-N computed (sec)	E-W/W-E computed (sec)	Measured * (sec)
10	45	53.1	54
23	19.6	23.1	24
50	9	10.6	11

* Letter n. 68.04215 from Interatom, dated 21/8/81.

TABLE II

N-S/S-N cloud passage, noon

$$\Delta t = \frac{\Delta y}{V} = \frac{25.0\ m}{V}$$

S-N	ϕ_p (W/cm^2)	$\Delta\phi_p$ (W/cm^2)	%	ϕ_{CT} (W/cm^2)	$\Delta\phi_{CT}$ (W/cm^2)	%	W_T (KW)	ΔW_T (KW)	%
54321	129	13	100	121	13	100	2810	450	100
5432	116	19	90	116	19	96	2360	720	84
543	97	48	75	97	48	80	1640	702	58
54	49	31	38	49	31	40	938	535	33
5	18	18	14	18	18	15	403	403	14

N-S	ϕ_p (W/cm^2)	$\Delta\phi_p$ (W/cm^2)	%	ϕ_{CT} (W/cm^2)	$\Delta\phi_{CT}$ (W/cm^2)	%	W_T (KW)	ΔW_T (KW)	%
12345	129	12	100	121	17	100	2810	450	100
1234	117	16	91	104	32	86	2400	530	85
123	101	25	78	72	48	59	1870	700	66
12	76	38	59	24	19	20	1170	728	42
1	38	38	29	5	5	4	442	442	16

ϕ_p = peak flux value

ϕ_{CT} = center target flux value

W T = power incident on the target

TABLE III

E-W/W-E cloud passage, noon

$$\Delta t = \frac{\Delta x}{V} = \frac{29.6\ m}{V}$$

E-W	ϕ_p (W/cm^2)	$\Delta\phi_p$ (W/cm^2)	%	ϕ_{CT} (W/cm^2)	$\Delta\phi_{CT}$ (W/cm^2)	%	W_T (KW)	ΔW_T (KW)	%
12345	134	15	100	124	22	100	2860	420	100
2345	119	25	89	102	27	82	2440	620	85
345	94	45	70	75	27	60	1820	780	64
45	49	26	37	48	25	39	1040	622	36
5	23	23	17	23	23	18	418	418	15

W-E	ϕ_p (W/cm^2)	$\Delta\phi_p$ (W/cm^2)	%	ϕ_{CT} (W/cm^2)	$\Delta\phi_{CT}$ (W/cm^2)	%	W_T (KW)	ΔW_T (KW)	%
12345	134	11	1.	124	23	1.	2860	420	1.
1234	123	34	.92	101	25	.81	2440	620	.85
123	89	35	.66	76	25	.61	1820	780	.64
12	54	31	.40	49	27	.40	1040	622	.36
1	23	23	.17	23	26	.19	418	418	.15

TABLE IV

E-W/W-E cloud passage, 9.30 a.m.

$$\Delta t = \frac{\Delta y}{V} = \frac{29.5\ m}{V}$$

E-W	ϕ_p (W/cm^2)	$\Delta\phi_p$ (W/cm^2)	%	ϕ_{CT} (W/cm^2)	$\Delta\phi_{CT}$ (W/cm^2)	%	W_T (KW)	ΔW_T (KW)	%
12345	77	5	100	73	19	100	1970	230	100
2345	72	12	93	68	18	93	1740	360	88
345	60	22	78	55	18	75	1370	551	70
45	38	18	49	36	17	51	819	477	41
5	20	20	26	20	20	27	342	342	17

W-E	ϕ_p (W/cm^2)	$\Delta\phi_p$ (W/cm^2)	%	ϕ_{CT} (W/cm^2)	$\Delta\phi_{CT}$ (W/cm^2)	%	W_T (KW)	ΔW_T (KW)	%
54321	77	17	1.	73	19	1.	1970	340	1.
4321	60	21	.78	54	18	.74	1630	480	.82
321	39	20	.51	36	17	.49	1150	551	.58
21	19	13	.25	19	13	.26	599	373	.30
1	6	6	.08	6	6	.08	226	226	.11

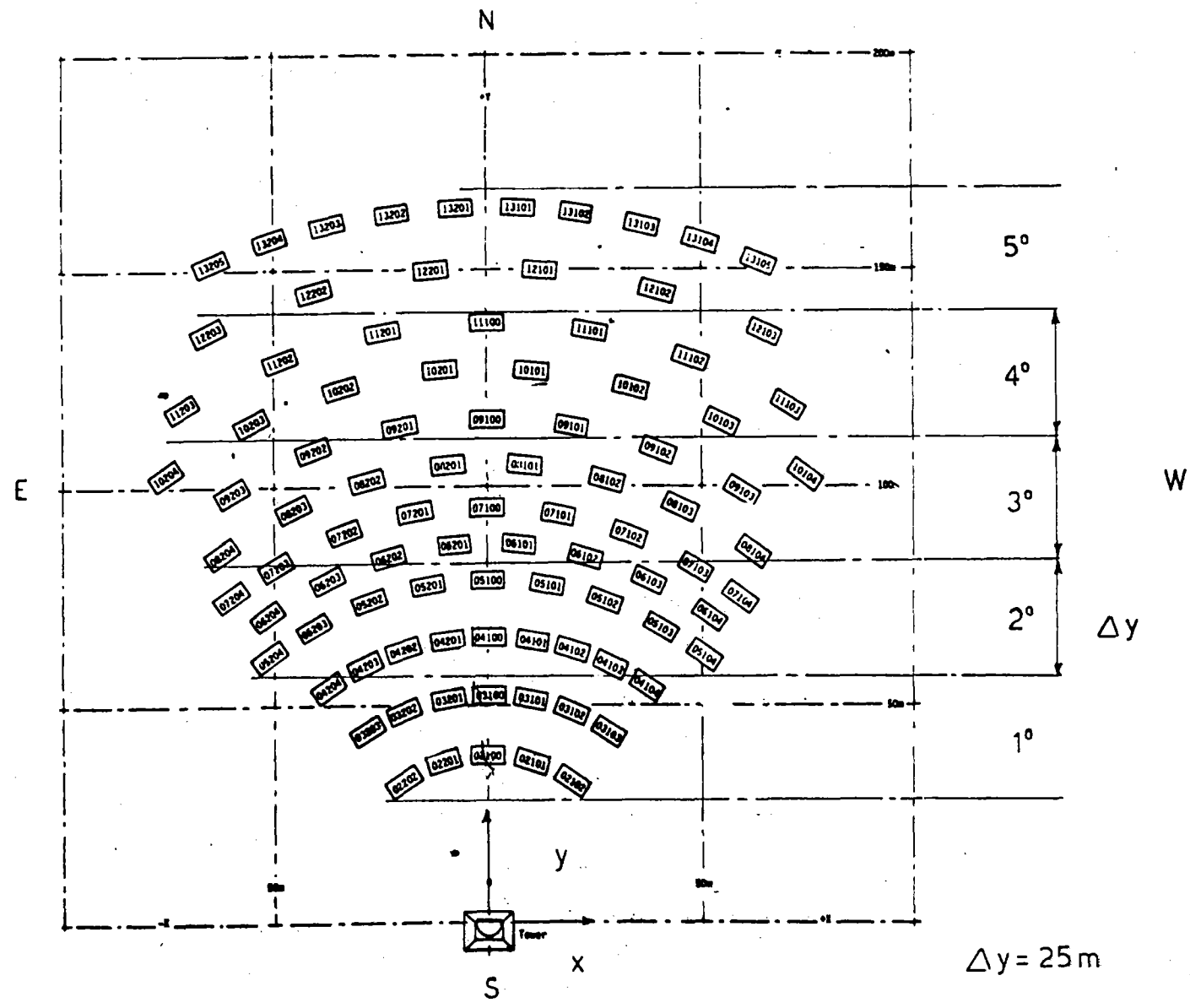

FIG. 2.1 - FIELD SUBDIVISION FOR CLOUD PASSAGE SIMULATION

1979 - 1990								
	N	NE	E	SE	S	SW	W	NW
APR	*	*	*	*	*	*	*	*
MAY	0%	40%	20%	0%	0%	0%	40%	0%
JUN	0%	14%	60%	4%	0%	18%	4%	0%
JUL	0%	0%	70%	5%	0%	10%	15%	0%
AUG	0%	10%	67%	0%	0%	10%	14%	0%
SEP	0%	11%	61%	0%	0%	11%	14%	4%
OCT	0%	13%	23%	0%	0%	30%	27%	7%
NOV	0%	7%	35%	0%	0%	24%	24%	10%
DEC	8%	8%	19%	4%	4%	15%	39%	4%
JAN	0%	11%	21%	4%	0%	25%	36%	4%
FEB	4%	28%	22%	0%	0%	20%	18%	4%
MAR	8%	8%	22%	0%	0%	22%	44%	0%
79-80	2%	11%	39%	2%	0%	10%	24%	4%

TOTAL DATA : 260 * NO DATA

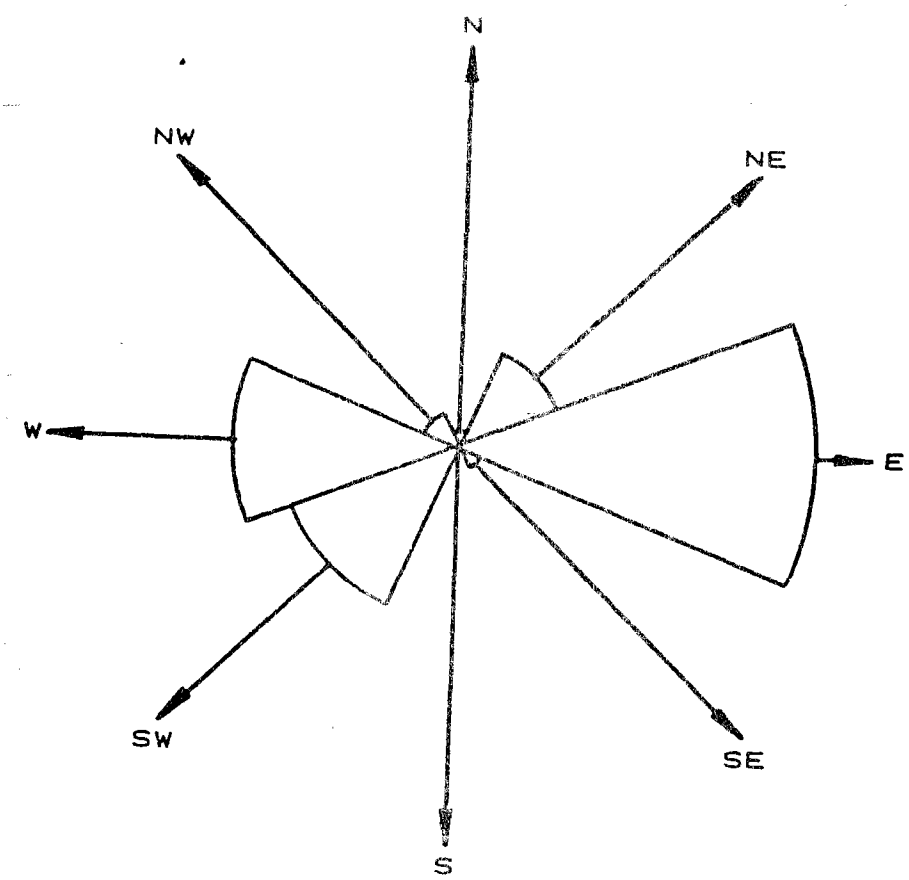

FIG. 2.2

BELGO BN NUCLEAIRE

SSPS - TABERNAS METEO DATA

MAIN WIND DIRECTION DURING DAYLIGHT PER MONTH

FOR THE YEAR 1979-1990

DFVLR

FIG. P.13

ALMERIA, 93 HELIOSTAT FIELD

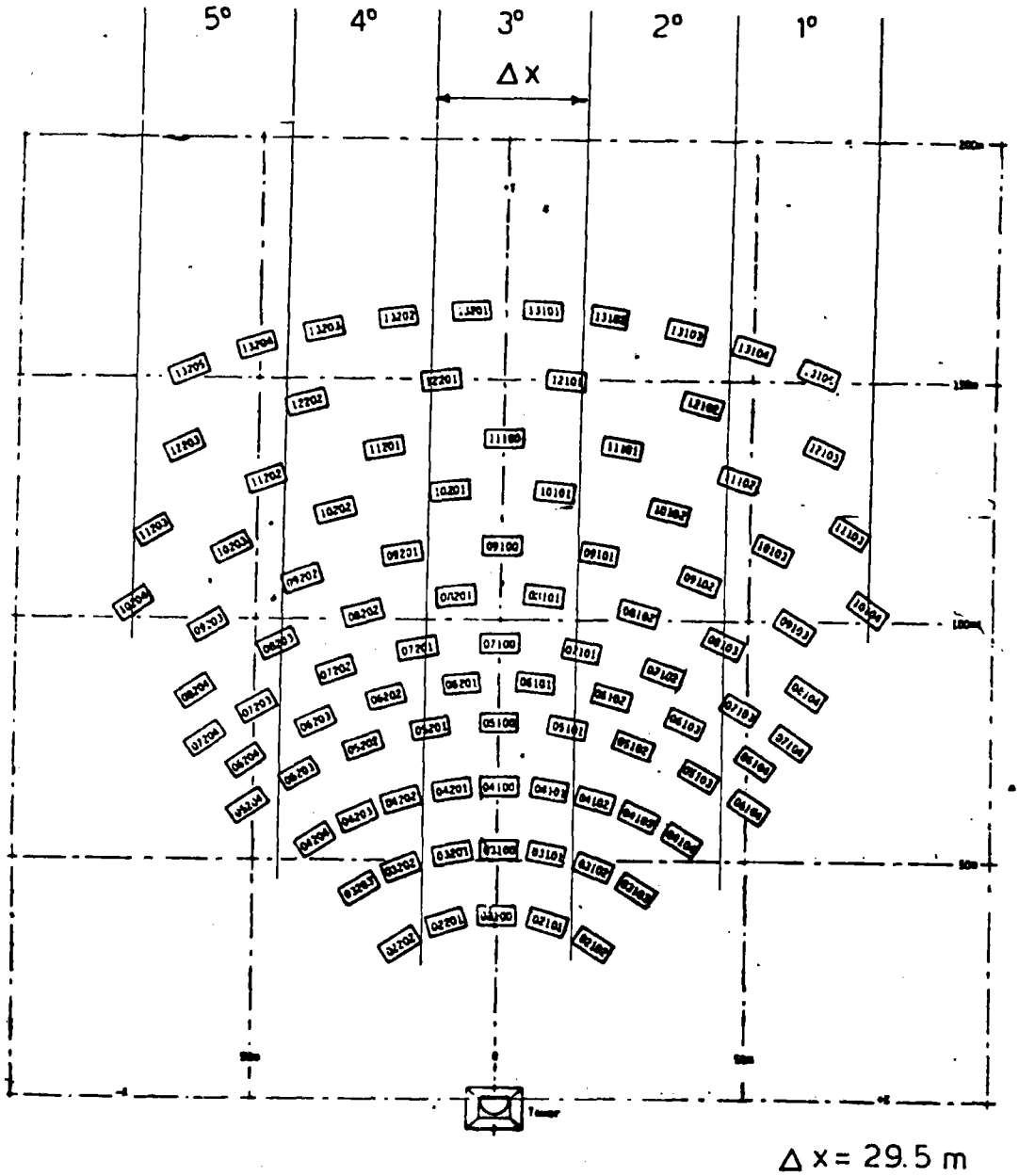

FIG.2.3-FIELD SUBDIVISION FOR E-W CLOUD PASSAGE

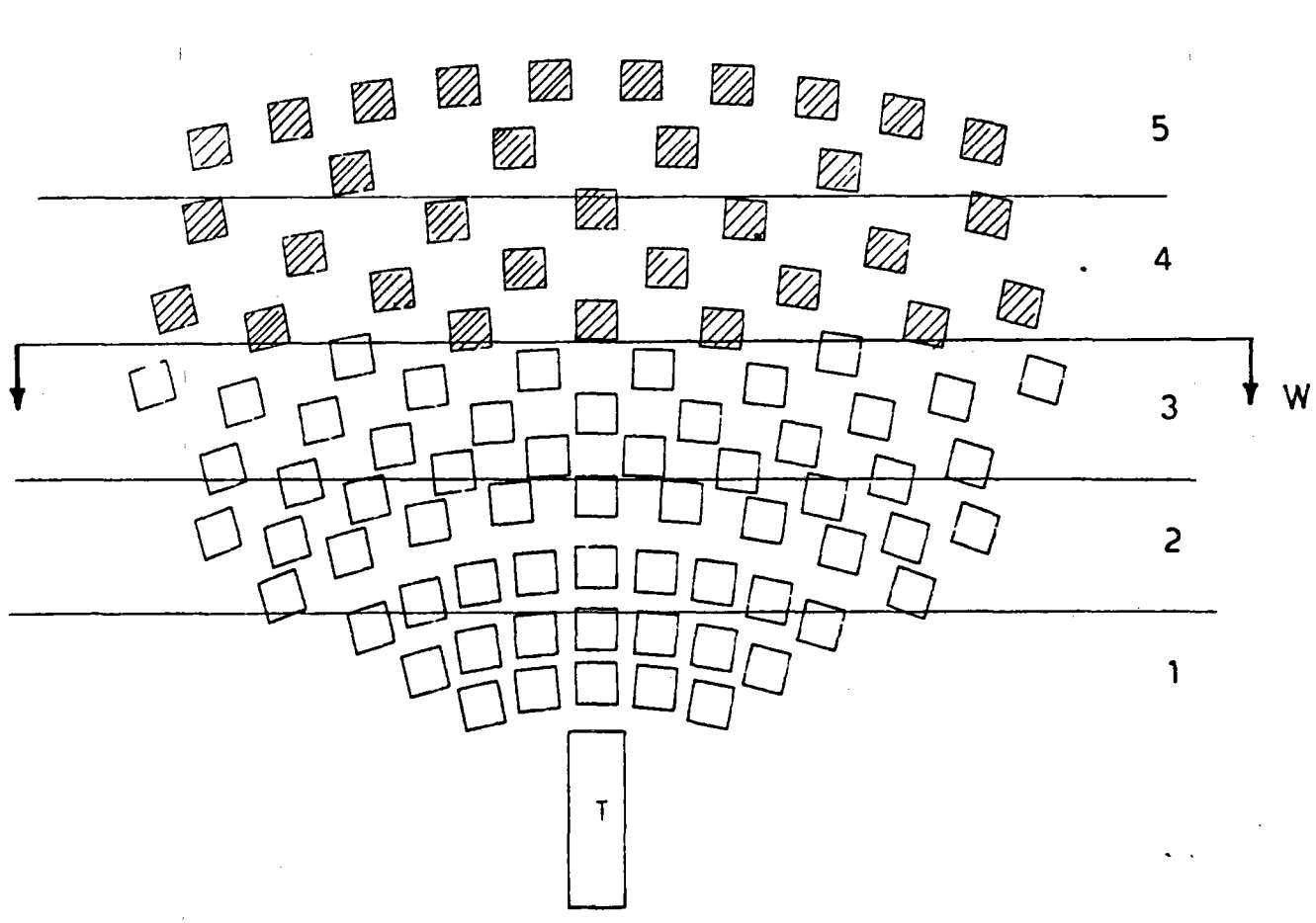

FIG.2.4 - MIRROR FIELD AS VIEW FROM SUN

ASR-ALMERIA 3.1 MAD 21/3 NOON

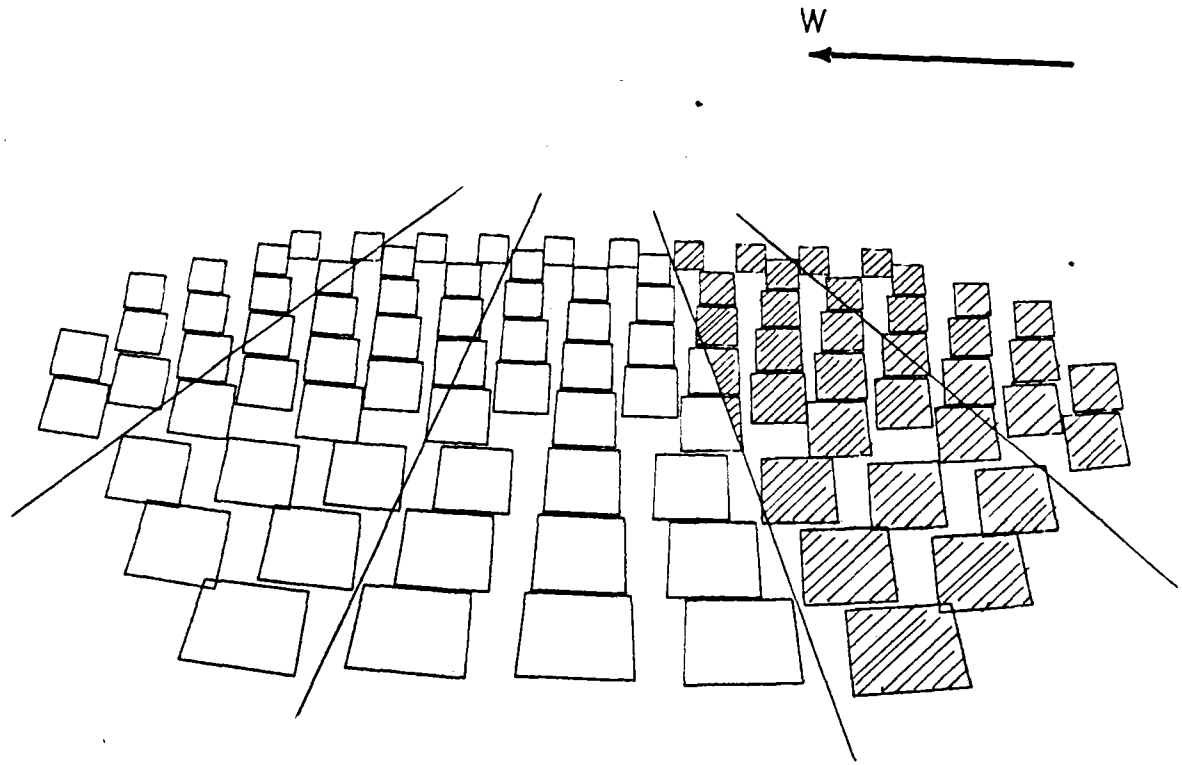

FIG.2.5 - MIRROR FIELD AS VIEW FROM TOWER

ALMERIA-ASR N-S (S-N) CLOUD PASSAGE SIMULATION

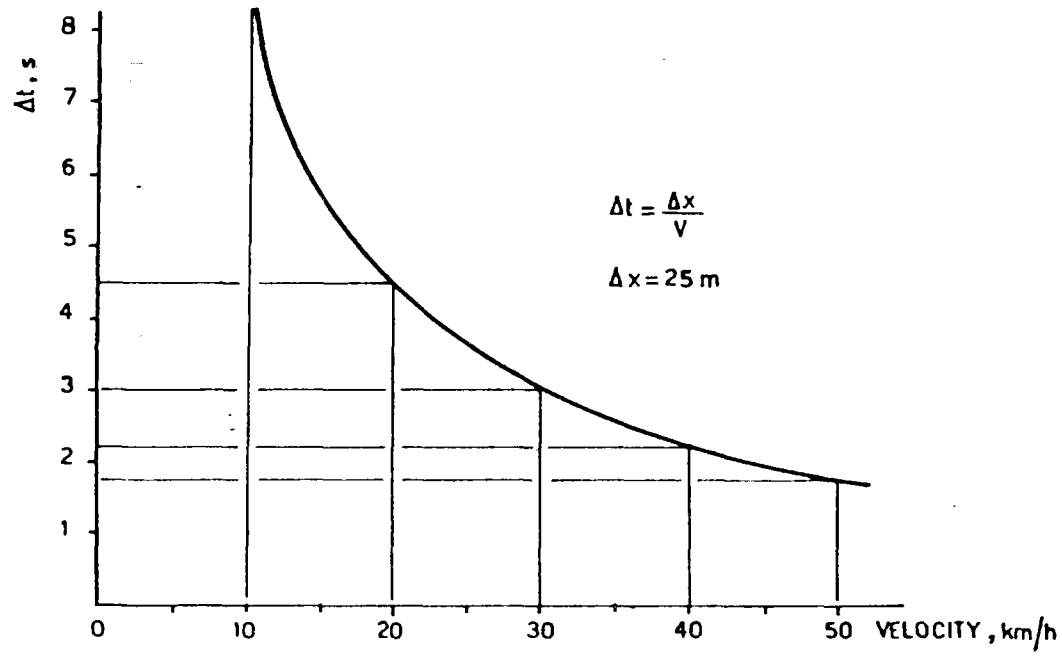

FIG. 2.6 - TIME STEP VS CLOUD VELOCITY

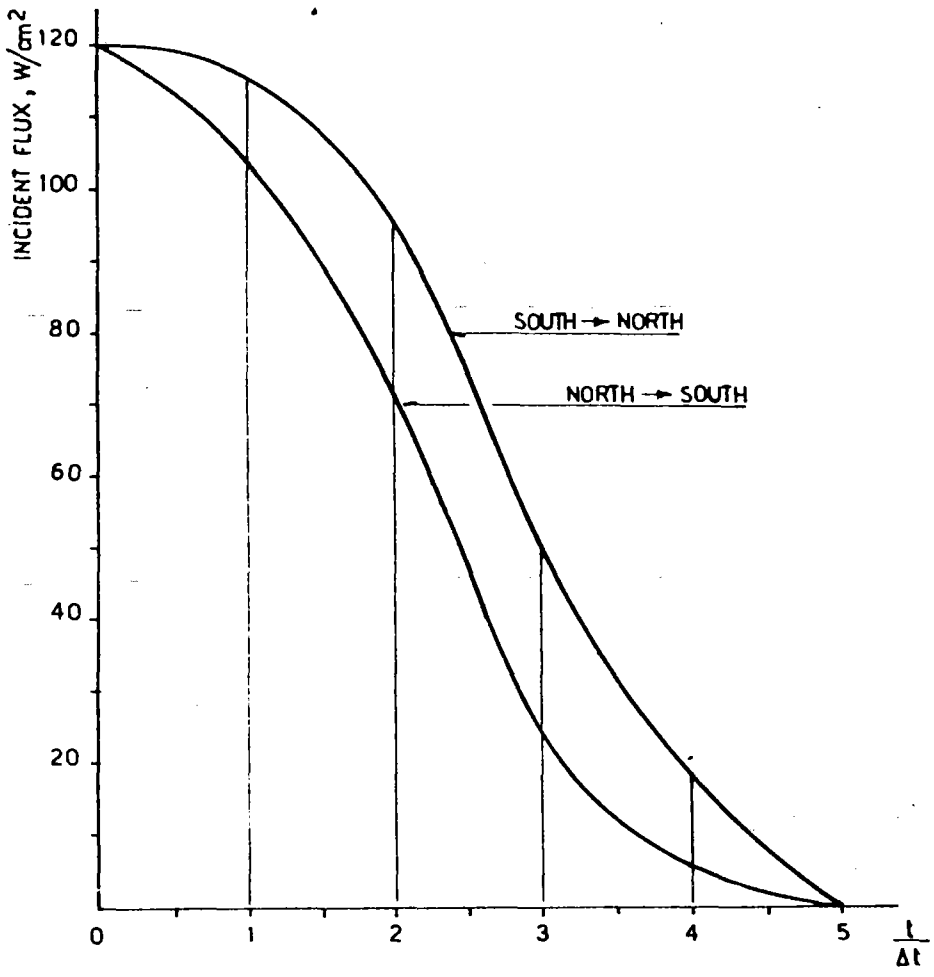

FIG. 2.7 - INCIDENT FLUX ON TARGET CENTER VS TIME

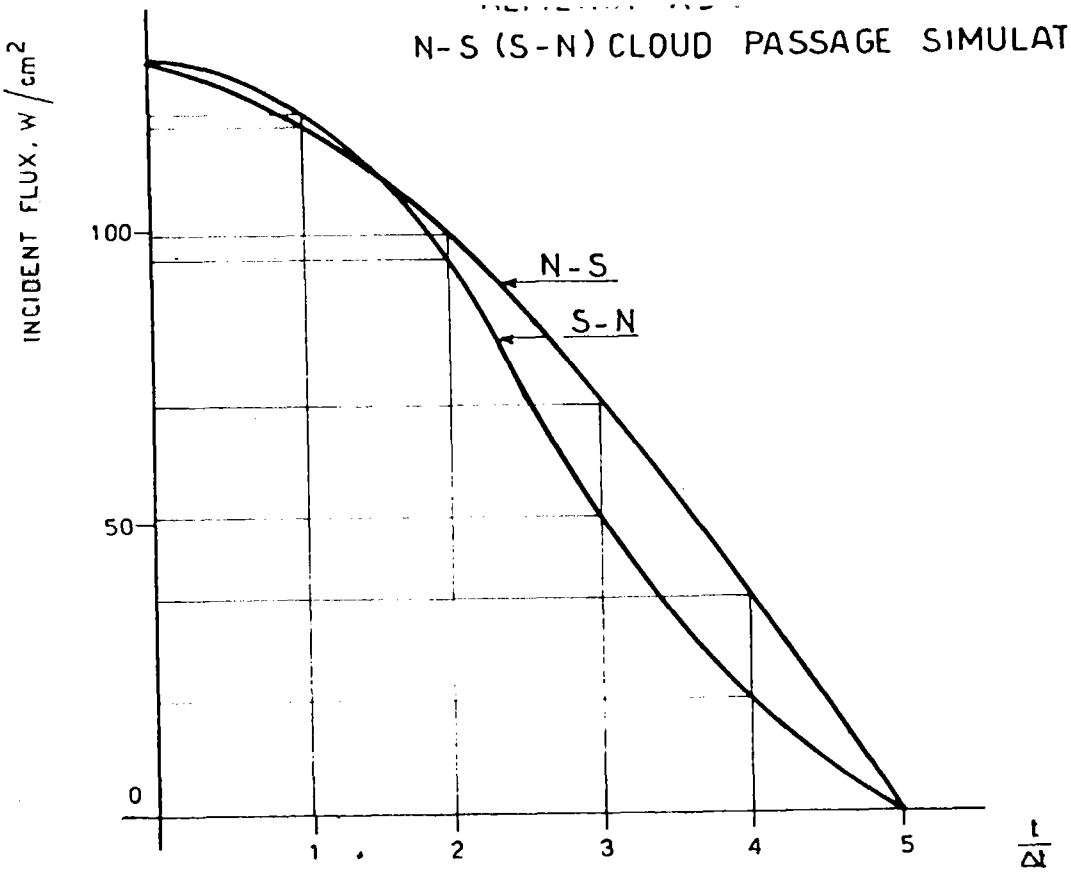

FIG. 2.8 - PEAK INCIDENT FLUX BEHAVIOUR VS TIME STEP

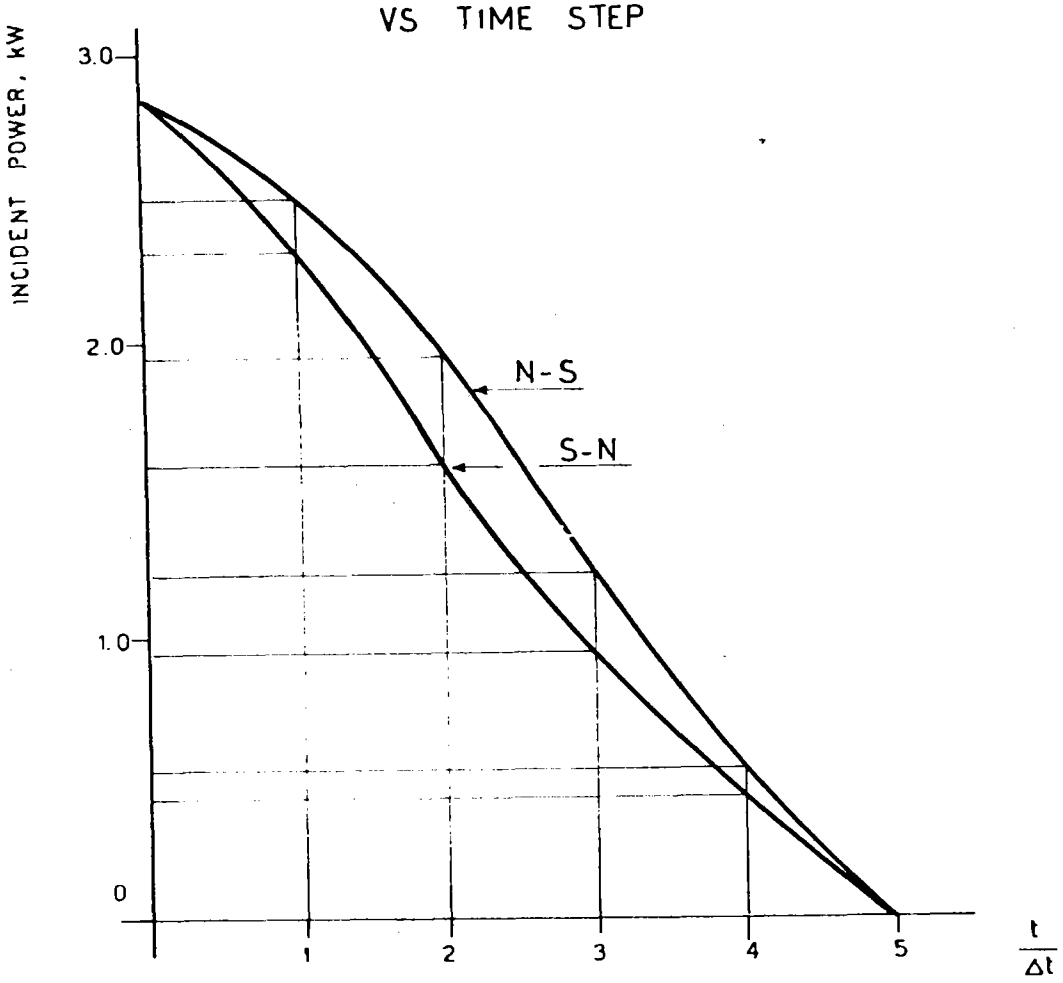

FIG. 2.9 - INCIDENT POWER VS TIME STEP

ALMERIA - A S R NORTH - SOUTH CLOUD PASSAGE SIMULATION

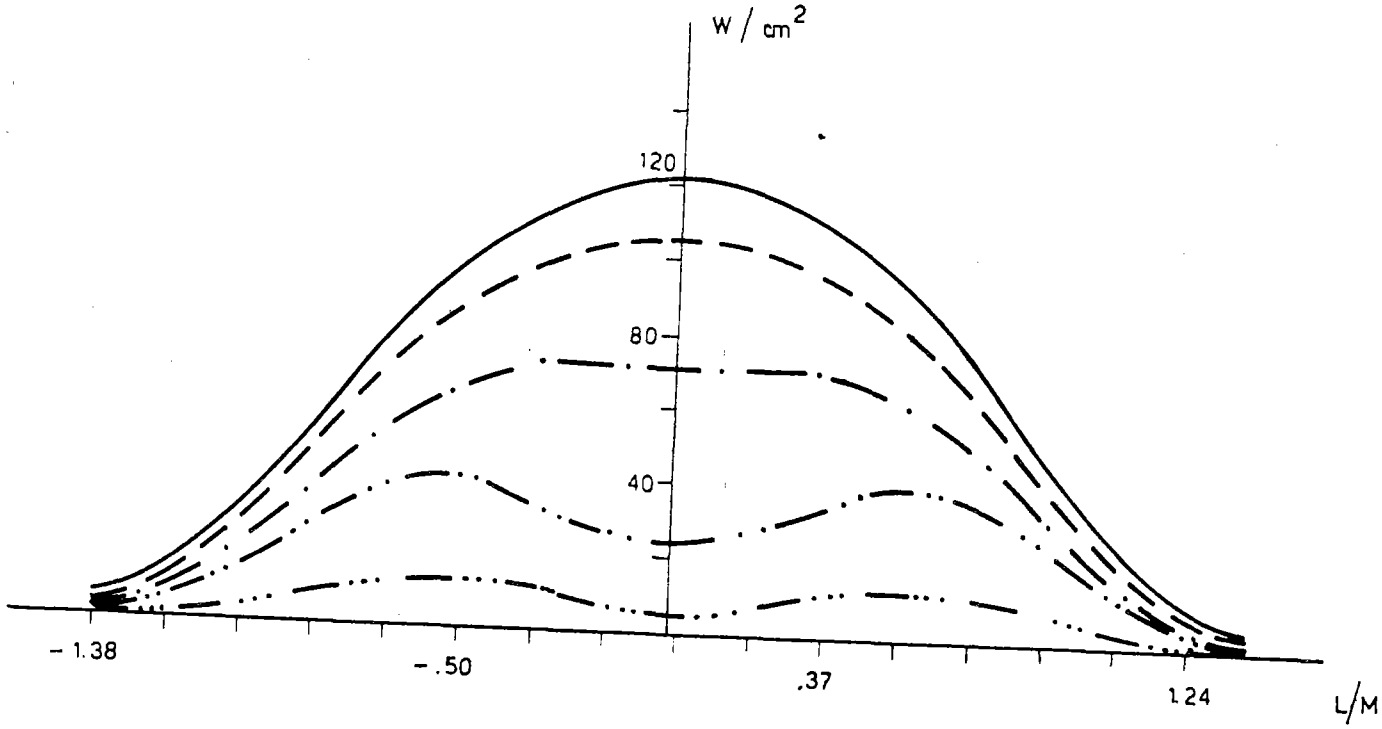

FIG. 2.10 - SOLAR FLUX ON TARGET SEC XX

ALMERIA - A S R SOUTH - NORTH CLOUD PASSAGE SIMULATION

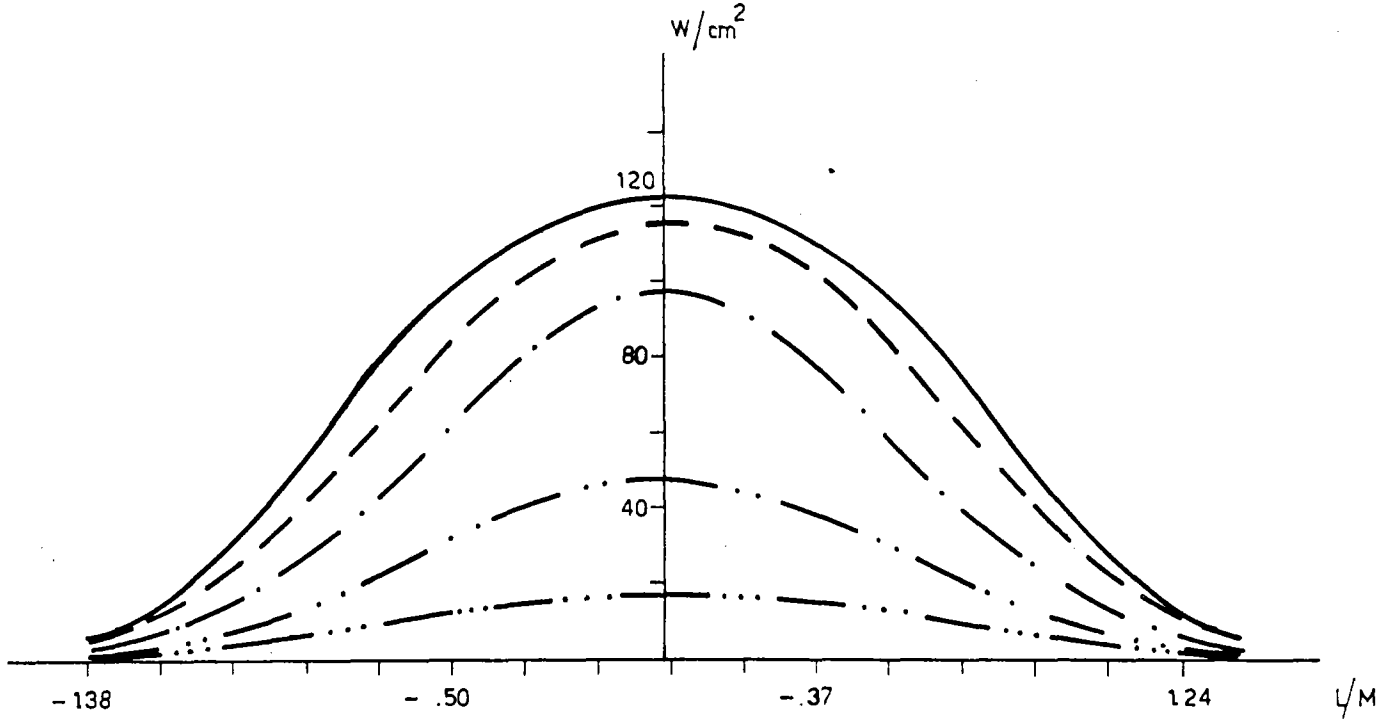

FIG. 2.11 - SOLAR FLUX ON TARGET SEC XX

ALMERIA-ARS NORTH-SOUTH CLOUD PASSAGE SIMULATION

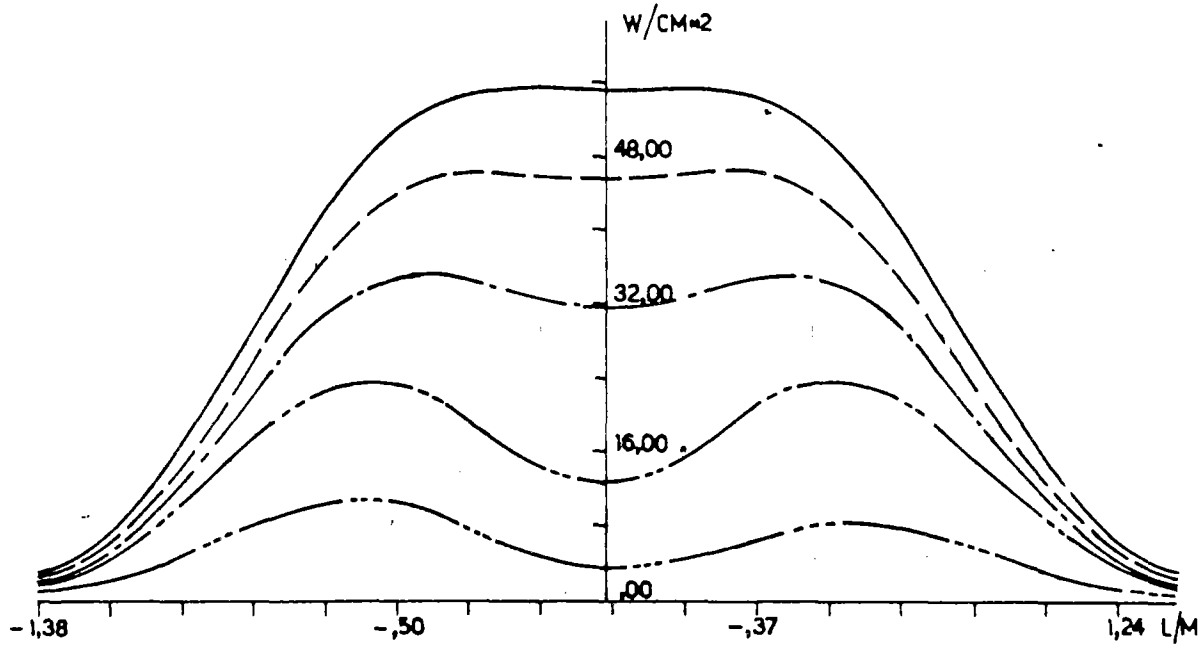

FIG.2.12-AVERAGE SOLAR FLUX ON VERTICAL STRIP (NOON)

ALMERIA-ASR SOUTH-NORTH CLOUD PASSAGE SIMULATION

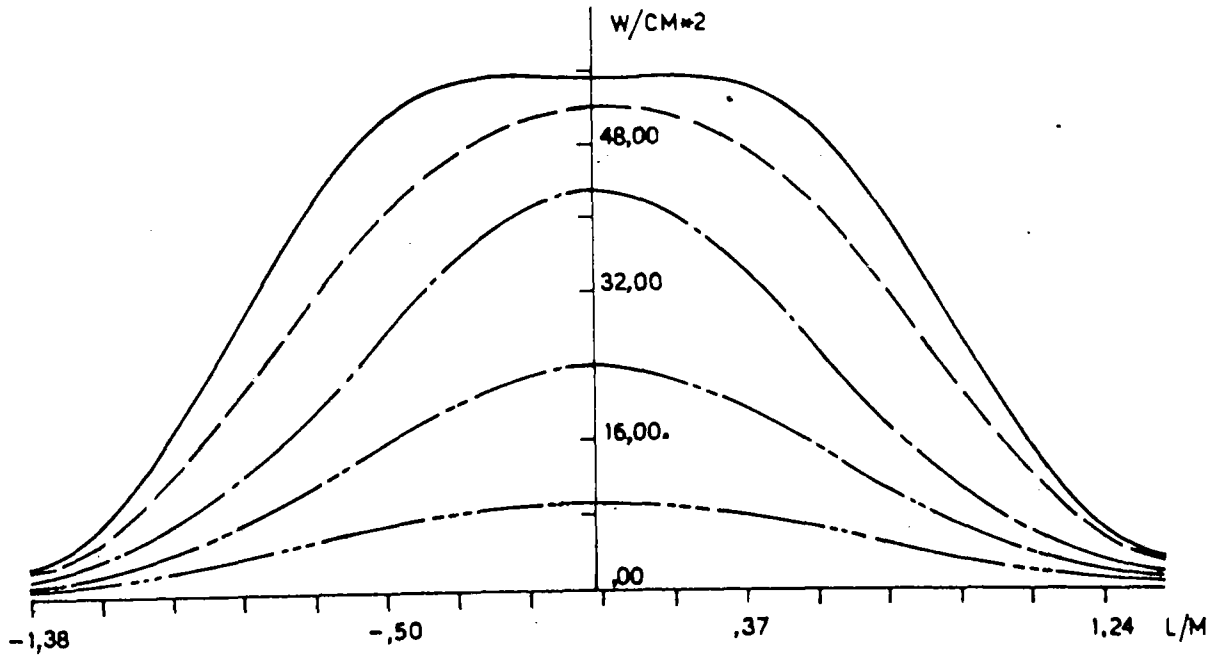

FIG.213-AVERAGE SOLAR FLUX ON VERTICAL STRIP (NOON)

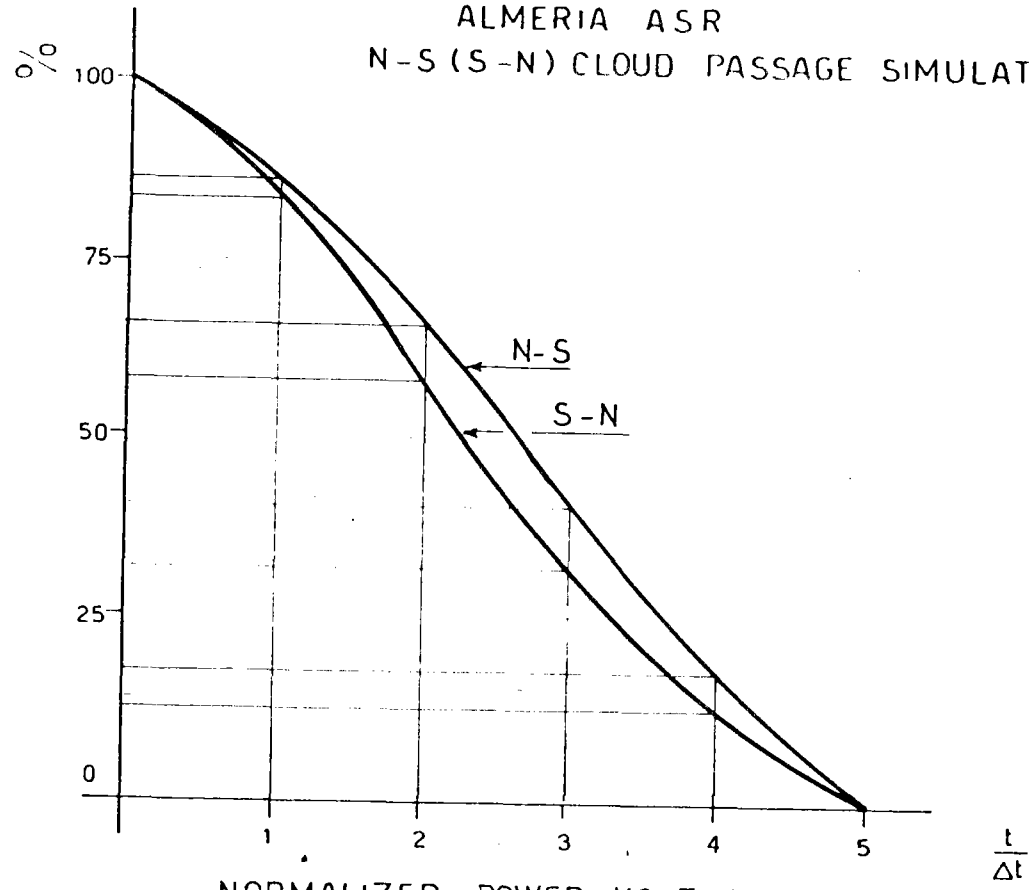

NORMALIZED POWER VS TIME STEP

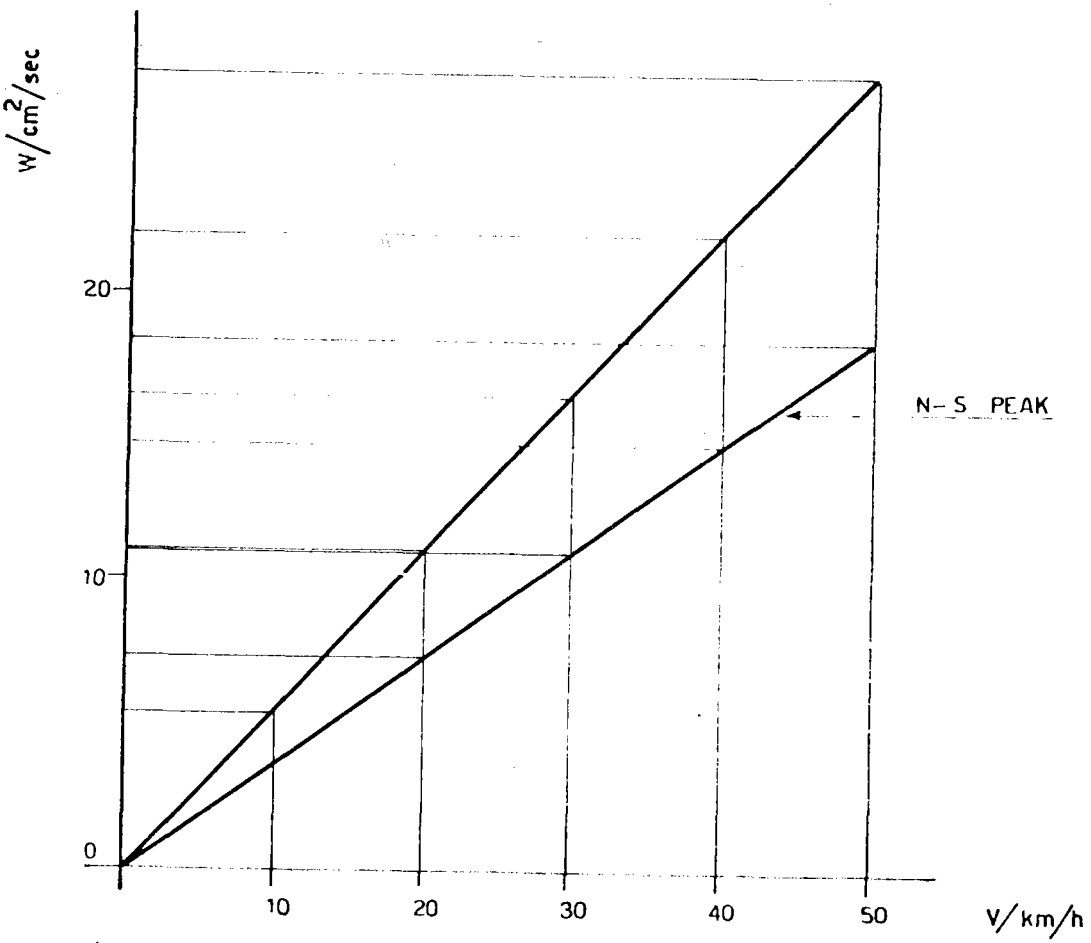

MAX TIME GRADIENT VS WIND VELOCITY

FIG. 2.14

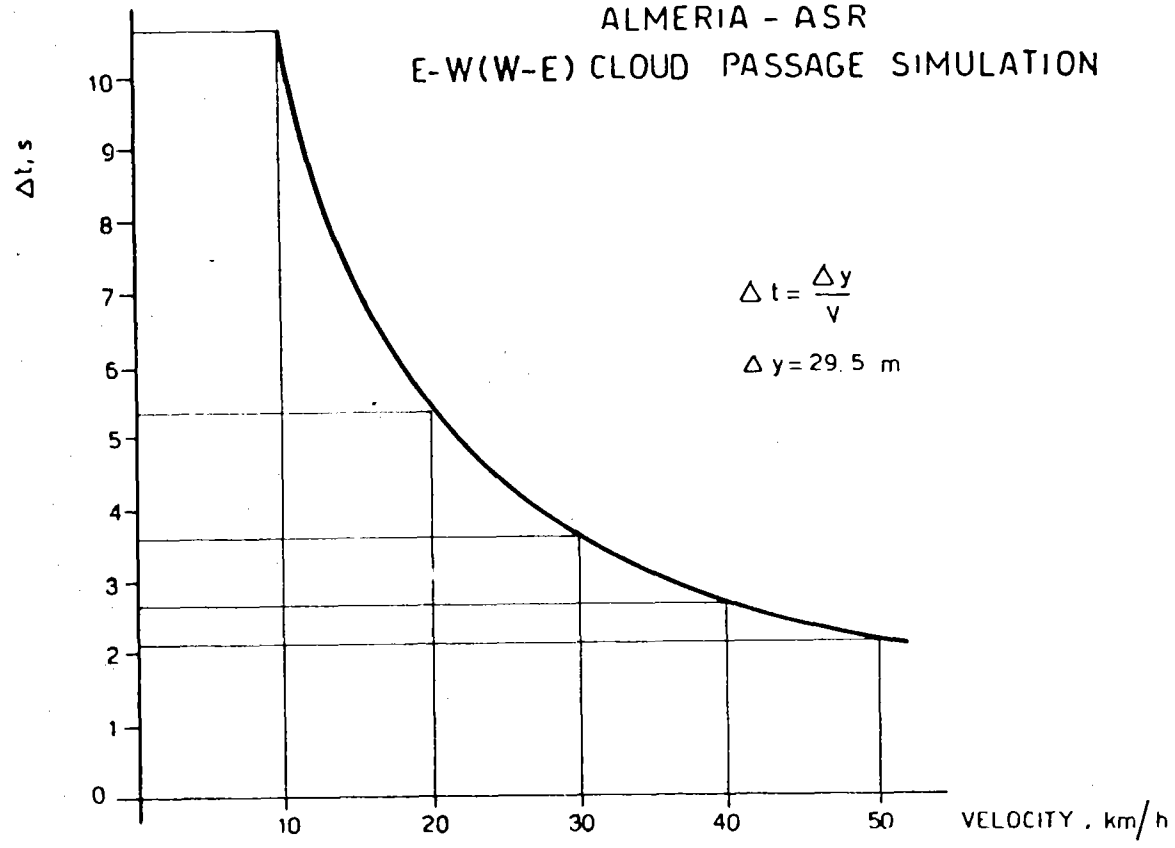

FIG. 2.15 - TIME STEP VS CLOUD VELOCITY

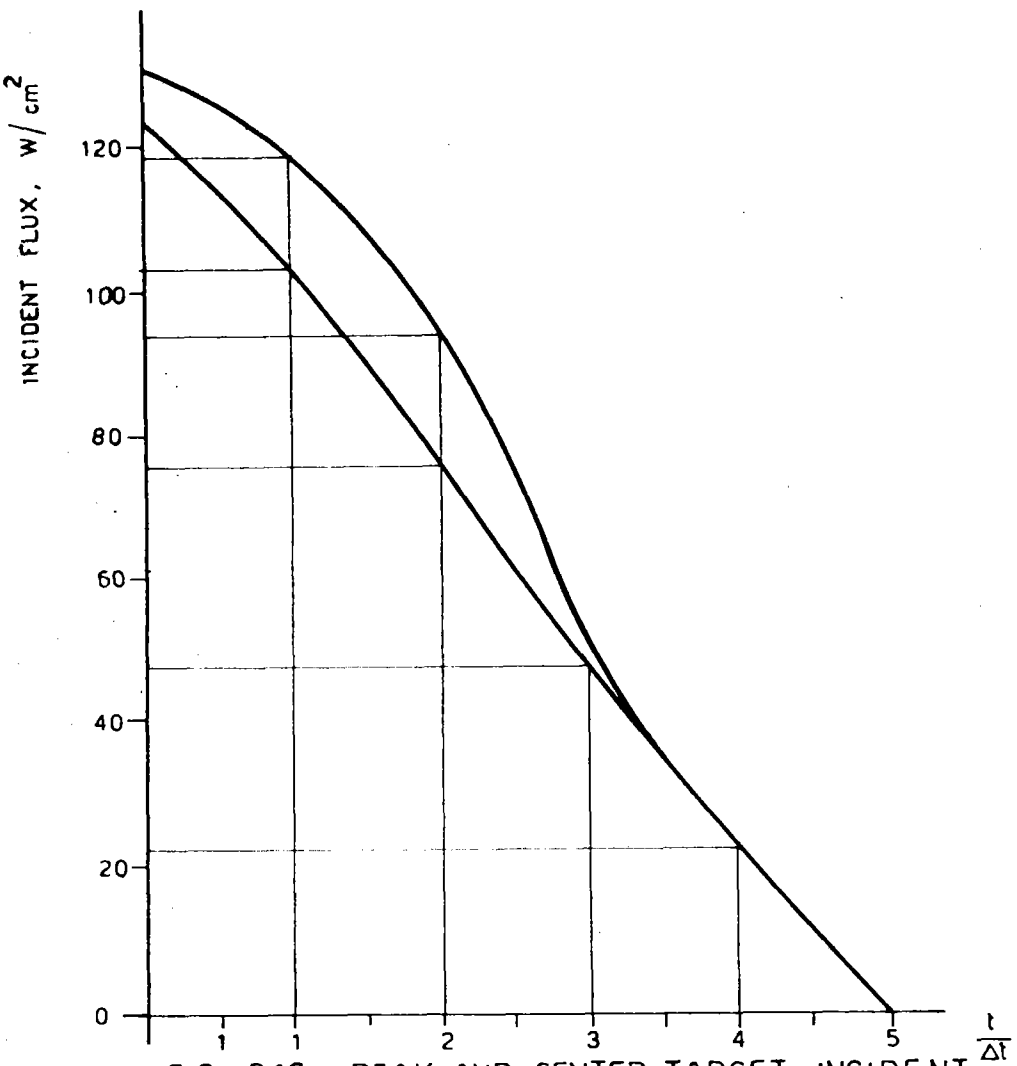

FIG. 2.16 - PEAK AND CENTER TARGET INCIDENT FLUX VS TIME STEP (NOON)

SNAMPROGETTI

ALMERIA - ASR

E - W (W - E) CLOUD PASSAGE SIMULATION

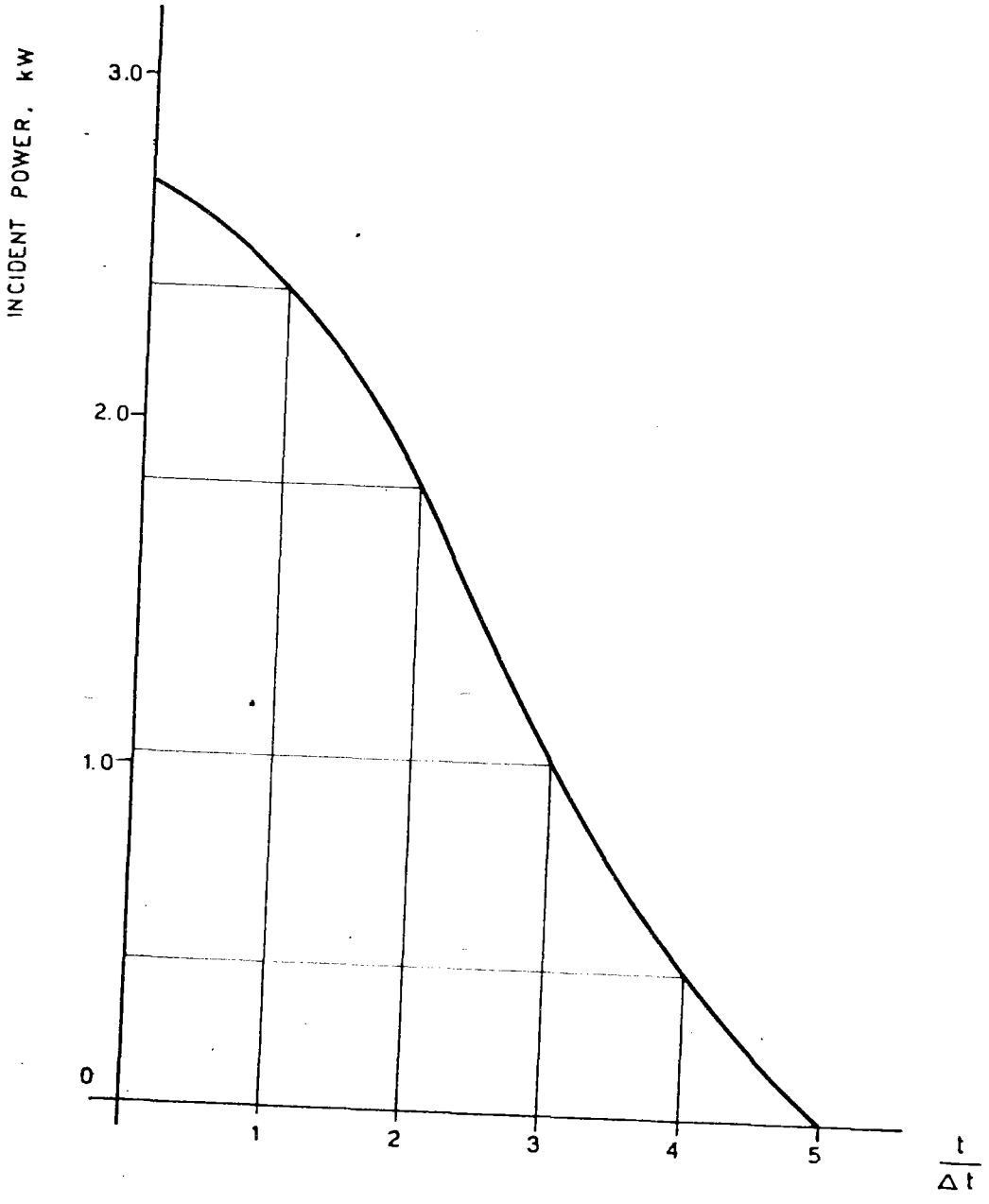

FIG. 2.17 - INCIDENT POWER VS TIME STEP (NOON)

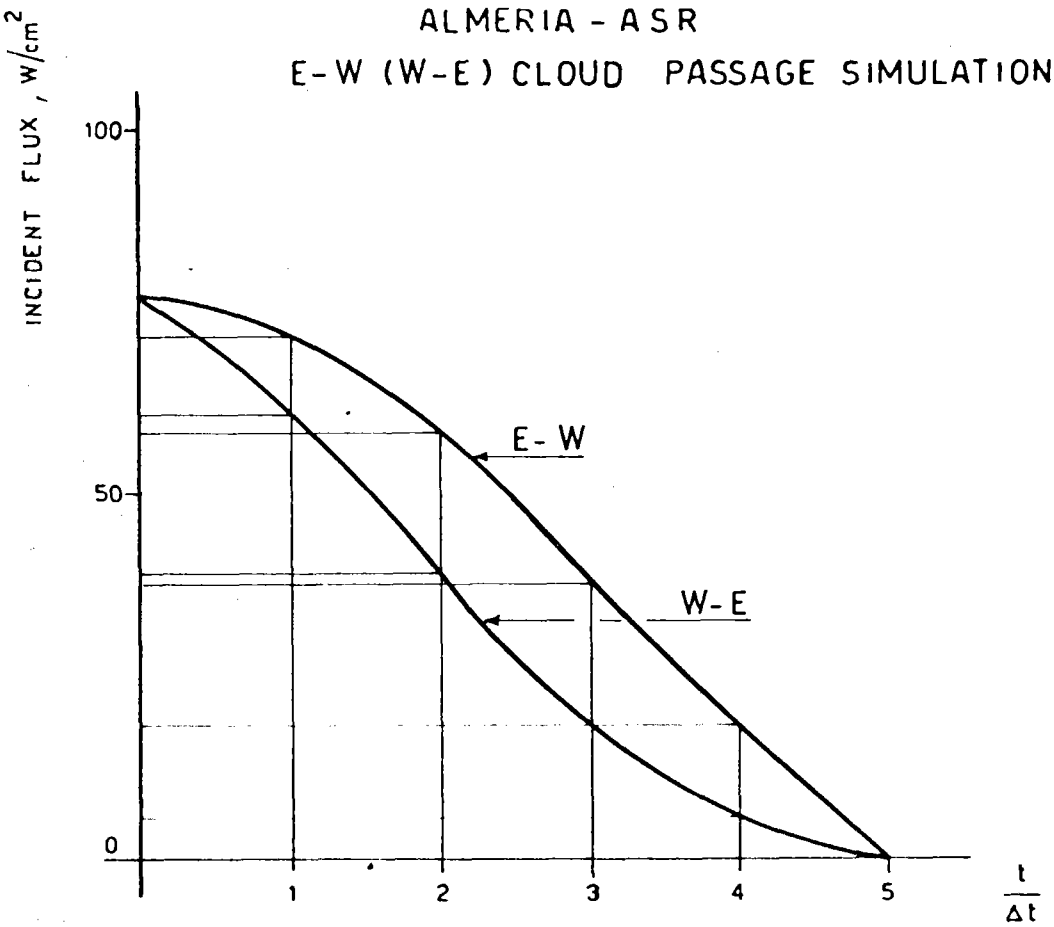

FIG. 2.18 - PEAK INCIDENT FLUX BENAVIOUR VS TIME STEP (9.30 AM)

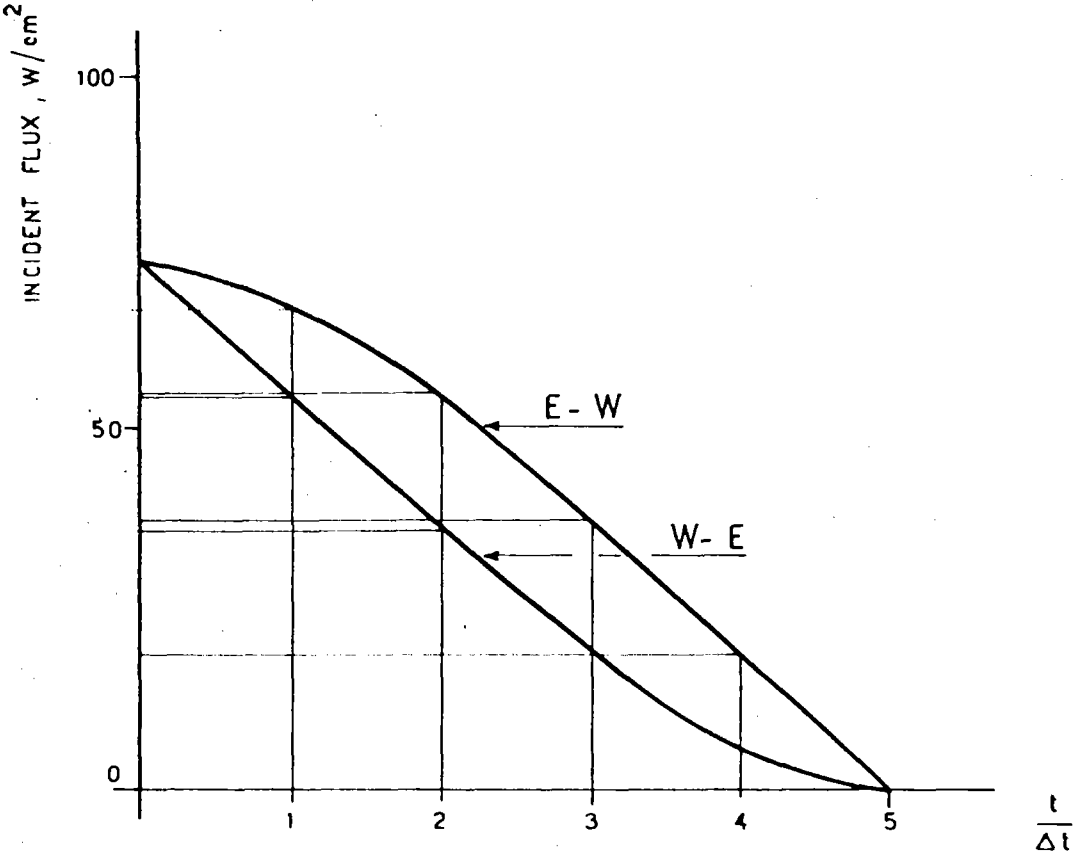

FIG. 2.19 - CENTER TARGET FLUX BENAVIOUR VS TIME STEP (9.30 AM)

ALMERIA - A S R

E-W (W-E) CLOUD PASSAGE SIMULATION

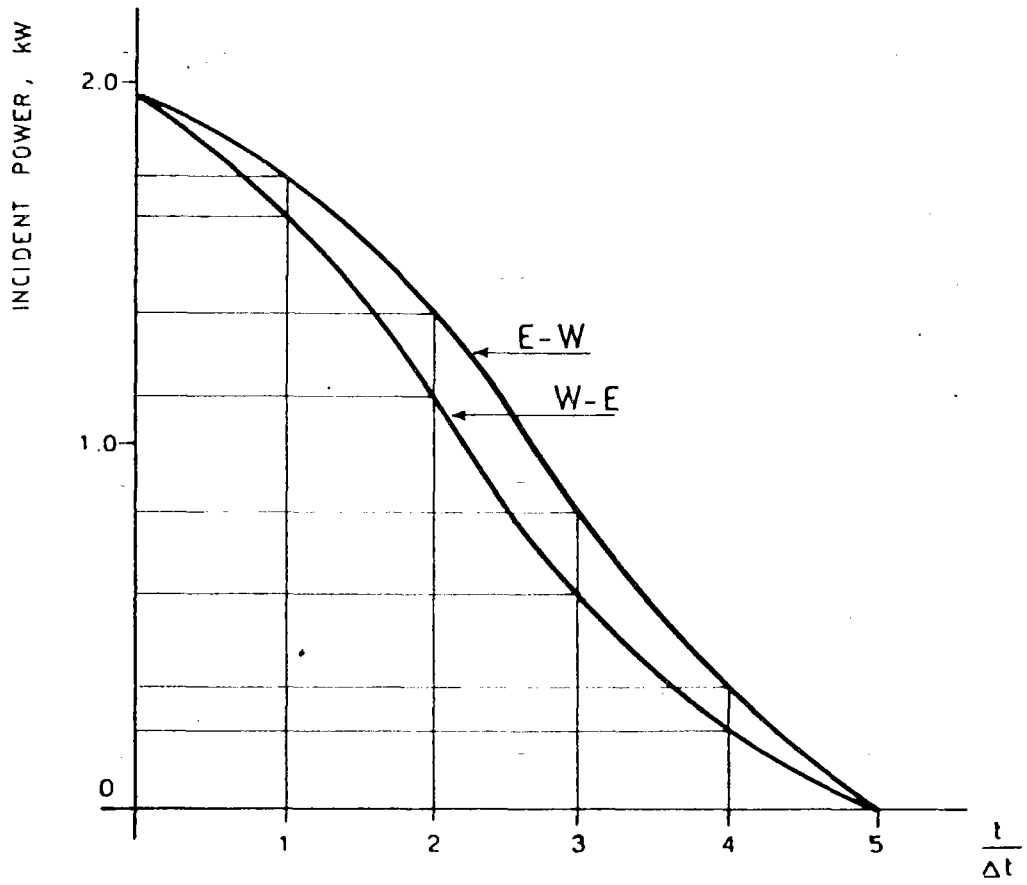

FIG. 2.20 - THERMAL POWER ON TARGET VS TIME STEP (9.30 AM)

ALMERIA - ASR E-W CLOUD PASSAGE SIMULATION

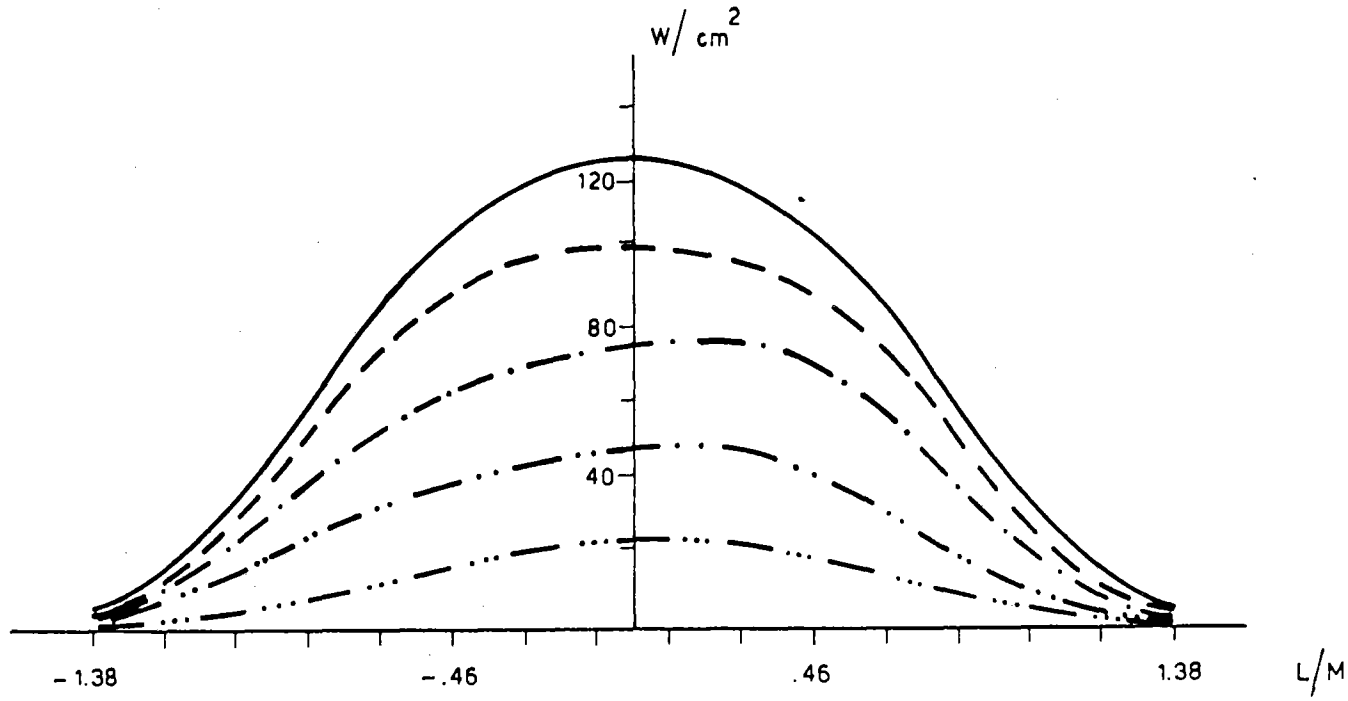

FIG. 2.21 - SOLAR FLUX ON TARGET SEC XX (NOON)

ALMERIA - A S R W-E CLOUD PASSAGE SIMULATION

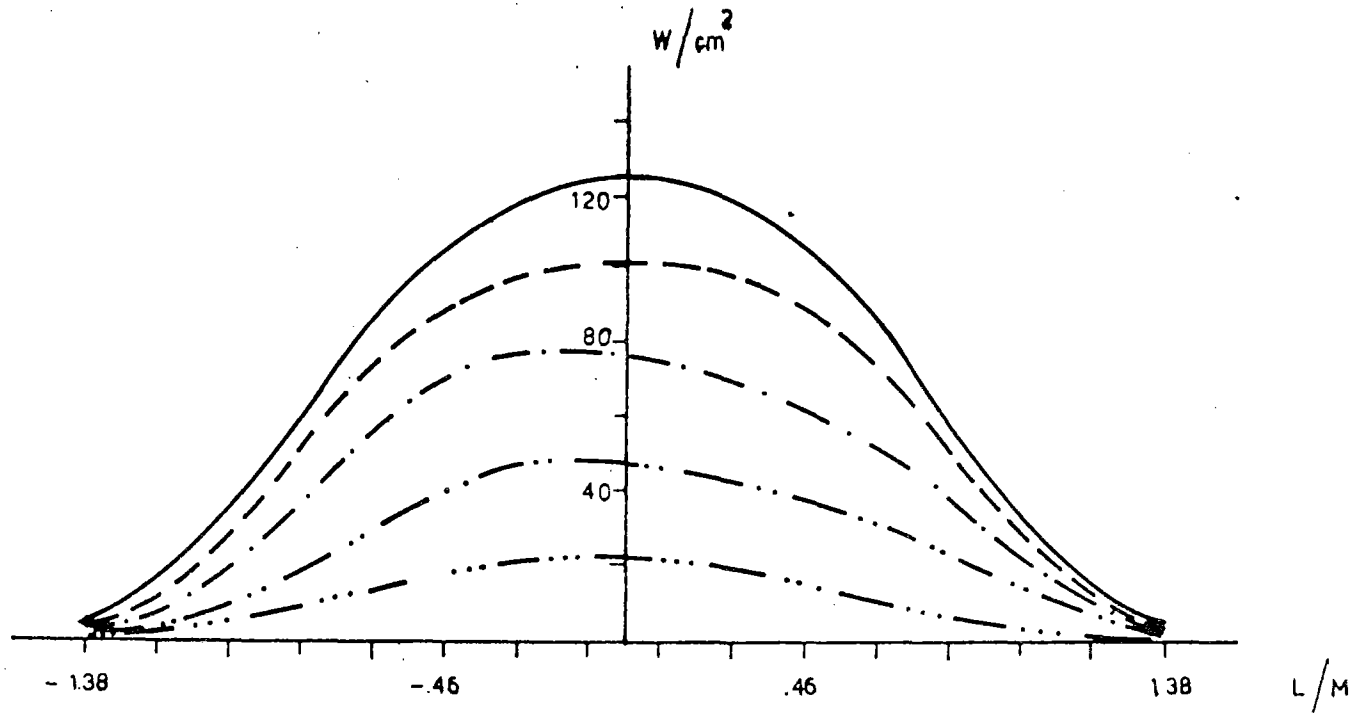

FIG. 2.22 - SOLAR FLUX ON TARGET SEC XX (NOON)

SNAMPROGETTI

ALMERIA - ASR E-W CLOUD PASSAGE SIMULATION

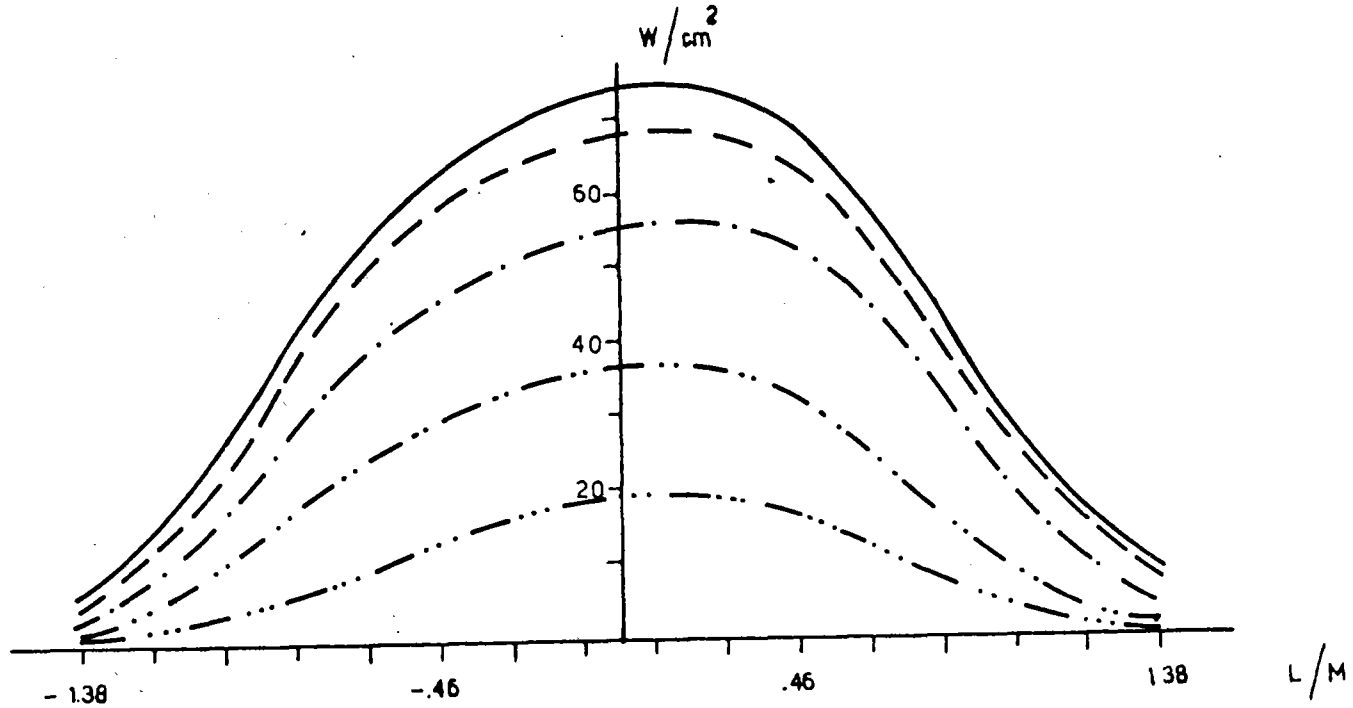

FIG.2.23 - SOLAR FLUX ON TARGET SEC XX (9.30)

ALMERIA - ASR W-E CLOUD PASSAGE SIMULATION

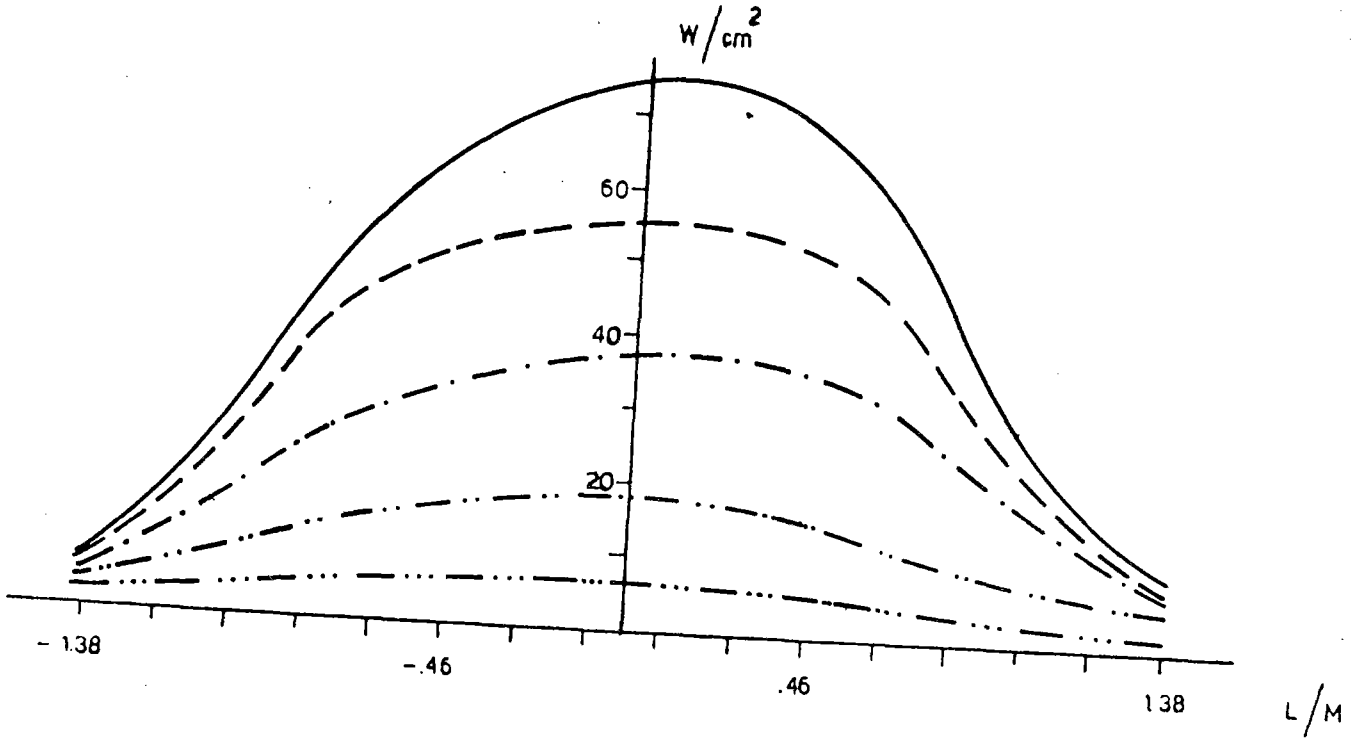

FIG. 2 24 - SOLAR FLUX ON TARGET SEC XX (9.70)

ALMERIA - AS R E-W CLOUD PASSAGE SIMULATION

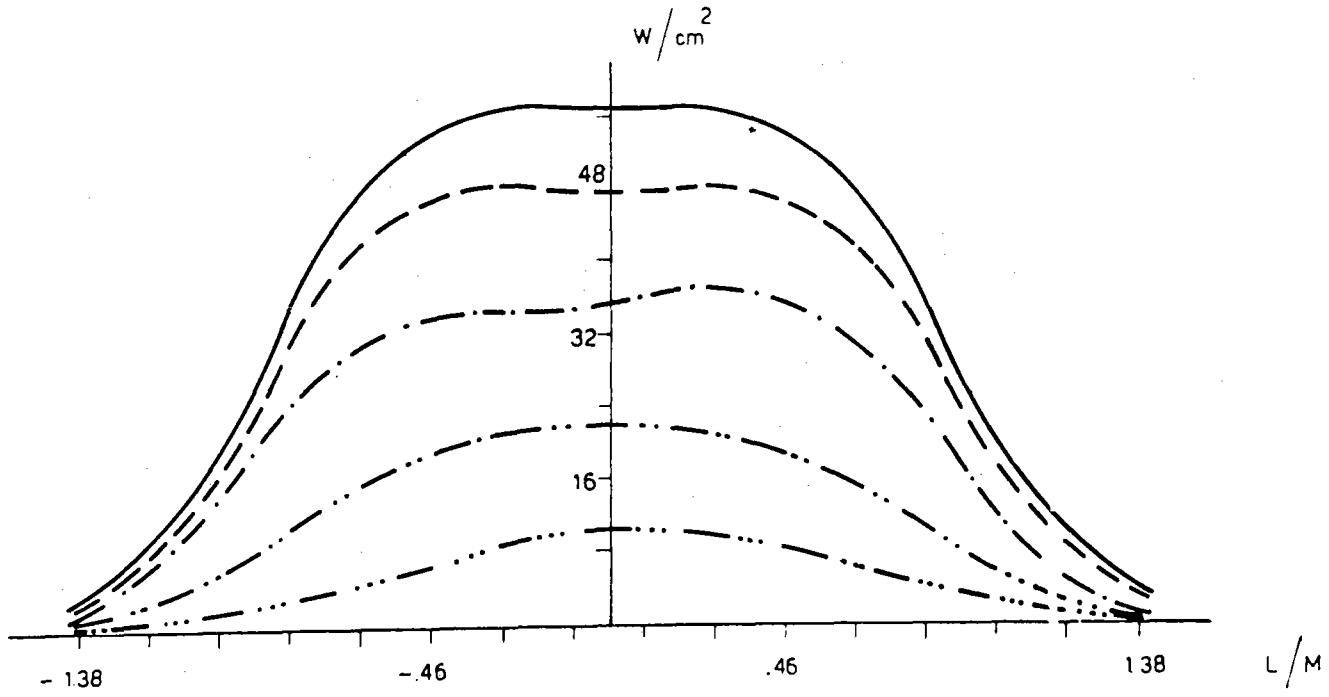

FIG. 2. 25 - AVERAGE SOLAR FLUX ON VERTICAL STRIP (NOON)

ALMERIA - AS R W-E CLOUD PASSAGE SIMULATION

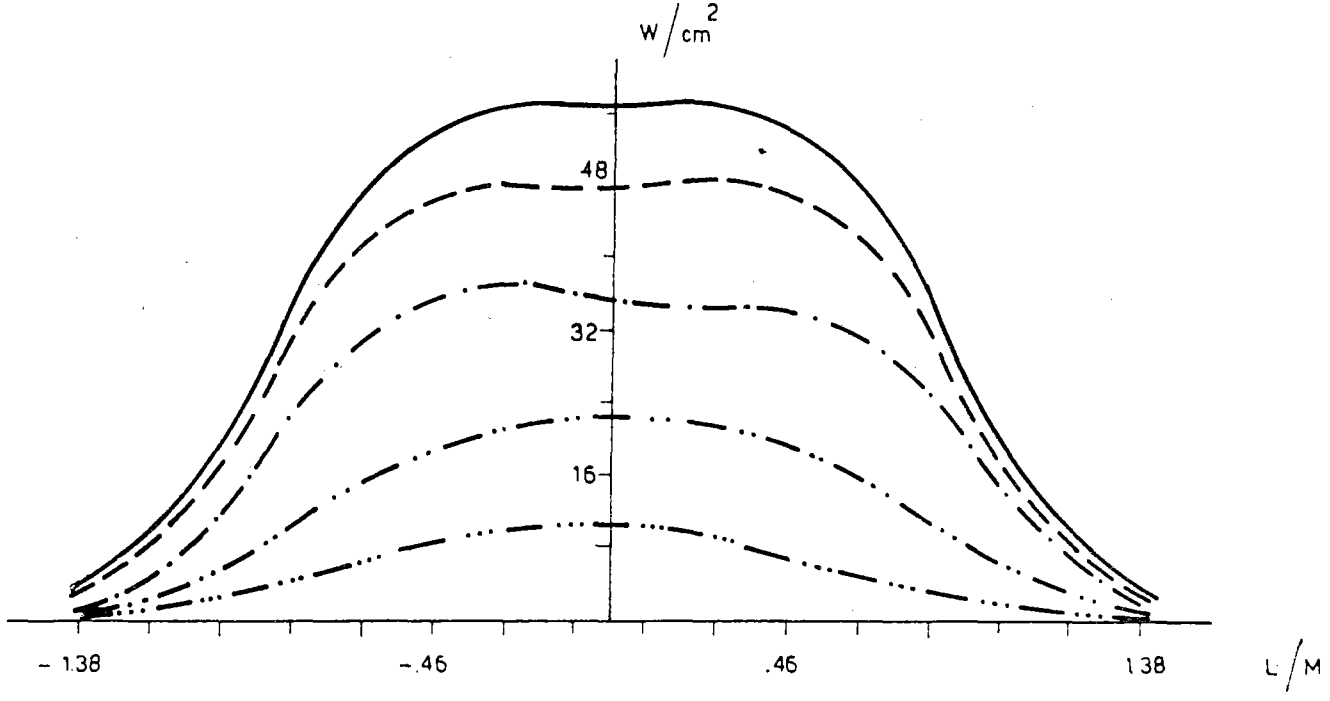

FIG. 2.26 - AVERAGE SOLAR FLUX ON VERTICAL STRIP (NOON)

SNAMPROGETTI

ALMERIA - A S R E - W CLOUD PASSAGE SIMULATION

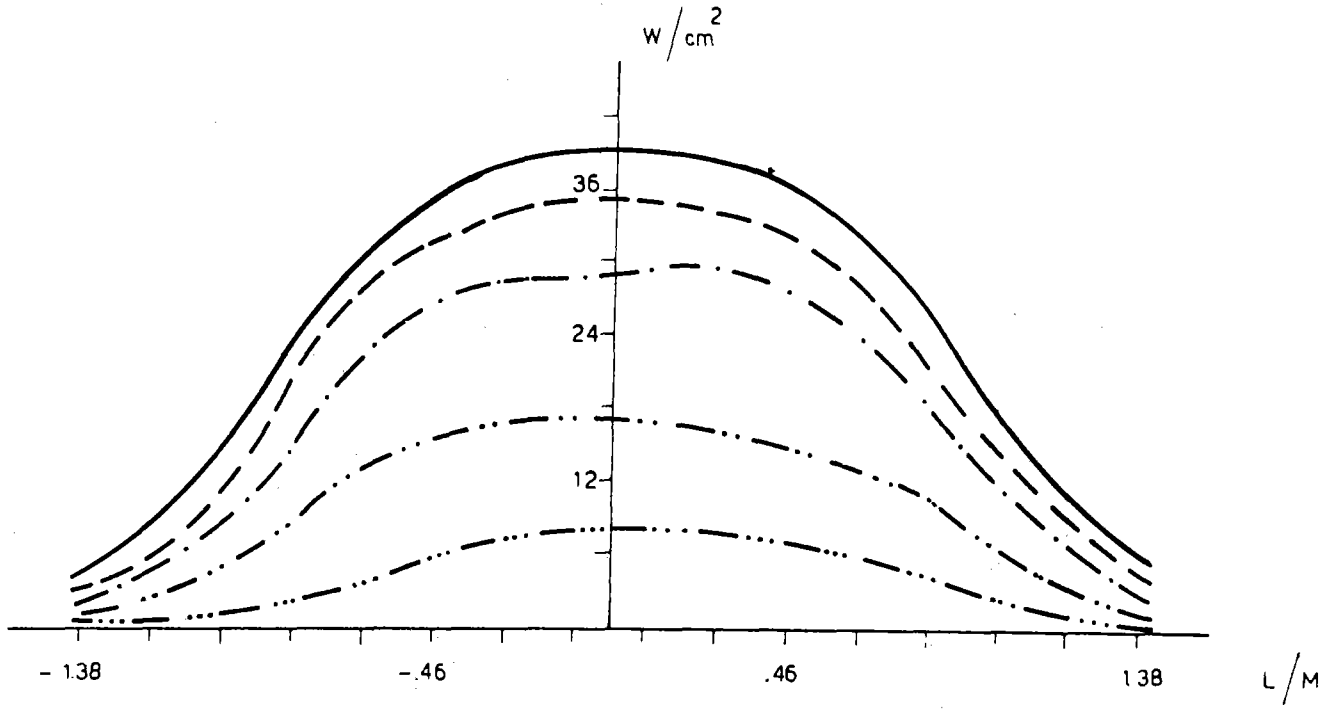

FIG. 2. 27 - AVERAGE SOLAR FLUX ON VERTICAL STRIP (9.30)

ALMERIA - AS R W-E CLOUD PASSAGE SIMULATION

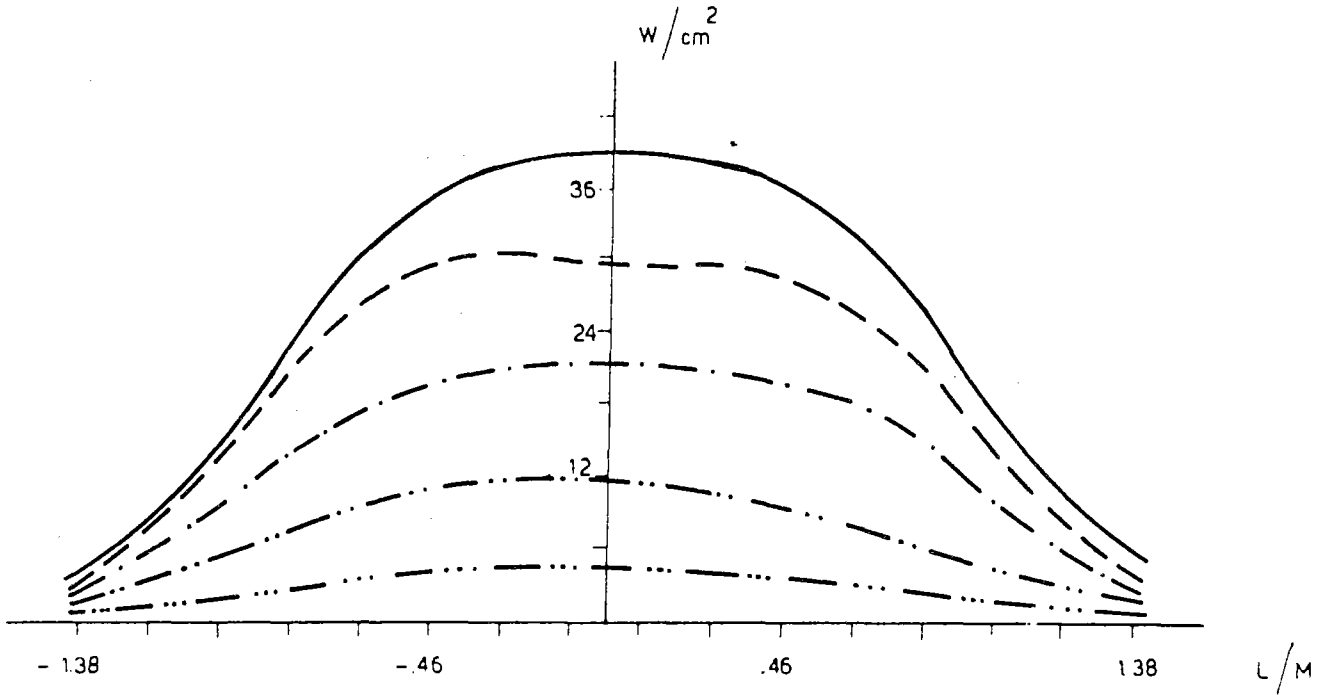

FIG. 2.28 - AVERAGE SOLAR FLUX ON VERTICAL STRIP (9.30)

SNAMPROGETTI

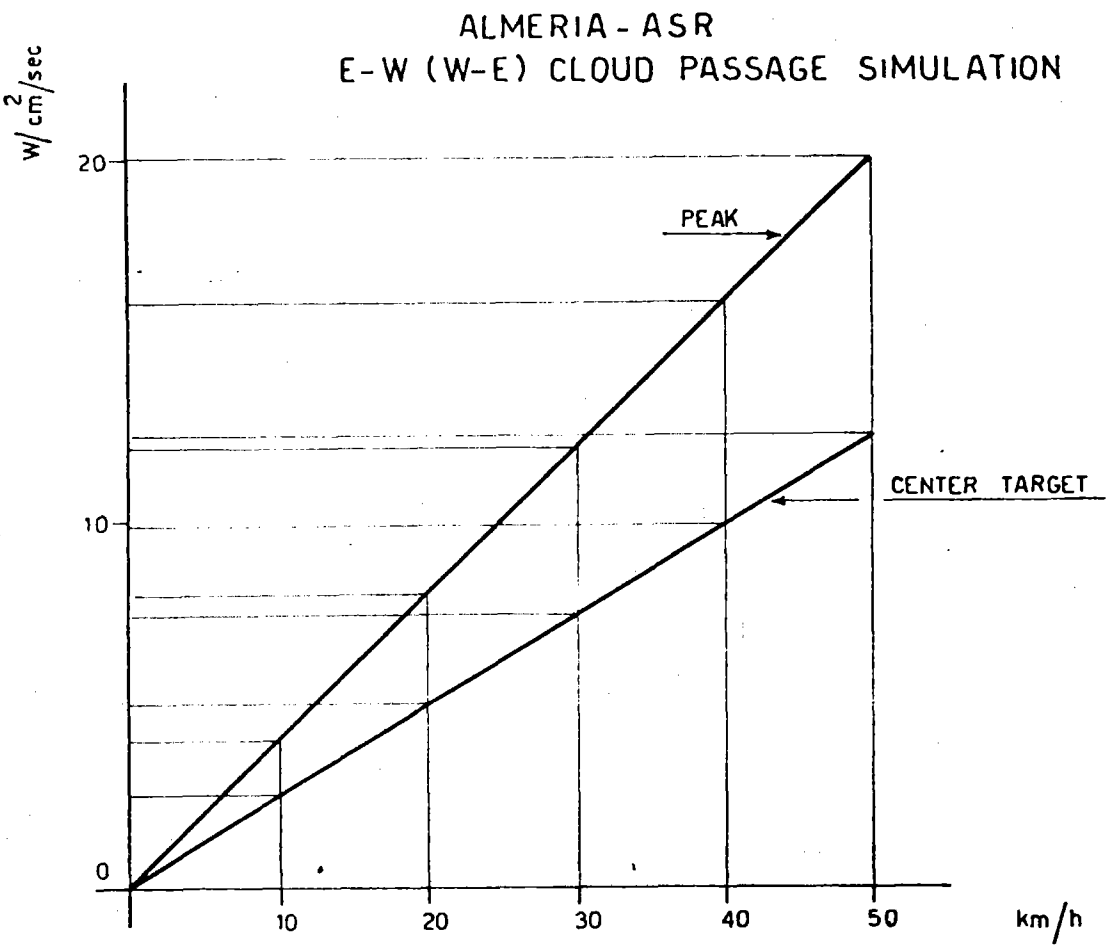

FIG. 2.29 - MAX FLUX TIME GRADIENT VS WIND VELOCITY

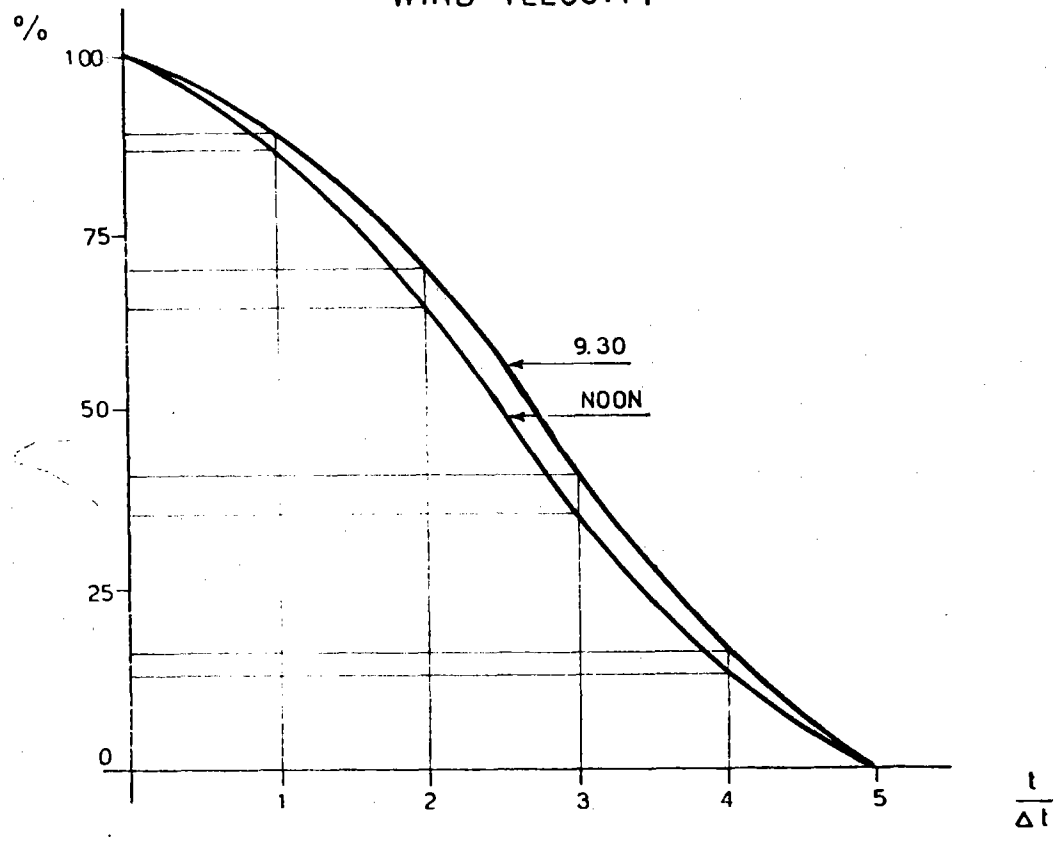

FIG. 2.30 - NORMALIZED POWER ON TARGET VS TIME STEP

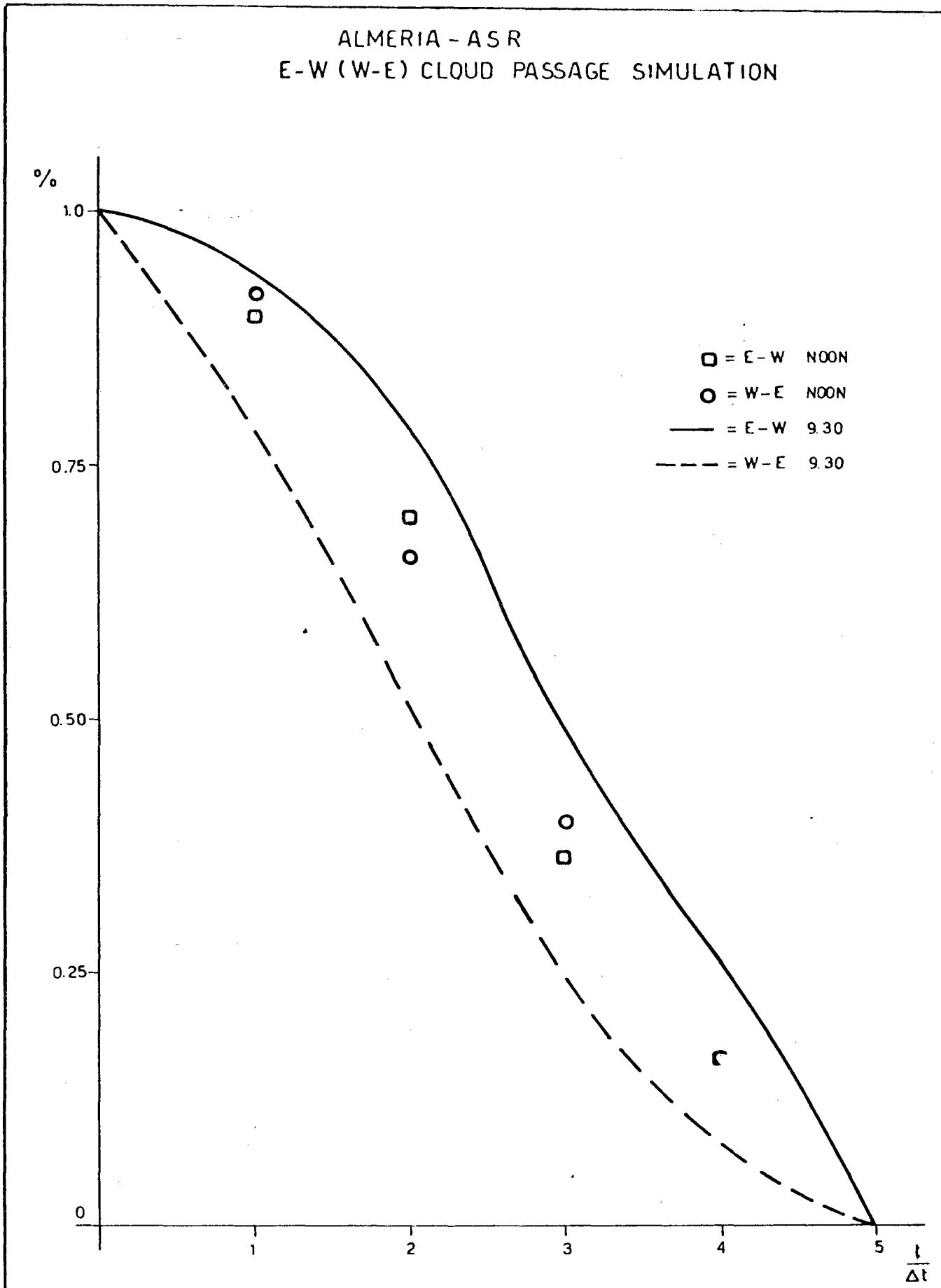

FIG. 2.31 - NORMALIZED PEAK FLUX VS TIME STEP

ALMERIA - ASR

E-W (W-E) CLOUD PASSAGE SIMULATION

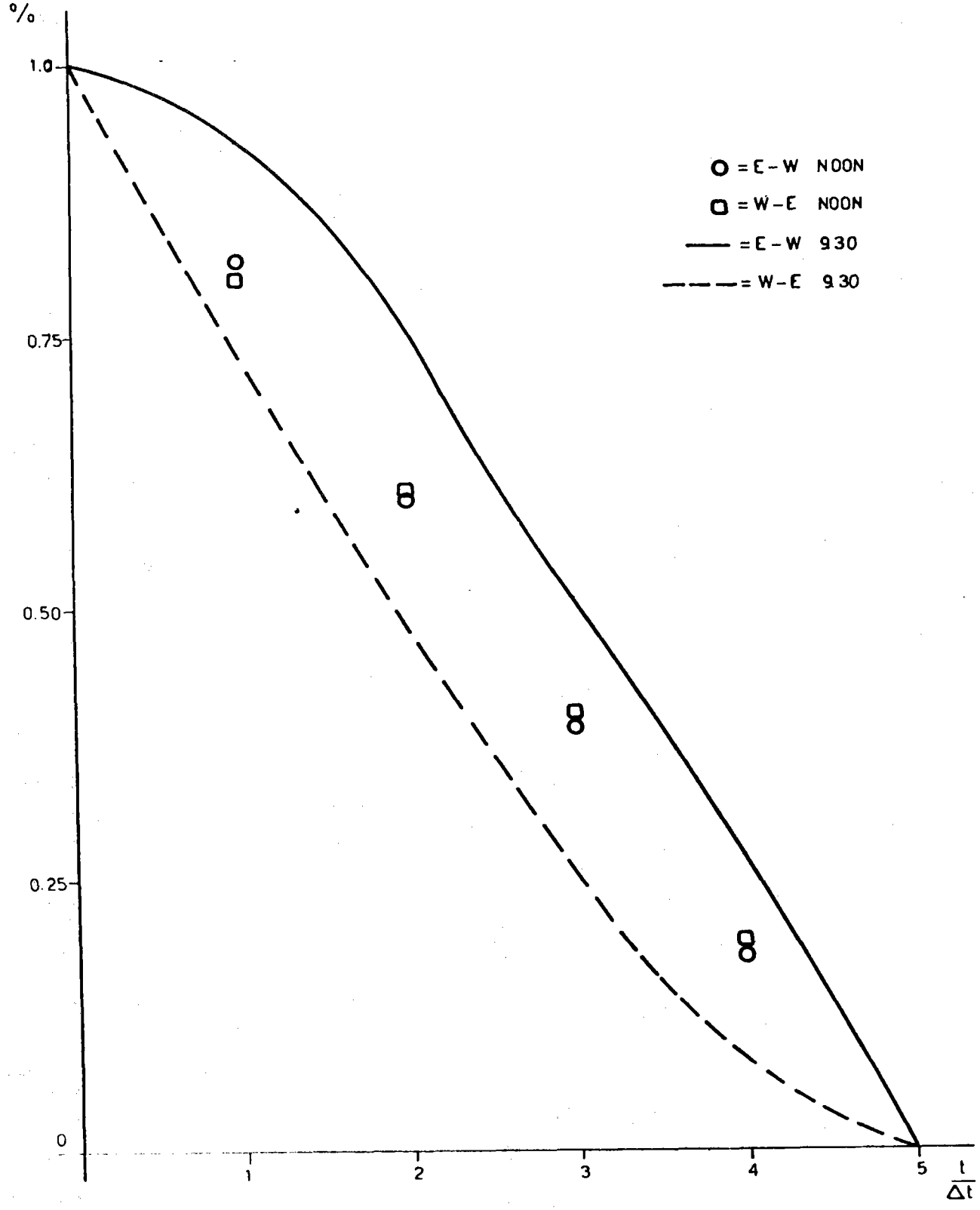

FIG. 2.32 - NORMALIZED CENTER TARGET FLUX VS TIME STEP

SNAMPROGETTI

ALMERIA - ASR

N-S (S-N) CLOUD PASSAGE SIMULATION

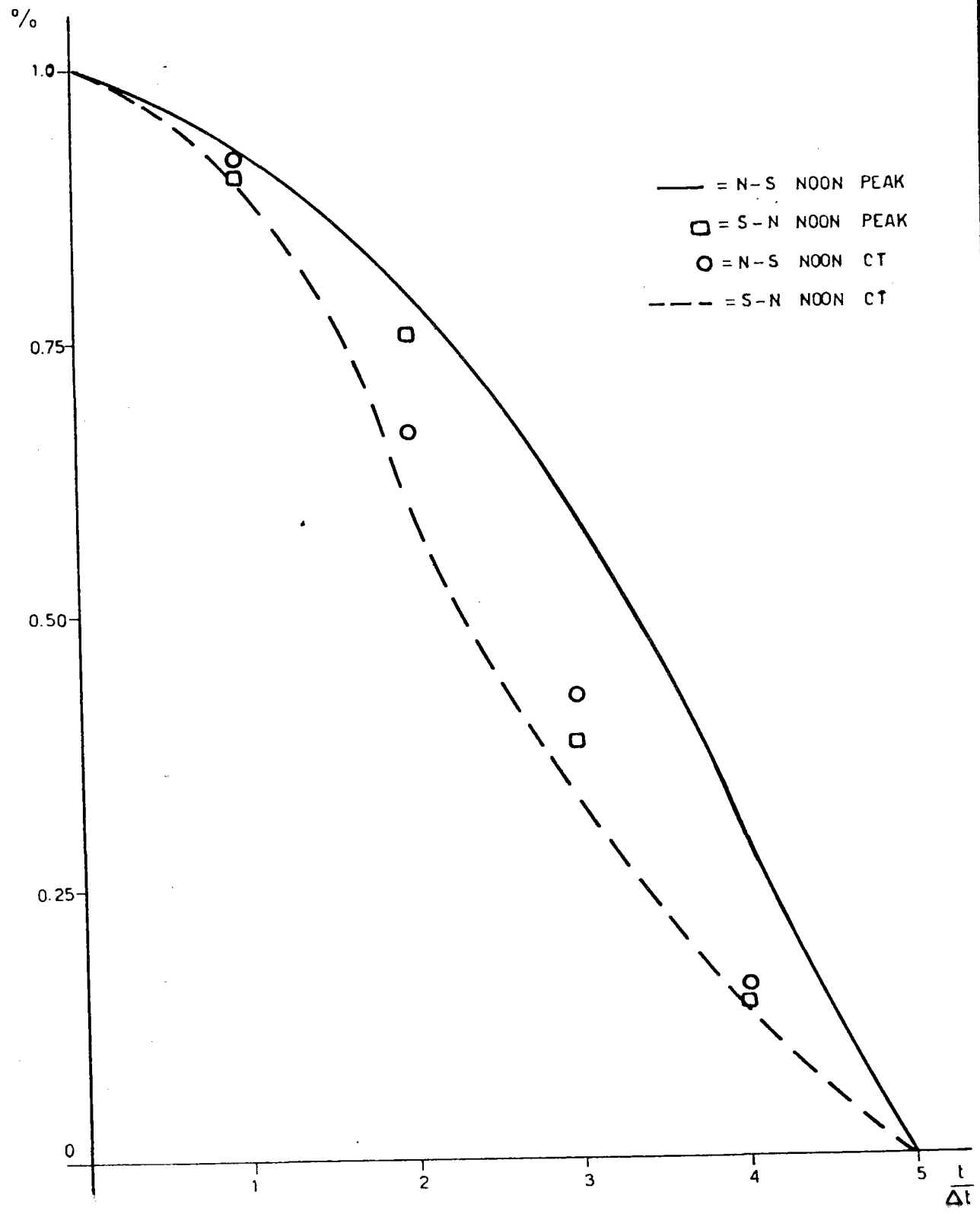

FIG. 2.33 - NORMALIZED FLUX VS TIME STEP

SNAMPROGETTI

ALMERIA-ASR E-W CLAUD PASSAGE GROUP12345

	,08	.23	,55	1,03	1,50	1,70	1,50	1,03	,55	.23	,08	
	,25	,68	2,15	4,10	5,09	6,95	6,07	4,09	2,14	,98	,25	
	.73	2,52	6,37	12,7	19,4	22,4	19,4	12,5	6,34	2,52	.73	
	1,72	5,68	14,7	30,0	46,5	54,0	46,5	30,0	14,7	5,70	1,77	
	3,25	11,5	29,7	57,0	93,5	94,5	93,5	57,1	29,5	11,5	3,31	
E.	5,45	22,5	59,0	97,7	120,	124,	119.	97,4	58,7	22,7	5,67	W.
	6,93	34,1	90,2	133.	134,	122.	132.	132.	88,3	33,5	7,25	
	6,07	30,5	79,6	111.	101,	85,0	99,6	110.	79,4	30,3	6,42	
	3,47	14,5	35,7	49,0	44,3	35,7	44,5	49,7	35,5	14,3	3,73	
	1,19	3,30	8,07	11,2	11,5	11,4	11,5	11,3	8,23	4,05	1,35	
	.23	,51	1,16	1,77	2,22	2,38	2,22	1,79	1,20	,55	,23	

BOT.

HELST. NO. 93,
INSOL. KW/M2 ,320
DAY NO. 80,
TIME HS. 12,
TOWER HEIGHT M 43,
TARGET DIM. M 2,5X2,5

AIM. NO. 3,
STD.DEV. MRAD. 2,60
INC.POW. KW 2380,
AVERG./PEAK ,27
SPILLAGE %

FIG.A.1 INCIDENT FLUX ON FLAT TARGET (W/CM2)

ALMERIA-ASR E-W CLOUD PASSAGE GROUP 12345

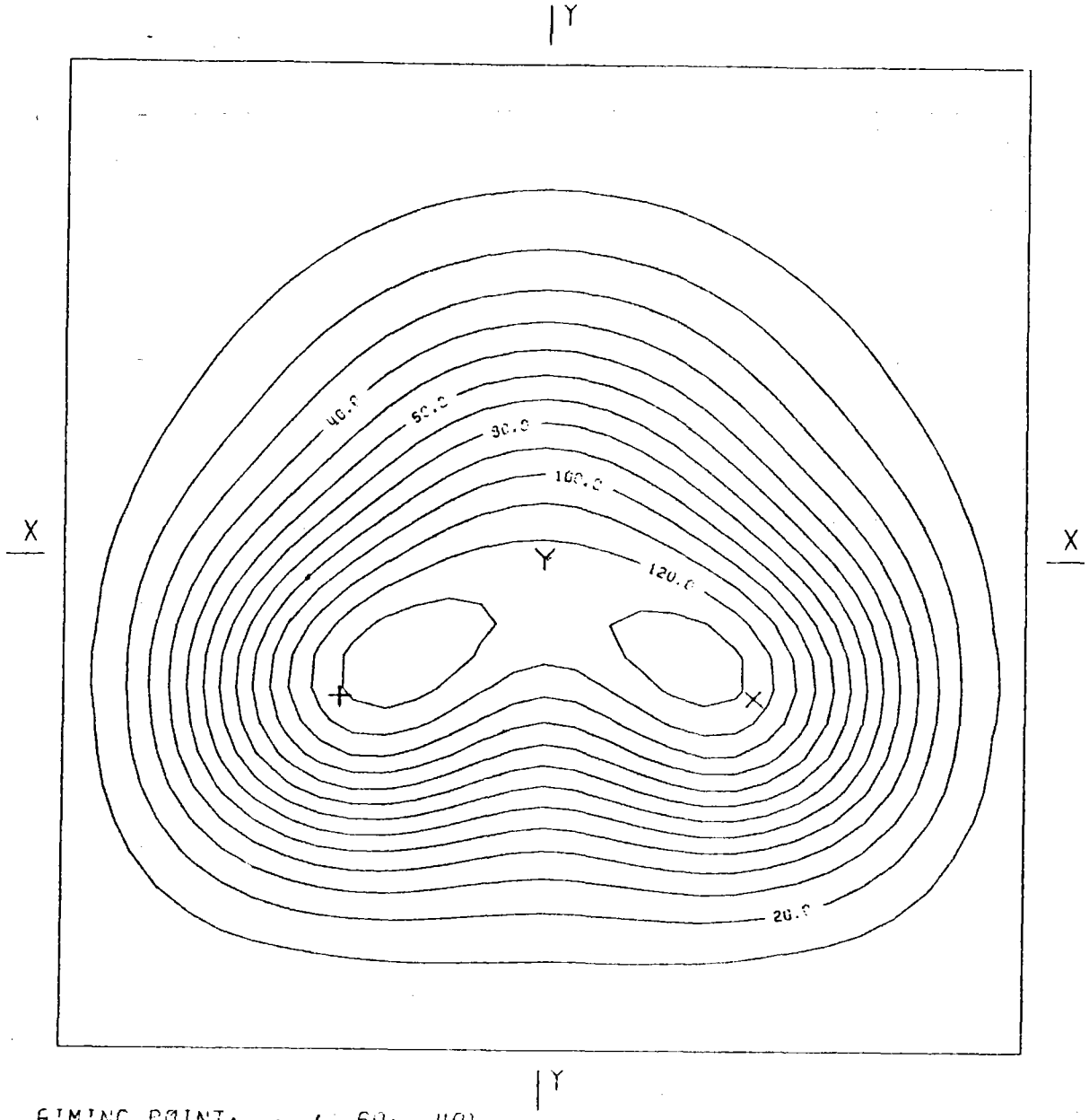

AIMING POINT: + (-,60; -,40)
× (,00; -,40)
Y (,00; ,00)

FIG.A.2 EQUIFLUX LINES, SPACING (W/CM2) 10,0

ALMERIA-ASR E-W CLAUD PASSAGE GROUP12345

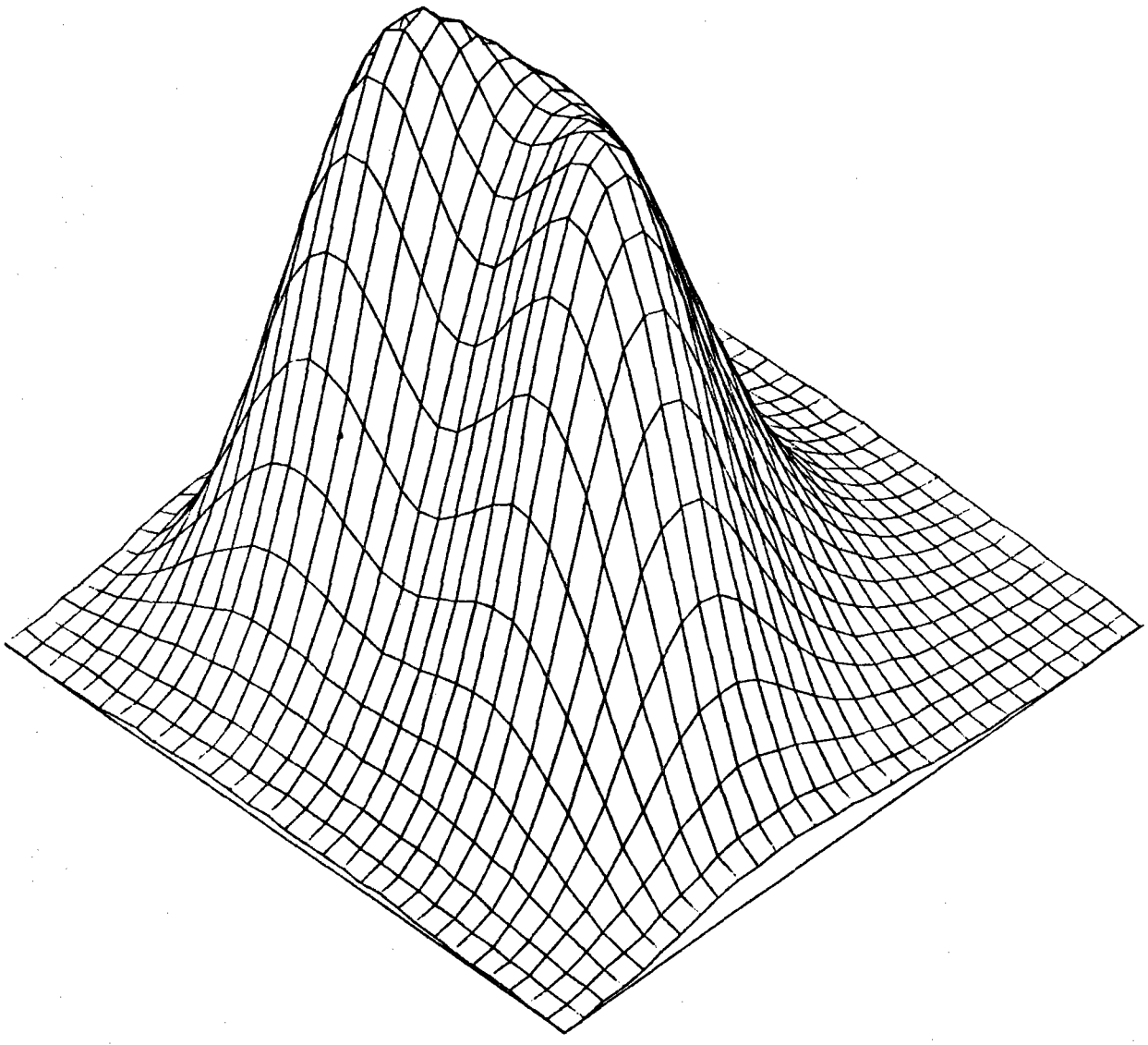

FIG.A.3 THREE-DIM. VIEW OF INCIDENT FLUX ON TARGET

SNAMPROGETTI

ALMERIA-ASR E-W CLAUD PASSAGE GROUP12345

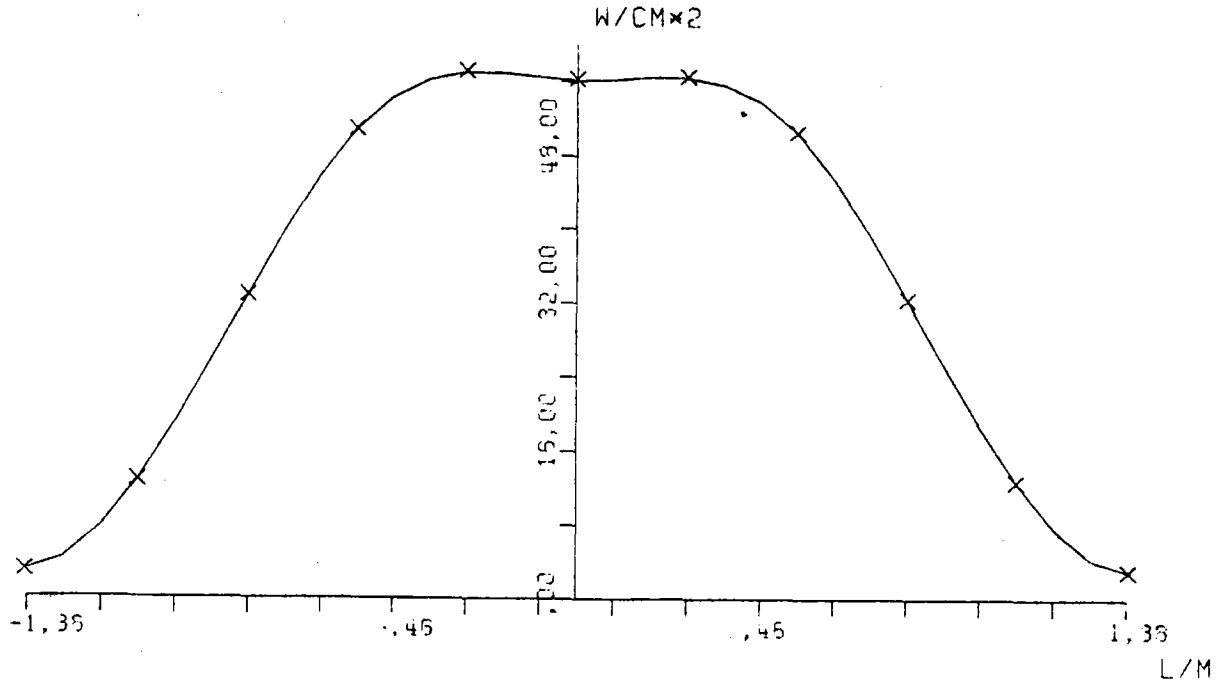

FIG.A.4 - AVERAGE SOLAR FLUX ON VERTICAL STRIP

SNGMPROGETTI

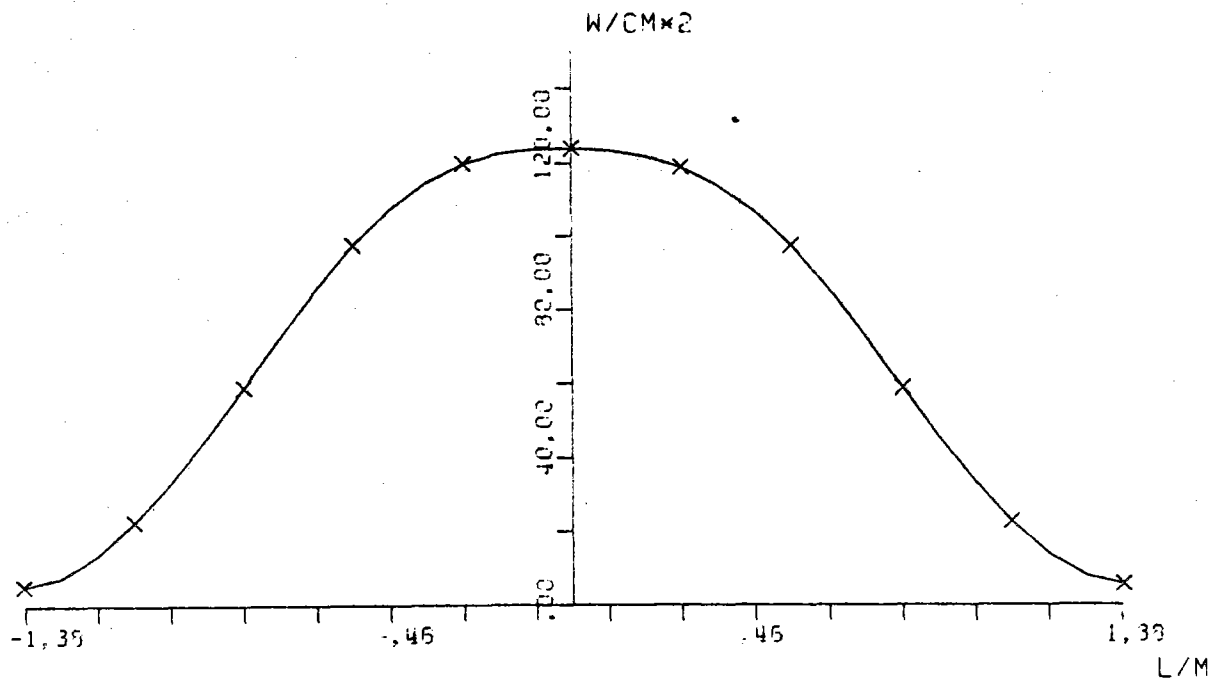

FIG.A.5 SOLAR FLUX ON TARGET SEC X-X

ALMERIA-ASR E-W CLAUD PASSAGE GROUP12345

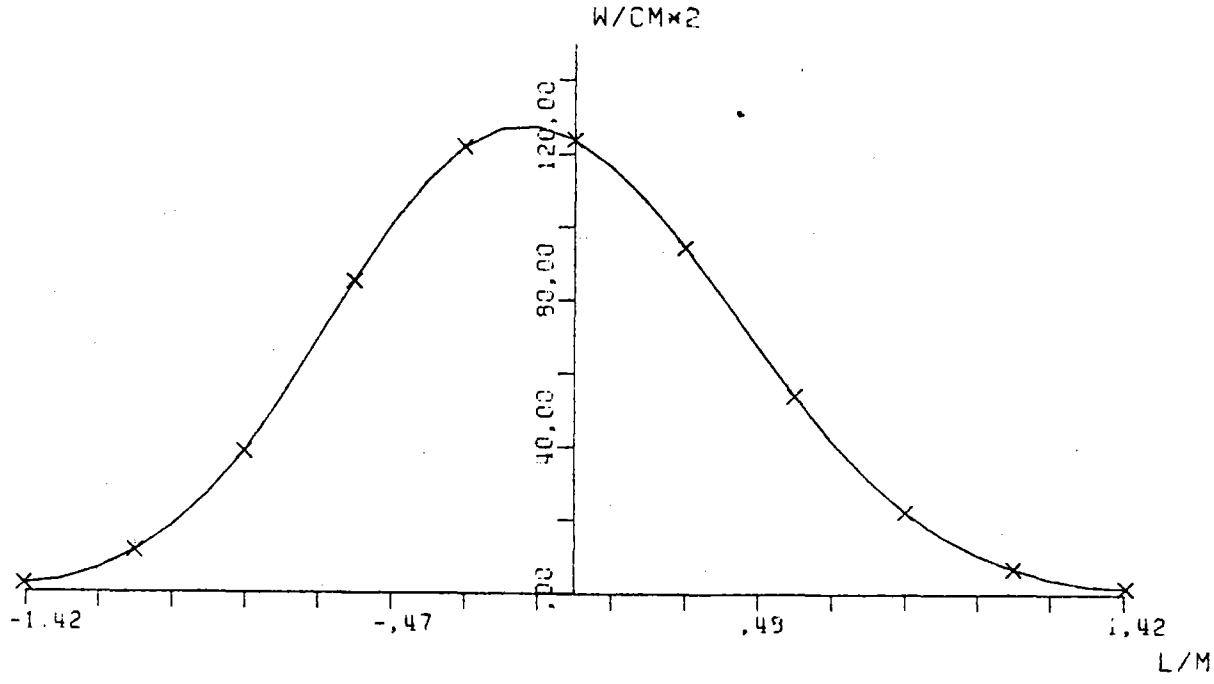

FIG.A.6 SOLAR FLUX ON TARGET SEC Y-Y

ALMERIA-ASR E-W CLAUD PASSAGE GROUP2345

	,07	,21	,48	,68	1,24	1,34	1,12	,72	,35	,13	,04	
	,25	,77	1,65	3,47	5,01	5,49	4,54	2,64	1,37	,51	,15	
	,69	2,17	5,42	10,6	15,9	17,6	14,6	8,94	4,14	1,51	,43	
	1,45	4,78	12,3	24,6	38,0	43,1	35,9	22,0	10,1	3,61	1,01	
	2,71	9,71	24,8	47,0	68,1	76,2	66,5	44,7	22,6	8,29	2,14	
E.	4,55	19,6	51,4	83,5	99,3	102,	98,9	82,9	50,2	18,6	4,10	W.
	5,70	30,3	81,5	118,	114,	102,	115,	119,	81,3	30,2	5,68	
	4,60	27,0	72,5	100,0	87,5	71,5	88,0	102,	73,5	28,0	5,64	
	2,57	12,7	31,7	43,5	36,5	32,3	39,0	44,9	33,4	14,0	3,45	
	,78	3,02	6,64	9,36	9,66	9,27	9,98	10,1	7,62	3,62	1,29	
	,13	,39	,83	1,33	1,71	1,67	1,61	1,54	1,09	,62	,28	

BOT.

HELST. NO. 79,
INSOL. KW/M2 ,920
DAY NO. 80,
TIME HR. 12,
TOWER HEIGHT M 43,
TARGET DIM. M 2,8X2,6

AIM. NO. 3,
STD.DEV. MRAD. 2,60
INC.POW. KW 2440,
AVERG./PEAK ,26
SPILLAGE %

FIG.A.7 INCIDENT FLUX ON FLAT TARGET (W/CM2)

ALMERIA-ASR E-W CLAUD PASSAGE GROUP2345

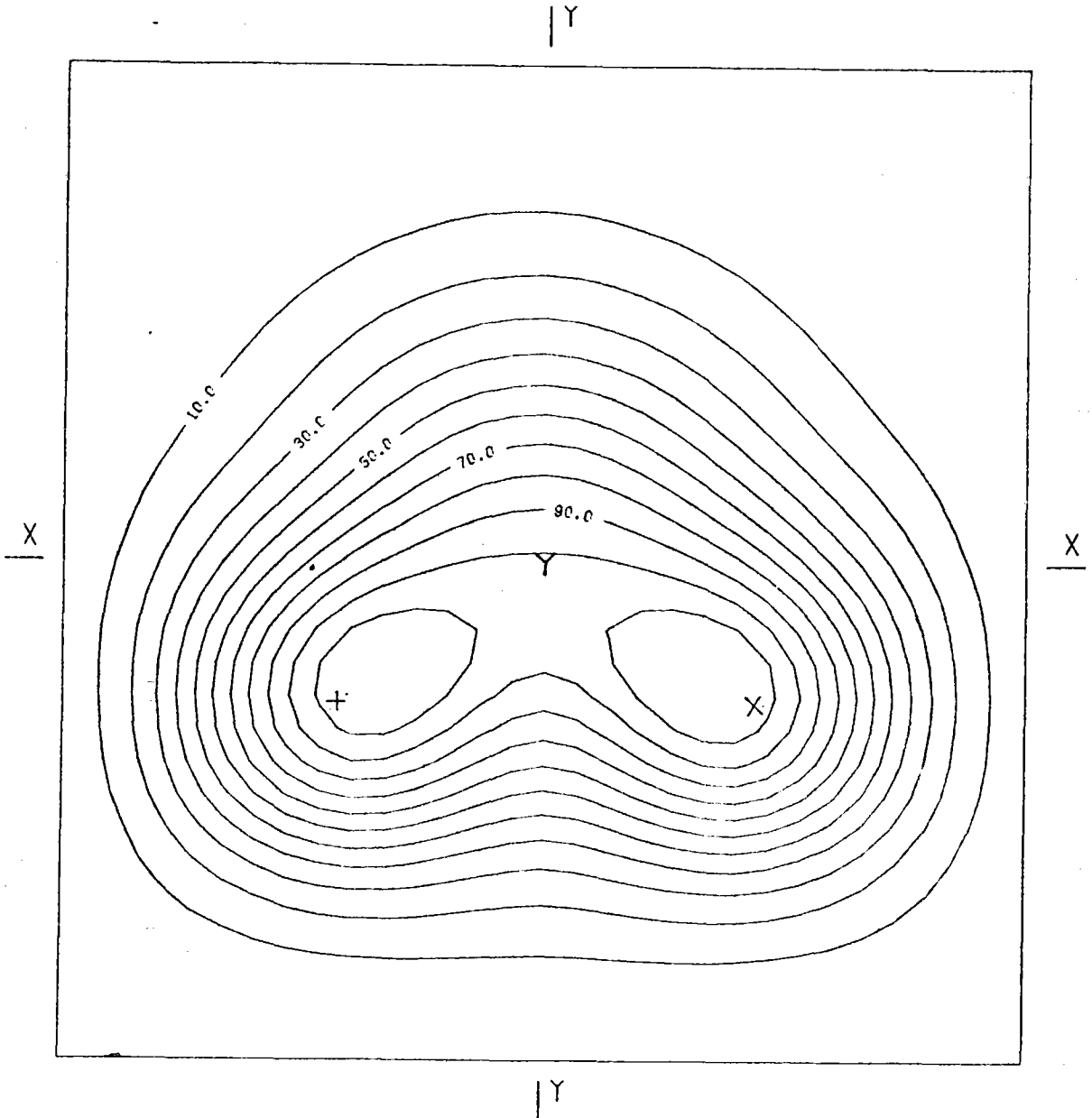

AIMING POINT: + (-,60; -,40)

× (,00; -,40)

Y (,00; ,00)

FIG.A.8 EQUIFLUX LINES, SPACING (W/CM2) 10,0

ALMERIA-ASR E-W CLAUD PASSAGE GROUP2345

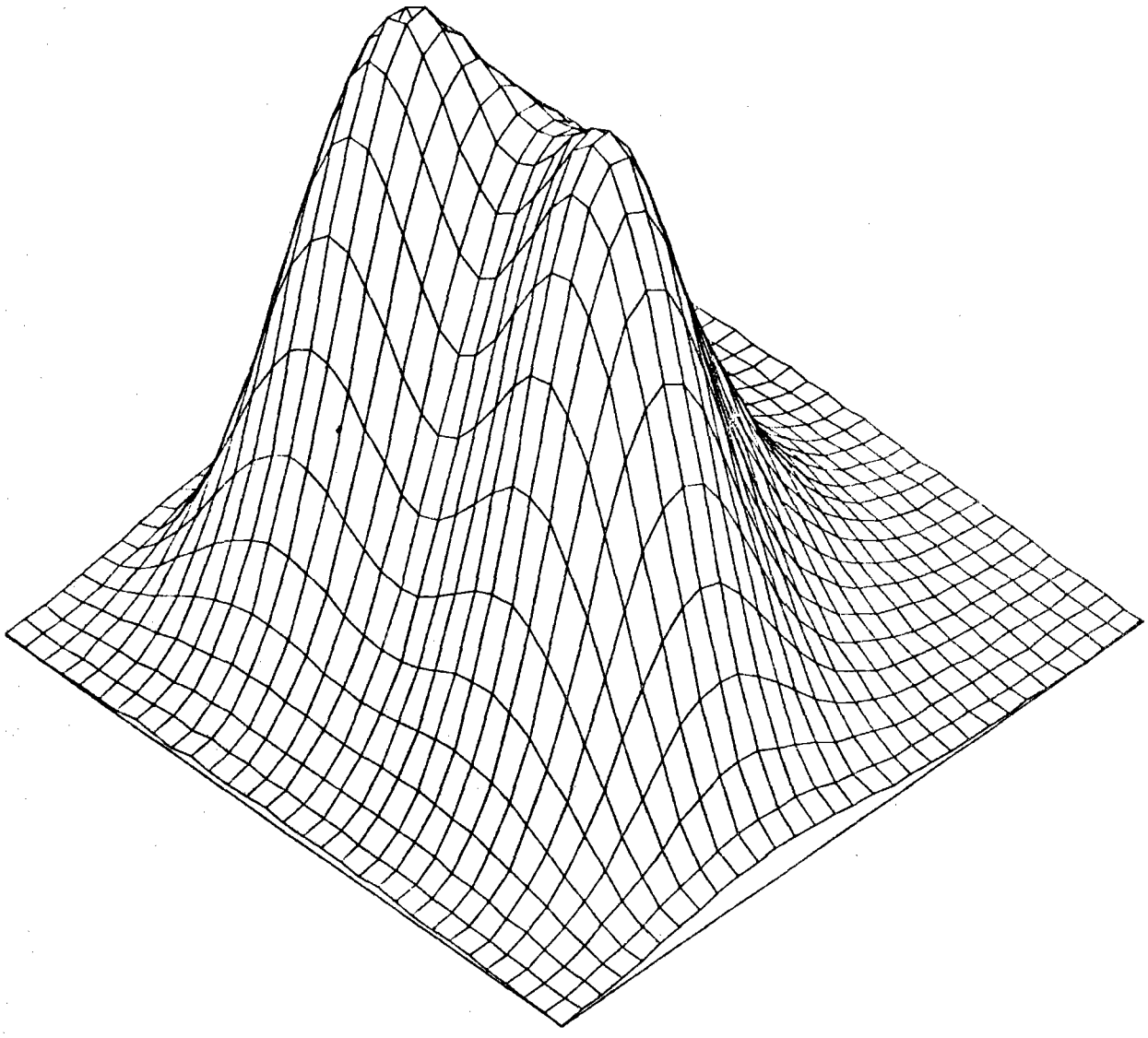

FIG.A.9 THREE-DIM. VIEW OF INCIDENT FLUX ON TARGET

ALMERIA-ASR E-W CLAUD PASSAGE GROUP2345

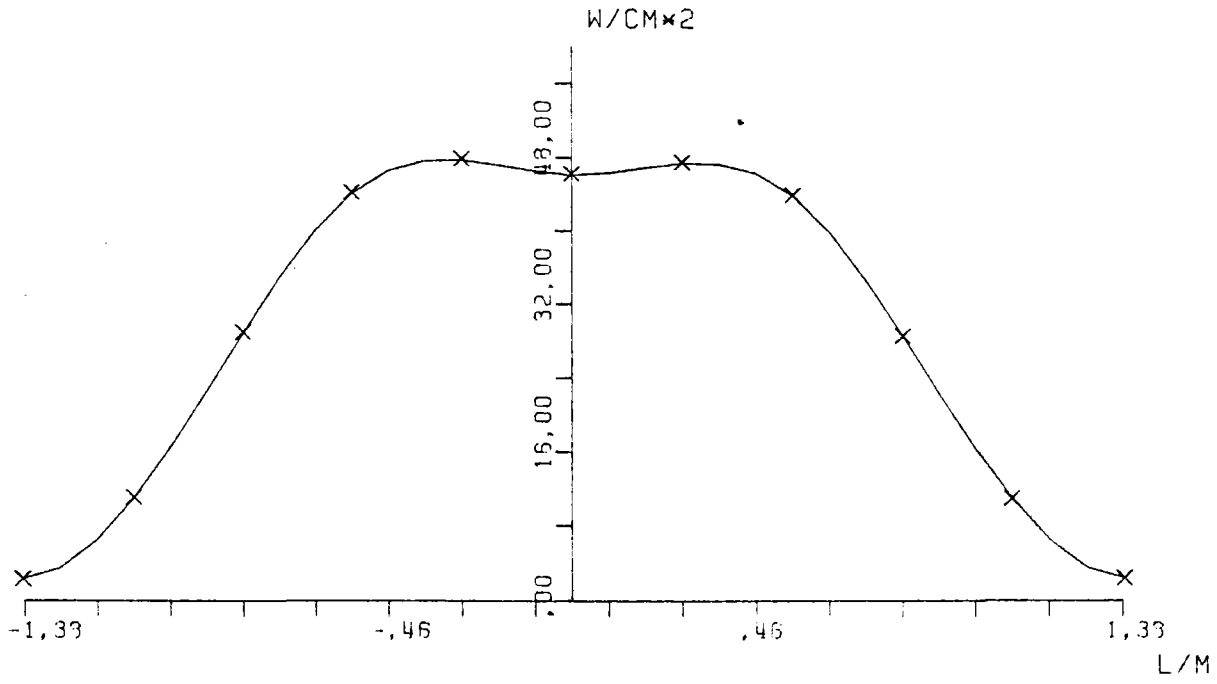

FIG.A.10 AVERAGE SOLAR FLUX ON VERTICAL STRIP

ALMERIA-ASR E-W CLOUD PASSAGE GROUP2345

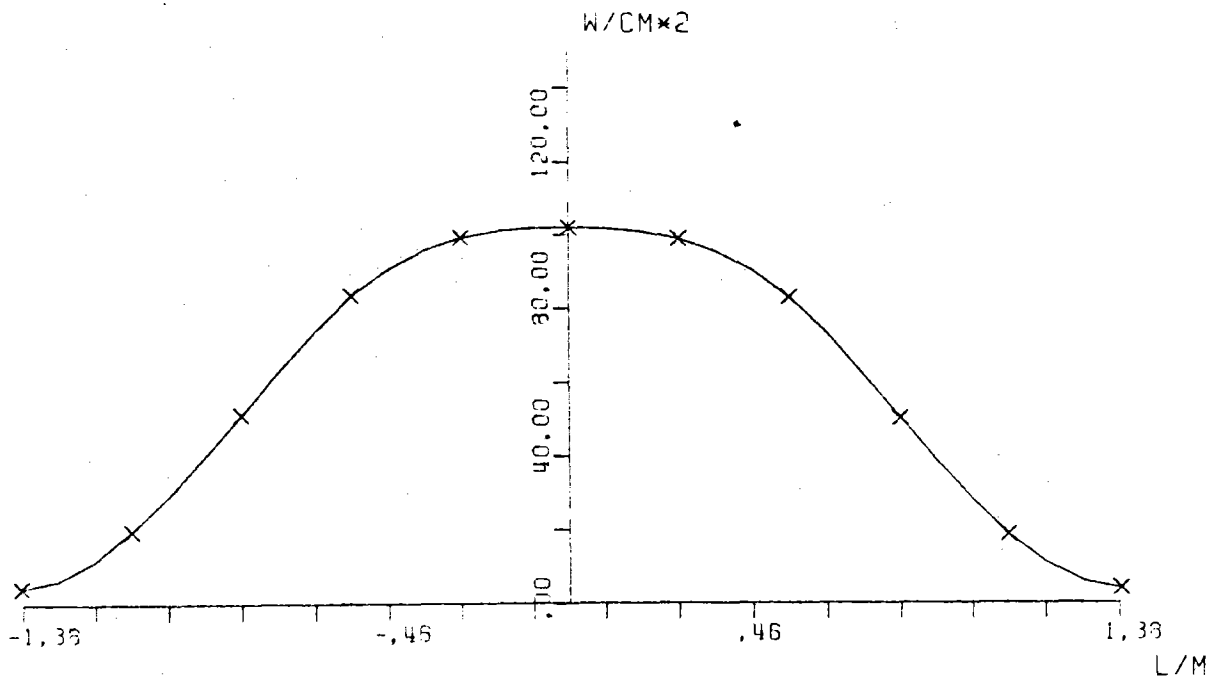

FIG.A.11 SOLAR FLUX ON TARGET SEC X-X

SNAMPROGETTI

ALMERIA-ASR E-W CLAUD PASSAGE GROUP2345

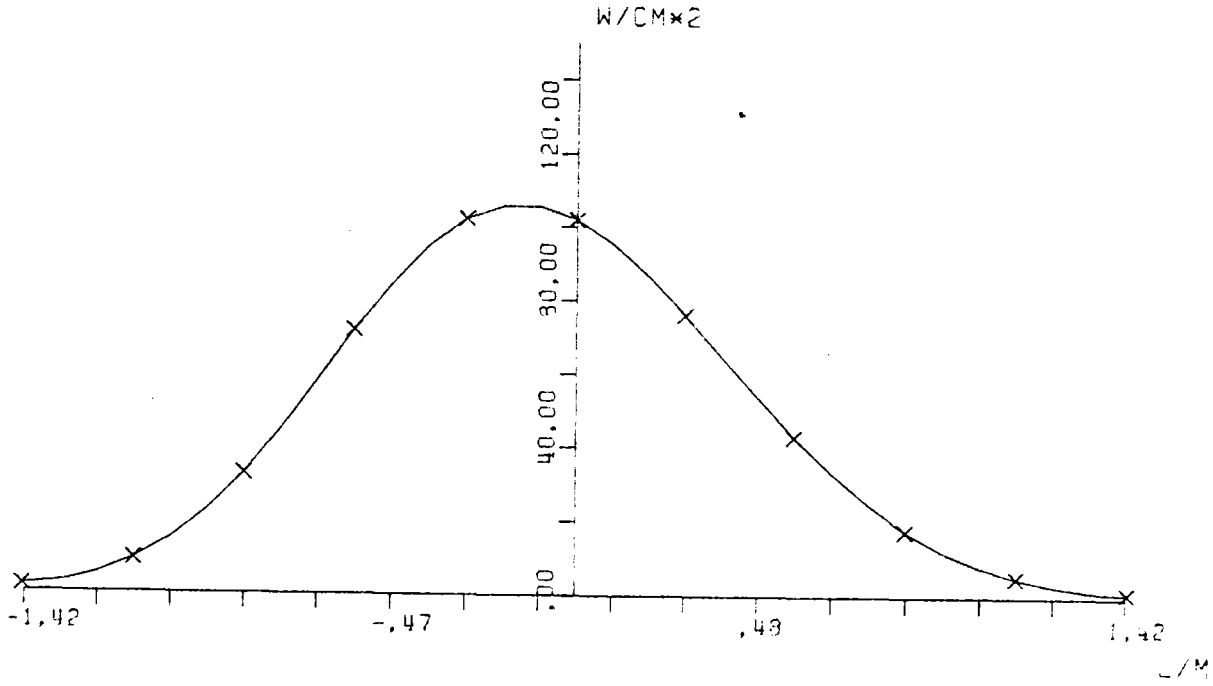

FIG.A.12 SOLAR FLUX ON TARGET SEC Y-Y

ALMERIA-ASR E-W CLAUD PASSAGE GROUP345

	,06	,18	,42	,73	1,00	1,04	,63	,51	,24	,09	,03	
	,23	,68	1,59	2,69	4,03	4,24	3,37	2,03	,95	,35	,10	
	,61	1,68	4,61	8,77	12,7	13,7	10,6	6,42	2,91	1,04	,29	
	1,27	4,11	10,3	20,0	29,7	32,6	26,7	16,0	7,21	2,50	,69	
	2,37	8,29	20,1	36,1	51,1	57,3	50,2	33,5	15,2	5,52	1,36	
E.	3,91	15,4	33,5	60,0	70,4	75,3	76,7	54,4	37,2	12,6	2,98	W.
	4,45	22,7	58,3	82,1	79,5	75,5	90,2	94,4	63,3	22,5	4,15	
	2,98	17,0	47,9	69,3	63,0	53,5	68,1	90,7	59,5	22,6	4,59	
	1,14	6,37	19,2	30,4	29,1	24,2	29,9	35,1	27,7	12,1	3,09	
	,26	1,28	3,53	6,66	7,49	6,92	7,18	7,77	6,43	3,45	1,21	
	,04	,17	,50	,96	1,31	1,41	1,35	1,21	,93	,57	,26	

BOT.

HELST. NO.	59,	AIM. NO.	3,
INSOL. KW/M2	,920	STD.DEV. MRAD.	2,60
DAY NO.	80,	INC.POW. KW	1820,
TIME HR.	12,	AVERG./PEAK	,25
TOWER HEIGHT M	43,	SPILLAGE %	
TARGET DIM. M	2,6X2,6		

FIG.A.13 INCIDENT FLUX ON FLAT TARGET (W/CM2)

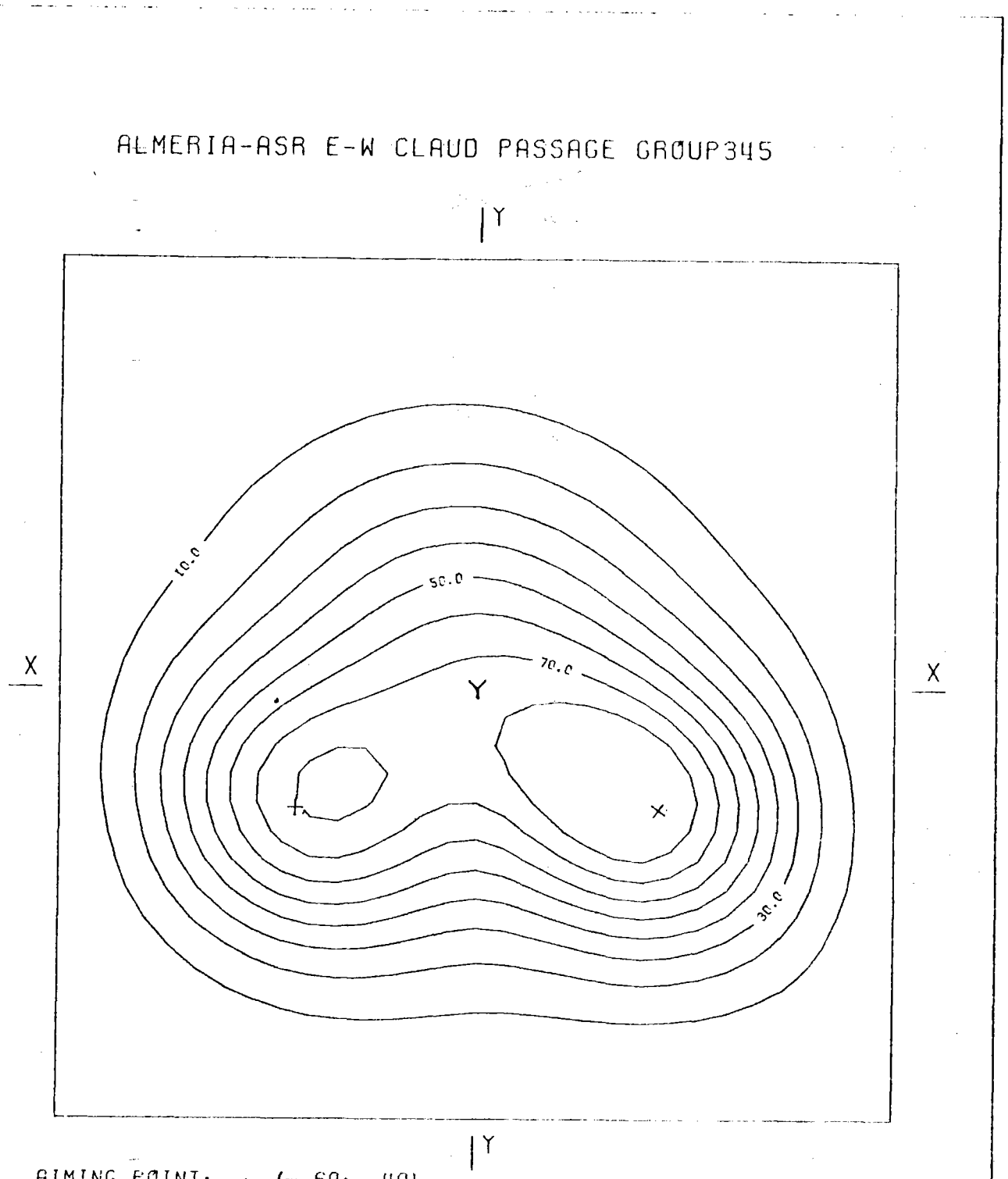

AIMING POINT: + (-,60;-,40)
× (,00;-,40)
Y (,00;,00)

FIG.A.14 EQUIFLUX LINES, SPACING (W/CM2) 10,0

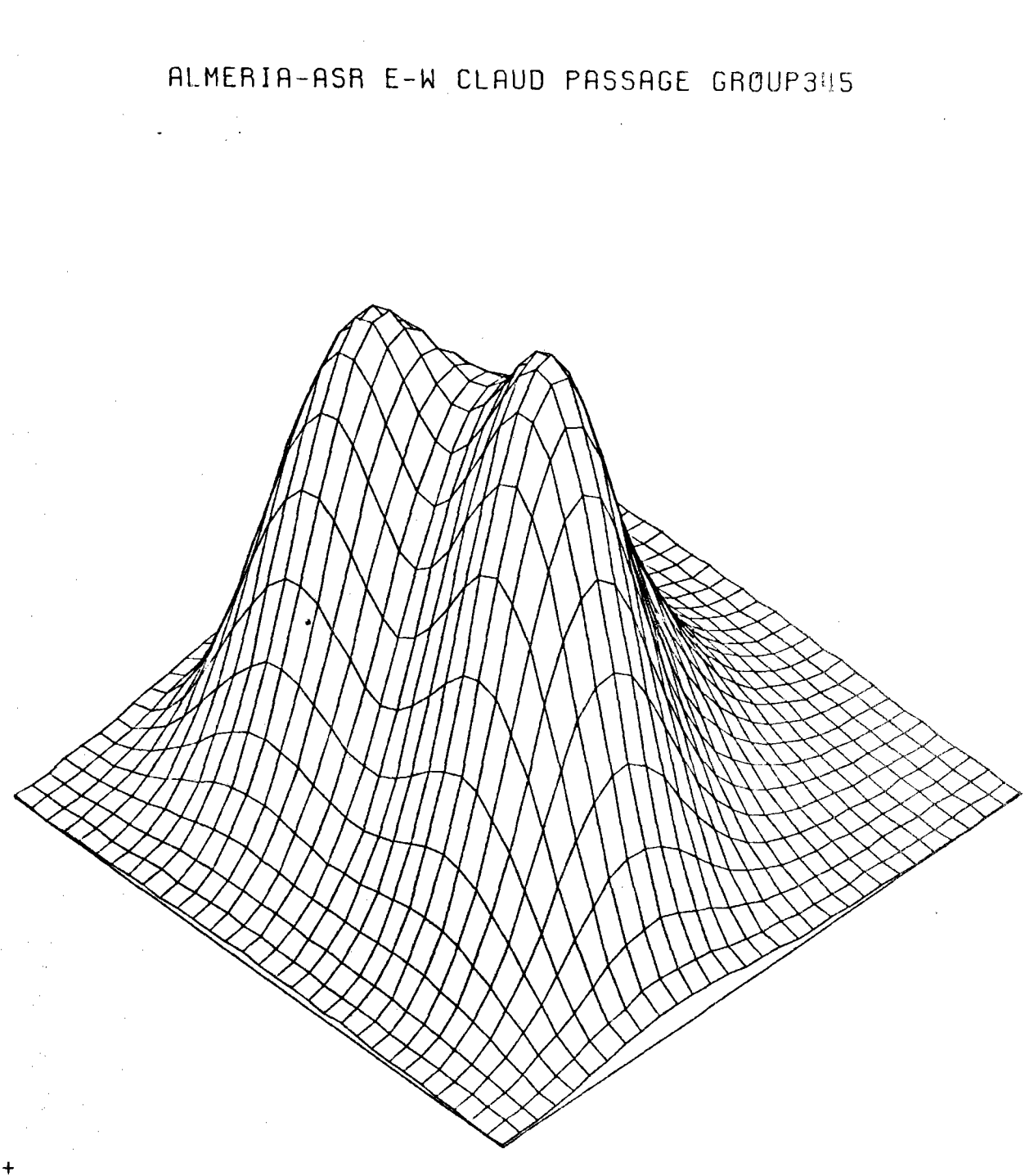

FIG.A.15 THREE-DIM. VIEW OF INCIDENT FLUX ON TARGET

ALMERIA-ASR E-W CLAUD PASSAGE GROUP345

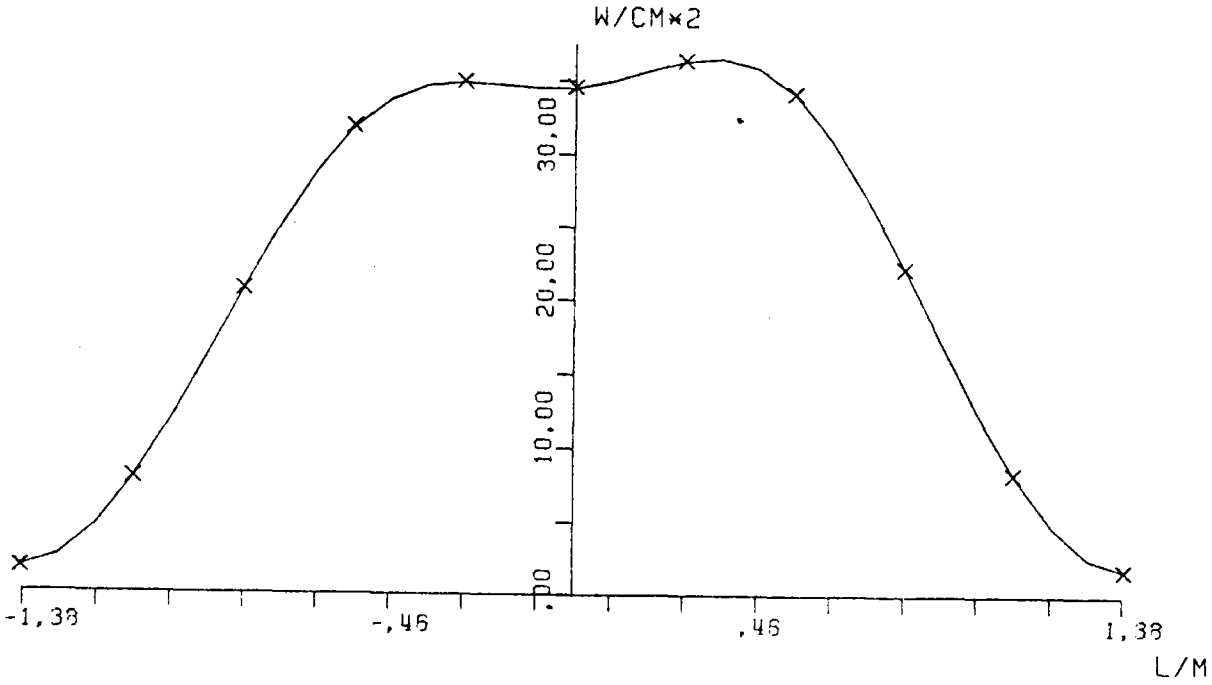

FIG.A.16 AVERAGE SOLAR FLUX ON VERTICAL STRIP

ALMERIA-ASR E-W CLAUD PASSAGE GROUP345

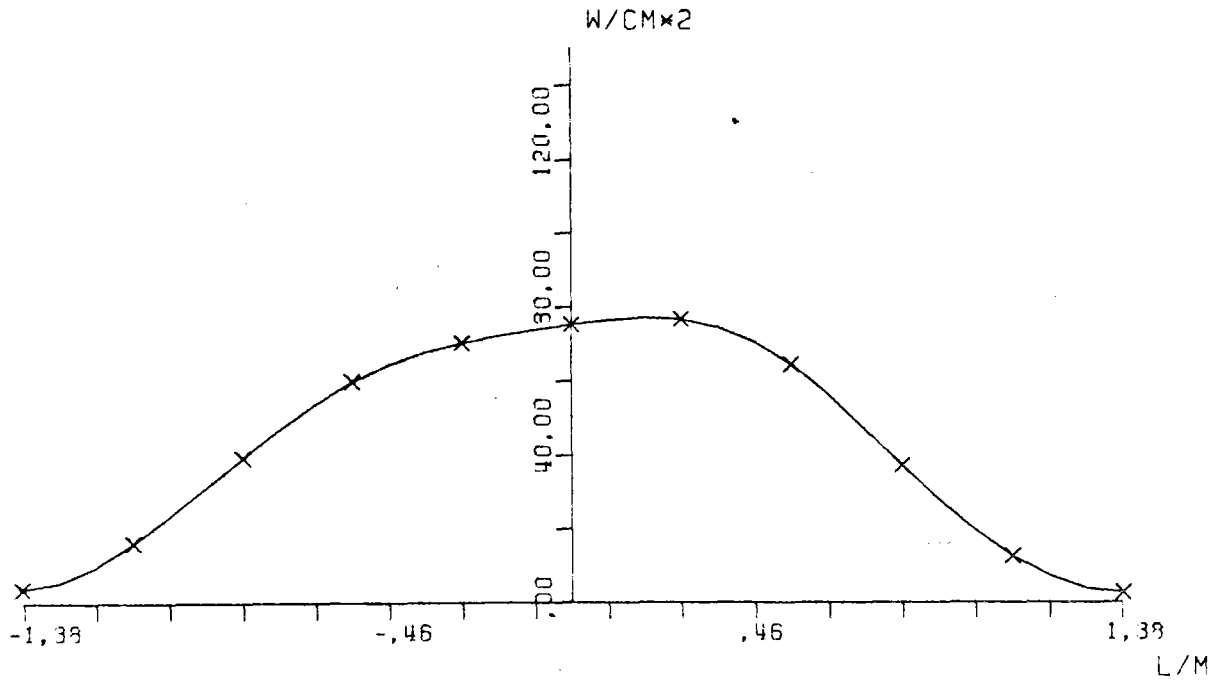

FIG.A.17 SOLAR FLUX ON TARGET SEC X-X

ALMERIA-ASR E-W CLAUD PASSAGE GROUP345

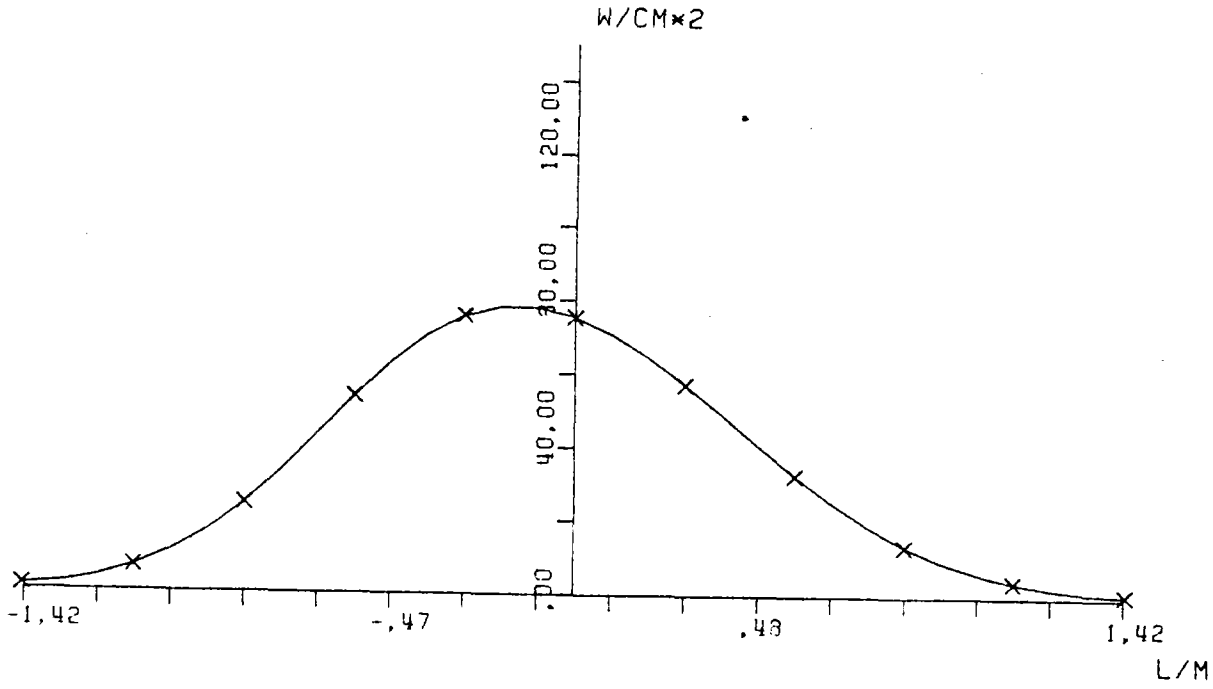

FIG.A.18 SOLAR FLUX ON TARGET SEC Y-Y

ALMERIA-ASR E-W CLOUD PASSAGE GROUP45

	.05	.15	.31	.53	.67	.66	.51	.30	.14	.02
	.19	.54	1,20	2,07	2,73	2,72	2,07	1,21	.56	.20	.06
	.50	1,48	3,46	6,25	8,59	8,61	6,74	3,90	1,76	.64	.18
	1,03	3,17	7,53	14,0	19,9	21,3	16,9	10,00	4,48	1,58	.45
	1,58	5,13	13,5	23,6	33,4	37,4	32,3	20,6	9,54	3,32	.89
E.	2,92	11,0	24,0	35,3	43,2	48,3	47,1	35,2	18,3	6,41	1,62	W
	2,92	13,2	31,5	44,1	45,5	46,2	49,4	44,0	27,1	10,5	2,64	
	1,63	6,35	23,6	35,9	35,7	31,6	34,3	35,5	26,1	11,6	3,25	
	.54	2,71	8,62	15,9	17,3	14,9	15,0	16,6	14,4	7,76	2,53	
	.12	.54	1,76	3,62	4,69	4,49	4,27	4,53	4,22	2,70	1,10	
	.02	.09	.26	.55	.63	.93	.69	.62	.71	.49	.25	

BOT.

HELST. NO. 34,
INSOL. KW/M2 ,920
DAY NO. 80,
TIME HR. 12,
TOWER HEIGHT M 43,
TARGET DIM. M 2,6X2,6

AIM. NO. 3,
STD.DEV. MRAD. 2,60
INC.POW. KW 1040,
AVERG./PEAK ,27
SPILLAGE %

FIG.A.19 INCIDENT FLUX ON FLAT TARGET (W/CM2)

ALMERIA-ASR E-W CLOUD PASSAGE GROUP45

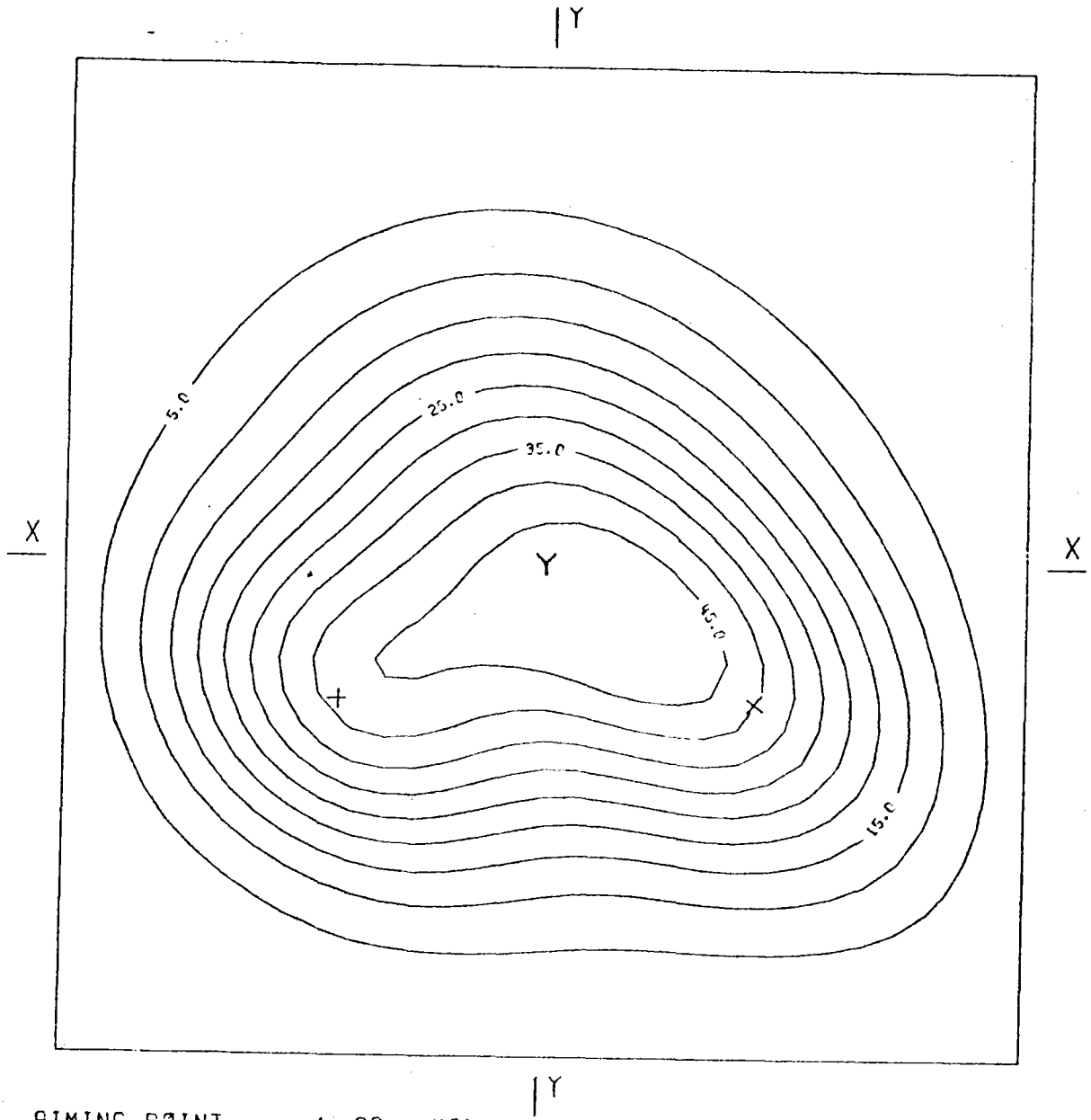

AIMING POINT: + (-,60;-,40)
× (,00;-,40)
Y (,00;,00)

FIG.A.20 EQUIFLUX LINES, SPACING (W/CM2) 5,0

ALMERIA-ASR E-W CLOUD PASSAGE GROUP45

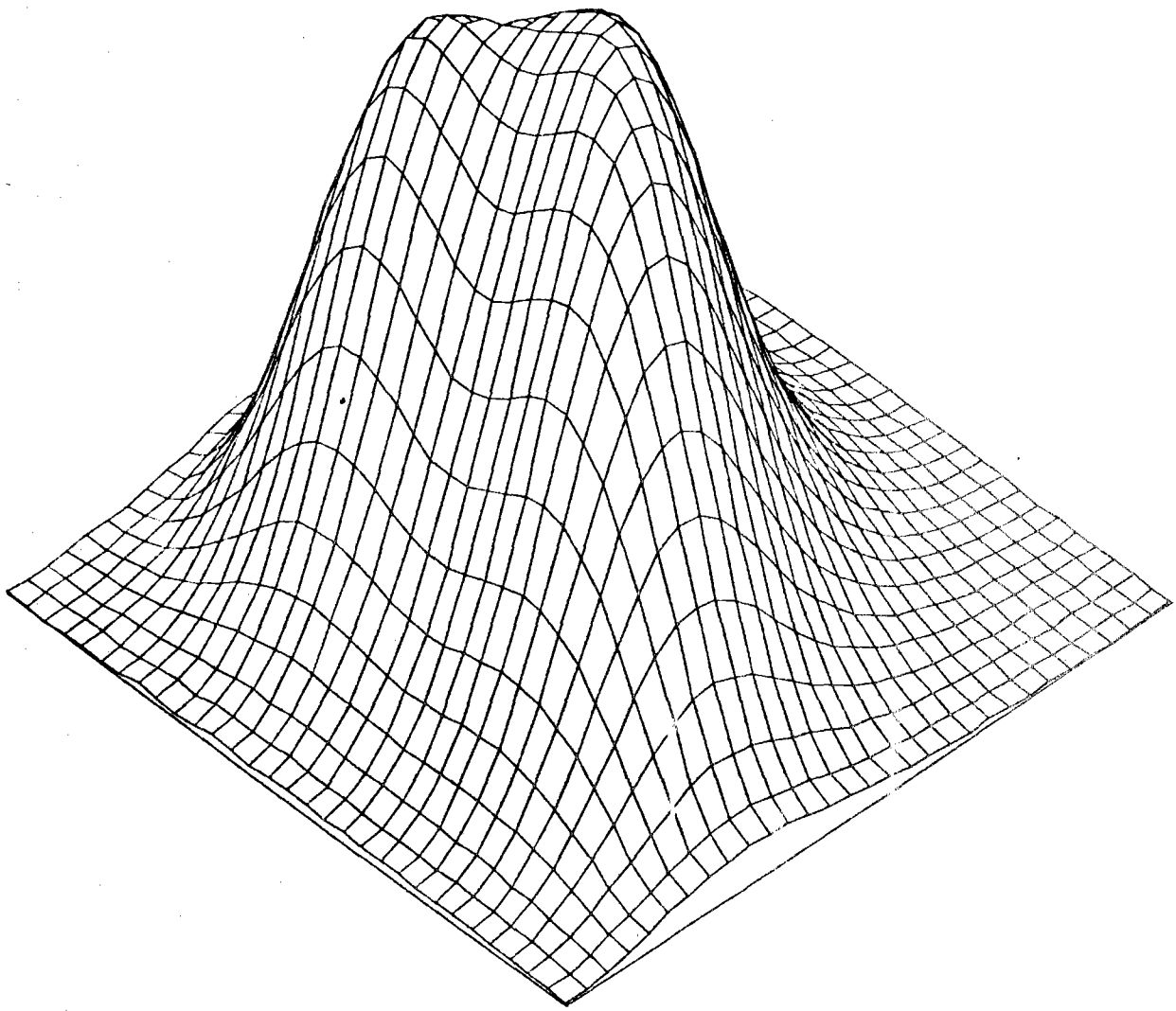

FIG.A.21 THREE-DIM. VIEW OF INCIDENT FLUX ON TARGET

ALMERIA-ASR E-W CLOUD PASSAGE GROUP45

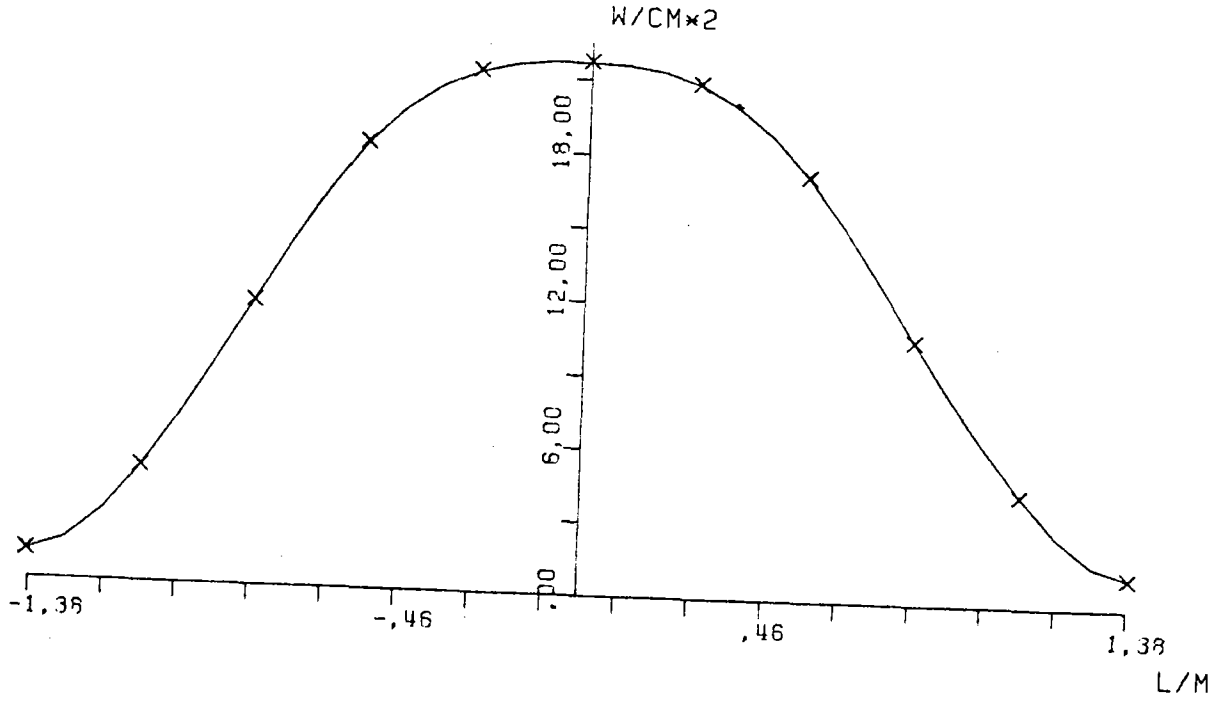

FIG.A.22 AVERAGE SOLAR FLUX ON VERTICAL STRIP

ALMERIA-ASR E-W CLOUD PASSAGE GROUP45

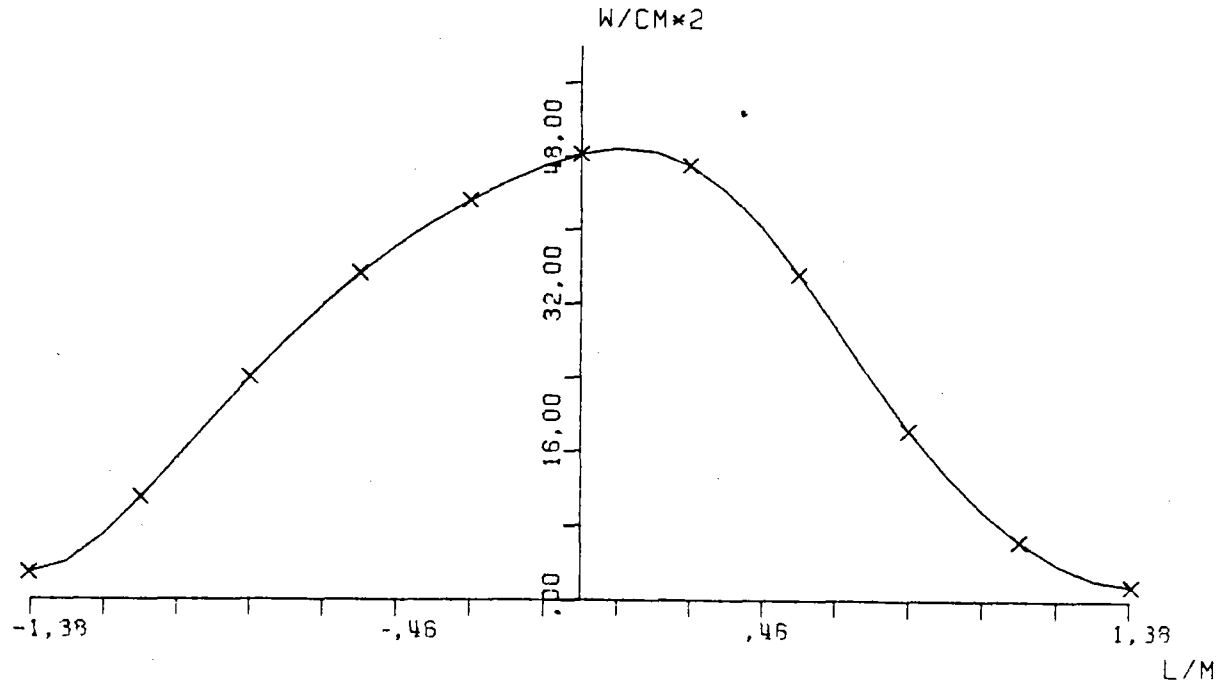

FIG.A.23 SOLAR FLUX ON TARGET SEC X-X

ALMERIA-ASR E-W CLOUD PASSAGE GROUP45

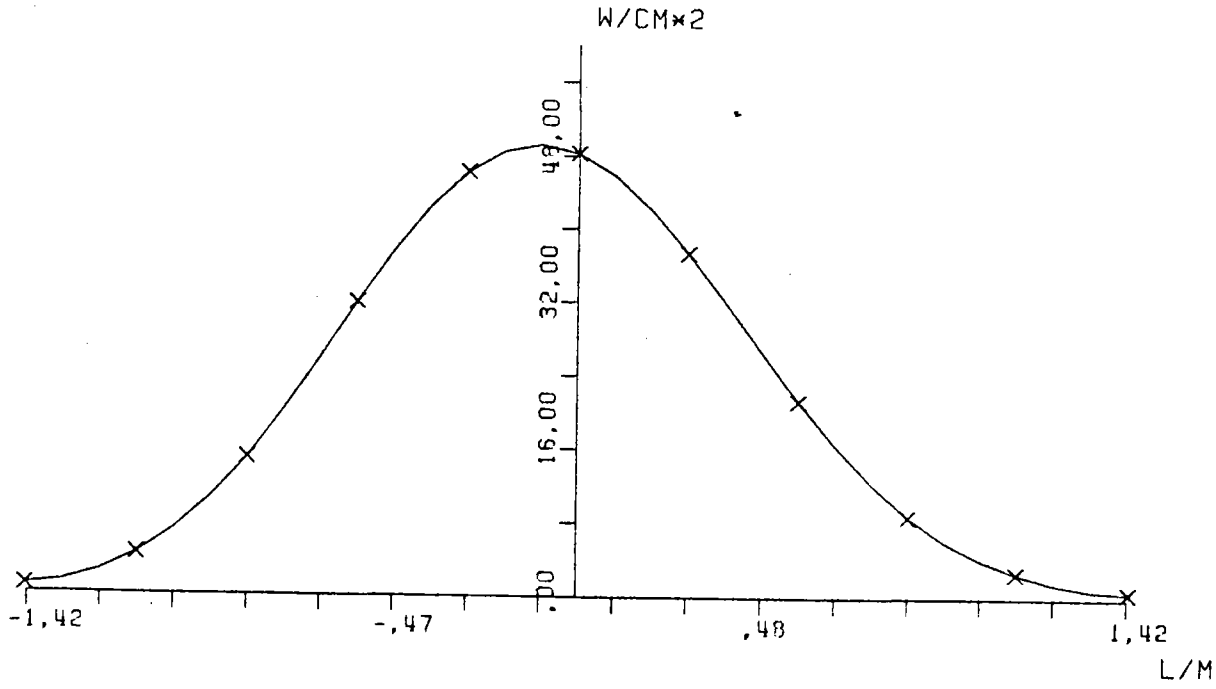

FIG.A.24: SOLAR FLUX ON TARGET SEC Y-Y

ALMERIA-ASR E-W CLOUD PASSAGE GROUP5

	,04	,10	,20	,32	,38	,36	,26	,15	,07	03	01	
	,14	,37	,78	1,25	1,55	1,47	1,09	,63	,29	,11	,03	
	,36	1,01	2,22	3,72	4,77	4,67	3,51	2,05	,95	,35	,10	
	,67	1,98	4,53	7,96	10,7	11,0	8,70	5,26	2,45	,90	,27	
	,90	2,76	6,58	12,1	17,1	18,9	16,1	10,5	5,13	1,90	,55	
E.	,67	2,75	6,61	13,1	19,6	23,4	21,9	15,6	8,51	3,42	,99	W.
	,62	1,99	5.09	10,3	15,4	20,9	21,5	17,4	10,6	4,34	1,57	
	,33	1,07	2,78	5,77	9,64	13,1	14,7	13,4	9,57	5,13	1,92	
	,14	,44	1,14	2,39	4,05	5,69	6.76	6,60	5,56	3,48	1,55	
	,04	,14	,36	,76	1,27	1,76	2,08	2,18	1,98	1,43	,75	
	,01	,04	,09	.19	,31	,42	,47	,46	,41	,32	,20	

BOT.

HELST. NO.	14,	AIM. NO.	3,
INSOL. KW/M2	,920	STO.DEV. MRAD.	2,60
DAY NO.	80,	INC.POW. KW	418,
TIME HR.	12,	AVERG./PEAK	,23
TOWER HEIGHT M	43,	SPILLAGE %	,13
TARGET DIM. M	2,6X2,6		

FIG.A.25INCIDENT FLUX ON FLAT TARGET (W/CM2)

ALMERIA-ASR E-W CLOUD PASSAGE GROUP5

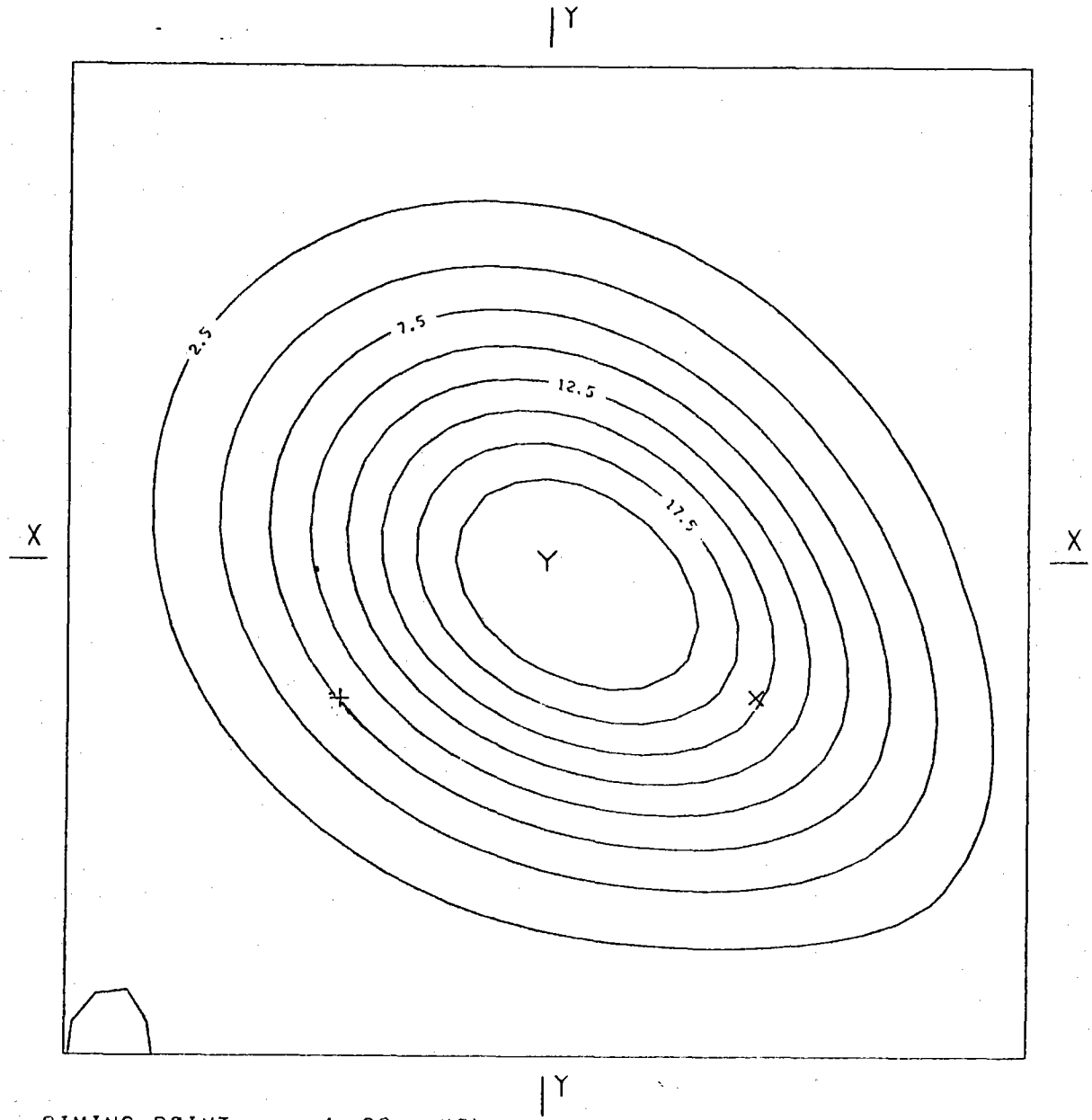

AIMING POINT: + (-,60;-,40)
× (,60;-,40)
Y (,00;,00)

FIG.A.26 EQUIFLUX LINES, SPACING (W/CM2) 2,5

ALMERIA-ASR E-W CLOUD PASSAGE GROUP5

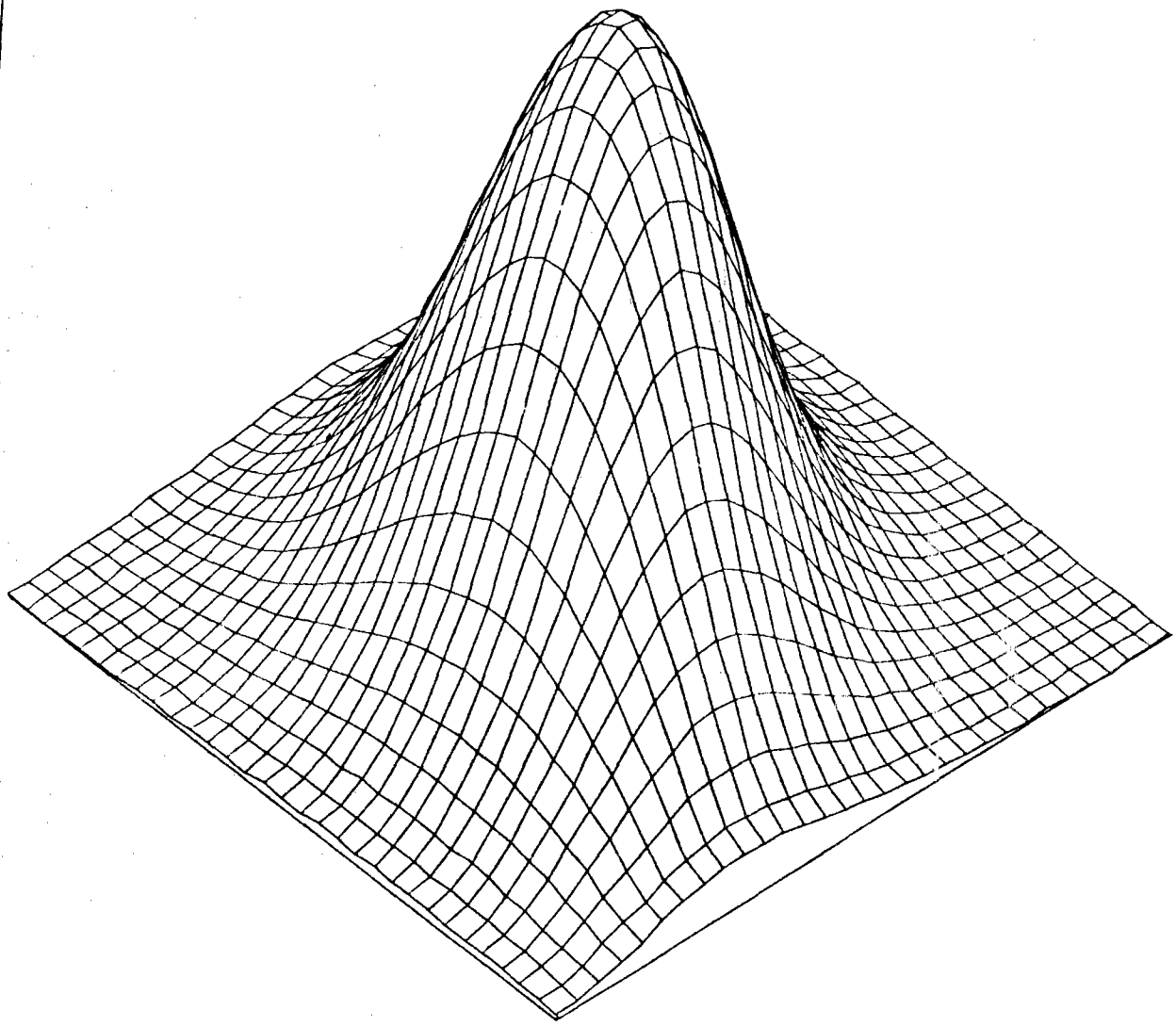

FIG.A.27 THREE-DIM. VIEW OF INCIDENT FLUX ON TARGET

SNAMPROGETTI

ALMERIA-ASR E-W CLOUD PASSAGE GROUP5

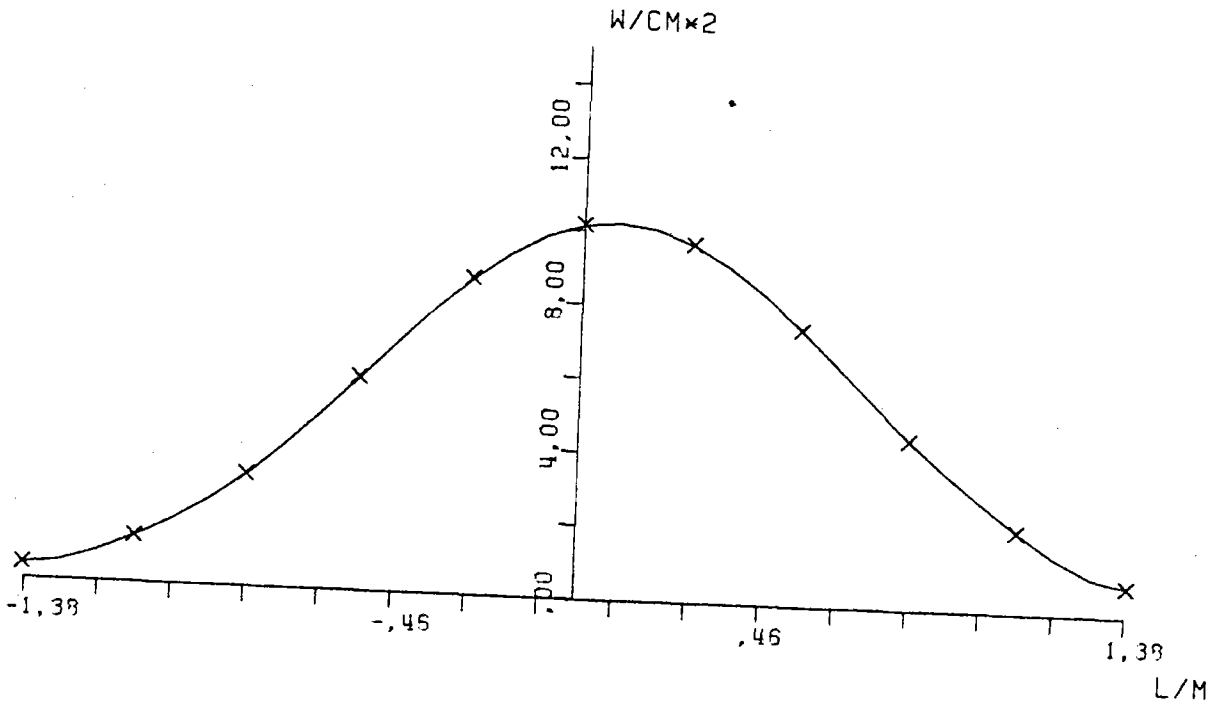

FIG.A.28 AVERAGE SOLAR FLUX ON VERTICAL STRIP

ALMERIA-ASR E-W CLOUD PASSAGE GROUP5

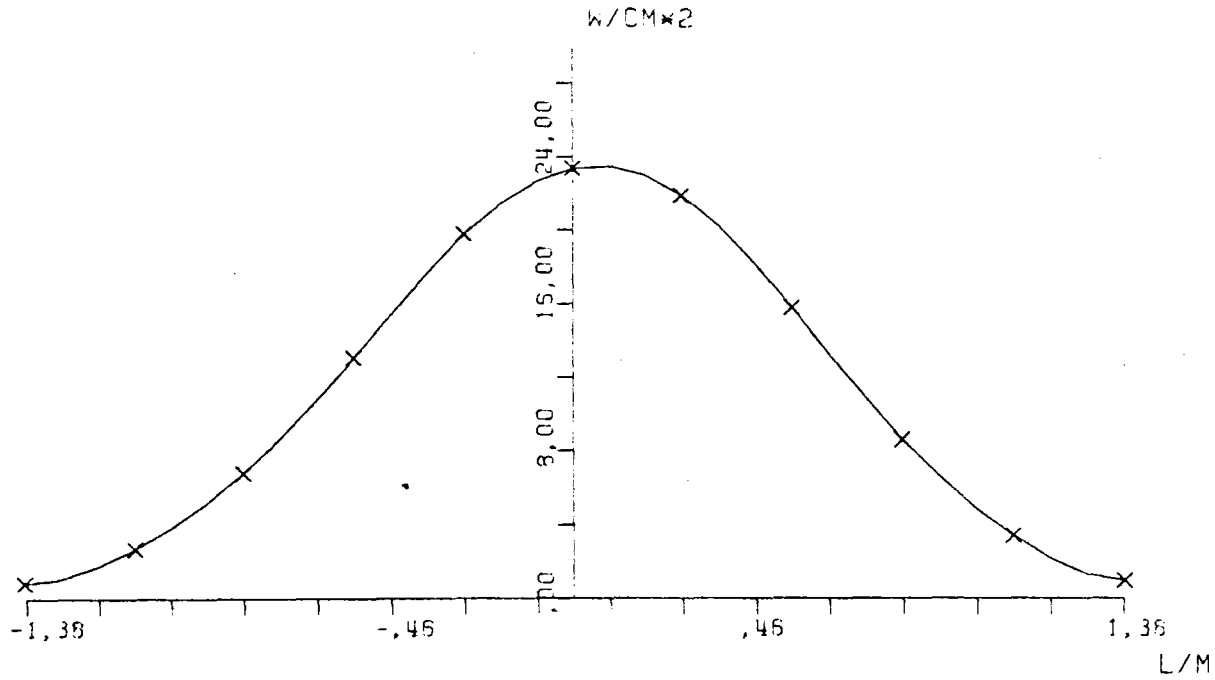

FIG.A.29 SOLAR FLUX ON TARGET SEC X-X

ALMERIA-ASR E-W CLOUD PASSAGE GROUPS

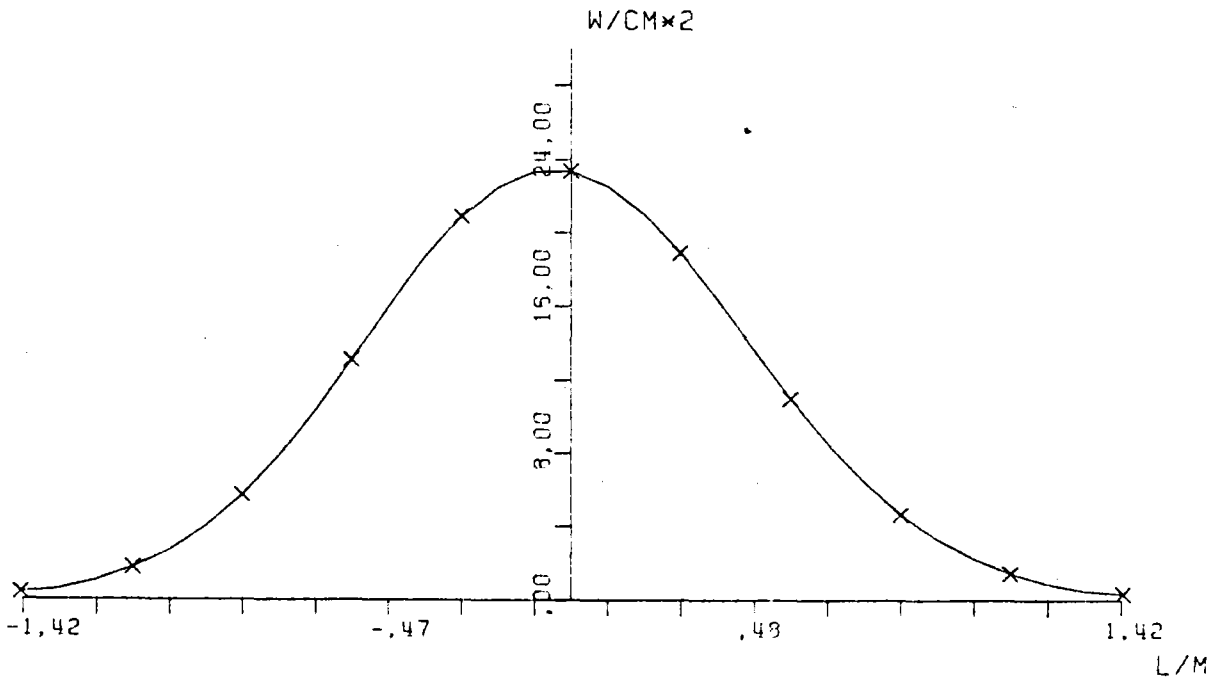

FIG.A.30 SOLAR FLUX ON TARGET SEC Y-Y

ALMERIA-ASR W-E CLOUD PASSAGE GROUP1234

	,04	,13	,35	,72	1,12	1,34	1,23	,67	,48	,20	,07
	,15	,51	1,37	2,65	4,54	5.48	4,38	3,45	1,84	,77	,25
	,43	1,51	4,15	8,05	14,6	17,7	15.8	10,6	5.33	2,15	,69
	1,05	3,70	10,2	22,0	35.6	43,0	37,6	24,7	12,3	4,90	1,60
	2,35	8.79	23,1	44,9	66,5	79.7	67,4	46.6	24,5	9,72	2,94
E.	4,58	20,0	52,2	84,6	99,6	101,	97,1	91,6	50,1	19,3	4,58	W.
	6.31	32,1	85,1	123,	117,	101,	111,	114,	78,1	28,9	5,68
	5,74	28.5	76,6	105,	91,2	71,9	84,9	96,5	68,6	25,2	4,50
	3,34	14,4	34,5	46,6	40,6	33,0	37,7	41,9	30,0	11,4	2,18
	1,14	3,75	7,71	10,5	10,5	9.67	9.71	9.13	6,25	2,62	,60
	,22	,57	1,07	1,58	1,91	1,96	1,75	1,33	,78	,34	,09

BØT.

HELST. NO. 79.
INSOL. KW/M2 ,920
DAY NO. 80,
TIME HR. 12,
TOWER HEIGHT M 43,
TARGET DIM. M 2,6X2,6

AIM. NO. 3,
STD.DEV. MRAD. 2,60
INC.POW. KW 2440,
AVERG./PEAK ,25
SPILLAGE %

FIG.A.31 INCIDENT FLUX ON FLAT TARGET (W/CM2)

ALMERIA-ASR W-E CLOUD PASSAGE GROUP1234

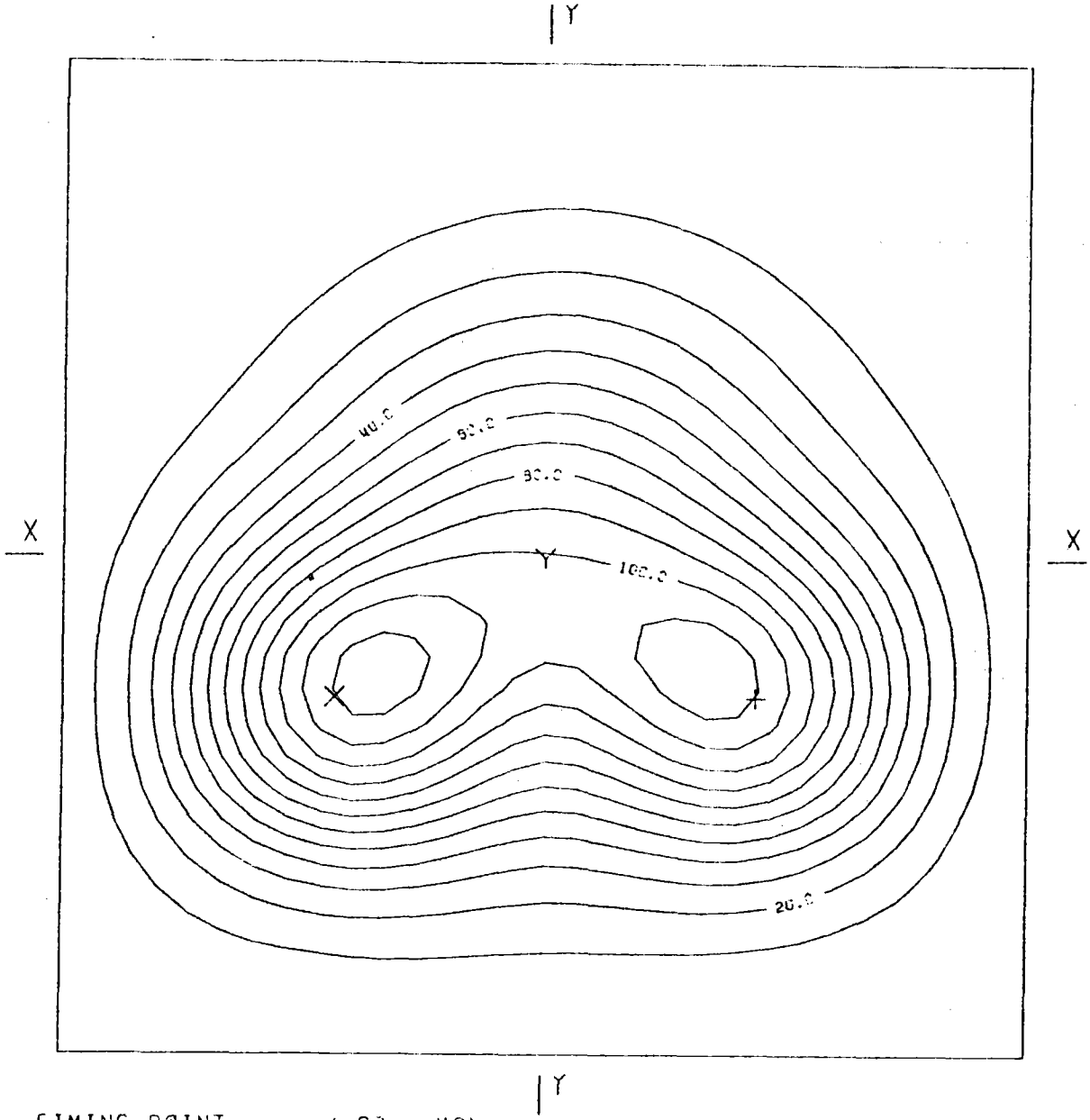

AIMING POINT: + (.60;-.40)

× (-.60;-.40)

Y (.00;.00)

FIG.A.32 EQUIFLUX LINES, SPACING (W/CM2) 10.0

ALMERIA-ASR W-E CLOUD PASSAGE GROUP1234

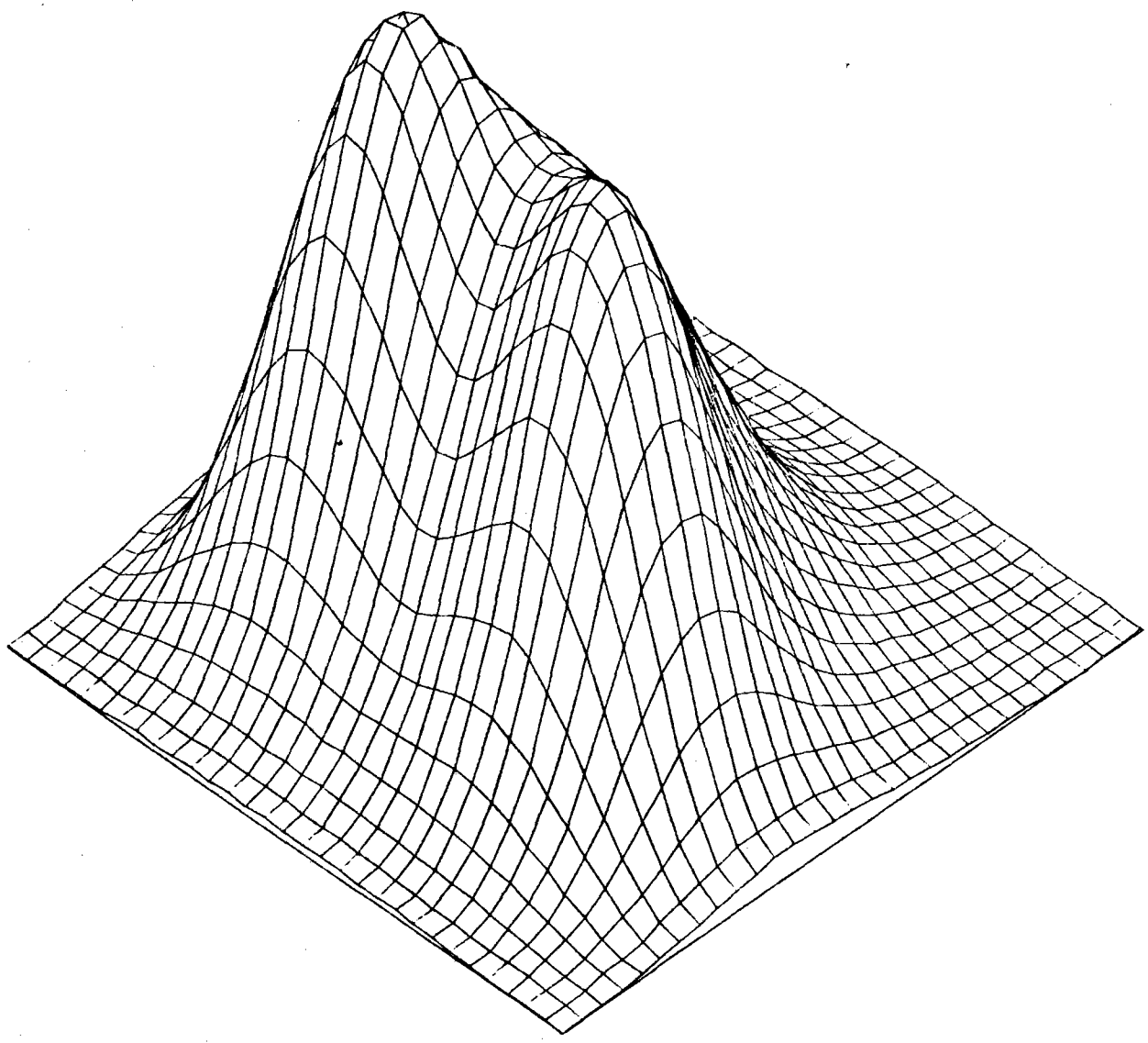

FIG.A.33 THREE-DIM. VIEW OF INCIDENT FLUX ON TARGET

SNAMPROGETTI

ALMERIA-ASR W-E CLOUD PASSAGE GROUP1234

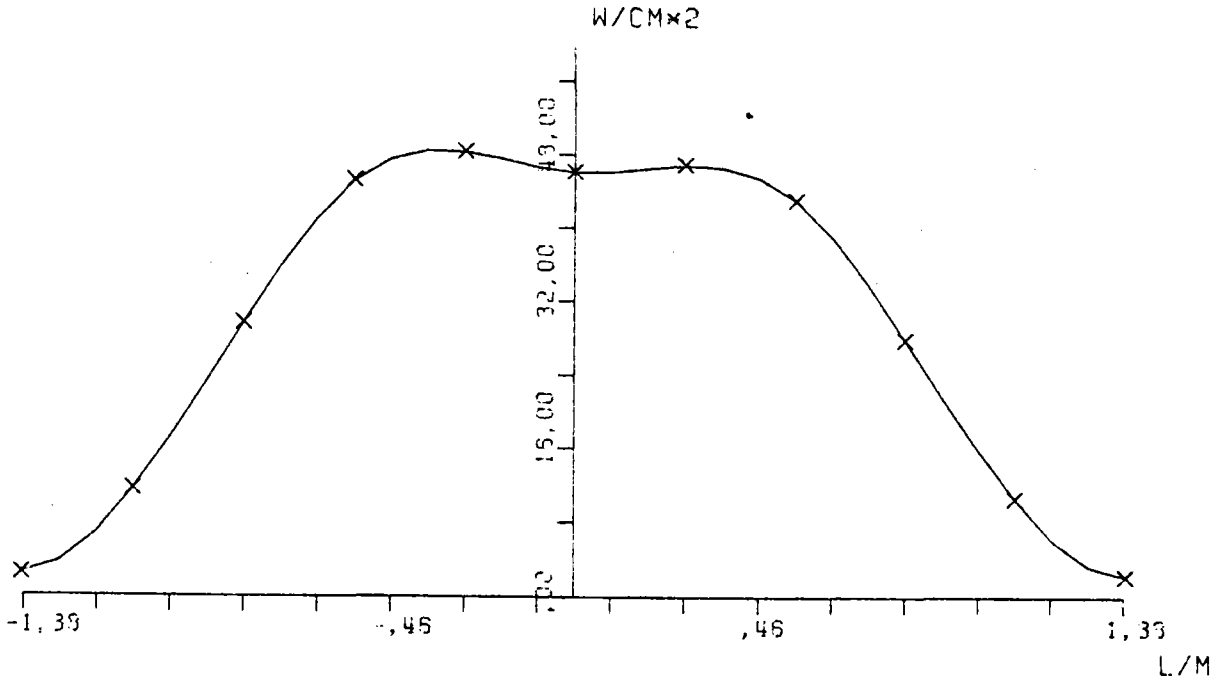

FIG.A.34 AVERAGE SOLAR FLUX ON VERTICAL STRIP

SNAMPROGETTI

ALMERIA-ASR W-E CLOUD PASSAGE GROUP1234

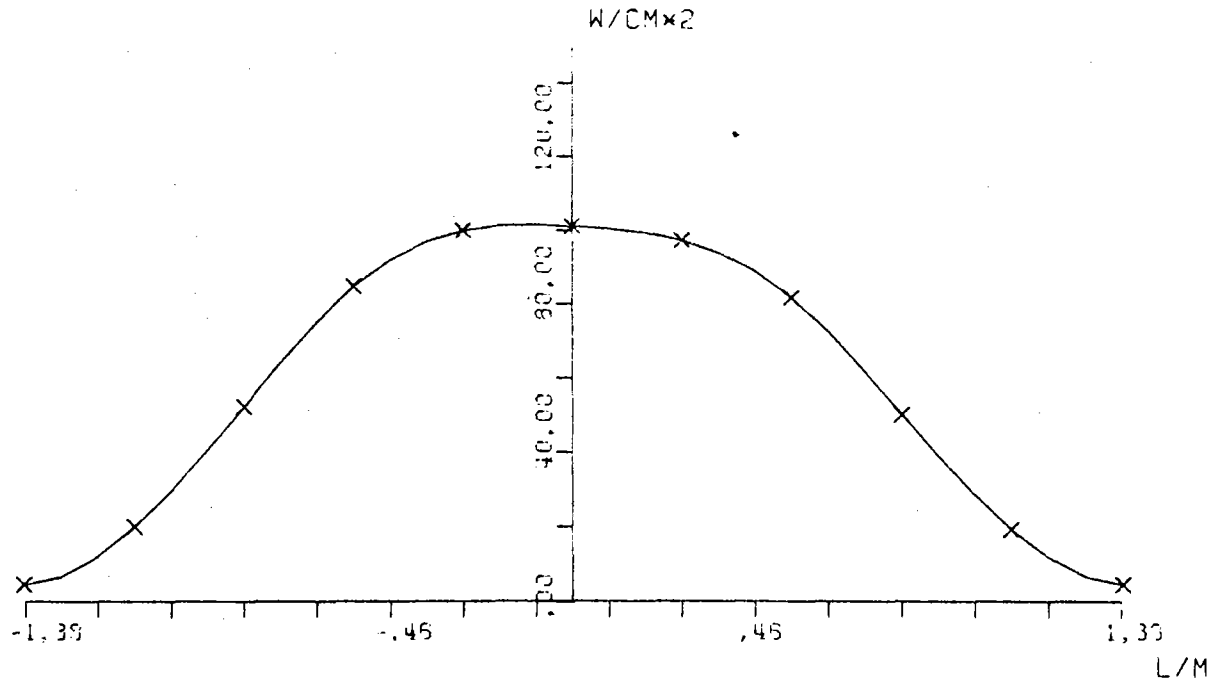

FIG.A.35 SOLAR FLUX ON TARGET SEC X-X

ALMERIA-ASR W-E CLOUD PASSAGE GROUP1234

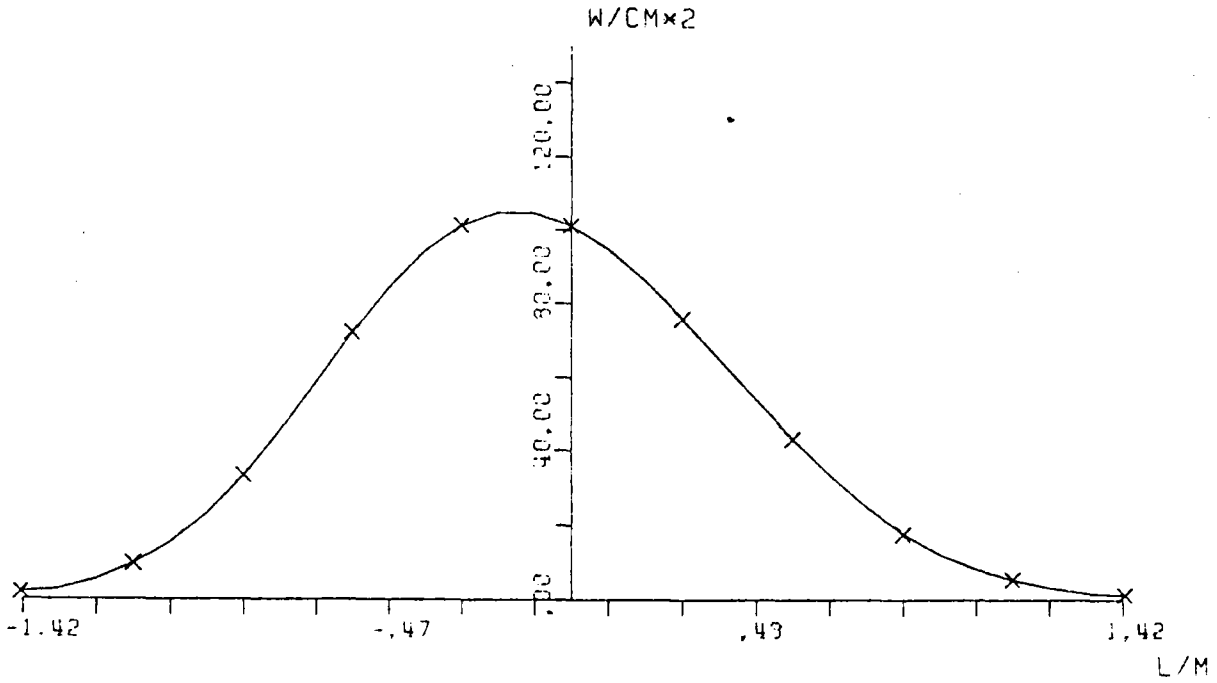

FIG.A.36 SOLAR FLUX ON TARGET SEC Y-Y

ALMERIA-ASR W-E CLOUD PASSAGE GROUP123

	,03	,09	.24	,51	,66	1,03	,89	.73	,41	,18	,05	
	.10	,35	.95	2,03	3,39	4,23	4,00	2,67	1,58	,67	.22	
	.29	1,04	2,31	5,42	10,5	13,5	12,6	8,73	4,58	1,68	,61	
	,69	2,51	7,22	16,0	25,5	32,7	29.5	19.9	10,3	4,13	1,32	
	1,37	5,41	15,9	33,2	50,2	67,2	61,2	39,3	20,1	8.30	2,49	
E.	2,53	11,5	35.0	62,4	76,4	75,9	71,9	62,2	40,4	16,3	4,05	W.
	4,01	20,9	58,7	89.1	88,2	76,2	93.0	87,7	61,5	23.3	4,61	
	4,44	22,2	56.0	75,5	65,1	53,2	65.3	74,4	52,3	18.5	3,14	
	2,93	12,1	26,6	33.1	27,5	23,6	29.5	32,0	21,1	7,11	1,19	
	1,07	3,39	5,31	7,62	7,12	6,34	7,52	6,75	4,01	1,35	.25	
	.21	,52	.90	1,22	1,39	1,45	1,33	.95	,50	,17	,04	

BOT.

HELST. NO. 59.
INSOL. KW/M2 ,320
DAY NO. 80,
TIME HR. 12,
TOWER HEIGHT M 43,
TARGET DIM. M 2,6X2,6

AIM. NO. 3,
STD.DEV. MRAD. 2,60
INC.POW. KW 1820,
AVERG./PEAK ,26
SPILLAGE %

FIG.A.37 INCIDENT FLUX ON FLAT TARGET (W/CM2)

SNAMPROGETTI

ALMERIA-ASR W-E CLOUD PASSAGE GROUP123

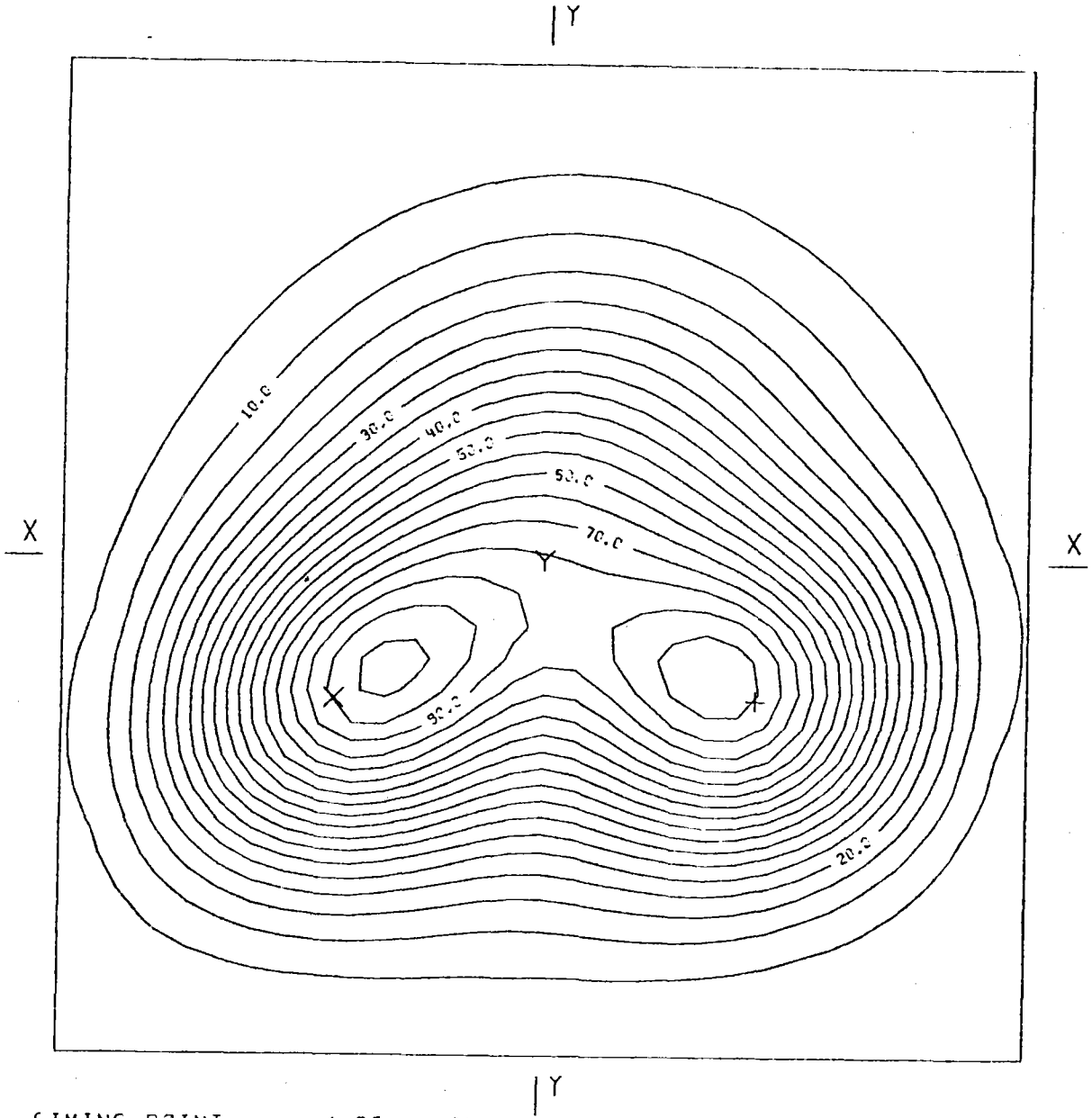

AIMING POINT: + (,60;-,40)

× (-,60;-,40)

Y (,00;,00)

FIG.A.38 EQUIFLUX LINES, SPACING (W/CM2) 5.0

ALMERIA-ASR W-E CLOUD PASSAGE GROUP123

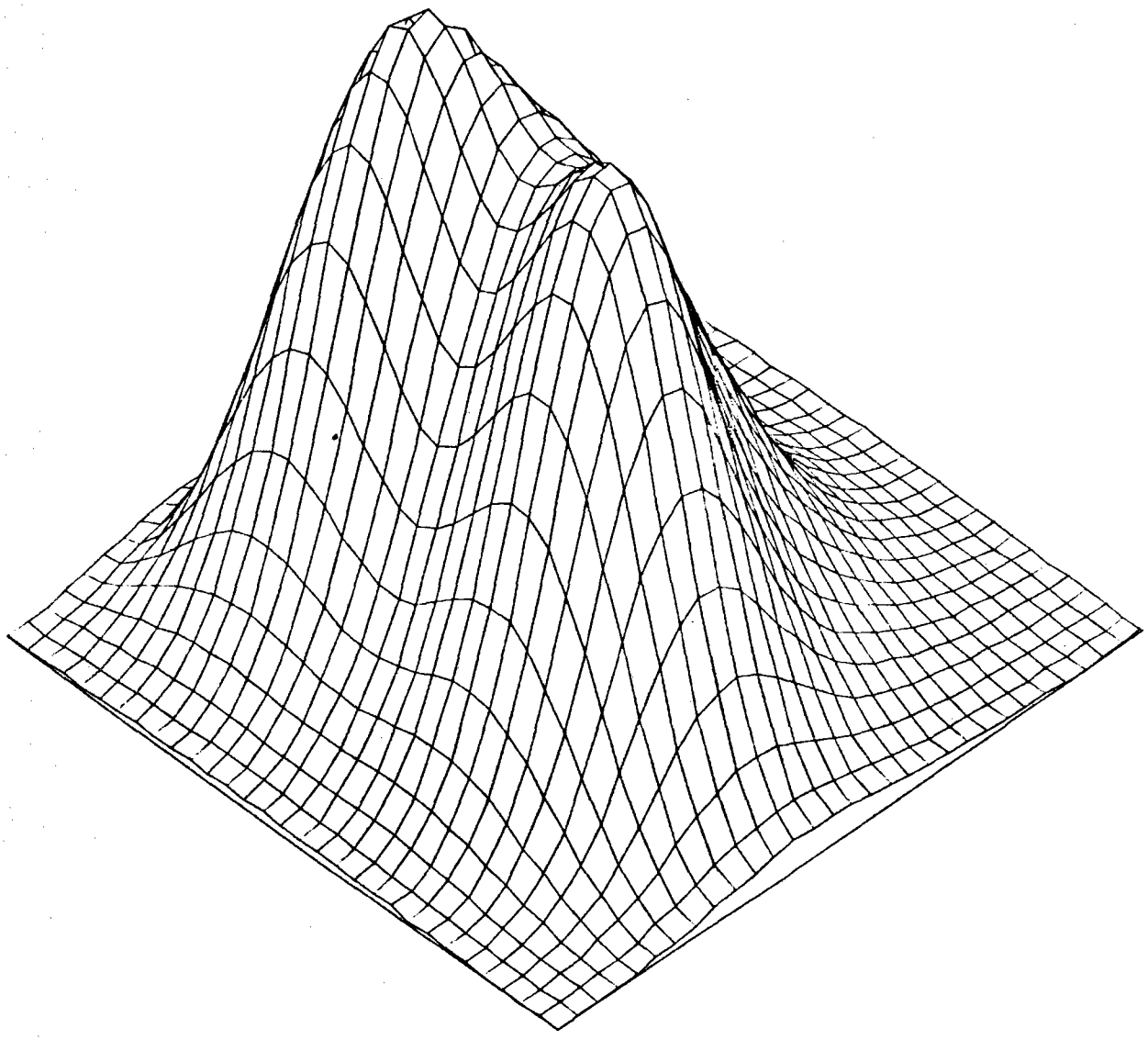

FIG.A.39 THREE-DIM. VIEW OF INCIDENT FLUX ON TARGET

SNAMPROGETTI

ALMERIA-ASR W-E CLOUD PASSAGE GROUP123

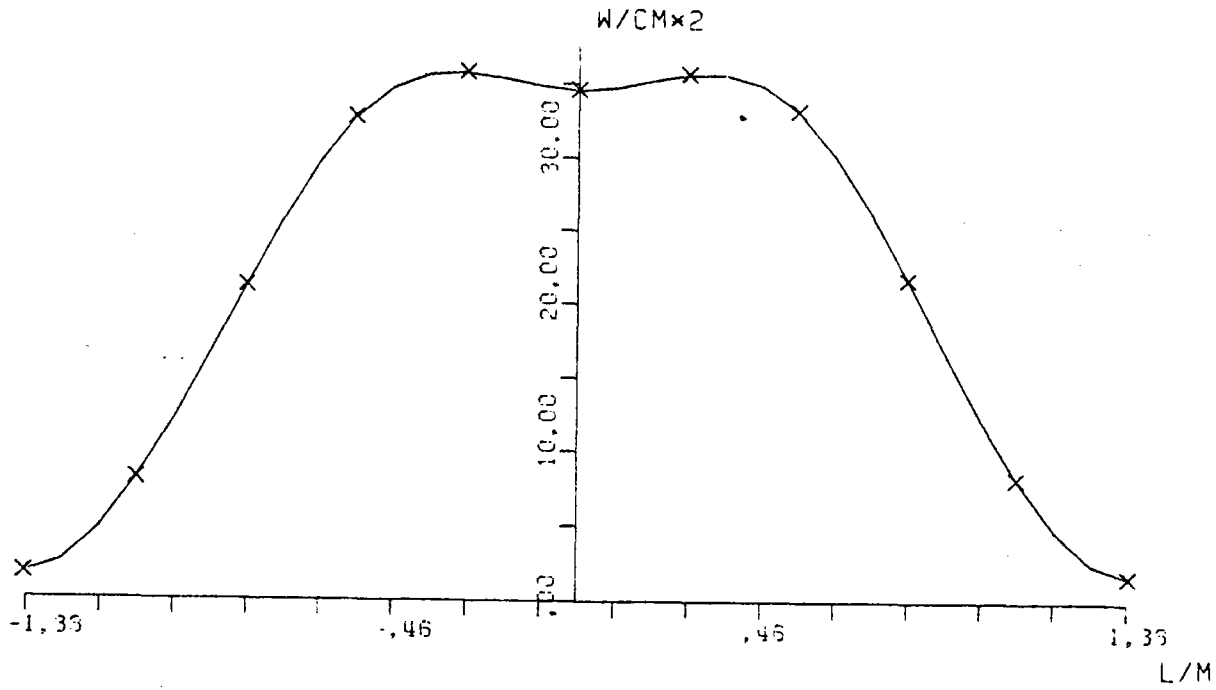

FIG.A.40 AVERAGE SOLAR FLUX ON VERTICAL STRIP

SNGMPROGETTI

ALMERIA-PSR W-E CLOUD PASSAGE GROUP123

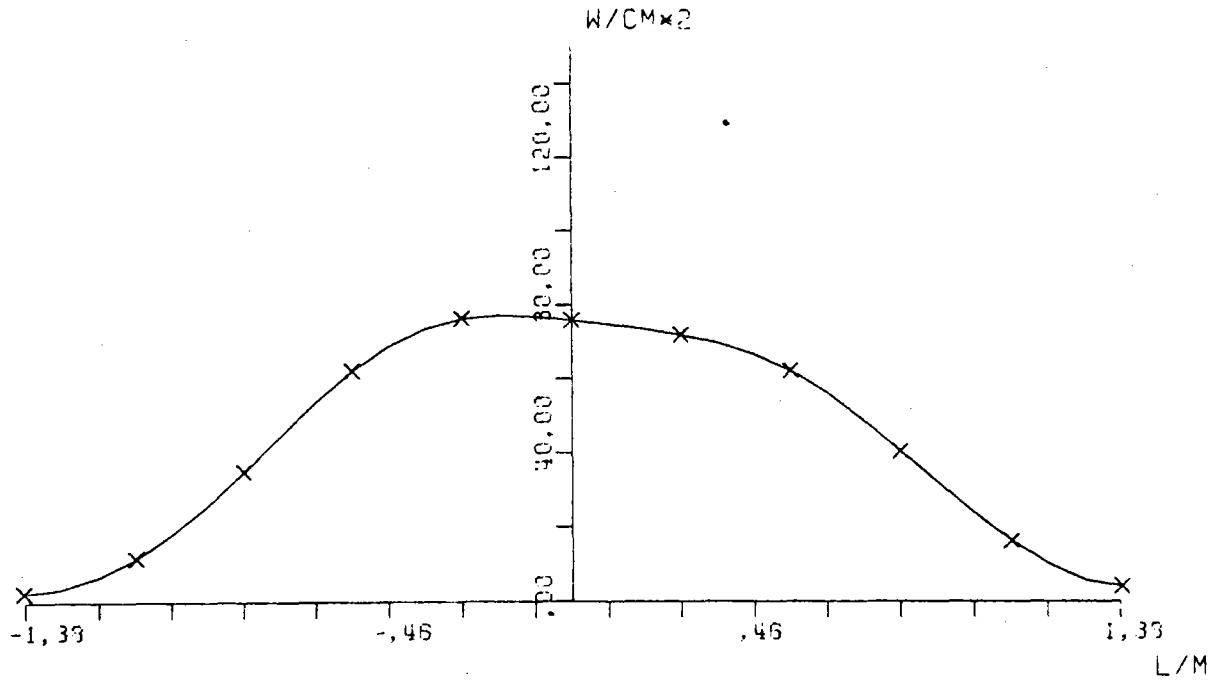

FIG.A.41 SOLAR FLUX ON TARGET SEC X-X

SNSMPROGLTT

ALMERIA-ASR W-E CLOUD PASSAGE GROUP123

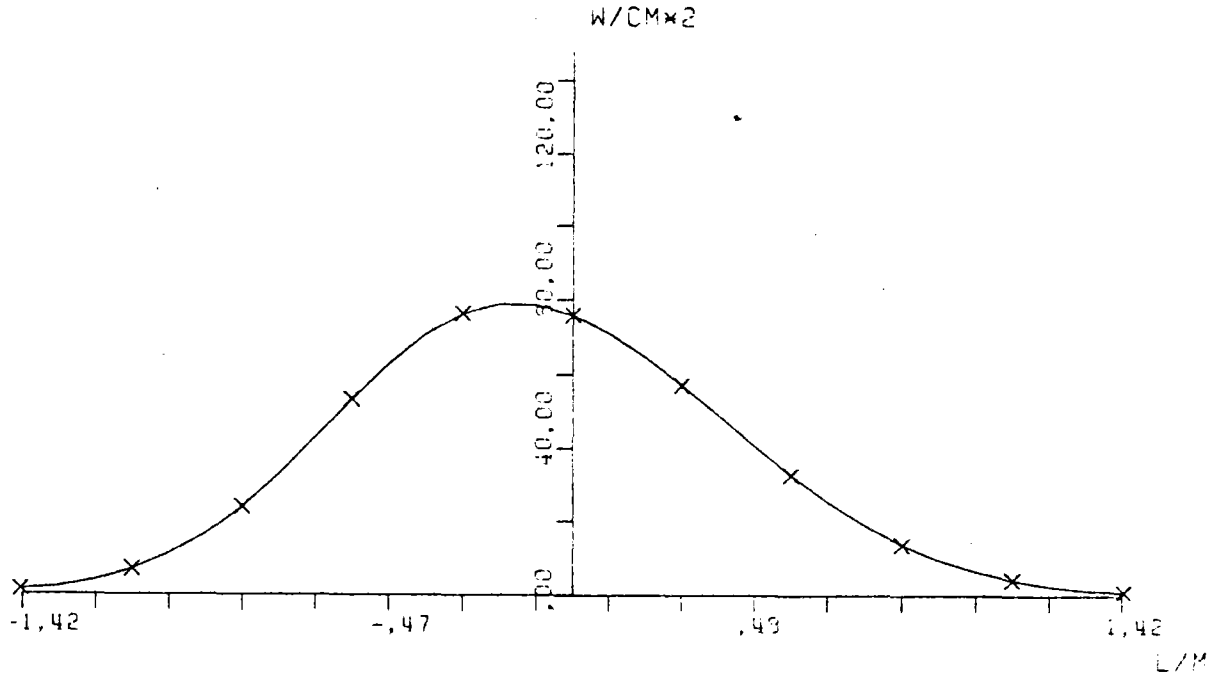

FIG.A.42 SOLAR FLUX ON TARGET SEC Y-Y

ALMERIA-ASR W-E CLOUD PASSAGE GROUP12

	,02	,05	,14	,30	,50	,66	,67	,52	,31	,14	,05	
	,05	,20	,56	1,21	2,05	2,71	2,70	2,05	1,19	,53	,18	
	,18	,64	1,76	3,30	5,71	8,76	8,53	5,21	3,43	1,47	,58	
	,45	1,57	4,47	9,37	16,3	21,2	19,5	13,3	7,53	3,20	1,08	
	,98	3,26	9,62	20,3	32,5	37,3	33,3	23,5	13,5	5,10	2,02	
E.	1,54	5,41	19,5	37,7	49,2	48,2	42,3	33,0	21,5	10,1	3,09	W.
	2,49	11,4	31,3	51,1	54,2	46,3	42,2	37,3	25,5	11,3	3 10	
	3,09	13,5	31,7	42,1	37,5	31,5	31,5	29,2	18,3	7,45	1,65	
	2,34	8,49	16,4	18,5	15,7	14,5	15,5	13,7	7,51	2,74	,63	
	,93	2,62	4,24	4,53	4,32	4,51	4,51	3,54	1,50	,50	,14	
	,19	,43	,65	,51	,32	,37	,57	,58	,28	,09	,02	

BOT.

HELST. NO. 34,
INSOL. KW/M2 ,920
DAY NO. 80,
TIME HR. 12,
TOWER HEIGHT M 43.
TARGET DIM. M 2,8X2,5

AIM. NO. 3,
STD.DEV. MRAD. 2,60
INC.POW. KW 1040,
AVERG./PEAK ,24
SPILLAGE %

FIG.A.43 INCIDENT FLUX ON FLAT TARGET (W/CM2)

ALMERIA-ASR W-E CLOUD PASSAGE GROUP12

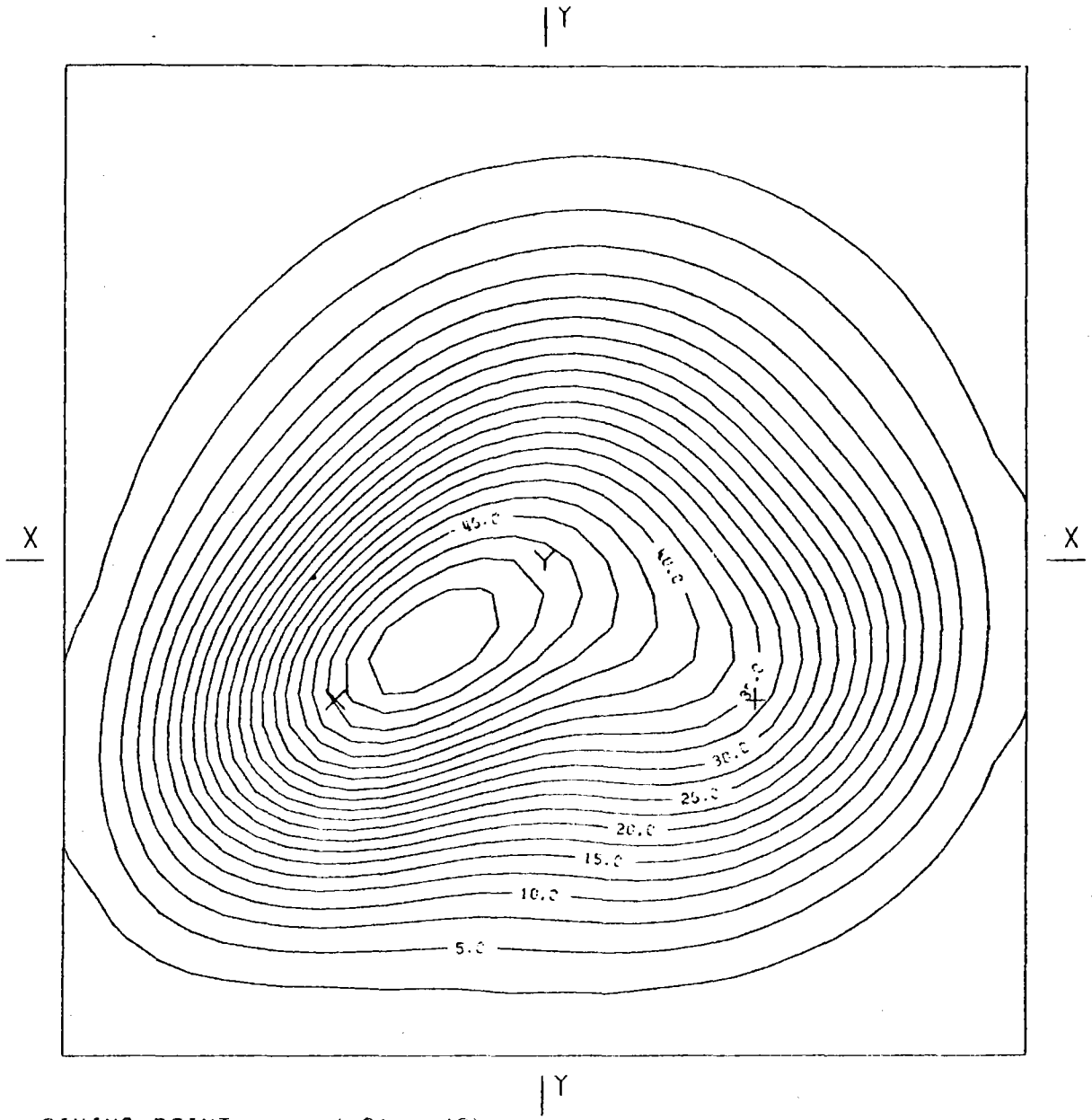

AIMING POINT: + (,60;-,40)

× (-,60;-,40)

Y (,00;,00)

FIG.A.44 EQUIFLUX LINES, SPACING (W/CM2) 2,5

ALMERIA-ASR W-E CLOUD PASSAGE GROUP12

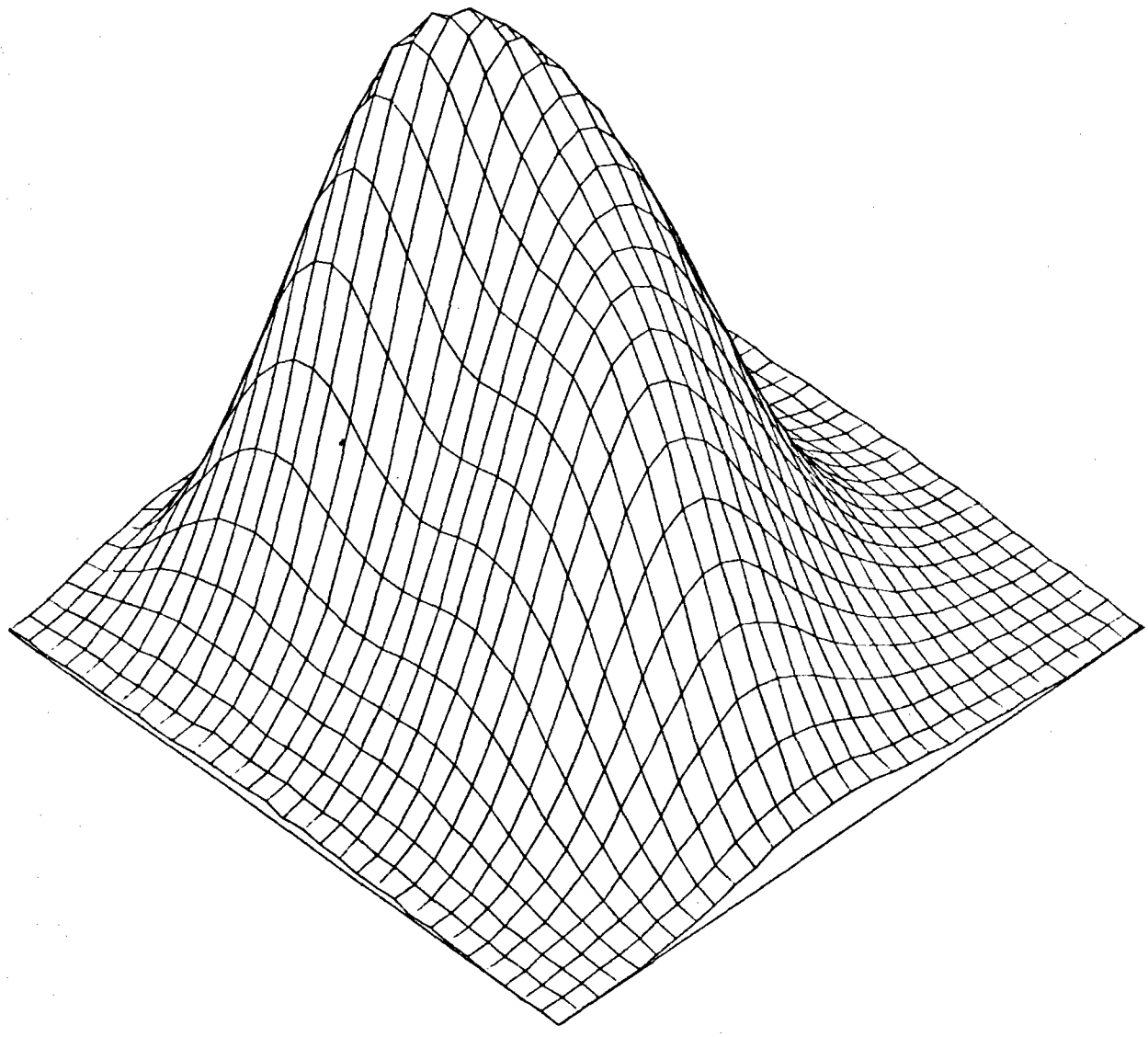

FIG.A.45 THREE-DIM. VIEW OF INCIDENT FLUX ON TARGET

ALMERIA-ASR W.-E CLOUD PASSAGE GROUP12

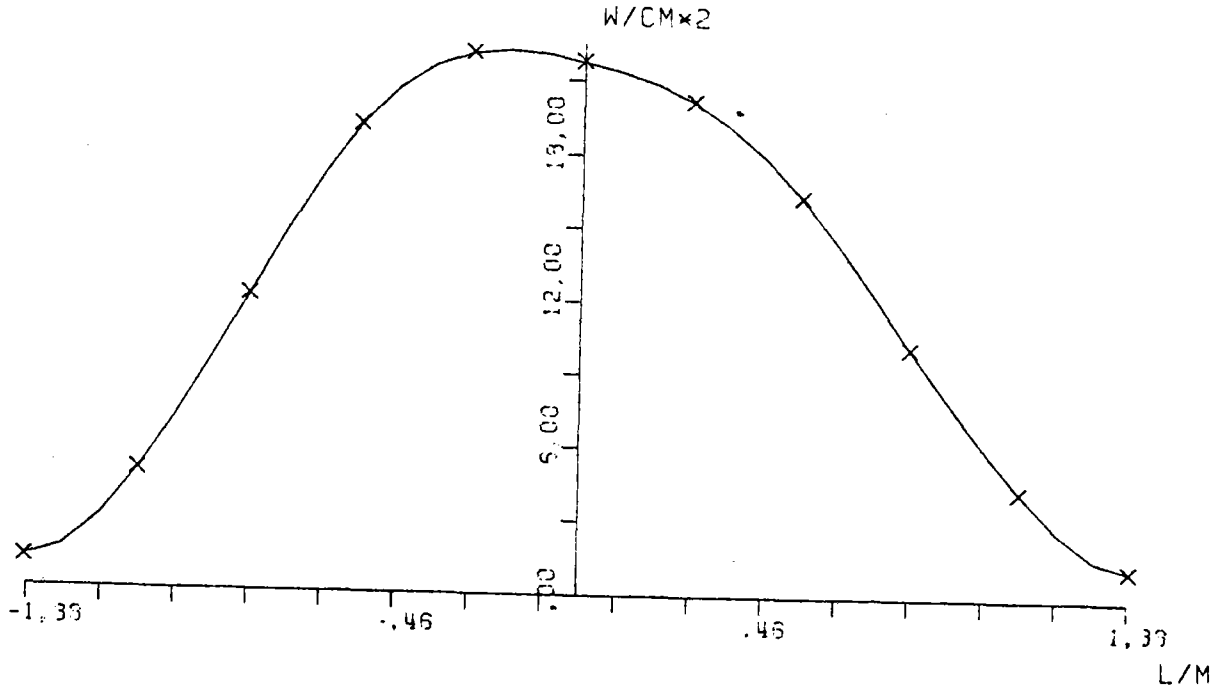

FIG.A.46 AVERAGE SOLAR FLUX ON VERTICAL STRIP

SNAMPROGETTI

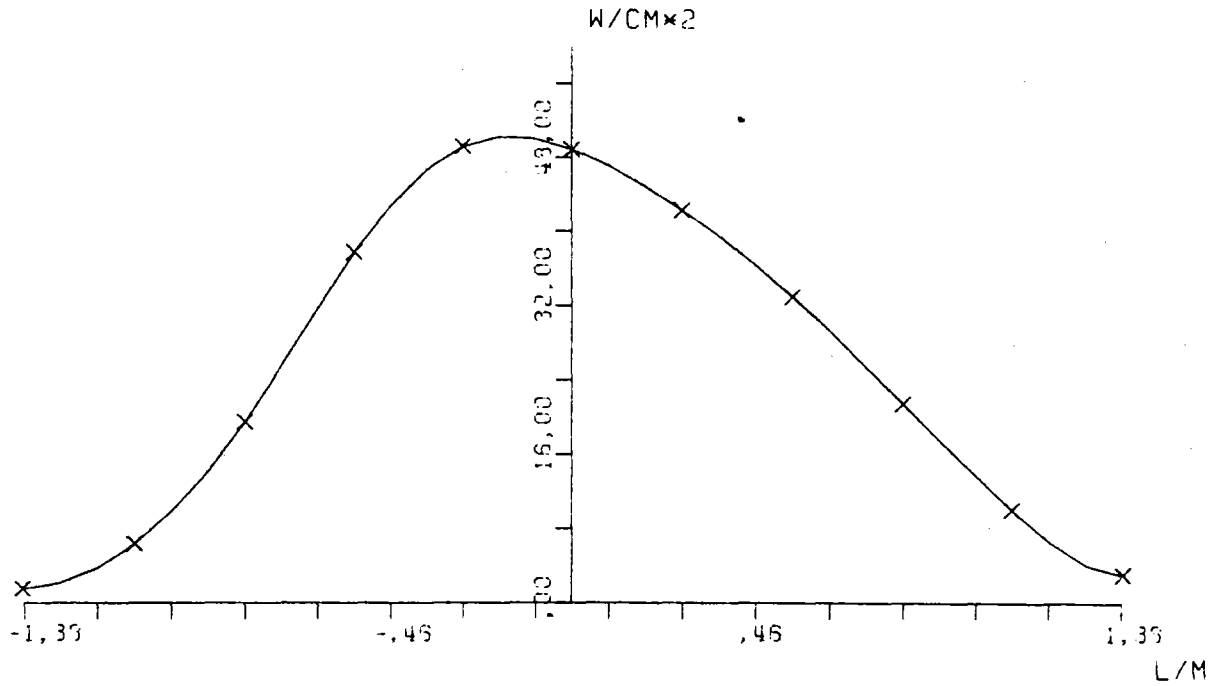

FIG.A.47 SOLAR FLUX ON TARGET SEC X-X

ALMERIA-ASR W-E CLOUD PASSAGE GROUP12

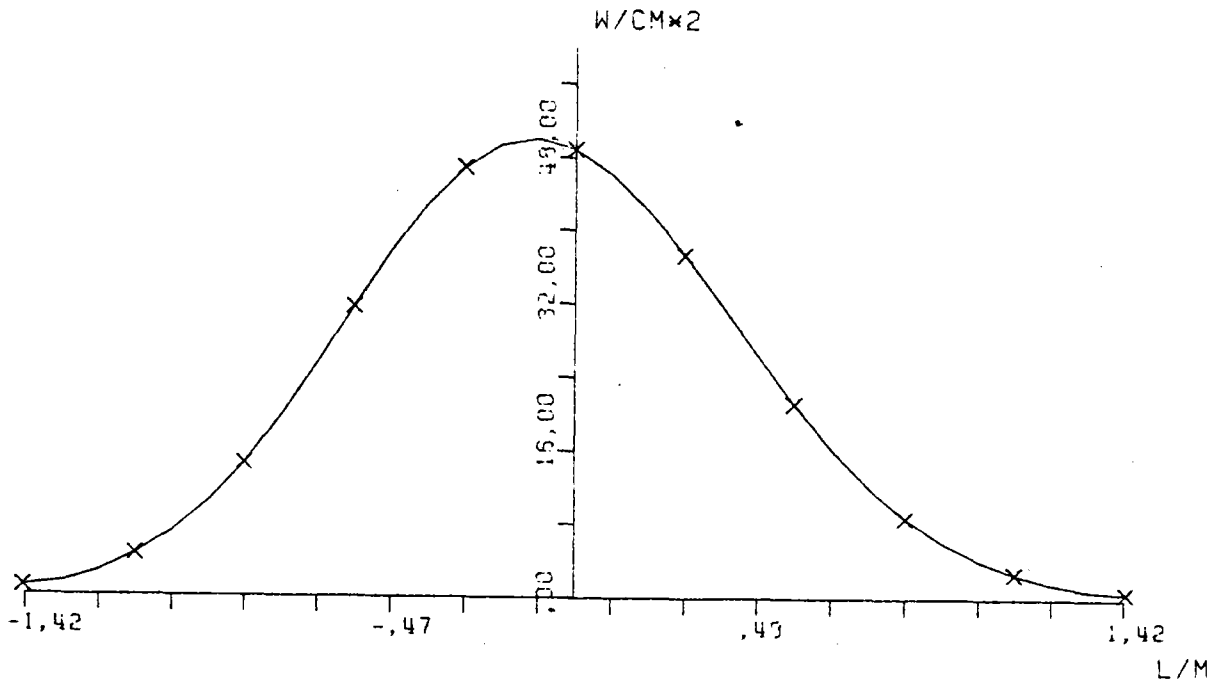

FIG.A.48 SOLAR FLUX ON TARGET SEC Y-Y

ALMERIA-ASR W-E CLOUD PASSAGE GROUP1

	,01	,03	,07	,15	,26	,36	,36	,31	,20	,10	,04
	,03	,11	,23	,53	1,06	1,46	1,53	1,24	,77	,36	,13
	,10	,35	,95	2,05	3,40	4,53	4,73	3,90	2,20	1,01	,35
	,27	,30	2,43	5,13	8,57	10,3	10,5	7,36	4,61	2,09	,76
	,54	1,53	4,59	8,33	15,5	18,4	17,0	12,4	7,19	3,33	1,25
E.	,90	3,02	7,53	14,2	20,3	22,5	20,1	14,5	8,50	4,06	1,57	W.
	1,23	3,54	8,59	14,7	19,4	20,4	17,7	12,7	7,53	3,57	1,37
	1,27	3,54	7,03	10,3	13,3	13,5	11,6	8,32	4,31	2,27	,78
	,91	2,21	3,35	5,52	6,41	6,40	5,47	3,90	2,16	,91	,28
	,40	,58	1,43	1,53	2,15	2,15	1,61	1,20	,51	,23	,06
	,10	,21	,33	,44	,52	,51	,41	,25	,12	,04	,01

BOT.

HELST. NO. 14,
INSOL. KW/M2 ,920
DAY NO. 80,
TIME HR. 12,
TOWER HEIGHT M 43,
TARGET DIM. M 2,6X2,6

AIM. NO. 3,
STD.DEV. MRAD. 2,60
INC.POW. KW 413,
AVERG./PEAK ,24
SPILLAGE %

FIG.A.49 INCIDENT FLUX ON FLAT TARGET (W/CM2)

ALMERIA-ASR WE CLOUD PASSAGE GROUP1

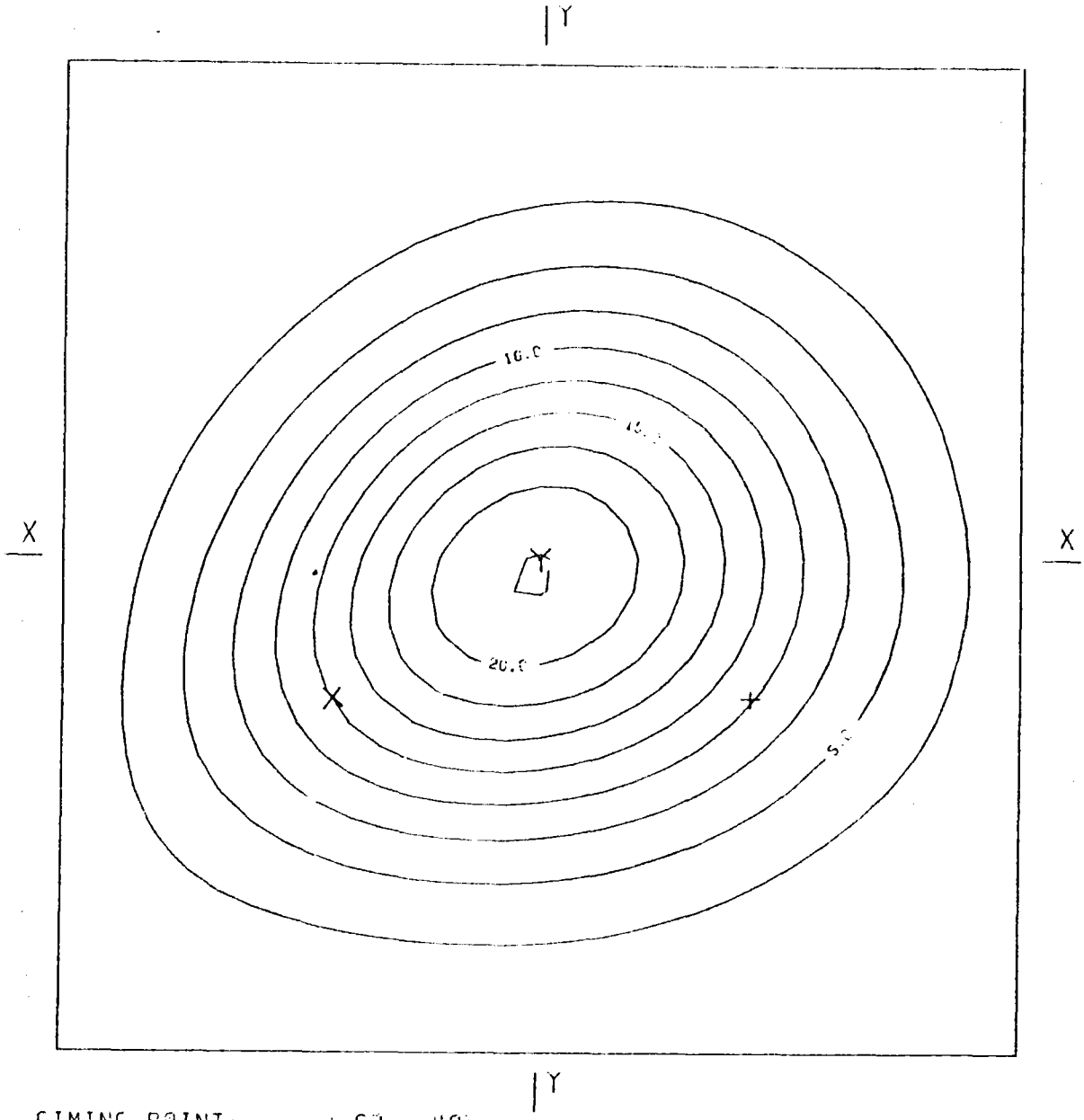

AIMING POINT: + (.50; -.40)
× (-.60; -.40)
Y (.00; .00)

FIG.A.50 EQUIFLUX LINES, SPACING (W/CM2) 2.5

ALMERIA-ASR W-E CLOUD PASSAGE GROUP1

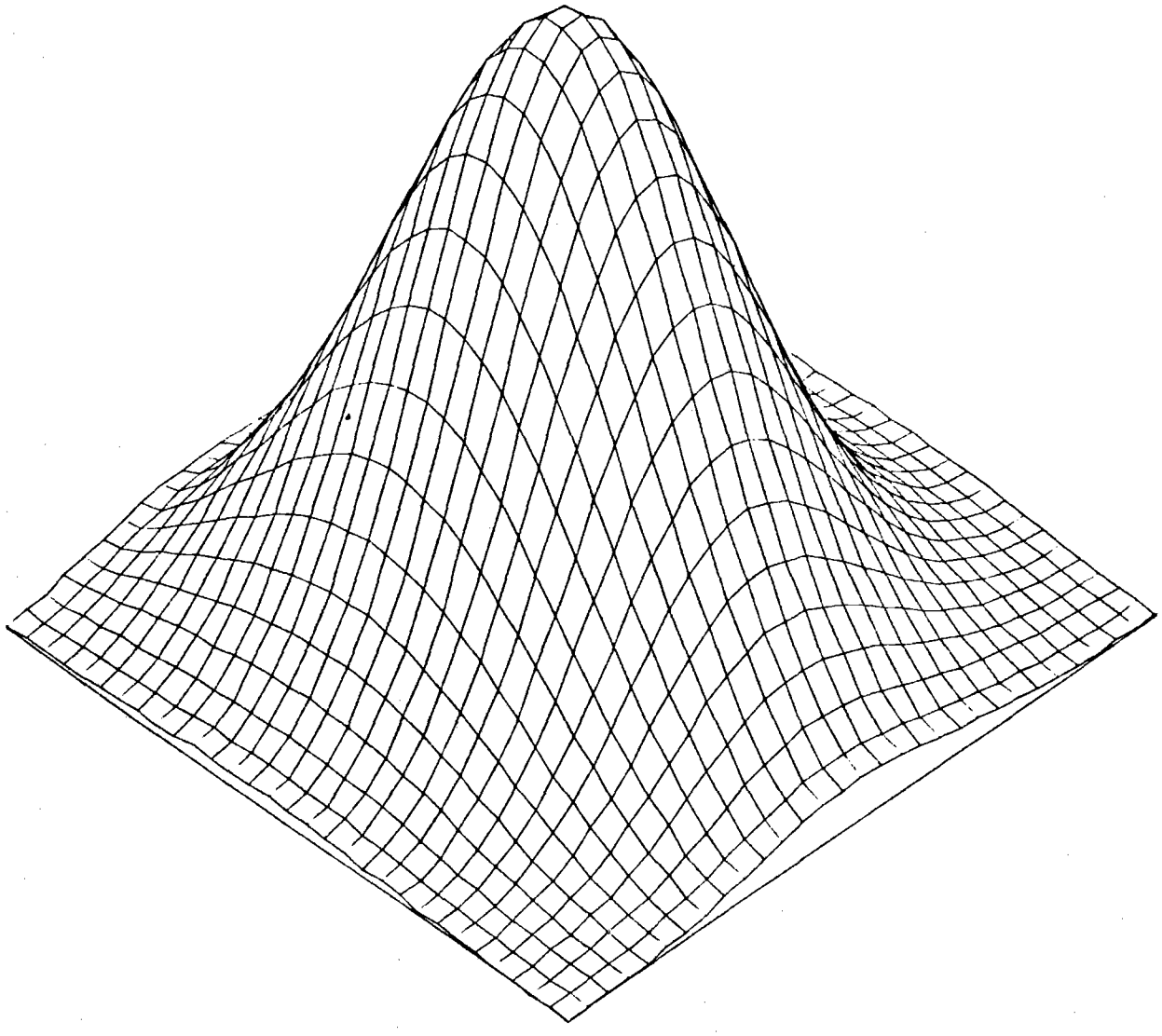

FIG A.51 TARGET DIM. VIEW OF INCIDENT FLUX ON TARGET

ALMERIA-ASR W-E CLOUD PASSAGE GROUP1

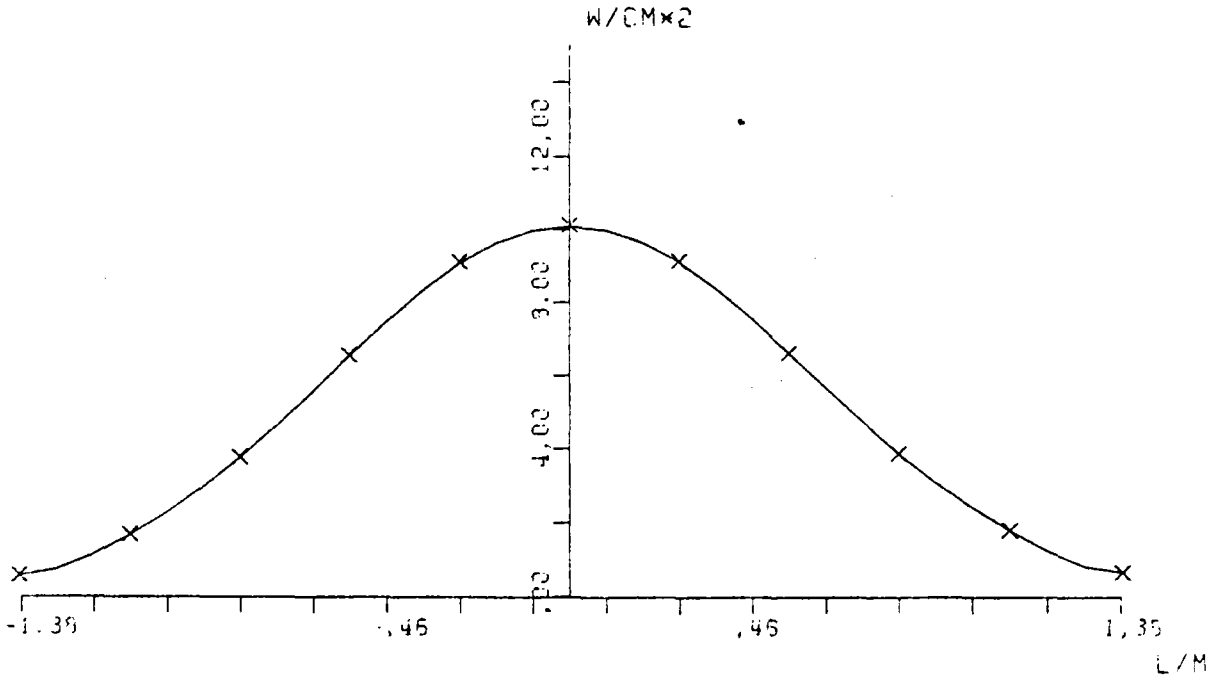

FIG.A.52 AVERAGE SOLAR FLUX ON VERTICAL STRIP

SNGMPROCETTI

ALMERIA-ASR W-E CLOUD PASSAGE GROUP1

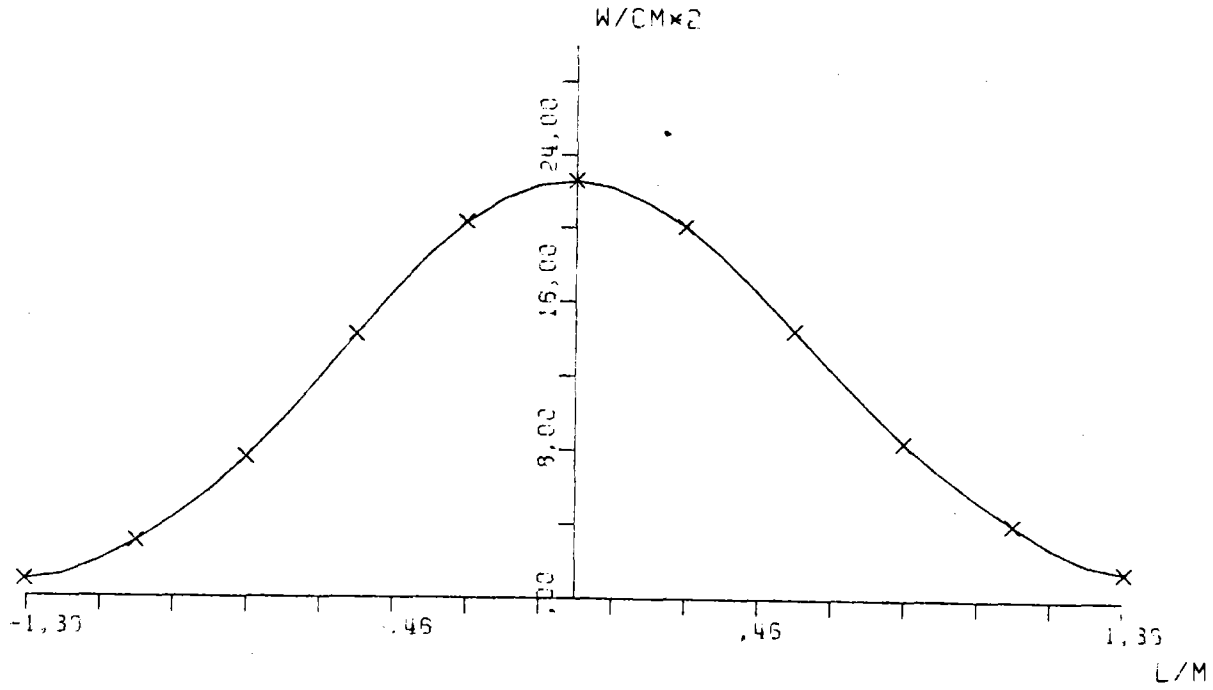

FIG.A.53 SOLAR FLUX ON TARGET SEC X-X

ALMERIA-ASR W-E CLOUD PASSAGE GROUP1

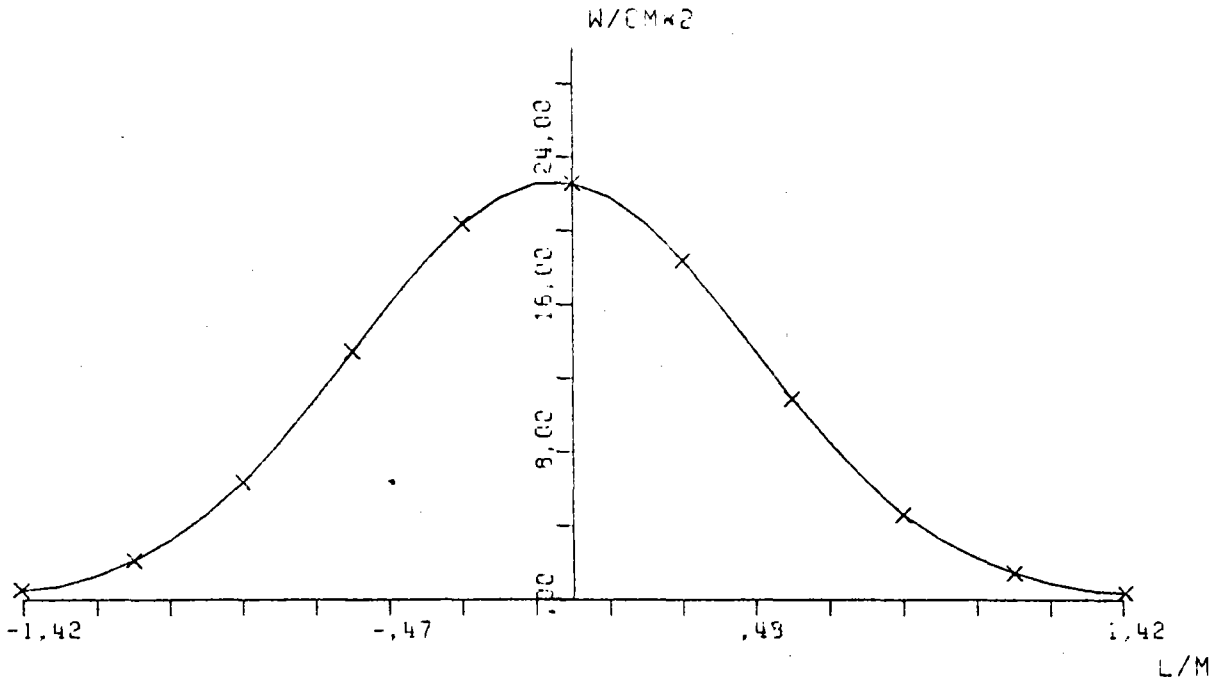

FIG.A.54 SOLAR FLUX ON TARGET SEC Y-Y

ASR-ALMERIA E-W CLOUD 21/3 H9.30 12345

	,15	.44	1,04	1,91	2,73	3,06	2,73	2,00	1,24	,68	.34	
	,47	1,34	3,07	5,48	7,55	8.17	7,12	5.17	3,24	1,60	,82	
	1,17	3,34	7,61	13,2	17,6	19,6	16,3	11,9	7,38	4,02	2,10	
	2,40	6,86	15.7	25.9	33,6	36,6	32,6	24,1	14,6	7,31	4,15	
	4,24	12,7	27,5	42,1	53,0	57,9	54,6	42,4	25,1	13,9	6,63	
E.	6,36	19.7	41,4	59.4	68,6	73,3	73,9	63,2	41,6	21,5	9.13	W.
	7,46	23,0	48,2	67,6	73,3	72,9	76,9	73,1	52.9	27,0	9.33	
	6,60	19.1	39.6	56,4	59.6	56,0	53,9	60,1	47,7	25,3	5,54	
	5,11	12,0	22,7	32,9	35.9	32,6	33,1	34,2	29.0	16,0	5,31	
	3,20	6,26	10,00	14,3	16,3	15.0	14,4	14,2	12,2	6,73	2,25	
	1,62	2,77	3,60	5,29	6,06	5.60	5,13	4,79	3,93	2,08	,67	

BOT.

HELST. NO. 93,
INSOL. KW/M2 ,750
DAY NO. 80,
TIME HR. 9.30
TOWER HEIGHT M 43,
TARGET DIM. M 2,6X2,6

AIM. NO. 5.
STD.DEV. MRAD. 2,60
INC.POW. KW 1970,
AVERG./PEAK ,33
SPILLAGE %

FIG.A.55INCIDENT FLUX ON FLAT TARGET (W/CM2)

ASR-ALMERIA E-W CLOUD 21/3 H9.30 12345

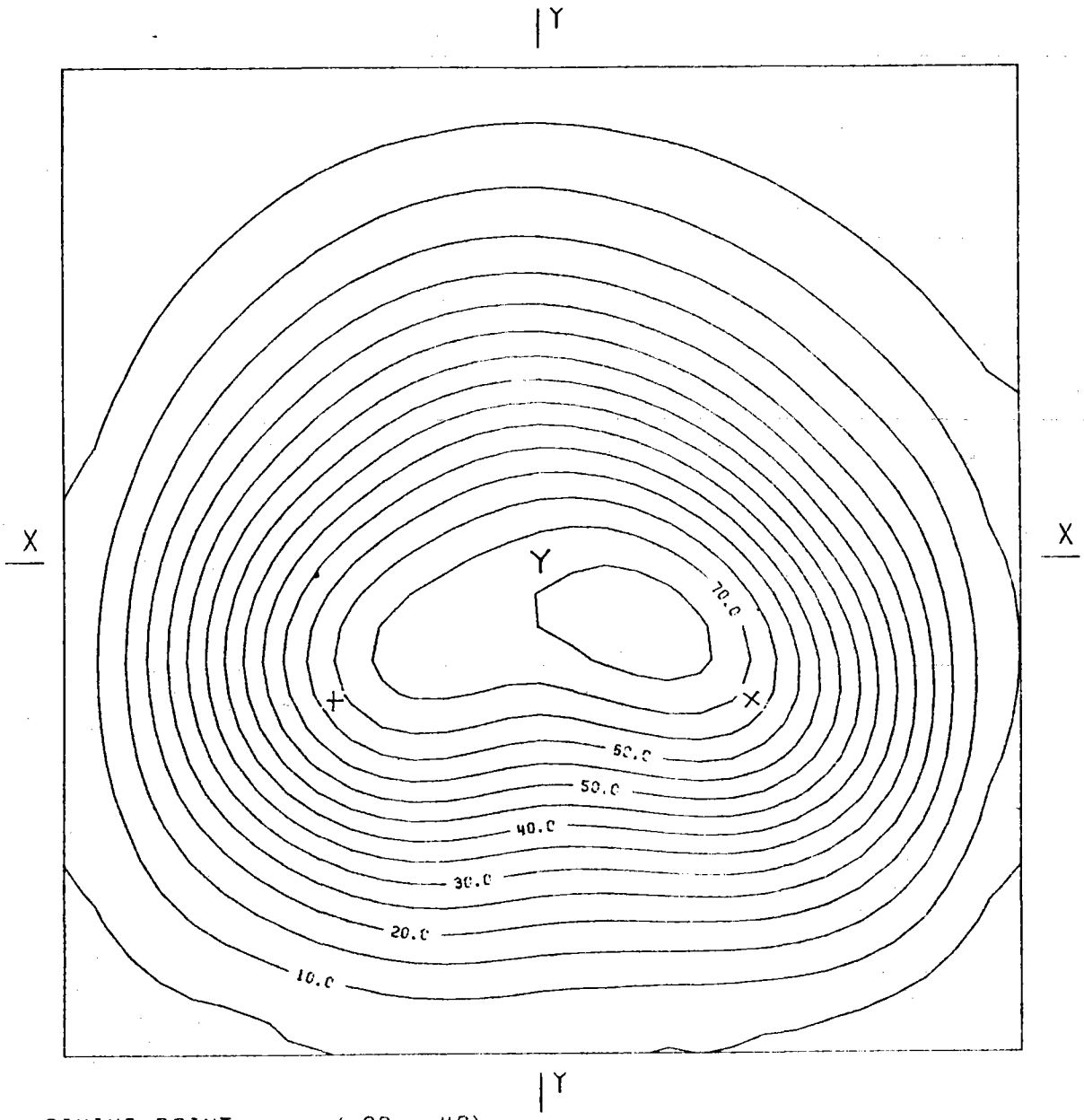

AIMING POINT: + (,60;-,40)

× (-,60;-,40)

Y (,00; ,00)

FIG.A.56 EQUIFLUX LINES, SPACING (W/CM2) 5.0

ASR-ALMERIA E-W CLOUD 21/3 H9.30 12345

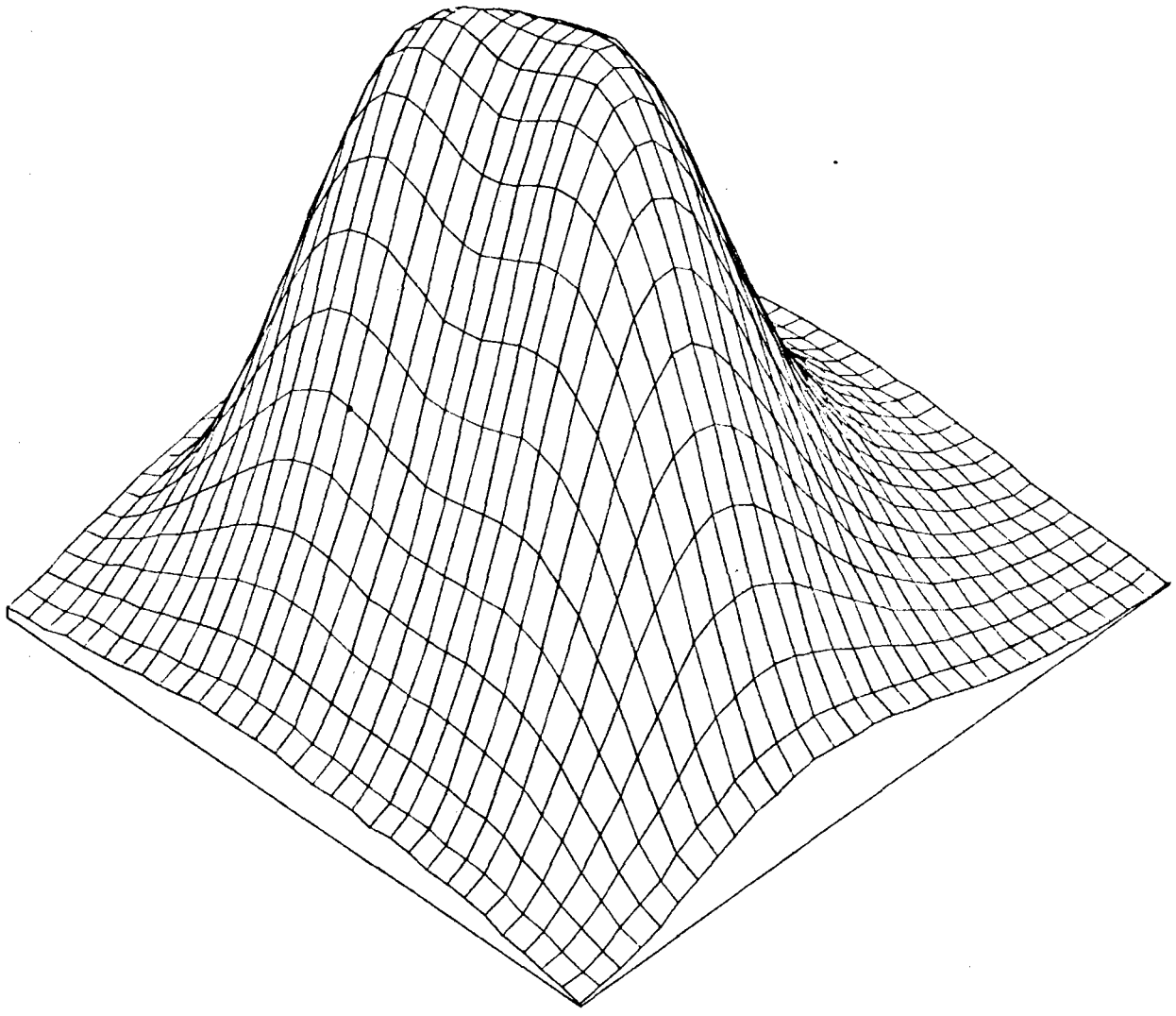

FIG.A.57 THREE-DIM. VIEW OF INCIDENT FLUX ON TARGET

SNAMPROGETTI

ASR-ALMERIA E-W CLOUD 21/3 H9.30 12345

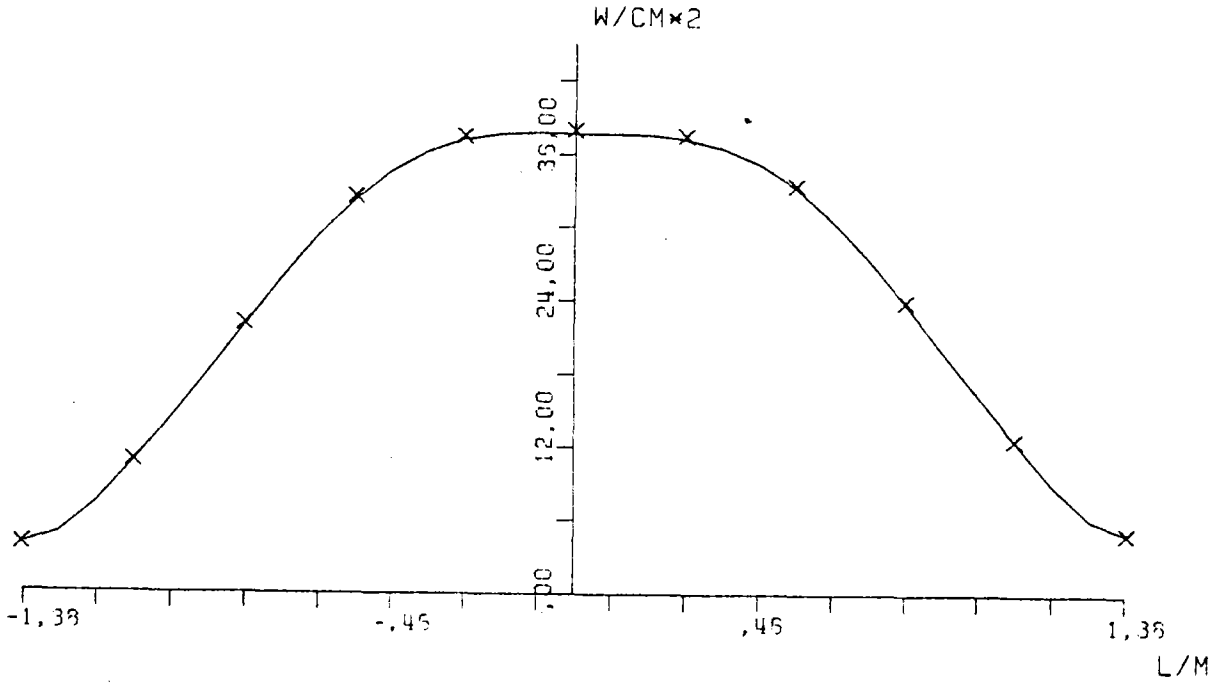

FIG.A.58 AVERAGE SOLAR FLUX ON VERTICAL STRIP

ASR-ALMERIA E-W CLOUD 21/3 H9.30 12345

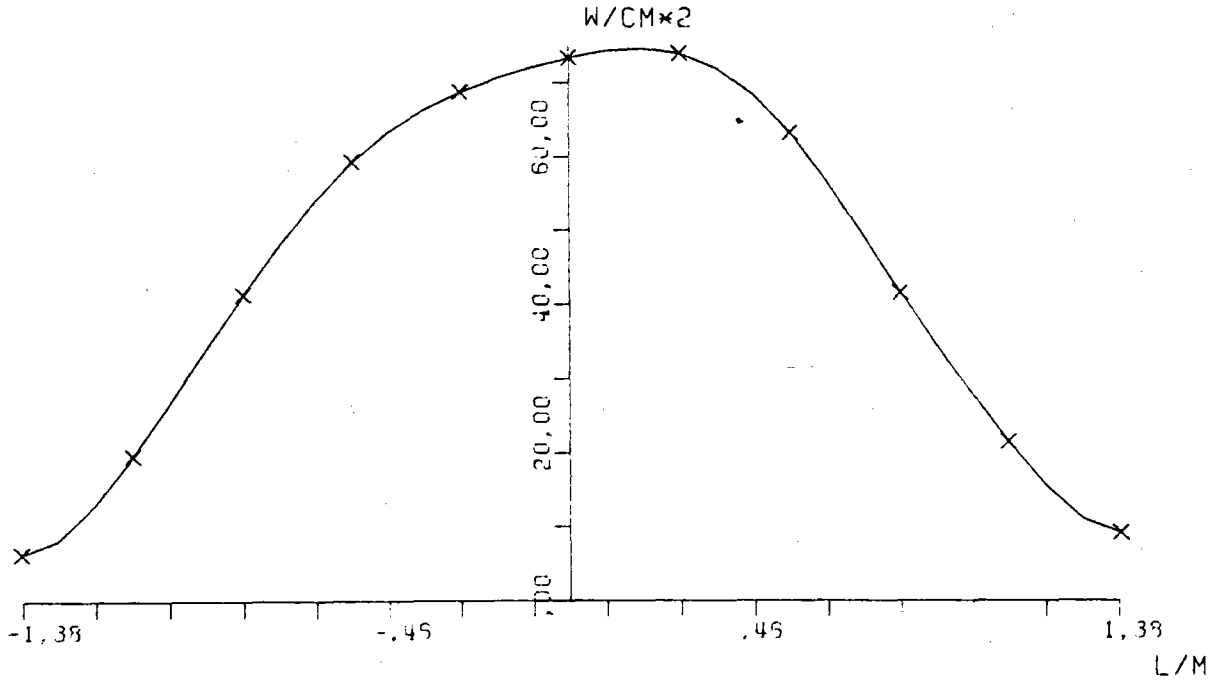

FIG.A.59 SOLAR FLUX ON TARGET SEC X-X

SNAMPROGETTI

ASR-ALMERIA E-W CLOUD 21/3 H9.30 12345

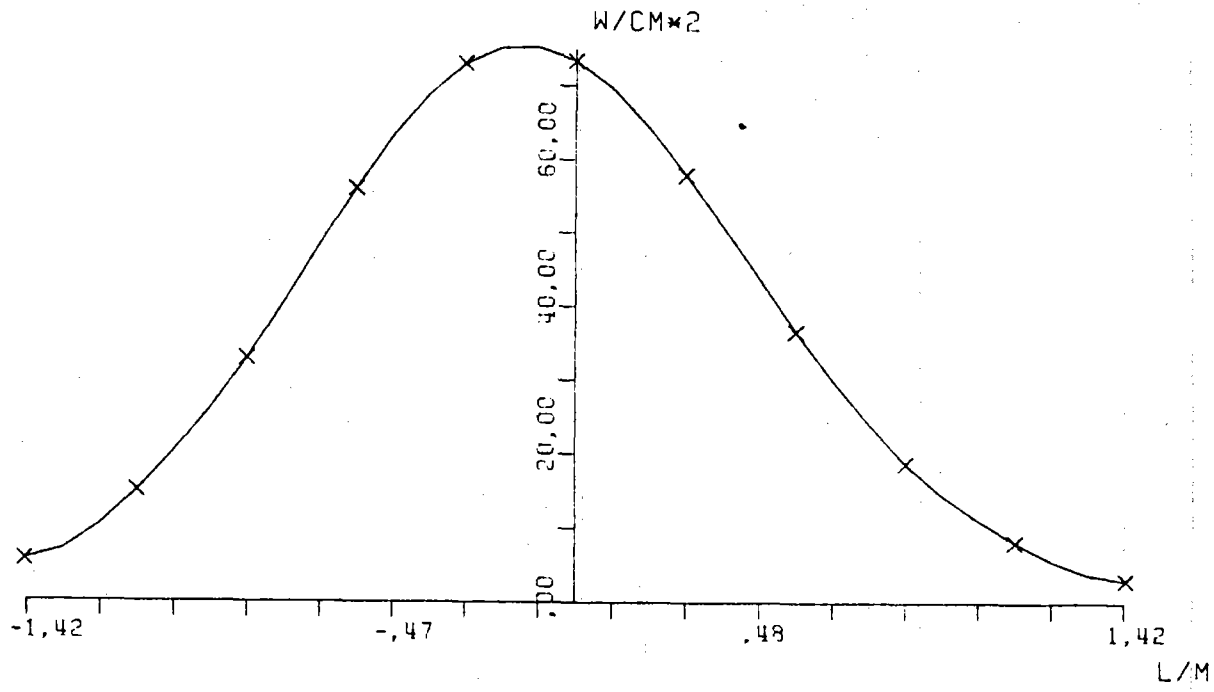

FIG.A.60 SOLAR FLUX ON TARGET SEC Y-Y

ASR-ALMERIA E-W CLOUD 21/3 H9.30 2345

	,09	.27	,63	1,17	1,66	1,93	1,55	1,04	,56	,25	.10
	,30	,69	2,12	3,59	5.42	5.62	4,90	3,31	1,63	,55	,32
	,76	2,33	5.60	10,4	14,2	15.2	12,9	8,92	4,33	2,28	.95
	1,59	5.23	12,3	22,0	29.3	31,9	29,1	20,0	11,3	5,40	2,41
	2,31	10,2	23,5	37,4	47,7	52,5	49.3	37,6	22,1	10,3	4,70
E.	4,52	16,7	37,3	54,4	63,3	67,6	68,4	58,2	37,5	18,4	6,96 W.
	5.35	19.5	44,1	63,0	68,0	67,4	71,6	63,5	49.2	24,3	8,09
	4,62	16,3	36,0	52,1	55,0	51,1	54,3	56,3	44,7	23,1	7,19
	3,59	9.30	20,0	29.5	32,0	29,9	29.6	31,3	26,6	14,6	4,47
	2,27	4,31	8,14	11,9	13,5	12,3	12,0	12,2	10,6	5,91	1,60
	1,15	2,02	2,68	3,66	4,50	4,03	3,76	3,53	3,16	1,63	,47

BØT.

HELST. NØ.	79.	AIM. NØ.	4,
INSØL. KW/M2	,750	STD.DEV. MRAD.	2,60
DAY NØ.	80,	INC.PØW. KW	1740,
TIME HR.	9.30	AVERG./PEAK	.31
TØWER HEIGHT M	43,	SPILLAGE %	
TARGET DIM. M	2,6X2,6		

FIG.A.61 INCIDENT FLUX ØN FLAT TARGET (W/CM2)

ASR-ALMERIA E-W CLOUD 21/3 H9.30 2345

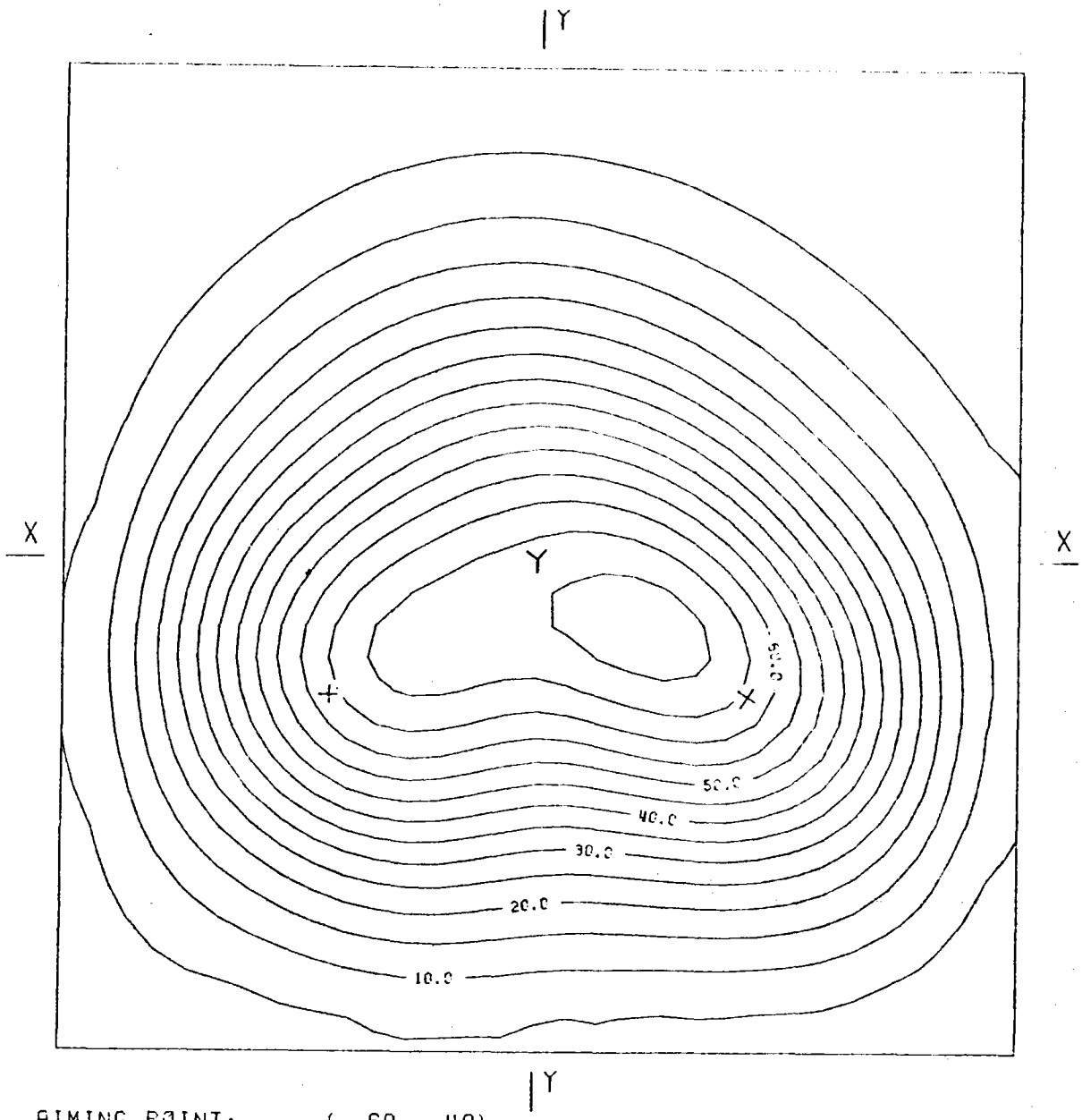

AIMING POINT: + (-,60;-,40)

× (,60;-,40)

Y (,00; ,00)

FIG.A.62 EQUIFLUX LINES, SPACING (W/CM2) 5.0

ASR-ALMERIA E-W CLOUD 21/3 H9.30 2345

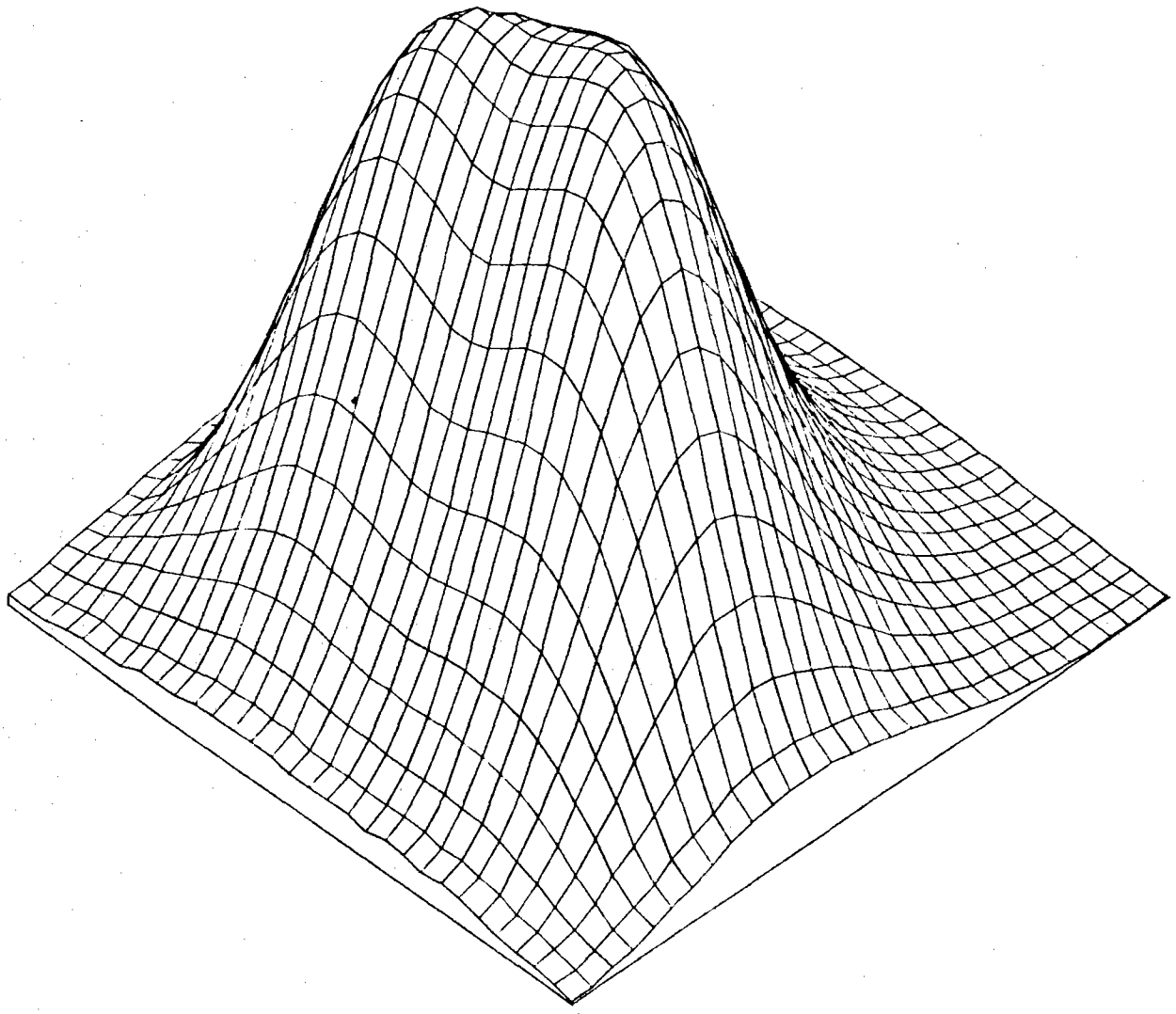

FIG.A.63 THREE-DIM. VIEW OF INCIDENT FLUX ON TARGET

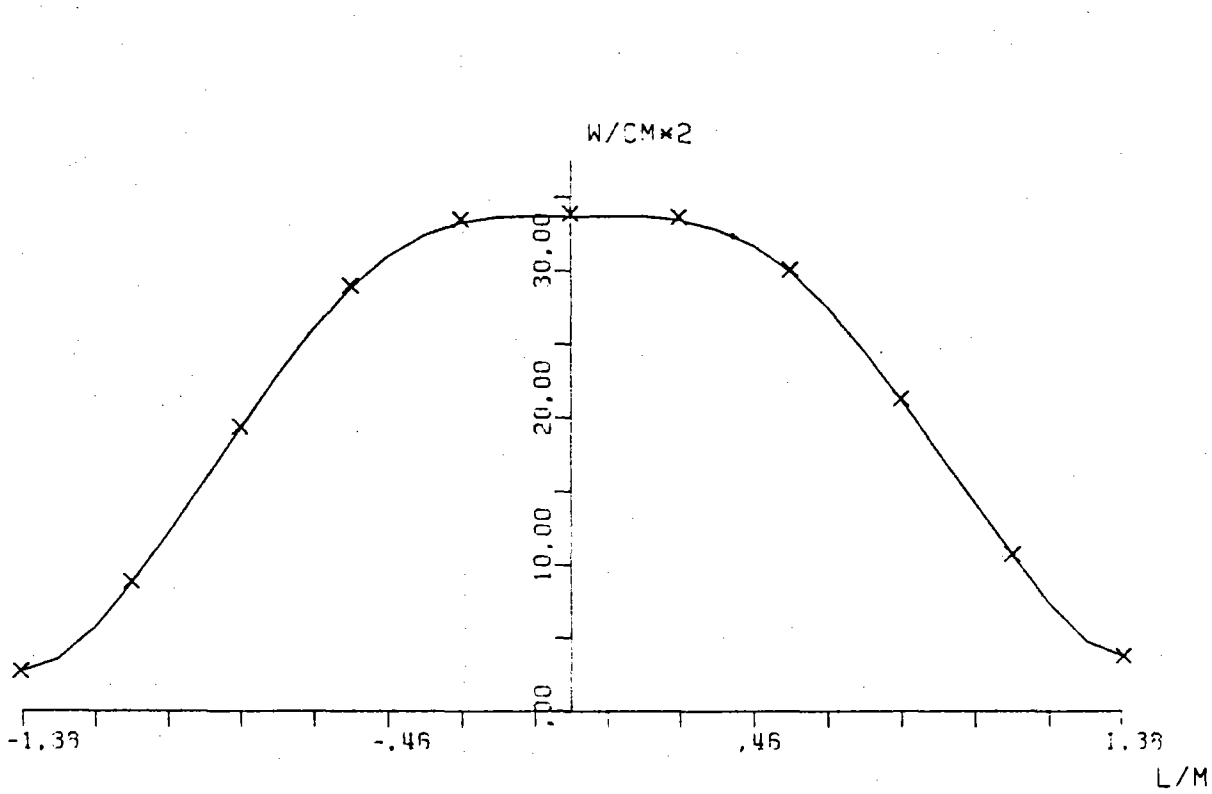

FIG.A.64 AVERAGE SOLAR FLUX ON VERTICAL STRIP

ASR-ALMERIA E-W CLOUD 21/3 H9.30 2345

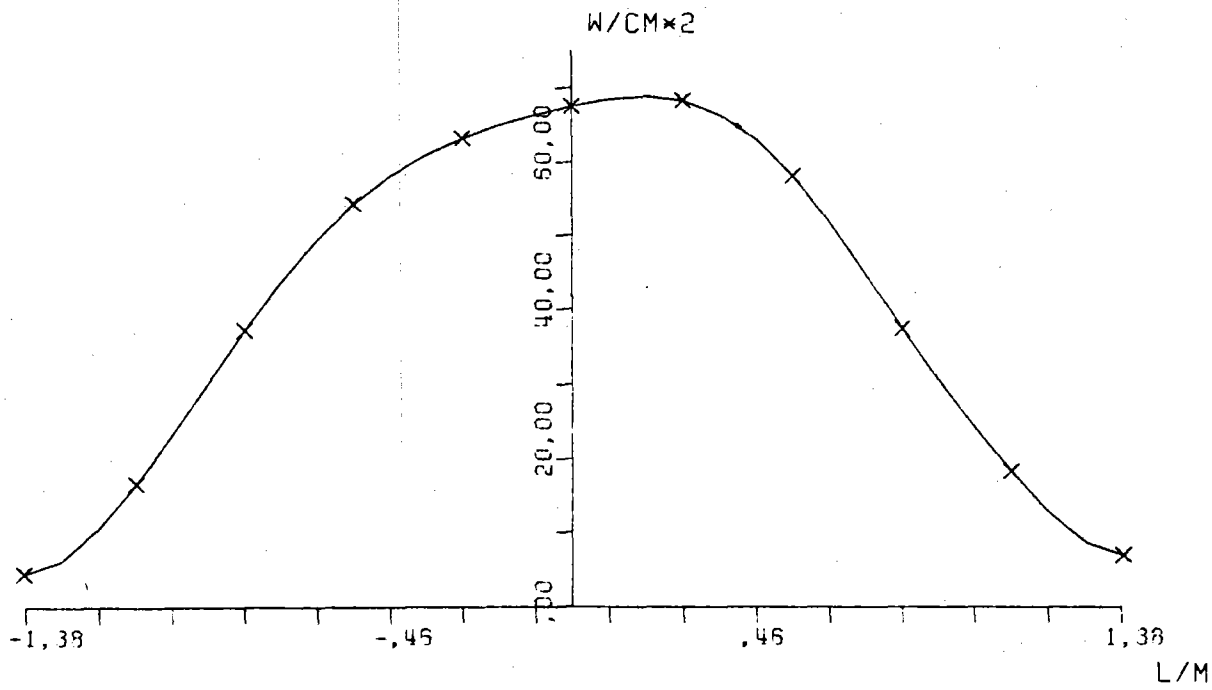

FIG.A.65 SOLAR FLUX ON TARGET SEC X-X

ASR-ALMERIA E-W CLOUD 21/3 H9.30 2345

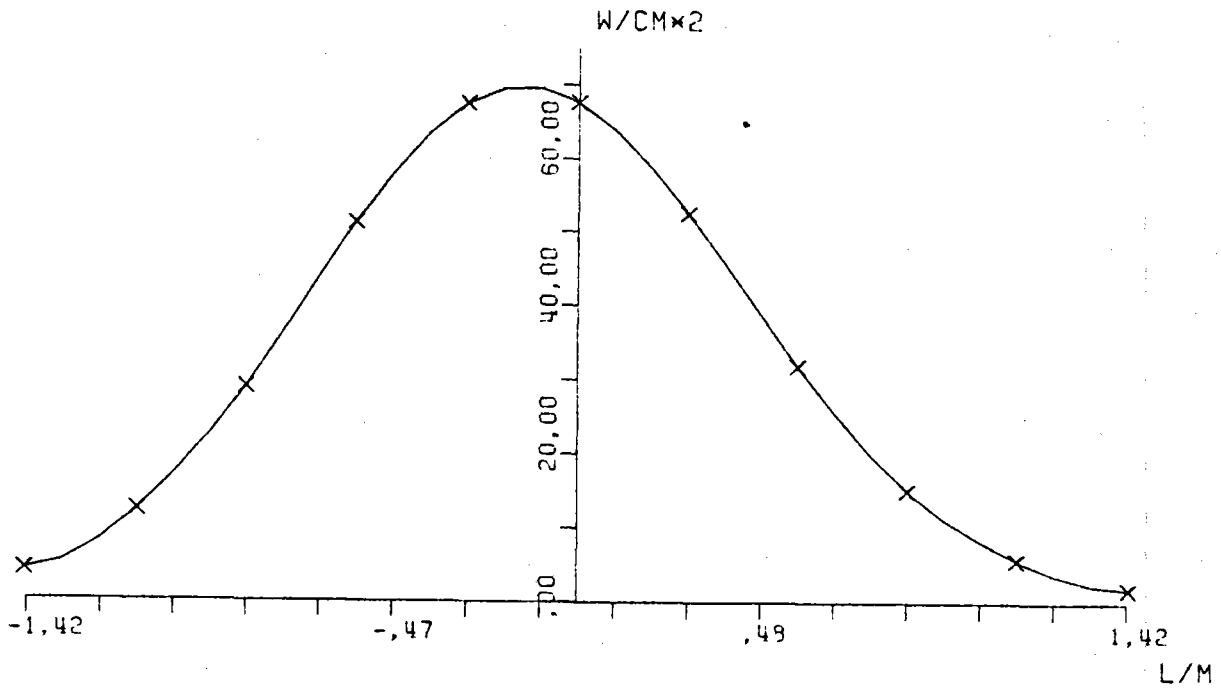

FIG.A.66 SOLAR FLUX ON TARGET SEC Y-Y

SNGMPROGLTT1

ASR-ALMERIA E-W CLOUD 21/3 H9.30 345

	,07	,19	,44	,77	1,06	1,12	,92	,59	,30	,12	,04	
	,22	,66	1,51	2,72	3,74	3,94	3,20	2,03	1,03	,42	,14	
	,57	1,73	4,14	7,58	10,5	11,2	9,14	5,64	2,95	1,20	,40	
	1,14	3,70	9,04	16,4	22,6	24,6	21,1	14,2	7,40	3,15	1,02	
	1,93	7,12	17,3	29,1	38,2	41,7	39,0	29,4	16,6	7,39	2,27	
E.	2,96	12,0	29,0	44,6	51,6	54,5	56,5	49,2	31,4	14,0	3,95	W.
	3,18	14,3	35,9	53,7	56,1	54,2	60,3	60,4	43,5	19,9	5,25	
	2,30	10,9	28,9	44,0	44,1	39,6	45,2	49,9	39,9	19,4	5,06	
	1,16	5,33	14,6	23,0	23,2	20,4	23,4	26,6	23,0	11,6	3,15	
	,41	1,74	4,63	7,40	7,76	7,35	8,52	9,35	8,16	4,19	1,14	
	,10	,37	,95	1,52	1,73	1,92	2,20	2,15	1,77	,65	,23	

BOT.

HELST. NO.	59.	AIM. NO.	3,
INSOL. KW/M2	,750	STD.DEV. MRAD.	2,60
DAY NO.	80,	INC.POW. KW	1370,
TIME HR.	9.30	AVERG./PEAK	,29
TOWER HEIGHT M	43,	SPILLAGE %	
TARGET DIM. M	2,6X2,6		

FIG.A.67 INCIDENT FLUX ON FLAT TARGET (W/CM2)

ASR-ALMERIA E-W CLOUD 21/3 H9.30 345

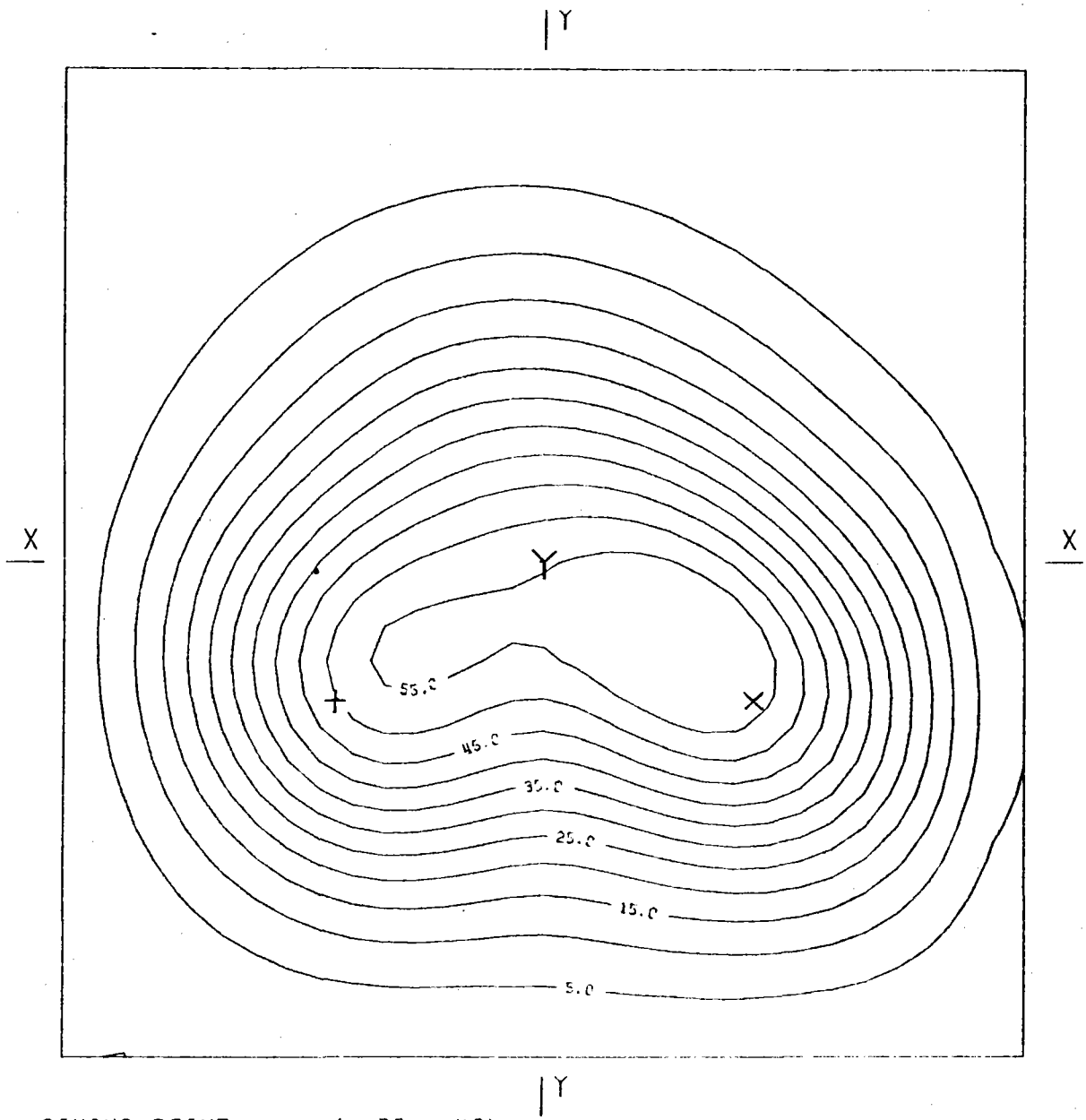

AIMING POINT: + (-,60;-,40)

× (,60;-,40)

Y (,00; ,00)

FIG.A.68 EQUIFLUX LINES, SPACING (W/CM2) 5.0

ASR-ALMERIA E-W CLOUD 21/3 H9.30 345

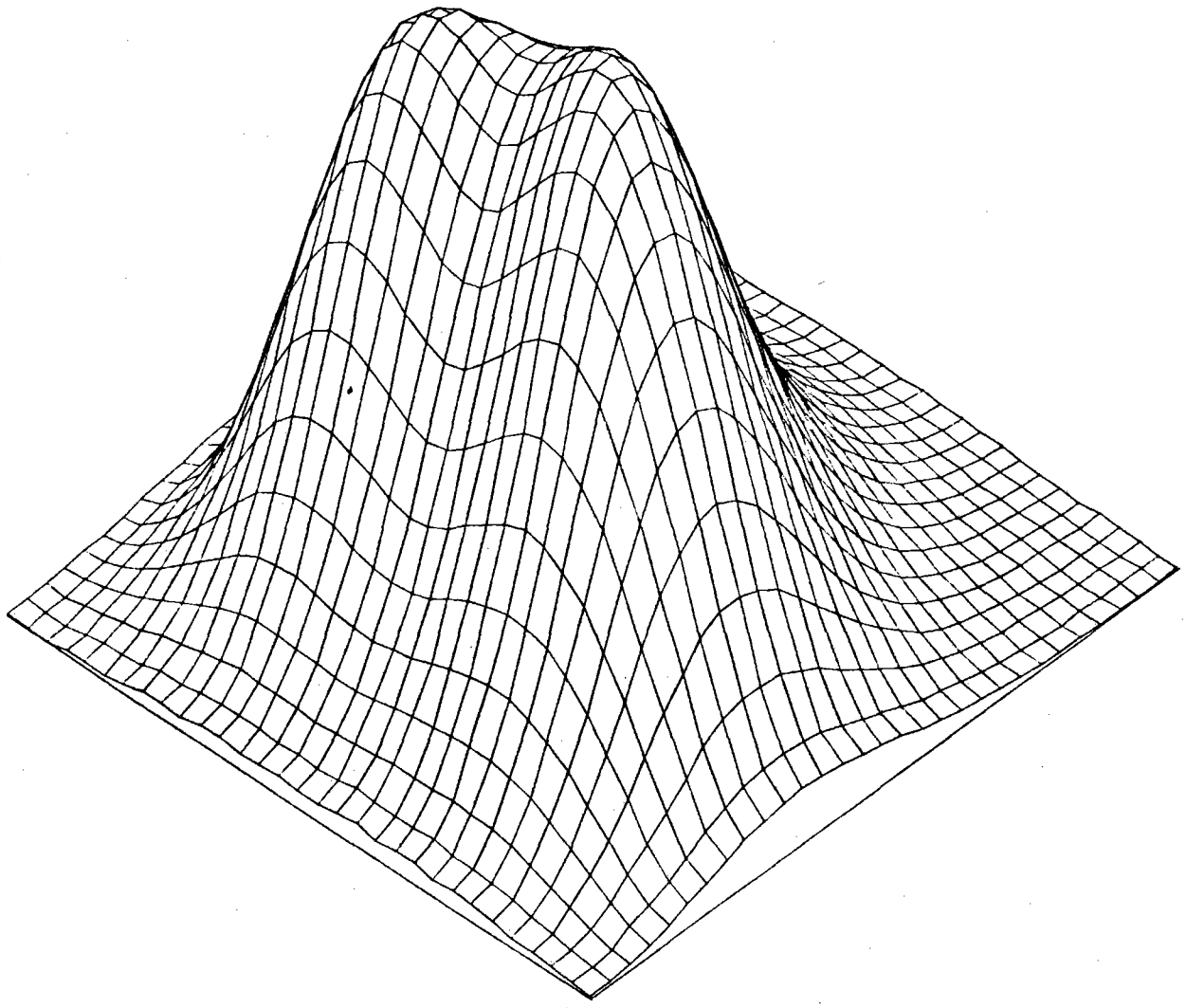

FIG.A.69 THREE-DIM. VIEW OF INCIDENT FLUX ON TARGET

SNAMPROGETTI

ASR-ALMERIA E-W CLØUD 21/3 H9.30 345

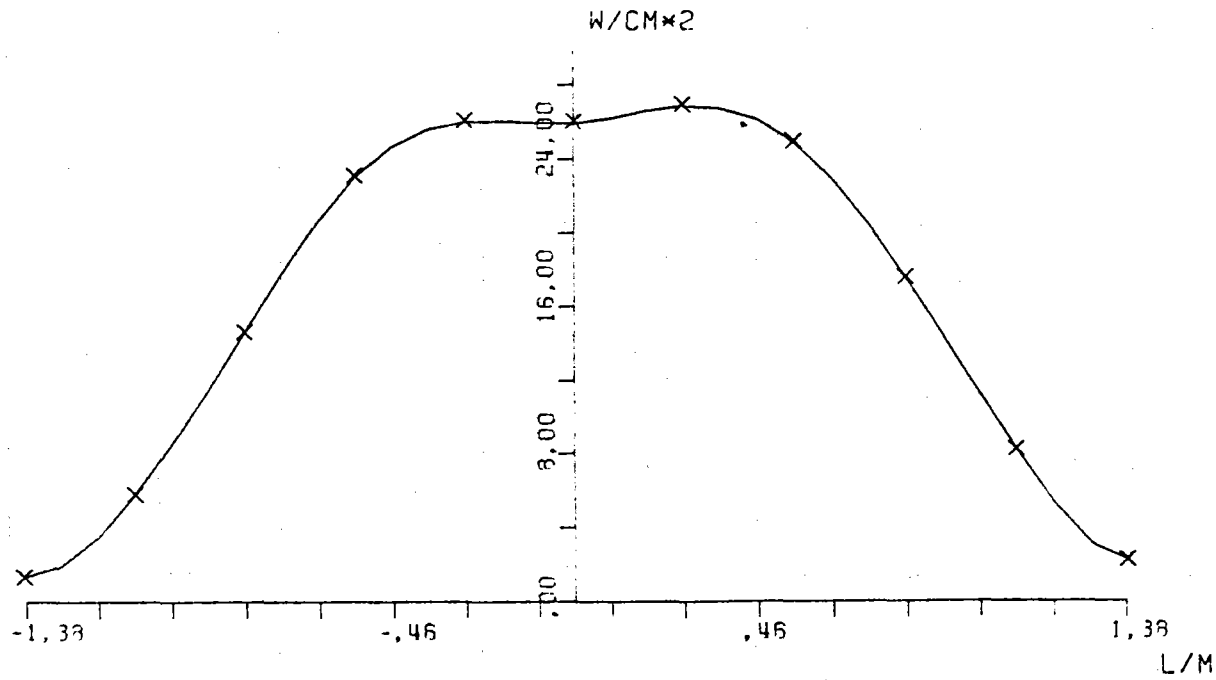

FIG.A.70 AVERAGE SOLAR FLUX ON VERTICAL STRIP

SNAMPROGETTI

ASR-ALMERIA E-W CLOUD 21/3 H9.30 345

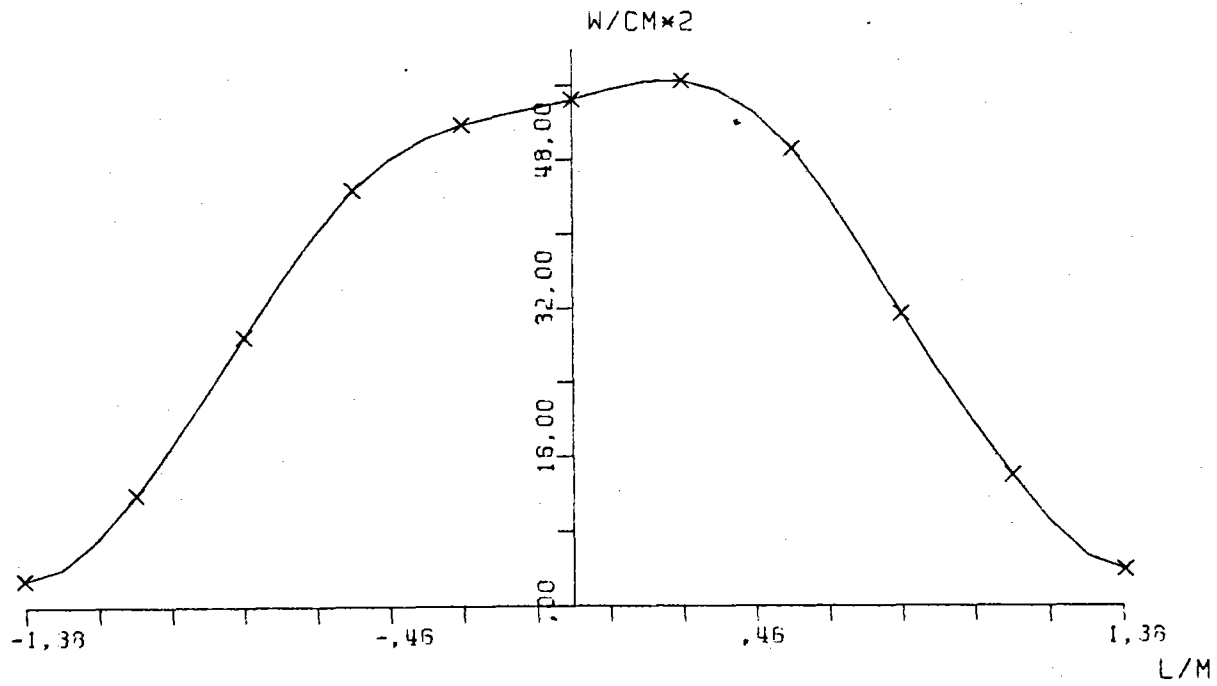

FIG.A.71 SOLAR FLUX ON TARGET SEC X-X

ASR-ALMERIA E-W CLØUD 21/3 H9.30 345

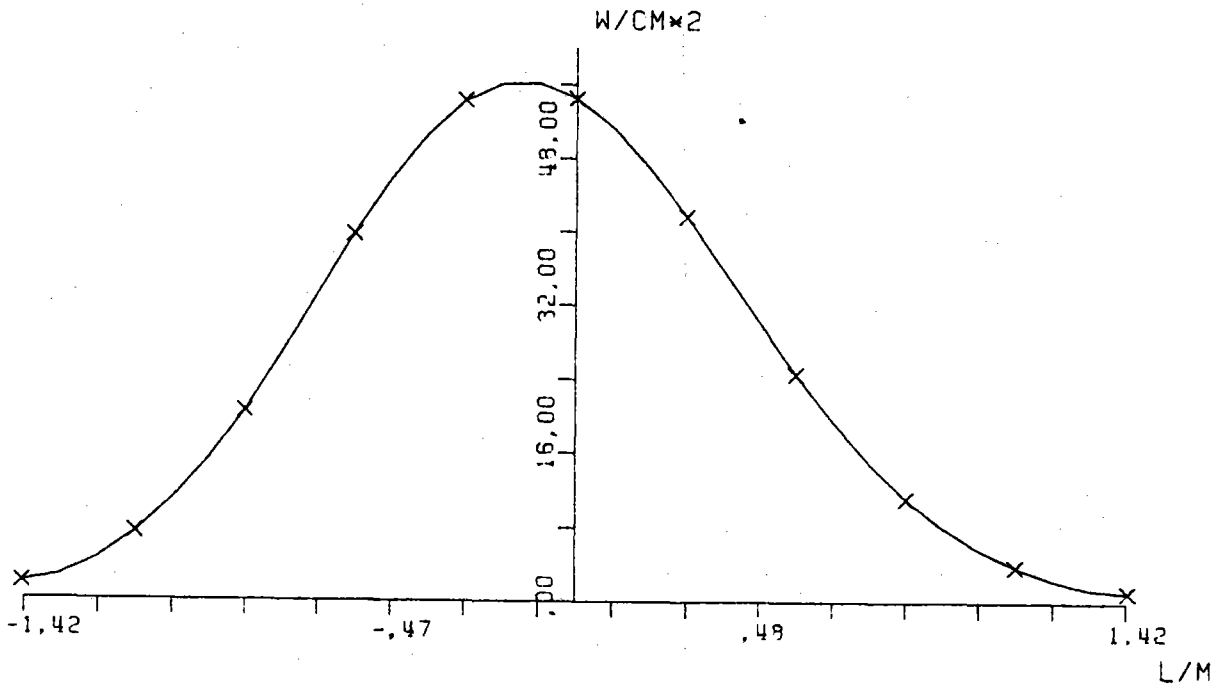

FIG.A.72 SØLAR FLUX ØN TARGET SEC Y-Y

ASR-ALMERIA E-W CLOUD 21/3 H9.30 45

	,05	,13	,27	,45	,58	,58	,46	,28	,14	,05	,02	
	,16	,45	1,00	1,71	2,25	2,27	1,77	1,07	,52	,20	,05	
	,41	1,20	2,61	5,05	6,59	7,11	5,56	3,34	1,58	,60	,19	
	,60	2,50	6,01	11,1	15,6	16,6	13,7	8,46	3,89	1,47	,44	
	1,33	4,52	10,5	18,9	25.9	28.8	25.7	17,5	8,67	3,14	,68	
E.	1,55	7,36	17,8	28,4	34,1	37,1	36,6	29.3	16,5	6,15	1,59	W.
	1,75	8,32	22,1	34,1	36,2	38.6	38,1	35.9	23,5	9 84	2,53	
	,96	5,43	16,6	27,0	27,5	24,4	26,5	28,5	22,0	10,3	2,67	
	,33	1,92	6,68	12,6	13,2	11,3	11,3	13,6	11,6	6,29	1,85	
	,09	,39	1,54	3,20	3,74	3,41	3,45	3,55	3,53	2,05	,72	
	,02	,06	,22	,50	,59	,75	,75	,73	,62	,37	,14	

BØT.

HELST. NØ. 34,
INSØL. KW/M2 ,750
DAY NØ. 80,
TIME HR. 9.30
TØWER HEIGHT M 43,
TARGET DIM. M 2,6X2,6

AIM. NØ. 2,
STD.DEV. MRAD. 2,60
INC.PØW. KW 819.
AVERG./PEAK ,27
SPILLAGE %

FIG.A.73 INCIDENT FLUX ØN FLAT TARGET (W/CM2)

SNAMPRØGETTI

ASR-ALMERIA E-W CLOUD 21/3 H9.30 45

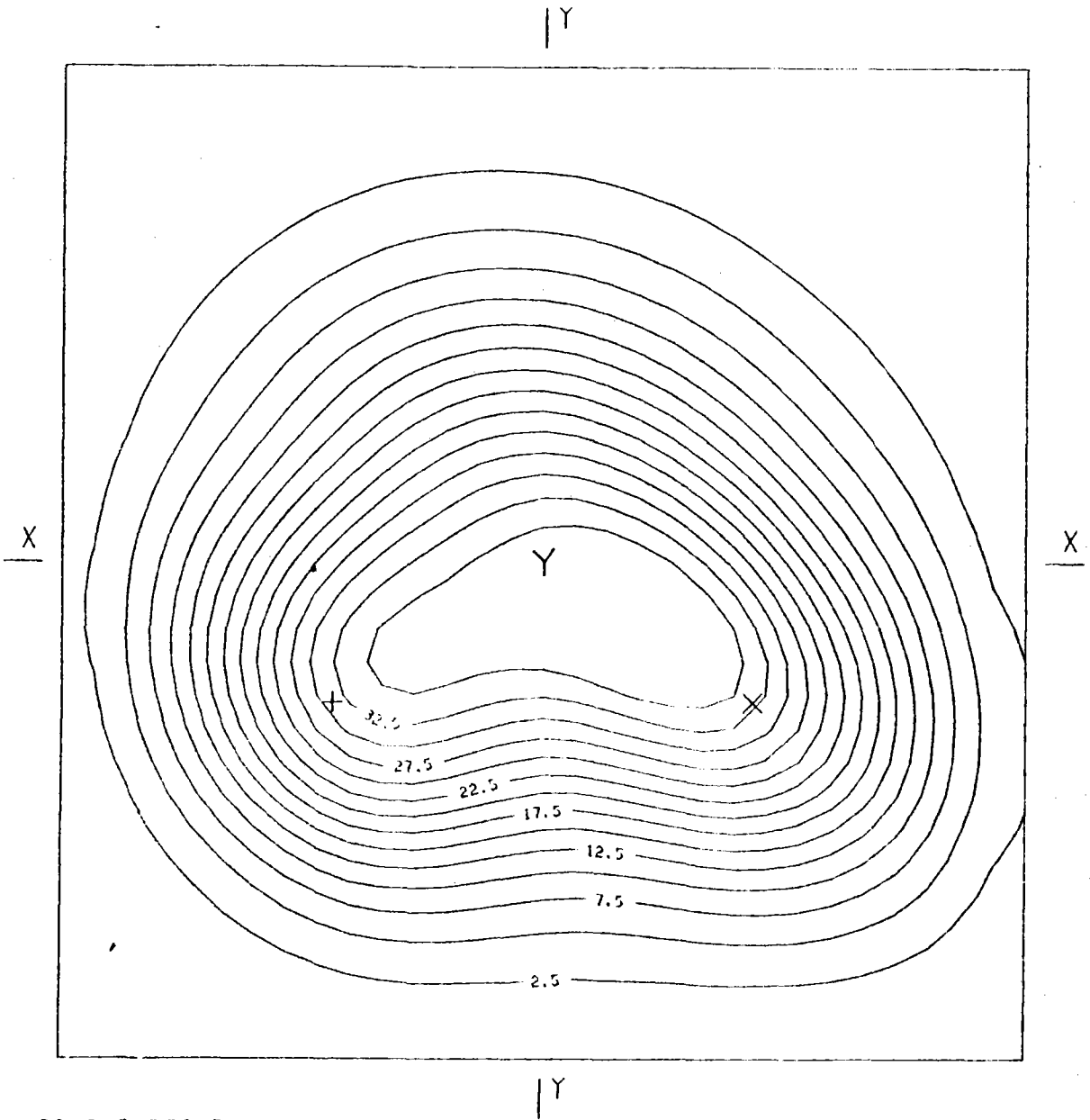

AIMING POINT: + (-,60; -,40)

× (,60; -,40)

Y (,00; ,00)

FIG.A.74 EQUIFLUX LINES, SPACING (W/CM2) 2,5

ASR-ALMERIA E-W CLOUD 21/3 H9.30 45

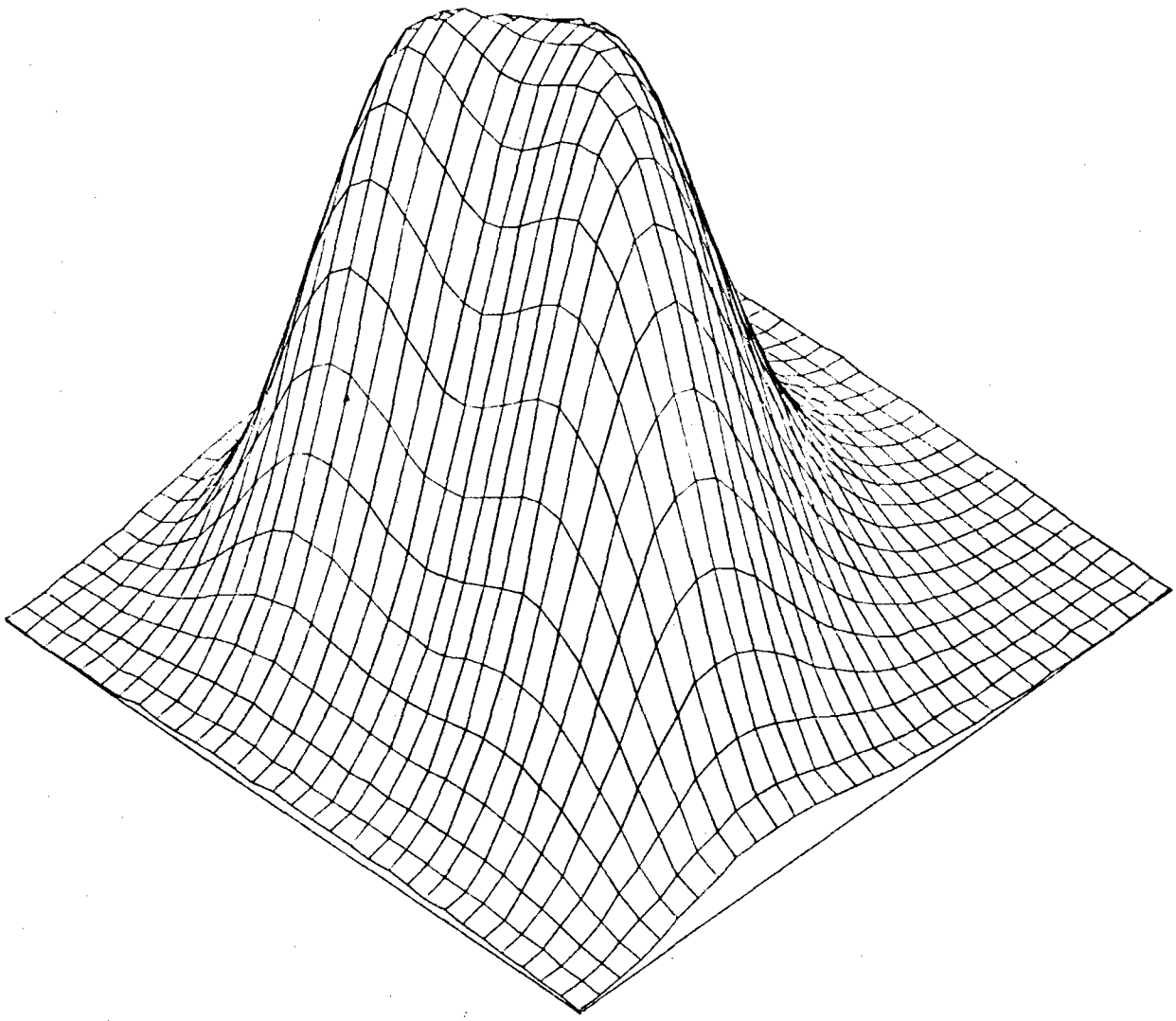

FIG.A.75 THREE-DIM. VIEW OF INCIDENT FLUX ON TARGET

ASR-ALMERIA E-W CLOUD 21/3 H9.30 45

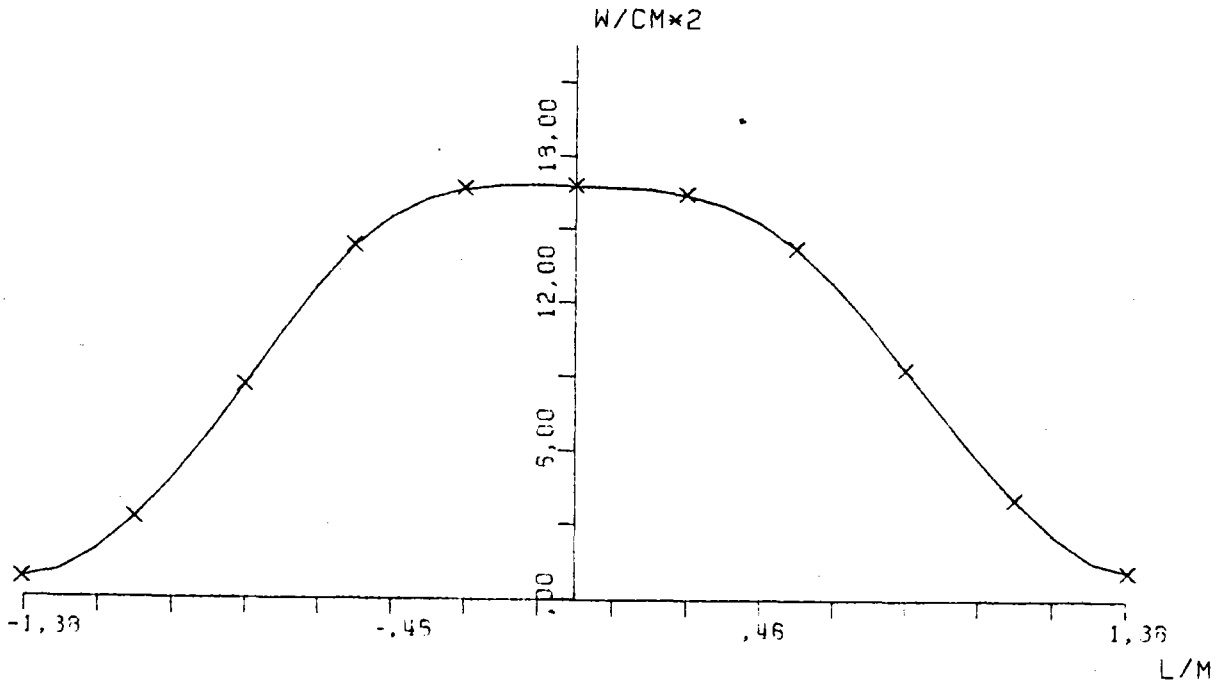

FIG.A.76 AVERAGE SOLAR FLUX ON VERTICAL STRIP

ASR-ALMERIA E-W CLOUD 21/3 H9.30 45

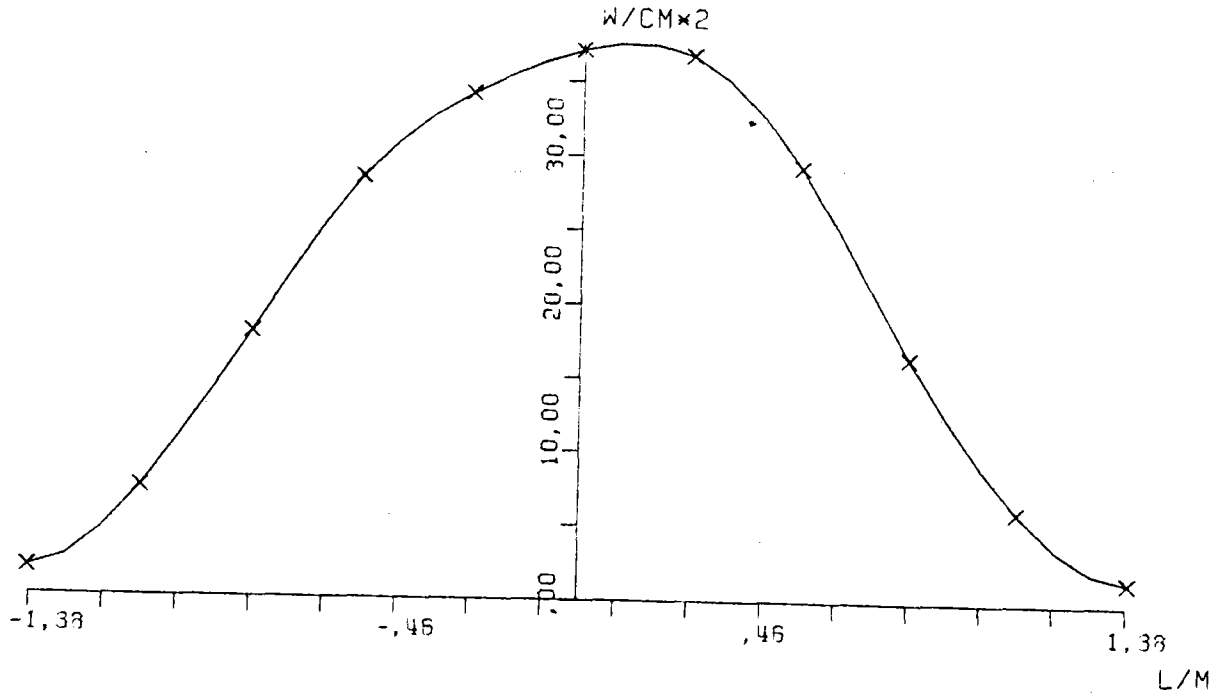

FIG.A.77 SOLAR FLUX ON TARGET SEC X-X

ASR-ALMERIA E-W CLOUD 21/3 H9.30 45

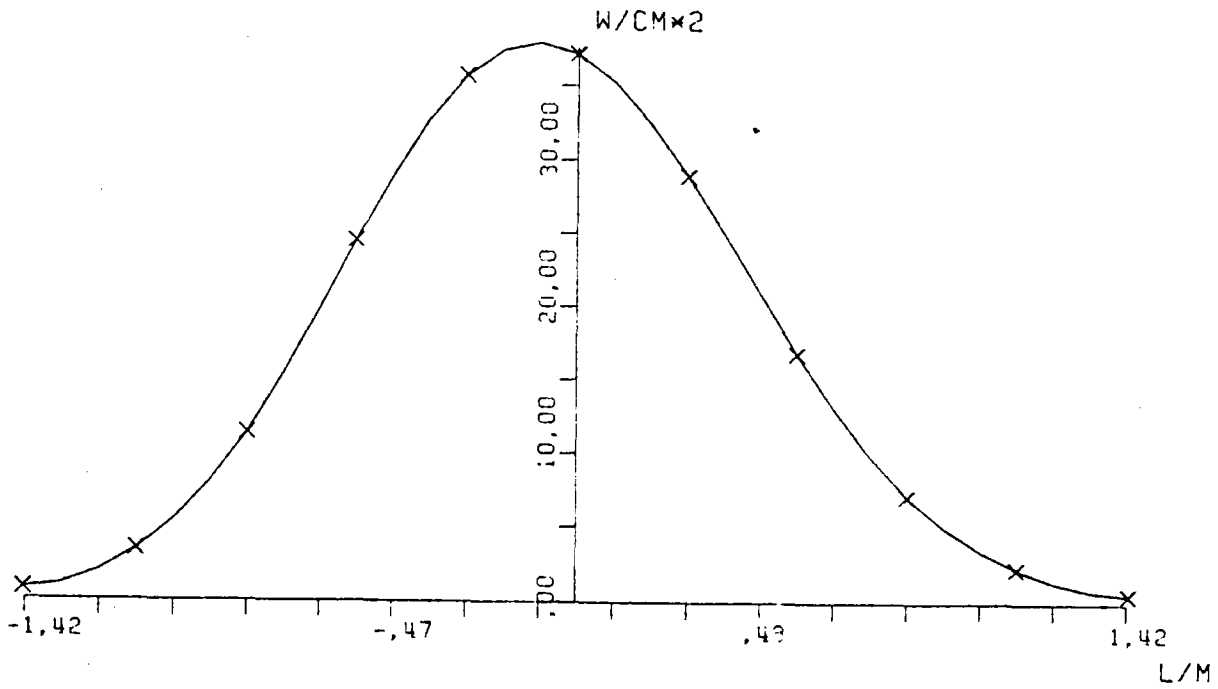

FIG.A.78 SOLAR FLUX ON TARGET SEC Y-Y

ASR-ALMERIA E-W CLOUD 21/3 H9.30 5

	,03	,08	,15	,24	,29	,29	,21	,13	,06	,02	,01	
	,10	,29	,60	,96	1,18	1,13	,55	,51	,24	,09	,03	
	,27	,77	1,72	2,91	3,75	3,69	2,50	1,66	,79	,30	,09	
	,49	1,51	3,56	6,37	8,67	9,00	7,16	4,36	2,05	,77	,23	
	,64	2,05	5,11	9,70	14,0	15,7	13,6	8,95	4,41	1,64	,47	
E.	,60	1,97	5,13	10,4	16,1	19,5	18,6	13,9	7,67	3,04	,86	W.
	,41	1,36	3,66	7,79	13,0	17,2	18,4	15,5	9,56	4,51	1,33	
	,21	,71	1,91	4,17	7,31	10,4	12,3	11,7	8,58	4,59	1,63	
	,09	,29	,76	1,66	2,92	4,27	5,32	5,60	4,70	2,68	1,17	
	,03	,09	,24	,52	,89	1,26	1,53	1,64	1,49	1,01	,46	
	,01	,02	,06	,13	,22	,30	,34	,32	,28	,19	,09	

BOT.

HELST. NO. 14,
INSOL. KW/M2 ,750
DAY NO. 80,
TIME HR. 9.30
TOWER HEIGHT M 43,
TARGET DIM. M 2,6X2,6

AIM. NO. 1,
STD.DEV. MRAD. 2,60
INC.POW. KW 342,
AVERG./PEAK ,22
SPILLAGE %

FIG.A.79 INCIDENT FLUX ON FLAT TARGET (W/CM2)

ASR-ALMERIA E-W CLOUD 21/3 H9.30 5

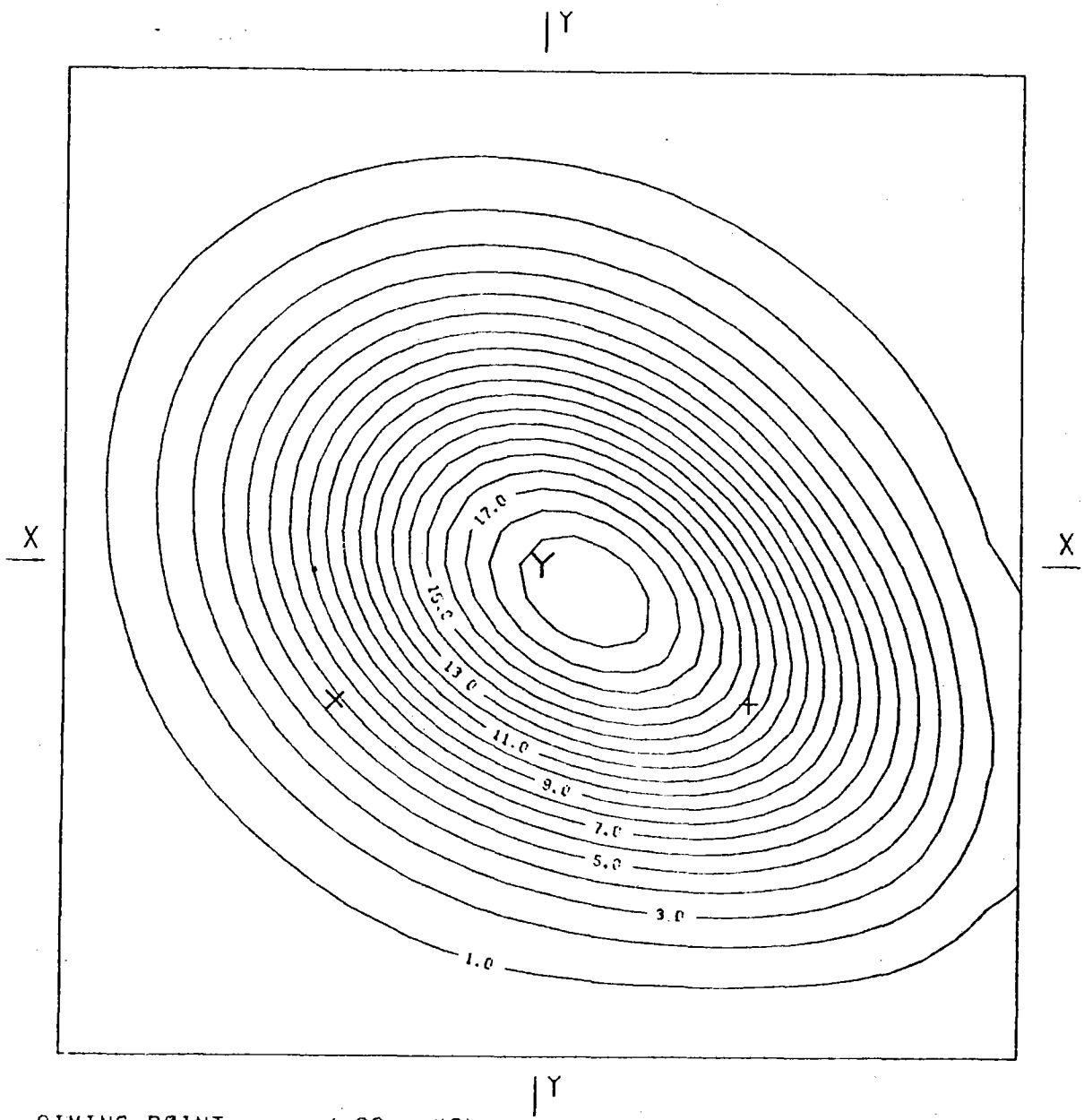

AIMING POINT: + (,60;-,40)
× (-,60;-,40)
Y (,00; ,00)

FIG.A.80 EQUIFLUX LINES, SPACING (W/CM2) 1,0

ASR-ALMERIA E-W CLOUD 21/3 H9.30 5

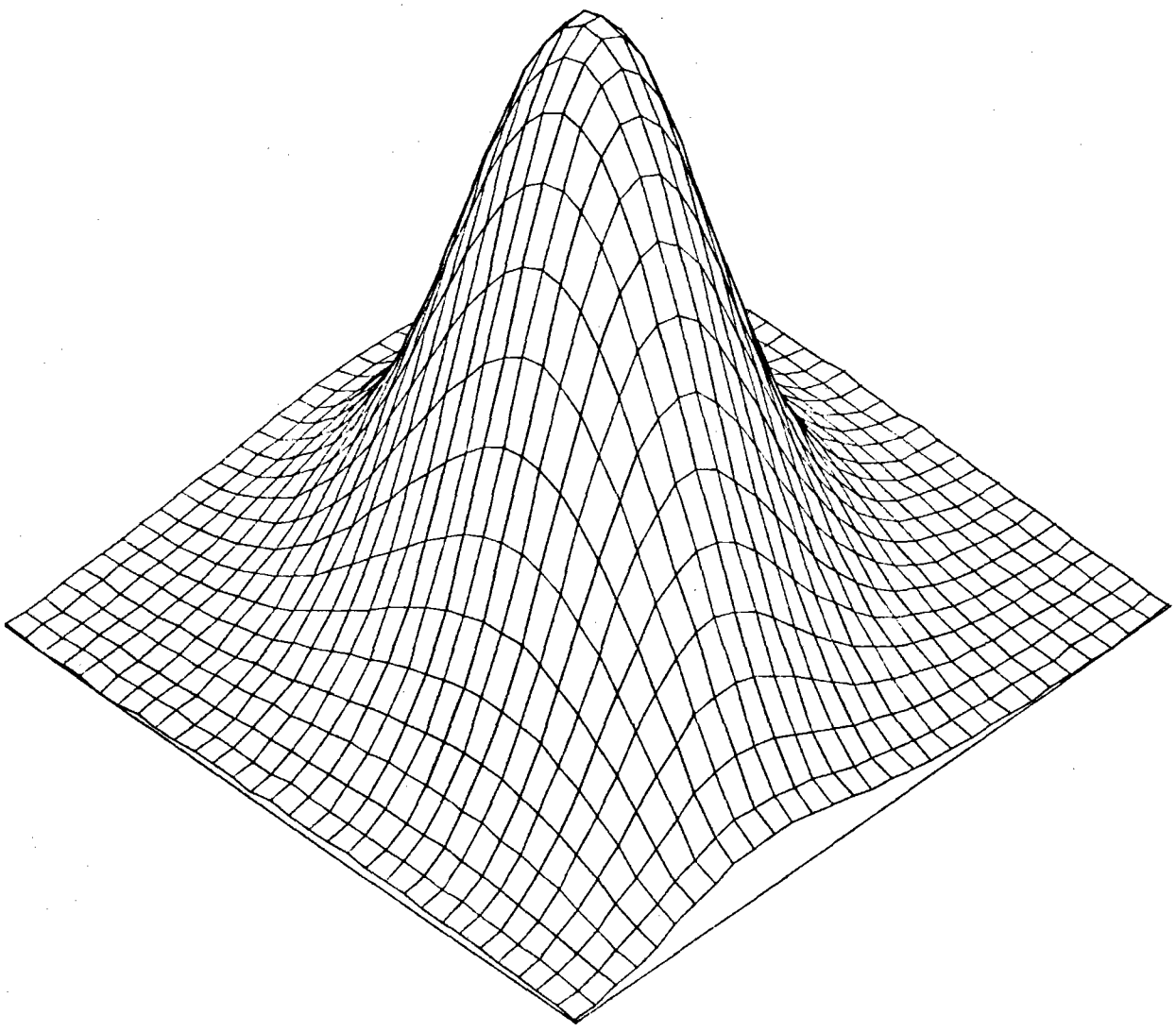

FIG.A.81 THREE-DIM. VIEW OF INCIDENT FLUX ON TARGET

ASR-ALMERIA E-W CLØUD 21/3 H9.30 5

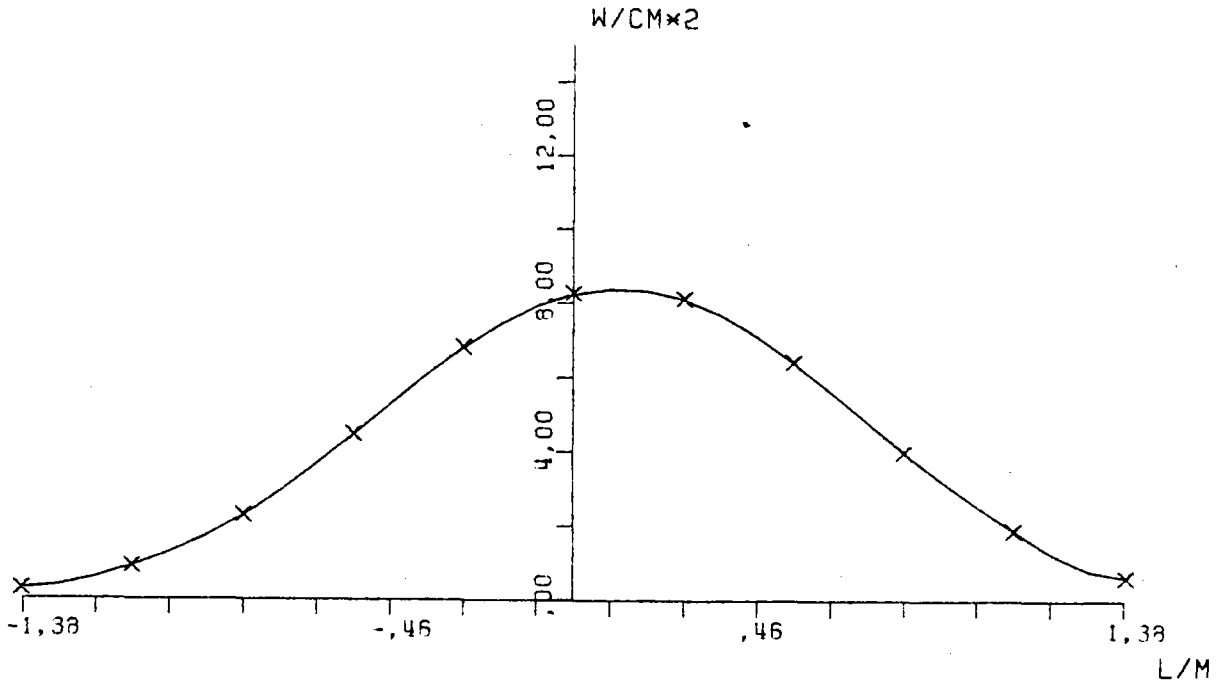

FIG.A.82 AVERAGE SØLAR FLUX ØN VERTICAL STRIP

SNAMPROGETTI

ASR-ALMERIA E-W CLØUD 21/3 H9.30 5

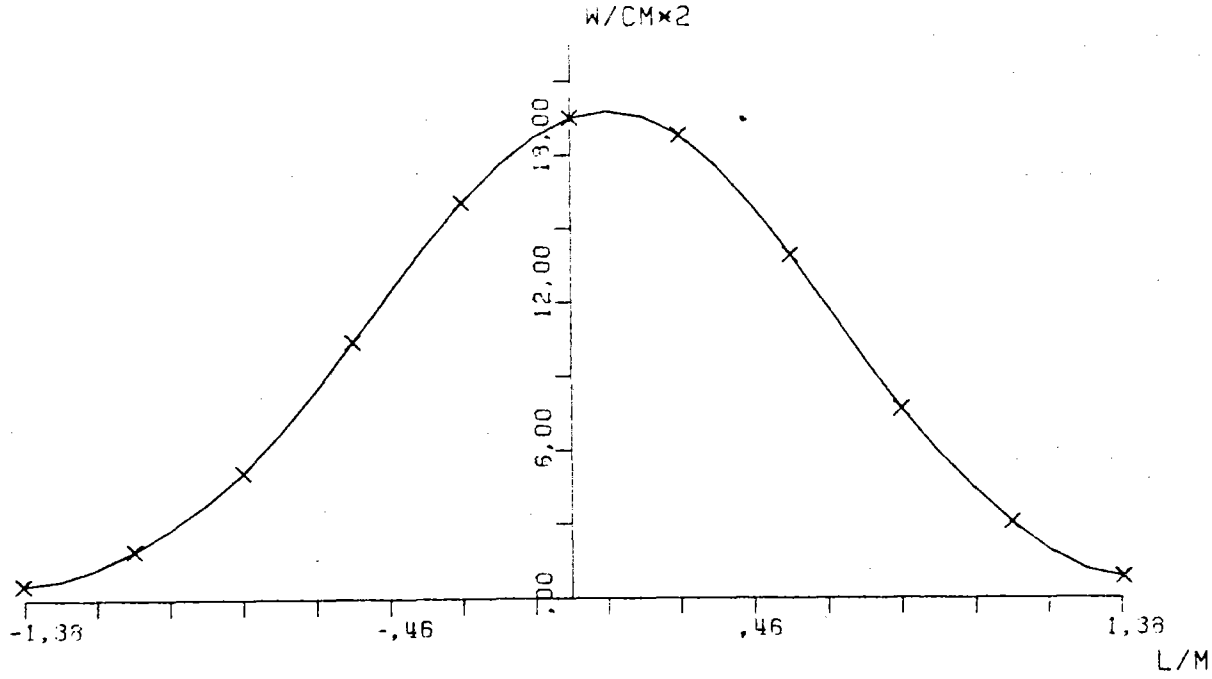

FIG.A.83 SØLAR FLUX ØN TARGET SEC X-X

ASR-ALMERIA E-W CLOUD 21/3 H9.30 5

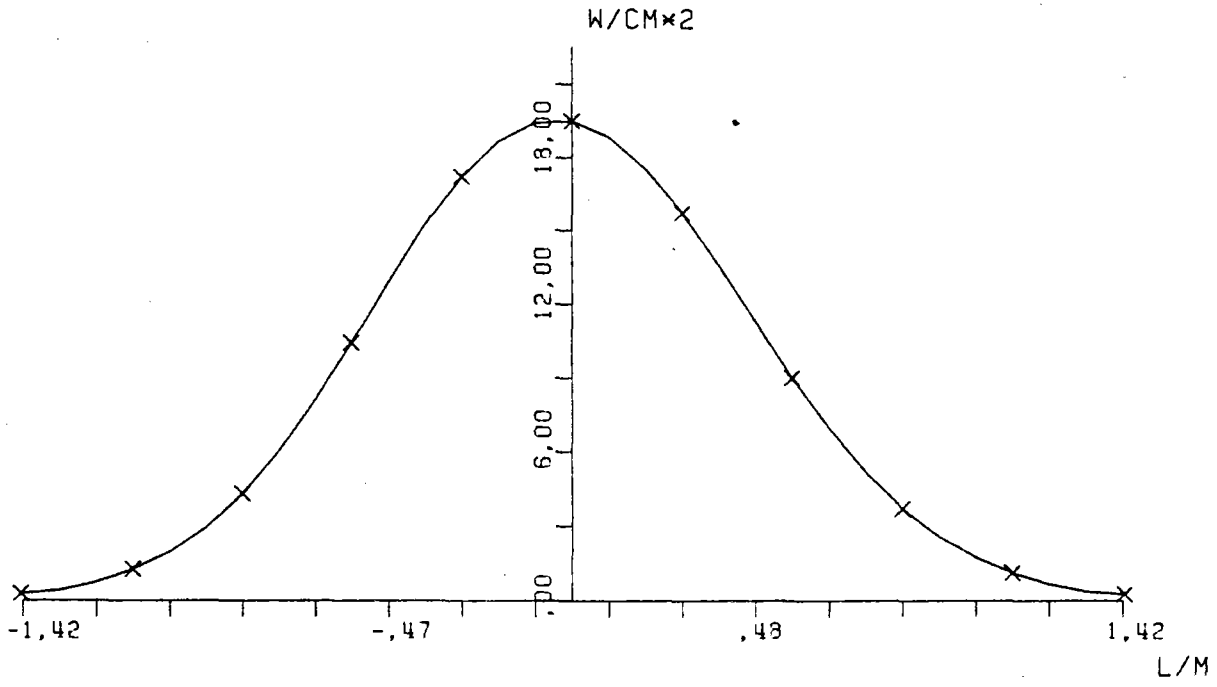

FIG.A.84 SOLAR FLUX ON TARGET SEC Y-Y

ASR-ALMERIA W-E CLOUD 21/3 H9.30 4321

	,12	,37	,88	1,67	2,44	2,78	2,52	1,67	1,18	,65	,33	
	,36	1,06	2,48	4,52	6,37	7,04	6,26	4,66	2,99	1,70	,69	
	,90	2,57	5,69	10,3	13,5	15,1	13,5	10,2	6,59	3,72	2,01	
	1,90	5,47	12,1	19,5	25,2	27,6	25,5	19,7	12,6	7,14	3,92	
	3,60	10,7	22,4	32,4	39,0	42,2	41,0	33,4	21,7	12,3	6,36	
E.	5,76	17,5	36,3	49,0	52,7	53,6	55,1	49,3	33,9	18,4	8,27	W.
	7,05	21,7	44,5	60,1	60,3	55,7	58,5	57,6	43,0	22,5	8,54	
	6,59	18,4	37,7	52,2	52,5	45,6	46,6	48,4	39,2	20,7	6,91	
	5,03	11,7	22,0	31,3	32,3	28,5	27,5	28,6	24,3	13,2	4,14	
	3,18	6,17	9,60	13,6	15,4	13,6	12,9	12,5	10,7	5,78	1,79	
	1,61	2,75	3,74	5,16	5,84	5,29	4,79	4,47	3,66	1,69	,58	

BOT.

HELST. NO. 79.
INSOL. KW/M2 ,750
DAY NO. 80,
TIME HR. 9.30
TOWER HEIGHT M 43,
TARGET DIM. M 2,6X2,6

AIM. NO. 4,
STD.DEV. MRAD. 2,60
INC.POW. KW 1630,
AVERG./PEAK ,34
SPILLAGE % 5,51

FIG.A.85 INCIDENT FLUX ON FLAT TARGET (W/CM2)

ASR-ALMERIA W-E CLOUD 21/3 H9.30 4321

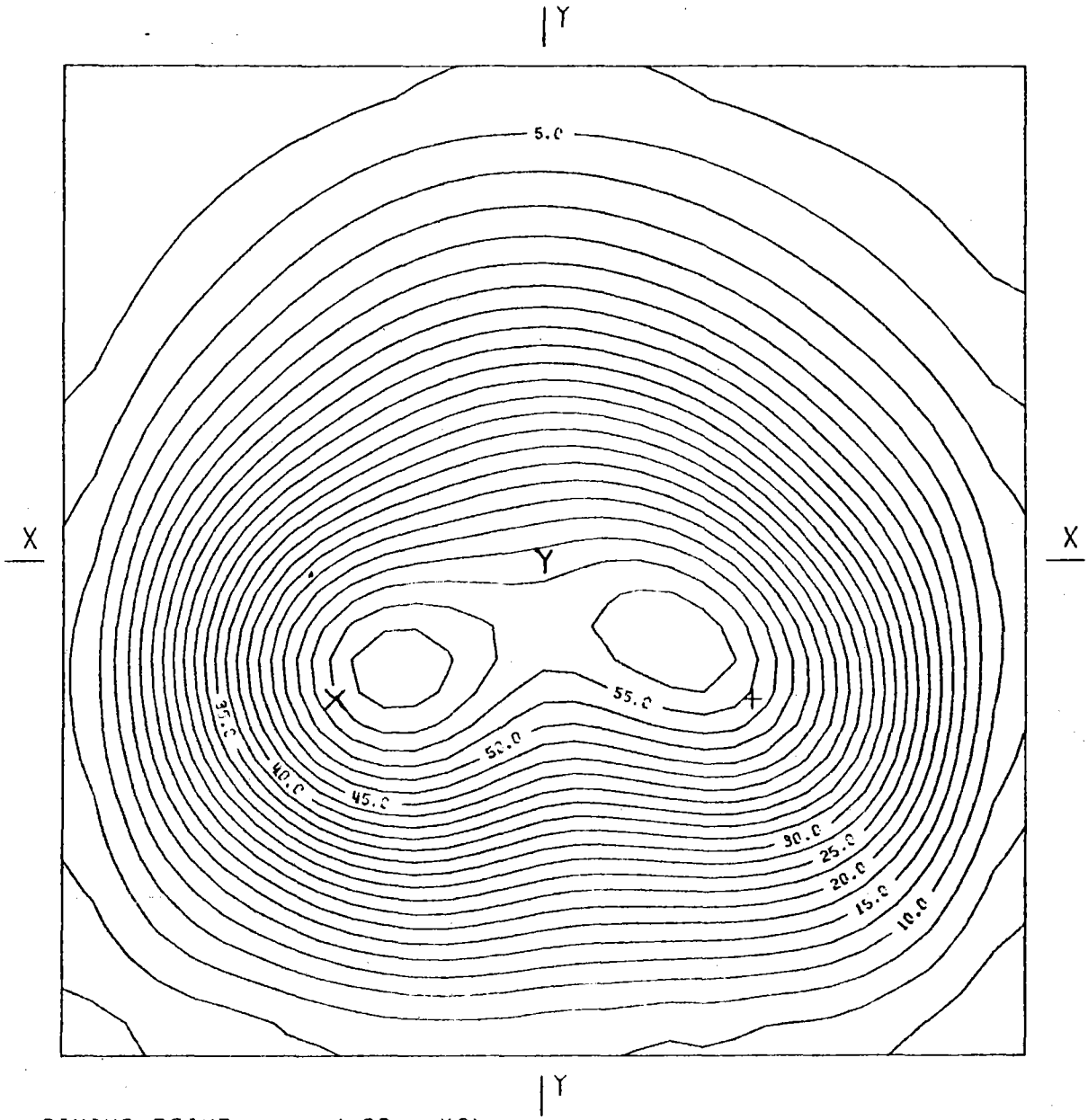

AIMING POINT: + (,60;-,40)

× (-,60;-,40)

Y (,00; ,00)

FIG.A.86 EQUIFLUX LINES, SPACING (W/CM2) 2,5

ASR-ALMERIA W-E CLOUD 21/3 H9.30 4321

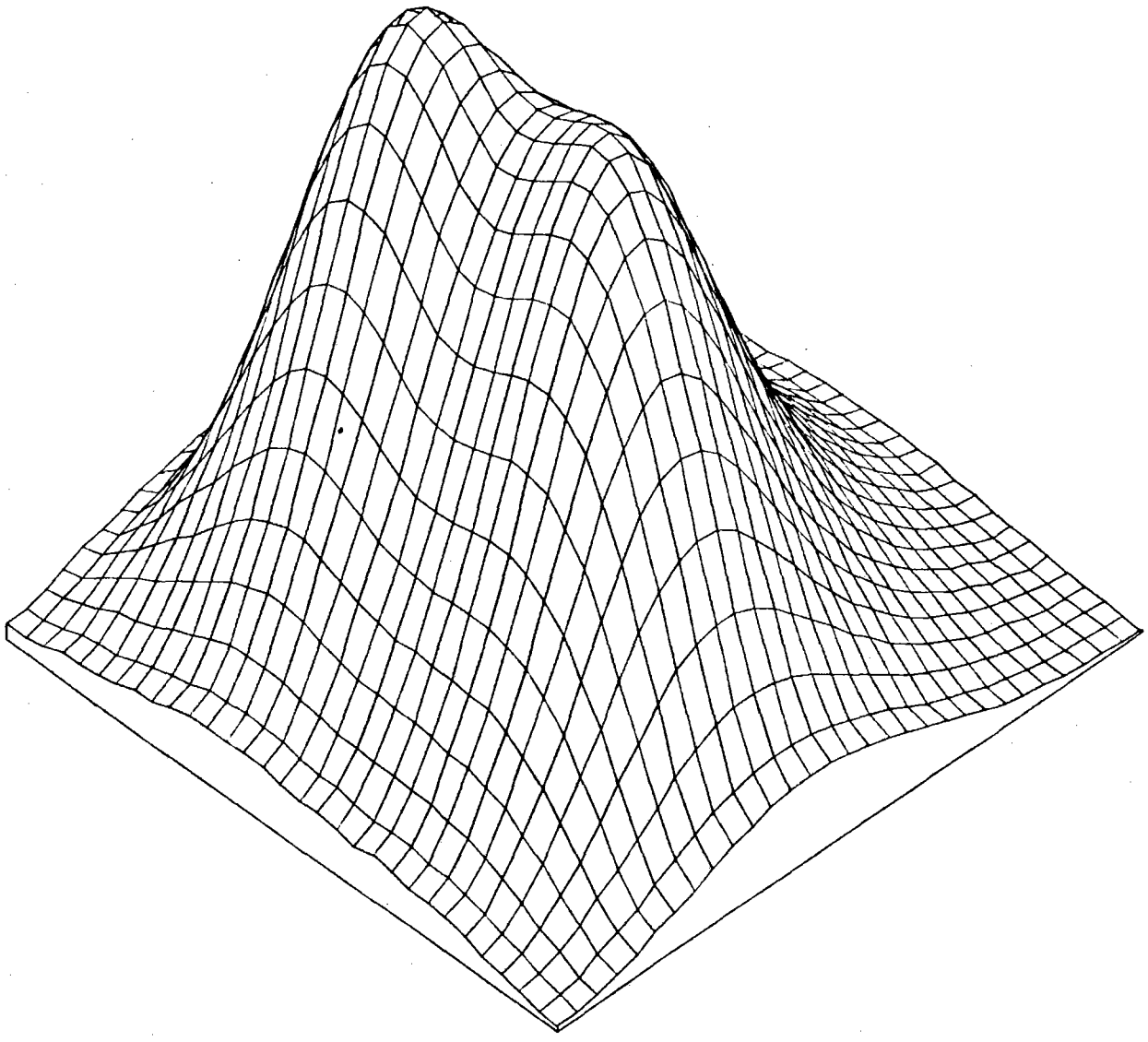

FIG.A.87 THREE-DIM. VIEW OF INCIDENT FLUX ON TARGET

ASR-ALMERIA W-E CLØUD 21/3 H9.30 4321

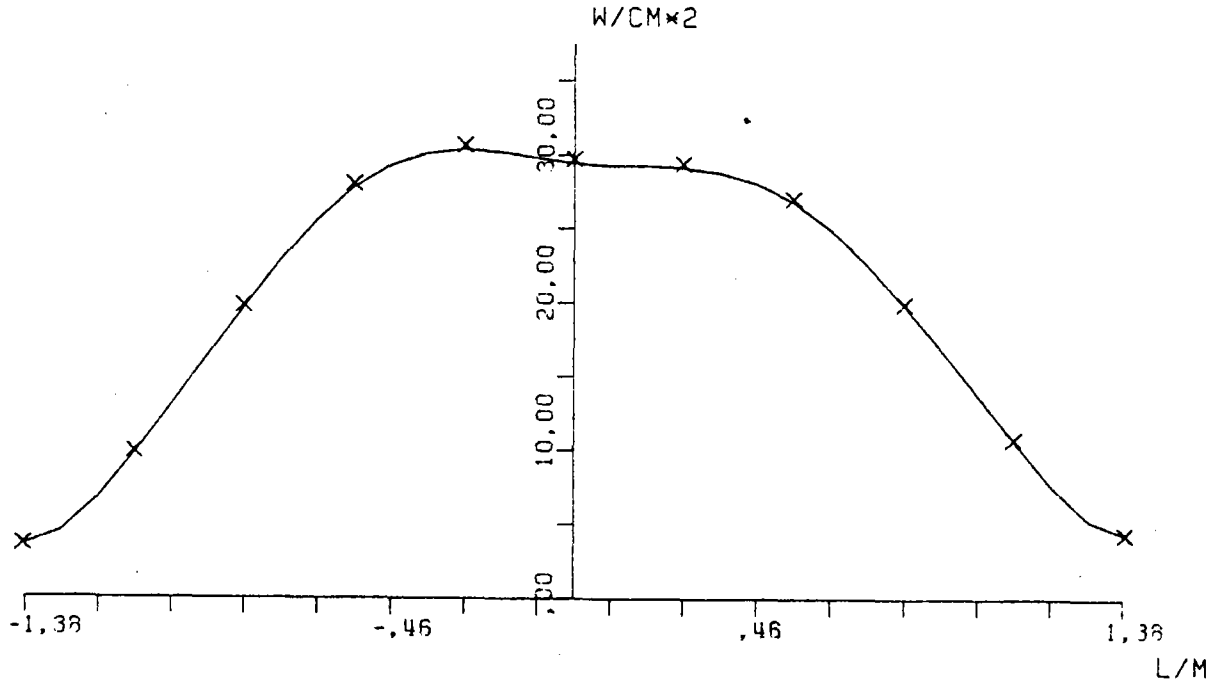

FIG.A.88 AVERAGE SOLAR FLUX ON VERTICAL STRIP

ASR-ALMERIA W-E CLOUD 21/3 H9.30 4321

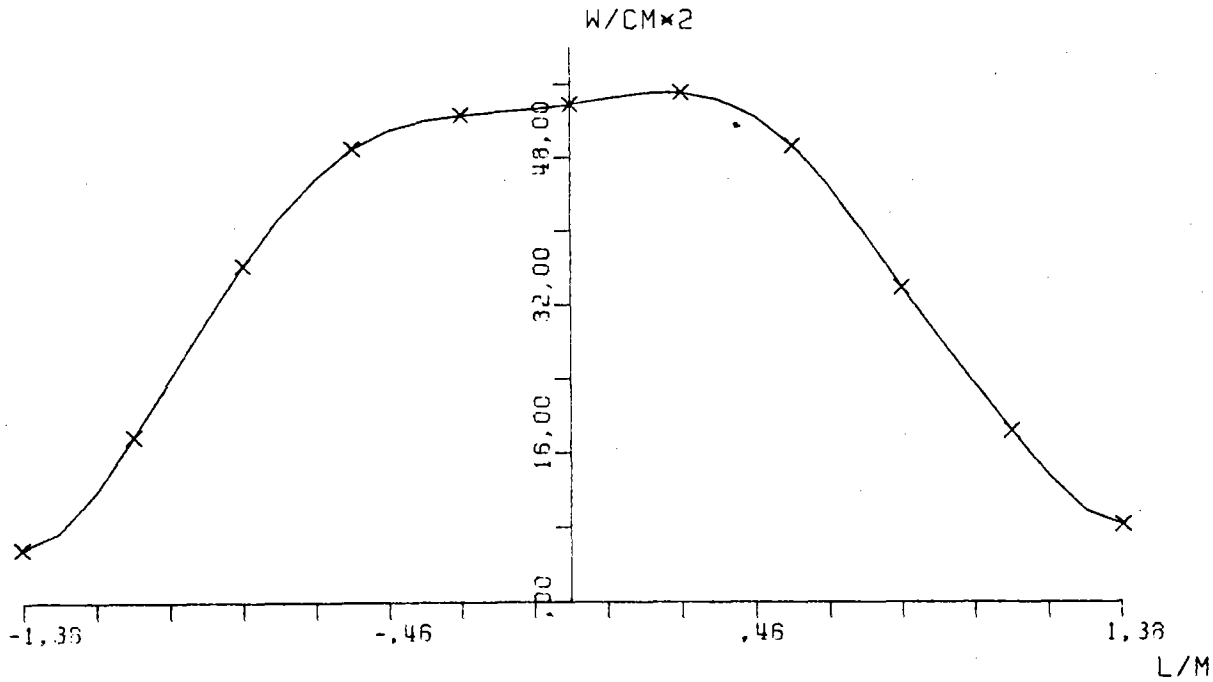

FIG.A.89 SOLAR FLUX ON TARGET SEC X-X

ASR-ALMERIA W-E CLOUD 21/3 H9.30 4321

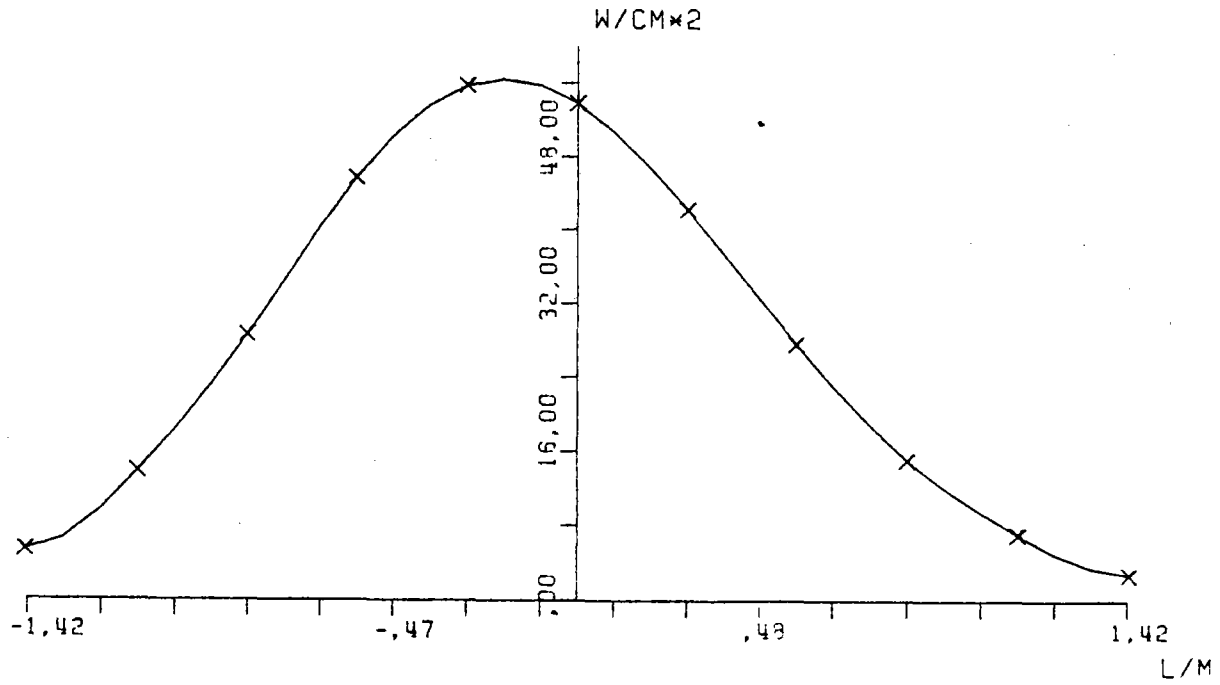

FIG.A.90 SOLAR FLUX ON TARGET SEC Y-Y

SNAMPROGETTI

ASR-ALMERIA W-E CLOUD 21/3 H9.30 321

	,11	,32	,76	1,45	2,15	2,47	2,29	1,71	1,10	,53	,32	
	,31	,59	2,08	3,77	5,30	5,90	5,35	4,10	2,72	1,60	,99	
	,76	2,14	4,60	8,13	10,7	11,7	10,6	8,67	5,60	3,42	1,31	
	1,60	4,48	9,67	14,6	18,2	19,6	18,9	15,6	10,6	6,44	3,71	
	2,31	8,20	16,7	23,2	27,1	29,0	28,9	24,9	17,4	10,6	5,96	
E.	4,50	12,4	23,5	31,0	34,7	36,2	37,1	33,9	25,1	15,3	7,54	W.
	5,70	14,7	25,1	33,5	37,1	37,3	39,5	37,2	29,1	17,2	7,40	
	5,62	13,7	23,0	29,4	32,3	31,6	32,4	31,6	25,6	14,3	5,67	
	4,78	10,1	15,9	20,4	22,6	21,5	21,3	20,6	17,2	9,77	3,37	
	3,13	5,57	8,50	11,1	12,5	11,6	11,0	10,3	8,67	4,74	1,53	
	1,60	2,71	3,58	4,79	5,37	4,65	4,39	4,06	3,32	1,71	,53	

BOT.

HELST. NO. 59.
INSOL. KW/M2 ,750
DAY NO. 80,
TIME HR. 9.30
TOWER HEIGHT M 43.
TARGET DIM. M 2,6X2,6

AIM. NO. 3,
STD.DEV. MRAD. 2,60
INC.POW. KW 1150,
AVERG./PEAK ,38
SPILLAGE %

FIG.A.91 INCIDENT FLUX ON FLAT TARGET (W/CM2)

ASR-ALMERIA W-E CLOUD 21/3 H9.30 321

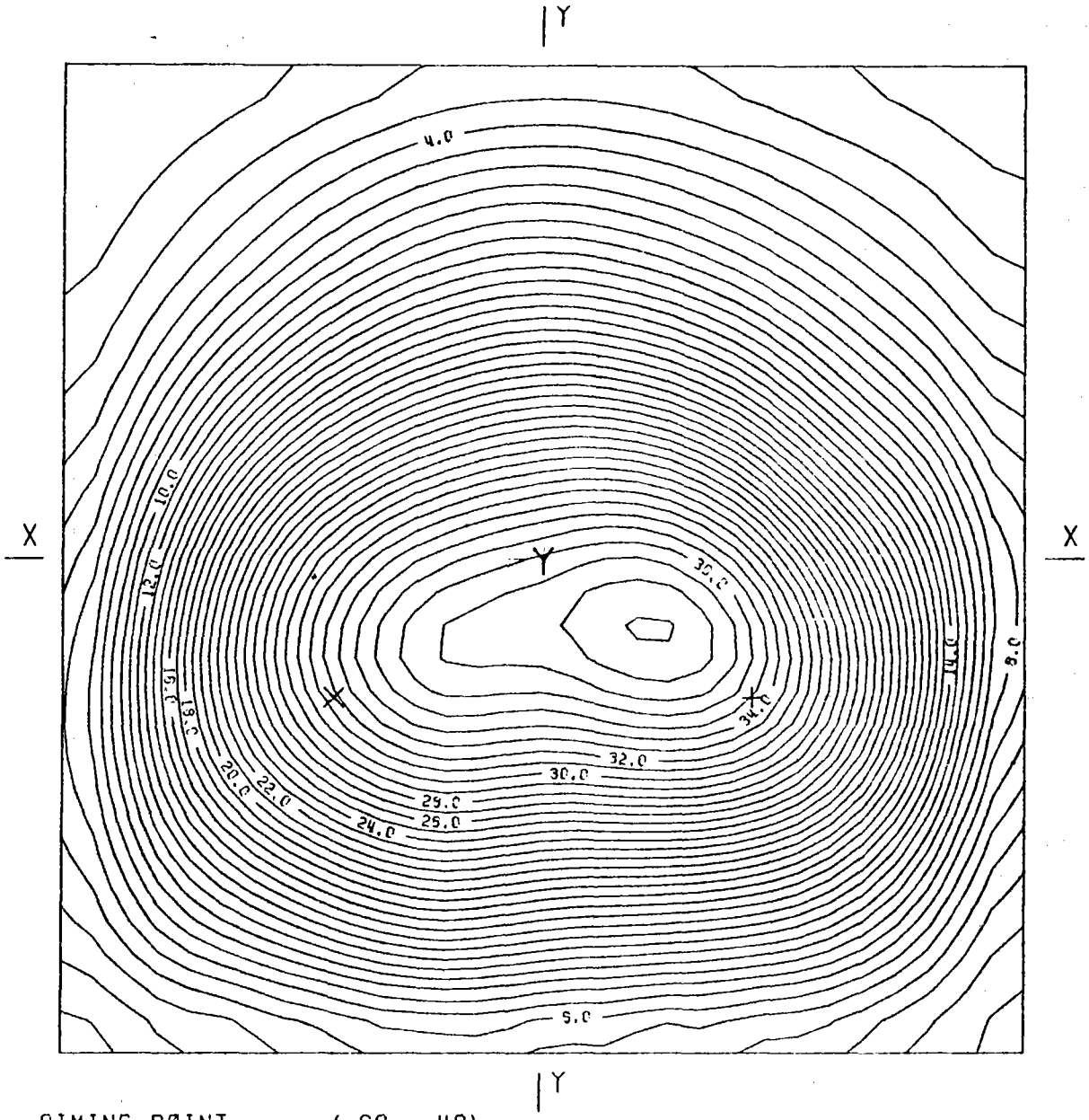

AIMING POINT: + (,60;-,40)

× (-,60;-,40)

Y (,00; ,00)

FIG.A.92 EQUIFLUX LINES, SPACING (W/CM2) 1,0

ASR-ALMERIA W-E CLOUD 21/3 H9.30 321

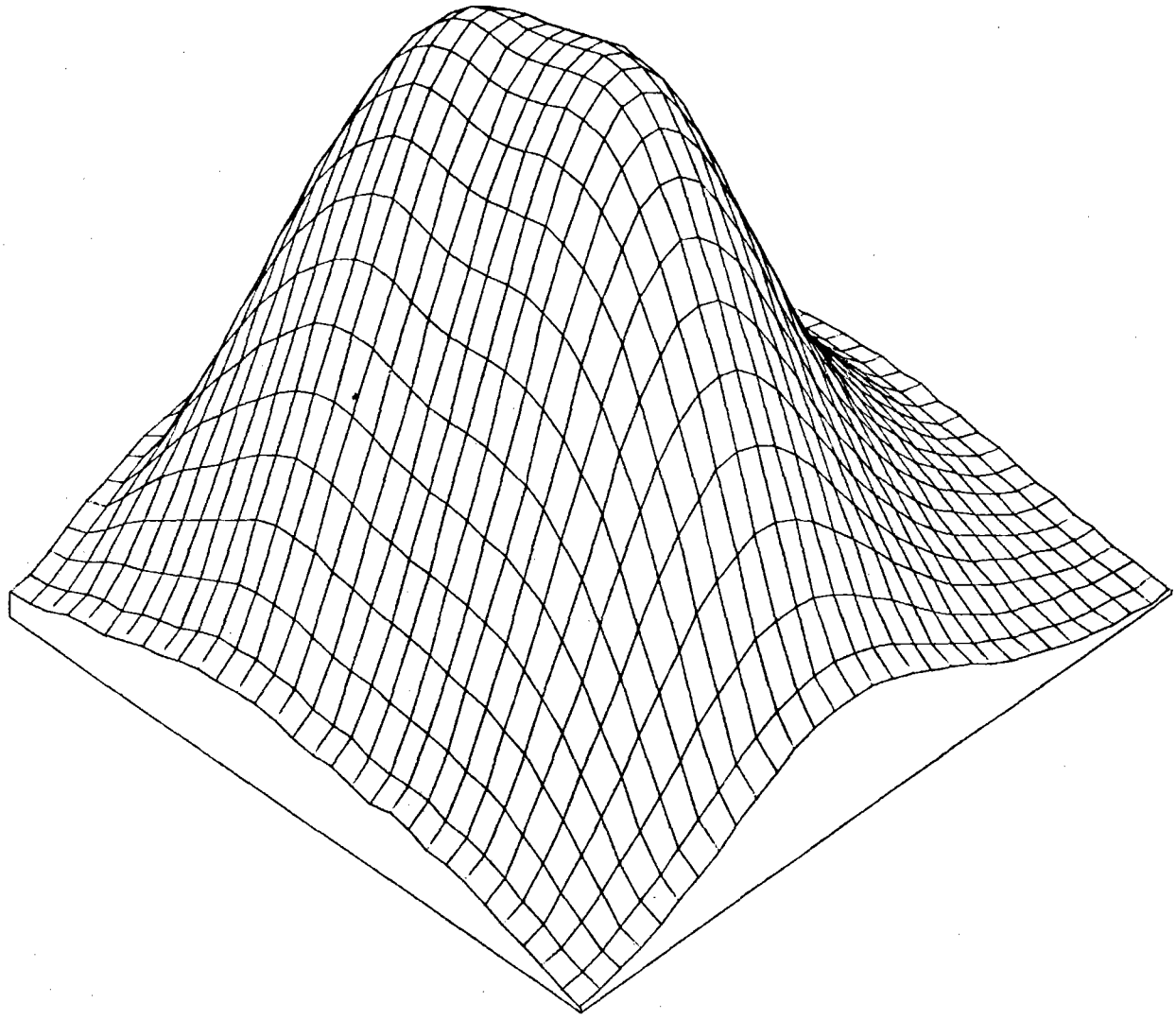

FIG.A.93 THREE-DIM. VIEW OF INCIDENT FLUX ON TARGET

SNAMPROGETTI

ASR-ALMERIA W-E CLOUD 21/3 H9.30 321

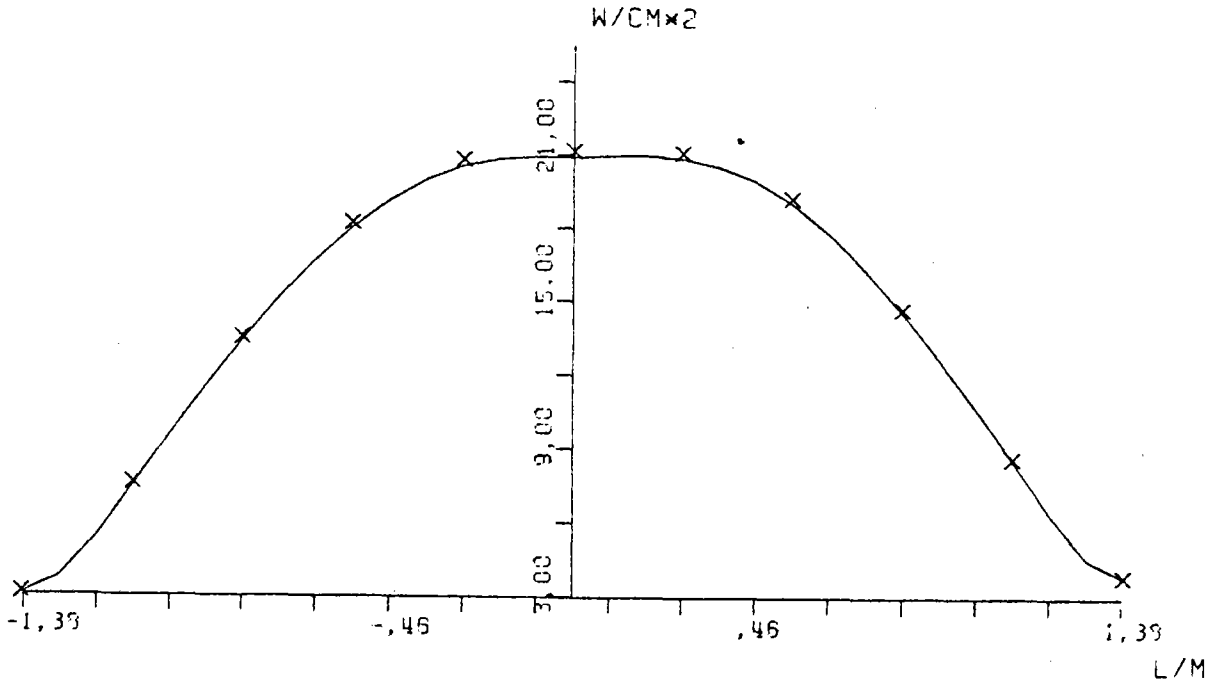

FIG.A.94 AVERAGE SOLAR FLUX ON VERTICAL STRIP

ASR-ALMERIA W-E CLOUD 21/3 H9.30 321

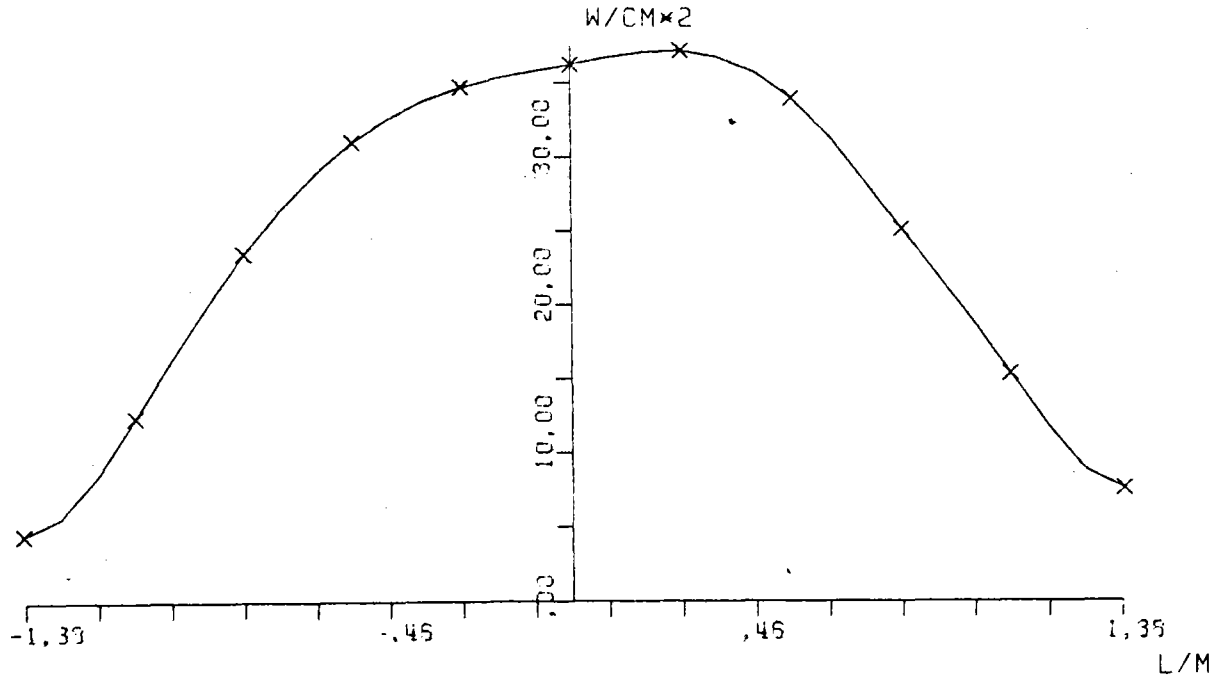

FIG.A.95 SOLAR FLUX ON TARGET SEC X-X

ASR-ALMERIA W-E CLOUD 21/3 H9.30 321

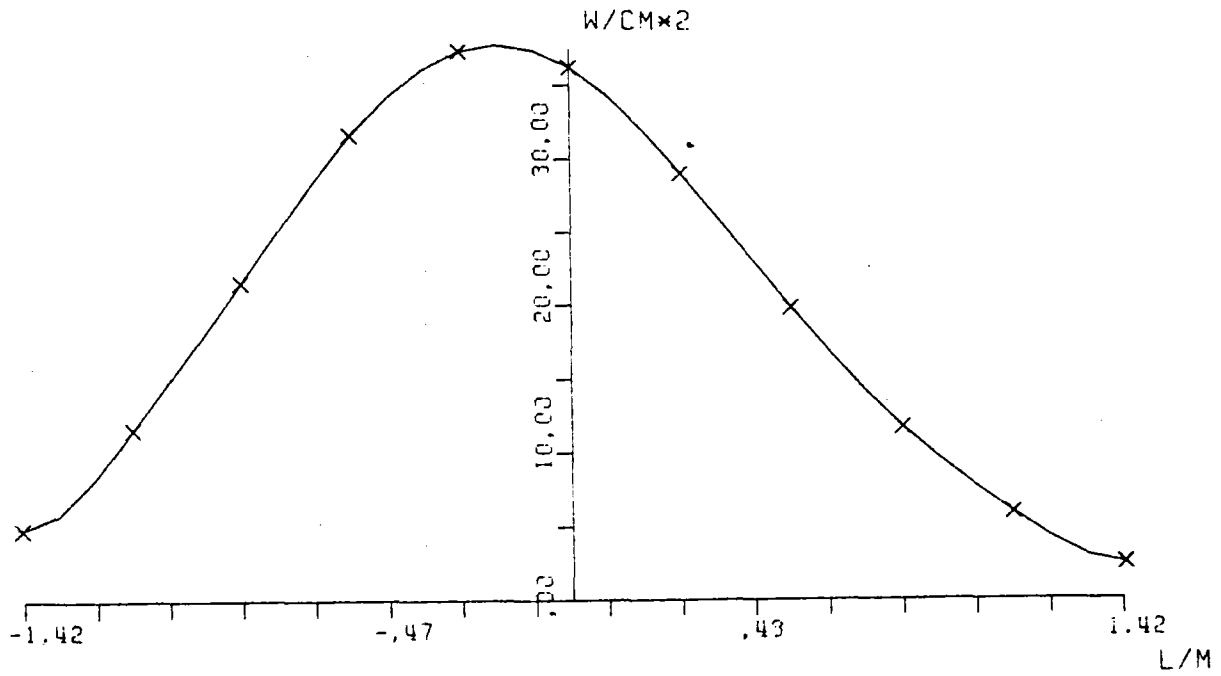

FIG.A.96 SOLAR FLUX ON TARGET SEC Y-Y

ASR-ALMERIA W-E CLOUD 21/3 H9.30 21

	,09	,25	,60	1,13	1,68	1,94	1,92	1,41	,94	,56	,30
	,25	,69	1,56	2,75	3,51	4,23	3,92	3,14	2,21	1,39	,79
	,60	1,62	3,47	5,90	7,06	7,63	7,21	6,07	4,43	2,62	1,70
	1,25	3,29	6,64	9,48	11,0	12,0	11,5	9,68	7,24	4,75	3,13
	2,25	5,60	10,2	13,0	14,6	16,2	15,6	13,0	9,45	6,56	4,56
E.	3,40	7,71	12,4	14,6	17,0	18,6	17,4	14,0	10,2	7,45	5,18 W.
	4,29	8,68	12,3	14,2	17,2	18,7	16,6	12,7	9,43	7,10	4,68
	4,60	8,25	10,7	12,4	15,7	16,4	13,7	10,2	7,67	5,67	3,48
	3,35	6,68	8,19	9,35	12,7	12,4	9,73	7,45	6,01	4,25	2,17
	2,60	4,62	5,41	6,30	8,49	7,67	5,90	4,64	4,04	2,60	1,11
	1,62	2,40	2,85	3,77	4,33	3,68	2,93	2,64	2,17	1,23	,44

BOT.

HELST. NO. 34,
INSOL. KW/M2 ,750
DAY NO. 80,
TIME HR. 9.30
TOWER HEIGHT M 43,
TARGET DIM. M 2,6X2,6

AIM. NO. 2,
STD.DEV. MRAD. 2,60
INC.POW. KW 599.
AVERG./PEAK ,41
SPILLAGE %

FIG.A97 INCIDENT FLUX ON FLAT TARGET (W/CM2)

ASR-ALMERIA W-E CLOUD 21/3 H9.30 21

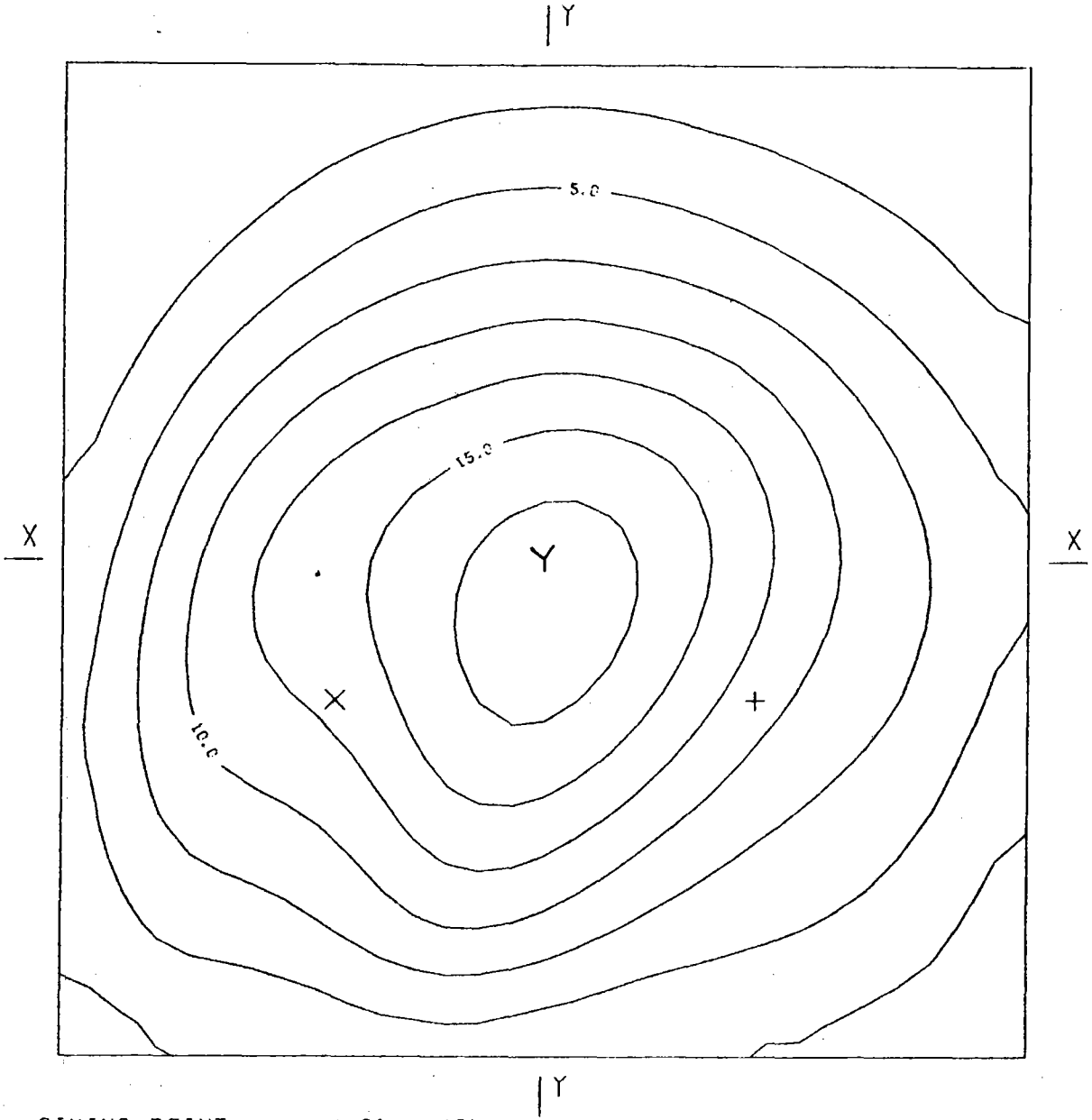

AIMING POINT: + (,60;-,40)

× (-,60;-,40)

Y (,00;,00)

FIG.A.98 EQUIFLUX LINES, SPACING (W/CM2) 2,5

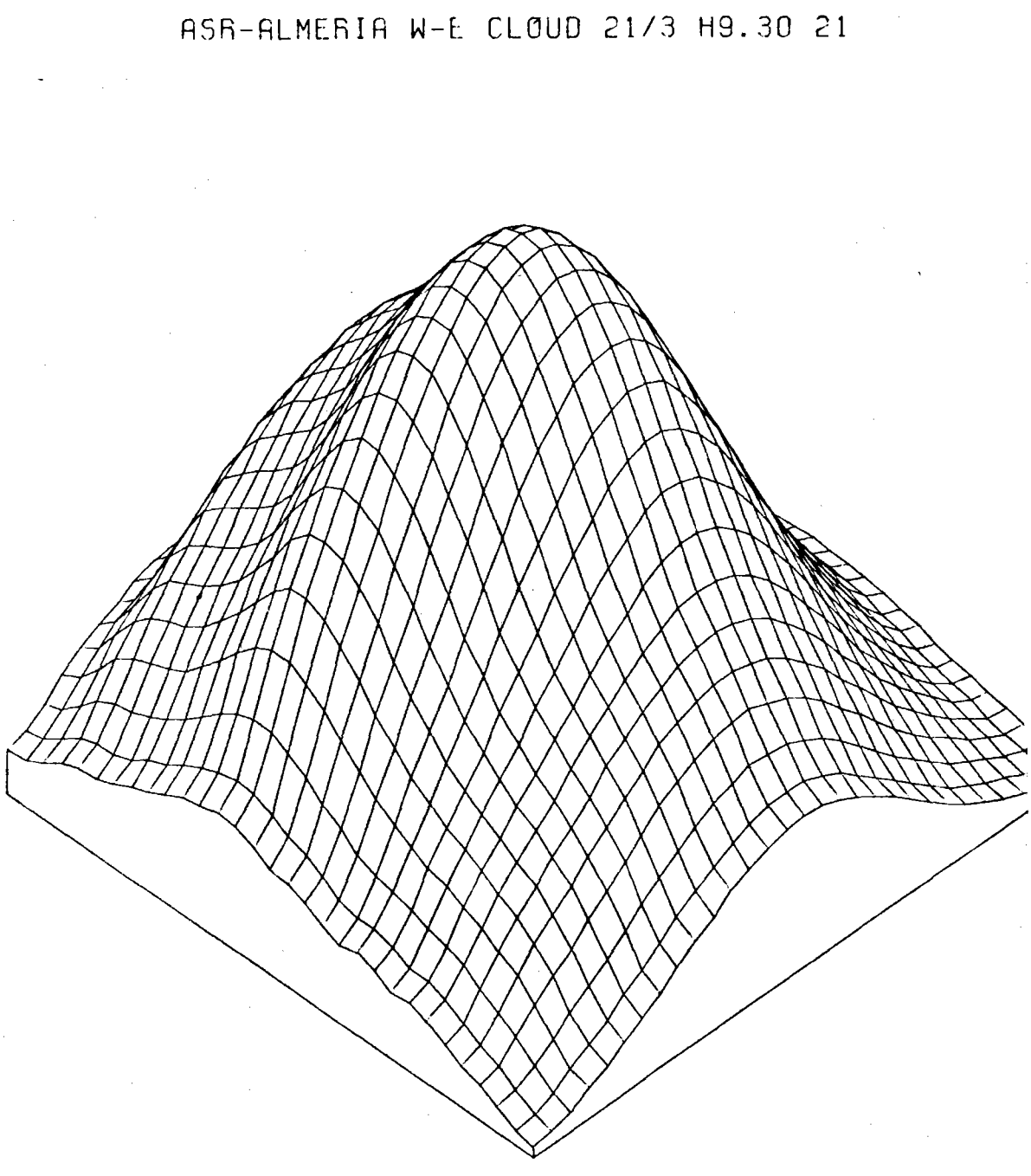

FIG.A.99 THREE-DIM. VIEW OF INCIDENT FLUX ON TARGE

ASR-ALMERIA W-E CLOUD 21/3 H9.30 21

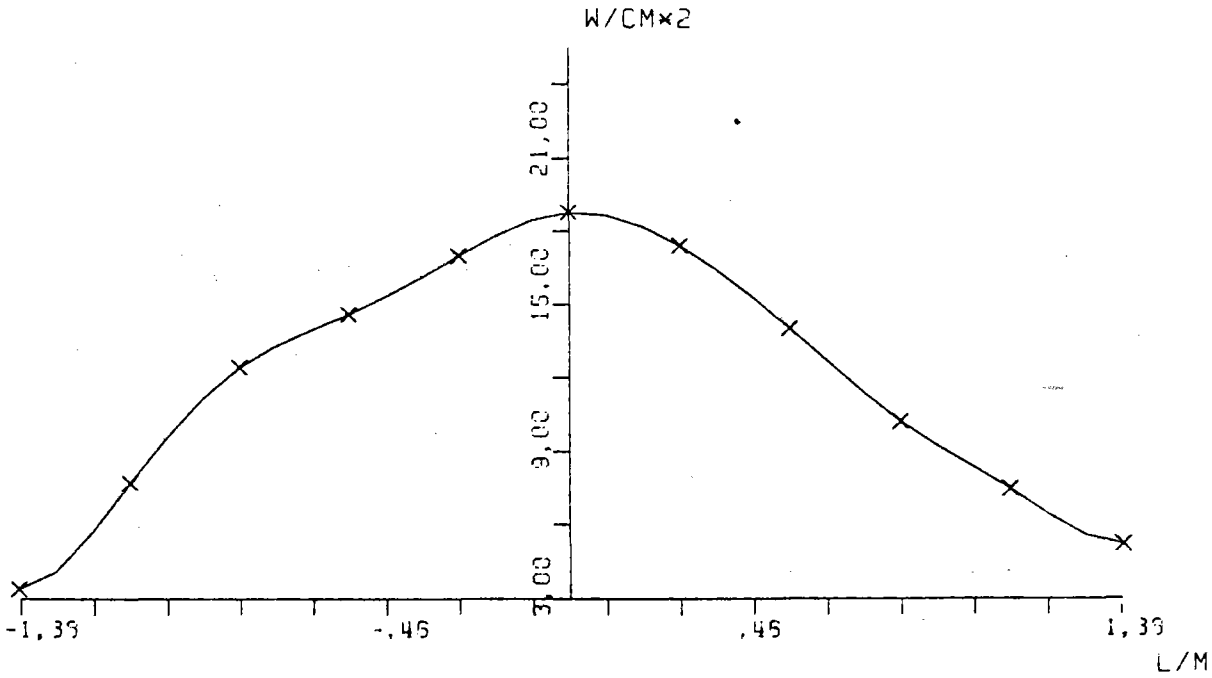

FIG.A.101 SOLAR FLUX ON TARGET SEC. X-X

ASR-ALMERIA W-E CLOUD 21/3 H9.30 21

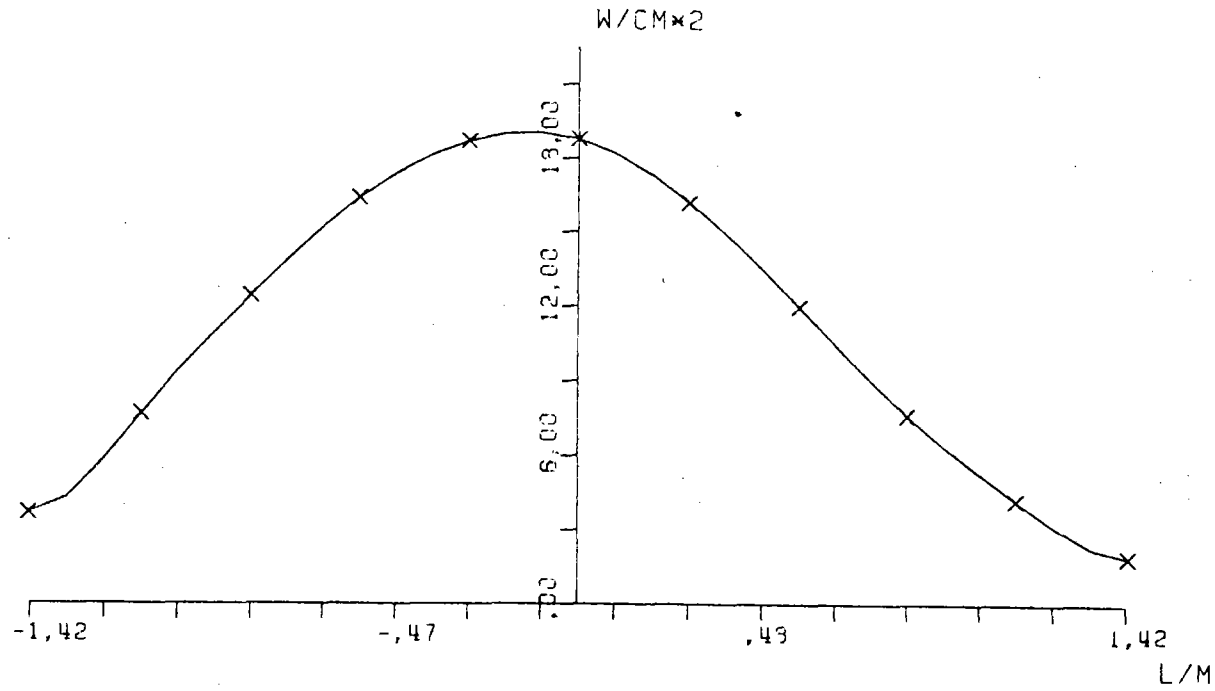

FIG.A.102 SOLAR FLUX ON TARGET SEC Y-Y

ASR-ALMERIA W-E CLOUD 21/3 H9.30 1

,06	,17	,40	,74	1,07	1,23	1,18	,95	,63	,43	,25
,17	,45	,96	1,59	2,13	2,35	2,22	1,9[illegible]	1,41	,97	,61
,41	,96	1,81	2,73	3,39	3,61	3,43	2,99	2,39	1,74	1,15
,80	1,69	2,62	3,59	4,50	4,69	4,52	4,05	3,35	2,51	1,74
1,33	2,47	3,70	4,66	5,21	5,39	5,26	4,77	3,97	3,02	2,13
1,64	3,05	4,18	4,99	5,48	5,68	5,53	4,96	4,08	3,10	2,17
2,11	3,19	4,13	4,55	5,35	5,54	5,30	4,63	3,72	2,75	1,55
1,96	2,62	3,60	4,31	4,62	4,95	4,60	3,69	3,03	2,14	1,35
1,52	2,11	2,78	3,45	3,80	3,92	3,55	2,93	2,20	1,47	,55
,94	1,35	1,90	2,43	2,72	2,68	2,39	1,95	1,41	,93	,45
,47	,75	1,12	1,43	1,56	1,52	1,37	1,11	,75	,44	,20

E.

W.

BOT.

HELST. NO. 14,
INSOL. KW/M2 ,750
DAY NO. 80,
TIME HR. 9.30
TOWER HEIGHT M 43,
TARGET DIM. M 2,6X2,6

AIM. NO. 1,
STD.DEV. MRAD. 2,60
INC.POW. KW 226,
AVERG./PEAK ,51
SPILLAGE %

FIG.A.03 INCIDENT FLUX ON FLAT TARGET (W/CM2)

ASR-ALMERIA W-E CLOUD 21/3 H9.30 1

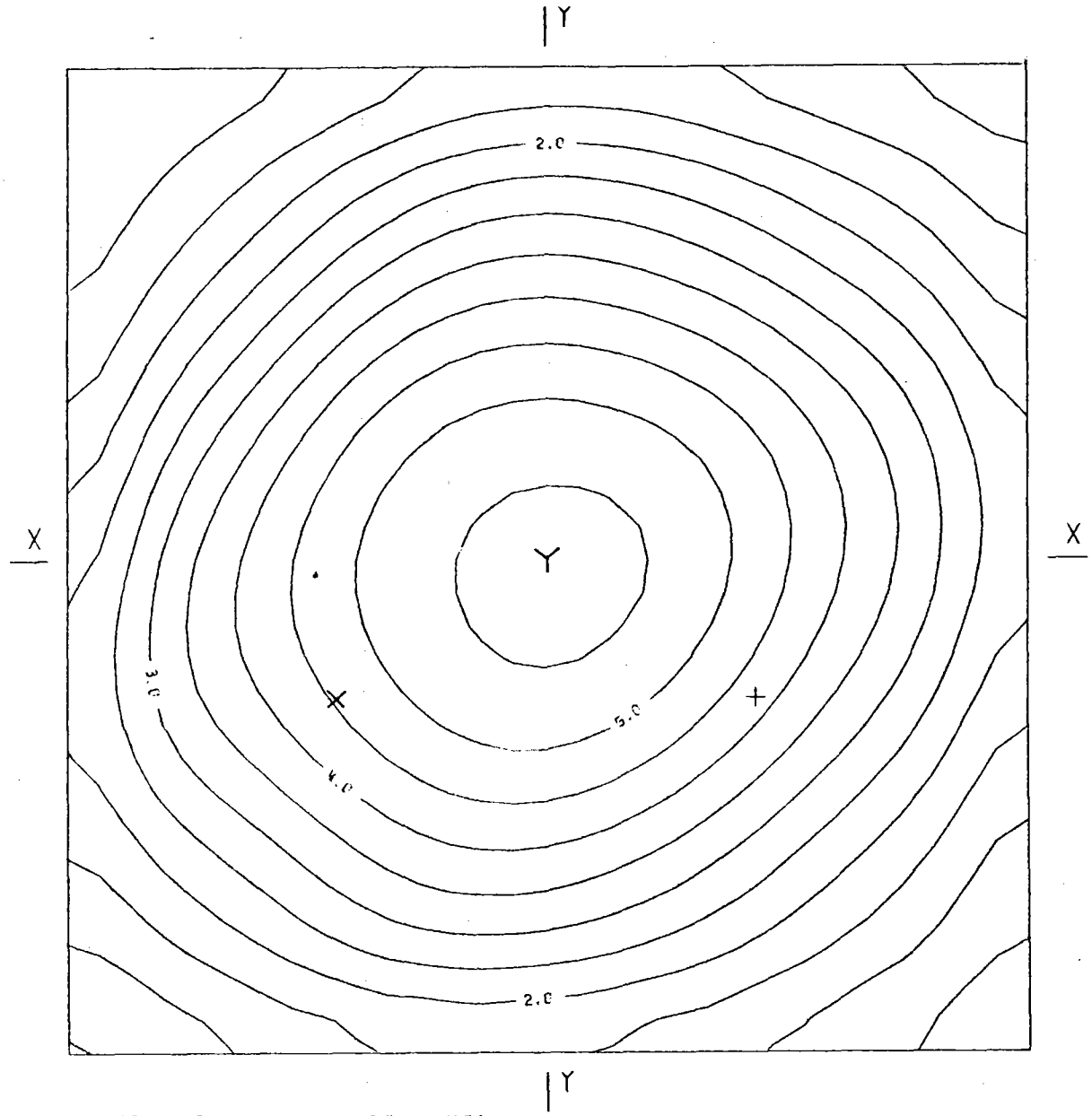

AIMING POINT: + (,60; -,40)
× (-,60; -,40)
Y (,00; 00)

FIG.A.104 EQUIFLUX LINES, SPACING (W/CM2) ,5

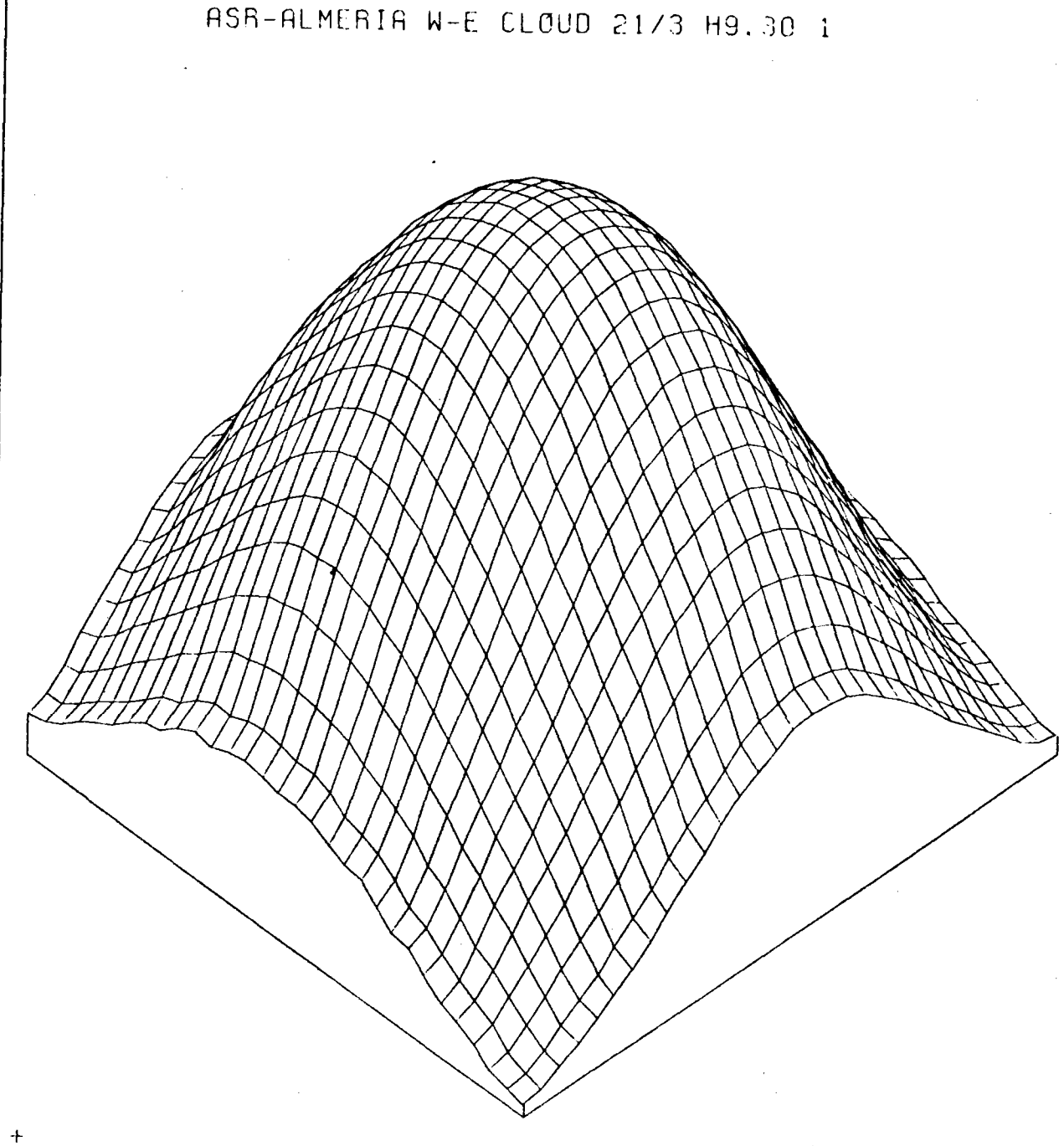

FIG.A.105 THREE-DIM. VIEW OF INCIDENT FLUX ON TARGET

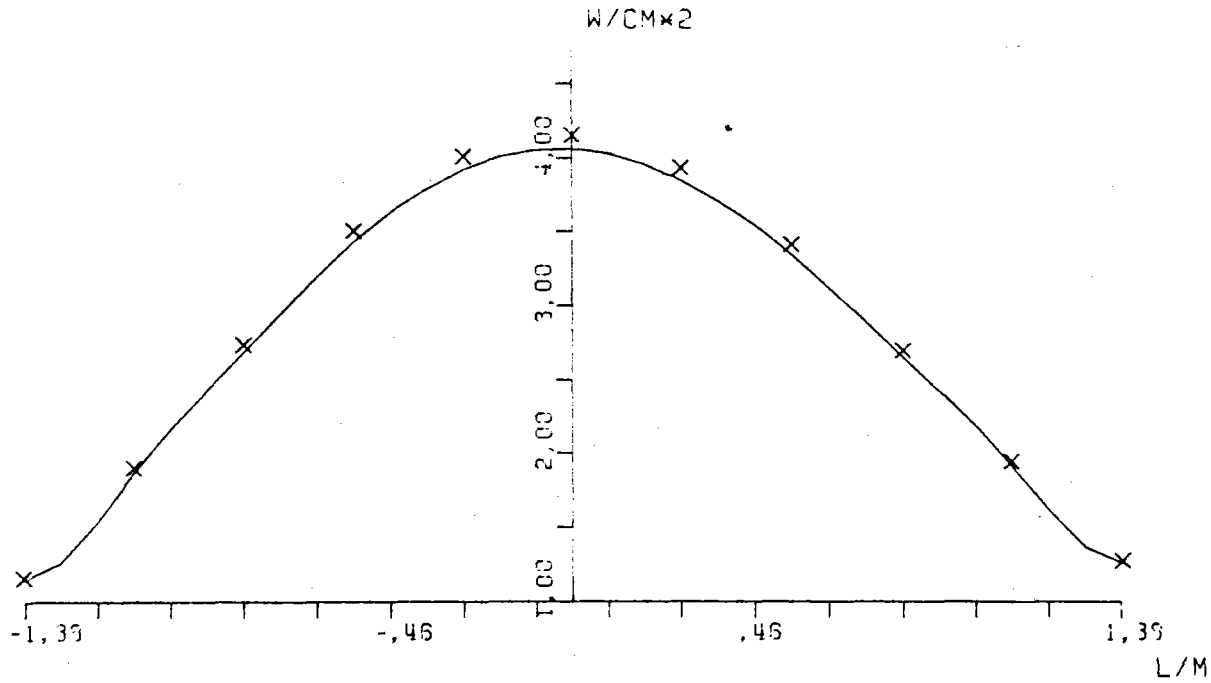

FIG.A.106 AVERAGE SOLAR FLUX ON VERTICAL STRIP

ASR-ALMERIA W-E CLOUD 21/3 H9.30 1

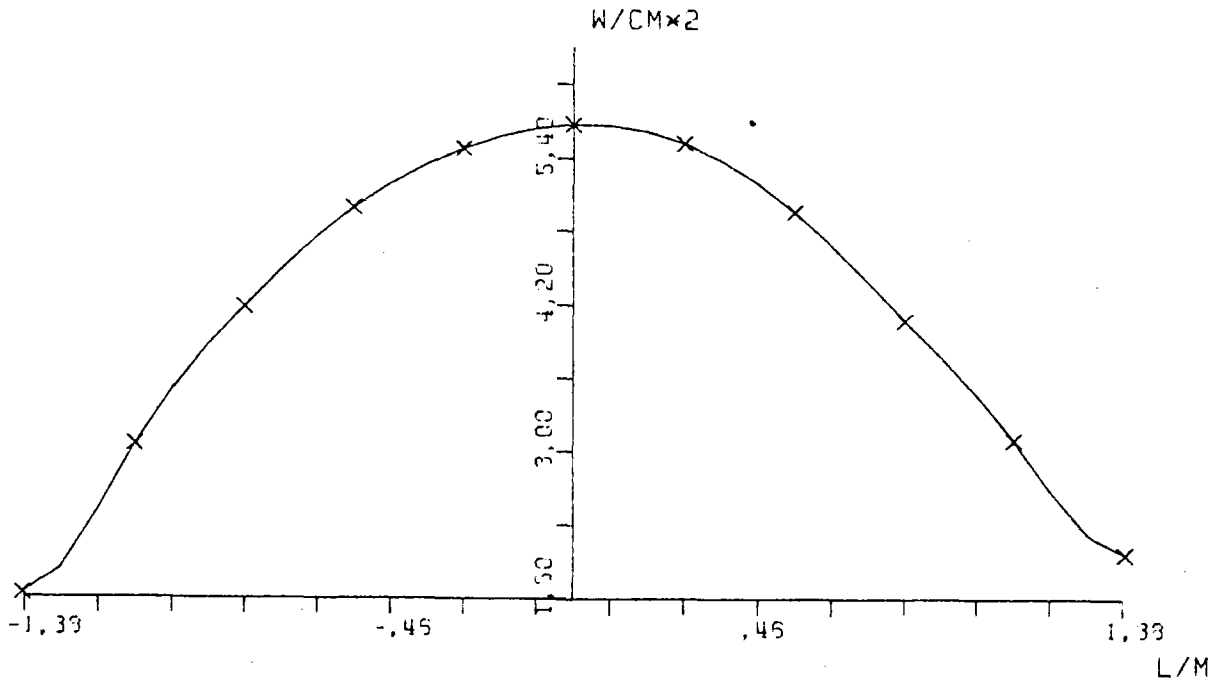

FIG.A.107 SOLAR FLUX ON TARGET SEC X-X

SNAMPROGETTI

ASR-ALMERIA W-E CLOUD 21/3 H9.30 1

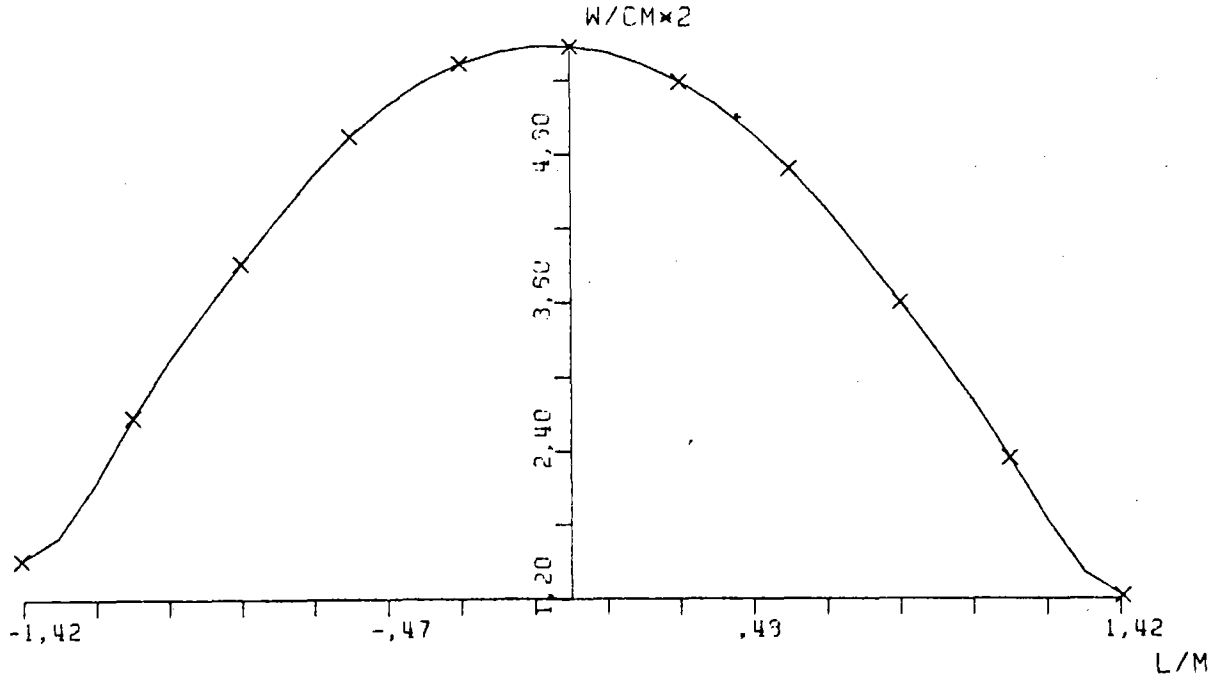

FIG.A.108 SOLAR FLUX ON TARGET SEC Y-Y

IEA ALMERIA PROJECT

ADVANCED SODIUM RECEIVER

ASR

Absorber thermal analysis

Topic Report No. 2

Revision 0

March 3rd, 1981

Prepared by: ENEL

FRANCO TOSI

SNAMPROGETTI

INDEX

Abstract

1. Introduction

2. Analysis

   2.1. Basic design data

   2.2. Incident heat flux maps

   2.3. Model features

   2.4. Heat transfer and removal: specific equations

3. Results and conclusions

References

Appendix A: Convection power loss correlations

Appendix B: Physical properties of ASTM 316 L austenitic steel

ABSTRACT

The report deals with the analytical determination of steady state temperature distribution in the ASR absorber panels.

The heat losses from the receiver are calculated. These include reflection of incident solar flux, I.R. radiation due to absorber surface temperature and convection to the atmosphere.

The approaches used in this study are presented. The most important results and graphs are shown.

1. INTRODUCTION

The absorbing surface analysed is flat, vertical, with rectangular shape, 2.73 m wide, 2.85 m high (fig. 1).

The piping arrangement is composed of 5 equal panels (fig. 2); each panel has 39 vertical side by side tubes with OD 14 mm and thickness 1 mm. Stainless steel AISI 316 L is the tube material.

Panels are connected in series and the flow is in the upward direction for all tubes (fig. 3); sodium first flows on lateral panels, than on intermediate panels and finally on the central panel.

The surfaces of the tubes exposed to solar flux are coated by Pyromark paint, having a solar absorptance of .95 and I.R. emittance of .90 .

2. ANALYSIS

2.1. Basic design data

- Design point: equinox noon
- Max power input: 2.7 thermal MW at design point
- Receiver sodium inlet temperature: 270 °C
- Receiver sodium outlet temperature: 530 °C
- Design pressure: 6 bar

2.2. Incident heat flux maps

The thermal analysis reported hereafter refers to heliostat field data and solar incident flux map shown in fig. 4, desumed from fig. 2.5 of Ref. 1.

Maximum heat flux on the absorber surface is 131 W/cm^2. Average heat flux is 30 W/cm^2. Fig. 5 shows the distribution of average solar flux on the absorber vertical strips.

2.3. Model features

Temperature distribution in the absorber tubes and performance of the receiver, considering reflected insolation, infrared radiation and convective losses, have been investigated.

For this purpose an iterative numerical technique has been emploied and the active length of each tube has been subdivided into 19 finite elements. Each panel has been characterized by 741 nodal points.

For each element, heat transfer processes taken into account for heat balance are:

- radiation absorption and emission
- conduction through tube thickness
- convection tube-to-sodium inside the receiver tubing
- convection tube-to-air outside the receiver tubing.

In the tube axial direction the heat transfer is assumed to be due to sodium mass flow only. No axial heat conduction has been taken into account.

The computer code developed for the absorber tubing thermal analysis, calculates the whole absorber (5 panels) in a single run taking into account the hydraulically coupling of panels and connection piping layout.

2.4. Heat transfer and removal: specific equations

Sodium outlet temperature and metal temperature are calculated by solving heat balance equations for each node at the absorber surface.

Consider a short section of the tube active length, the incident solar flux will be assumed not to change in the axial direction of this element. The heat flow into the element will substantially be radial.

A heat balance may be written for the case of steady state heat transfer as follows:

$$\begin{aligned}(\text{incident power}) = {} & (\text{reflected power}) + \\ & +(\text{reradiated power}) + \\ & +(\text{convection power losses}) + \\ & +(\text{absorbed power})\end{aligned} \qquad [1]$$

To evaluate the temperatures of metal and coolant at any one cross section of the tube, a heat balance in the axial direction must be written too:

$$\begin{aligned}(\text{absorbed power}) = {} & (\text{sensible heat gain by} \\ & \text{sodium})\end{aligned} \qquad [2]$$

Let us now consider each bracketed term of equations [1] and [2] separately.

- Incident power $= F \cdot A_p$

  where

  F Incident solar flux (W/m^2)

  A_p Node area $= \Delta x \cdot \Delta z$ (m^2)

  Δx Node width = tube O.D. (m)

  Δz Node height (m)

- Reflected power = $F \cdot A_p \cdot RO$

  RO — Tube coating reflectivity. For Pyromark paint the value .05 is assumed.

- Reradiated power = $\varepsilon \cdot \sigma \cdot A_p(TTE^4 - T_a^4)$

  ε — Tube coating I.R. emittance, for Pyromark paint the value .90 is assumed.

  σ — Stefan-Boltzman constant = $5.73 \cdot 10^{-8}$ $(W/m^2/°K^4)$

  TTE — Outside tube wall temperature (°K).

  T_a — Ambient air temperature = 293 (°K).

- Convection power losses = $H(TTE - T_a) \cdot A_p$

  H — Outside tube surface film coefficient $(W/m^2/°K)$. H takes into account both natural convection (H_n) and forced convection (H_f).
  The flat plate heat transfer correlations used for H_n and H_f evaluation are reported in Appendix A.

- Absorber power = $U \cdot S(TTE - TFM)$

  TFM — Average sodium temperature (°K).

  U — Overall tube thermal conductance referenced to the tube OD, d_e .

S Effective heat transfer area = $\frac{\pi \cdot d_e \cdot \Delta z}{2}$

$$\frac{1}{U} = \frac{d_e}{d_i\ h} + \frac{d_e\ \ln(d_e/d_i)}{2\ K}$$

d_i Tube ID (m).

h Sodium film coefficient calculated from the Skupinski correlation (Ref. 2)

$Nu = 4.82 + 0.0185 \cdot P_e^{0.827}$ $(W/m^2/°K)$

K Tube conductivity (W/m/°K) (see Appendix B for SS AISI 316 L).

. Sodium sensible heat gain = $\dot{M}$ CP (TFO – TFI)

$\dot{M}$ Sodium flow rate (Kg/sec).

CP Sodium specific heat (J/Kg/K).

TFO Sodium outlet temperature (°K).

TFI Sodium inlet temperature (°K).

From equations [1] and [2] it is possible to determine:

TTE Outside tube wall temperature (°C).

TTI Inside tube wall temperature (°C).

TFM Average sodium temperature (°C).

TTM Average tube wall temperature (°C).

TEMAX Maximum outside wall temperature (°C).

DTMAX Maximum temperature difference across the tube wall (°C).

For TEMAX and DTMAX a semplified evaluation is performed by the code taking no account of circumferential conduction and assuming a complete mixing of sodium in the section.

Under these assumptions the equation [1] (one dimensional) may be written and solved at any fixed node around the tube wall accounting for the circumferential heat flux distribution. The code performs this analysis for the midpoint node of the tube hot side.

The results of this procedure were tested by a two dimensional heat transfer analysis performed using the finite element computer code FLHE.

The comparison of the results showed a very good accordance between predictions of these two analytical procedures confirming the validity of the formulated assumptions.

3. RESULTS AND CONCLUSIONS

All 195 tubes of the receiver have been analysed. Each tube is identifiable by a progressive number from 1 to 195 moving from east to west along the width of absorber surface.

Figures from 6 to 20 show the plots of the extreme and middle tubes of each panel. For the same tubes tables from 1 to 15 summarize the computer input data and the predicted thermal performance.

The same analysis performed at equinox noon has been performed at 7.15 and 9.30 on March 21 to evaluate thermal performance of the receiver at partial loads. The resultant curve of receiver efficiency versus absorbed power is shown in fig. 21.

Owing to the flow rate adjustment according to the absorbed power, convection and reradiated power losses increase in percentage at partial loads significantly.

Fig. 22 shows the graph of receiver thermal losses as function of the absorbed power.

REFERENCES

1 - Advanced sodium receiver ASR - Progress Report No. 6, 16 Dec. 1980

2 - E. Skupinski, J. Tortel et L. Vautrey: Determination des coefficientes de convection d'un alliage sodium-potassium dans un tube circulare, Int. J. Heat Mass Transfer, Vol. 8, 1965

3 - Conceptual design of advanced central receiver power systems, Final Technical Report, SAN/20500-1, June 1979

4 - E.M. Sparrow and J.L. Gregg: Buoyancy effects in forced convection flow and heat transfer, Trans. ASME, Journal of Applied Mechanics, Ser.E, Vol. 81, 1959

5 - F. Kreith: Principles of heat transfer, Third Edition, Intext Educational Publisher, New York, 1973

6 - Conceptual design of advanced central receiver power systems, Sodium cooled receiver concept, Final Report, SAN/1483-1/3, 1979

7 - Sandvik steel catalogue, 1,842E - 3R60, Sandviken September 1975

FIG. 1

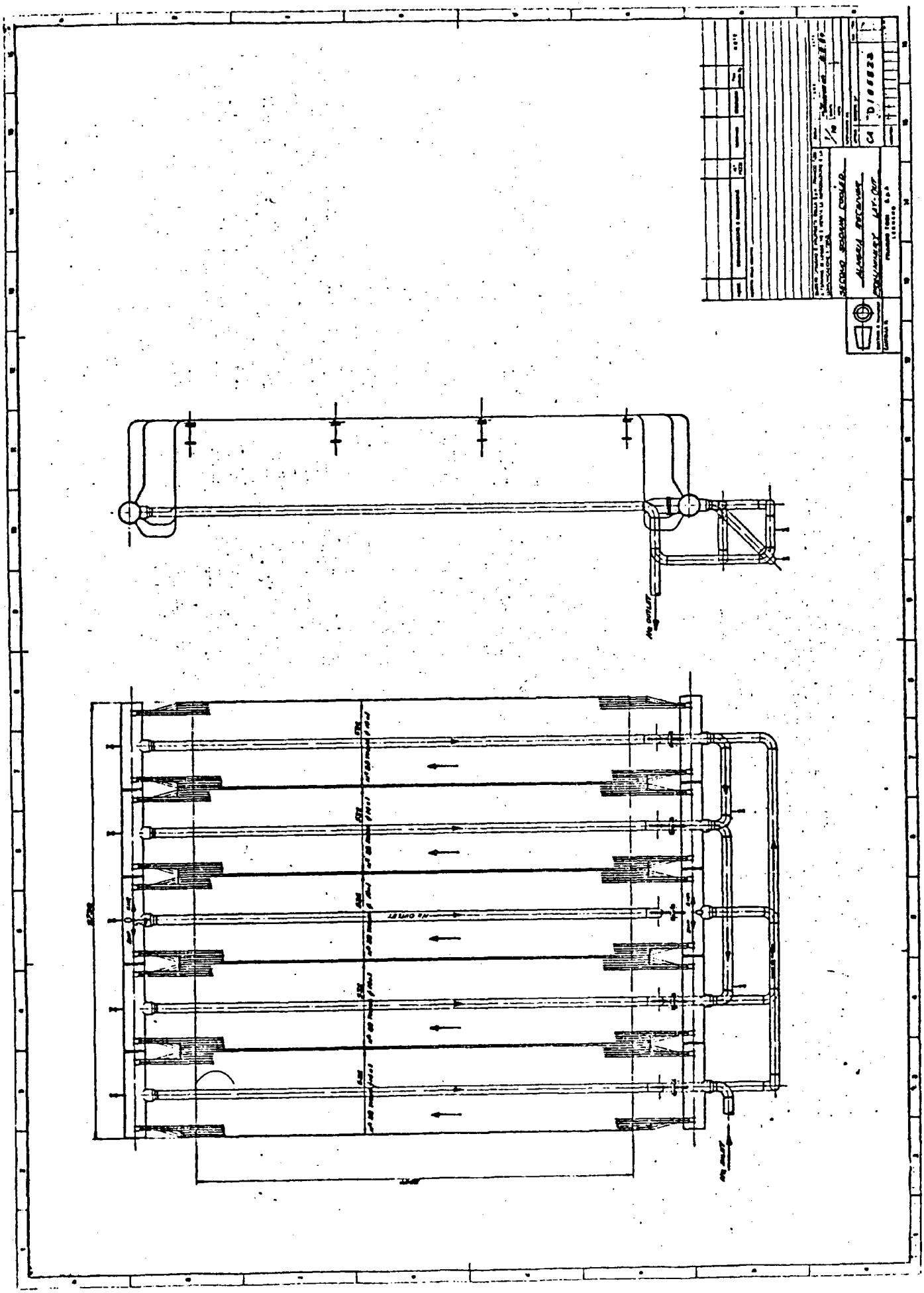

FIG. 2

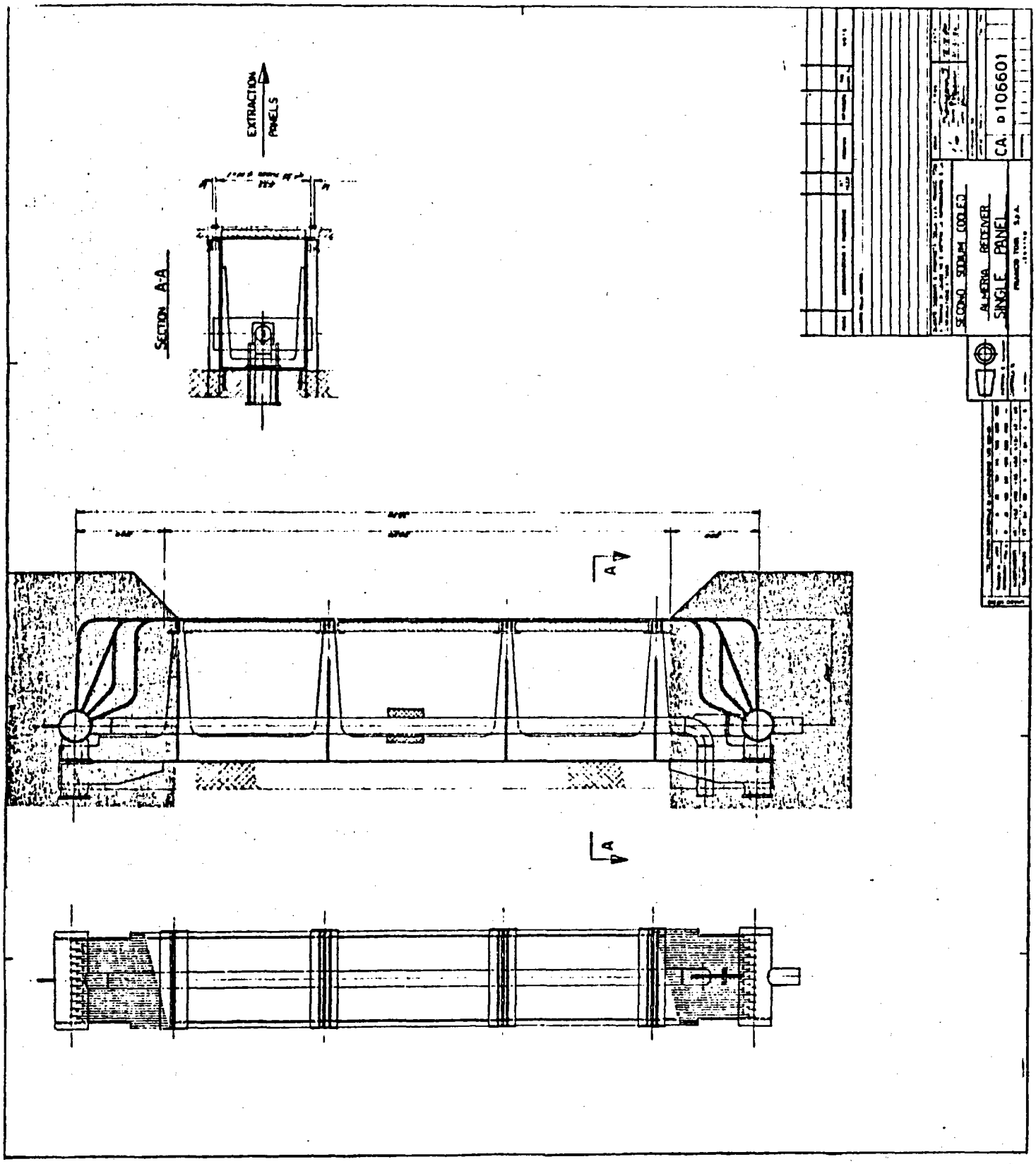
EXTRACTION
PANELS
SECTION A-A
A
A
SECOND SOLIDIFIED
ALUMINA REFINERY
SINGLE PANEL
CA. D106601

FIG. 3

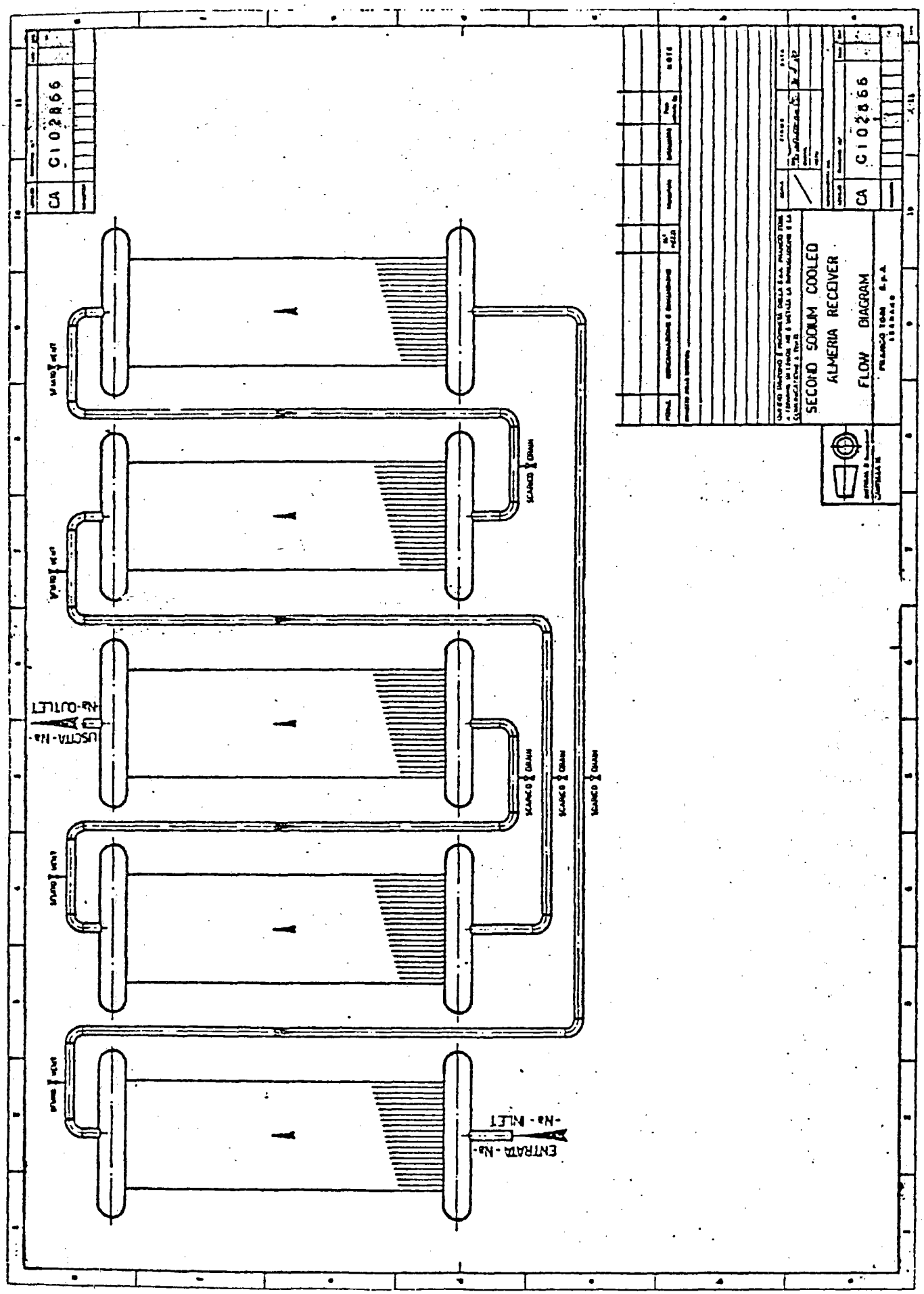
CA C102866
SECOND SODIUM COOLED
ALMERIA RECOVER
FLOW DIAGRAM
CA C102866
USCITA - Na - OUTLET
ENTRATA - Na - INLET
SCARICO DRAIN

ALMERIA ,93HLS., DAY 81, H 12, S.O.2,6MR., TN= 20°C

	.00	.10	.30	.50	1.00	1.10	1.00	.50	.30	.10	.00	
	.10	.50	1.30	2.70	4.20	5.00	4.20	2.70	1.30	.50	.10	
	.40	1.40	4.10	9.20	15.5	19.4	15.5	9.20	4.10	1.40	.40	
	.50	3.30	10.2	24.2	41.6	50.0	41.6	24.2	10.2	3.30	.50	
	1.50	5.90	22.2	49.7	90.1	93.5	90.0	49.7	22.2	6.90	1.60	
EAST	2.30	13.5	47.2	91.7	119.	124.	119.	91.3	46.9	13.6	2.50	WEST
	2.60	13.1	71.6	126.	131.	119.	130.	125.	70.6	19.2	2.90	
	2.20	15.6	57.9	96.7	91.0	75.1	90.1	96.0	57.2	15.9	2.40	
	1.20	6.90	22.0	35.5	34.2	29.3	33.9	35.3	21.9	7.00	1.30	
	.40	1.60	3.90	6.20	7.10	7.10	7.10	6.30	4.00	1.70	.50	
	.00	.20	.50	.80	1.20	1.30	1.20	.80	.50	.20	.10	

BOTTOM

HEL.N.	93	AIM. N.	3,
INSOL. KW/M2	0.92	STD.DEV. MRAD	2.6
DAY N.	81,	INC.POW. MW	2.77
TIME H.	12,	AVERG./PEAK	0.25
TOWER M	43,	SPILLAGE %	0.62
TARGET M	3,3,		

INCIDENT FLUX ON FLAT TARGET (W/CM2)

— FIG. 4 —

ALMERIA,93HLS.,DAY 81,H 12,S.O.2.6MR.,TN

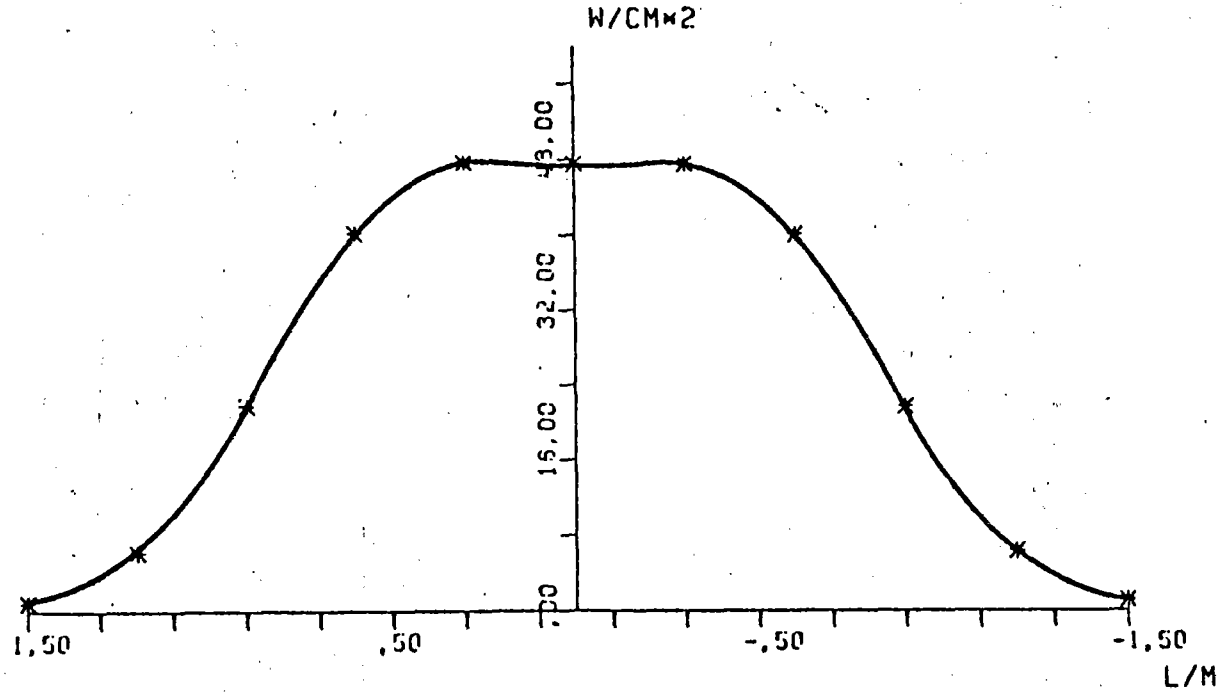

FIG. 5

AVERAGE SOLAR FLUX ON VERTICAL STRIP

SNAMPROGETT

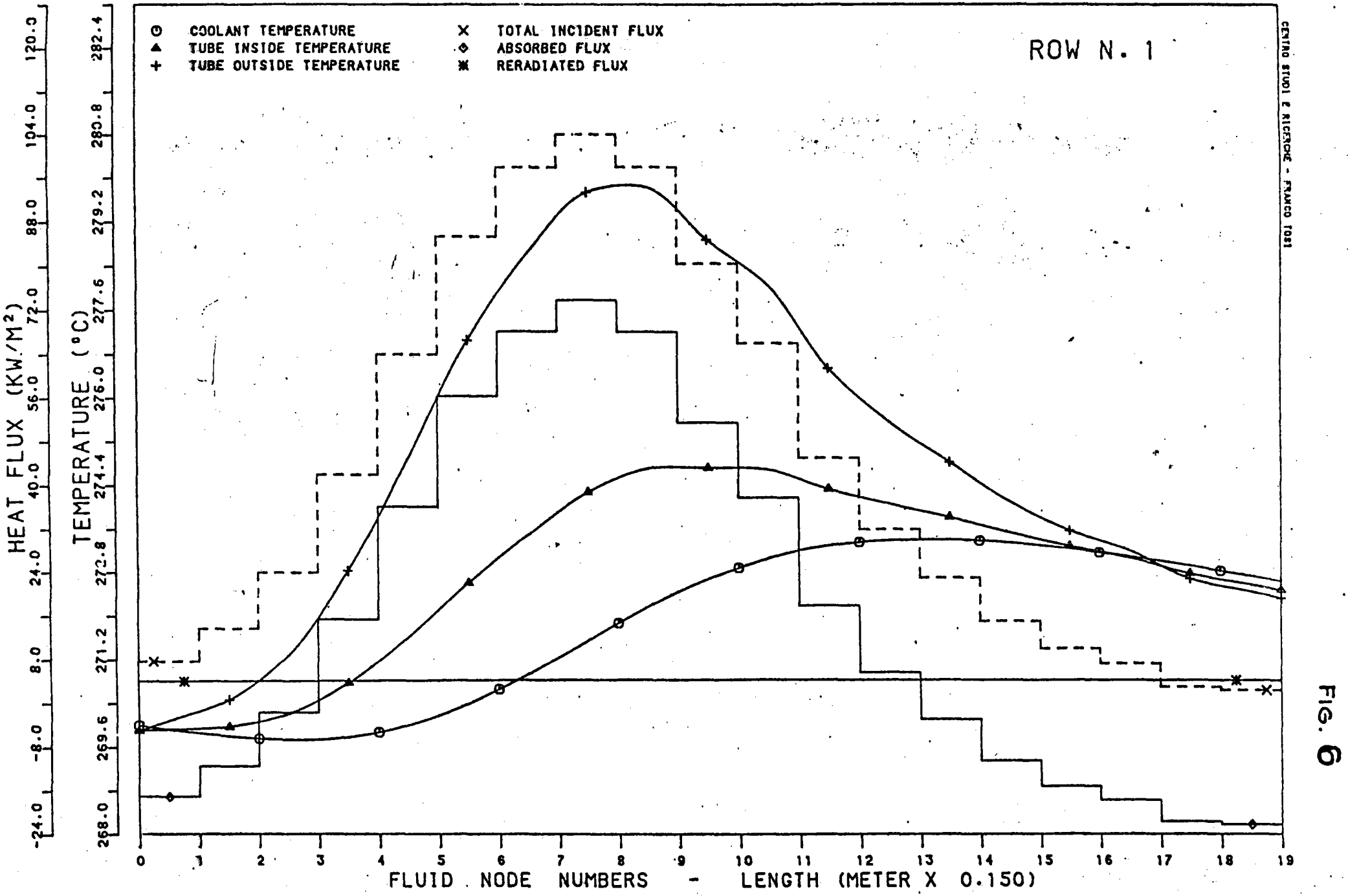
COOLANT TEMPERATURE
TUBE INSIDE TEMPERATURE
TUBE OUTSIDE TEMPERATURE
TOTAL INCIDENT FLUX
ABSORBED FLUX
RERADIATED FLUX
ROW N. 1
HEAT FLUX (KW/M²)
TEMPERATURE (°C)
-24.0
-8.0
8.0
24.0
40.0
56.0
72.0
88.0
104.0
120.0
268.0
269.6
271.2
272.8
274.4
276.0
277.6
279.2
280.8
282.4
0
1
2
3
4
5
6
7
8
9
10
11
12
13
14
15
16
17
18
19
FLUID NODE NUMBERS - LENGTH (METER X 0.150)
CENTRO STUDI E RICERCHE - FIAMCO 1981

FIG. 6

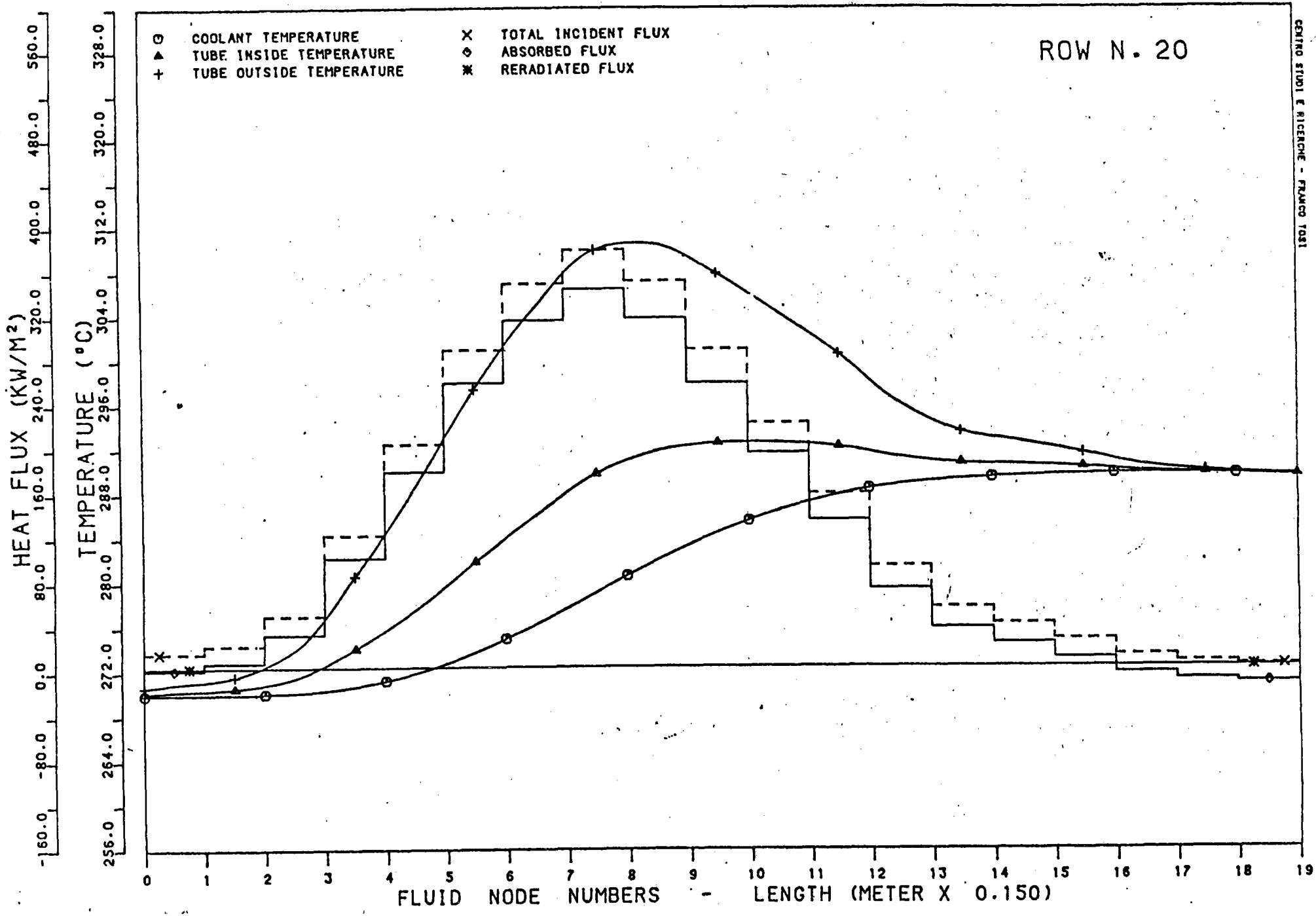
COOLANT TEMPERATURE
TUBE INSIDE TEMPERATURE
TUBE OUTSIDE TEMPERATURE
TOTAL INCIDENT FLUX
ABSORBED FLUX
RERADIATED FLUX
ROW N. 20
HEAT FLUX (KW/M²)
TEMPERATURE (°C)
-160.0
-80.0
0.0
80.0
160.0
240.0
320.0
400.0
480.0
560.0
256.0
264.0
272.0
280.0
288.0
296.0
304.0
312.0
320.0
328.0
0 1 2 3 4 5 6 7 8 9 10 11 12 13 14 15 16 17 18 19
FLUID NODE NUMBERS - LENGTH (METER X 0.150)
CENTRO STUDI E RICERCHE - FRANCO TOSI

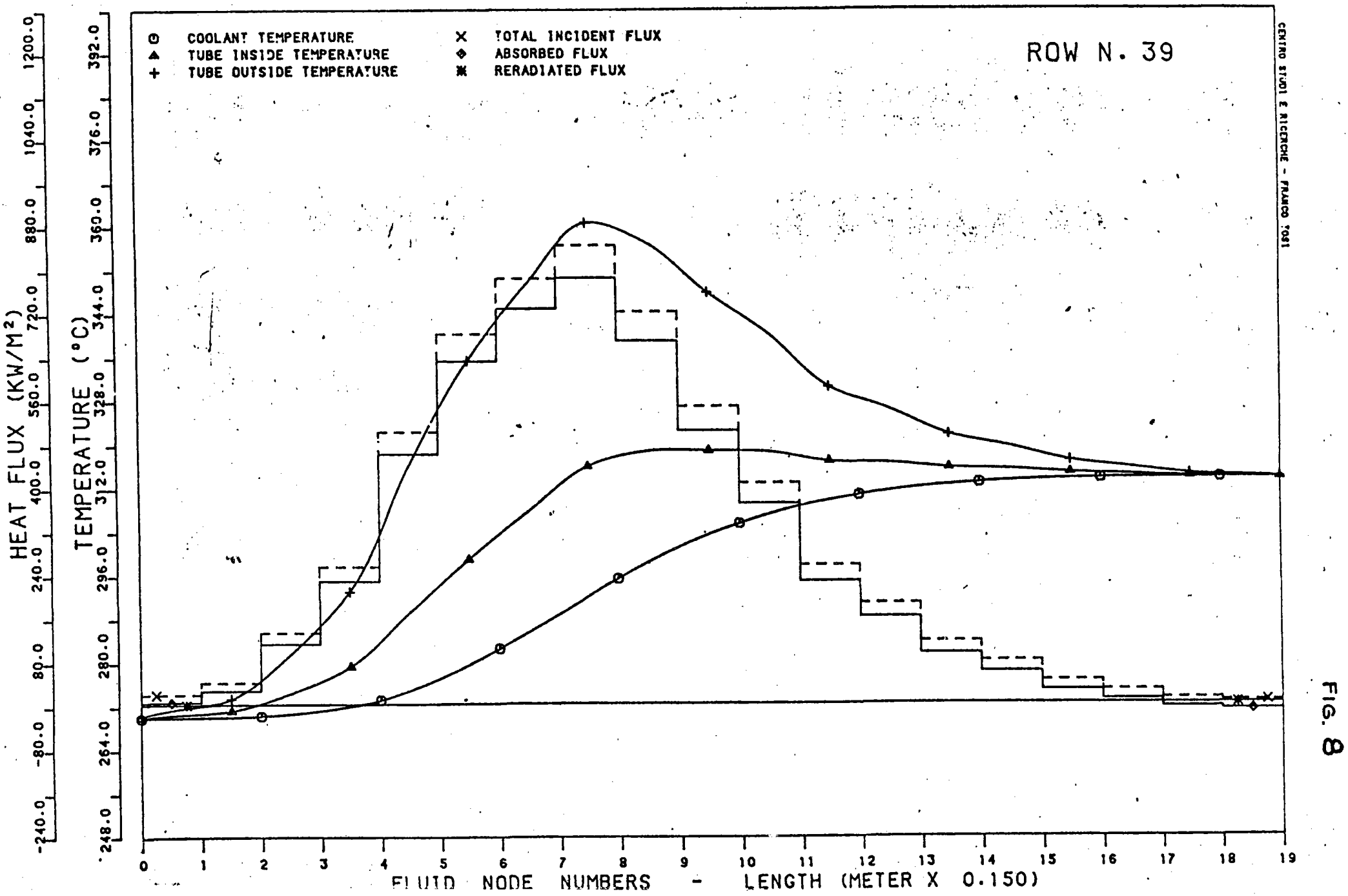
COOLANT TEMPERATURE
TUBE INSIDE TEMPERATURE
TUBE OUTSIDE TEMPERATURE
TOTAL INCIDENT FLUX
ABSORBED FLUX
RERADIATED FLUX
ROW N. 39
CENTRO STUDI E RICERCHE - FRANCO 1981
HEAT FLUX (KW/M²)
-240.0
-80.0
80.0
240.0
400.0
560.0
720.0
880.0
1040.0
1200.0
TEMPERATURE (°C)
248.0
264.0
280.0
296.0
312.0
328.0
344.0
360.0
376.0
392.0
0 1 2 3 4 5 6 7 8 9 10 11 12 13 14 15 16 17 18 19
FLUID NODE NUMBERS - LENGTH (METER X 0.150)

FIG. 8

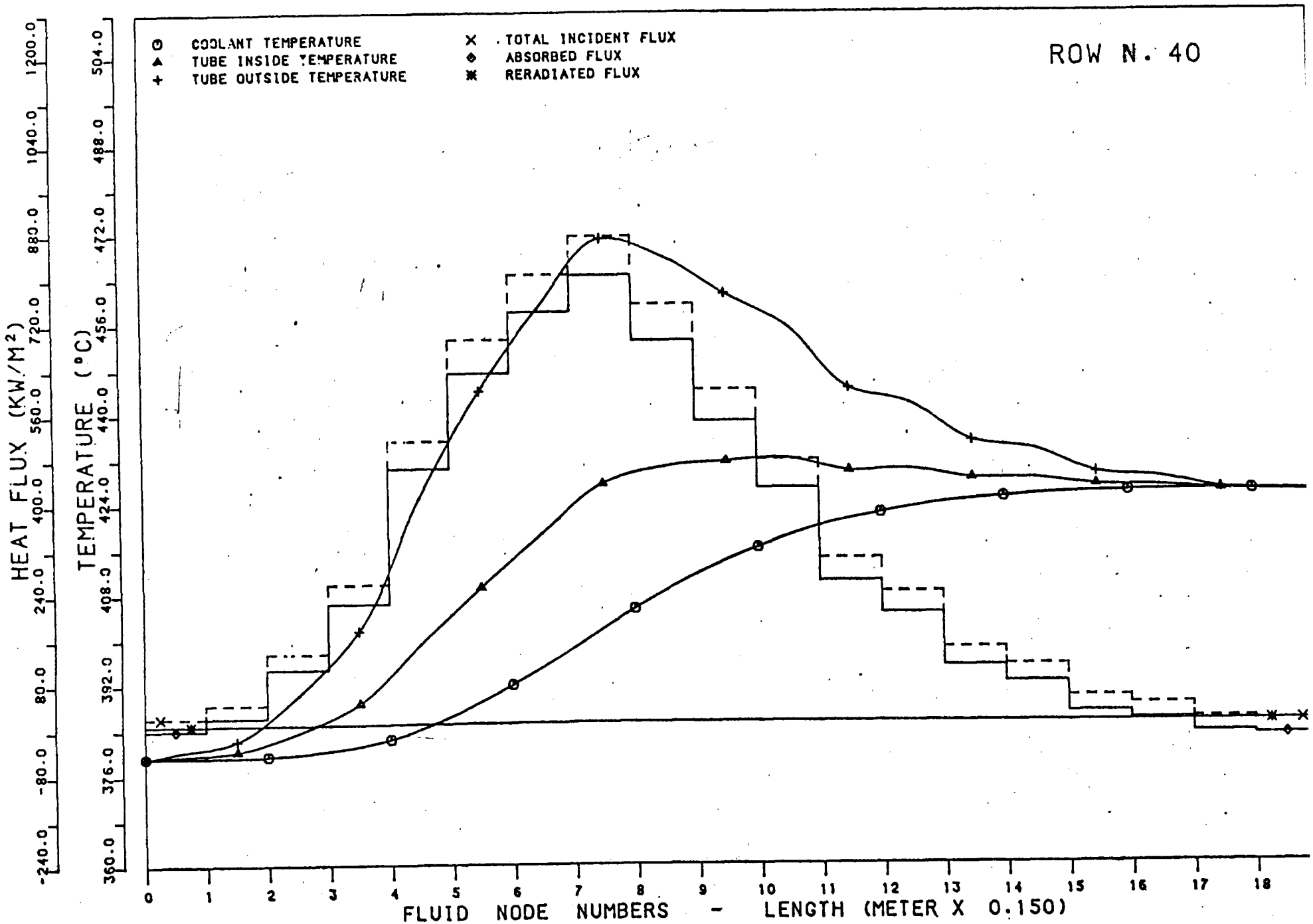
COOLANT TEMPERATURE
TUBE INSIDE TEMPERATURE
TUBE OUTSIDE TEMPERATURE
TOTAL INCIDENT FLUX
ABSORBED FLUX
RERADIATED FLUX
ROW N. 40
HEAT FLUX (KW/M²)
-240.0
-80.0
80.0
240.0
400.0
560.0
720.0
880.0
1040.0
1200.0
TEMPERATURE (°C)
360.0
376.0
392.0
408.0
424.0
440.0
456.0
472.0
488.0
504.0
0 1 2 3 4 5 6 7 8 9 10 11 12 13 14 15 16 17 18
FLUID NODE NUMBERS - LENGTH (METER X 0.150)

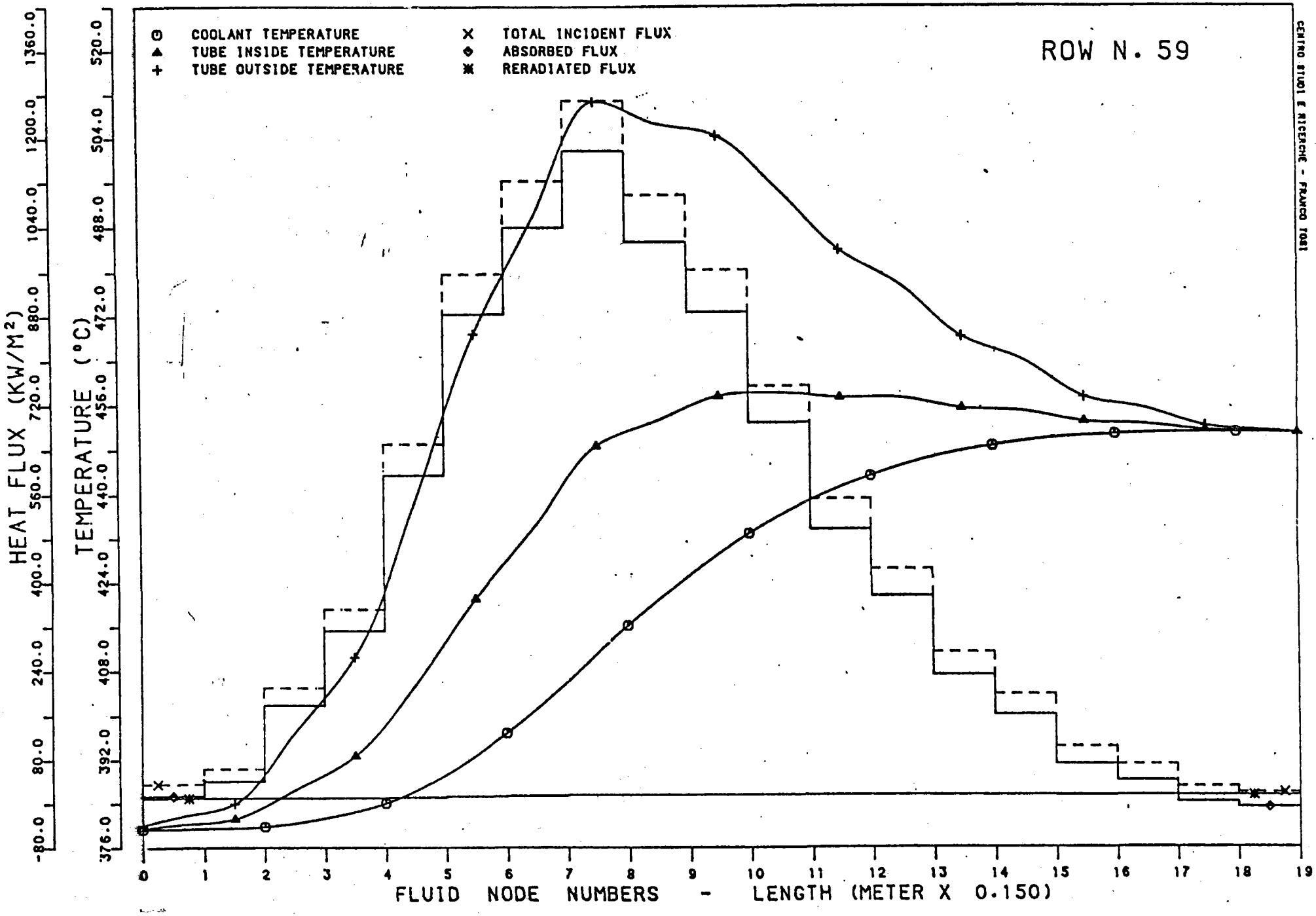
COOLANT TEMPERATURE
TUBE INSIDE TEMPERATURE
TUBE OUTSIDE TEMPERATURE
TOTAL INCIDENT FLUX
ABSORBED FLUX
RERADIATED FLUX
ROW N. 59
HEAT FLUX (KW/M²)
TEMPERATURE (°C)
-80.0
80.0
240.0
400.0
560.0
720.0
880.0
1040.0
1200.0
1360.0
376.0
392.0
408.0
424.0
440.0
456.0
472.0
488.0
504.0
520.0
0
1
2
3
4
5
6
7
8
9
10
11
12
13
14
15
16
17
18
19
FLUID NODE NUMBERS - LENGTH (METER X 0.150)
CENTRO STUDI E RICERCHE - FRANCO TOSI

FIG. 10

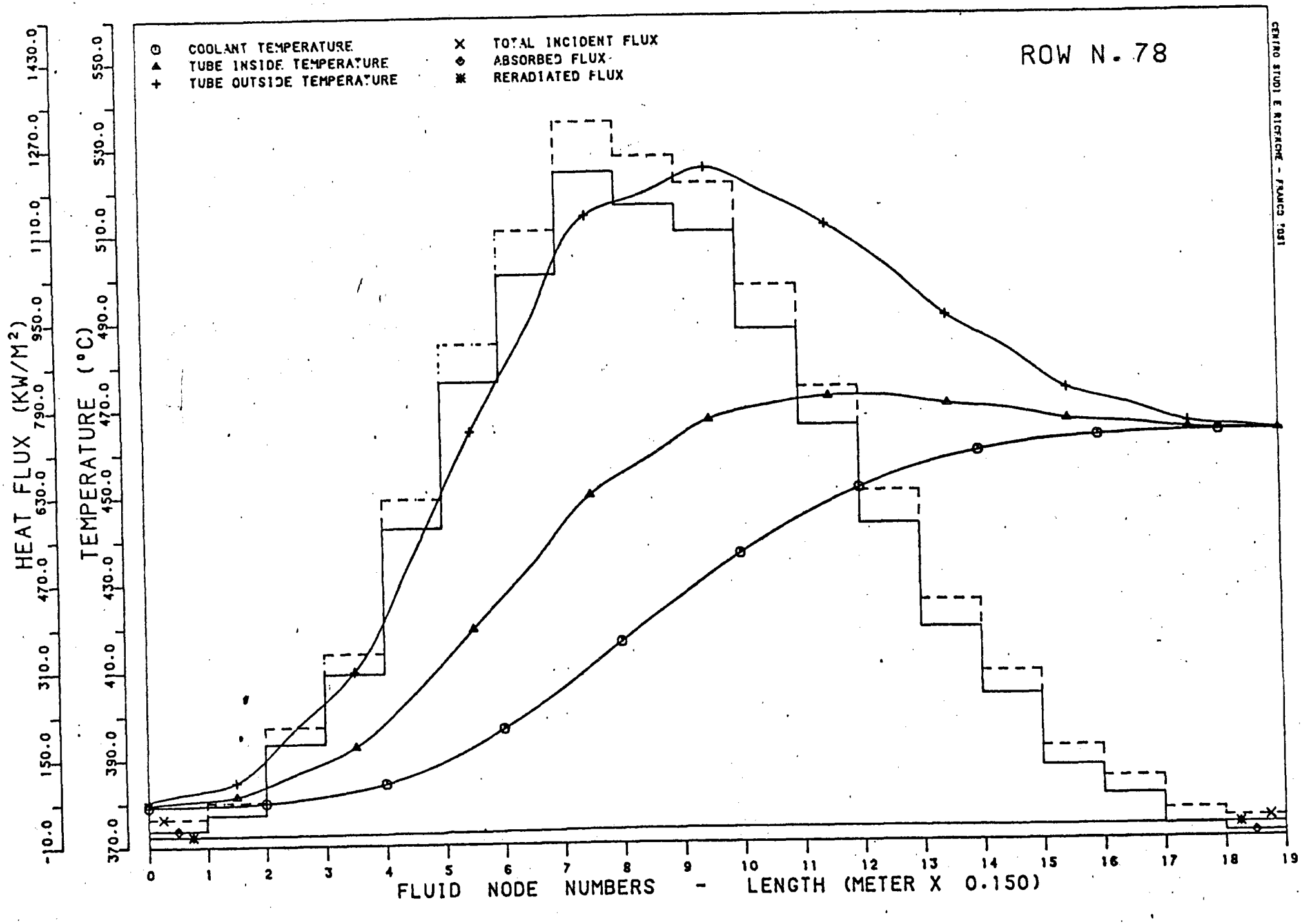
ROW N. 78
COOLANT TEMPERATURE
TUBE INSIDE TEMPERATURE
TUBE OUTSIDE TEMPERATURE
TOTAL INCIDENT FLUX
ABSORBED FLUX
RERADIATED FLUX
HEAT FLUX (KW/M²)
TEMPERATURE (°C)
FLUID NODE NUMBERS - LENGTH (METER X 0.150)
CENTRO STUDI E RICERCHE - FRANCO 1981

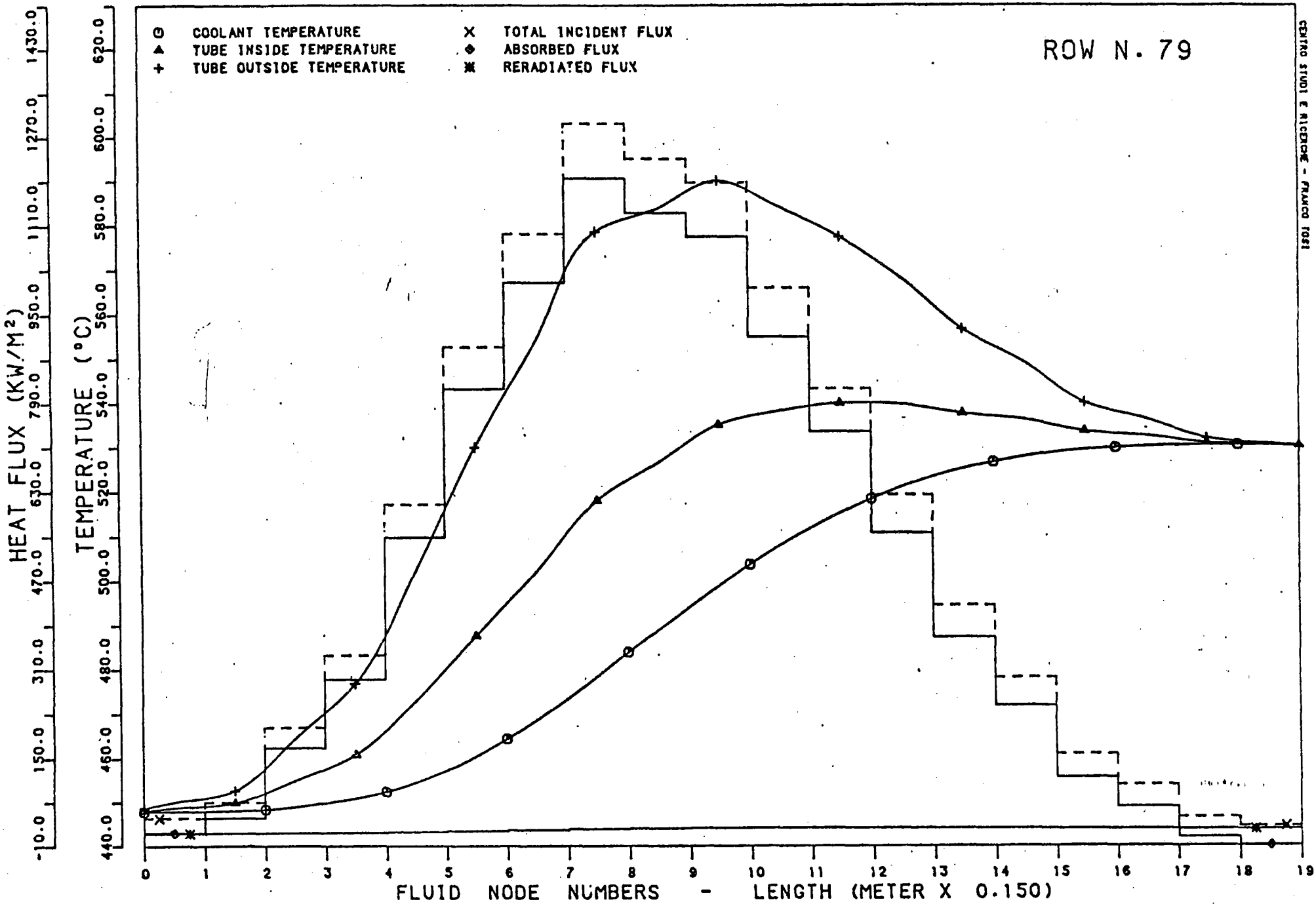
COOLANT TEMPERATURE
TUBE INSIDE TEMPERATURE
TUBE OUTSIDE TEMPERATURE
TOTAL INCIDENT FLUX
ABSORBED FLUX
RERADIATED FLUX
ROW N. 79
HEAT FLUX (KW/M²)
TEMPERATURE (°C)
FLUID NODE NUMBERS - LENGTH (METER X 0.150)
CENTRO STUDI E RICERCHE - FRANCO 1981

FIG. 12

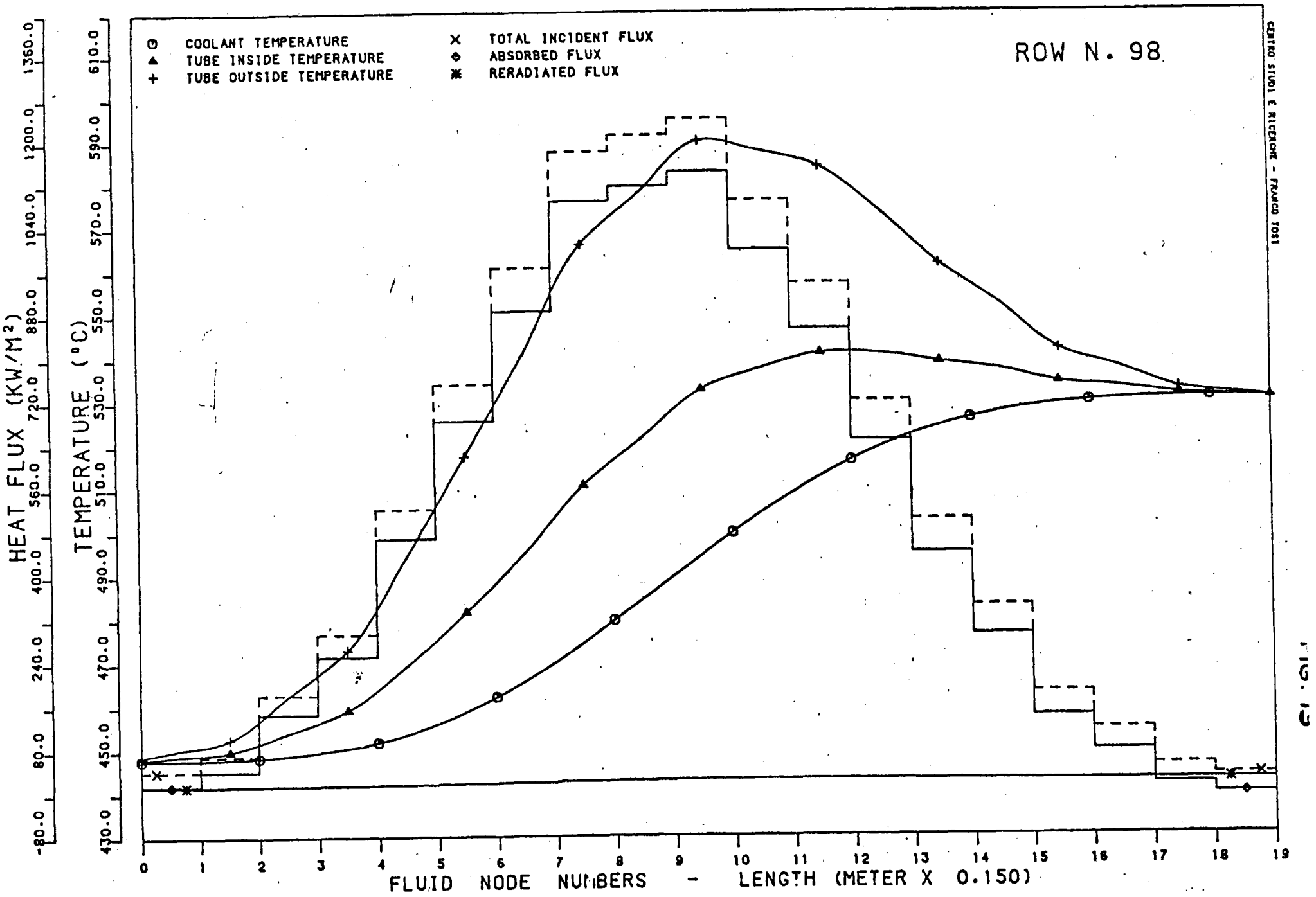
COOLANT TEMPERATURE
TUBE INSIDE TEMPERATURE
TUBE OUTSIDE TEMPERATURE
TOTAL INCIDENT FLUX
ABSORBED FLUX
RERADIATED FLUX
ROW N. 98
HEAT FLUX (KW/M²)
TEMPERATURE (°C)
-80.0 80.0 240.0 400.0 560.0 720.0 880.0 1040.0 1200.0 1360.0
430.0 450.0 470.0 490.0 510.0 530.0 550.0 570.0 590.0 610.0
0 1 2 3 4 5 6 7 8 9 10 11 12 13 14 15 16 17 18 19
FLUID NODE NUMBERS - LENGTH (METER X 0.150)
CENTRO STUDI E RICERCHE - FRASCO 1081

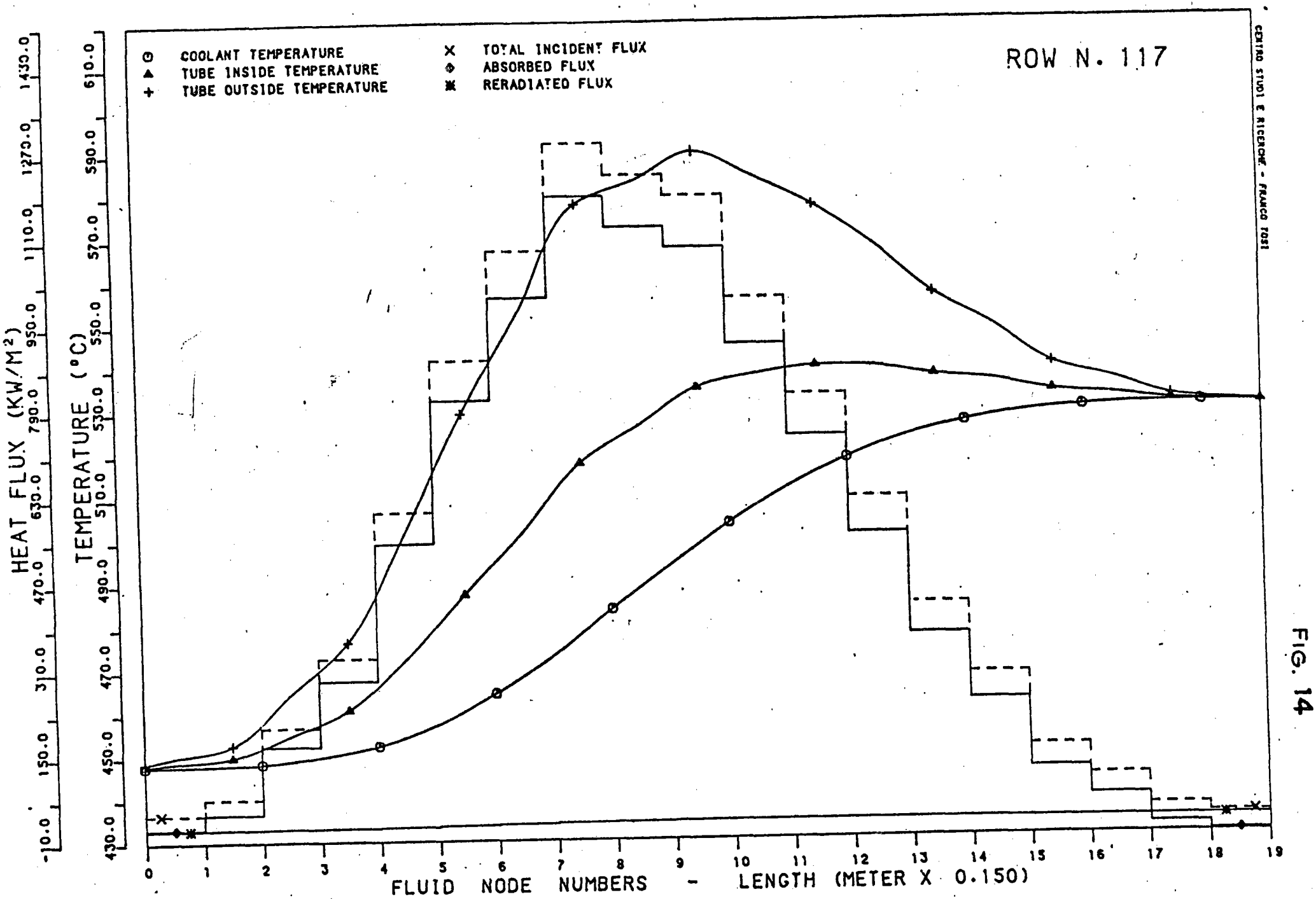
COOLANT TEMPERATURE
TUBE INSIDE TEMPERATURE
TUBE OUTSIDE TEMPERATURE
TOTAL INCIDENT FLUX
ABSORBED FLUX
RERADIATED FLUX
ROW N. 117
HEAT FLUX (KW/M²)
TEMPERATURE (°C)
FLUID NODE NUMBERS - LENGTH (METER X 0.150)
CENTRO STUDI E RICERCHE - FRANCO TOSI

FIG. 14

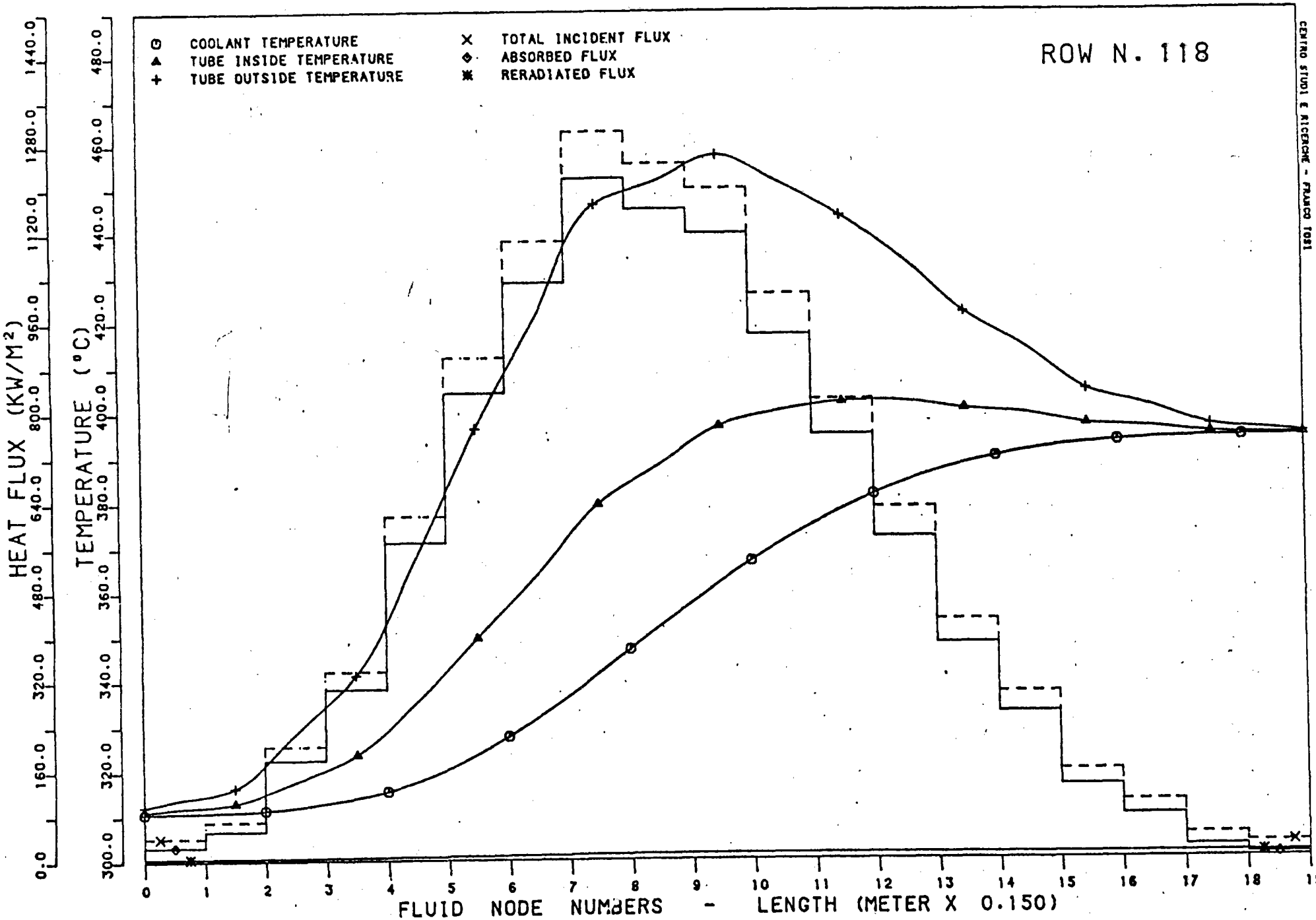
COOLANT TEMPERATURE
TUBE INSIDE TEMPERATURE
TUBE OUTSIDE TEMPERATURE
TOTAL INCIDENT FLUX
ABSORBED FLUX
RERADIATED FLUX
ROW N. 118
HEAT FLUX (KW/M²)
TEMPERATURE (°C)
FLUID NODE NUMBERS - LENGTH (METER X 0.150)
CENTRO STUDI E RICERCHE - FIAMCO 1981

FIG. 15

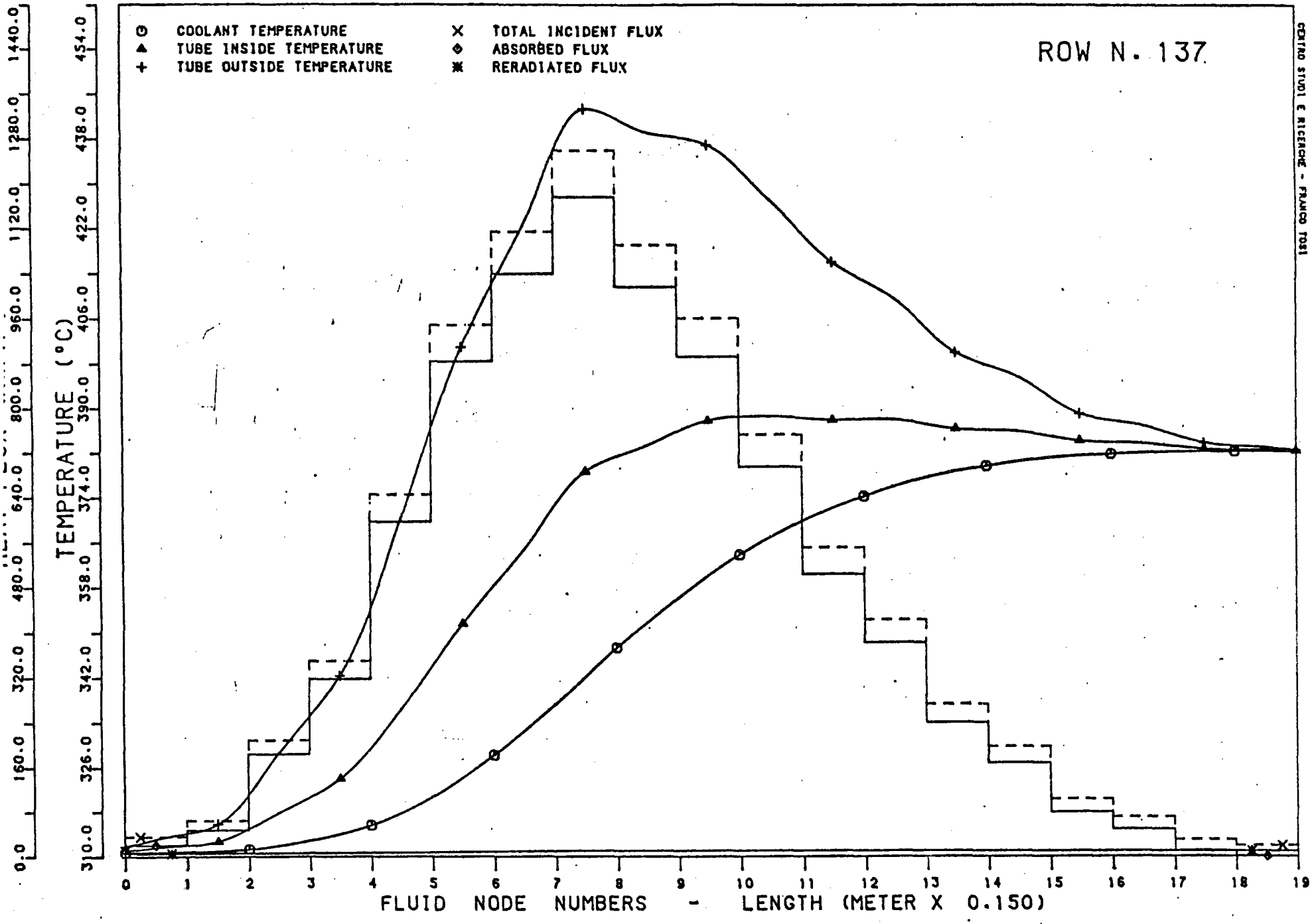
COOLANT TEMPERATURE
TUBE INSIDE TEMPERATURE
TUBE OUTSIDE TEMPERATURE
TOTAL INCIDENT FLUX
ABSORBED FLUX
RERADIATED FLUX
ROW N. 137
TEMPERATURE (°C)
310.0
326.0
342.0
358.0
374.0
390.0
406.0
422.0
438.0
454.0
0.0
160.0
320.0
480.0
640.0
800.0
960.0
1120.0
1280.0
1440.0
0 1 2 3 4 5 6 7 8 9 10 11 12 13 14 15 16 17 18 19
FLUID NODE NUMBERS - LENGTH (METER X 0.150)
CESNO STUDI E RICERCHE - FRANCO TOSI

FIG. 16

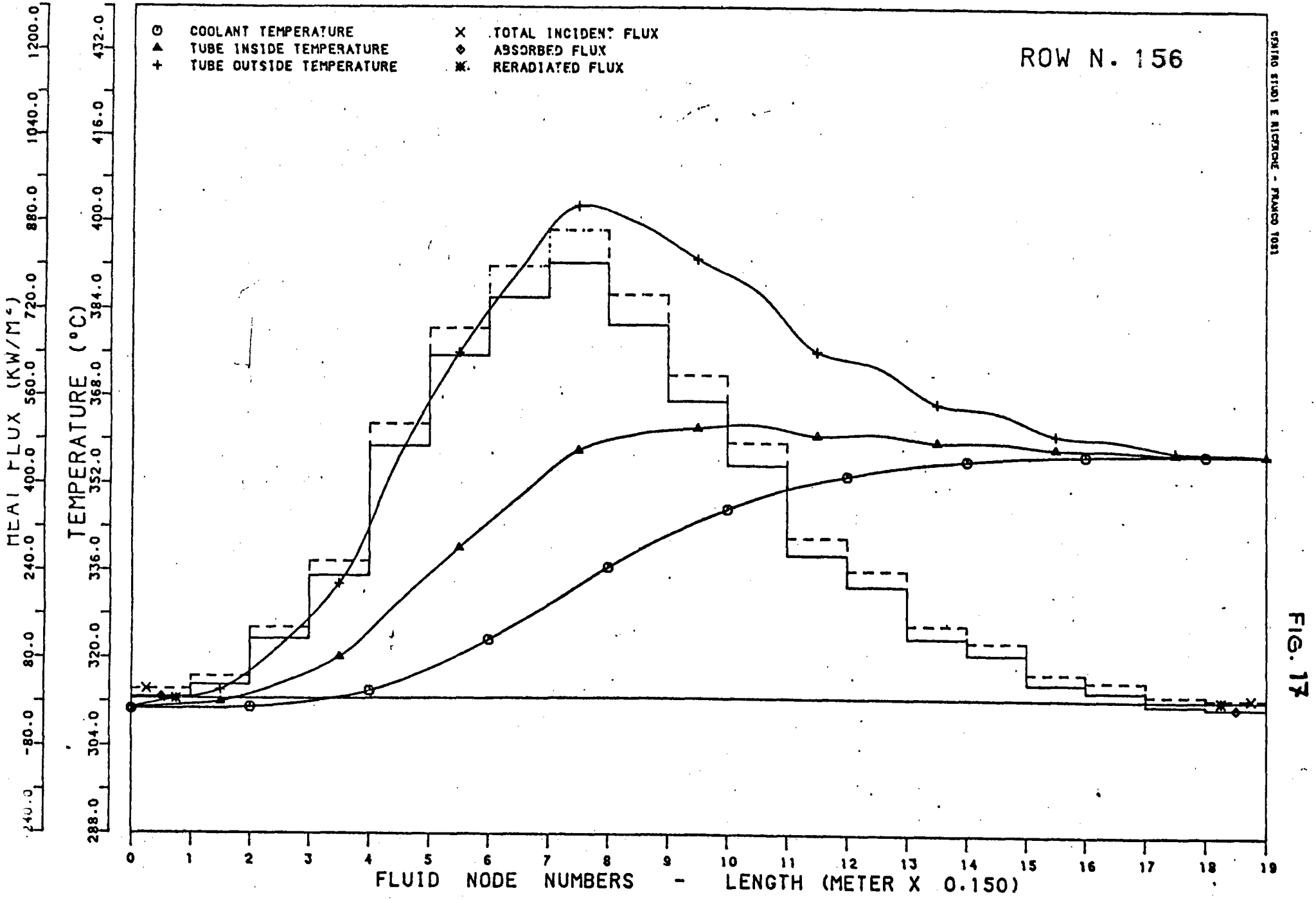
COOLANT TEMPERATURE
TUBE INSIDE TEMPERATURE
TUBE OUTSIDE TEMPERATURE
TOTAL INCIDENT FLUX
ABSORBED FLUX
RERADIATED FLUX
ROW N. 156
HEAT FLUX (KW/M²)
TEMPERATURE (°C)
FLUID NODE NUMBERS - LENGTH (METER X 0.150)
CERCA SIGEL E RICERCHE - FRASCO 1981

FIG. 17

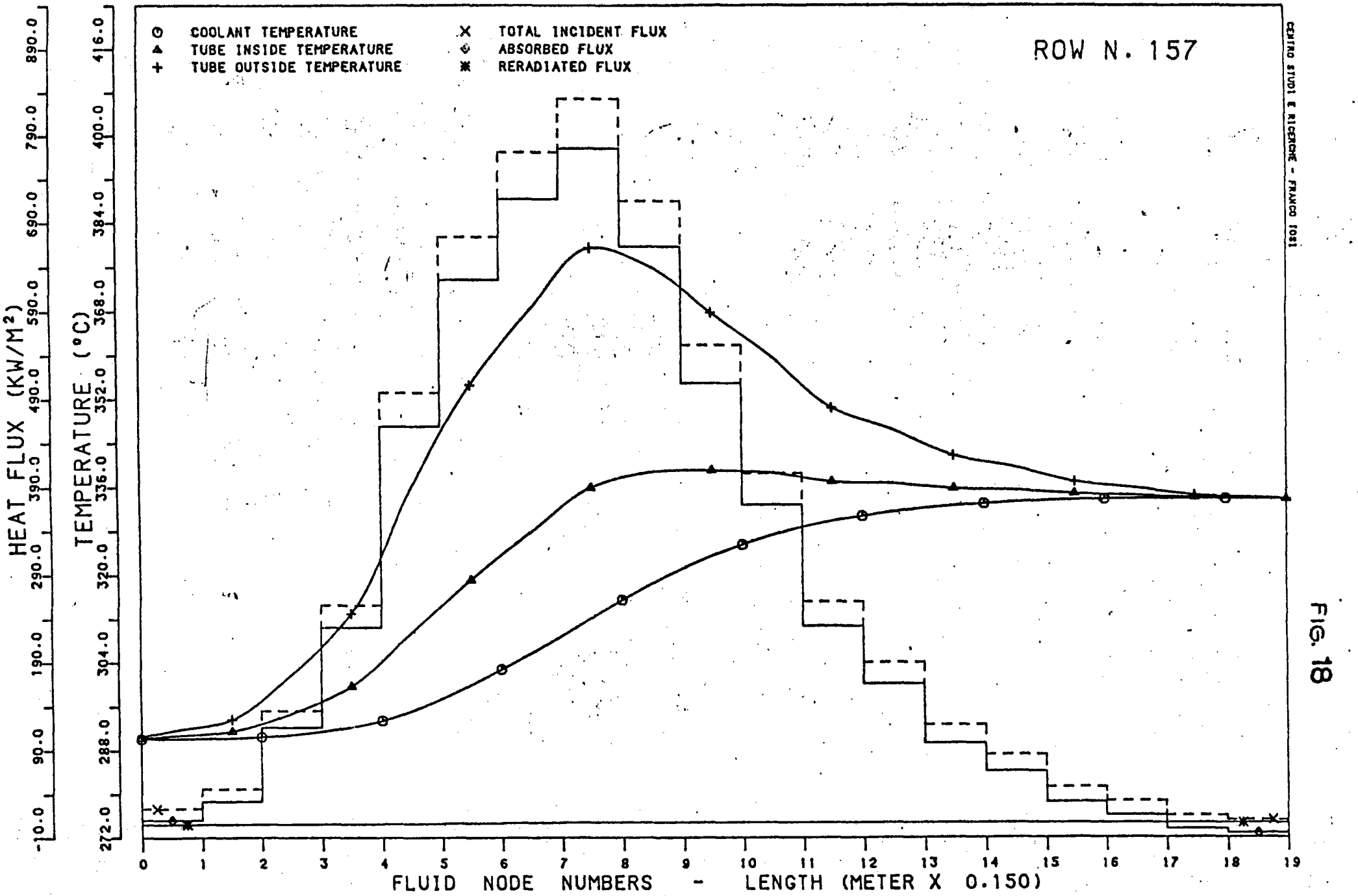
COOLANT TEMPERATURE
TUBE INSIDE TEMPERATURE
TUBE OUTSIDE TEMPERATURE
TOTAL INCIDENT FLUX
ABSORBED FLUX
RERADIATED FLUX
ROW N. 157
CENTRO STUDI E RICERCHE - FRANCO TOSI
HEAT FLUX (KW/M²)
-10.0
90.0
190.0
290.0
390.0
490.0
590.0
690.0
790.0
890.0
TEMPERATURE (°C)
272.0
288.0
304.0
320.0
336.0
352.0
368.0
384.0
400.0
416.0
0 1 2 3 4 5 6 7 8 9 10 11 12 13 14 15 16 17 18 19
FLUID NODE NUMBERS - LENGTH (METER X 0.150)

FIG. 18

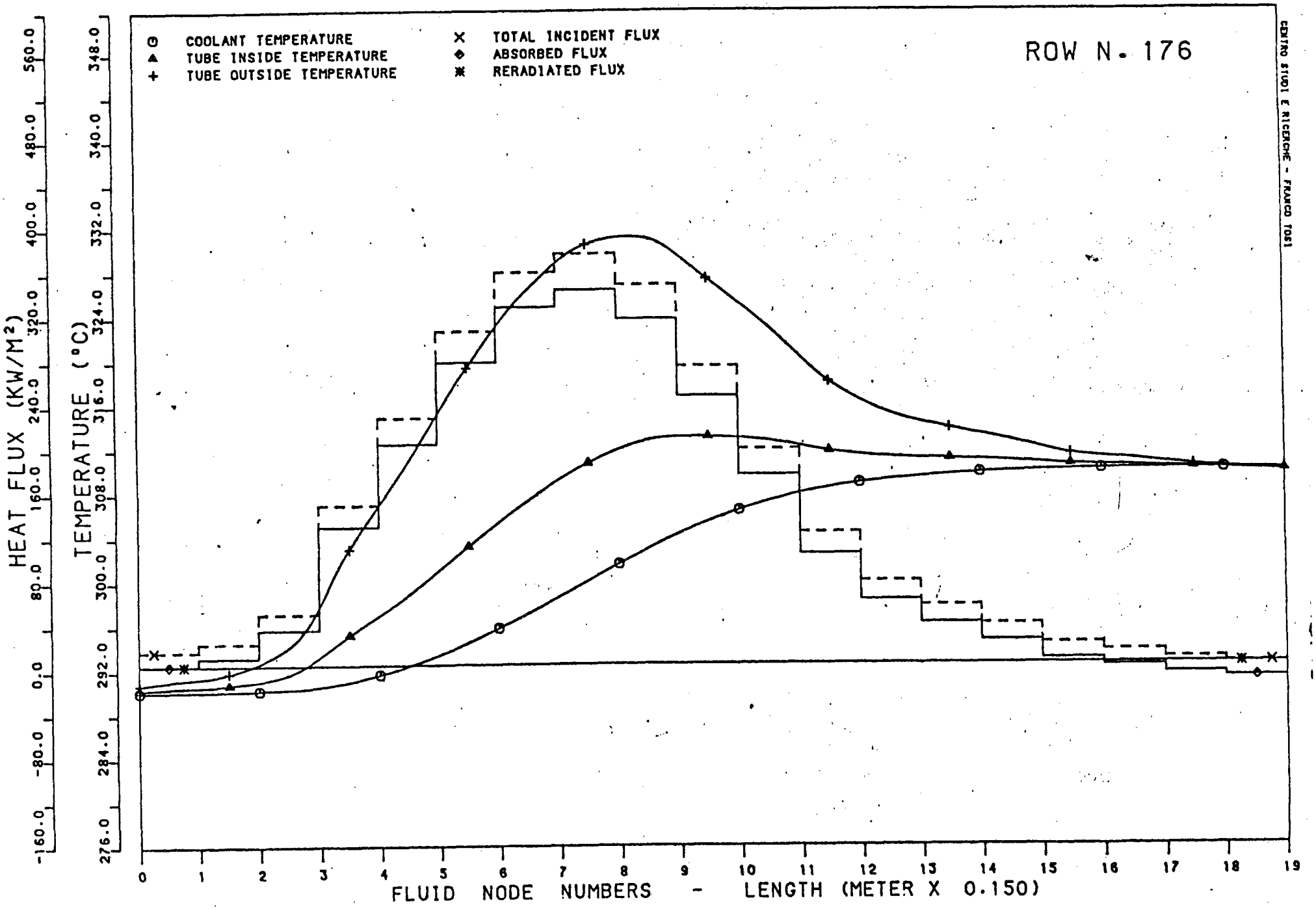
COOLANT TEMPERATURE
TUBE INSIDE TEMPERATURE
TUBE OUTSIDE TEMPERATURE
TOTAL INCIDENT FLUX
ABSORBED FLUX
RERADIATED FLUX
ROW N. 176
HEAT FLUX (KW/M²)
TEMPERATURE (°C)
FLUID NODE NUMBERS - LENGTH (METER X 0.150)
CENTRO STUDI E RICERCHE - FRANCO TOSI

FIG. 20

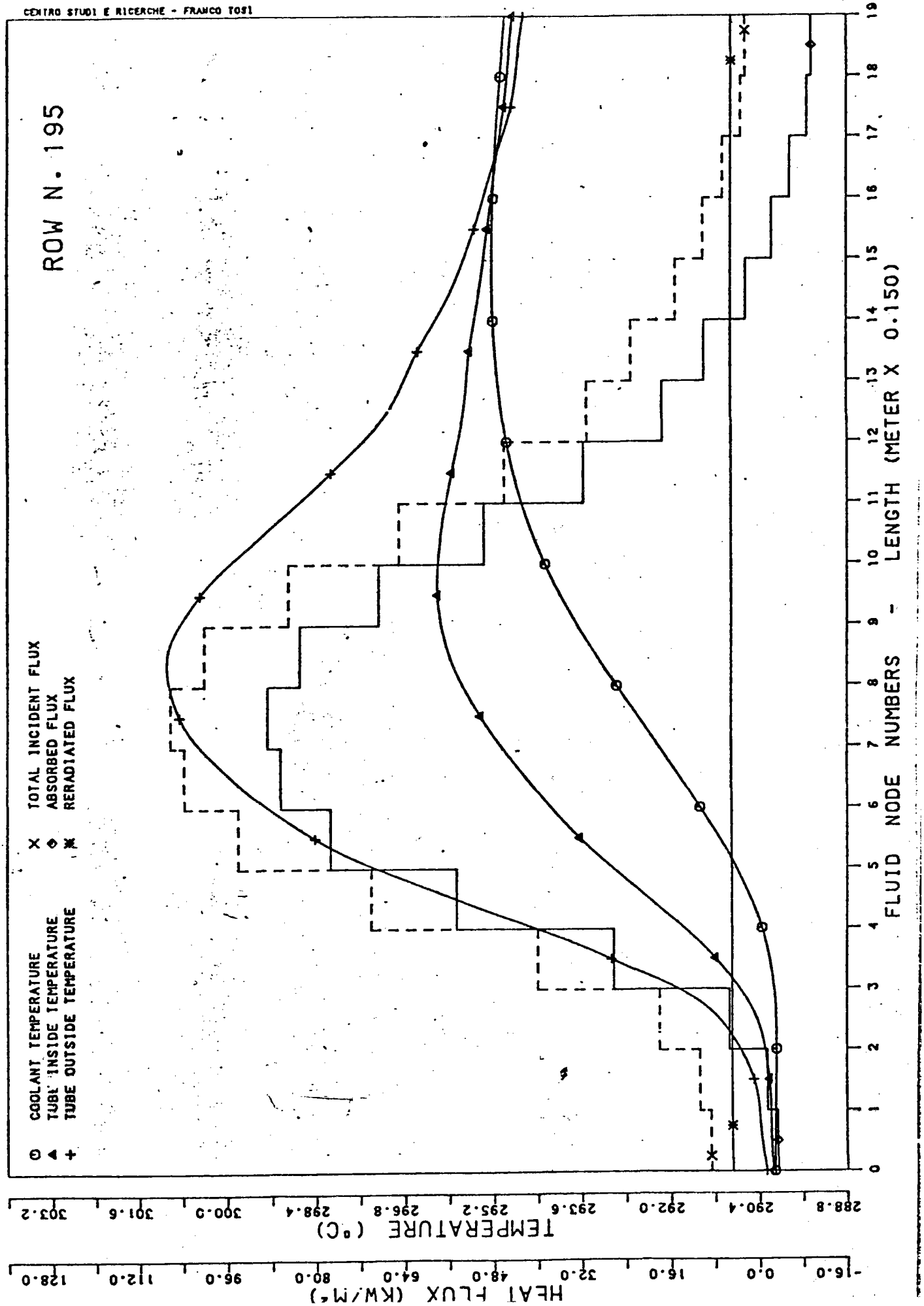
CENTRO STUDI E RICERCHE - FRANCO TOSI
ROW N. 195
COOLANT TEMPERATURE
TUBE INSIDE TEMPERATURE
TUBE OUTSIDE TEMPERATURE
TOTAL INCIDENT FLUX
ABSORBED FLUX
RERADIATED FLUX
FLUID NODE NUMBERS - LENGTH (METER X 0.150)
TEMPERATURE (°C)
HEAT FLUX (KW/M²)

RECEIVER PERFORMANCE ANALISYS

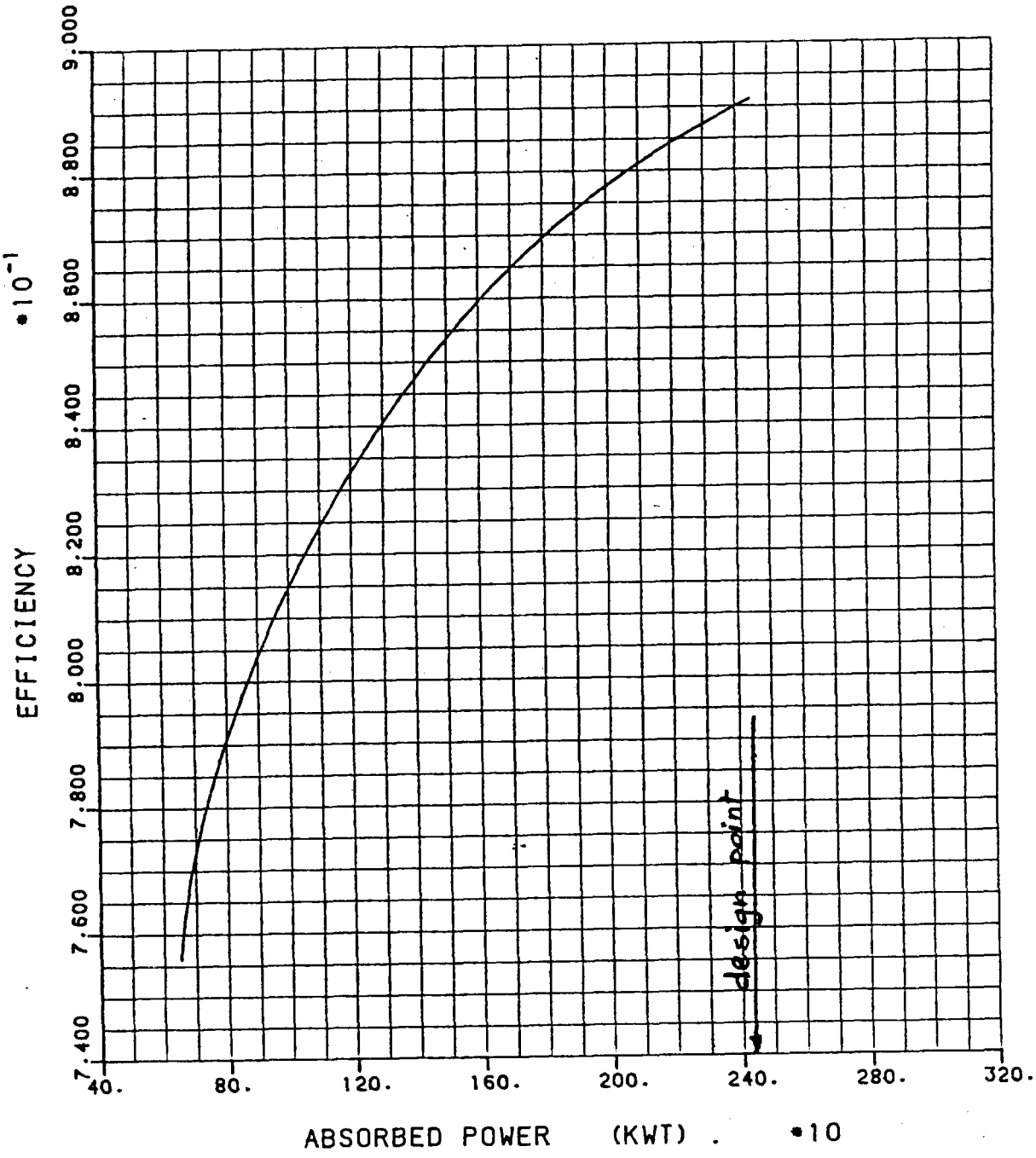

FIG. 21

		CALC.	VERIF.	03/03/81

HEAT LOSSES FROM RECEIVER

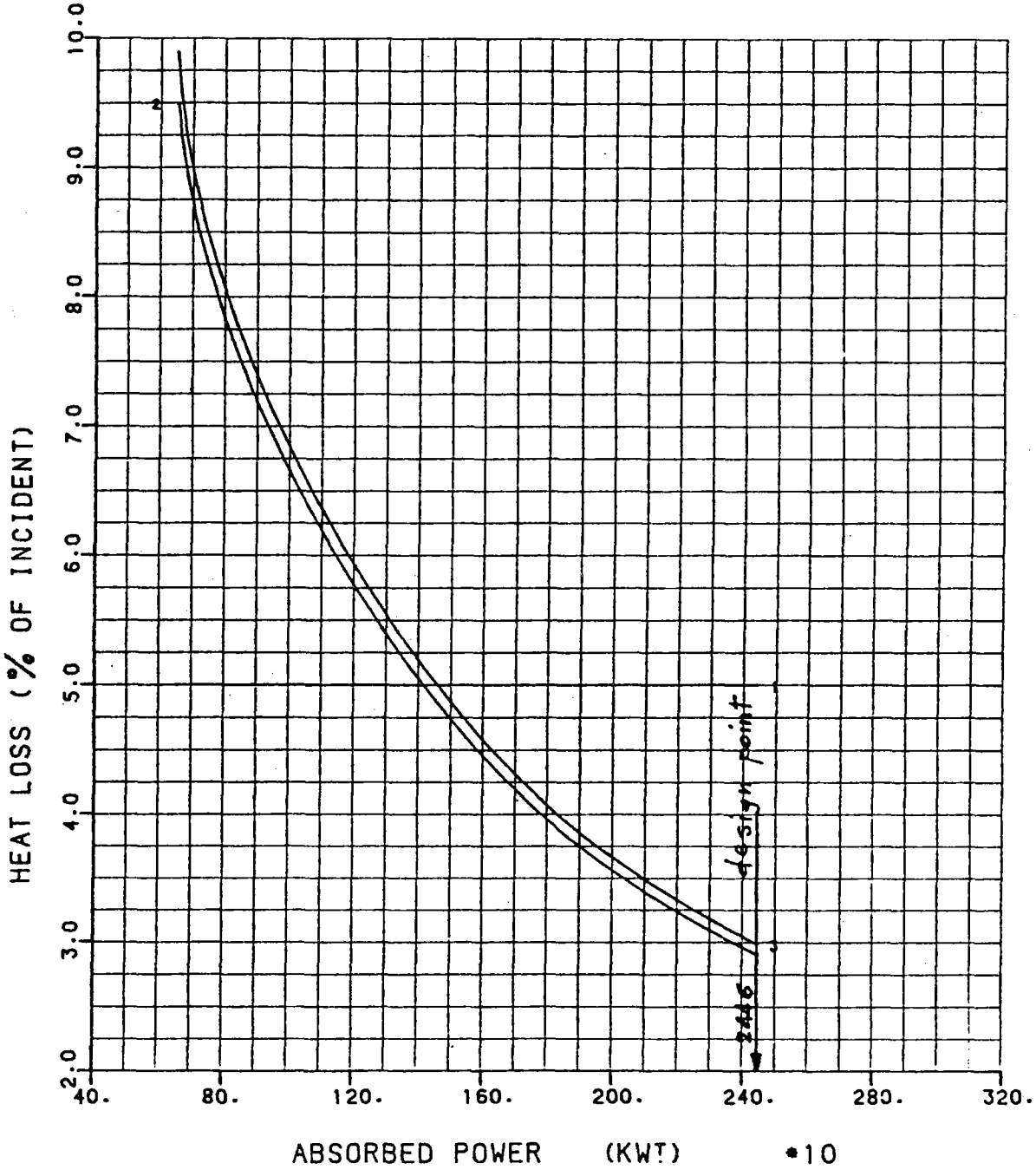

CURVA 1/ REFLECTION **
CURVA 2/ I.R. **
CURVA 3/ CONVECTION **

FIG. 22

MAPPA DEL FLUSSO DIRETTO

****
N.FILA TUBI = 1
****

COEF.ASS.TUBI	0.95	
EMISSIVITA'	0.90	
NUMERO TUBI	1.0	
DIAM.EST.TUBI	0.0140	M
DIAM.INT.TUBI	0.0120	M
PASSO	0.0140	M
TEMP.ARIA EST.	20.0	GR.CENT.
VEL.ARIA EST.	5.0	M/SEC
TEMP.SODIO IN	270.0	GR.CENT.
LUNG.TUBO	2.0500	M
LARG.FILA	0.0140	M
VEL.SODIO IN	1.867	M/SEC
PRESSIONE	5.25	BAR
COEFF.CONV.	45663.5	W/MQD*C
REYNOLDS	54789.	
PERDITA CARICO	0.08	BAR
RENDIMENTO	0.378	
T.MED.METALLO	272.1	GR.CENT.
ALLUNG. MEDIO	13.47	MM

N.	FTOT*	FASS*	FIRR*	T.SODIO+	TTE+	TTI+	TTM+	TEMAX+	DTMAX+
1	7.7	-17.1	4.1	269.9	269.0	269.6	269.6	270.1	0.2
2	13.7	-11.4	4.1	269.8	269.2	269.6	269.6	270.5	0.5
3	24.0	-1.6	4.1	269.7	269.6	269.7	269.7	271.3	1.1
4	42.0	15.4	4.2	269.9	270.6	270.0	270.1	272.8	2.1
5	64.0	36.2	4.2	270.2	271.9	270.6	270.6	274.9	3.3
6	85.4	56.4	4.2	270.7	273.4	271.3	271.4	277.1	4.4
7	98.0	68.2	4.3	271.2	274.6	272.0	272.1	278.6	5.1
8	104.1	73.9	4.3	271.9	275.5	272.7	272.8	279.7	5.5
9	98.0	68.1	4.3	272.4	275.8	273.2	273.3	279.8	5.1
10	80.5	51.5	4.3	272.9	275.4	273.5	273.6	278.9	4.2
11	66.0	37.8	4.3	273.2	275.0	273.6	273.7	278.1	3.4
12	45.0	17.9	4.3	273.4	274.2	273.6	273.6	276.5	2.2
13	32.0	5.6	4.3	273.4	273.7	273.5	273.5	275.6	1.5
14	23.0	-2.5	4.2	273.4	273.2	273.3	273.3	274.8	1.0
15	15.0	-10.4	4.2	273.3	272.8	273.1	273.1	274.1	0.6
16	10.0	-15.2	4.2	273.2	272.4	273.0	273.0	273.6	0.3
17	7.2	-17.8	4.2	273.0	272.1	272.8	272.8	273.2	0.1
18	3.0	-21.7	4.2	272.8	271.7	272.5	272.5	272.7	-0.1
19	2.4	-22.3	4.2	272.6	271.5	272.4	272.3	272.4	-0.1

(*) KW/MQD
MQC PIANO EQUIV.
(+) GRADI CENT.

TAB. 1

****
N.FILA TUBI = 20
****

COEF.ASS.TUBI	0.95	
EMISSIVITA'	0.90	
NUMERO TUBI	1.0	
DIAM.EST.TUBI	0.0140	M
DIAM.INT.TUBI	0.0120	M
PASSO	0.0140	M
TEMP.ARIA EST.	20.0	GR.CENT.
VEL.ARIA EST.	5.0	M/SEC
TEMP.SODIO IN	270.0	GR.CENT.
LUNG.TUBO	2.8500	M
LARG.FILA	0.0140	M
VEL.SODIO IN	1.867	M/SEC
PRESSIONE	5.25	BAR
COEFF.CONV.	45430.4	W/MQD*C
REYNOLDS	56064.	
PERDITA CARICO	0.08	BAR
RENDIMENTO	0.844	
T.MED.METALLO	283.6	GR.CENT.
ALLUNG. MEDIO	14.08	MM

N.	FTOT*	FASS*	FIRR*	T.SODIO+	TTE+	TTI+	TTM+	TEMAX+	DTMAX+
1	17.3	2.4	4.1	270.0	270.1	270.0	270.0	271.0	0.1
2	24.3	9.0	4.1	270.1	270.5	270.2	270.2	271.6	1.1
3	50.8	34.1	4.2	270.4	272.0	270.6	270.8	274.0	2.1
4	122.4	102.7	4.5	271.3	276.3	272.5	272.6	280.6	6.1
5	205.0	180.0	4.5	272.8	281.6	274.9	275.1	288.6	10.1
6	290.0	260.3	4.7	275.0	287.7	278.1	278.4	297.4	15.1
7	350.0	316.9	4.9	277.7	293.1	281.5	281.8	304.7	18.1
8	380.0	345.1	5.1	280.6	297.4	284.8	285.1	310.0	20.1
9	352.0	318.4	5.2	283.4	298.8	287.2	287.5	310.5	18.1
10	290.0	259.5	5.1	285.6	298.1	288.7	288.9	307.8	15.1
11	223.3	196.3	5.1	287.2	296.7	289.6	289.8	304.2	11.1
12	160.0	136.3	5.0	288.4	295.0	290.0	290.2	300.5	8.1
13	95.0	74.7	4.9	289.0	292.6	289.9	290.0	296.1	4.1
14	57.8	39.5	4.9	289.4	291.3	289.8	289.9	293.5	2.1
15	43.2	25.6	4.9	289.6	290.8	289.9	289.9	292.6	2.1
16	29.1	12.2	4.8	289.7	290.3	289.8	289.9	291.6	1.1
17	15.0	-1.1	4.8	289.7	289.6	289.7	289.7	290.4	0.1
18	9.0	-6.8	4.8	289.6	289.3	289.5	289.5	289.9	0.1
19	5.9	-9.7	4.8	289.6	289.1	289.4	289.4	289.6	0.1

(*) KW/MQD
MQD PIANO EQUIV.
(+) GRADI CENT.

TAB. 2

****
N.FILA TUBI = 39
****

COEF.ASS.TUBI	0.95	
EMISSIVITA'	0.90	
NUMERO TUBI	1.0	
DIAM.EST.TUBI	0.0140	M
DIAM.INT.TUBI	0.0120	M
PASSO	0.0140	M
TEMP.ARIA EST.	20.0	GR.CENT.
VEL.ARIA EST.	5.0	M/SEC
TEMP.SODIO IN	270.0	GR.CENT.
LUNG.TUBO	2.8500	M
LARG.FILA	0.0140	M
VEL.SODIO IN	1.867	M/SEC
PRESSIONE	5.25	BAR
COEFF.CONV.	45099.2	W/MQD*C
REYNOLDS	58099.	
PERDITA CARICO	0.08	BAR
RENDIMENTO	0.899	
T.MED.METALLO	300.0	GR.CENT.
ALLUNG. MEDIO	15.00	MM

N.	FTOT*	FASS*	FIRR*	T.SODIO+	TTE+	TTI+	TTN+	TEMAX+	DTMAX+
1	22.7	8.7	4.1	270.1	270.5	270.2	270.2	271.5	1.0
2	44.7	29.5	4.2	270.3	271.8	270.7	270.7	273.5	2.2
3	135.2	115.2	4.4	271.3	276.9	272.7	272.8	281.6	7.2
4	257.2	230.6	4.6	273.3	284.5	276.0	276.3	293.1	13.8
5	503.8	463.9	5.2	277.2	299.8	282.8	283.3	316.1	26.8
6	683.3	633.5	5.7	282.6	313.3	290.2	290.8	335.4	36.3
7	785.0	729.3	6.2	288.8	324.0	297.6	298.3	349.4	41.5
8	845.5	786.1	6.6	295.5	333.4	305.1	305.7	360.7	44.6
9	723.5	670.2	6.6	301.3	333.5	309.4	309.9	357.0	38.1
10	550.0	505.7	6.5	305.6	329.9	311.8	312.1	347.9	28.9
11	410.0	372.9	6.3	308.8	326.7	313.3	313.6	340.2	21.5
12	259.7	230.5	6.1	310.8	321.8	313.6	313.7	330.5	13.5
13	189.5	163.9	6.0	312.2	320.0	314.2	314.3	326.4	9.8
14	119.0	97.1	5.9	313.0	317.7	314.2	314.2	321.8	6.0
15	83.5	63.4	5.9	313.5	316.6	314.3	314.4	319.6	4.1
16	47.7	29.5	5.8	313.8	315.2	314.1	314.2	317.0	2.2
17	30.0	12.8	5.8	313.9	314.5	314.0	314.1	315.7	1.3
18	15.0	-1.5	5.8	313.9	313.8	313.8	313.9	314.6	0.5
19	10.0	-6.2	5.8	313.8	313.5	313.7	313.7	314.1	0.2

(*) KW/MQD
MQD PIANO EQUIV.
(+) GRADI CENT.

TAB. 3

****
N.FILA TUBI = 40
****

COEF.ASS.TUBI	0.95	
EMISSIVITA'	0.90	
NUMERO TUBI	2.0	
DIAM.EST.TUBI	0.0140	M
DIAM.INT.TUBI	0.0120	M
PASSO	0.0140	M
TEMP.ARIA EST.	20.0	GR.CENT.
VEL.ARIA EST.	5.0	M/SEC
TEMP.SODIO IN	379.3	GR.CENT.
LUNG.TUBO	2.8500	M
LARG.FILA	0.0140	M
VEL.SODIO IN	1.925	M/SEC
PRESSIONE	4.53	BAR
COEFF.CONV.	42825.7	W/MQD*L
REYNOLDS	76155.	
PERDITA CARICO	0.08	BAR
RENDIMENTO	0.874	
T.MED.METALLO	411.7	GR.CENT.
ALLUNG. MEDIO	20.91	MM

N.	FTOT*	FASS*	FIRR*	T.SODIO+	TTE+	TTI+	TTM+	TEMAX+	DTMAX+
1	22.3	0.6	9.0	379.3	379.3	379.3	379.3	380.3	0.6
2	45.7	22.8	9.1	379.5	380.6	379.8	379.8	382.3	1.9
3	136.2	108.3	9.4	380.5	385.6	381.8	381.9	390.2	6.6
4	259.6	224.9	9.8	382.4	393.2	385.3	385.3	401.7	13.0
5	513.3	464.5	10.8	386.5	408.6	392.4	392.5	425.1	25.9
6	692.8	633.8	11.7	392.0	422.2	400.1	400.2	444.2	34.8
7	807.1	741.3	12.5	396.4	433.6	407.9	408.0	459.1	40.3
8	875.6	805.3	13.2	405.4	443.5	415.8	415.8	471.1	43.4
9	753.6	689.4	13.3	411.5	444.0	420.4	420.3	467.8	37.3
10	602.5	546.1	13.1	416.2	442.0	423.3	423.2	461.2	29.7
11	477.5	427.6	13.0	420.0	440.1	425.5	425.5	455.4	23.4
12	302.7	262.0	12.6	422.3	434.6	425.7	425.6	444.4	14.7
13	242.7	205.1	12.5	424.1	433.7	426.7	426.7	441.6	11.6
14	143.1	110.8	12.3	425.0	430.2	426.5	426.4	435.0	6.6
15	112.6	81.9	12.2	425.7	429.6	426.8	426.8	433.4	5.1
16	56.0	28.3	12.1	426.0	427.3	426.3	426.3	429.3	2.2
17	42.0	15.1	12.0	426.1	426.8	426.3	426.3	428.3	1.5
18	17.1	-8.4	11.9	426.0	425.6	425.9	425.9	426.4	0.2
19	12.1	-13.2	11.9	425.9	425.3	425.7	425.7	425.9	-0.0

(*) KW/MQD
MQD PIANO EQUIV.
(+) GRADI CENT.

TAB. 4

****
N.FILA TUBI = 59
****

COEF.ASS.TUBI	0.95	
EMISSIVITA'	0.90	
NUMERO TUBI	1.0	
DIAM.EST.TUBI	0.0140	M
DIAM.INT.TUBI	0.0120	M
PASSO	0.0140	M
TEMP.ARIA EST.	20.0	GR.CENT.
VEL.ARIA EST.	5.0	M/SEC
TEMP.SODIO IN	379.3	GR.CENT.
LUNG.TUBO	2.8500	M
LARG.FILA	0.0140	M
VEL.SODIO IN	1.925	M/SEC
PRESSIONE	4.93	BAR
COEFF.CONV.	42515.0	W/MQD*C
REYNOLDS	77786.	
PERDITA CARICO	0.08	BAR
RENDIMENTO	0.897	
T.MED.METALLO	427.8	GR.CENT.
ALLUNG. MEDIO	21.77	MM

N.	FTOT*	FASS*	FIRR*	T.SODIO+	TTE+	TTI+	TTM+	TEMAX+	DTMAX+
1	35.1	13.5	9.0	379.4	380.1	379.6	379.6	381.4	1.3
2	63.6	40.5	9.1	379.8	381.7	380.3	380.3	384.0	2.8
3	210.1	179.0	9.6	381.3	389.9	383.6	383.7	396.8	10.4
4	352.7	313.6	10.2	384.1	399.0	388.1	388.1	410.5	17.7
5	650.7	595.2	11.4	389.2	417.6	396.8	396.9	438.3	32.8
6	956.7	883.8	12.9	396.9	438.9	408.3	408.3	468.8	47.7
7	1122.5	1039.8	14.1	406.0	455.1	419.4	419.3	490.0	55.4
8	1269.0	1177.1	15.5	416.3	471.6	431.5	431.3	510.7	62.0
9	1097.5	1014.1	15.6	425.1	472.6	438.4	438.1	506.7	53.5
10	964.3	887.4	15.7	432.9	474.4	444.6	444.3	504.5	46.8
11	754.3	688.3	15.5	438.9	471.1	448.0	447.8	494.8	36.6
12	551.7	496.3	15.1	443.3	466.5	449.9	449.7	484.0	26.6
13	424.2	375.4	14.9	446.6	464.2	451.6	451.4	477.6	20.3
14	273.3	232.5	14.5	448.7	459.6	451.7	451.6	468.3	12.9
15	198.3	161.5	14.4	450.1	457.6	452.2	452.1	464.0	9.1
16	103.3	71.6	14.1	450.7	454.1	451.6	451.6	457.4	4.4
17	70.8	40.8	14.0	451.1	453.0	451.6	451.6	455.3	2.8
18	29.7	1.9	13.8	451.1	451.2	451.1	451.1	452.2	0.7
19	15.2	-8.0	13.8	451.0	450.6	450.9	450.9	451.3	0.2

(*) KW/MQD
MQD PIANO ECUIV.
(+) GRADI CENT.

TAB. 5

****
N.FILA TUBI = 78
****

COEF.ASS.TUBI	0.95	
EMISSIVITA*	0.90	
NUMERO TUBI	1.0	
DIAM.EST.TUBI	0.0140	M
DIAM.INT.TUBI	0.0120	M
PASSO	0.0140	M
TEMP.ARIA EST.	20.0	GR.CENT.
VEL.ARIA EST.	5.0	M/SEC
TEMP.SODIO IN	379.3	GR.CENT.
LUNG.TUBO	2.8500	M
LARG.FILA	0.0140	M
VEL.SODIO IN	1.925	M/SEC
PRESSIONE	4.53	BAR
COEFF.CONV.	42414.0	W/MQD*C
REYNOLDS	78327.	
PERDITA CARICO	0.08	BAR
RENDIMENTO	0.904	
T.MED.METALLO	433.5	GR.CENT.
ALLUNG. MEDIO	22.08	MM

N.	FTOT*	FASS*	FIRR*	T.SODIO+	TTE+	TTI+	TTM+	TEMAX+	DTMAX+
1	41.9	20.5	9.1	379.5	380.5	379.7	379.8	382.0	1.7
2	71.6	48.6	9.2	379.9	382.2	380.5	380.5	384.7	3.2
3	207.1	176.7	9.6	381.5	389.9	383.7	383.7	396.7	10.2
4	341.1	303.3	10.1	384.1	398.6	387.9	388.0	409.7	17.1
5	622.2	568.8	11.3	389.0	416.2	396.3	396.4	435.9	31.3
6	906.2	836.7	12.7	396.3	436.1	407.0	407.1	464.4	45.2
7	1113.3	1031.7	14.1	405.3	454.1	418.6	418.6	488.6	55.0
8	1313.3	1219.7	15.7	415.9	473.3	431.8	431.6	513.7	64.2
9	1248.3	1157.2	16.3	426.1	480.2	441.2	440.8	518.7	60.6
10	1197.5	1108.2	16.9	435.8	487.5	450.3	449.9	524.4	57.8
11	1008.0	928.2	16.5	443.9	487.2	456.2	455.8	518.5	48.6
12	821.3	750.9	16.7	450.5	485.5	460.5	460.1	511.1	39.4
13	628.8	568.5	16.4	455.5	482.0	463.1	462.8	501.7	30.1
14	427.6	377.9	15.9	458.9	476.5	463.9	463.7	490.0	20.3
15	297.1	254.4	15.6	461.1	473.0	464.5	464.4	482.4	13.9
16	159.2	123.9	15.2	462.2	468.0	463.9	463.8	473.1	7.1
17	102.7	70.4	15.0	462.8	466.1	463.8	463.7	469.4	4.3
18	43.0	14.0	14.8	462.9	463.6	463.1	463.1	465.0	1.3
19	27.0	-1.2	14.8	462.9	462.9	462.9	462.9	463.8	0.5

(*) KW/MQD
MQD PIANO EQUIV.
(+) GRADI CENT.

TAB. 6

****
N.FILA TUBI = 79
****

COEF.ASS.TUBI	0.95	
EMISSIVITA'	0.90	
NUMERO TUBI	1.0	
DIAM.EST.TUBI	0.0140	M
DIAM.INT.TUBI	0.0120	M
PASSO	0.0140	M
TEMP.ARIA EST.	20.0	GR.CENT.
VEL.ARIA EST.	5.0	M/SEC
TEMP.SODIO IN	448.0	GR.CENT.
LUNG.TUBO	2.8500	M
LARG.FILA	0.0140	M
VEL.SODIO IN	1.962	M/SEC
PRESSIONE	4.30	BAR
COEFF.CONV.	40593.6	W/MQD*C
REYNOLDS	88260.	
PERDITA CARICO	0.07	BAR
RENDIMENTO	0.890	
T.MED.METALLO	501.3	GR.CENT.
ALLUNG. MEDIO	25.73	MM

N.	FTOT*	FASS*	FIRR*	T.SODIO+	TTE+	TTI+	TTM+	TEMAX+	DTMAX+
1	41.6	14.2	13.6	448.1	448.7	448.2	448.2	450.1	1.3
2	71.0	41.9	13.8	448.4	450.4	449.0	449.0	452.7	2.8
3	206.5	169.9	14.4	449.9	457.9	452.2	452.1	464.5	9.5
4	336.4	292.5	15.1	452.5	466.2	456.4	456.3	476.9	15.9
5	608.0	548.6	16.5	457.3	483.0	464.6	464.4	502.0	29.0
6	892.0	816.2	18.3	464.5	502.6	475.4	475.0	530.0	42.4
7	1095.3	1007.2	20.1	473.4	520.1	486.9	486.3	553.7	51.7
8	1295.3	1194.8	22.1	484.0	539.1	500.1	499.2	578.6	60.6
9	1230.3	1132.1	22.9	494.0	546.1	509.4	508.4	583.7	57.3
10	1186.8	1089.8	23.8	503.7	553.8	518.6	517.5	590.0	55.0
11	997.3	909.8	23.7	511.8	553.6	524.4	523.4	584.2	46.0
12	816.2	737.9	23.6	518.4	552.3	528.6	527.8	577.4	37.5
13	623.7	555.5	23.2	523.3	548.9	531.1	530.4	568.1	28.4
14	425.5	368.0	22.6	526.6	543.6	531.8	531.3	556.7	19.1
15	295.0	244.5	22.2	528.8	540.1	532.2	531.9	549.2	12.9
16	158.3	115.2	21.7	529.8	535.2	531.4	531.3	540.0	6.5
17	101.8	61.8	21.4	530.4	533.2	531.3	531.2	536.3	3.8
18	42.9	6.2	21.2	530.5	530.7	530.5	530.5	532.0	1.0
19	26.9	-8.9	21.1	530.4	529.9	530.2	530.3	530.7	0.2

(*) Kw/MQD
MQD PIANO EQUIV.
(+) GRADI CENT.

TAB. 7

****
N.FILA TUBI = 98
****

COEF.ASS.TUBI	0.95	
EMISSIVITA'	0.90	
NUMERO TUBI	1.0	
DIAM.EST.TUBI	0.0140	M
DIAM.INT.TUBI	0.0120	M
PASSO	0.0140	M
TEMP.ARIA EST.	20.0	GR.CENT.
VEL.ARIA EST.	5.0	M/SEC
TEMP.SODIO IN	440.0	GR.CENT.
LUNG.TUBO	2.3500	M
LARG.FILA	0.3140	M
VEL.SODIO IN	1.962	M/SEC
PRESSIONE	4.30	BAR
COEFF.CONV.	41032.9	W/MQD*C
REYNOLDS	87997.	
PERDITA CARICO	0.07	BAR
RENDIMENTO	0.891	
T.MED.METALLO	499.6	GR.CENT.
ALLUNG. MEDIO	25.64	MM

N.	FTOT*	FASS*	FIRR*	T.SODIO+	TTE+	TTI+	TTM+	TEMAX+	DTMAX+
1	42.0	15.0	13.6	448.1	448.8	448.3	448.3	450.2	1.4
2	71.0	42.4	13.8	448.5	450.4	449.0	449.0	452.7	2.8
3	182.0	147.2	14.3	449.8	456.7	451.7	451.6	462.5	8.3
4	293.0	251.9	14.9	452.0	463.8	455.3	455.2	473.1	13.8
5	522.0	468.0	16.1	456.1	478.0	462.3	462.1	494.3	24.9
6	751.0	683.8	17.5	462.1	494.0	471.2	470.9	517.3	35.8
7	965.5	885.5	19.1	469.9	511.1	481.8	481.2	540.8	45.7
8	1180.0	1087.0	21.1	479.5	529.8	494.2	493.4	565.9	55.4
9	1210.0	1114.2	22.3	489.4	540.7	504.5	503.5	577.7	56.5
10	1240.0	1141.1	23.6	499.5	552.0	515.1	514.0	589.8	57.5
11	1087.5	996.0	23.8	508.4	554.1	522.1	521.0	587.4	50.2
12	935.0	850.9	23.9	516.0	555.0	527.7	526.8	583.7	43.0
13	717.5	644.9	23.5	521.7	551.3	530.7	529.9	573.4	32.8
14	500.0	439.0	22.8	525.6	545.8	531.8	531.2	561.2	22.6
15	342.0	289.4	22.4	528.2	541.6	532.3	531.9	552.1	15.1
16	184.0	140.1	21.7	529.5	535.9	531.4	531.3	541.6	7.7
17	117.0	76.7	21.5	530.2	533.7	531.2	531.1	537.2	4.5
18	50.0	13.4	21.2	530.3	530.9	530.5	530.4	532.3	1.3
19	30.5	-5.0	21.1	530.2	530.0	530.1	530.2	530.8	0.4

(*) KW/MQD
MQD PIANO EQUIV.
(+) GRADI CENT.

TAB. 8

****
N.FILA TUBI = 117
****

COEF.ASS.TUBI	0.95	
EMISSIVITA'	0.90	
NUMERO TUBI	1.0	
DIAM.EST.TUBI	0.0140	M
DIAM.INT.TUBI	0.0120	M
PASSO	0.0140	M
TEMP.ARIA EST.	20.0	GR.CENT.
VEL.ARIA EST.	5.0	M/SEC
TEMP.SODIO IN	440.0	GR.CENT.
LUNG.TUBO	2.8500	M
LARG.FILA	0.0140	M
VEL.SODIO IN	1.962	M/SEC
PRESSIONE	4.30	BAR
COEFF.CONV.	40597.2	W/MQD*C
REYNOLDS	88237.	
PERDITA CARICO	0.07	BAR
RENDIMENTO	0.891	
T.MED.METALLO	501.1	GR.CENT.
ALLUNG. MEDIO	25.72	MM

N.	FTOT*	FASS*	FIRR*	T.SODIO+	TTE+	TTI+	TTM+	TEMAX+	DTMAX+
1	41.6	15.0	13.6	448.1	448.8	448.3	448.3	450.1	1.3
2	71.0	42.7	13.8	448.5	450.4	449.0	449.0	452.8	2.8
3	205.0	169.3	14.4	449.9	457.9	452.2	452.1	464.4	9.5
4	333.8	290.8	15.0	452.5	466.1	456.4	456.2	476.7	15.8
5	603.0	544.8	16.5	457.3	482.8	464.5	464.3	501.6	28.8
6	884.0	809.6	18.3	464.4	502.2	475.2	474.8	529.4	42.0
7	1086.9	1000.3	20.0	472.3	519.6	486.7	486.0	552.9	51.3
8	1286.4	1187.4	22.0	483.8	538.6	499.8	498.9	577.8	60.2
9	1226.4	1129.5	22.8	493.8	545.7	509.1	508.1	583.2	57.1
10	1186.8	1090.8	23.7	503.5	553.6	518.4	517.3	589.8	55.0
11	996.8	910.4	23.7	511.6	553.4	524.1	523.1	583.9	46.0
12	815.3	733.1	23.6	518.2	552.1	528.4	527.5	577.1	37.4
13	622.8	555.7	23.2	523.1	548.7	530.8	530.2	567.8	28.4
14	424.6	369.1	22.6	526.4	543.3	531.5	531.1	556.4	19.1
15	294.6	245.1	22.2	528.6	539.9	532.0	531.7	548.9	12.5
16	158.3	116.2	21.6	529.6	535.0	531.2	531.1	539.8	6.5
17	101.8	62.7	21.4	530.2	533.1	531.1	531.0	536.1	3.8
18	42.9	7.1	21.2	530.3	530.6	530.3	530.3	531.8	1.0
19	26.9	-8.0	21.1	530.2	529.8	530.1	530.1	530.5	0.2

(*) Kw/MQD
MQD PIANO EQUIV.
(+) GRADI CENT.

TAB. 9

****
N.FILA TUBI = 118
****

COEF.ASS.TUBI	0.95	
EMISSIVITA'	0.90	
NUMERO TUBI	1.0	
DIAM.EST.TUBI	0.0140	M
DIAM.INT.TUBI	0.0120	M
PASSO	0.0140	M
TEMP.ARIA EST.	20.0	GR.CENT.
VEL.ARIA EST.	5.0	M/SEC
TEMP.SODIO IN	310.7	GR.CENT.
LUNG.TUBO	2.8500	M
LARG.FILA	0.0140	M
VEL.SODIO IN	1.838	M/SEC
PRESSIONE	4.76	BAR
COEFF.CONV.	43833.8	W/MQD*C
REYNOLDS	67619.	
PERDITA CARICO	0.08	BAR
RENDIMENTO	0.916	
T.MED.METALLO	364.7	GR.CENT.
ALLUNG. MEDIO	18.40	MM

N.	FTOT*	FASS*	FIRR*	T.SODIO+	TTE+	TTI+	TTM+	TEMAX+	DTMAX+
1	41.9	26.1	5.7	310.9	312.2	311.2	311.3	313.7	1.9
2	71.5	54.1	5.8	311.4	314.0	312.0	312.1	316.5	3.5
3	205.5	180.9	6.1	313.0	321.7	315.2	315.3	328.5	10.6
4	338.1	306.3	6.5	315.6	330.3	319.3	319.5	341.4	17.6
5	616.1	569.2	7.3	320.5	347.8	327.4	327.8	367.7	32.2
6	897.1	834.7	8.3	327.6	367.7	337.9	338.4	396.3	46.6
7	1103.8	1029.7	9.4	336.5	385.8	349.2	349.8	420.8	57.1
8	1303.3	1217.6	10.6	347.0	405.1	362.1	362.7	446.2	66.8
9	1243.3	1160.0	11.0	357.0	412.2	371.5	371.9	451.4	63.4
10	1197.8	1116.1	11.5	366.6	419.8	380.7	381.0	457.3	60.7
11	1007.8	935.6	11.5	374.7	419.2	386.6	386.8	451.0	51.0
12	820.2	757.6	11.4	381.3	417.3	391.0	391.1	443.3	41.5
13	627.7	575.0	11.1	386.3	413.7	393.7	393.7	433.7	31.7
14	426.5	384.4	10.7	389.6	408.0	394.6	394.6	421.7	21.4
15	296.5	261.2	10.5	391.9	404.4	395.3	395.3	414.0	14.8
16	159.2	131.2	10.2	393.1	399.3	394.7	394.8	404.5	7.7
17	102.7	77.6	10.1	393.7	397.4	394.7	394.7	400.8	4.8
18	43.0	21.1	9.9	393.9	394.9	394.2	394.2	396.4	1.7
19	27.0	6.0	9.9	394.0	394.2	394.0	394.0	395.2	0.8

(*) KW/MQD
MQD PIANO EQUIV.
(+) GRADI CENT.

TAB. 10

****
N.FILA TUBI = 137
****

COEF.ASS.TUBI	0.95	
EMISSIVITA'	0.90	
NUMERO TUBI	1.0	
DIAM.EST.TUBI	0.0140	M
DIAM.INT.TUBI	0.0120	M
PASSO	0.0140	M
TEMP.ARIA EST.	20.0	GR.CENT.
VEL.ARIA EST.	5.0	M/SEC
TEMP.SODIO IN	310.7	GR.CENT.
LUNG.TUBO	2.8500	M
LARG.FILA	0.0140	M
VEL.SODIO IN	1.888	M/SEC
PRESSIONE	4.76	BAR
COEFF.CONV.	43931.4	W/MQD*C
REYNOLDS	67203.	
PERDITA CARICO	0.08	BAR
RENDIMENTO	0.913	
T.MED.METALLO	359.1	GR.CENT.
ALLUNG. MEDIO	18.10	MM

N.	FTOT*	FASS*	FIRR*	T.SODIO+	TTE+	TTI+	TTM+	TEMAX+	DTMAX+
1	35.6	20.3	5.7	310.9	311.8	311.1	311.1	313.2	1.6
2	64.4	47.6	5.8	311.3	313.6	311.9	311.9	315.8	3.1
3	209.4	184.9	6.1	312.9	321.8	315.1	315.3	328.7	10.8
4	350.5	318.3	6.5	315.6	330.9	319.5	319.7	342.4	18.3
5	645.9	597.6	7.4	320.7	349.5	323.1	328.5	370.3	33.7
6	949.4	884.4	8.5	326.3	370.8	339.2	339.8	401.0	49.3
7	1114.0	1039.5	9.4	337.3	387.0	350.2	350.7	422.4	57.6
8	1259.0	1175.9	10.5	347.4	403.5	362.1	362.6	443.3	64.6
9	1090.5	1015.8	10.5	356.2	404.6	368.9	369.3	439.2	55.9
10	961.1	852.6	10.6	363.9	406.4	375.1	375.4	436.9	49.1
11	753.1	695.3	10.4	369.9	403.0	378.7	378.9	427.1	38.4
12	551.6	504.3	10.1	374.3	398.3	380.7	380.8	416.1	28.1
13	424.1	383.3	10.0	377.6	395.9	382.5	382.6	409.6	21.5
14	273.1	240.3	9.7	379.7	391.2	382.7	382.8	400.0	13.7
15	198.1	169.2	9.6	381.2	389.2	383.3	383.3	395.7	9.8
16	103.3	79.5	9.4	381.8	385.6	382.8	382.9	389.1	4.9
17	70.8	48.7	9.3	382.3	384.6	382.9	382.9	387.0	3.2
18	29.7	9.7	9.2	382.3	382.8	382.5	382.5	383.9	1.0
19	19.2	-0.2	9.2	382.3	382.3	382.3	382.3	383.1	0.5

(*) Kw/MQD
MQD PIANO EQUIV.
(+) GRADI CENT.

TAB. 11

****
N.FILA TUBI = 156
****

COEF.ASS.TUBI	0.95	
EMISSIVITA'	0.90	
NUMERO TUBI	1.0	
DIAM.EST.TUBI	0.0140	M
DIAM.INT.TUBI	0.0120	M
PASSO	0.0140	M
TEMP.ARIA EST.	20.0	GR.CENT.
VEL.ARIA EST.	5.0	M/SEC
TEMP.SODIO IN	310.7	GR.CENT.
LUNG.TUBO	2.6500	M
LARG.FILA	0.0140	M
VEL.SODIO IN	1.338	M/SEC
PRESSIONE	4.76	BAR
COEFF.CONV.	44229.0	W/MQD*C
REYNOLDS	65118.	
PERDITA CARICO	0.00	BAR
RENDIMENTO	0.900	
T.MED.METALLO	343.3	GR.CENT.
ALLUNG. MEDIO	17.25	MM

N.	FTOT*	FASS*	FIRK*	T.SODIO+	TTE+	TTI+	TTM+	TEMAX+	DTMAX+
1	22.8	3.4	5.7	310.8	311.2	310.9	310.9	312.1	0.9
2	46.7	31.1	5.7	311.1	312.5	311.4	311.4	314.2	2.2
3	136.2	115.8	5.9	312.0	317.6	313.4	313.5	322.2	6.9
4	258.3	231.3	6.3	314.0	325.2	316.8	317.0	333.7	13.4
5	509.3	468.7	7.0	318.0	340.6	323.8	324.1	357.1	26.6
6	685.8	635.4	7.6	323.5	354.0	331.3	331.7	376.1	35.8
7	798.6	741.7	8.2	329.9	365.4	339.0	339.5	391.0	41.5
8	865.6	804.7	8.8	336.8	375.3	346.8	347.2	403.0	44.8
9	747.1	692.0	8.8	342.8	375.8	351.4	351.7	399.8	38.6
10	599.3	551.7	8.7	347.5	373.9	354.4	354.6	393.2	30.9
11	475.7	434.5	8.6	351.3	372.1	356.7	356.9	387.4	24.5
12	302.7	270.5	8.3	353.6	366.5	357.0	357.1	376.4	15.4
13	242.7	213.6	8.2	355.4	365.7	358.1	358.2	373.6	12.3
14	143.1	119.2	8.0	356.5	362.2	358.0	358.0	366.9	7.1
15	112.6	90.3	8.0	357.3	361.6	358.4	358.4	365.3	5.5
16	56.0	36.7	7.9	357.6	359.3	358.0	358.0	361.3	2.5
17	42.0	23.4	7.9	357.8	358.9	358.0	358.1	360.4	1.8
18	17.1	-0.1	7.8	357.8	357.7	357.7	357.8	358.4	0.4
19	12.1	-4.8	7.8	357.7	357.5	357.6	357.7	358.0	0.2

(*) KW/MQD
MQD PIANO EQUIV.
(+) GRADI CENT.

TAB. 12

****
N.FILA TUBI = 157
****

COEF.ASS.TUBI	0.95	
EMISSIVITA'	0.90	
NUMERO TUBI	1.0	
DIAM.EST.TUBI	0.0140	M
DIAM.INT.TUBI	0.0120	M
PASSO	0.0140	M
TEMP.ARIA EST.	20.0	GR.CENT.
VEL.ARIA EST.	5.0	M/SEC
TEMP.SODIO IN	290.1	GR.CENT.
LUNG.TUBO	2.8500	M
LARG.FILA	0.0140	M
VEL.SODIO IN	1.677	M/SEC
PRESSIONE	5.00	BAR
COEFF.CONV.	44683.9	W/MQD*C
REYNOLDS	61264.	
PERDITA CARICO	0.08	BAR
RENDIMENTO	0.901	
T.MED.METALLO	320.8	GR.CENT.
ALLUNG. MEDIO	16.06	MM

N.	FTOT*	FASS*	FIRR*	T.SODIO+	TTE+	TTI+	TTM+	TEMAX+	DTMAX+
1	23.2	10.1	4.9	290.2	290.7	290.3	290.3	291.6	1.0
2	45.7	31.3	4.9	290.5	292.0	290.8	290.9	293.6	2.2
3	135.2	116.0	5.1	291.5	297.1	292.9	293.0	301.6	7.0
4	255.8	230.1	5.4	293.4	304.6	296.2	296.4	313.0	13.4
5	497.4	458.7	6.0	297.4	319.5	302.9	303.3	335.6	26.2
6	673.9	625.5	6.6	302.7	332.8	310.2	310.8	254.6	35.5
7	770.8	716.9	7.1	308.8	343.3	317.6	318.1	368.1	40.4
8	832.8	775.1	7.6	315.5	352.7	325.0	325.5	379.4	43.6
9	714.3	662.6	7.6	321.2	352.9	329.2	329.7	375.9	37.3
10	551.1	507.8	7.4	325.5	349.9	331.8	332.1	367.7	28.7
11	405.5	369.7	7.2	328.7	346.4	333.3	333.5	359.6	21.0
12	259.7	231.5	7.0	330.7	341.8	333.5	333.7	350.3	13.4
13	189.7	165.1	6.9	332.1	340.0	334.1	334.2	346.3	9.7
14	119.0	98.1	6.8	332.9	337.7	334.2	334.2	341.6	5.9
15	85.0	65.9	6.8	333.5	336.7	334.3	334.4	339.6	4.1
16	47.7	30.5	6.7	333.8	335.2	334.1	334.2	336.9	2.1
17	31.7	15.4	6.7	333.9	334.6	334.1	334.1	335.8	1.3
18	15.0	-0.5	6.6	333.9	333.9	333.9	333.9	334.5	0.4
19	10.0	-5.2	6.6	333.9	333.6	333.8	333.8	334.1	0.1

(*) KW/MQD
MQD PIANO EQUIV.
(+) GRADI CENT.

TAB. 13

****
N.FILA TUBI = 176
****

COEF.ASS.TUBI	0.95	
EMISSIVITA*	0.90	
NUMERO TUBI	1.0	
DIAM.EST.TUBI	0.0140	M
DIAM.INT.TUBI	0.0120	M
PASSO	0.0140	M
TEMP.ARIA EST.	20.0	GR.CENT.
VEL.ARIA EST.	5.0	M/SEC
TEMP.SODIO IN	290.1	GR.CENT.
LUNG.TUBO	2.8500	M
LARG.FILA	0.0140	M
VEL.SODIO IN	1.877	M/SEC
PRESSIONE	5.00	BAR
COEFF.CONV.	45008.3	W/MQD*C
REYNOLDS	59102.	
PERDITA CARICO	0.08	BAR
RENDIMENTO	0.859	
T.MED.METALLO	304.2	GR.CENT.
ALLUNG. MEDIO	15.18	MM

N.	FTOT*	FASS*	FIRR*	Y.SODIO+	TTE+	TTI+	TTM+	TEMAX+	DTMAX+
1	17.8	5.1	4.8	290.2	290.4	290.2	290.2	291.1	0.7
2	25.3	12.2	4.9	290.3	290.8	290.4	290.4	291.8	1.1
3	51.8	37.3	4.9	290.6	292.4	291.0	291.1	294.2	2.1
4	150.0	130.2	5.1	291.7	298.0	293.3	293.4	303.0	7.1
5	229.0	205.0	5.3	293.5	303.4	295.9	296.1	310.9	12.1
6	307.7	279.3	5.6	295.8	309.3	299.2	299.5	319.4	16.2
7	360.5	329.2	5.8	298.6	314.5	302.6	302.9	326.3	19.1
8	377.0	344.7	5.9	301.6	318.2	305.8	306.1	330.5	19.1
9	349.0	318.0	6.0	304.3	319.6	308.2	308.4	331.0	18.1
10	275.0	247.7	6.0	306.4	318.4	309.5	309.6	327.4	14.1
11	199.5	176.1	5.9	307.9	316.4	310.1	310.2	323.0	10.3
12	124.1	104.6	5.8	308.8	313.9	310.1	310.2	318.0	6.3
13	80.0	62.9	5.7	309.4	312.4	310.1	310.2	315.1	3.9
14	57.8	41.8	5.7	309.7	311.7	310.2	310.3	313.8	2.8
15	41.0	25.9	5.7	310.0	311.2	310.3	310.3	312.7	1.1
16	23.7	9.5	5.6	310.0	310.5	310.1	310.2	311.4	0.1
17	17.0	3.1	5.6	310.1	310.2	310.1	310.1	310.9	0.1
18	10.0	-3.5	5.6	310.0	309.8	310.0	310.0	310.3	0.1
19	5.9	-7.4	5.6	310.0	309.6	309.9	309.9	309.9	-0.1

(*) KW/MQ
MQD PIANO EQUIV.
(+) GRADI CENT.

TAB. 14

****
N.FILA TUBI = 135
****

COEF.ASS.TUBI	0.95	
EMISSIVITA'	0.90	
NUMERO TUBI	1.0	
DIAM.EST.TUBI	0.0140	M
DIAM.INT.TUBI	0.0120	M
PASSO	0.0140	M
TEMP.ARIA EST.	20.0	GR.CENT.
VEL.ARIA EST.	5.0	M/SEC
TEMP.SODIO IN	290.1	GR.CENT.
LUNG.TUBO	2.8500	M
LARG.FILA	0.0140	M
VEL.SODIO IN	1.377	M/SEC
PRESSIONE	5.00	BAR
COEFF.CONV.	45214.9	W/MQD*C
REYNOLDS	57803.	
PERDITA CARICO	0.08	BAR
RENDIMENTO	0.679	
T.MED.METALLO	293.6	GR.CENT.
ALLUNG. MEDIO	14.62	MM

N.	FTOT*	FASS*	FIRR*	T.SODIO+	TTE+	TTI+	TTM+	TEMAX+	DTMAX+
1	8.7	-3.4	4.8	290.1	289.9	290.0	290.0	290.3	0.2
2	10.7	-1.5	4.8	290.1	290.0	290.0	290.1	290.5	0.3
3	18.0	5.4	4.8	290.1	290.4	290.2	290.2	291.1	0.7
4	40.0	26.2	4.9	290.4	291.6	290.6	290.7	293.1	1.9
5	70.0	54.6	5.0	290.8	293.5	291.5	291.5	295.9	3.5
6	94.0	77.3	5.0	291.5	295.2	292.4	292.5	298.4	4.8
7	103.7	86.4	5.1	292.2	296.4	293.2	293.3	299.5	5.3
8	106.2	88.8	5.1	293.0	297.3	294.0	294.1	300.9	5.4
9	100.0	82.9	5.1	293.7	297.7	294.7	294.7	301.1	5.1
10	85.0	68.6	5.1	294.3	297.6	295.1	295.1	300.5	4.3
11	65.0	49.7	5.1	294.7	297.1	295.3	295.3	299.3	3.2
12	46.0	31.7	5.1	295.0	296.5	295.3	295.4	298.1	2.2
13	31.0	17.4	5.1	295.1	295.9	295.3	295.3	297.1	1.4
14	23.0	9.9	5.0	295.2	295.7	295.3	295.3	296.6	0.9
15	15.0	2.3	5.0	295.2	295.3	295.2	295.2	295.9	0.5
16	10.0	-2.5	5.0	295.2	295.1	295.1	295.2	295.5	0.2
17	6.5	-5.8	5.0	295.1	294.8	295.1	295.1	295.2	0.0
18	3.2	-8.9	5.0	295.1	294.6	294.9	294.9	294.9	-0.1
19	2.4	-9.7	5.0	295.0	294.5	294.8	294.8	294.7	-0.2

(*) KW/MQD
MQD PIANO EQUIV.
(+) GRADI CENT.

TAB. 15

APPENDIX A

Convection power loss correlations

To evaluate the effect of forced convection the following correlation for flat plate has been considered (see Ref. 3)

$$Nu_x = 0.0592(Pr)^{0.6}.(Re_x)^{0.8}.(\frac{TTE}{T_a})^{-0.4}$$

where: Nu_x Nusselt number at point x

Pr Prandtl number

Re_x Reynolds number at point x

TTE Outside tube wall temperature

T_a Ambient air temperature

In this expression, to take into account the roughness effect of the absorber surface, in comparison with the smooth flat plate case, a roughness factor of 2, based on cylinder correlation (Achenbach's data), has been included.

A wind velocity at ground $W_g = 5$ m/sec has been considered. At receiver elevation z , the wind velocity

has been calculated according to the expression (Ref. 3)

$$W = W_g \cdot \left(\frac{z}{10}\right)^{0.15}$$

$$W = 5 \cdot \left(\frac{43}{10}\right)^{.15} = 6.2 \text{ m/sec}$$

The average value of forced convection coefficient taking into account absorber temperature distribution is:

$$H_f = 29 \text{ W/m}^2/^\circ\text{K}$$

To have an indication of the relative contribution of natural and forced convection to the total convection power loss, consider tha ratio (Ref. 4, 5)

$$\alpha = \frac{Gr_L}{(Re_L)^2}$$

where: $$Gr_L = \frac{g\beta L^3(T - Ta)}{\nu^2}$$

$$Re_L = \frac{W \cdot L}{\nu}$$

g	Gravity acceleration (m/sec^2)
β	Coefficient of volumetric expansion($1/^\circ K$)
L	Height of vertical surface (m)
T	Surface temperature ($^\circ K$)
ν	Cinematic viscosity (m^2/sec)

substituting

$T = 400\ °C$

$L = 3\ m$

$\nu\ (T = 210\ °C) = 0.36 \cdot 10^{-4}\ \ (m^2/sec)$

$\beta\ (T = 210\ °C) = 2.07 \cdot 10^{-3}\ \ (1/°K)$

$$Gr_L = \frac{(9.8)(2.07 \cdot 10^{-3})(3)^3 \cdot (380)}{(0.36 \cdot 10^{-4})^2}$$

$$Re_L = \frac{(6.2) \cdot (3)}{(0.36 \cdot 10^{-4})} = 5.2 \cdot 10^5$$

$$\alpha = \frac{1.6 \cdot 10^{11}}{(5.2 \cdot 10^5)^2} \cong 0.6$$

The α value shows the predominant effect of forced convection in comparison with natural convection. However natural convection effect has been taken into account according to the expression (Ref. 6)

$$H = \sqrt{H_n^2 + H_f^2}$$

To evaluate the natural convection effect the correlation shown in the diagram of fig. A/1 has been used (Ref. 5)

$Pr(T = 210) = 0.689$

$$Gr \cdot Pr = (0.689) \cdot (1.6 \cdot 10^{11}) = 1.1 \cdot 10^{11}$$

$Nu \cong 600$ (from diagram of fig. A/1)

$$H_n = \frac{K_f \, Nu}{L} = \frac{(0.037)(600)}{(3)} = 7.4 \ W/m^2 \cdot {}^\circ K$$

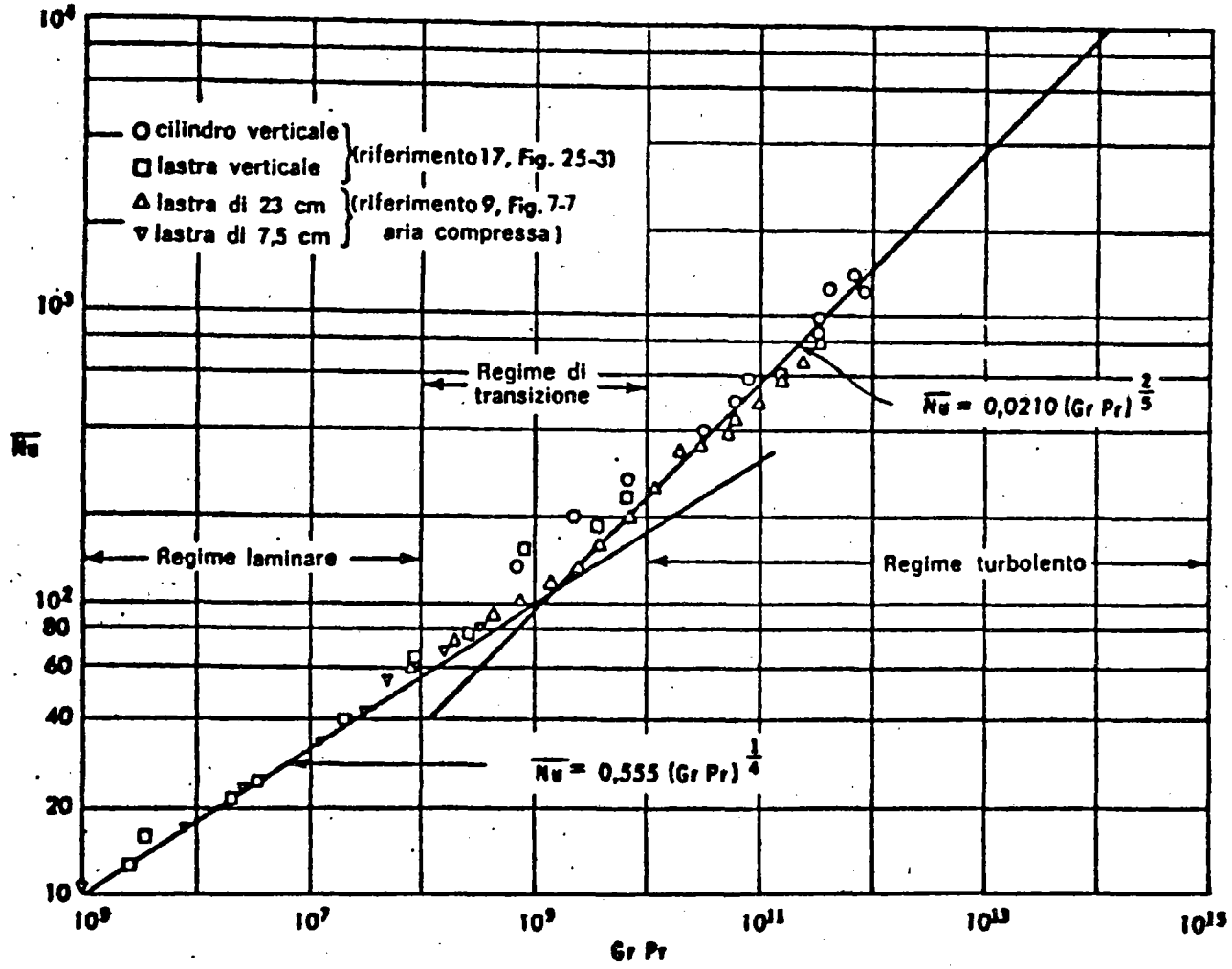

FIG. A/1 – CORRELATION OF DATA ON HEAT TRASFER BY NATURAL CONVECTION FROM VERTICAL PLATES AND CYLINDERS

APPENDIX B

ASTM Type 316 L physical properties

The data sheet reported in Tab. B/1 and reproduced from Ref. 7, summarize the physical properties of ASTM Type 316 L austenitic steel.

This data has been used to perform absorber tubing thermal analysis.

Physical properties

Density 8.0 g/cm³, 0.29 lb/in³

Thermal conductivity

Temperature °C	Temperature °F	W/m · °C	kcal/m · h · °C	Btu/ft · h · °F
20	68	15	13	9
100	210	16	14	9.5
300	570	19	16	10.5
500	930	21	18	12
700	1290	23	20	13.5

Specific heat capacity, mean values

Temperature °C	Temperature °F	J/kg · °C	kcal/kg · °C	Btu/lb · °F
50—100	120—210	500	0.12	0.12
600—700	1110—1290	630	0.15	0.15

Thermal expansion, mean values (x10⁻⁶)

Temperature °C	Temperature °F	Per °C	Per °F
20—100	68—210	16.0	8.9
20—200	68—390	17.0	9.5
20—300	68—570	17.5	9.7
20—400	68—750	17.8	9.9
20—500	68—930	18.0	10.0
20—600	68—1110	18.2	10.1
20—700	68—1290	18.5	10.3

Modulus of elasticity

Temperature °C	Temperature °F	N/mm²	kg/mm²	ksi
20	68	200 000	20 000	28 500
400	750	170 000	17 000	24 000
600	1110	150 000	15 000	19 000

TAB. B/1 – PHYSICAL PROPERTIES OF ASTM TYPE 316 L AUSTENITIC STEEL

IEA ALMERIA PROJECT

ADVANCED SODIUM RECEIVER
ASR

Tube panel stress analysis

Topic Report No. 3

Revision 0

March 3th 1981

Prepared by: ENEL
FRANCO TOSI
SNAMPROGETTI

INDEX

Abstract

1. Introduction

2. Tube panel stress analysis
   - 2.1. Analysis limits
   - 2.2. Description of structure and its boundary conditions
   - 2.3. Thermal load basic data
   - 2.4. Mechanical load basic data
   - 2.5. Material basic data
   - 2.6. Hypothesis and calculation method
   - 2.7. Results

3. Code stress limits compliance
   - 3.1. Analysis limits
   - 3.2. Operating conditions
   - 3.3. Stress table following ASME criteria
   - 3.4. Bursting analysis
   - 3.5. Shake-down analysis
   - 3.6. Ratcheting analysis
   - 3.7. Creep-fatigue analysis

4. Conclusions

Appendix 1

Annex 1

Annex 2

ABSTRACT

The main contents of this report are:

1) Detailed elastic stress analysis of the most stressed tube due to thermal heat flux and mechanical loads during normal operations (dayly cycling).

2) Compliance analysis of the tube stresses with the code limits and in accordance to the contract.

1. INTRODUCTION

With purpose to introduce the problems studied in this report, is usefull to refer to the summary description of the system, reported in the Topic Report n° 2, Section 1.

2. TUBE PANEL STRESS ANALYSIS

2.1. Analysis limits

The analysis regards the hottest tube, subject to thermal flux conditions and to stationary mechanical load, corresponding to max. loads.

We have assumed that attainment of these conditions is so slow as not to cause any overstresses; therefore the considered stress condition is also the severest one.

2.2. Description of structure and its boundary conditions

The structure under consideration is the receiver tube (D_e = 14 mm, tichn = 1 mm), restrained in the rectilinear portion by means of support, and clamped in the header connection points.

In fig. 1 are shown the 3 kinds of tube, alternately assembled.

The suitable length of down comer supplies a cold-spring effect in the tubes, in the erection conditions.

In the considered running conditions, this cold-spring effect nullifies the stresses which would occur as a result of the different expansion in the tubes and in the down comer.

Another cold-spring effect has been imposed with a misalignement of the two central restraints in respect to laterals, with the purpose to reduce thermal stresses.

In fig. 1 are shown the sketchs of the applied cold-springs.

2.3. Thermal load basic data

The receiver flux map used as a basis for these calculations is the equinox noon heat flux map reported in Progress Report n° 6 at section 2-7.

Fig. 2 shows the trend of the absorbed flux and the sodium temperature.

These data are assumed as a basis for the thermal calculation of section 2.6.

2.4. Mechanical load basic data

The mechanical loads which act on the structure are:

- tube and sodium weight (0,424 kg/m);
- internal pressure (6,11 kg/cm2);
- cold-spring effects (see section 2.2);
- wind load at full power operation.

2.5. Material basic data

The receiver tube material is SANDVIK Alloy 3R60 corresponding to the ASTM 316L type.

The material features have been taken from the manufacturer's documentation.

In the Appendix 1 the material is completely specified.

2.6. Hypothesis and calculation method

On the basis of the outside flux conditions and internal sodium temperature data given in Section 2.3, we have determined, by means of a finite elements calculation program (FLHE of the BERSAFE series), the temperature field on every point of the section.

This calculation has been performed on a certain number of sections, with the purpose of determining the complete temperatures field on the tube.

In fig. 3 is shown the 2-D mesh used in these thermal calculations.

In the assumption of linear elastic behaviore of the material, the stress condition has been determined by means of superimposition of 3 effects:

1) stresses due to internal pressure;

2) self equilibrating stresses in every section, due to non-linear temperature distribution on the section;

3) stresses due to partial restraint of expansion and deflections on the tube, due to the linear portion of temperature;

4) stresses due to weight and wind.

Stresses at point 1) can easily be determined by formulas.

Stresses at point 2) can be found by imposing the temperature field previously determined on a portion of tube isostatically bounded, and discretized by shell finite elements, with SAP V structural analysis code (fig. 4).

Resultant displacements allow moreover to determine on equivalent linear temperature distribution on the section for different flux values.

Stresses at point 3) and 4) are determined by a flexibility calculation using a beam element discretization, whose loading condition consists in the previously found linear temperature distribution.

In fig. 5, 6, 7 are shown the meshs and the deformed shapes of the 3 types of tube.

2.7. Results

In Table 1 are shown the stresses obtained in the most stressed structure point (the outer point of max flux on the most radiated section).

Pressure stresses are of little importance; stresses due to non linear temperature distribution on section are considerable, and cannot be reduced because they are not influenced by boundary conditions.

Stresses due to partial expansion restraint have been reduced by suitable disposition and number of boundaries, in compliance with other requirements.

3. CODE STRESS LIMITS COMPLIANCE

3.1. Analysis limits

In compliance with Contract Section A-7.1, since the tube is a sodium containing component, the design has been carried out by following criteria:

a) Primary membrane stress is limited to prevent bursting, according to par. UG-27, ASME Section VIII, Division 1.

b) An extention of the shakedown limit is imposed on primary and secondary stresses, to prevent noticeable distortions, that is: $P_L + P_B + Q < 3\ S_m$, according to par. 4-134, Appendix 4, ASME Section VIII, Division 2.

c) To satisfy the distortion limits by using an elastic analysis, and particularly to limit the inelastic strain amount that can occur during the service life of the component, Test No. 3, par. T-1324, Appendix T, Code Case N-47-17 has been applied. This analysis is not strictly required by the Contract, but is necessary in order to make possible the use of subsequent creep-fatigue analysis on elastic basis.

d) For component service life time evaluations, that is to evaluate creep-fatigue interaction effects, it has

been imposed the limit by eq. (5) of the par. T-1411, Appendix T, Code Case N-47-17, for elastic analysis.

Note

1. With reference to c) and d) above, some modifications have been brought with respect to that requested by Code Case, taken in account that we deal with a solar receiver and not a nuclear component, as forecast by Contract.

2. The creep-fatigue damage calculated hereafter, is only the damage portion of dayly cycling; the damages due to other operating conditions will be analyzed in other documents.

3.2. Operating conditions

The trend of the principals parameters during the dayly cycle (referred to 21 March and to the hottest section of the tube) is reported in fig. 8.

These data are:

- metal wall average temperature on the hottest radial section of the tube;
- sodium temperature;
- absorbed heat flux.

3.3. Stress table following ASME criteria

In table 2 are shown the stresses with their classification.

With a large conservatisme, the effects of non linear temperature distribution on the cross section of the tube have been classified as secondary stresses Q.

Actually, part or all the stresses due to that non-linearity, since doesn't produce any distortion, could be classified as F, by definitions in 3213.11 and 3213.13(b)(2), Code Case N-47-17.

3.4. Bursting analysis

The joint efficiency E, requested in UG-27, ASME Section VIII, Division 1, is equal to 1.

The allowable stress value S_m is determined conservatively corresponding with the maximum metal wall-averaged temperature on the hottest cross section (see table 3).

3.5. Shake down analysis

The S_m value is taken as average of the two S_m values at maximum and minimum cycle temperatures, as it results

from Note (1), fig. 4-130.1, Appendix 4, ASME Section VIII, Division 2, because all secondary stress is a thermal stress (see table 3).

3.6. Ratcheting analysis

We have excluded the presence of "Elastic follow-op", by which the thermal stresses due to linear temperature distribution on the tube cross section, responsible of the strain, would be classified as P_L for purpose of Test No. 3, T+1324, Code Case N-47-17. Such assumption is justified in the sollowing points:

a) The possible plasticity doesn't affect the total tube cross section but only a portion; therefore the plastic portion cannot reach noticeable strains, because of the internal restrains caused by the elastic core of the section.

b) The thermal stress distribution along the tube lenght has a quite mooth trend without picks in the most stressed section.

The step by step procedure proposed by par. T-1321 and T-1324 in the Appendix T of Code Case N-47-17 has been followed and the results are shown in table 4.

Non axisymmetric loads has been included as axisymmetric loads, and the curves of fig. T-1324-1 has been used, according with T-1324(a), Appendix T, Code Case N-47-17.

3.7. Creep-fatigue analysis

The following assumptions have been held:

- the total allowable creep-fatigue damage is $D = 1$, for elastic analysis (T-1431(b));
- the factor $K' = 0.9$ has been neglected in the evaluation of effective creep-fatigue damage, for the determination of the allowable time duration T_d (table T-1411-1);
- allowable number of cycles to use in equation (5), T-1411, is taken from curves of fig. T-1420-1B, Code Case N-47-17, removing excessive conservatisme of curves of fig. T-1430, according to the Contract statement (see point A-7.1);
- the step by step procedure suggest in T-1410 in the Appendix T of Code Case N-47-17 has been carried out and the results are described in table 5.

Note:
The elastic analysis rules applied in this note may be used because elastic ratcheting rules have been satisfied as shown in 3.6 .

4. CONCLUSIONS

All tests are complied, particularly the tube is prevented against the creep-fatigue interaction, which is the most dangerous failure mechanism for the component under examination.

Available margins of safety allow to foresee the component withstands accidents, at present not undertaken.

Points of particular conservativisme will be stressed as follow:

- elastic analysis has been applied;
- creep in compression has been considered as dangerous as creep in tension;
- creep-fatigue verification has been carried out considering relaxation-fatigue as dangerous as creep-fatigue. The actual phenomenon on the tube is relaxation-fatigue which has been demonstrated to be less dangerous (1) then creep-fatigue.

---

(1) E.P. Esztergar - Oak Ridge National Laboratory "Creep-fatigue interaction and cumulative damage evaluations for type 304 Stainless Steel"

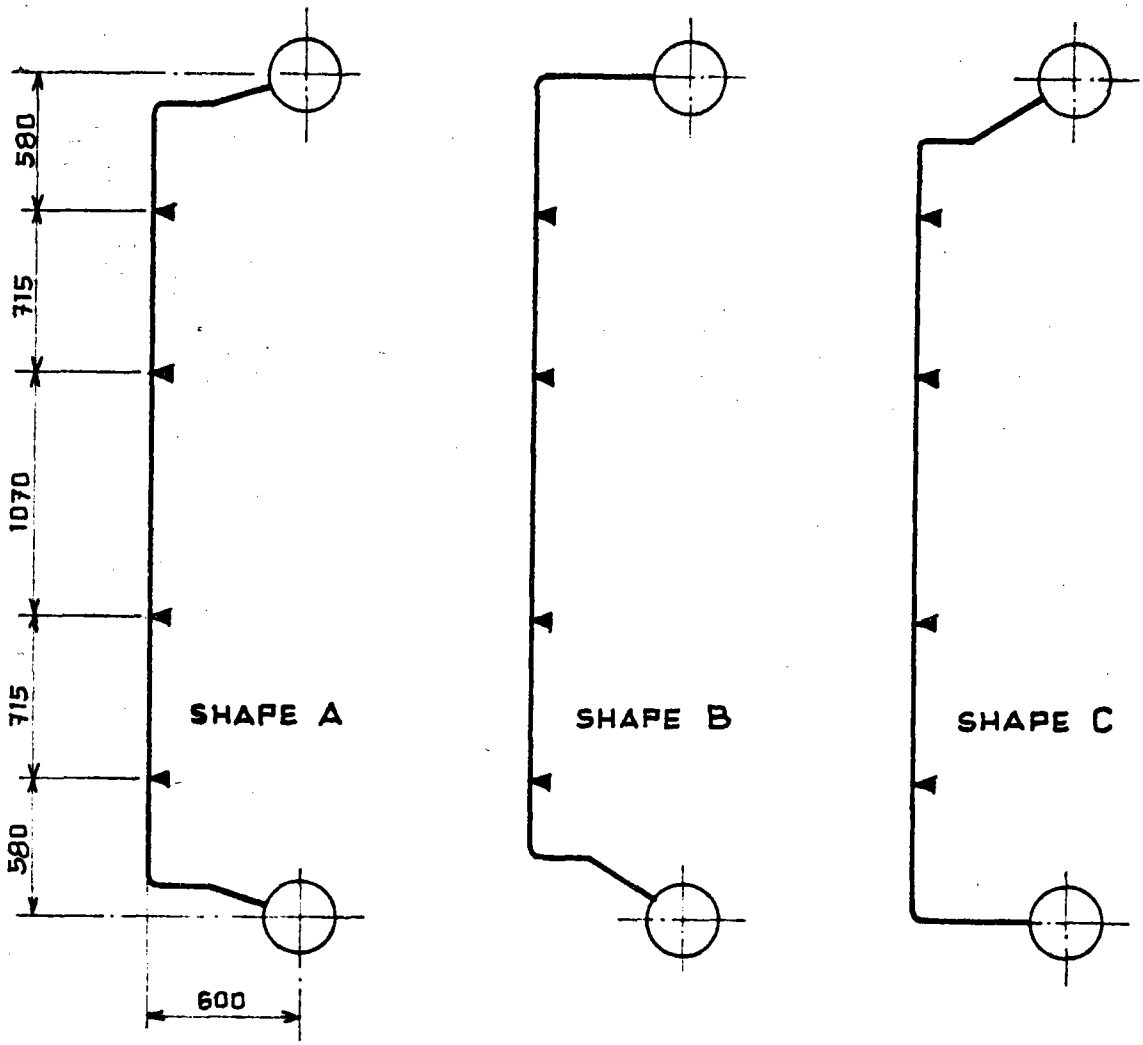

COLD SPRING EFFECT N° 1

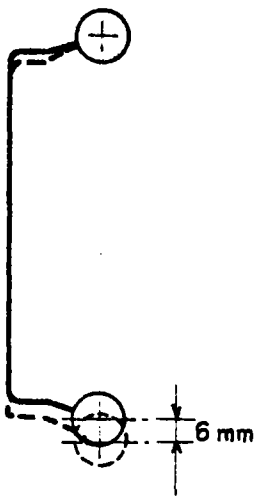

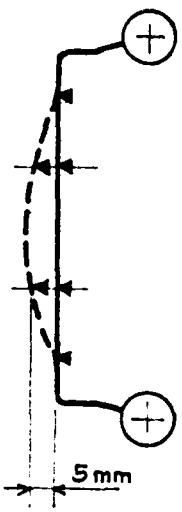

COLD SPRING EFFECT N° 2

— FIG. 1 —

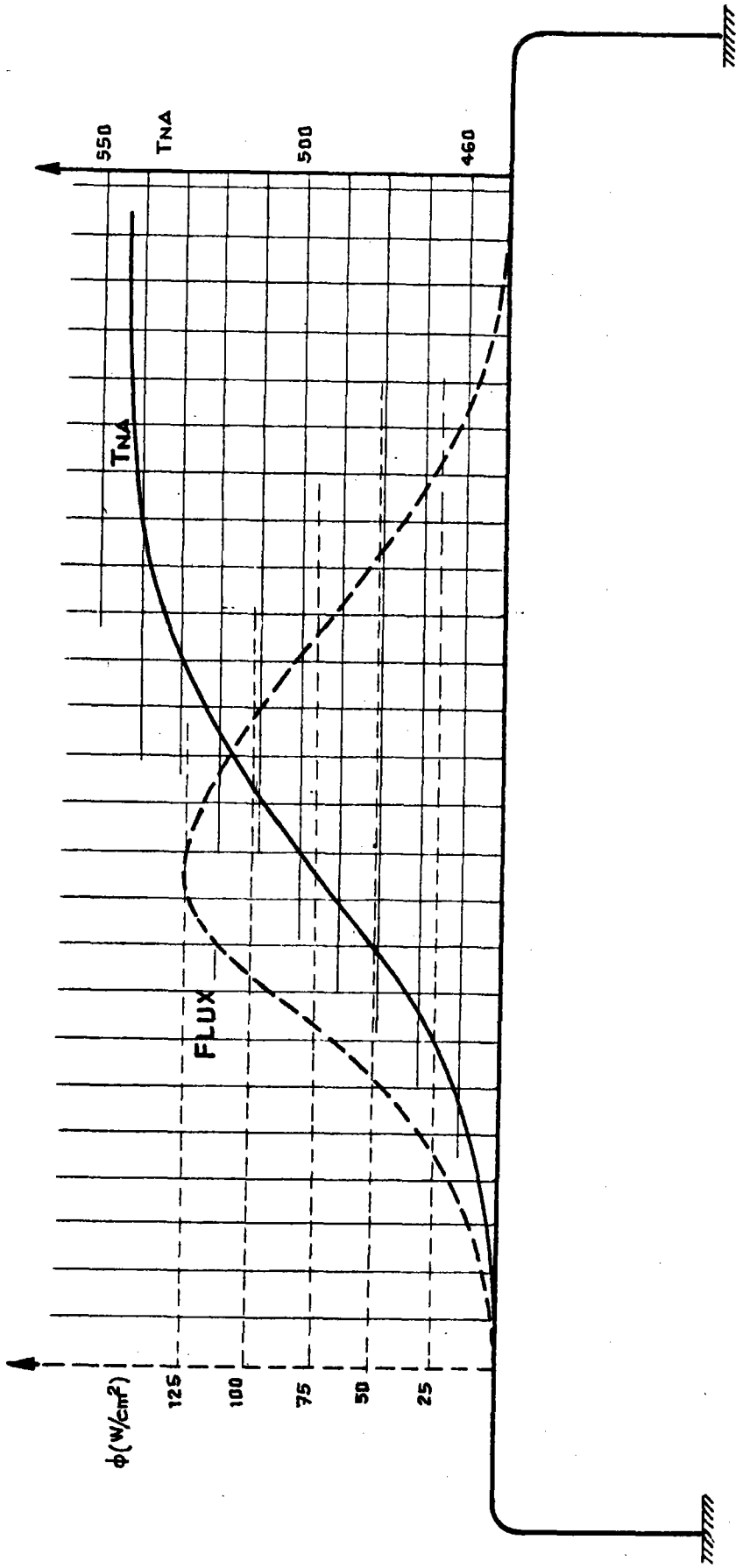

— FIG. 2 —

FT

LEGNANO

*** 1/2 TUBO - ELEM. TIPO 4 ***
UNDEFORMED SHAPE
FEBRUARY 25. 1981 09:19:56
IAXIS= 3 ALPHA= 0.00 BETA= 0.00

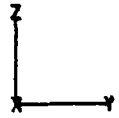

FIG. 3

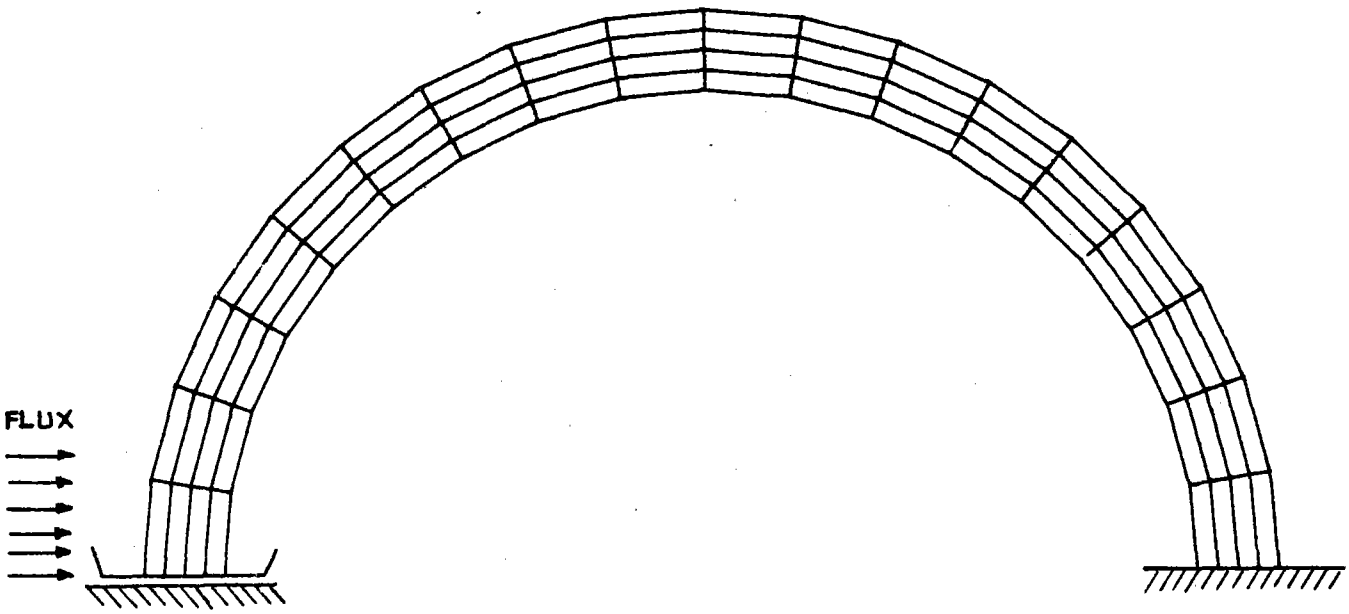

LEGNANO

• ALMERIA SOLAR RECEIVER • HALF-TUBE DISCRETISATION WITH SHELL ELEMENTS
UNDEFORMED SHAPE
DECEMBER 11, 1980 15:24:12
IAXIS= 2 ALPHA= 30.00 BETA= 30.00

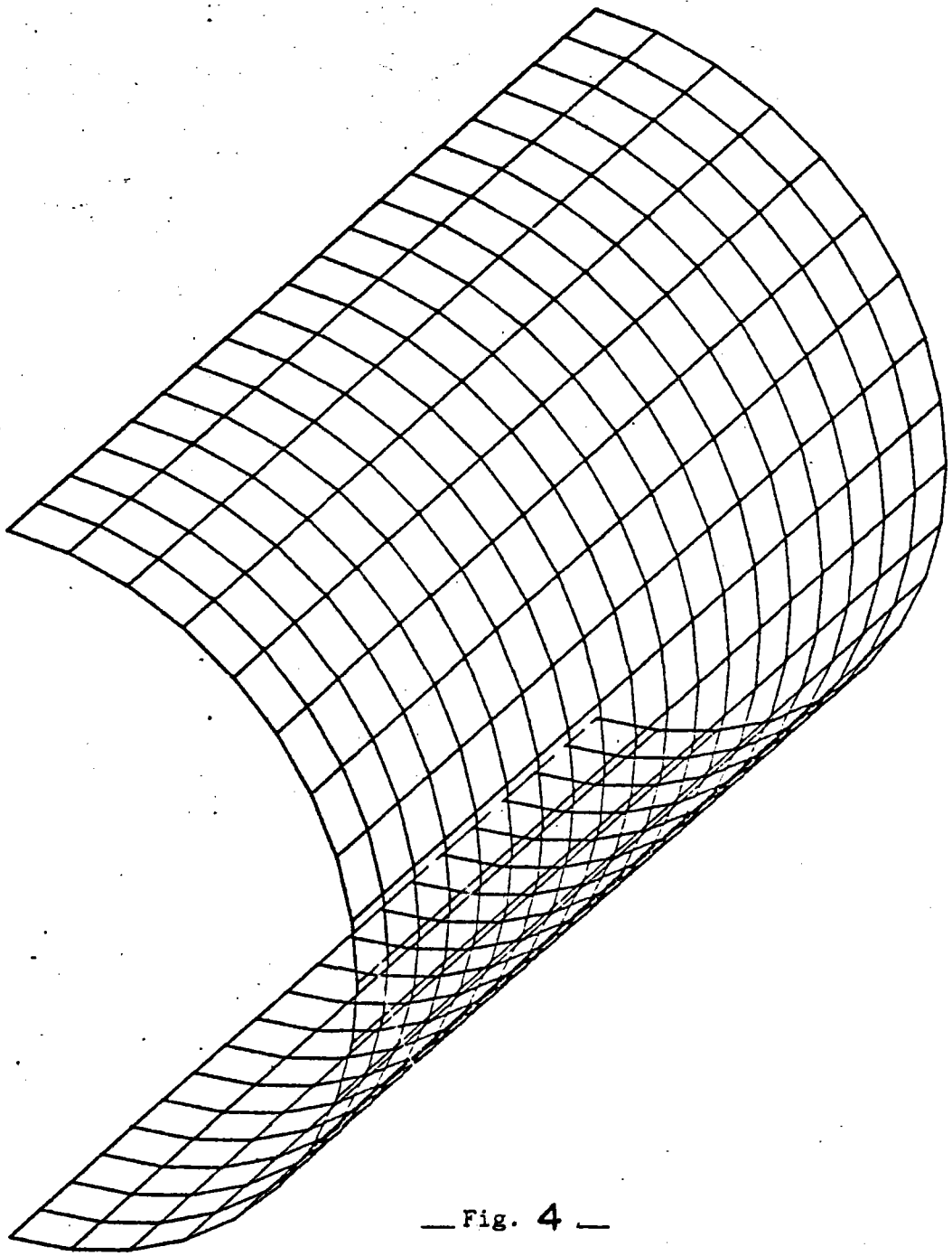

Fig. 4

LEGNANO

ALMERIA-
STATIC LOAD CASE 4
DECEMBER 20, 1980 01:24:29
IAXIS= 1 ALPHA= 0.00 BETA= 90.00
DEFLECTION SCALE FACTOR= 0.53873 E-1

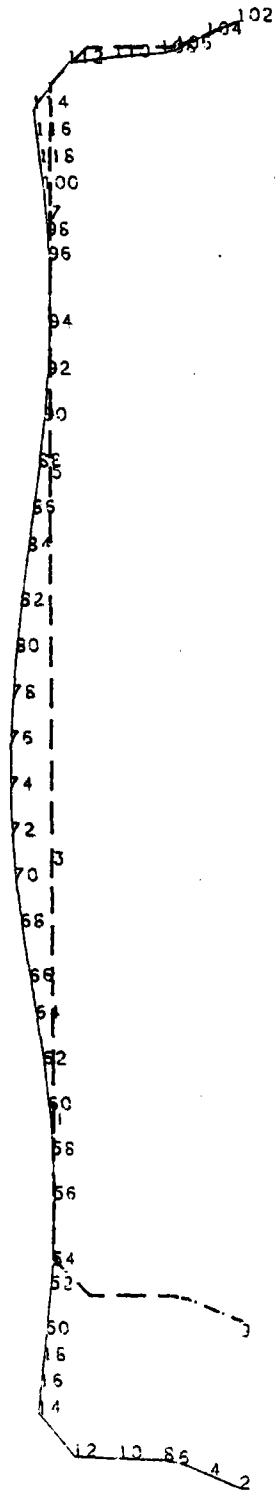

FIG. 5 - BEAM CALCULATION - SHAPE A

LEGNANO

ALMERIA-
STATIC LOAD CASE 4
DECEMBER 23, 1980 16:09:12
IAXIS= 1 ALPHA= 0.00 BETA= 90.00
DEFLECTION SCALE FACTOR= 0.53873 E-1

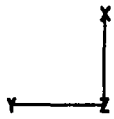

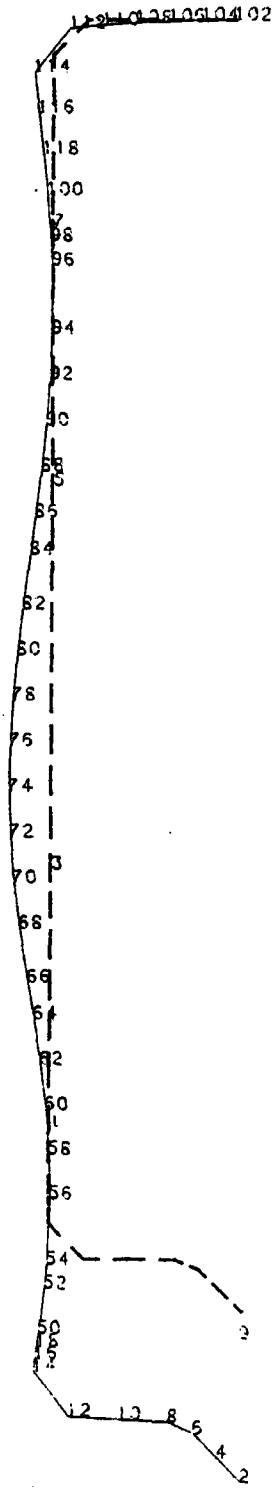

FIG. 6 _ BEAM CALCULATION - SHAPE B

LEGNANO

ALMERIA-
STATIC LOAD CASE 4
DECEMBER 23, 1980 09:57:44
1AXIS= 1 ALPHA= 0.00 BETA= 90.00
DEFLECTION SCALE FACTOR= 0.53586 E-1

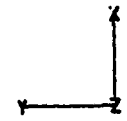

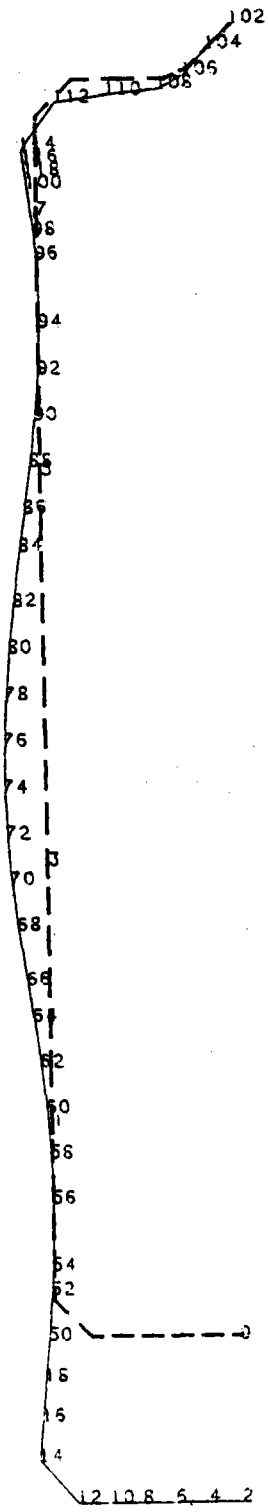

FIG. 7 - BEAM CALCULATION - SHAPE C

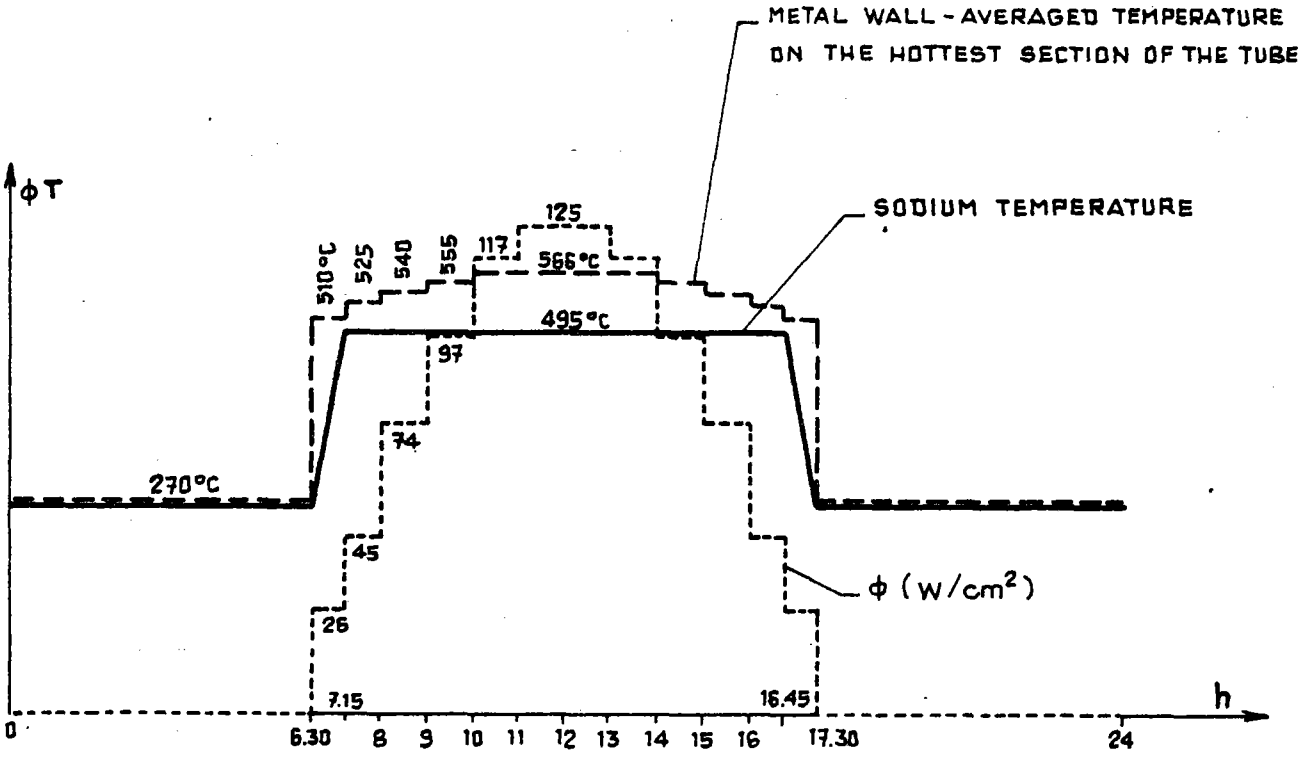

METAL TEMPERATURE	DAILY HOURS	TOTAL HOURS
270 °C	13.	42510.
510 °C	1.5	4905.
525 °C	1.5	4905.
540 °C	2.	6540.
555 °C	2.	6540.
566 °C	4.	13080.

_ FIG. 8 _

	STRESSES (kg/cm^2)								
	SHAPE A			SHAPE B			SHAPE C		
	σ_z	σ_ϑ	σ_R	σ_z	σ_ϑ	σ_R	σ_z	σ_ϑ	σ_R
Thermal stresses due to nonlinear distribution of temperatures	-14.49	-9.27	0	-14.49	-9.27	0	-14.49	-9.27	0
Pressure	0.17	0.34	0	0.17	0.34	0	0.17	0.34	0
Restraint stresses due to equivalent linear distribution of temperature on the tube	-9.58	0	0	-9.4	0	0	-9.68	0	0
Cold spring effect n° 1 (increase 6 mm in center distance of the headers)	-0.11	0	0	-0.14	0	0	-0.09	0	0
Cold spring effect n° 2 (misalignement of 5 mm of the two central restraints)	1.42	0	0	1.45	0	0	1.40	0	0
Weight	0.06	0	0	0.06	0	0	0.06	0	0
Wind	Neglegibles								

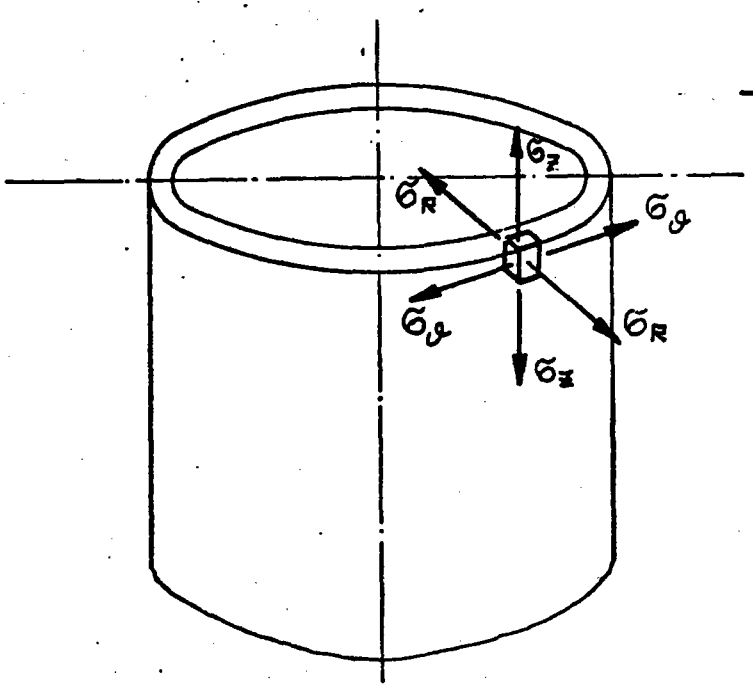

_ TAB. 1 _

Stresses in the most stressed point on the cross section, corresponding to the highest metal temperature during the dayly cycling.

Loads	Axial	Circumf.	Radial	Classif.
Weight	0.06	0.	0.	P_m
Pressure	0.17	0.34	0.	P_m
Restraints	-9.68	0.	0.	Q
Thermal	-14.49	-9.27	0.	Q
Cold spring effect n° 1	-0.06	0.	0.	Q
Cold spring effect n° 2	0.93	0.	0.	Q

Highest metal temperature in a point of cross section:

$$T_{max} = 596\ °C$$

Note: the stresses due to cold spring effects have been reduced to $\frac{2}{3}$, according to .3672(g) of N47 Code Case.

- TABLE 2 -

BURSTING ANALYSIS

Maximum metal wall-averaged temperature on the hottest hoop section ..... $T_{max_{h.s.}} = 566\ °C$

Maximum allowable stress at $T_{max_{h.s.}}$ ..... $S_m = 7.62\ Kp/mm^2$

Minimum required thickness of shell ..... t

Design pressure ..... $P = 0.0611\ Kp/mm^2$

Inside radius of shell ..... $R = 12\ mm$

Circumferential stress: $$t = \frac{PR}{S-0.6P} = \frac{0.0611 \times 12}{7.62-0.6 \times 0.0611} = 0.10\ mm$$

Longitudinal stress : $$t = \frac{PR}{2S+0.4P} = \frac{0.0611 \times 12}{2 \times 7.62+0.4 \times 0.0611} = 0.05\ mm$$

The actual tube tickness is: $t_a = 1\ mm$

SHAKE DOWN ANALYSIS

Highest metal temperature in a point of the cross section ..... $T_{max} = 596\ °C$

Lowest metal temperature in a point of the cross section ..... $T_{min} = 270\ °C$

Maximum allowable stress at T_{max} ..... $S_m(T_{max}) = 7.48\ Kp/mm^2$

Minimum allowable stress at T_{min} ..... $S_m(T_{min}) = 9.84\ Kp/mm^2$

Allowable stress for TEST B ..... $S_m = 8.66\ Kp/mm^2$

$$P_L+P_B+Q = 14.49 + 9.68 - 0.17 - 0.06 + 0.06 - 0.93 =$$

$$= 23.07\ Kp/mm^2 < 3\,S_m = 3 \times 8.66 = 25.98\ Kp/mm^2$$

- TABLE 3 -

REATCHETING ANALYSIS

Maximum metal wall-averaged temperature on the hottest hoop section ..... T_{max} = 566 °C

Minimum metal wall-averaged temperature .... T_{min} = 270 °C

Yeld stenght at T_{min} ..... S_y = 8.45 Kp/mm^2

$$X = (P_L + \frac{P_b}{K_T}) + S_y \quad ; \qquad Y = \frac{(Q_R)max}{S_y} \quad ;$$

$$K_T = 1 + K_S(1 - \frac{P_L}{S_t}) \simeq 1 + K_S \quad (*) \quad ; \qquad K_S = \alpha(K-1) \quad ;$$

K = 1.27 (from ASME Section III, Appendix A, Table A-9221(a)-1);

$\alpha = 0.5$; $K_S = 0.5(1.27-1) = 0.135$;

P_L	P_b	Q_R	K_T	X	Y	Z	c
0.34	0.	24.17	1.135	0.04	2.86	0.114	1.21

$\sigma_c = 1.25\ Z\ S_y$

Entering the isochronous stress-strain curves at temperature 566 °C, and for any time, by σ_c, we read no significant strain, % due to creep.

(*) Smallnes of $\frac{P_L}{S_T}$ justifies this position.

- TABLE 4 -

FATIGUE ANALYSIS

$$\varepsilon_t = \left(\frac{S^*}{S}\right) K^2 \varepsilon_n + K\varepsilon_c + K_T\varepsilon_F \quad ; \quad \text{where} \quad \frac{S^*}{S} = 1$$

$K = 1$

$\varepsilon_n = .207E-2$

$\varepsilon_c = 0$

$\varepsilon_F = 0$

$\varepsilon_t = .207E-2$

$T = 596\ ^\circ C$

$N_d = 13172$ by T-1420-1A,1B

$n = 3270$

$\sum \frac{n}{N_d} = 0.248$

CREEP ANALYSIS

$T_{min} = 270\ ^\circ C$

$T_{max} = 567\ ^\circ C$

$S_y/K = 9.76\ Kg/mm^2$

$P_m/K = 0.34\ Kg/mm^2$

$S_r/K = 23\ Kg/mm^2$

$(P_L+P_B+Q)_{SS} = 22.80\ Kg/mm^2$

$P_m/K + 0.5\ S_r/K = 11.87\ Kg/mm^2$

$S_K = 12.2\ Kg/mm^3$

CREEP DAMAGE OF AN HALF CYCLE OF A DAY

Time interval	Interval lenght:t	T (°C)	T_d	t/T_d
6.30-7.1	0.75 h	510	5000000	1.5E-7
7.15-8	0.75	525	2500000	3.E-7
8 - 9	1	540	1800000	5.5E-7
9 - 10	1	555	770000	1.3E-6
10 - 11	1	566	450000	2.2E-6
11 - 12	1	566	450000	2.2E-6

$\Sigma = 6.7E-6$

Number of years : 10
Number of sunny days : 182
Number of cloudy days: 145

$$\Sigma \frac{t}{T_d} = 2x\ (6.7E-6)x\ 182x\ 10 + 2x\ (6.7E-6)x\ \frac{145}{2}\ x\ 10 = 0.034$$

TOTAL CREEP-FATIGUE DAMAGE

$D = 0.248 + 0.034 = 0.282$

APPENDIX 1

Mechanical characteristics of tube material

In the thermoelastic calculations the following assumptions are made:

- density: the values are assumed from phisical properties in the SANDVIK 3R60 fish reported in Annex 1;
- thermal conductivity: as before;
- specific heat capacity: as before;
- istantaneous coefficient of thermal expansion: the values are assumed from Table I-14.8 of ASME Code Case N47-17;
- modulus of elasticity: the values are assumed from SANDVIK 3R60 fish reported in Annex 1.

In the code compliance analysis the following assumptions are made:

- yield strenght: the values are assumed from fig. 1 in Annex 2;

. allowable stress S_m: the values are represented in fig. A1/1 as the minimum value between:

- 1/3 of the tensile strength at temperature;
- 90% of the yield strenght at temperature but not exced 2/3 of the specified minimum yield strenght at noon temperature;

the yield and the tensile strenght are desumed from fig. 1 and fig. 2 in Annex 2;

. fatigue curves: the values are assumed from fig. T-1420 1B of ASME Code Case N47-17;

. isochronous curves: the values are assumed from fig. T-1800-B of ASME Code Case N47-17;

. minimum time to rupture: the values are assumed ad the lower bound of the curves represented in fig. 3 in Annex 2.

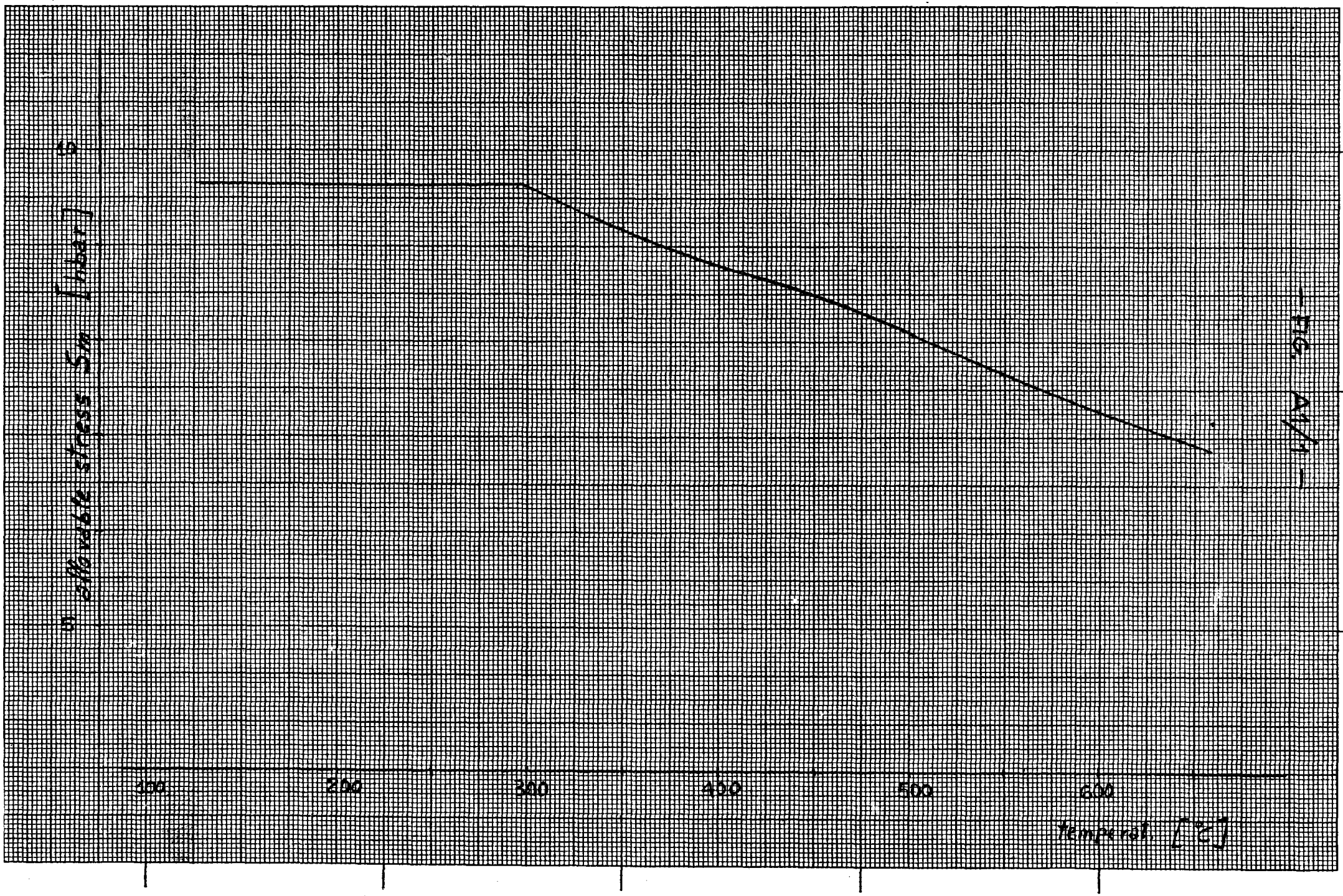
10
8
6
200
300
400
500
600
Temperat. [°C]

SANDVIK 3R60

ASTM type 316 L

Austenitic stainless ELC-steel

Sandvik · Sandviken · Sweden

SANDVIK
Tube

1,842 E

SANDVIK steel catalogue

FSI, September 1975
Cancels edition of September 1971
(1,8 E - 3R60)

SANDVIK 3R60 is a molybdenum-alloyed austenitic ELC-steel.

On request the material can also be supplied in a variant for the urea industry, Urea Grade, which has a guaranteed low ferrite content and meets the requirements in Huey-testing according to ASTM A262, practice C. This has been achieved by means of a well balanced chemical composition and an extremely low impurity content.

The steel is also delivered in a nitrogen-alloyed variant having higher strength, SANDVIK 3R69. See data sheet 1,846 E.

This data sheet gives information on mechanical properties, corrosion resistance and welding. For data on chipforming machining of SANDVIK 3R60 hollow bar, please refer to the data sheet 1,45 E - 3R60.

Chemical composition (nominal), %

C max	Si	Mn	P max	S max	Cr	Ni	Mo
0.030	0.6	1.7	0.030	0.030	17.5[a]	13.5[b]	2.7

[a] Cr = 17% for welded tube and pipe; [b] Ni = 13% for welded tube and pipe

Specifications

ASTM A213, A249, A269, A312, A511
BS 3605
DIN 17440, 2463, 2464

Type of steel

ASTM	AISI	DIN	W.-Nr.	BS	SIS
TP316L		X 2 CrNiMo 18 12	1.4435	316S14	2353
MT316L	316L		(1.4404)	316S22	

AFNOR Z 2 CND 17.13

Forms of supply, finishes and dimensions

Seamless tube and pipe

Tube and pipe are supplied in the quench-annealed and white-pickled or in the bright-annealed condition. The latter alternative applies as a rule to small sizes. The principal size range can be seen from Figure 1, but also certain other sizes can be delivered on request.

Hollow bar

These tubes are supplied quench-annealed and white-pickled in the size range 32—250 mm (1.3—9.8 inch) O.D.

Welded tube and pipe

Longitudinally welded and calibrated

Tube and pipe are delivered quench-annealed and white-pickled or bright-annealed. In the range above 10 mm (0.4 inch) I.D. tube and pipe can be supplied internally bead rolled. The principal size range can be seen from Figure 2, but also certain other sizes can be delivered on request.

Longitudinally welded and cold-drawn

The tubes are supplied quench-annealed and white-pickled or bright-annealed with maximum O.D. = 87 mm (3.4 inch).

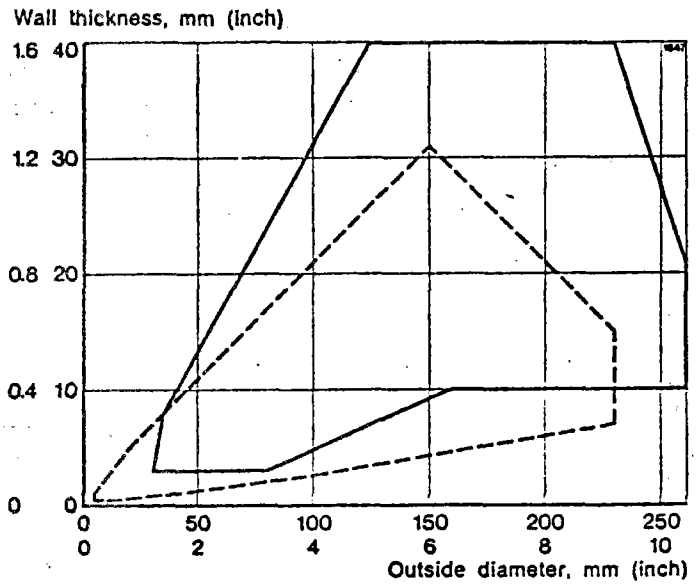

Figure 1 Size range for seamless tube and pipe
Solid line = hot-worked
Broken line = cold-worked

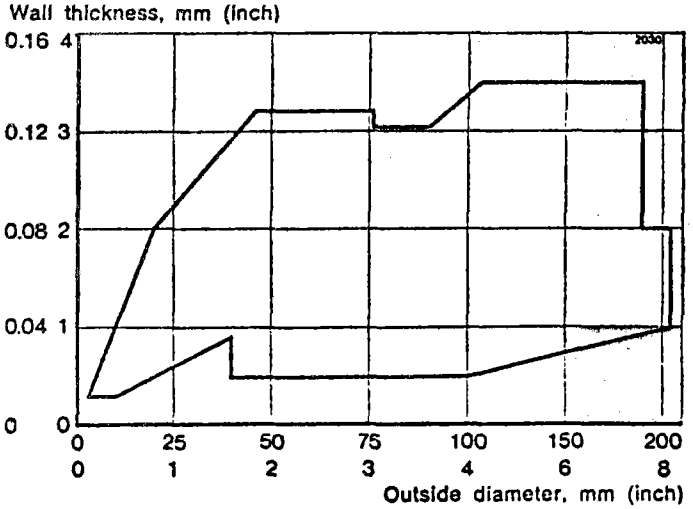

Figure 2 Size range for longitudinally welded, calibrated tube and pipe

Fabricated

Starting material is annealed and white-pickled sheet.

The size range of *tube* is:
outside diameter = 205—1200 mm (7.9—47 inch)
wall thickness = ≥2.5 mm (0.1 inch)

Pipe is made according to ANSI B36.10 and B36.19 in the following size range:
nominal pipe size = 3½"—24"
wall thickness = Schedule 5—Schedule 80

Spiral-welded

Starting material is annealed and white-pickled strip.

Size range:
outside diameter = 90—508 mm (3.5—20 inch)
wall thickness = 1.5—5 mm (0.06—0.2 inch)

Pipe fittings

Fittings are available in SANDVIK 3R60 comprising butt-weld fittings according to ISO and ANSI standards, as well as SANDVIK couplings.

Sizes in stock

Seamless tube and pipe

Seamless tube and pipe are stocked in a large number of sizes according to ISO R1127, ISO R65 medium series and ANSI B36.19. See our brochure 1,10 E.

Hollow bar

Hollow bar are stocked in a large number of sizes.

Longitudinally welded tube and pipe

Longitudinally welded tube and pipe are stocked in sizes according to ISO R1127. See our brochure 1,10 E.

Fabricated tube and pipe

These types are stocked in frequent sizes.

Pipe fittings

Sandvik's pipe fittings are stocked in a large number of sizes and finishes. See our brochures 1,13 E, 1,14 E and 1,15 E.

Mechanical properties

At 20°C (68°F)

Metric units

Yield strength 0.2% offset N/mm² min	Yield strength 0.2% offset kg/mm² min	Yield strength 1.0% offset N/mm² min	Yield strength 1.0% offset kg/mm² min	Tensile strength N/mm²	Tensile strength kg/mm²	Elong.[a] A5 % min	Hardness Vickers nom.
195	20	235	24	500–650	51–66	45	150

[a] A5 corresponds to $5.65\sqrt{S_0}$

The impact energy at —60°C is min 157 J, 16.0 kgm, and the transition temperature (transition from ductile to brittle fracture) is lower than —200°C.

English units

Yield strength 0.2% offset N/mm² min	Yield strength 0.2% offset ksi min	Yield strength 1.0% offset N/mm² min	Yield strength 1.0% offset ksi min	Tensile strength N/mm²	Tensile strength ksi	Elong.[a] A5 % min	Hardness Vickers nom.
195	28	235	34	500–650	73–94	45	150

The impact energy at —75°F is min 157 J, 116 ft-lb, and the transition temperature (transition from ductile to brittle fracture) is lower than —330°F.

At high temperatures

Temperature °C	Temperature °F	Yield strength 0.2% offset N/mm² min	Yield strength 0.2% offset kg/mm² min	Yield strength 0.2% offset ksi min	Yield strength 1.0% offset N/mm² min	Yield strength 1.0% offset kg/mm² min	Yield strength 1.0% offset ksi min
100	210	172	17.5	24.9	206	21.0	29.9
200	390	147	15.0	21.3	177	18.0	25.6
300	570	128	13.0	18.5	157	16.0	22.8
400	750	118	12.0	17.1	147	15.0	21.3
500	930	108	11.0	15.6	137	14.0	19.9
600	1110	98	10.0	14.2	128	13.0	18.5

Physical properties

Density 8.0 g/cm³, 0.29 lb/in³

Thermal conductivity

Temperature °C	Temperature °F	W/m · °C	kcal/m · h · °C	Btu/ft · h · °F
20	68	15	13	9
100	210	16	14	9.5
300	570	19	16	10.5
500	930	21	18	12
700	1290	23	20	13.5

Specific heat capacity, mean values

Temperature °C	Temperature °F	J/kg · °C	kcal/kg · °C	Btu/lb · °F
50—100	120—210	500	0.12	0.12
600—700	1110—1290	630	0.15	0.15

Thermal expansion, mean values (x10⁻⁶)

Temperature °C	Temperature °F	Per °C	Per °F
20—100	68—210	16.0	8.9
20—200	68—390	17.0	9.5
20—300	68—570	17.5	9.7
20—400	68—750	17.8	9.9
20—500	68—930	18.0	10.0
20—600	68—1110	18.2	10.1
20—700	68—1290	18.5	10.3

Modulus of elasticity

Temperature °C	Temperature °F	N/mm²	kg/mm²	ksi
20	68	200 000	20 000	28 500
400	750	170 000	17 000	24 000
600	1110	150 000	15 000	19 000

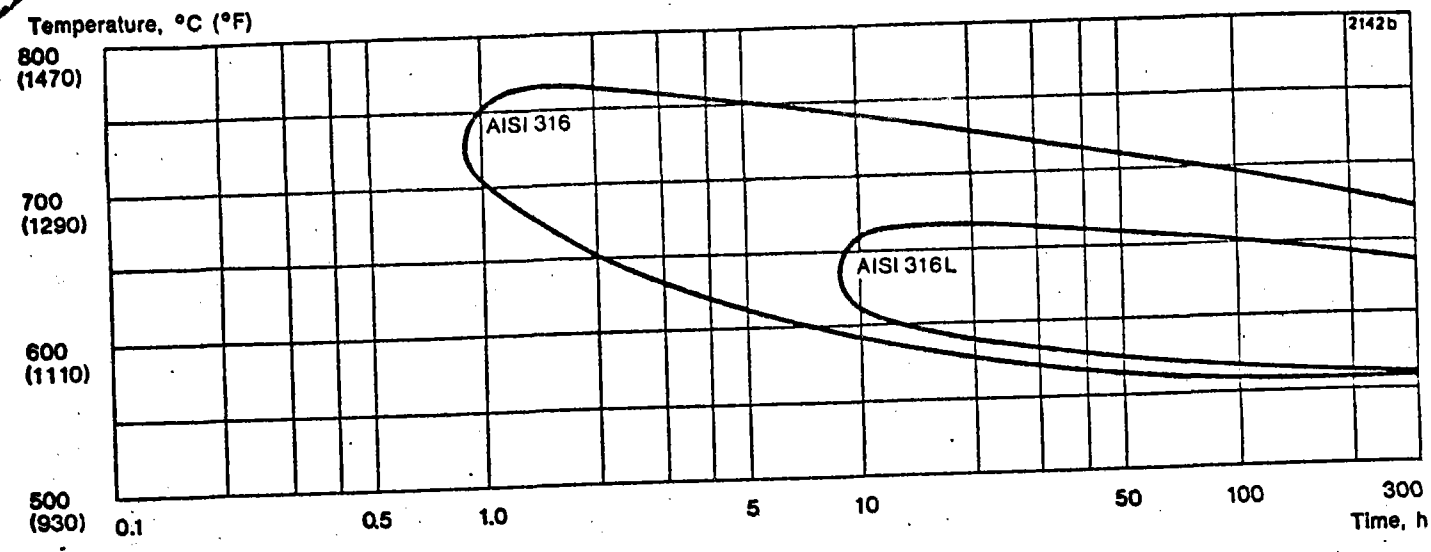

Figure 3 TTC-diagram for SANDVIK 3R60 (AISI 316L) and AISI 316.

Corrosion resistance

General corrosion

SANDVIK 3R60 has good resistance to

organic acids, e.g. citric, lactic, formic, tartaric and acetic acids, at high concentrations and temperatures

inorganic acids, e.g. boric, phosphoric, nitric and sulphurous acids, at moderate concentrations and temperatures. The steel can also be used in sulphuric acid at low temperature and concentrations below 10% or above 90%

salts, e.g. sulphates, sulphides and sulphites

solutions of carbamate in urea processes.

SANDVIK 3R60 is unsuitable for use in hydrochloric acid.

Pitting

Resistance to pitting improves with increasing molybdenum content and SANDVIK 3R60, containing about 2.7% of molybdenum, has substantially higher resistance to pitting than steels of the 18/8 type.

Intergranular corrosion

Thanks to its low carbon content SANDVIK 3R60 has better resistance to intergranular corrosion than steels of type AISI 316.

The TTC-diagram — Figure 3 — shows the results of corrosion testing for 24 hours in boiling Strauss-solution (12% sulphuric acid, 6% copper sulphate). As can be seen in the diagram the resistance to grain boundary attacks is much better for SANDVIK 3R60 than for a corresponding steel with higher carbon content (AISI 316). This is of course an advantage in complicated welding operations.

Stress corrosion cracking

Austenitic steels are susceptible to stress corrosion cracking. This may occur at temperatures above about 70°C (160°F), if the steel is subjected to tensile stresses and at the same time comes into contact with certain solutions, particularly those containing chlorides. Such service conditions should therefore be avoided. Also when plants are shut down the conditions must be considered, as the condensates which are then formed can develop a chloride content that leads to both stress corrosion cracking and pitting.

Mechanical stresses are set up e.g. in bending or welding. Therefore, the risk of stress corrosion cracking can be reduced by stress relieving bends and welds.

Where good resistance to stress corrosion cracking is required, the choice should be another stainless steel, e.g. a ferritic or a ferritic-austenitic steel or a material of high nickel content.

Heat treatment

Stress relieving

850—950°C (1560—1740°F), 10—15 minutes, cooling in air

Quench annealing

1000—1100°C (1830—2010°F), 5—20 minutes, rapid cooling in air or water.

Welding

The weldability of SANDVIK 3R60 is good. Suitable fusion-welding methods are manual metal-arc welding with coated electrodes or gas-shielded arc welding, with the TIG and MIG methods as first choice. No preheating is required in normal cases, and as a rule post-weld heat treatment is not necessary.

Since the material has low thermal conductivity and high thermal expansion, welding must be carried out with a low heat input and with welding plans well thought out in advance, so that the deformation of the welded joint can be kept under control. If, despite these precautions, it is foreseen that the residual stresses might impair the functioning of the structure, we recommend that the entire structure be stress-relieved.

As filler material for gas-shielded arc welding we recommend wire of SANDVIK grades 2R61 (AWS ER 316L), 3RS63 (AWS ER 316L Si) or, when a ferrite-free weld metal is desired, SANDVIK 3RS69 (AWS ER 316L Si). In manual metal-arc welding we recommend coated electrodes of type ESAB OK 63.30, SMIT Arosta 316L, PHILIPS RS 316 or OERLIKON Inox BWL. In the urea industry filler metal of the type 19Cr/15Ni/MnMo, e.g. SANDVIK 3RM69, is often used for welds in contact with the process solution.

Bending

Annealing after cold bending is not normally necessary, but this point must be decided with regard to the degree of bending and the operating conditions. Heat treatment, if any, should take the form of stress relieving or quench annealing, see those headings.

Hot bending is carried out at 1100—850°C (2010—1560°F) and should be followed by quench annealing.

ANNEX 2

The annex hereafter consists of a part of the SANDVIK document No. K0605/3.

Date		Reg. No. / Page
1977-11-21		Page 1/4
Prepared by: TRH/Andersson	DOSSIER DE CARACTERISATION	Spec. No.: Rev. 4
Approved by: TR/Gullberg		Supersedes: 1977-10-19

TOSI COMMANDE 77/383

TUBES SANS SOUDURE SANDVIK 3R60 (TYPE 316L)

SANDVIK COMMANDE: 345-47566, 47567

DOCUMENTATION NO: K 0605/3

1.5 Structure micrographique

- grosseur du grain: 3-7 avec la possibilité de fournir tubes avec grosseur du grain 8.

2. CARACTERISTIQUES MECANIQUES

Les caractéristiques mécaniques pour SANDVIK 3R60 à la température ambiante (20°C) sont indiquées dans paragraphe 2.1 et pour températures élevées dans paragraphe 2.2.

Toutes les valeurs représentent des valeurs minimales que nous pouvons garantir.

2.1 $R \geqslant 490$ MPa
E 0,2% $\geqslant 172$ MPa
A5 $\geqslant 40$ %

2.2 Les valeurs minimales aux températures élevées que nous pouvons garantir sont indiquées en fig. 1 - limite élastique et en fig. 2 - résistance à la traction. Interpolation entre 500 et 600°C donne les valeurs minimales suivantes à 550°C

$R \geqslant 378$ MPa
E 0,2% $\geqslant$ 85 MPa

2.3 Fluage

4 coulées différantes de SANDVIK 3R60 ont été soumises à des essais de fluage à 550°C, 600°C et 700°C.

Fig. 3 indique les contraintes conduisant à la rupture. A la température de 550°C une extrapolation jusqu'à 100.000 heures donne la valeur 165 MPa pour la contrainte moyenne conduisant à la rupture.

Fig. 4 indique les contraintes donnant 1 % d'élongation en t heures pour température T. Les valeurs représentent des valeurs moyennes.

3. TENUE A LA CORROSION VIS A VIS DU FLUIDE

La tenue à la corrosion vis à vis du sodium en contact à 550°C est très bonne.

Références: - Faisceau tubulaire des échangeurs intermédiaires de Phénix.

- G.A. WHITLOW, J.C. CWYNAR, S.L. SCHROCK - "Sodium corrosion behavior of alloys for fast reactor application" - Proceedings Symp, Detroit, Michigan, Oct 19-20, 1971

- E. BERKEY, G.A. WHITLOW - "Microstructural and compositional changes in sodium exposed stainless steel by scanning electron microscopy"-id-

- P.A. BACUE, L.J. CHAMPEIX, E.T. HONNORAT - "Compositionnal changes in austenitic steels after corrosion in sodium at 700°C" -id-

- A. LAFON - "Compatibilité d'aciers austenitiques avec le sodium dynamique à 700°C" - "Quelques aspects métallurgiques" - R. STRS 029 - Fév. 73 -

4. SOUDAGE

Le SANDVIK 3R60 a une bonne soudabilité. Pour tubes avec une épaisseur de paroi de 1 mm on recommande soudage automatique ou manuel selon la méthode TIG. Comme métal d'apport on recommande du fil en SANDVIK 2R61 (AWS ER 316L), 3RS63 (AWS ER 316L Si) ou quand le métal déposé ne doit pas contenir de ferrite, 3RS69 (AWS ER 316L Si).

Fig. 1

Limite élastique

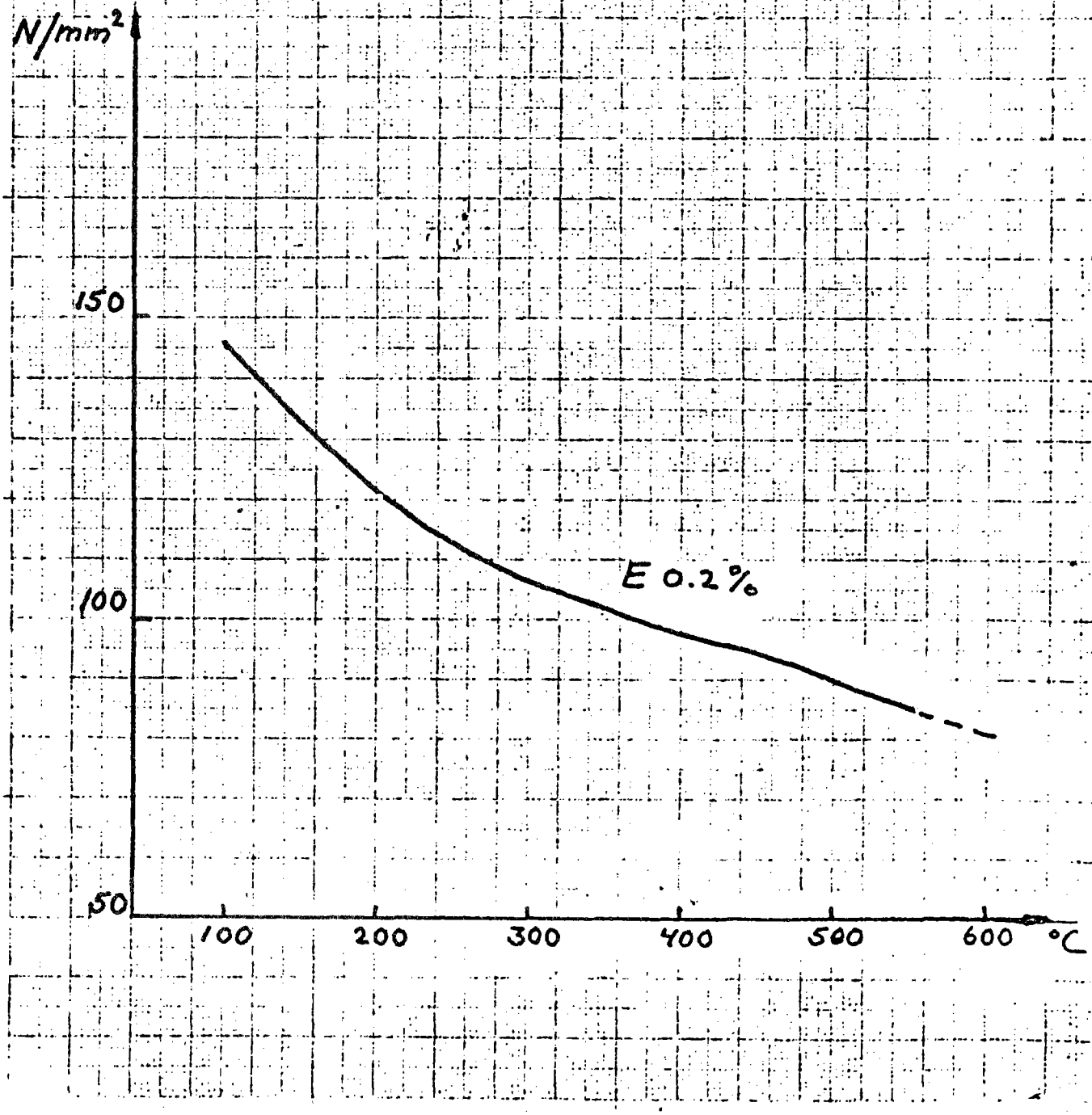

Fig. 2

SANDVIK 3R60

Résistance à la traction

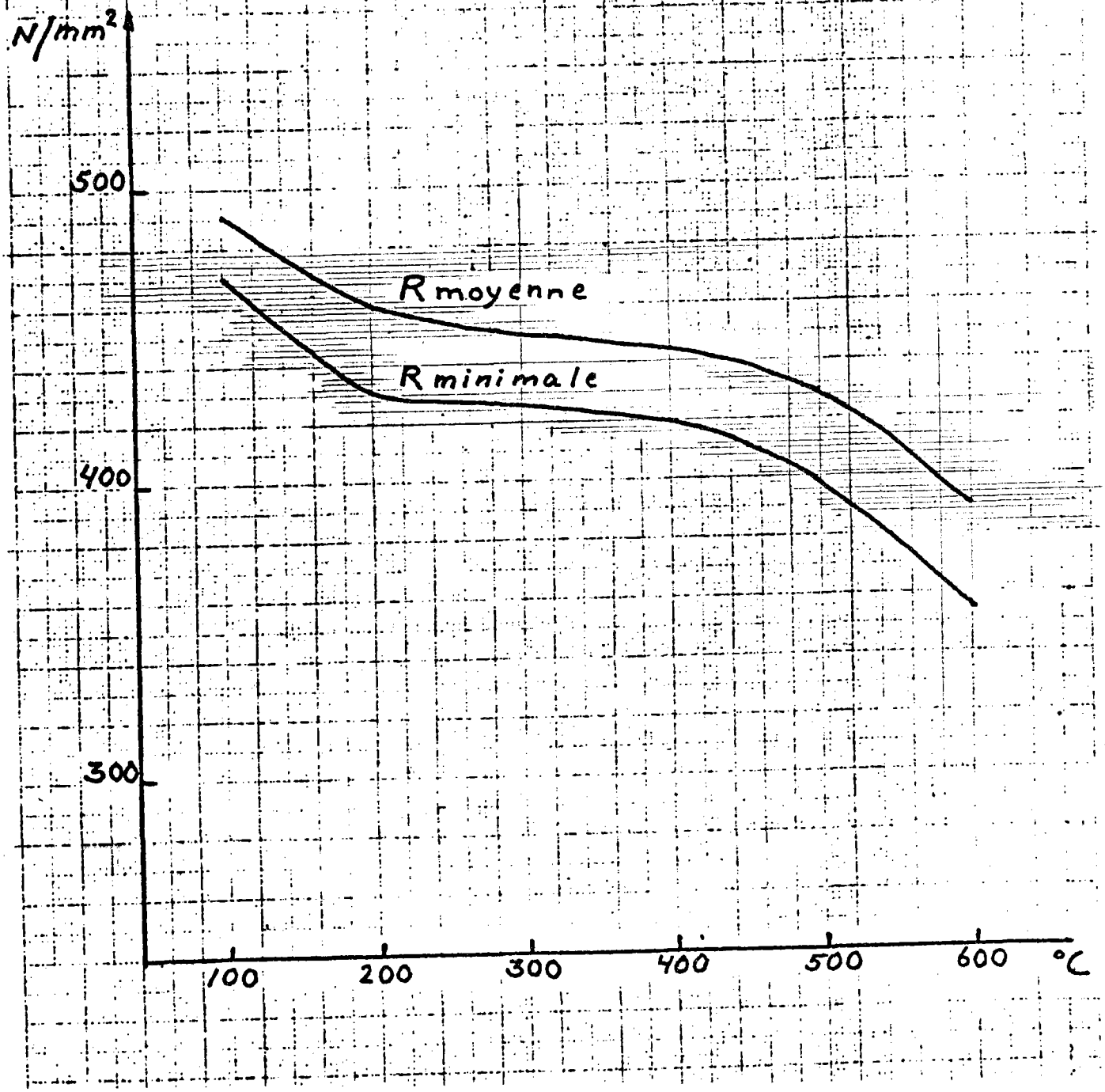

SANDVIK 3R60

Contraintes conduisant à la rupture

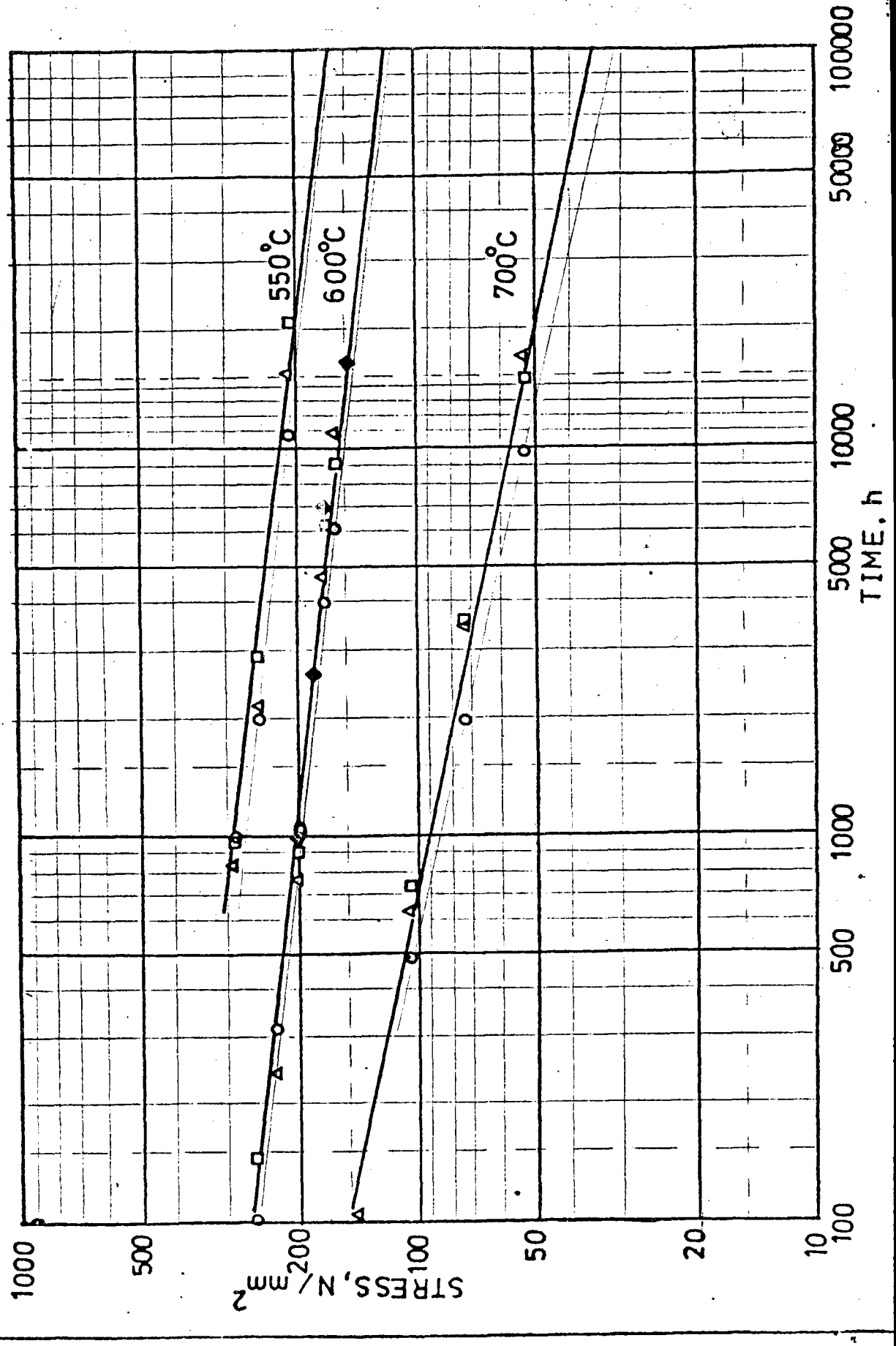

Fig. 4

SANDVIK 3R60

Contraintes donnant 1 % d'élongation
en t heures pour température T.

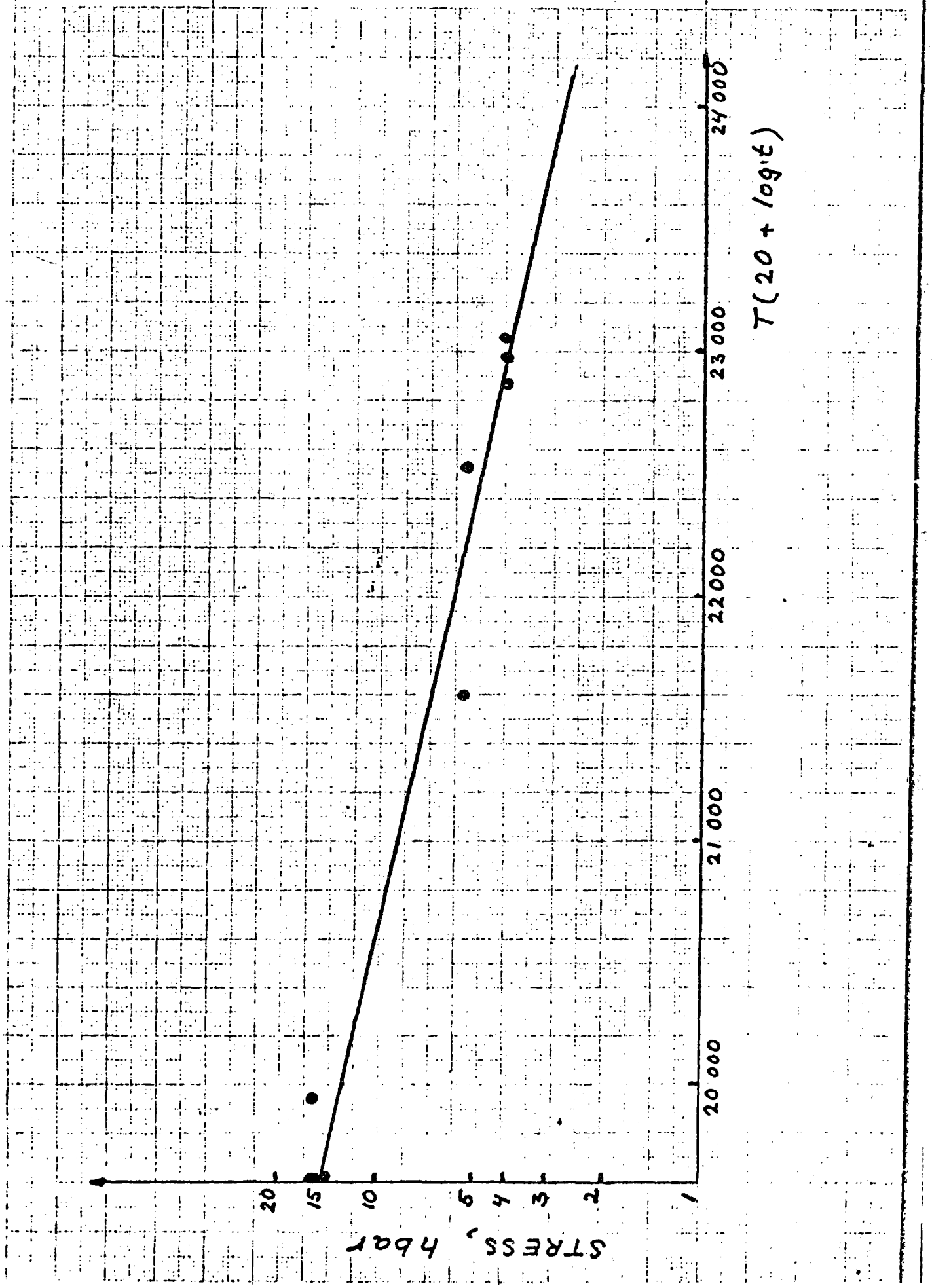

IEA ALMERIA PROJECT

ADVANCED SODIUM RECEIVER

ASR

TOPIC REPORT N. 4

REVISION 0

JUNE 1981

Prepared by ENEL

FRANCO TOSI

SNAM PROGETTI

INDEX

FOREWORD

1. DYNAMIC MODEL
2. FRICTION LOSSES AND FLOW RATE COMPUTATION
3. THERMAL FIELD COMPUTATION IN CASE OF SUDDEN FLUX INCREASE
4. PRELIMINARY STUDIES FOR CONTROL SYSTEM DESIGN
5. TRANSFER FUNCTION COMPUTATION
   - 5.1. FIRST METHOD (LINEARIZATION)
   - 5.2. SECOND METHOD (IDENTIFICATION)
6. CONCLUDING REMARKS
7. NOMENCLATURE

Foreword

This report concerns the work about ASR dynamic analysis and control performed from february to may 1981.
With reference to the situation described in ASR report n. 6 (Dec. 1980), the following developments have been made:

- The receiver model has been completed: a more accurate calculation of the friction losses and the equations for the feed pump with its associated driving motor have been included.
- The transfer functions needed for control system design have been obtained; they relate the temperature variations at the outlet of each radiated panel with pump speed.
- A preliminary study has begun with the aim of making a choice among different possible control strategies. Regulator parameters have been computed for many possible receiver operating conditions and simulations are being done to check the behaviour of the controlled system.

1. Dynamic model

Hereafter a brief summary is reported of model characteristics, which were described with more detail in report n. 6 (Dec. 1980).
The model consists of the following subsystems (see fig. 1):

- Radiated pipes (one average pipe for each of the five panels)
- Connecting pipes among the five panels
- Inlet and outlet headers
- Riser and downcomer tubes
- Receiver feed pump
- Driving motor
- Regulators.

The basic assumptions have been the following:

- The incident heat flux in every section of the radiated tubes is supposed as circumferentially uniform, equal to the average value of the actual circumferential flux distribution. Owing to this assumption, only the average metal temperature in every section is computed. The exact radial and circumferential temperature distribution can be computed by other codes which make use of the real incident flux and of the sodium temperature computed by means of the present model.
  The flux map used in nominal conditions is reported in fig. 2.
- Sodium properties are considered as temperature functions and vary with time and tube spatial coordinate.
- Sodium flow rate is considered only as a time function (uncompressible flow) and, at every instant, is the same in every radiated pipe (total flow divided by the number of tubes in each panel).
- For what concerns the thermal field computation, radiated pipes and connecting pipes have been considered as distributed parameter, one dimensional systems. Headers have been considered as a single lump in which a perfect mixing is assumed. The thermal behaviour of the riser tube has not been taken into account because it is considered that temperature variations of the sodium in the riser represent only a low frequency disturb for the receiver.

Hereafter the last developments performed are reported.

2. Friction losses and flow rate computation

For flow rate computation, the following relationships have been used:

1) $$\frac{dw}{dt} \sum_i \frac{r_i L_i}{A_i} = \Delta p + g \sum_i \rho_i L_i - \Delta p_a$$

2) $$\Delta p = \left(\frac{\Omega}{\Omega_n}\right)^2 \Delta p_n - \left(K_{p1} w + K_{p2} w^2\right)$$

3) $$\frac{1}{2} J \frac{\partial \Omega^2}{\partial t} = Mm\,\Omega - \frac{W \Delta p}{\rho \eta}$$

4) $$Mm = \frac{k_{M1} V - \Omega}{k_{M2}}$$

Equations 3) and 4) and the numerical values of the associated constants are the same used by INTERATOM for the simulation of the first receiver loop.

For the computation of friction losses Δp_a we have:

$$\Delta p_a = \Delta p_{irr} + \Delta p_{ce} + \Delta p_{cr} + \Delta p_{rd}$$

with

$$\Delta p_{irr} = \frac{f_{irr} L}{2D} \frac{1}{S^2} W^2 \sum_i \frac{L_i}{\rho_i}$$

$$\Delta p_{ce} = \frac{f_{ce}}{2 D_{ce}} \frac{1}{S_{ic}^2} W^2 \sum_i \frac{L_i}{\rho_i}$$

$$\Delta p_{cr} = \frac{3}{2} \sum_i \rho_i \frac{1}{S_{irr}^2} \left(\frac{W}{n}\right)^2 \frac{1}{\rho_i}$$

$$\Delta p_{rd} = k_{rd}\, W^2$$

Coefficients f_{irr} and f_{ce} depend on the tube relative roughness and Reynolds number.

Pressure drops Δp_{rd} in risers and downcomer tubes have been computed from data reported in INTERATOM CRS Document 2105.1.

A diagram of total friction losses as a function of sodium flow rate is shown in fig. 3.

From Fig. 3 it can be seen that friction losses can be considered as a parabolic function of the sodium flow rate

$$\Delta p_a = a W + b W^2$$

3. Thermal field computation in case of a sudden flux increase

This situation occurs when clouds which cover the sun suddenly disappear. In this case it is convenient to obtain the maximum allowable power from the receiver without causing too fast temperature increases which could give rise to unbearable stresses.

Since the speed of flux increase depends not only on cloud speed but also on helidstats control strategy it may be interesting to calculate the thermal field on the receiver for different values of the flux speed. This will serve as a basis for thermal stress computation in the most critical points of the receiver.

The results of the simulation are shown in figures 4 + 12.

The flux is supposed to increase from zero to its maximum (nominal) value linearly in 10 seconds (fig.s 4÷6), 20 seconds (fig.s 7÷9) and 30 seconds (with the same ratio in every point of the receiver)(fig.s 10÷12).

The initial temperature in the whole receiver has been suppoed to be equal to the sodium inlet temperature (270°C) owing to the absence of flux.

The sodium flow rate has been supposed to vary from 10% (technical minimum) to its maximum value with an average speed related to the heat flux speed. This has been obtained by using the measure of flux as a feedforward action (PD) to drive the pump motor.

The maximum temperature gradients have been found to be near the outlet of each panel; in fig.s 4, 7, 10 are shown the temperatures at the outlet of the 5th panel for the three assumed flux increase speeds; in fig.s 5, 8, 11 and 6, 9, 12, the sodium flow rate and flux increase are shown, respectively.

The simulations give a preliminary information about the transient behaviour of the temperatures; it seems desirable, however, to take into account the effect of the shape of the flux map, which may vary during the transient.

The thermal stress computations will be made on the basis of these new simulations.

4. Preliminary studies for control system design

The main design goals for receiver control system are:

- during start-up, to reach as soon as possible the desired operating conditions (maximum allowable power), while keeping temperature gradients not too high;
- during steady state (or quasi steady state), to compensate the disturbancies due to cloud passages, to keep temperature variations at receiver outlet as low as possible.

The control system must be fast and stable from technical minimum to maximum load; to improve system performances it may be convenient to use temperature measurements not only at the outlet but also in intermediate points of the receiver and a feedforward signal bound to heat flux measure.
The first step necessary for control system design is to evaluate the transfer functions between the temperatures and the control variable (pump driving motor voltage).
This has been done as described below.

5. Transfer function computation

The computation has been done following two different kinds of approach; this has allowed to accurately verify the obtained results.
The first method is based on linearization of system equations about fixed equilibrium points (which may vary from 10% to 100% of receiver power). The second method is based on the identification of model responses: starting from a steady state condition, a step variation is given to the control variable (pump motor voltage) and the time responses of the selected sodium temperatures are recorded; a suitable L-transform is then assumed for these responses and, by a numerical code based on the Fletcher and Powell algorithm, the values of poles, zeros and pure lags are computed which minimize the difference between the time behaviour of the assumed fun-

tions and that of the temperatures given by the model. The fitting is very good, if the form of the L-transform has been properly chosen.

5.1. First method (Linearization)

For the radiated tubes, the energy equations have been written in the following way:

5) $$c_m A_m \rho_m \frac{\partial T_m(x,t)}{\partial t} = Q_{irr}(x,t) - \gamma w \left[T_m(x,t) - T(x,t)\right]$$

6) $$c A \rho \frac{\partial T(x,t)}{\partial t} + c w \frac{\partial T(x,t)}{\partial x} = \gamma w \left[T_m(x,t) - T(x,t)\right]$$

with $$\gamma = \left[5 + 0.025 (Re\, Pr)^{0.8}\right] \frac{\lambda}{D}$$

In 5) and 6) the sodium specific heat c, density ρ and heat transfer coefficient γ are temperature functions and vary with time and space; the same is true for the absorbed power $Q_{irr}(x,t)$. Writing equations 5) and 6) for a short pipe segment of lenght ℓ, the parameters c, ρ, γ and the input $Q_{irr}(x,t)$ can be assumed as constant along the segment. Linearizing 5) and 6) about an equilibrium point we obtain:

5') $$c_m A_m \rho_m \frac{\partial}{\partial t} \Delta T_m(x,t) = \Delta Q_{irr}(x,t) - \gamma w \left[\Delta T_m(x,t) - \Delta T(x,t)\right.$$

6') $$c A \rho \frac{\partial}{\partial t} \Delta T(x,t) + c w \frac{\partial}{\partial x} \Delta T(x,t) + c \frac{\partial T}{\partial x} \Delta w =$$
$$= \gamma w \left[\Delta T_m(x,t) - \Delta T(x,t)\right]$$

where

$$\Delta T_m(x,t) \triangleq T_m(x,t) - T_m(x,0)$$

$$\Delta T(x,t) \triangleq T(x,t) - T(x,0)$$

$$\Delta Q_{irr}(x,t) \triangleq Q_{irr}(x,t) - Q_{irr}(x,0)$$

L-transforming 5') and 6') and solving the resulting space equation, we obtain:

$$7)\quad \frac{\Delta T(\ell,s)}{\Delta W} = \frac{\ell}{\bar{W}} \frac{\bar{Q}_{irr}}{c\bar{W}} \frac{1}{s\tau\left(1+\frac{\tau_m/\tau_a}{1+s\tau_m}\right)} \left[1 - e^{-\tau\left(1+\frac{\tau_m/\tau_a}{1+s\tau_m}\right)s}\right]$$

$$8)\quad \frac{\Delta T(\ell,s)}{\Delta T(0,s)} = e^{-\tau\left(1+\frac{\tau_m/\tau_a}{1+s\tau_m}\right)s}$$

where $$\tau = \frac{A\rho\ell}{\bar{W}}$$

$$\tau_m = \frac{c_m A_m \rho_m}{\gamma w} \quad ; \quad \tau_a = \frac{cA\rho}{\gamma w}$$

and the overlined variables refer to steady state values.

The transfer function between the sodium flow rate and the temperature at a panel outlet can be obtained dividing the tube in a suitable number of nodes (fig. 13).

For the node i we have:

$$\Delta T(x_i,s) = -\frac{\ell}{\bar{W}} \frac{Q_{irr_i}}{c_i W} \frac{1}{s\tau_i\left(1+\frac{\tau_m/\tau_a}{1+s\tau_m}\right)} \left[1 - e^{-\tau_i\left(1+\frac{\tau_m/\tau_a}{1+s\tau_m}\right)s}\right] \Delta$$

$$10)\quad + \Delta T(x_{i-1},s)\, e^{-\tau_i\left(1+\frac{\tau_m/\tau_{a_i}}{1+s\tau_m}\right)s}$$

Thus, $\Delta T(L,s)$ can be computed in a recursive way if $\Delta T(x_0,s)$ is known.

For every radiated tube, $\Delta T(x_0,s)$ represents the temperature at the outlet of its inlet header. The headers have been considered as a single lump, for which the following relations have been used:

$$11)\quad M_m c_m \dot{T}_{mc} = -\gamma_c S_i (T_{mc} - T_{uc})$$

$$12)\quad c\rho V_c \dot{T}_u = \gamma_c S_i (T_{mc} - T_{uc}) + W(h_{ic} - h_{uc})$$

Linearizing 11) and 12 we have:

11') $$\Delta \dot{T}_{mc} = \frac{-\gamma_c S_i}{M_m C_m} (\Delta T_{mc} - \Delta T_{uc})$$

12') $$\Delta \dot{T}_u = \frac{\gamma_c S_i}{c \rho V_c} (\Delta T_{mc} - \Delta T_{uc}) + \frac{\bar{W}}{\rho V_c} (\Delta T_{ic} - \Delta T_{uc}) + \frac{1}{\rho V_c} (\bar{T}_{ic} - \bar{T}_{uc}) \Delta W$$

Since $T_{ic} - T_{uc}$ is zero at steady state, the last term in 12') is zero and the header outlet temperature can vary only if the inlet temperature ΔT_i varies. Laplace transforming 11') and 12') we obtain:

13) $$\frac{\Delta T_{uc}}{\Delta T_{ic}} = \frac{1 + s\tau_1}{\tau_1 \tau_3 s^2 + \frac{\tau_1\tau_2 + \tau_1\tau_3 + \tau_2\tau_3}{\tau_2} s + 1}$$

with

$$\tau_1 = \frac{M_m C_m}{\gamma_c S_i} \; ; \; \tau_2 = \frac{c \rho V_c}{\gamma_c S_i} \; ; \; \tau_3 = \frac{\rho V}{\bar{W}}$$

For the connecting pipes among the radiated panels equations 5), 6), 7) and 8) still hold, with the incident heat flux set to zero.
As for the headers, also in this case the outlet temperature varies only for variation of the inlet temperature of the tube.
Since at steady state the temperature and the sodium properties are uniform along the tube, it is not necessary to divide the tube into nodes and the transfer function between inlet and outlet temperature is given by eq. 7), in which represents now the total lenght of the considered tube.
Taking into account the cascade connection of these elements in the receiver, the global transfer function between receiver outlet temperature and sodium flow rate has been computed with a recursive procedure; it is worth noticing that in this way it is possible to compute the transfer function between any selected temperature and the sodium flow rate, by simply stopping the procedure at the desired point.

Since the control variable is not sodium flow rate but pump driving motor voltage, the transfer function $\Delta W/\Delta V$ has been computed too, by linearizing eq.s 1), 2), 3), 4).

A block diagram which graphically represents the frequency domain behaviour of the receiver is shown in fig. 14. Here, the inlet temperature of the receiver has been considered constant and so the main variable affecting receiver temperatures are the absorbed heat flux per unit lenght Q_{inc} and the pump motor voltage V .

G_{TWV} represents the transfer function between sodium flow rate and pump driving motor voltage; it is of the type:

$$G_{WV}(s) = \frac{\mu_{WV}}{(1+s\tau_{p1})(1+s\tau_{p2})}$$

(τ_{p1} = 0.88 sec, τ_{p2} = 0,166 sec at maximum load).

$G_{TW1}, G_{TW2}, G_{TW3}, G_{TW4}, G_{TW5}$ are the high frequency components of the transfer functions between the temperatures T1, T2, T3, T4, T5 (at the outlet of panels 1, 2, 3, 4, 5) and sodium flow rate. These five functions are very similar among them, the only differences being due to fluid phisical properties variation along the receiver and to the shape of thermal flux map on each panel.

The static gains of the five functions, which are proportional to the thermal power absorbed by each panel, are (at maximum load):

$\mu_{TW1} \cong \mu_{TW2} \cong 1.5$ [°C/kg/s]

$\mu_{TW3} \cong \mu_{TW4} \cong 10$ [°C/kg/s]

$\mu_{TW5} \cong 12.1$ [°C/kg/s]

$G_{TQ1}, G_{TQ2}, G_{TQ3}, G_{TQ4}, G_{TQ5}$ are the high frequency components of the transfer functions between the temperatures at the outlet of the five panels and the absorbed thermal power per unit lenght. These five functions are very similar to the other group of functions $G_{TW1}, G_{TW2}, G_{TW3}, G_{TW4}, G_{TW5}$ and their static gains are proportional to $\mu_{TW1}, \mu_{TW2}, \mu_{TW3}, \mu_{TW4}, \mu_{TW5}$ respectively.

GT21, GT32, GT43, GT54 are the transfer functions between the outlet temperature of a panel and that of the preceding one. They essentially describe the mass transport phenomena across the connecting tubes, the headers and radiated tube. More precisely, the pure lag is much higher than the transport delay (mass divided by flow rate) because of the presence of the metal and of the high heat transfer coefficient between sodium and metal. For example, in a radiated tube one has $\tau_{al} = 2.7\,\tau_{del}$, where τ_{al} is the true lag and τ_{del} the lag due to transport.

The whole computation has been done by a numerical program, developed for this purpose, which gives modulus and phase of the required functions in a selectable frequency range.

In figures 15, 16, 17, 18, 19, are shown the modulus and phase diagrams for the temperature at the outlet of panel 5, 4, 3, 2, 1, respectively.

5.2) Second method (Identification)

In Fig. 20 is shown the time response (obtained from the digital model) in a selected point of the receiver (outlet of panel 4) to a step input (negative) variation of the control variable. Before this perturbation the receiver was at steady state, full load (100%). This curve can be considered as the sum of two responses: the first (fig. 21) is delayed with respect to the step of about 2 sec and has then a very fast rise followed by a flat zone. It represents only the effect of the initial unbalancing between sodium flow rate and heat flux on panel 4 (no temperature variation at inlet of panel has still occurred).

The second response (fig. 22) is delayed of about 16 sec with respect to the step and has a slower rise; it represents the temperature wave coming from panels 1 , 2 , 3 .

It has been assumed that response of fig. 21 can be approximated by a third order system plus a pure lag, and response of fig. 22 with a second order system plus another (larger) pure lag.

The automatic identification code, starting from initial tentatively chosen values for the eigenvalues and the pure lags of the two systems, computes the final values of these parameters which give the best fitting between the model response and the response of the assumed simplified systems. The differences found are negligible.

In the example shown, the required transfer function found is the following:

$$\frac{\Delta T_u(s)}{\Delta V(s)} = \left[-\frac{0.306}{s+0.812} + \frac{1.364}{(s+0.812)^2} - \frac{0.155}{(s+0.812)^3}\right] e^{-2.6s} + \left[\frac{0.113}{s+0.174} + \frac{0.056}{s+0.04}\right] e^{-13.7s}$$

In fig. 23) are shown the Bode diagrams (modulus and phase) of the function computed in this way; with reference to the diagrams of fig. 16, the differences are negligible, and this fact represents a good check for the digital simulation program. The same kind of computation has been performed for other operating conditions of the receiver . In fig. 24 and 25 are shown, for an example, the Bode diagrams for the receiver outlet temperature, obtained analitically with reference to operating points of 10% and 50%.

6) Concluding remarks

The work done till now is the basis on which the synthesis of the temperature regulator is being carried out.

From the Bode diagrams shown, quantitative information about the frequency domain behaviour of the receiver and about the required characteristics of the control system can be drawn. Thus, for instance, since the frequency band of the transfer functions becomes narrower at low loads, it seems necessary to use regulators with load varying parameters, in order to better match the load-varying receiver response; this will be done by means of the heat flux measure, which will be used to vary regulator gains according to a single function which has been computed on the basis of receiver frequency responses at various operating points. In order to avoid unstabilities, a precise measure at the heat flux is needed.

Symbols list

x = Tube spatial coordinate

t = Time

c_m = Specific heat capacity of metal

c = Specific heat capacity of sodium

A_m = Tube metal cross section

A = Sodium flow cross section

ρ_m = Metal density

ρ = Sodium density

ω = Tube inner perimeter

γ = Metal to sodium heat transfer coefficient

Q_{in} = Absorbed power per unit lenght

T_m = Metal average temperature

T = Sodium temperature

λ = Sodium conductivity

D = Tube internal diameter

W = Sodium flow rate

M_m = Mass of header metal

S_i = Internal header surface

T_{mc} = Metal temperature of the header

T_{uc} = Sodium outlet temperature of the header

V_c = Header inner volume

h_{ic} = Sodium inlet enthalpy

h_{uc} = Sodium outlet enthalpy

Δp = Pump head

η = Pump efficiency

g = Gravity acceleration

L_i = i-th tube lenght

Δp_a = Total pressure drop due to friction

Ω = Angular velocity of the pump

Ω_n = Nominal angular velocity of the pump

Δp_{irr} = Pressure drop due to friction in radiated tubes

Δp_{cl} = Pressure drop due to friction in connecting tubes

Δp_{cT} = Pressure drop in the headers

$\Delta p_{s,d}$ = Pressure drop due to friction in downcomer and riser tubes

η_i = Ratio between sodium flow rate in a radiated tube and total sodium flow rate

M_m = Motor torque

K_{m1}, K_{m2} = Motor constants

V = Motor voltage

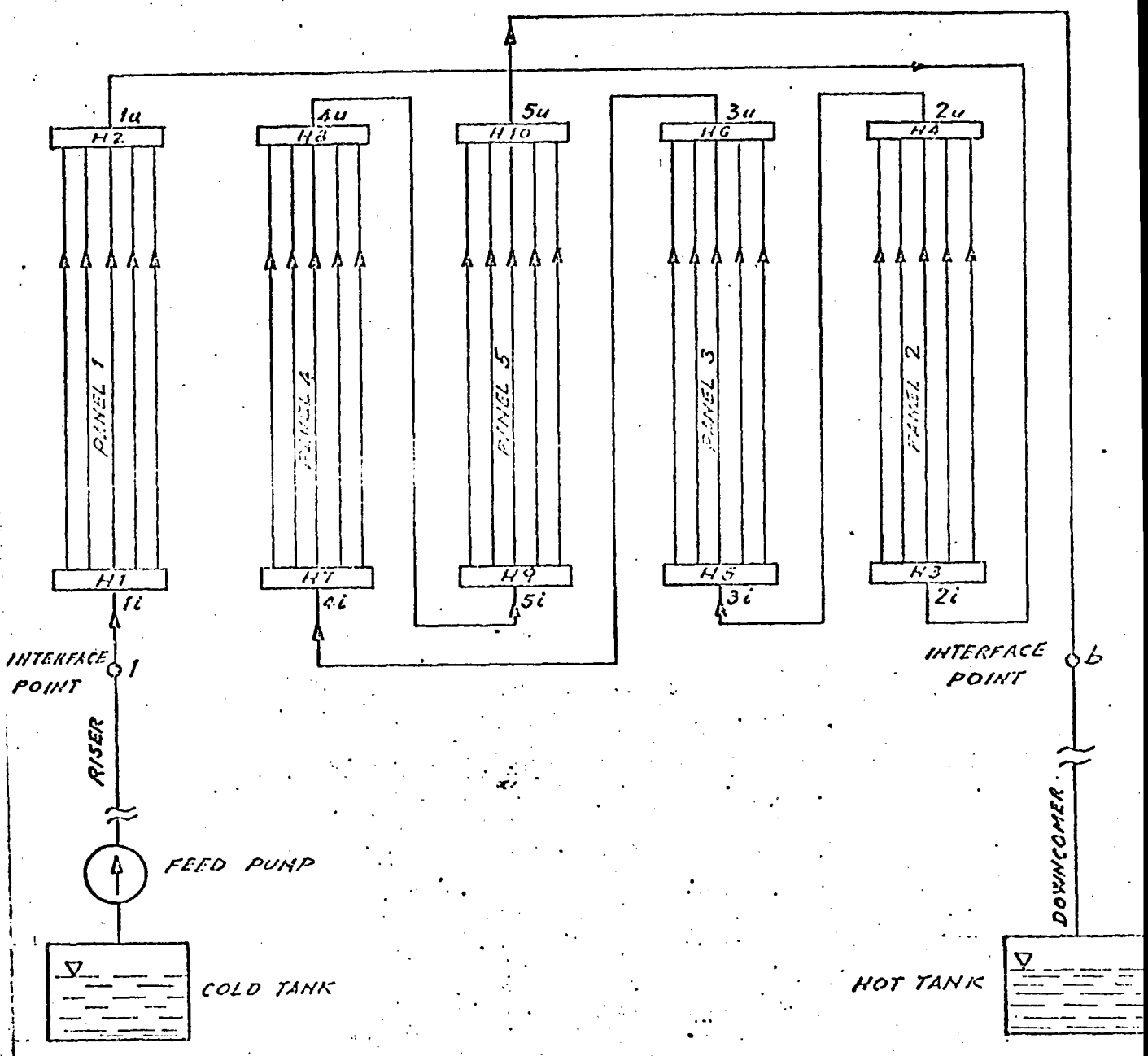

Fig. 1 TRANSIENT MODEL SCHEMATIC

ALMERIA ,93HLS., DAY 81, H 12, S.D.2,6MR., TN

	.00	.10	.30	.50	1.00	1.10	1.00	.50	.30	.10	.00	
	.10	.50	1.30	2.70	4.20	5.00	4.20	2.70	1.30	.50	.10	
	.40	1.40	4.10	9.20	15.5	19.4	15.5	9.20	4.10	1.40	.40	
	.80	3.30	10.2	24.2	41.6	50.0	41.6	24.2	10.2	3.30	.80	
	1.50	6.90	22.2	49.7	80.1	93.5	80.0	49.7	22.2	6.90	1.60	
EAST	2.30	13.5	47.2	91.7	118.	124.	118.	91.3	46.9	13.6	2.50	WEST
	2.60	19.1	71.6	126.	131.	118.	130.	125.	70.8	19.2	2.90	
	2.20	15.8	57.9	96.7	91.0	75.1	90.1	96.0	57.2	15.9	2.40	
	1.20	6.90	22.0	35.5	34.2	29.3	33.9	35.3	21.9	7.00	1.30	
	.40	1.60	3.90	6.20	7.10	7.10	7.10	6.30	4.00	1.70	.50	
	.00	.20	.50	.80	1.20	1.30	1.20	.80	.50	.20	.10	

BOTTOM

HEL.N.	93	AIM. N	3,
INSOL. KW/M2	0.92	STD.DEV. MRAD	2.6
DAY N.	81,	INC.POW. MW	2.77
TIME H.	12,	AVERG./PEAK	0.25
TOWER M	43,	SPILLAGE %	0.62
TARGET M	3,3,		

FIG.2 INCIDENT FLUX ON FLAT TARGET (W/CM2)

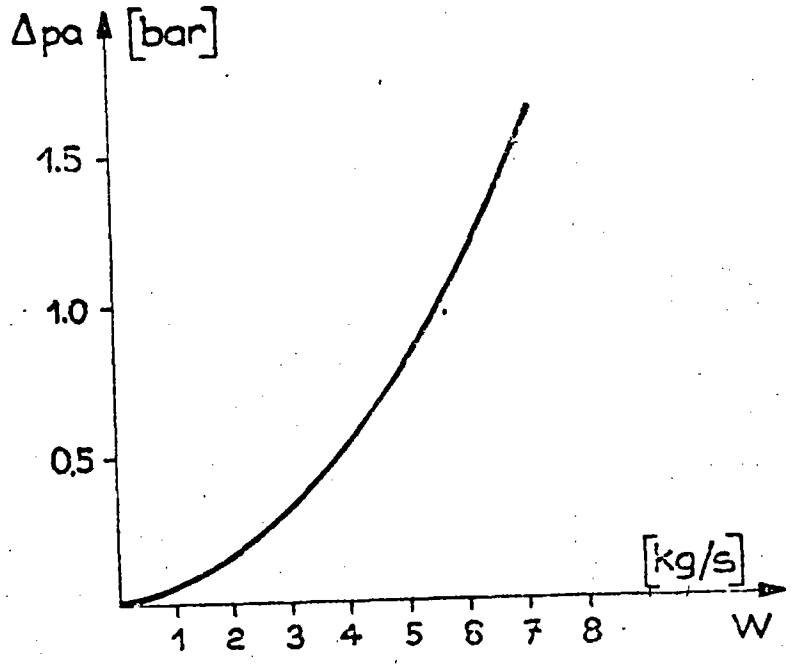

Fig. 3- FRICTION LOSSES

FIG. 4 – Panel 5 sodium outlet temperature.

Flux ramp lenght 10 S (°C).

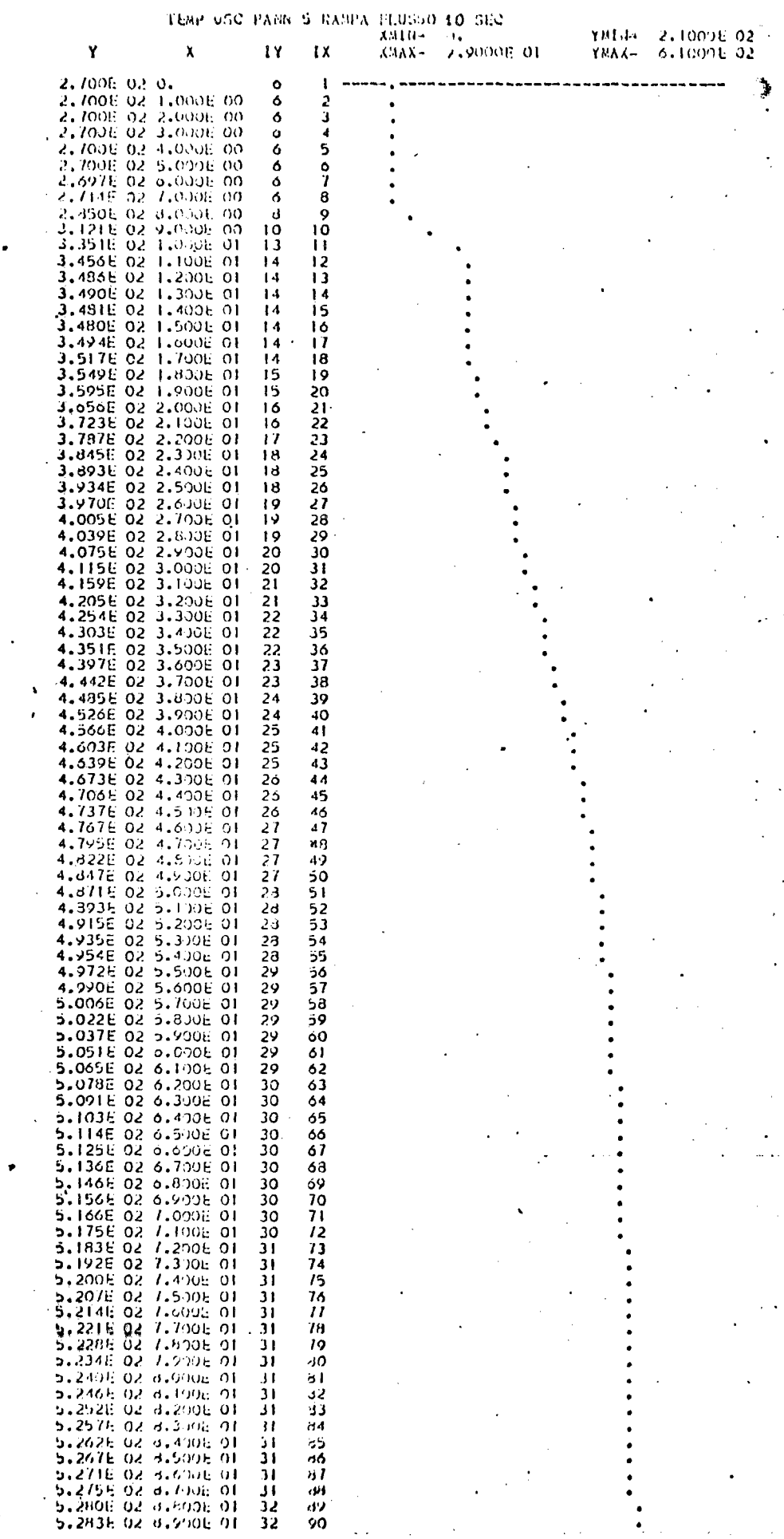

Y	X	IY	IX
2.700E 02	0.	0	1
2.700E 02	1.000E 00	6	2
2.700E 02	2.000E 00	6	3
2.700E 02	3.000E 00	6	4
2.700E 02	4.000E 00	6	5
2.700E 02	5.000E 00	6	6
2.697E 02	6.000E 00	6	7
2.714E 02	7.000E 00	6	8
2.850E 02	8.000E 00	8	9
3.121E 02	9.000E 00	10	10
3.351E 02	1.000E 01	13	11
3.456E 02	1.100E 01	14	12
3.486E 02	1.200E 01	14	13
3.490E 02	1.300E 01	14	14
3.481E 02	1.400E 01	14	15
3.480E 02	1.500E 01	14	16
3.494E 02	1.600E 01	14	17
3.517E 02	1.700E 01	14	18
3.549E 02	1.800E 01	15	19
3.595E 02	1.900E 01	15	20
3.656E 02	2.000E 01	16	21
3.723E 02	2.100E 01	16	22
3.787E 02	2.200E 01	17	23
3.845E 02	2.300E 01	18	24
3.893E 02	2.400E 01	18	25
3.934E 02	2.500E 01	18	26
3.970E 02	2.600E 01	19	27
4.005E 02	2.700E 01	19	28
4.039E 02	2.800E 01	19	29
4.075E 02	2.900E 01	20	30
4.115E 02	3.000E 01	20	31
4.159E 02	3.100E 01	21	32
4.205E 02	3.200E 01	21	33
4.254E 02	3.300E 01	22	34
4.303E 02	3.400E 01	22	35
4.351E 02	3.500E 01	22	36
4.397E 02	3.600E 01	23	37
4.442E 02	3.700E 01	23	38
4.485E 02	3.800E 01	24	39
4.526E 02	3.900E 01	24	40
4.566E 02	4.000E 01	25	41
4.603E 02	4.100E 01	25	42
4.639E 02	4.200E 01	25	43
4.673E 02	4.300E 01	26	44
4.706E 02	4.400E 01	26	45
4.737E 02	4.500E 01	26	46
4.767E 02	4.600E 01	27	47
4.795E 02	4.700E 01	27	48
4.822E 02	4.800E 01	27	49
4.847E 02	4.900E 01	27	50
4.871E 02	5.000E 01	28	51
4.893E 02	5.100E 01	28	52
4.915E 02	5.200E 01	28	53
4.935E 02	5.300E 01	28	54
4.954E 02	5.400E 01	28	55
4.972E 02	5.500E 01	29	56
4.990E 02	5.600E 01	29	57
5.006E 02	5.700E 01	29	58
5.022E 02	5.800E 01	29	59
5.037E 02	5.900E 01	29	60
5.051E 02	6.000E 01	29	61
5.065E 02	6.100E 01	29	62
5.078E 02	6.200E 01	30	63
5.091E 02	6.300E 01	30	64
5.103E 02	6.400E 01	30	65
5.114E 02	6.500E 01	30	66
5.125E 02	6.600E 01	30	67
5.136E 02	6.700E 01	30	68
5.146E 02	6.800E 01	30	69
5.156E 02	6.900E 01	30	70
5.166E 02	7.000E 01	30	71
5.175E 02	7.100E 01	30	72
5.183E 02	7.200E 01	31	73
5.192E 02	7.300E 01	31	74
5.200E 02	7.400E 01	31	75
5.207E 02	7.500E 01	31	76
5.214E 02	7.600E 01	31	77
5.221E 02	7.700E 01	31	78
5.228E 02	7.800E 01	31	79
5.234E 02	7.900E 01	31	80
5.240E 02	8.000E 01	31	81
5.246E 02	8.100E 01	31	82
5.252E 02	8.200E 01	31	83
5.257E 02	8.300E 01	31	84
5.262E 02	8.400E 01	31	85
5.267E 02	8.500E 01	31	86
5.271E 02	8.600E 01	31	87
5.275E 02	8.700E 01	31	88
5.280E 02	8.800E 01	32	89
5.283E 02	8.900E 01	32	90

FIG. 5 - Sodium flow rate (Kh/s).

Flux ramp lenght 10 s.

PORTATA SODIO RAMPA FLUSSO 10 SEC

XMIN= 0. YMIN= 6.0000E-01

XMAX= 9.9000E 01 YMAX= 8.6000E 00

Y	X	IY	IX
7.134E-01	0.	1	1
7.134E-01	1.000E 00	1	2
7.134E-01	2.000E 00	1	3
1.100E 00	3.000E 00	3	4
1.759E 00	4.000E 00	6	5
2.561E 00	5.000E 00	10	6
3.436E 00	6.000E 00	14	7
4.319E 00	7.000E 00	19	8
5.154E 00	8.000E 00	23	9
5.920E 00	9.000E 00	26	10
6.634E 00	1.000E 01	30	11
7.332E 00	1.100E 01	33	12
8.029E 00	1.200E 01	37	13
7.529E 00	1.300E 01	34	14
7.270E 00	1.400E 01	33	15
7.189E 00	1.500E 01	33	16
7.162E 00	1.600E 01	32	17
7.151E 00	1.700E 01	32	18
7.144E 00	1.800E 01	32	19
7.137E 00	1.900E 01	32	20
7.127E 00	2.000E 01	32	21
7.116E 00	2.100E 01	32	22
7.104E 00	2.200E 01	32	23
7.092E 00	2.300E 01	32	24
7.081E 00	2.400E 01	32	25
7.072E 00	2.500E 01	32	26
7.064E 00	2.600E 01	32	27
7.057E 00	2.700E 01	32	28
7.050E 00	2.800E 01	32	29
7.043E 00	2.900E 01	32	30
7.036E 00	3.000E 01	32	31
7.028E 00	3.100E 01	32	32
7.019E 00	3.200E 01	32	33
7.010E 00	3.300E 01	32	34
7.001E 00	3.400E 01	32	35
6.992E 00	3.500E 01	32	36
6.982E 00	3.600E 01	32	37
6.973E 00	3.700E 01	32	38
6.964E 00	3.800E 01	32	39
6.956E 00	3.900E 01	31	40
6.948E 00	4.000E 01	31	41
6.940E 00	4.100E 01	31	42
6.933E 00	4.200E 01	31	43
6.926E 00	4.300E 01	31	44
6.919E 00	4.400E 01	31	45
6.913E 00	4.500E 01	31	46
6.907E 00	4.600E 01	31	47
6.901E 00	4.700E 01	31	48
6.895E 00	4.800E 01	31	49
6.890E 00	4.900E 01	31	50
6.885E 00	5.000E 01	31	51
6.880E 00	5.100E 01	31	52
6.876E 00	5.200E 01	31	53
6.872E 00	5.300E 01	31	54
6.868E 00	5.400E 01	31	55
6.864E 00	5.500E 01	31	56
6.860E 00	5.600E 01	31	57
6.857E 00	5.700E 01	31	58
6.854E 00	5.800E 01	31	59
6.851E 00	5.900E 01	31	60
6.848E 00	6.000E 01	31	61
6.845E 00	6.100E 01	31	62
6.842E 00	6.200E 01	31	63
6.839E 00	6.300E 01	31	64
6.837E 00	6.400E 01	31	65
6.835E 00	6.500E 01	31	66
6.832E 00	6.600E 01	31	67
6.830E 00	6.700E 01	31	68
6.828E 00	6.800E 01	31	69
6.826E 00	6.900E 01	31	70
6.824E 00	7.000E 01	31	71
6.822E 00	7.100E 01	31	72
6.820E 00	7.200E 01	31	73
6.819E 00	7.300E 01	31	74
6.817E 00	7.400E 01	31	75
6.815E 00	7.500E 01	31	76
6.814E 00	7.600E 01	31	77
6.812E 00	7.700E 01	31	78
6.811E 00	7.800E 01	31	79
6.810E 00	7.900E 01	31	80

FIG. 6 – Flux ramp in the middle of panel 5 (W/M).

FLUSSO A META PANN 5

XMIN= 0. YMIN= 0.
XMAX= 7.9000E 01 YMAX= 2.0000E 04

Y	X	IY	IX
0.	0.	1	1
0.	1.000E 00	1	2
1.585E 03	2.000E 00	4	3
3.185E 03	3.000E 00	7	4
4.786E 03	4.000E 00	10	5
6.386E 03	5.000E 00	13	6
7.987E 03	6.000E 00	16	7
9.587E 03	7.000E 00	19	8
1.119E 04	8.000E 00	22	9
1.279E 04	9.000E 00	25	10
1.439E 04	1.000E 01	29	11
1.599E 04	1.100E 01	32	12
1.601E 04	1.200E 01	32	13
1.601E 04	1.300E 01	32	14
1.601E 04	1.400E 01	32	15
1.601E 04	1.500E 01	32	16
1.601E 04	1.600E 01	32	17
1.601E 04	1.700E 01	32	18
1.601E 04	1.800E 01	32	19
1.601E 04	1.900E 01	32	20
1.601E 04	2.000E 01	32	21
1.601E 04	2.100E 01	32	22
1.601E 04	2.200E 01	32	23
1.601E 04	2.300E 01	32	24
1.601E 04	2.400E 01	32	25
1.601E 04	2.500E 01	32	26
1.601E 04	2.600E 01	32	27
1.601E 04	2.700E 01	32	28
1.601E 04	2.800E 01	32	29
1.601E 04	2.900E 01	32	30
1.601E 04	3.000E 01	32	31
1.601E 04	3.100E 01	32	32
1.601E 04	3.200E 01	32	33
1.601E 04	3.300E 01	32	34
1.601E 04	3.400E 01	32	35
1.601E 04	3.500E 01	32	36
1.601E 04	3.600E 01	32	37
1.601E 04	3.700E 01	32	38
1.601E 04	3.800E 01	32	39
1.601E 04	3.900E 01	32	40

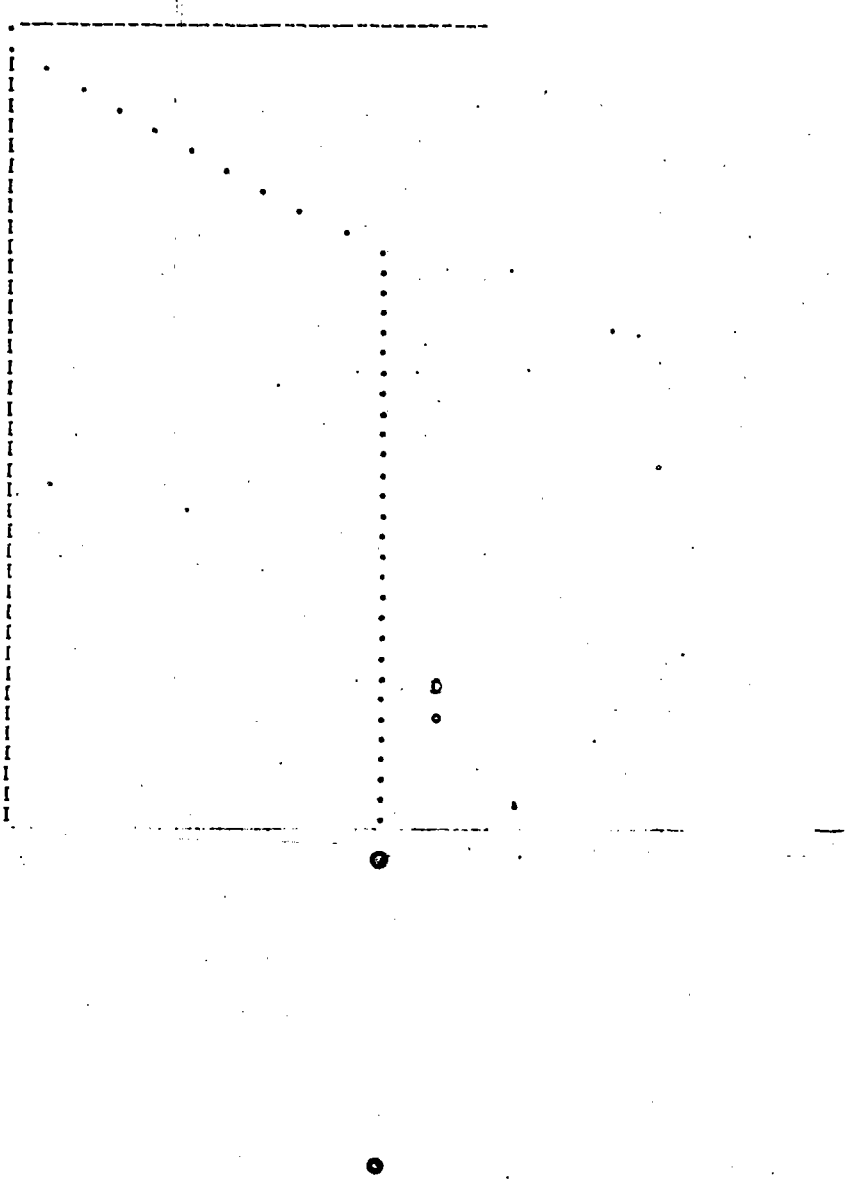

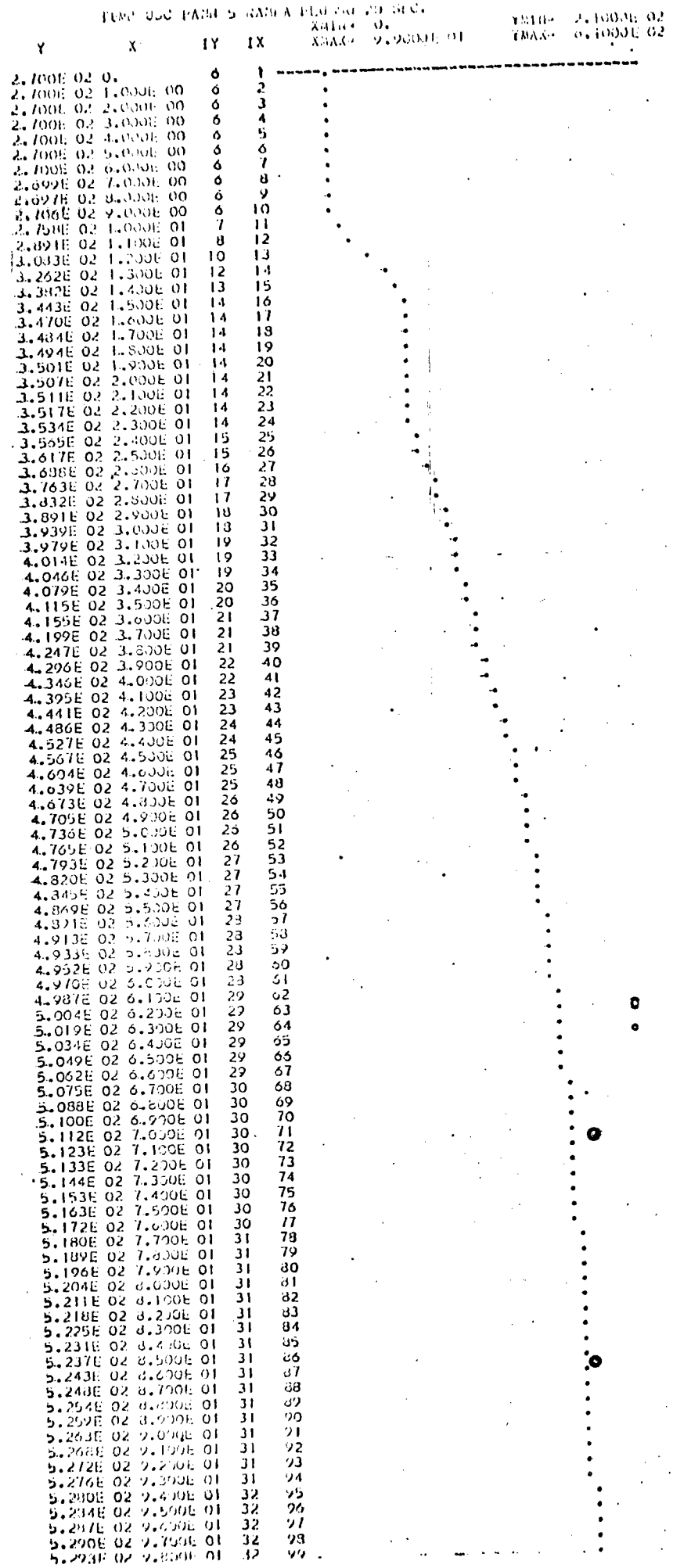

FIG. 7 – Panel 5 sodium outlet temperature (°C). Flux ramp lenght 20 s.

FIG. 8 – Sodium flow rate (Kg/s).

Flux ramp lenght 20 s.

FLUSSO A META' PANN 5

XMIN= 0. YMIN= 0.
XMAX= 9.9000E 01 YMAX= 2.0000E 04

Y	X	IY	IX
0.	0.	1	1
0.	1.000E 00	1	2
7.923E 02	2.000E 00	2	3
1.593E 03	3.000E 00	4	4
2.393E 03	4.000E 00	5	5
3.193E 03	5.000E 00	7	6
3.993E 03	6.000E 00	8	7
4.794E 03	7.000E 00	10	8
5.594E 03	8.000E 00	11	9
6.394E 03	9.000E 00	13	10
7.195E 03	1.000E 01	15	11
7.995E 03	1.100E 01	16	12
8.795E 03	1.200E 01	18	13
9.595E 03	1.300E 01	19	14
1.040E 04	1.400E 01	21	15
1.120E 04	1.500E 01	22	16
1.200E 04	1.600E 01	24	17
1.280E 04	1.700E 01	25	18
1.360E 04	1.800E 01	27	19
1.440E 04	1.900E 01	29	20
1.520E 04	2.000E 01	30	21
1.600E 04	2.100E 01	32	22
1.601E 04	2.200E 01	32	23
1.601E 04	2.300E 01	32	24
1.601E 04	2.400E 01	32	25
1.601E 04	2.500E 01	32	26
1.601E 04	2.600E 01	32	27
1.601E 04	2.700E 01	32	28
1.601E 04	2.800E 01	32	29
1.601E 04	2.900E 01	32	30
1.601E 04	3.000E 01	32	31
1.601E 04	3.100E 01	32	32
1.601E 04	3.200E 01	32	33
1.601E 04	3.300E 01	32	34
1.601E 04	3.400E 01	32	35
1.601E 04	3.500E 01	32	36
1.601E 04	3.600E 01	32	37
1.601E 04	3.700E 01	32	38
1.601E 04	3.800E 01	32	39
1.601E 04	3.900E 01	32	40

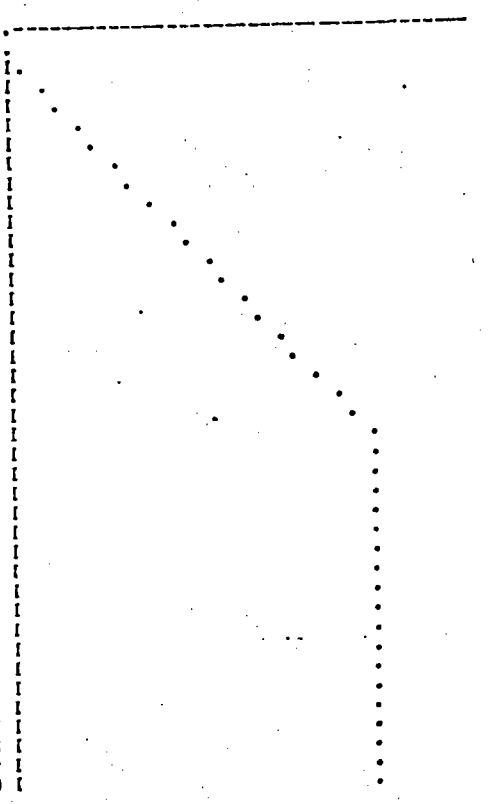

FIG. 9 - Flux ramp in the middle of panel 5 (W/M).

PORTATA SODIO

XMIN= 0. YMIN= 4.0000E-01
XMAX= 9.9000E 01 YMAX= 8.4000E 00

Y	X	IY	IX
7.134E-01	0.	2	1
7.134E-01	1.000E 00	2	2
7.134E-01	2.000E 00	2	3
8.627E-01	3.000E 00	3	4
1.107E 00	4.000E 00	4	5
1.412E 00	5.000E 00	5	6
1.767E 00	6.000E 00	7	7
2.157E 00	7.000E 00	9	8
2.567E 00	8.000E 00	11	9
2.983E 00	9.000E 00	13	10
3.391E 00	1.000E 01	15	11
3.776E 00	1.100E 01	17	12
4.134E 00	1.200E 01	19	13
4.471E 00	1.300E 01	20	14
4.802E 00	1.400E 01	22	15
5.140E 00	1.500E 01	24	16
5.486E 00	1.600E 01	25	17
5.836E 00	1.700E 01	27	18
6.188E 00	1.800E 01	29	19
6.539E 00	1.900E 01	30	20
6.848E 00	2.000E 01	32	21
7.235E 00	2.100E 01	34	22
7.590E 00	2.200E 01	36	23
7.341E 00	2.300E 01	34	24
7.209E 00	2.400E 01	34	25
7.161E 00	2.500E 01	33	26
7.138E 00	2.600E 01	33	27
7.121E 00	2.700E 01	33	28
7.106E 00	2.800E 01	33	29
7.093E 00	2.900E 01	33	30
7.082E 00	3.000E 01	33	31
7.073E 00	3.100E 01	33	32
7.065E 00	3.200E 01	33	33
7.058E 00	3.300E 01	33	34
7.051E 00	3.400E 01	33	35
7.044E 00	3.500E 01	33	36
7.037E 00	3.600E 01	33	37
7.029E 00	3.700E 01	33	38
7.021E 00	3.800E 01	33	39
7.012E 00	3.900E 01	33	40

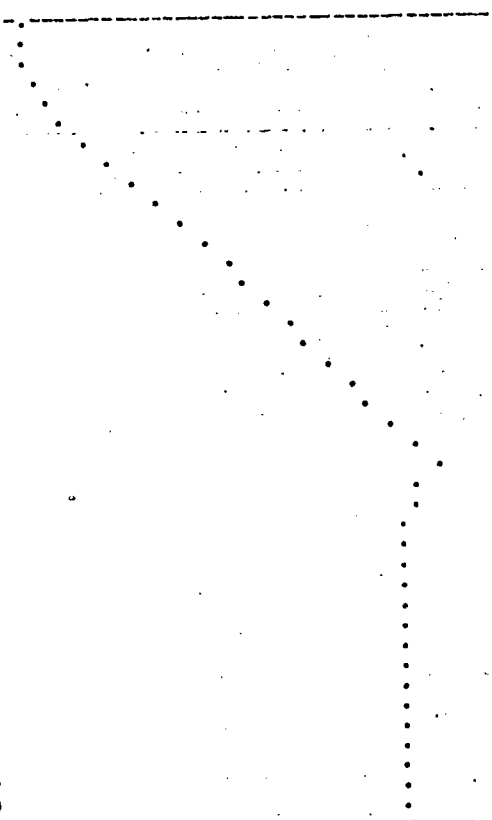

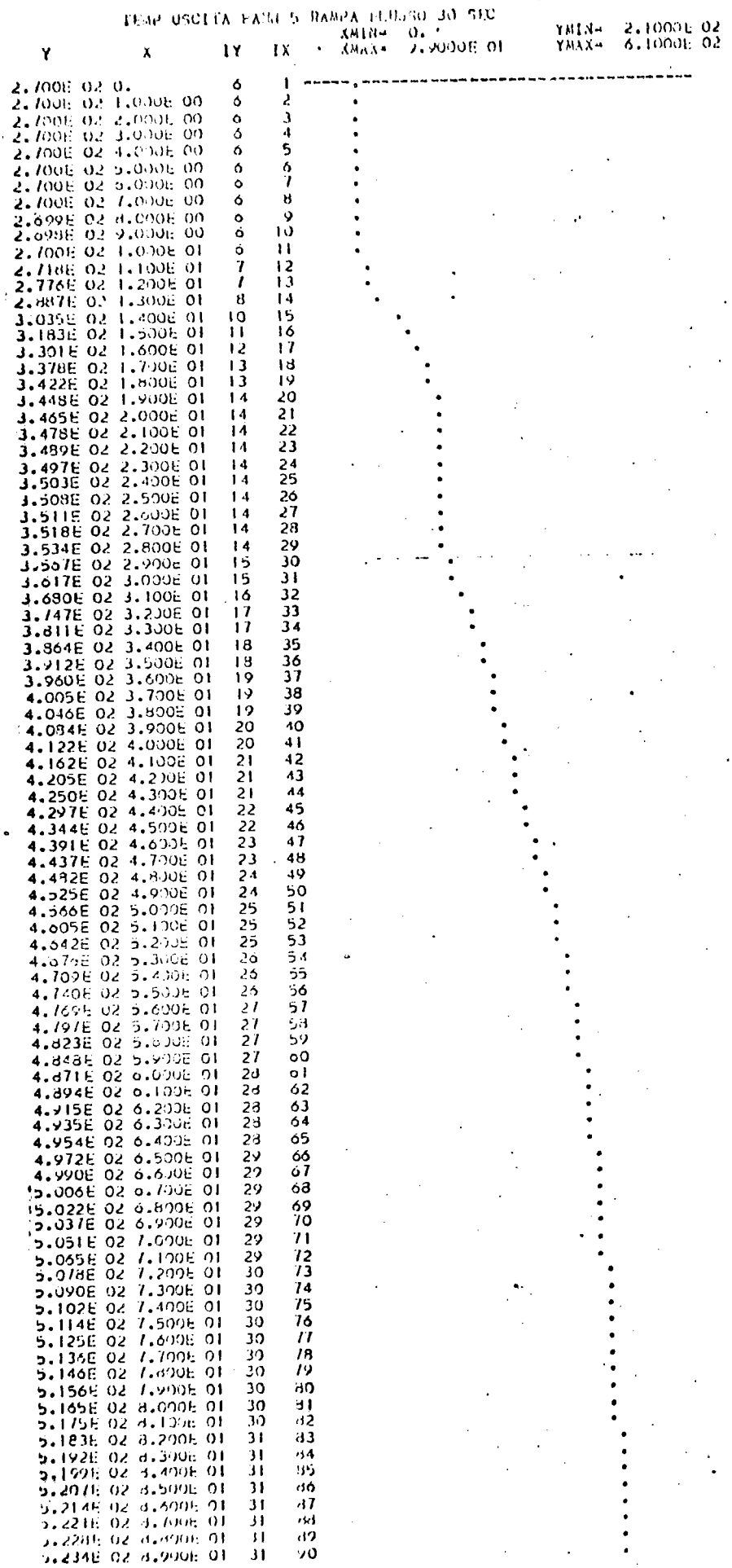

FIG. 10 - Panel 5 sodium outlet temperature (°C).

Flux ramp lenght 30 s.

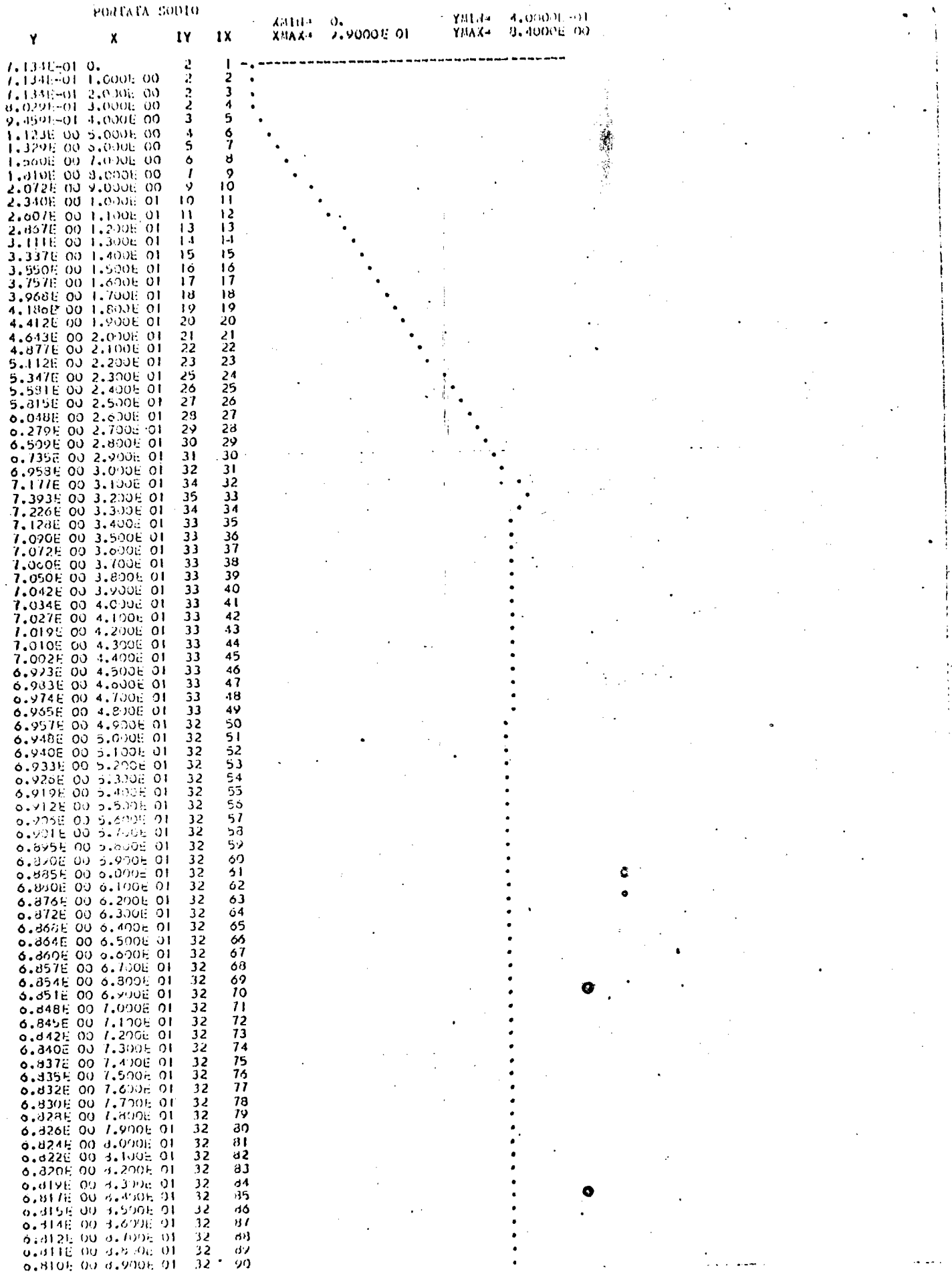

FIG. 11 – Sodium flow rate (Kg/S).

Flux ramp lenght 30 S.

FIG. 12 – Fluw ramp in the middle of panel 5 (W/M).

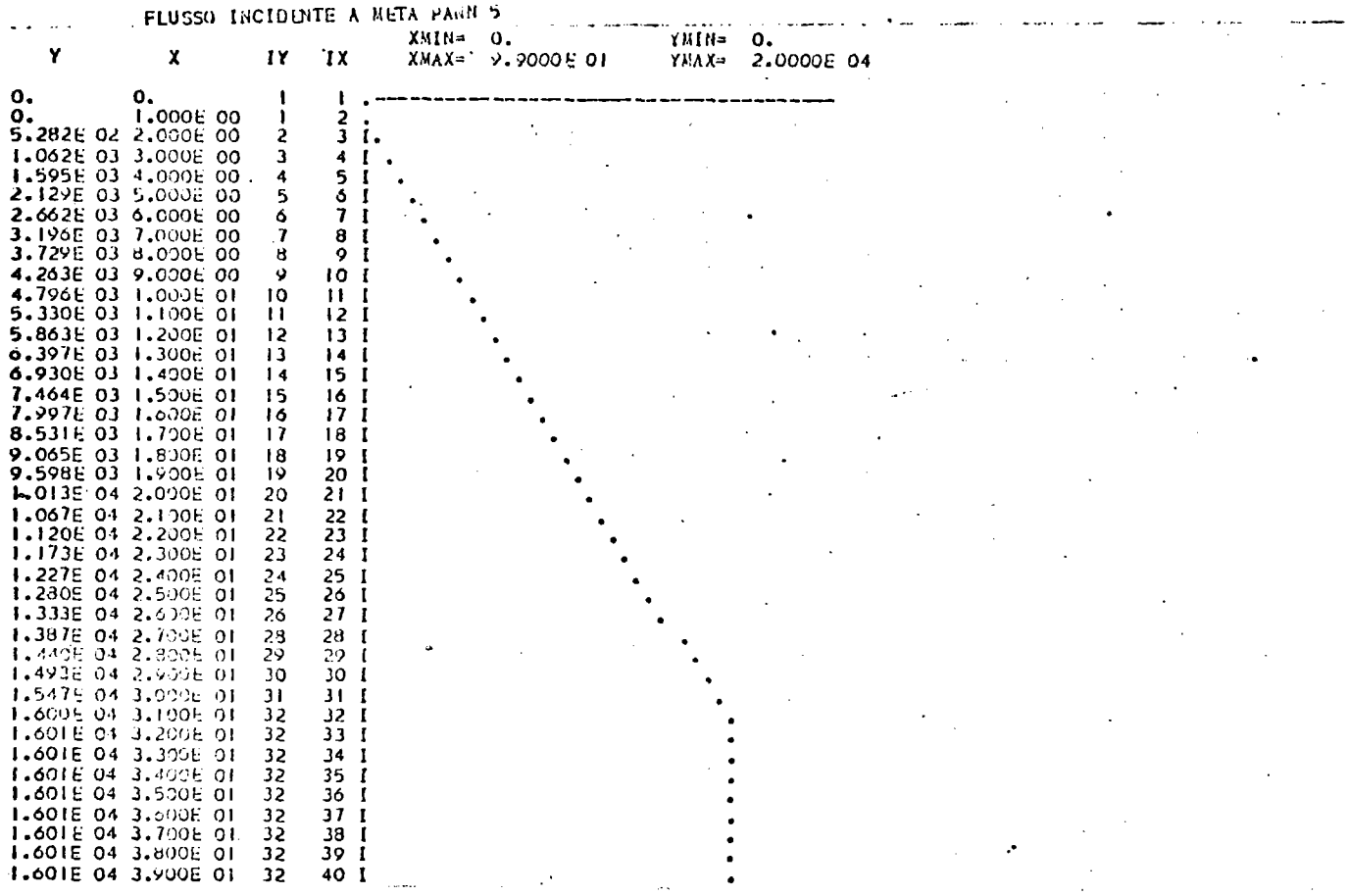

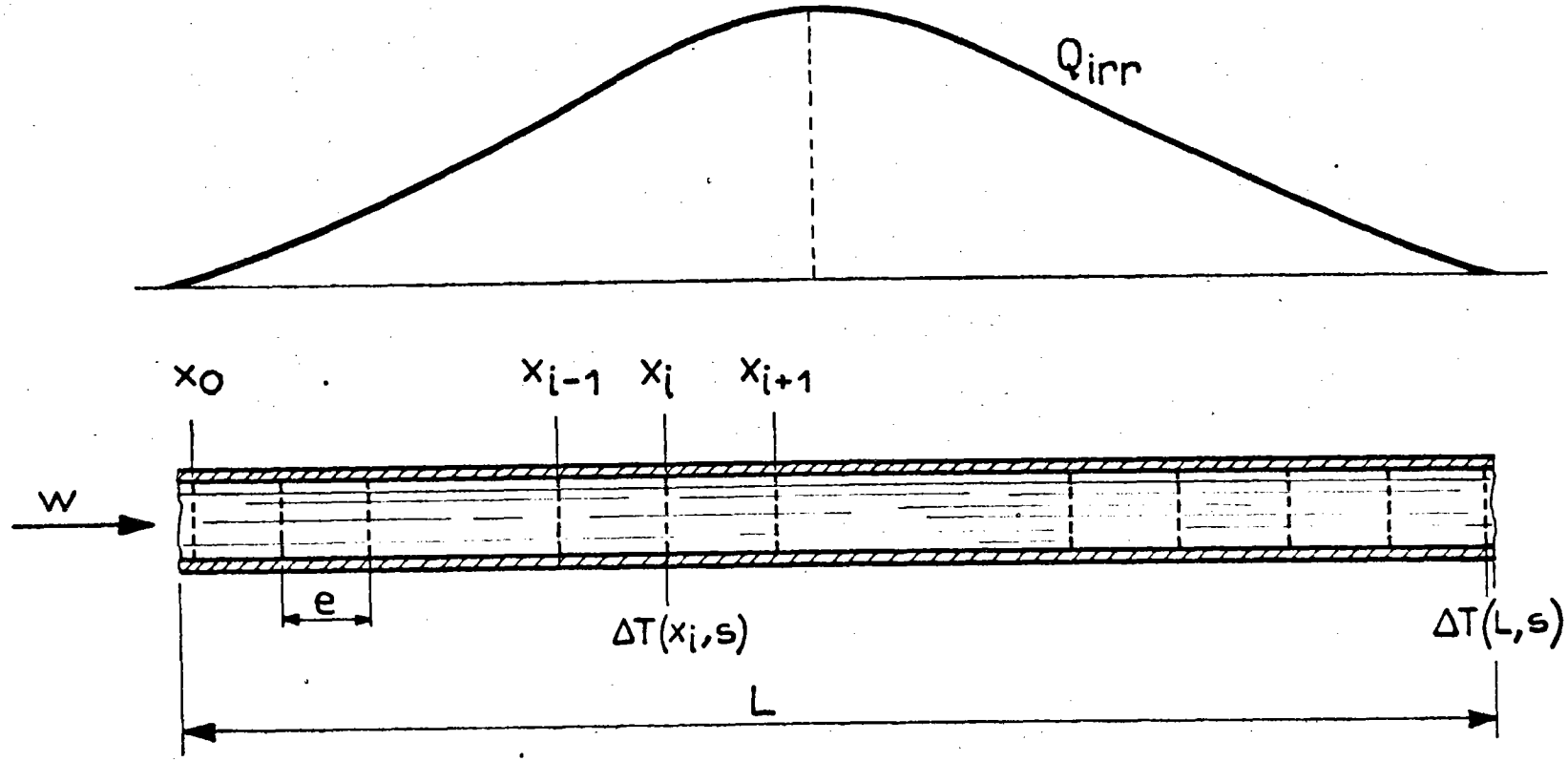

Fig.13- RADIATED PIPE SCHEMATIC

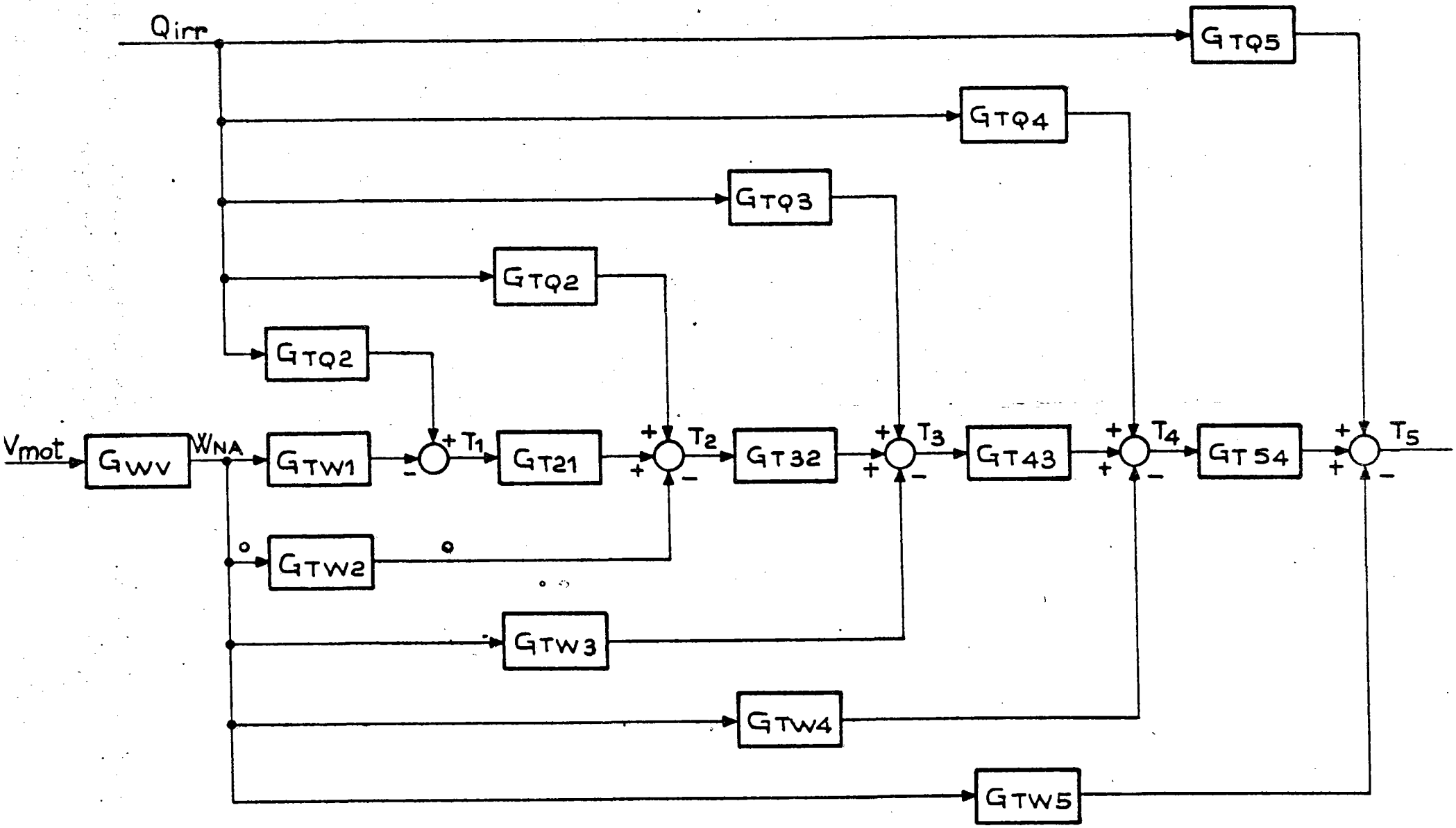

Fig. 14 - BLOCK DIAGRAM OF THE RECEIVER

XMIN= -3.0000E 00 YMIN= 0.
XMAX= 4.8398E-01 YMAX= 2.0000E 00

Y	X	IY	IX
9.997E-01	0.1000E-02	20	1
9.993E-01	0.1200E-02	20	2
9.988E-01	0.1440E-02	20	3
9.982E-01	0.1728E-02	20	4
9.975E-01	0.2074E-02	20	5
9.967E-01	0.2488E-02	20	6
9.957E-01	0.2986E-02	20	7
9.946E-01	0.3583E-02	20	8
9.934E-01	0.4300E-02	20	9
9.920E-01	0.5160E-02	20	10
9.903E-01	0.6192E-02	20	11
9.883E-01	0.7430E-02	20	12
9.859E-01	0.8916E-02	20	13
9.830E-01	0.1070E-01	19	14
9.795E-01	0.1284E-01	19	15
9.753E-01	0.1541E-01	19	16
9.702E-01	0.1849E-01	18	17
9.641E-01	0.2219E-01	17	18
9.568E-01	0.2662E-01	16	19
9.480E-01	0.3195E-01	15	20
9.376E-01	0.3834E-01	14	21
9.252E-01	0.4601E-01	12	22
9.105E-01	0.5521E-01	10	23
8.931E-01	0.6625E-01	8	24
8.725E-01	0.7950E-01	6	25
8.481E-01	0.9540E-01	4	26
8.192E-01	0.1145	4	27
7.850E-01	0.1374	5	28
7.445E-01	0.1648	5	29
7.016E-01	0.1978	5	30
6.568E-01	0.2374	5	31
6.093E-01	0.2849	5	32
5.589E-01	0.3418	6	33
5.059E-01	0.4102	6	34
4.513E-01	0.4922	5	35
3.956E-01	0.5907	4	36
3.394E-01	0.7088	3	37
2.833E-01	0.8506	2	38
2.284E-01	1.021	2	39
1.753E-01	1.225	1	40
1.253E-01	1.470	1	41
8.088E-02	1.764	1	42
4.516E-02	2.116	1	43
2.041E-02	2.540	1	44
7.497E-03	3.048	1	45

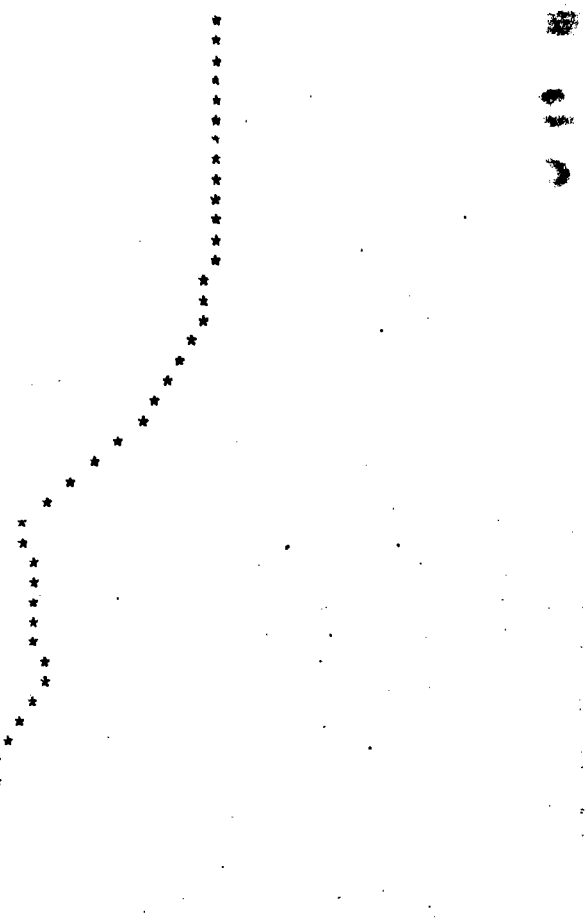

PHASE

XMIN= -3.0000E 00 YMIN= -3.8002E 00
XMAX= 4.8398E-01 YMAX= 4.2002E 00

Y	X	IY	IX
-3.031E-02	0.1000E-02	20	1
-3.635E-02	0.1200E-02	20	2
-4.363E-02	0.1440E-02	20	3
-5.235E-02	0.1728E-02	20	4
-6.281E-02	0.2074E-02	20	5
-7.536E-02	0.2488E-02	20	6
-9.041E-02	0.2986E-02	20	7
-1.085E-01	0.3583E-02	20	8
-1.301E-01	0.4300E-02	20	9
-1.560E-01	0.5160E-02	20	10
-1.870E-01	0.6192E-02	20	11
-2.241E-01	0.7430E-02	19	12
-2.683E-01	0.8916E-02	19	13
-3.210E-01	0.1070E-01	19	14
-3.836E-01	0.1284E-01	19	15
-4.574E-01	0.1541E-01	18	16
-5.439E-01	0.1849E-01	18	17
-6.442E-01	0.2219E-01	17	18
-7.585E-01	0.2662E-01	17	19
-8.855E-01	0.3195E-01	16	20
-1.021E 000	0.3834E-01	16	21
-1.157E 000	0.4601E-01	15	22
-1.281E 000	0.5521E-01	14	23
-1.372E 000	0.6625E-01	14	24
-1.395E 000	0.7950E-01	14	25
-1.265E 000	0.9540E-01	14	26
-9.829E-01	0.1145	16	27
-8.824E-01	0.1374	16	28
-1.006E 000	0.1648	16	29
-1.174E 000	0.1978	15	30
-1.285E 000	0.2374	14	31
-1.430E 000	0.2849	14	32
-1.761E 000	0.3418	12	33
-2.290E 000	0.4102	9	34
-2.861E 000	0.4922	7	35
-2.954E 000	0.5907	34	36
-2.495E 000	0.7088	32	37
-1.898E 000	0.8506	29	38
-1.161E 00	1.021	25	39
-4.110E-01	1.225	22	40
3.795E-01	1.470	19	41
1.202E 00	1.764	15	42
2.000E 00	2.116	11	43
2.731E 00	2.540	7	44
2.939E 00	3.048	34	45

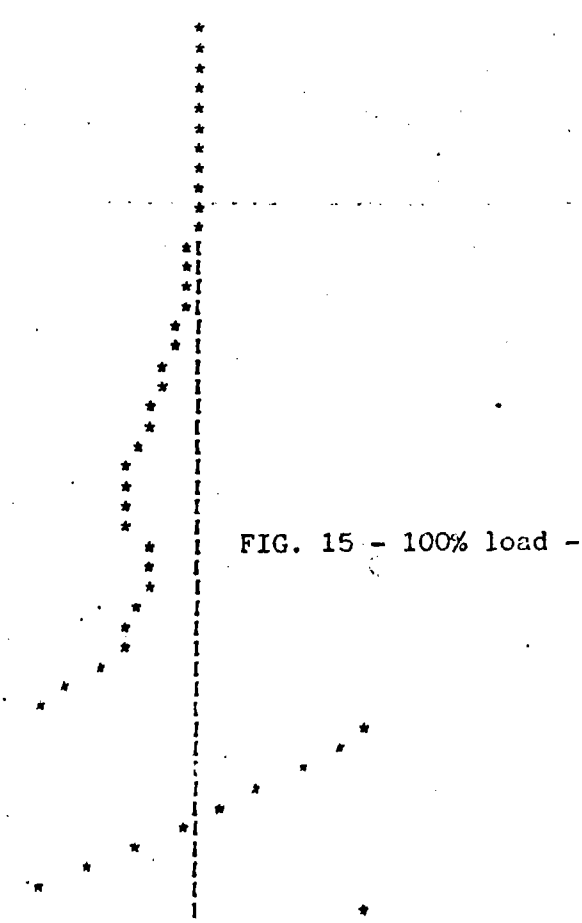

FIG. 15 - 100% load - $\Delta T_s/\Delta V$

Y	X	IY	IX
9.998E-01	0.1000E-02	20	1
9.997E-01	0.1200E-02	20	2
9.996E-01	0.1440E-02	20	3
9.994E-01	0.1728E-02	20	4
9.992E-01	0.2074E-02	20	5
9.988E-01	0.2488E-02	20	6
9.983E-01	0.2986E-02	20	7
9.976E-01	0.3583E-02	20	8
9.965E-01	0.4300E-02	20	9
9.950E-01	0.5160E-02	20	10
9.928E-01	0.6192E-02	20	11
9.897E-01	0.7430E-02	20	12
9.852E-01	0.8916E-02	20	13
9.788E-01	0.1070E-01	20	14
9.698E-01	0.1284E-01	19	15
9.571E-01	0.1541E-01	19	16
9.393E-01	0.1849E-01	19	17
9.147E-01	0.2219E-01	18	18
8.816E-01	0.2662E-01	18	19
8.382E-01	0.3195E-01	17	20
7.834E-01	0.3834E-01	16	21
7.180E-01	0.4601E-01	15	22
6.457E-01	0.5521E-01	13	23
5.719E-01	0.6625E-01	12	24
5.002E-01	0.7950E-01	10	25
4.269E-01	0.9540E-01	9	26
3.445E-01	0.1145	7	27
2.581E-01	0.1374	6	28
2.028E-01	0.1648	4	29
2.161E-01	0.1978	5	30
2.672E-01	0.2374	6	31
3.183E-01	0.2849	7	32
3.505E-01	0.3418	7	33
3.386E-01	0.4102	7	34
2.760E-01	0.4922	6	35
1.985E-01	0.5907	4	36
1.475E-01	0.7088	3	37
1.155E-01	0.8506	3	38
7.781E-02	1.021	2	39
4.427E-02	1.225	1	40
2.264E-02	1.470	1	41
9.741E-03	1.764	1	42
3.454E-03	2.116	1	43
9.934E-04	2.540	1	44
2.274E-04	3.048	1	45

FASE

XMIN= -3.0000E 00 YMIN= -4.0000E 00
XMAX= 4.8390E-01 YMAX= 4.0000E 00

Y	X	IY	IX
-2.238E-02	0.1000E-02	21	1
-2.684E-02	0.1200E-02	21	2
-3.221E-02	0.1440E-02	21	3
-3.865E-02	0.1728E-02	21	4
-4.638E-02	0.2074E-02	21	5
-5.564E-02	0.2488E-02	21	6
-6.675E-02	0.2986E-02	21	7
-8.008E-02	0.3583E-02	21	8
-9.605E-02	0.4300E-02	21	9
-1.152E-01	0.5160E-02	21	10
-1.381E-01	0.6192E-02	21	11
-1.655E-01	0.7430E-02	21	12
-1.982E-01	0.8916E-02	21	13
-2.371E-01	0.1070E-01	20	14
-2.834E-01	0.1284E-01	20	15
-3.380E-01	0.1541E-01	20	16
-4.022E-01	0.1849E-01	20	17
-4.768E-01	0.2219E-01	19	18
-5.621E-01	0.2662E-01	19	19
-6.579E-01	0.3195E-01	18	20
-7.619E-01	0.3834E-01	18	21
-8.706E-01	0.4601E-01	17	22
-9.790E-01	0.5521E-01	17	23
-1.085E 00	0.6625E-01	16	24
-1.194E 00	0.7950E-01	16	25
-1.313E 00	0.9540E-01	15	26
-1.429E 00	0.1145	15	27
-1.465E 00	0.1374	14	28
-1.304E 00	0.1648	15	29
-1.109E 00	0.1978	16	30
-1.165E 00	0.2374	16	31
-1.426E 00	0.2849	15	32
-1.842E 00	0.3418	13	33
-2.382E 00	0.4102	10	34
-2.968E 00	0.4922	7	35
2.767E 00	0.5907	34	36
2.319E 00	0.7088	32	37
1.993E 00	0.8506	29	38
9.177E-01	1.021	29	39
1.051E-01	1.225	21	40
-7.541E-01	1.470	18	41
-1.673E 00	1.764	13	42
-2.995E 00	2.116	9	43
2.902E 00	2.540	34	44
2.019E 00	3.048	30	45

FIG. 16 - 100% load - $\Delta T_4/\Delta V$

Y	X	IY	IX
9.999E-01	0.1000E-02	20	1
9.998E-01	0.1200E-02	20	2
9.997E-01	0.1440E-02	20	3
9.996E-01	0.1728E-02	20	4
9.995E-01	0.2074E-02	20	5
9.992E-01	0.2488E-02	20	6
9.989E-01	0.2986E-02	20	7
9.984E-01	0.3583E-02	20	8
9.977E-01	0.4300E-02	20	9
9.967E-01	0.5160E-02	20	10
9.953E-01	0.6192E-02	20	11
9.932E-01	0.7430E-02	20	12
9.903E-01	0.8916E-02	20	13
9.861E-01	0.1070E-01	20	14
9.801E-01	0.1284E-01	20	15
9.716E-01	0.1541E-01	19	16
9.597E-01	0.1849E-01	19	17
9.433E-01	0.2219E-01	19	18
9.208E-01	0.2662E-01	18	19
8.910E-01	0.3195E-01	18	20
8.530E-01	0.3834E-01	17	21
8.074E-01	0.4601E-01	16	22
7.575E-01	0.5521E-01	15	23
7.111E-01	0.6625E-01	14	24
6.785E-01	0.7950E-01	14	25
6.660E-01	0.9540E-01	13	26
6.679E-01	0.1145	14	27
6.679E-01	0.1374	14	28
6.527E-01	0.1648	13	29
6.226E-01	0.1978	13	30
5.919E-01	0.2374	12	31
5.721E-01	0.2849	12	32
5.531E-01	0.3418	11	33
5.093E-01	0.4102	10	34
4.358E-01	0.4922	9	35
3.538E-01	0.5907	7	36
2.746E-01	0.7088	6	37
2.014E-01	0.8506	4	38
1.334E-01	1.021	3	39
7.784E-02	1.225	2	40
3.960E-02	1.470	1	41
1.701E-02	1.764	1	42
6.006E-03	2.116	1	43
1.705E-03	2.540	1	44
3.791E-04	3.048	1	45

FASE

XMIN= -3.0000E 00 YMIN= -4.0000E 00
XMAX= 4.8393E-01 YMAX= 4.0000E 00

Y	X	IY	IX
-1.414E-02	0.1000E-02	21	1
-1.694E-02	0.1200E-02	21	2
-2.034E-02	0.1440E-02	21	3
-2.441E-02	0.1728E-02	21	4
-2.928E-02	0.2074E-02	21	5
-3.513E-02	0.2488E-02	21	6
-4.214E-02	0.2986E-02	21	7
-5.055E-02	0.3583E-02	21	8
-6.063E-02	0.4300E-02	21	9
-7.270E-02	0.5160E-02	21	10
-8.714E-02	0.6192E-02	21	11
-1.044E-01	0.7430E-02	21	12
-1.250E-01	0.8916E-02	21	13
-1.495E-01	0.1070E-01	21	14
-1.785E-01	0.1284E-01	21	15
-2.127E-01	0.1541E-01	20	16
-2.527E-01	0.1849E-01	20	17
-2.989E-01	0.2219E-01	20	18
-3.512E-01	0.2662E-01	20	19
-4.088E-01	0.3195E-01	20	20
-4.695E-01	0.3834E-01	19	21
-5.291E-01	0.4601E-01	19	22
-5.816E-01	0.5521E-01	19	23
-6.223E-01	0.6625E-01	18	24
-6.547E-01	0.7950E-01	18	25
-6.979E-01	0.9540E-01	18	26
-7.779E-01	0.1145	18	27
-9.063E-01	0.1374	17	28
-1.073E 00	0.1648	16	29
-1.260E 00	0.1978	15	30
-1.461E 00	0.2374	14	31
-1.701E 00	0.2849	13	32
-2.022E 00	0.3418	12	33
-2.434E 00	0.4102	10	34
-2.901E 00	0.4922	7	35
2.876E 00	0.5907	35	36
2.309E 00	0.7088	32	37
1.659E 00	0.8506	29	38
9.138E-01	1.021	25	39
9.990E-02	1.225	21	40
-7.709E-01	1.470	18	41
-1.702E 00	1.764	13	42
-2.645E 00	2.116	9	43
2.719E 00	2.540	34	44
1.879E 00	3.048	30	45

FIG. 17 - 100% load - $\Delta T_3 / \Delta V$

Y	X	IY	IX
9.999E-01	0.1000E-02	20	1
9.999E-01	0.1200E-02	20	2
9.998E-01	0.1440E-02	20	3
9.997E-01	0.1728E-02	20	4
9.996E-01	0.2074E-02	20	5
9.994E-01	0.2488E-02	20	6
9.991E-01	0.2986E-02	20	7
9.988E-01	0.3583E-02	20	8
9.982E-01	0.4300E-02	20	9
9.975E-01	0.5160E-02	20	10
9.963E-01	0.6192E-02	20	11
9.947E-01	0.7430E-02	20	12
9.924E-01	0.8916E-02	20	13
9.891E-01	0.1070E-01	20	14
9.844E-01	0.1284E-01	20	15
9.776E-01	0.1541E-01	20	16
9.679E-01	0.1849E-01	19	17
9.542E-01	0.2219E-01	19	18
9.349E-01	0.2662E-01	19	19
9.077E-01	0.3195E-01	18	20
8.702E-01	0.3834E-01	17	21
8.194E-01	0.4601E-01	16	22
7.519E-01	0.5521E-01	15	23
6.656E-01	0.6625E-01	13	24
5.601E-01	0.7950E-01	11	25
4.402E-01	0.9540E-01	9	26
3.203E-01	0.1145	7	27
2.350E-01	0.1374	5	28
2.347E-01	0.1648	5	29
3.019E-01	0.1978	6	30
3.756E-01	0.2374	8	31
4.213E-01	0.2849	9	32
4.215E-01	0.3418	9	33
3.707E-01	0.4102	8	34
2.870E-01	0.4922	6	35
2.158E-01	0.5907	5	36
1.788E-01	0.7088	4	37
1.388E-01	0.8506	3	38
8.990E-02	1.021	2	39
5.336E-02	1.225	2	40
2.802E-02	1.470	1	41
1.233E-02	1.764	1	42
4.508E-03	2.116	1	43
1.322E-03	2.540	1	44
3.011E-04	3.048	1	45

XMIN= -3.0000E 00 YMIN= 0.
XMAX= 4.8398E-01 YMAX= 2.0000E 00

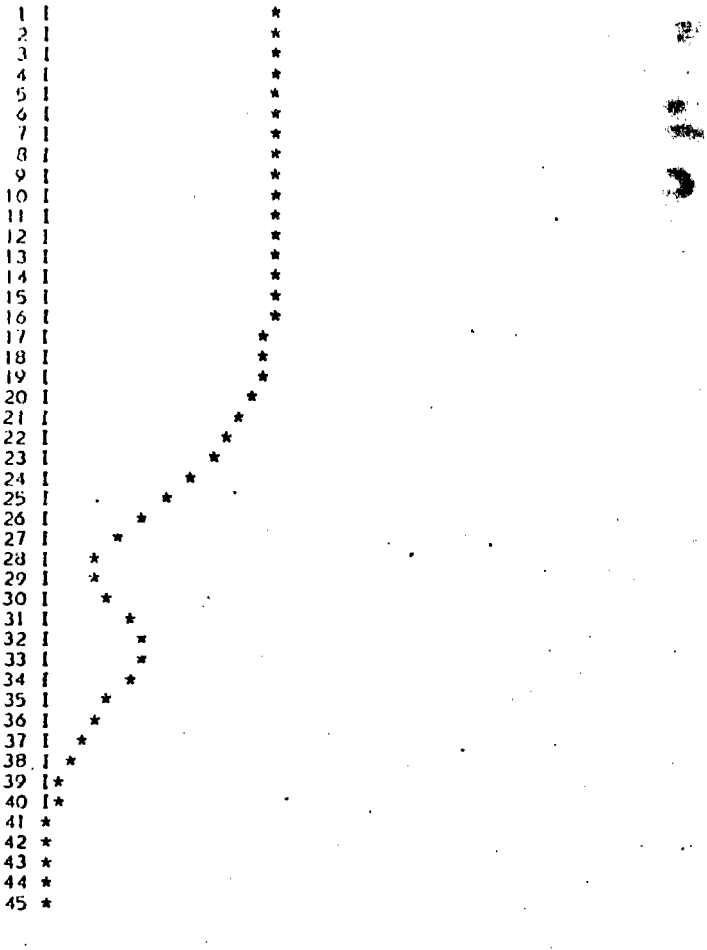

FASE

Y	X	IY	IX
-1.848E-02	0.1000E-02	21	1
-2.215E-02	0.1200E-02	21	2
-2.659E-02	0.1440E-02	21	3
-3.191E-02	0.1728E-02	21	4
-3.829E-02	0.2074E-02	21	5
-4.594E-02	0.2488E-02	21	6
-5.512E-02	0.2986E-02	21	7
-6.614E-02	0.3583E-02	21	8
-7.936E-02	0.4300E-02	21	9
-9.522E-02	0.5160E-02	21	10
-1.142E-01	0.6192E-02	21	11
-1.370E-01	0.7430E-02	21	12
-1.643E-01	0.8916E-02	21	13
-1.971E-01	0.1070E-01	21	14
-2.362E-01	0.1284E-01	20	15
-2.830E-01	0.1541E-01	20	16
-3.389E-01	0.1849E-01	20	17
-4.053E-01	0.2219E-01	20	18
-4.841E-01	0.2662E-01	19	19
-5.769E-01	0.3195E-01	19	20
-6.855E-01	0.3834E-01	18	21
-8.108E-01	0.4601E-01	18	22
-9.524E-01	0.5521E-01	17	23
-1.107E 00	0.6625E-01	16	24
-1.265E 00	0.7950E-01	15	25
-1.400E 00	0.9540E-01	15	26
-1.450E 00	0.1145	14	27
-1.222E 00	0.1374	15	28
-2.965E-01	0.1648	17	29
-9.587E-01	0.1978	17	30
-1.180E 00	0.2374	16	31
-1.552E 00	0.2849	14	32
-2.021E 00	0.3418	12	33
-2.547E 00	0.4102	9	34
-3.063E 00	0.4922	7	35
2.780E 00	0.5907	34	36
2.277E 00	0.7098	32	37
1.567E 00	0.8506	28	38
7.841E-01	1.021	24	39
-2.266E-02	1.225	21	40
-9.249E-01	1.470	17	41
-1.665E 00	1.764	12	42
-2.817E 00	2.116	8	43
2.563E 00	2.540	33	44
1.807E 00	3.048	29	45

XMIN= -3.0000E 00 YMIN= -4.0000E 00
XMAX= 4.8398E-01 YMAX= 4.0000E 00

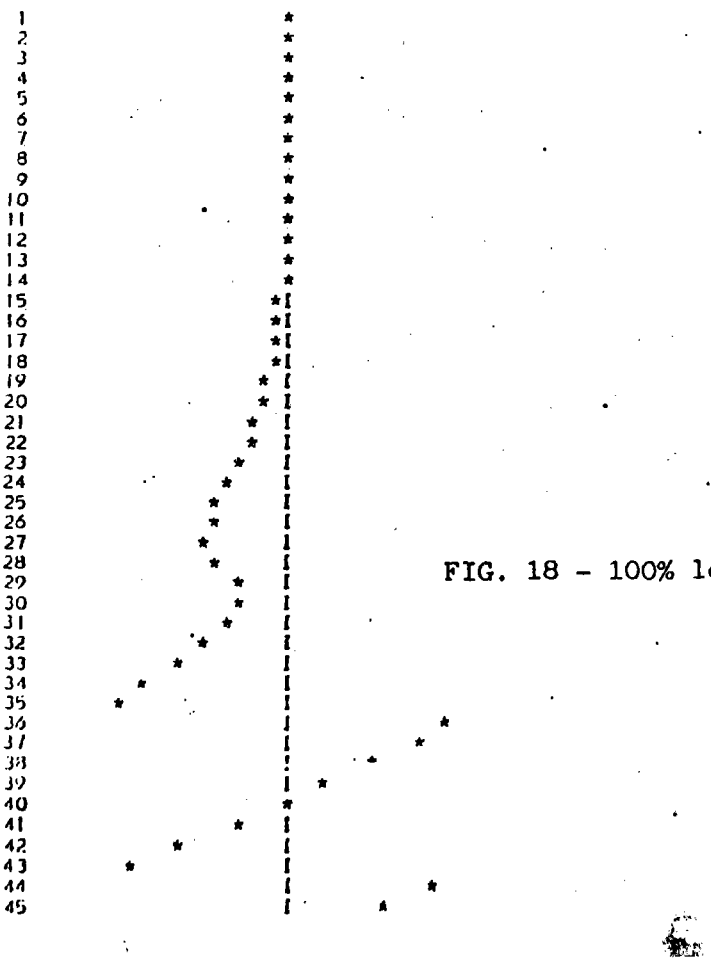

FIG. 18 - 100% load - $\Delta T_2 / \Delta V$

XMIN= -3.0000E 00 YMIN= 0.
XMAX= 4.8398E-01 YMAX= 2.0000E 00

Y	X	IY	IX
1.000E 00	0.1000E-02	20	1
1.000E 00	0.1300E-02	20	2
1.000E 00	0.1440E-02	20	3
1.000E 00	0.1728E-02	20	4
1.000E 00	0.2074E-02	20	5
1.000E 00	0.2488E-02	20	6
9.999E-01	0.2986E-02	20	7
9.999E-01	0.3583E-02	20	8
9.999E-01	0.4300E-02	20	9
9.998E-01	0.5160E-02	20	10
9.998E-01	0.6192E-02	20	11
9.997E-01	0.7430E-02	20	12
9.995E-01	0.8916E-02	20	13
9.993E-01	0.1070E-01	20	14
9.990E-01	0.1284E-01	20	15
9.985E-01	0.1541E-01	20	16
9.979E-01	0.1849E-01	20	17
9.970E-01	0.2219E-01	20	18
9.957E-01	0.2662E-01	20	19
9.938E-01	0.3195E-01	20	20
9.912E-01	0.3834E-01	20	21
9.876E-01	0.4601E-01	20	22
9.825E-01	0.5521E-01	20	23
9.755E-01	0.6625E-01	20	24
9.662E-01	0.7950E-01	19	25
9.539E-01	0.9540E-01	19	26
9.381E-01	0.1145	19	27
9.182E-01	0.1374	18	28
8.936E-01	0.1648	18	29
8.634E-01	0.1978	17	30
8.265E-01	0.2374	17	31
7.812E-01	0.2849	16	32
7.254E-01	0.3418	15	33
6.573E-01	0.4102	13	34
5.760E-01	0.4922	12	35
4.827E-01	0.5907	10	36
3.819E-01	0.7089	8	37
2.806E-01	0.8506	6	38
1.880E-01	1.021	4	39
1.125E-01	1.225	3	40
5.861E-02	1.470	2	41
2.589E-02	1.764	1	42
9.433E-03	2.116	1	43
2.755E-03	2.540	1	44
6.207E-04	3.048	1	45

FASE

XMIN= -3.0000E 00 YMIN= -4.0000E 00
XMAX= 4.8398E-01 YMAX= 4.0000E 00

Y	X	IY	IX
-6.810E-03	0.1000E-02	21	1
-8.149E-03	0.1200E-02	21	2
-9.783E-03	0.1440E-02	21	3
-1.175E-02	0.1728E-02	21	4
-1.409E-02	0.2074E-02	21	5
-1.691E-02	0.2484E-02	21	6
-2.029E-02	0.2986E-02	21	7
-2.434E-02	0.3583E-02	21	8
-2.921E-02	0.4300E-02	21	9
-3.505E-02	0.5160E-02	21	10
-4.206E-02	0.6192E-02	21	11
-5.047E-02	0.7430E-02	21	12
-6.056E-02	0.8916E-02	21	13
-7.266E-02	0.1070E-01	21	14
-8.718E-02	0.1284E-01	21	15
-1.046E-01	0.1541E-01	21	16
-1.255E-01	0.1849E-01	21	17
-1.505E-01	0.2219E-01	21	18
-1.804E-01	0.2662E-01	21	19
-2.162E-01	0.3195E-01	20	20
-2.591E-01	0.3834E-01	20	21
-3.102E-01	0.4601E-01	20	22
-3.711E-01	0.5521E-01	20	23
-4.435E-01	0.6625E-01	19	24
-5.293E-01	0.7950E-01	19	25
-6.308E-01	0.9540E-01	18	26
-7.505E-01	0.1145	18	27
-8.916E-01	0.1374	17	28
-1.058E 00	0.1648	16	29
-1.254E 00	0.1978	15	30
-1.486E 00	0.2374	14	31
-1.760E 00	0.2849	13	32
-2.084E 00	0.3418	11	33
-2.465E 00	0.4102	9	34
-2.910E 00	0.4922	7	35
2.454E 00	0.5907	34	36
2.264E 00	0.7089	32	37
1.591E 00	0.8506	28	38
8.361E-01	1.021	25	39
4.056E-03	1.225	21	40
-4.956E-01	1.470	17	41
-1.042E 00	1.764	13	42
-2.802E 00	2.116	8	43
2.563E 00	2.540	31	44
1.741E 00	3.048	29	45

FIG. 19 - 100% load $-\Delta T_1/\Delta V$

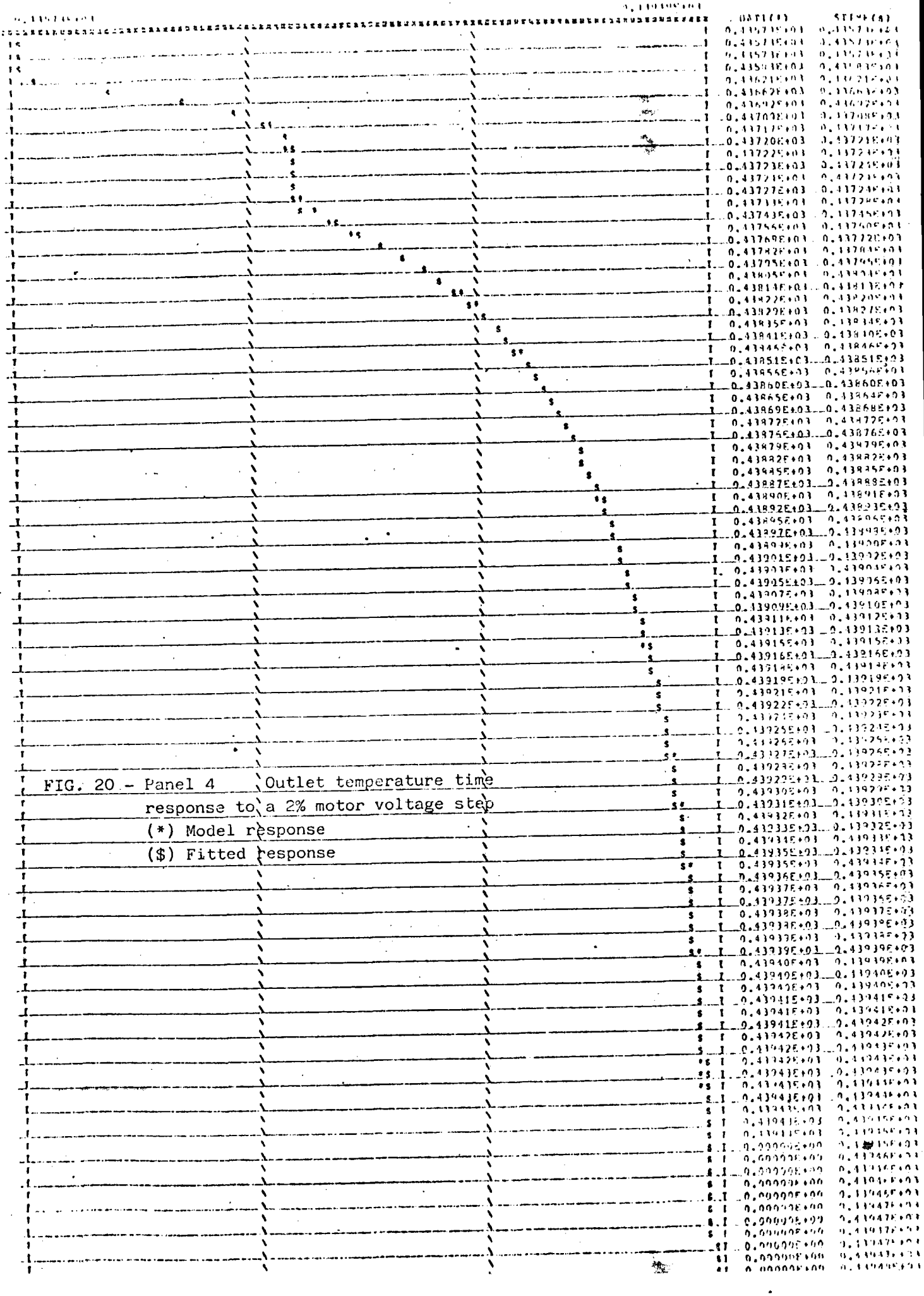

FIG. 20 - Panel 4 Outlet temperature time response to a 2% motor voltage step
(*) Model response
($) Fitted response

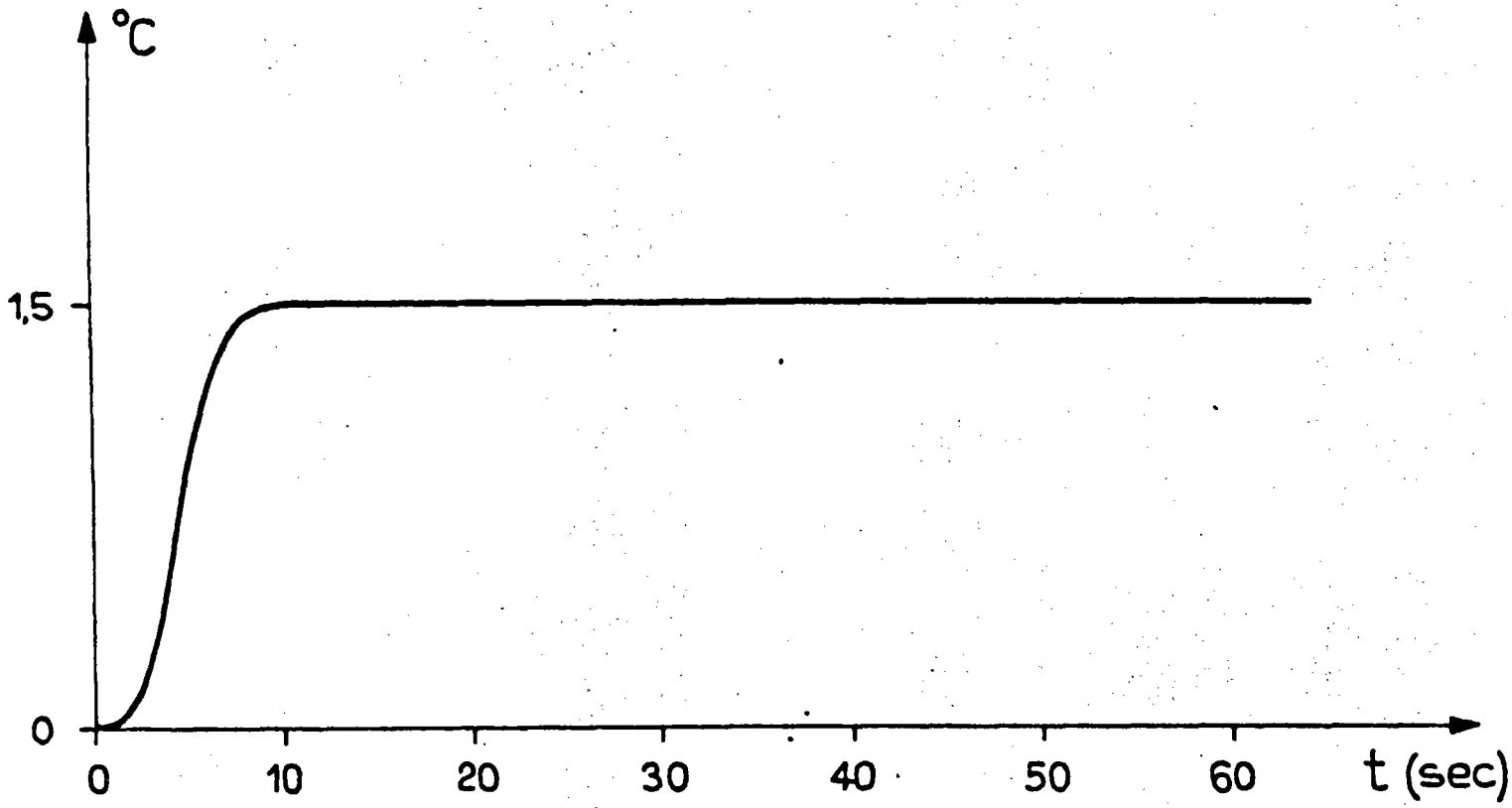

Fig. 21 - FIRST SYSTEM

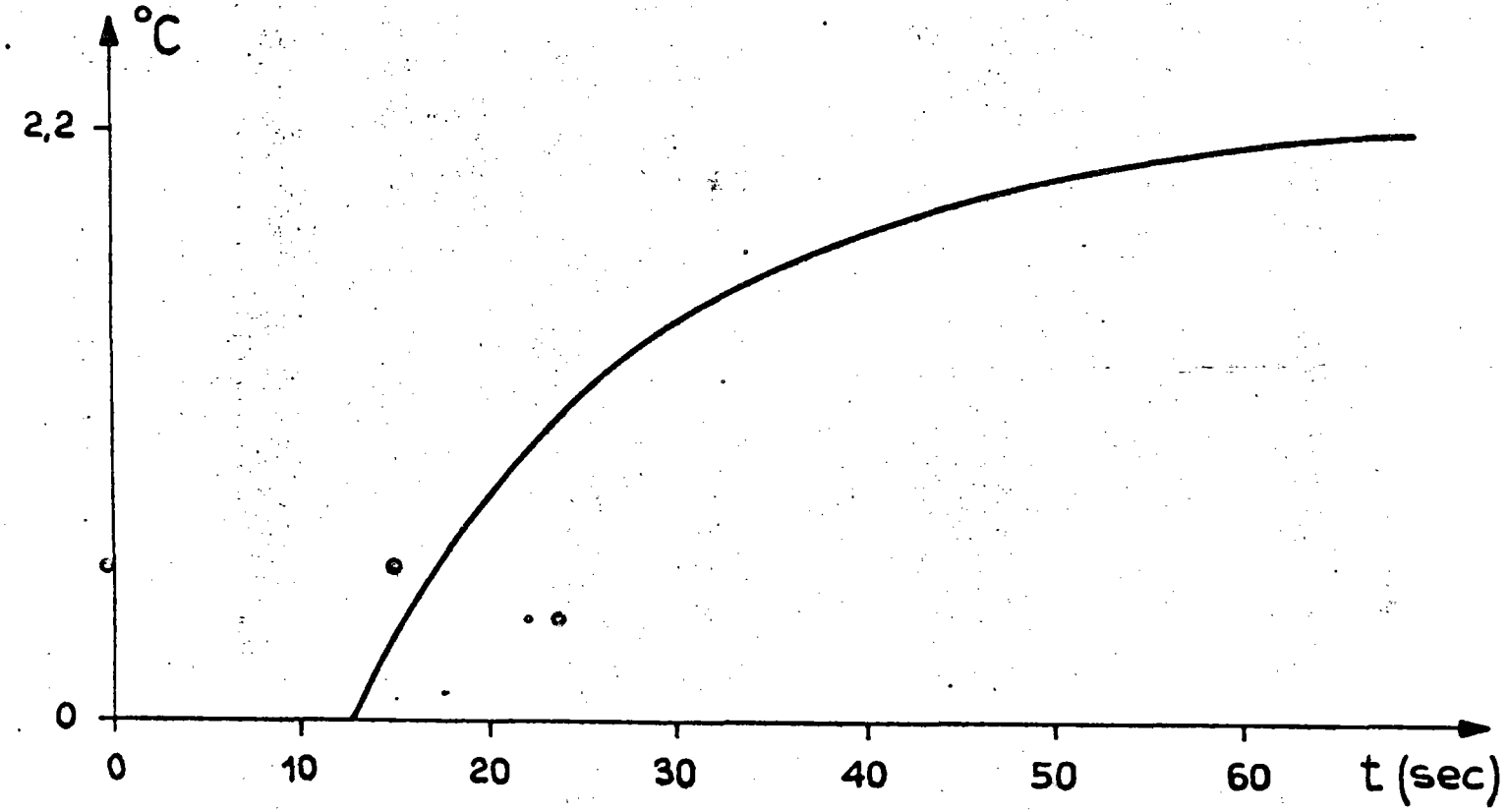

Fig. 22 - SECOND SYSTEM

XMIN= -3.0000E 00 YMIN= 0.
XMAX= 4.8398E-01 YMAX= 2.0000E 00

Y	X	IY	IX
1.000E 00	0.1000E-02	20	1
9.999E-01	0.1200E-02	20	2
9.997E-01	0.1440E-02	20	3
9.995E-01	0.1728E-02	20	4
9.992E-01	0.2074E-02	20	5
9.987E-01	0.2488E-02	20	6
9.980E-01	0.2986E-02	20	7
9.971E-01	0.3583E-02	20	8
9.957E-01	0.4300E-02	20	9
9.937E-01	0.5160E-02	20	10
9.909E-01	0.6192E-02	20	11
9.868E-01	0.7430E-02	20	12
9.811E-01	0.8916E-02	20	13
9.731E-01	0.1070E-01	19	14
9.620E-01	0.1284E-01	19	15
9.467E-01	0.1541E-01	19	16
9.263E-01	0.1849E-01	19	17
8.995E-01	0.2219E-01	18	18
8.655E-01	0.2662E-01	17	19
8.238E-01	0.3195E-01	17	20
7.750E-01	0.3834E-01	16	21
7.199E-01	0.4601E-01	15	22
6.601E-01	0.5521E-01	13	23
5.969E-01	0.6625E-01	12	24
5.310E-01	0.7950E-01	11	25
4.623E-01	0.9540E-01	10	26
3.904E-01	0.1145	8	27
3.163E-01	0.1374	7	28
2.445E-01	0.1648	5	29
1.903E-01	0.1978	4	30
1.827E-01	0.2374	4	31
2.287E-01	0.2849	5	32
2.959E-01	0.3418	6	33
3.532E-01	0.4102	7	34
3.763E-01	0.4922	8	35
3.448E-01	0.5907	7	36
2.528E-01	0.7088	5	37
1.505E-01	0.8506	3	38
1.696E-01	1.021	4	39
1.756E-01	1.225	4	40
7.788E-02	1.470	2	41
1.114E-01	1.764	3	42
4.367E-02	2.116	1	43
5.230E-02	2.540	2	44
5.058E-02	3.048	1	45

FASE

XMIN= -3.0000E 00 YMIN= -4.0000E 00
XMAX= 4.8398E-01 YMAX= 4.0000E 00

Y	X	IY	IX
-2.234E-02	0.1000E-02	21	1
-2.680E-02	0.1200E-02	21	2
-3.216E-02	0.1440E-02	21	3
-3.858E-02	0.1728E-02	21	4
-4.629E-02	0.2074E-02	21	5
-5.552E-02	0.2488E-02	21	6
-6.659E-02	0.2986E-02	21	7
-7.985E-02	0.3583E-02	21	8
-9.572E-02	0.4300E-02	21	9
-1.147E-01	0.5160E-02	21	10
-1.373E-01	0.6192E-02	21	11
-1.643E-01	0.7430E-02	21	12
-1.963E-01	0.8916E-02	21	13
-2.340E-01	0.1070E-01	20	14
-2.784E-01	0.1284E-01	20	15
-3.299E-01	0.1541E-01	20	16
-3.893E-01	0.1849E-01	20	17
-4.566E-01	0.2219E-01	19	18
-5.316E-01	0.2662E-01	19	19
-6.138E-01	0.3195E-01	19	20
-7.021E-01	0.3834E-01	18	21
-7.956E-01	0.4601E-01	18	22
-8.941E-01	0.5521E-01	17	23
-9.977E-01	0.6625E-01	17	24
-1.107E 000	0.7950E-01	16	25
-1.222E 000	0.9540E-01	16	26
-1.337E 000	0.1145	15	27
-1.436E 000	0.1374	14	28
-1.478E 000	0.1648	14	29
-1.382E 000	0.1978	15	30
-1.162E 000	0.2374	16	31
-1.107E 000	0.2849	16	32
-1.324E 000	0.3418	15	33
-1.736E 000	0.4102	13	34
-2.292E 000	0.4922	10	35
-2.960E 000	0.5907	7	36
2.616E 000	0.7088	33	37
2.193E 000	0.8506	31	38
1.909E 00	1.021	30	39
7.856E-01	1.225	24	40
-1.156E-01	1.470	21	41
-9.079E-01	1.764	17	42
-1.984E 00	2.116	12	43
2.484E 00	2.540	33	44
1.103E 00	3.048	26	45

FIG. 23 - 100% load $-\Delta T_4/\Delta V$ (identified)

XMIN= -3.0000E 00 YMIN= 6.4271E-12
XMAX= 4.8320E-01 YMAX= 2.0000E 00

Y	X		IY	IX
9.739E	0.1000E-02	00	19	1
9.627E	0.1200E-02	00	19	2
9.466E	0.1440E-02	00	19	3
9.244E	0.1728E-02	00	19	4
8.933E	0.2074E-02	00	18	5
8.506E	0.2488E-02	00	17	6
7.932E	0.2986E-02	00	16	7
7.187E	0.3583E-02	00	15	8
6.263E	0.4300E-02	00	13	9
5.186E	0.5160E-02	00	11	10
4.027E	0.6192E-02	00	8	11
2.857E	0.7430E-02	00	6	12
1.707E	0.8916E-02	00	4	13
1.216E	0.1070E-01	00	3	14
2.192E	0.1284E-01	00	5	15
2.684E	0.1541E-01	00	6	16
2.092E	0.1849E-01	00	5	17
2.159E	0.2219E-01	00	5	18
3.390E	0.2662E-01	00	7	19
3.825E	0.3195E-01	00	8	20
2.749E	0.3834E-01	00	6	21
1.973E	0.4601E-01	00	4	22
1.760E	0.5521E-01	00	4	23
1.621E	0.6625E-01	00	4	24
1.318E	0.7950E-01	00	3	25
9.975E	0.9540E-01	00	2	26
7.354E	0.1145	00	2	27
4.986E	0.1374	00	1	28
3.021E	0.1648	00	1	29
1.568E	0.1978	00	1	30
6.413E	0.2374	00	1	31
1.780E	0.2849	00	1	32
2.358E	0.3418	00	1	33
3.866E	0.4102	00	1	34
7.530E	0.4922	00	1	35
2.625E	0.5907	00	1	36
6.634E	0.7088	00	1	37
4.514E	0.8506	00	1	38
3.194E	1.021	00	1	39
1.907E	1.225	00	1	40
3.871E	1.470	00	1	41
2.407E	1.764	00	1	42
4.052E	2.116	00	1	43
5.705E	2.540	00	1	44
6.427E	3.048	00	1	45

FASE

XMIN= -3.0000E 00 YMIN= -3.8000E 00
XMAX= 4.8320E-01 YMAX= 4.2000E 00

Y	X		IY	IX
-2.974E	0.1000E-02	00	19	1
-3.552E	0.1200E-02	00	19	2
-4.256E	0.1440E-02	00	18	3
-5.080E	0.1728E-02	00	18	4
-6.049E	0.2074E-02	00	18	5
-7.176E	0.2488E-02	00	17	6
-8.469E	0.2986E-02	00	16	7
-9.916E	0.3583E-02	00	16	8
-1.147E	0.4300E-02	00	15	9
-1.304E	0.5160E-02	00	14	10
-1.447E	0.6192E-02	00	13	11
-1.551E	0.7430E-02	00	13	12
-1.505E	0.8916E-02	00	13	13
-7.903E	0.1070E-01	00	17	14
-9.531E	0.1284E-01	00	18	15
-9.121E	0.1541E-01	00	16	16
-1.124E	0.1849E-01	00	15	17
-8.861E	0.2219E-01	00	16	18
-1.115E	0.2662E-01	00	15	19
-1.800E	0.3195E-01	00	12	20
-2.397E	0.3834E-01	00	9	21
-2.660E	0.4601E-01	00	8	22
-2.963E	0.5521E-01	00	6	23
2.824E	0.6625E-01	00	33	24
2.190E	0.7950E-01	00	30	25
1.525E	0.9540E-01	00	27	26
7.564E	0.1145	00	23	27
-1.542E	0.1374	00	20	28
-1.209E	0.1648	00	15	29
-2.440E	0.1978	00	9	30
2.406E	0.2374	00	31	31
7.131E	0.2849	00	23	32
-1.470E	0.3418	00	13	33
1.251E	0.4102	00	26	34
-1.952E	0.4922	00	20	35
-7.175E	0.5907	00	17	36
-1.220E	0.7088	00	15	37
-1.617E	0.8505	00	13	38
-3.001E	1.021	00	6	39
1.089E	1.225	00	25	40
-2.098E	1.470	00	10	41
3.072E	1.764	00	21	42
3.070E	2.116	00	34	43
7.239E	2.540	00	23	44
-1.366E	3.048	00	14	45

FIG. 24 - 10% load - $\Delta T_5/\Delta V$

XMIN= -3.0000E 00 YMIN= 0.
XMAX= 4.8398E-01 YMAX= 2.0000E 00

Y	X	IY	IX
9.989E-01	0.1000E-02	20	1
9.984E-01	0.1200E-02	20	2
9.977E-01	0.1440E-02	20	3
9.966E-01	0.1728E-02	20	4
9.952E-01	0.2074E-02	20	5
9.930E-01	0.2488E-02	20	6
9.900E-01	0.2986E-02	20	7
9.856E-01	0.3583E-02	20	8
9.794E-01	0.4300E-02	20	9
9.705E-01	0.5160E-02	19	10
9.578E-01	0.6192E-02	19	11
9.400E-01	0.7430E-02	19	12
9.150E-01	0.8916E-02	18	13
8.805E-01	0.1070E-01	18	14
8.336E-01	0.1284E-01	17	15
7.718E-01	0.1541E-01	16	16
6.931E-01	0.1849E-01	14	17
5.982E-01	0.2219E-01	12	18
4.915E-01	0.2662E-01	10	19
3.807E-01	0.3195E-01	8	20
2.737E-01	0.3834E-01	6	21
1.828E-01	0.4601E-01	4	22
1.609E-01	0.5521E-01	4	23
2.150E-01	0.6625E-01	5	24
2.436E-01	0.7950E-01	5	25
2.277E-01	0.9540E-01	5	26
2.265E-01	0.1145	5	27
2.620E-01	0.1374	6	28
2.899E-01	0.1648	6	29
2.700E-01	0.1978	6	30
2.168E-01	0.2374	5	31
1.693E-01	0.2849	4	32
1.383E-01	0.3418	3	33
1.129E-01	0.4102	3	34
8.200E-02	0.4922	2	35
5.203E-02	0.5907	2	36
3.019E-02	0.7088	1	37
1.478E-02	0.8506	1	38
5.900E-03	1.021	1	39
1.809E-03	1.225	1	40
3.994E-04	1.470	1	41
6.378E-05	1.764	1	42
1.277E-05	2.116	1	43
4.021E-06	2.540	1	44
1.304E-06	3.043	1	45

FASE

XMIN= -3.0000E 00 YMIN= -3.8000E 00
XMAX= 4.8398E-01 YMAX= 4.2000E 00

Y	X	IY	IX
-6.036E-02	0.1000E-02	20	1
-7.243E-02	0.1200E-02	20	2
-8.690E-02	0.1440E-02	20	3
-1.042E-01	0.1728E-02	20	4
-1.250E-01	0.2074E-02	20	5
-1.500E-01	0.2488E-02	20	6
-1.798E-01	0.2986E-02	20	7
-2.156E-01	0.3583E-02	19	8
-2.583E-01	0.4300E-02	19	9
-3.092E-01	0.5160E-02	19	10
-3.698E-01	0.6192E-02	19	11
-4.417E-01	0.7430E-02	18	12
-5.263E-01	0.8916E-02	18	13
-6.253E-01	0.1070E-01	17	14
-7.394E-01	0.1284E-01	17	15
-8.684E-01	0.1541E-01	16	16
-1.010E 00	0.1849E-01	16	17
-1.157E 00	0.2219E-01	15	18
-1.298E 00	0.2662E-01	14	19
-1.414E 00	0.3195E-01	14	20
-1.469E 00	0.3834E-01	13	21
-1.341E 00	0.4601E-01	14	22
-8.979E-01	0.5521E-01	16	23
-7.695E-01	0.6625E-01	17	24
-9.620E-01	0.7950E-01	16	25
-1.124E 00	0.9540E-01	15	26
-1.173E 00	0.1145	15	27
-1.346E 00	0.1374	14	28
-1.744E 00	0.1648	12	29
-2.254E 00	0.1978	10	30
-2.743E 00	0.2374	7	31
3.112E 00	0.2849	35	32
2.648E 00	0.3418	32	33
2.046E 00	0.4102	29	34
1.303E 00	0.4922	26	35
5.062E-01	0.5907	22	36
-3.749E-01	0.7088	19	37
-1.351E 00	0.8506	14	38
-2.407E 00	1.021	9	39
2.803E 00	1.225	33	40
1.817E 00	1.470	28	41
1.189E 00	1.764	25	42
1.153E 00	2.116	25	43
9.947E-01	2.540	24	44
6.779E-01	3.043	23	45

FIG. 25 – 50% load $-\Delta T_5/\Delta V$

9.0. DYNAMIC ANALYSIS AND CONTROL

Foreword

In the following paragraphs the planning of the job, the tools up to now carried out and the results obtained are briefly presented.

INTRODUCTION

The dynamic simulation of the receiver and of the related primary sodium circuit allows the most critical conditions of this part of the plant to be tested previous to the plant operation.

Then the aims of the simulation are:

i. to supply a suitable tool for receiver outlet sodium temperature control system design;

ii. to study dynamic behaviour in normal operating conditions such as start-up and cloud passages;

iii. to determine the transient thermal field in emergency operating conditions, as pump failure or control system failure, so that the computation of thermal stresses on the receiver can be obtained.

The temperature distribution in the receiver metal and of the sodium is determined.

Two different time scales of the transient phenomena with two corresponding models are being considered.

a) Slow phenomena due to energy transport and storage in sodium and metal (the energy diffusion in the receiver pipes metal, can be simplified because the time scale of this phenomena is relatively fast (see point b)).

b) Fast phenomena related to the energy diffusion in radial and Azimuthal direction of a pipe section.

The model describing fast phenomena, obtained with an analitical-finite differences method is presented in Ref. /1/.

Here after we present the model describing slow transient phenomena.

MODEL FEATURES AND GENERAL ASSUMPTIONS

The dynamic analysis of the receiver is being performed according to the following criteria:

- The whole receiver is divided into subsystems.
- Each subsystem is represented by an associated set of differential and/or algebraic equations.
- The boundary conditions for every set of differential equations are chosen in order to be consistent with the physical coupling among the subsystems.

The subsystems considered up till now are:

- The receiver feed pump
- The riser and downcomer pipes
- The radiated pipes of each panel of receiver
- The headers at the inlet and the outlet of each radiated panel
- The connecting pipes among the panels.

The remaining subsystems (hot and cold storages, valves and temperature controllers) will be included in the model in the next future.

A scheme of the simulated loop is shown in fig. 1.

For each of the five heated panels an average pipe is considered, with its associated incident power and its inlet-outlet headers; the non radiated connecting pipes 1-1i, 1u-2i, 2u-3i, 3u-4i, 4u-5i and 5u-b are also considered.

The riser and downcomer pipes have been included only for purposes of sodium flow and pressure drop caldulation but their thermal behaviour has not been simulated. It is considered that their temperature will vary slowly in time because the storage tanks will almost completely decouple the primary and secondary loop.

Each heated pipe and coupling pipe has been divided into a suitable number of nodes (15 nodes for radiated pipes and 10 nodes for connecting pipes).

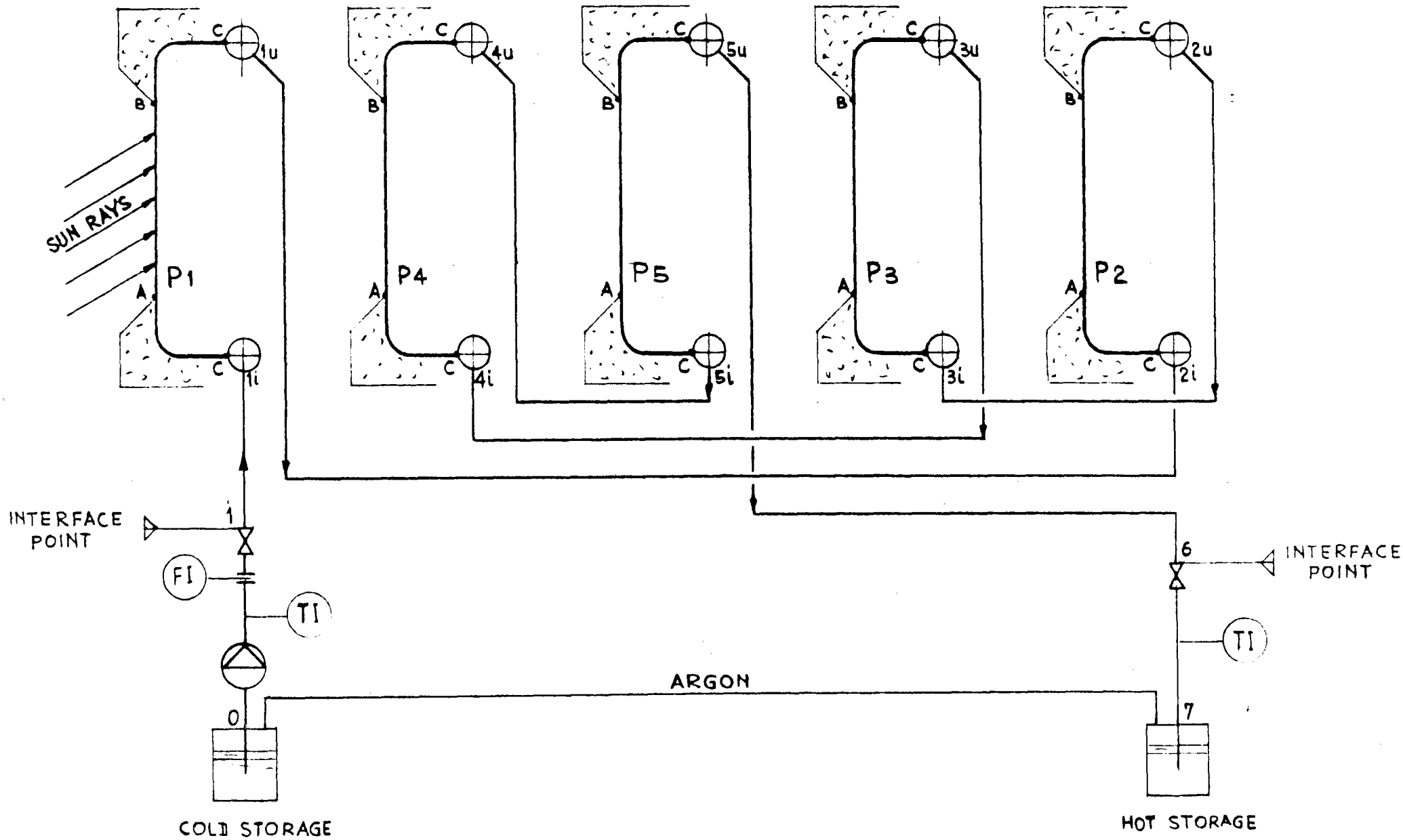
SUN RAYS
P1
P2
P3
P4
P5
A
B
C
1u
1i
2u
2i
3u
3i
4u
4i
5u
5i
INTERFACE POINT
1
FI
TI
0
ARGON
6
INTERFACE POINT
TI
7
COLD STORAGE
HOT STORAGE

PIPE SEGMENT	SOLAR FLUX	PIPE I.D. mm	PIPE LENGTH m	PIPE THK. mm	PIPE ROUGH. mm		NOTE
$0 \rightarrow 1$	/	88.9	85	4.78	$5 \cdot 10^{-3}$		
$1 \rightarrow 1i$	/	88.9	1.5	4.78	"		
INLET HEADER P_1	/	168.3	0.55	7.11	0.1		
$C \rightarrow A$	/	12	0.7	1	$1.25 \cdot 10^{-3}$		39 PIPES
$A \rightarrow B$	YES	12	3	1	"		"
$B \rightarrow C$	/	12	0.7	1	"		"
OUTLET HEADER P_1	/	168.3	0.55	7.11	0.1		
$1u \rightarrow 2i$	/	88.9	7.55	4.78	$5 \cdot 10^{-3}$		
INLET HEADER P_2	/	168.3	0.55	7.11	0.1		
$C \rightarrow A$	/	12	0.7	1	$1.25 \cdot 10^{-3}$		39 PIPES
$A \rightarrow B$	YES	12	3	1	"		"
$B \rightarrow C$	/	12	0.7	1	"		"
OUTLET HEADER P_2	/	168.3	0.55	7.11	0.1		
$2u \rightarrow 3i$	/	88.9	4.97	4.78	$5 \cdot 10^{-3}$		
INLET HEADER P_3	/	168.3	0.55	7.11	0.1		
$C \rightarrow A$	/	12	0.7	1	$1.25 \cdot 10^{-3}$		39 PIPES
$A \rightarrow B$	YES	12	3	1	"		"
$B \rightarrow C$	/	12	0.7	1	"		"
OUTLET HEADER P_3	/	168.3	0.55	7.11	0.1		
$3u \rightarrow 4i$	/	88.9	5.50	4.78	$5 \cdot 10^{-3}$		
INLET HEADER P_4	/	168.3	0.55	7.11	0.1		
$C \rightarrow A$	/	12	0.7	1	$1.25 \cdot 10^{-3}$		39 PIPES
$A \rightarrow B$	YES	12	3	1	"		"
$B \rightarrow C$	/	12	0.7	1	"		"
OUTLET HEADER P_4	/	168.3	0.55	7.11	0.1		
$4u \rightarrow 5i$	/	88.9	5.65	4.78	$5 \cdot 10^{-3}$		
INLET HEADER P_5	/	168.3	0.55	7.11	0.1		
$C \rightarrow A$	/	12	0.7	1	$1.25 \cdot 10^{-3}$		39 PIPES
$A \rightarrow B$	YES	12	3	1	"		"
$B \rightarrow C$	/	12	0.7	1	"		"
OUTLET HEADER P_5	/	168.3	0.55	7.11	0.1		
$5u \rightarrow 6$	/	88.9	3.65	4.78	$5 \cdot 10^{-3}$		
$6 \rightarrow 7$	/	88.9	85	4.78	$5 \cdot 10^{-3}$		

For every node, the average metal and sodium temperatures, together with their derivatives, are evaluated at every time integration step. The partial derivative energy equations for a one-dimensional system are used for this purpose (see paragraph 2 for more detailed description). The incident power on the radiated pipes (from which radiation, reflection and convection lorses are subtracted) is a function of the abscissa X and time and can be varied at any instant to simulate the most typical disturbances (I;e. cloud passages).

The sodium properties are considered as temperature functions and vary with time and space.

The headers have been considered as a single lump in which a perfect mixing is assumed. The total sodium flow is considered only a function of time and not of space (uncompressible flow). It is calculated, together with its derivative, by a momentum equation for the whole loop. An equal sodium flow is assumed in each heated pipe (total flow divided by the number of pipes in a panel).

SPECIFIC EQUATIONS

A) Thermal

The same equations hold for radiated pipes and non radiated pipes; in the last the incident power is set to zero.

The energy equation for the pipe metal is:

$$C_m A_m \rho_m \frac{\partial T_m(x,t)}{\partial t} = Q(x,t) - \gamma\omega\left[T_m(x,t) - T(x,t)\right] \qquad (1)$$

The energy equation for the sodium is given by:

$$CA\rho \frac{\partial T(x,t)}{\partial t} + CW\frac{\partial T(x,t)}{\partial x} = \gamma\omega\left(T_m(x,t) - T(x,t)\right) \qquad (2)$$

where

x = tube axial coordinate

t = time

C_m = specific heat capacity of metal

A_m = pipe metal cross section

A = sodium flow cross section

C = specific heat of sodium

ρ_m, ρ = metal and sodium density, respectively

W = sodium flow

ω = pipe inner perimeter

γ = metal to sodium heat transfer coefficient

Q = absorbed power per unit lenght

T_m, T = metal and sodium temperatures, respectively.

As it can be seen from equation (2), the axial energy diffusion term has been neglected.

The following relations are used for sodium properties calculation:

$$C = 1436.715 - 0.5805379.T + 4.627274.10^{-4}T^2$$

$$\rho = 950.0483 - 0.2297537.T - 14.6045.10^{-6}T^2$$

$$\gamma = \left[5 + 0.025\ (Re \times Pr)^{0.8}\right]\frac{\lambda}{D}$$

where

λ = sodium conductivity

D = Pipe internal diameter

$$\lambda = 92.951 - 5.8087.10^{-2}T$$

For the headers the energy equations, according to the "perfect mixing" assumption, have been written as follows:

$$M_m C_m \frac{dT_{mc}}{dt} = -\gamma S_i (T_{mc} - T_{uc}) \qquad \text{(metal)} \qquad (3)$$

$$\rho V_c \frac{dT_{uc}}{dt} = \gamma S_i (T_{mc} - T_{uc}) + W(h_{ic} - h_{uc}) \quad \text{(sodium)} \quad (4)$$

where:

M_m = mass of header metal

S_i = internal header surface

T_{mc} = metal temperature

T_{uc} = sodium outlet temperature

V_c = header inner volume

h_{ic} = sodium inlet enthalpy

h_{uc} = sodium outlet enthalpy.

The metal to sodium heat transfer coefficient has been calculated assuming an average flow in the header given by approximately a fourth of the total flow.

B) Hydraulics

Sodium flow is calculated by means of a momentum balance applied to the whole loop. We have started with the general equation, given by:

$$\rho A \frac{\partial u}{\partial t} + \rho A u \frac{\partial u}{\partial x} + \rho A g + A \frac{\partial P}{\partial x} = -\frac{f}{D} \rho A \frac{u^2}{2} \qquad (5)$$

where

u = sodium velocity

g = gravity acceleration

P = pressure

f = friction coefficient

D = inner diameter.

The other symbols have the same meaning already stated above.

We can integrate equation (5) between two coordinates X_1 and X_2 (the initial and final coordinate of a single pipe for instance) and make the following symplifying assumtpions:

- sodium density ρ and velocity u are not a space function between X_1 and X_2 and are only function of time,
- the flow $W = \rho A u$ is not a function of X but only of time.

Thus, we obtain:

$$(x_2 - x_1)\frac{dW}{dt} + \rho A g (x_1 - x_2) + A[P(x_2) - P(x_1)] = -\frac{f}{D}\frac{W^2}{2\rho A}(x_2 - x_1)$$

Writing this equation for every pipe of the loop and summing the equations, we obtain:

$$\sum_i \frac{L_i}{A_i}\frac{dw_i}{dt} = \Delta P + g\sum_i \rho_i L_i - \sum_i \frac{f_i}{D_i}\frac{w_i^2 L_i}{2\rho_i A_i}$$

where ΔP is the pump head, L_i the lenght of every pipe segment and the subscript i refers to the various pipes.

Letting $w_i = r_i W$ with $r_i = 1$ for riser, downcomers and coupling pipes and $r_i = 1/n$ for the heated pipes (n=41, the number of pipes for each panel) we finally obtain:

$$\frac{dW}{dt}\sum_i \frac{L_i r_i}{A_i} = \Delta P + g\sum_i \rho_i L_i - W^2 \sum_i \frac{f_i}{D_i}\frac{L_i}{2\rho_i A_i} \qquad (6)$$

The expression of the pump head has been deduced by the pump characteristics as a function of sodium flow and normalized angular speed Ω/Ω_o (Ω_o = 314.159 rad/s corresponding to 3000 r.p.m.):

$$\Delta P = a\frac{W^2}{\rho} + b\rho\left(\frac{\Omega}{\Omega_o}\right)^2$$

The angular velocity is calculated by:

$$J\frac{d\Omega}{dt} = Cm - \frac{W\Delta P}{\eta\rho\Omega}$$

where

J = moment of hynertia of pump and associated servomotor

Cm = motor torque

η = pump efficiency

The motor torque is supposed to be a function of armature current Ia and speed: $Cm = f(Ia, \Omega)$

The exact knowledge of the type of motor employed and its characteristics will allow to obtain a definitive expression for motor torque.

NUMERICAL TREATMENT

The equation system describing receiver and primary loop thermoidraulic is solved with a finite-differences numerical method.

The distributed parameter energy equations, for a heated or a connecting pipe, was discretized with a scheme semi-implicit in time and space, in detail described in appendix 1.

We have found that such a scheme is convergent and its stability region is very broad.

The problem considered deals with temperature wave propagation, so an accurate solution requires a large number of nodes and consequently a proportionally small time integration step is needed for good transient accuracy.

The number of nodes was chosen to accurately match, in a wide frequency range, numerically evaluated responses and analytical responses.

The last was obtained directly from linearized partial differential equation, with uniform heat flux distribution, by Laplace- transform techniques.

Time integration step lenght was analitically evaluated on the basis of single node time constants magnitude.

The momentum equation for the loop, the pump and motor equations, as well as the lumped parameters energy equations for the headers were solved by an explicit method (Euler).

This was deemed the most convenient since the time step lenght, which is fixed by the integration of the distributed parameter equations, is small enough to assure stability and adequate accuracy.

TEMPERATURE CONTROL

A preliminary study of outlet sodium temperature regulation was performed, using standard PID or more general controllers with a larger number of poles and zeros.

The analyzed situation was the following:

- a single pipe segment, with the same geometrical characteristics as the receiver heated pipes;
- sodium flow rate used as control variable;
- tree different types of heat flux distribution Q (see fig. 2)
  a) most of radiation impinging on the first part of the pipe
  b) uniform radiation
  c) most of radiation impinging on the second part of the pipe

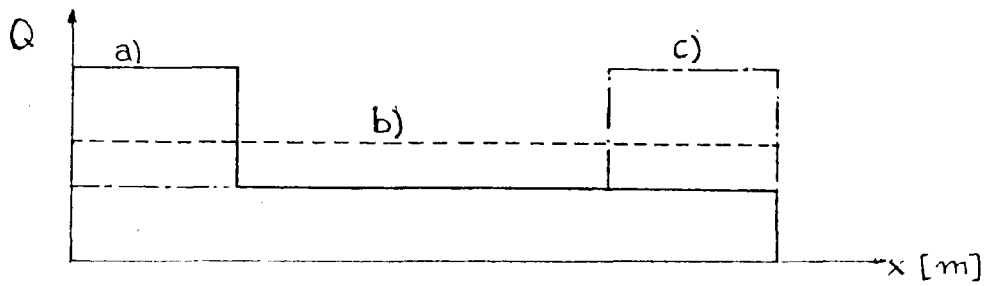

Fig. 2 - Heat flux distribution along the pipe.

The main results of the preliminary study were that:

1) The thermal power distribution strongly affects receiver dynamics and, consequently, controlled system performances.
   Case c) proved to be the most favourable, and case a) viceversa, was the most unfavourable, because the negative effects on temperature dynamics due to transport delay and other non minimal phase phenomena were strongly relevant in it.
   As well known, heat flux distribution of type c) is also preferable for static efficiency reasons and, viceversa, unpleasant with regard to thermal stresses.

In this way the need of a joint design for process and control system is pointed out.

2) To achieve a good improvement of controlled system performances, more sophisticated control structures seem desirable which, for instance, make use of intermediate feedback and feedforward actions, and of load varying parameter regulators (see ref. 2).

The future work will take into account the above mentioned points.

RESULTS

The first transient examined using the model are: a 10% step change in incident flux and a -10% step variation in pump motor voltage, which causes a corresponding decrease in sodium flow.
For each of the two transients, the following output variables are plotted as a function of time:

1) Panel 1 Sodium outlet temperature, together with header H2 sodium outlet temperature and connecting pipe 1u-2i;
2) Panel 2 sodium outlet temperature, together with header H4 and connecting pipe 2u-3i sodium outlet temperature;
3) Panel 3 sodium outlet temperature;
4) Panel 4 sodium outlet temperature;
5) Panel 5 sodium outlet temperature;
6) sodium flow.

Other output variables could have been plotted too, as for instance the metal and sodium temperature in any node of the radiated and connecting pipes, pumps speed and head, incident flux. It is also possible to plot some variables as a function of space for any given instant of time (metal and sodium temperatures along a pipe and incident power).

Diagrams 1) and 2) were generated to show the non negligible lag caused by the headers and connecting pipes on the sodium temperature at the end of a radiated pipe.

This will influence the control system design.

For both the transients examined the time of the input step variation is at t= 1 sec.

As it can be seen from diagrams 1a, 2a, 3a, 4a, 5a and 1b; 2b, 3b, 4b, 5b, the temperature at the outlet of the first and second panel vary of a low quantity due to the low thermal flux, while the outlet temperatures of the other panels are subjected to higher variations. The speed of variation, however, is high for the first panel outlet temperature; the other temperatures experience an initial fast variation, due to the effect of flow or flux variation on the associated panel, followed by a flat zone, after which a new temperature rise follows, due to the arrival of a wave coming from the preceding panels.

APPENDIX

Numerical integration of the one-dimension energy equation for sodium and metal

The integration is performed by means of a finite difference method.

The equations are:

$$\tau_m \frac{\partial T_m(x,t)}{\partial t} = Q(x,t) - h\left[T_m(x,t) - T(x,t)\right]$$

$$\tau \frac{\partial T(x,t)}{\partial t} + \tau_x \frac{\partial T(x,t)}{\partial t} = h\left[T_m(x,t) - T(x,t)\right]$$

The solution is to be obtained in the nodal points of a mesh by the lines $t = n\Delta t$, $x = J\Delta x$

where the symbol P_j^n means the couple of temperatures $\left(T(x=j\Delta x, t=n\Delta t), T_m(x=j\Delta x, t=n\Delta t)\right)$

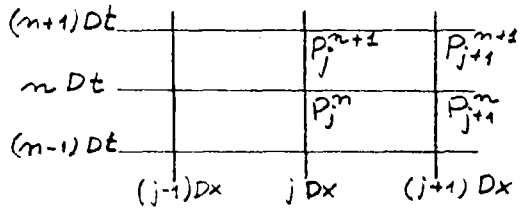

The equations were first discretized with respect to time using a semi-implicit scheme, where the computation of the time derivative in the point $(x,(n+1)\Delta t)$ is performed by considering constant in every time step coefficients τ_m, τ, τ_x, h which are evaluated at $(x, n\Delta t)$.

Thus, we obtained:

$$\tau_m \frac{\Delta_t T_{mx}^n}{\Delta t} = Q(x,n) - h\left[T_m(x,n) + \varepsilon \Delta_t T_{mx}^n - T(x,n) - \varepsilon \Delta t T_x^n\right]$$

$$\tau \frac{\Delta_t T_x^n}{\Delta t} + \tau_x \frac{d}{dx}\left[T(x,n) + \varepsilon \Delta_t T_x^n\right] = h\left[T_m(x,n) + \varepsilon \Delta_t T_{mx}^n - T(x,n) - \varepsilon \Delta_t\right.$$

Where $\Delta_t T_{mx}^n \triangleq T_m(x,n+1) - T_m(x,n)$

$\Delta_t T_x^n \triangleq T(x,n+1) - T(x,n)$; $0 \le \varepsilon \le 1$

This system of two equations in the two variables $\Delta_t T_x^n$, $\Delta_t T_{mx}^n$ was solved by sostitution, eliminating ΔT_{mx}^n from the second equation.

The equation so obtained was:

$$\frac{d}{dx}\left(T_x^n + \varepsilon \Delta_t T_x^n\right) = f\left(T_x^n, T_{mx}^n, \Delta_t T_x^n\right)$$

and was discretized with respect to space coordinate x by means of a semi-implicit scheme:

$$\frac{T_{j+1}^n + \varepsilon \Delta_t T_{j+1}^n - T_j^n - \varepsilon \Delta_t T_j^n}{Dx} = (1-\alpha) f\left(T_j^n, T_{mj}^n, \Delta_t T_j^n\right) + \alpha f\left(T_{j+1}^n, T_{mj+1}^n, \Delta_t T_{j+1}^n\right)$$

Again, by considering constant the coefficients τ_m, τ, τ_x, h between x_j and x_{j+1} and calculating them at (jDx, nDt) a linear equation was obtained in the unknown variable $\Delta_t T_{j+1}^n$ which can be written as a function of the terms P_j^n, P_{j+1}^n; these are known or calculated at the preceding time or space step. From the metal energy equation discretized with respect to time the unknown variable $\Delta_t T_{mx}^n$ is then evaluated at $x = (j+1)Dx$

REFERENCES

/1/ A. Macchi, "CILL2D: Programma per il calcolo del campo termico in sezioni piane circolari con condizioni al contorno non simmetriche utilizzando un metodo misto analitico - differenze finite" Internal ENEL Report N. 740/427 - 1, february 1980.

/2/ A. Siniscalchi, R. Squatiti , "Controllo di temperatura in un ricevitore solare", Thesis, November 1980.

/3/ C. Maffezzoni, F. Parigi, "Eurelios solar power plant: dynamic analysis and control system design", ENEL internal report 340/120-1.

/4/ A. Leonard Gould - "Chemical process control - Theory and Application", Addison Wesley Publishing Company, 1969.

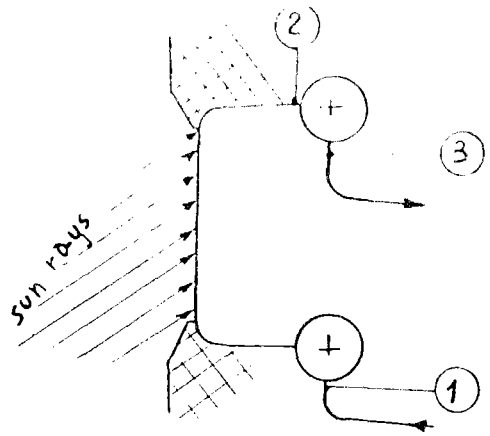

OPEN LOOP TRANSIENT

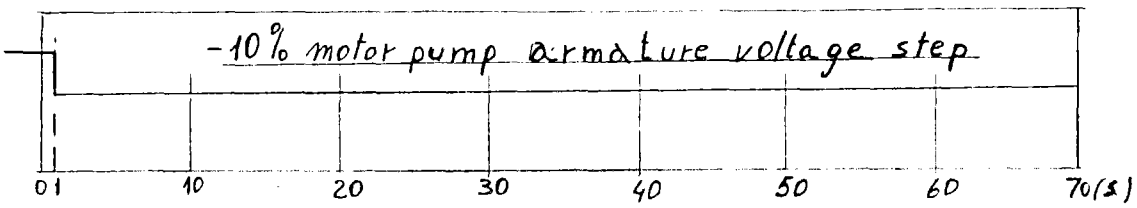

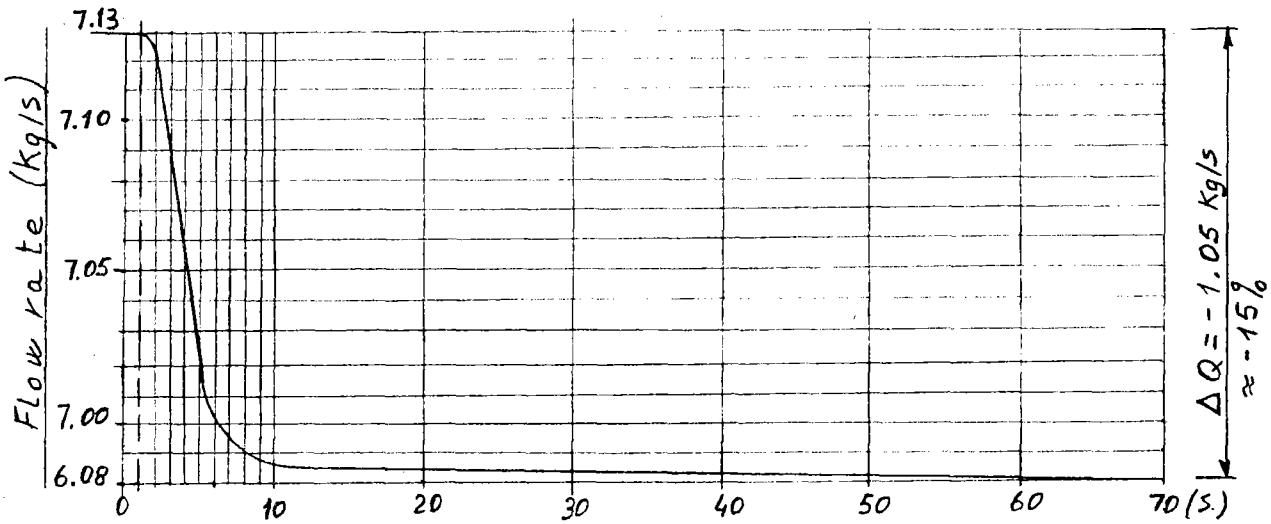

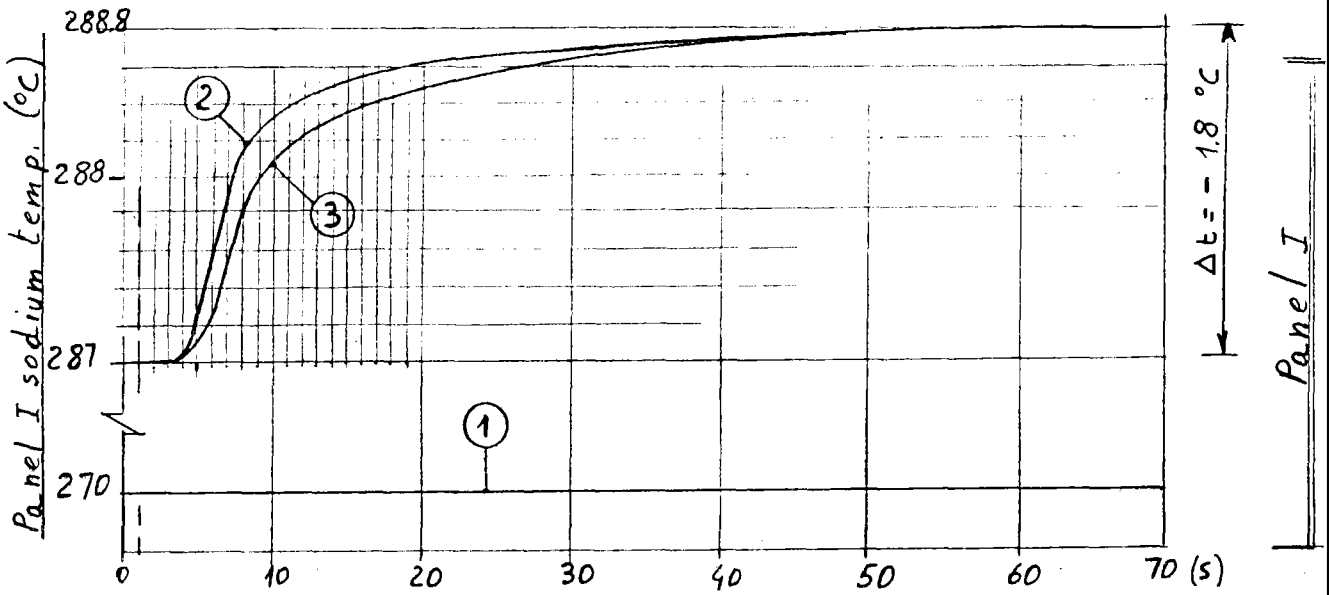

FIG. 9.1 - 10% m.p. armature voltage step / Receiver flow transient
Panel I sodium temp. transient

Fig. 9.2 - 10% M.P. armature voltage step
Receiver flow transient panels II - III sodium
temperature transient

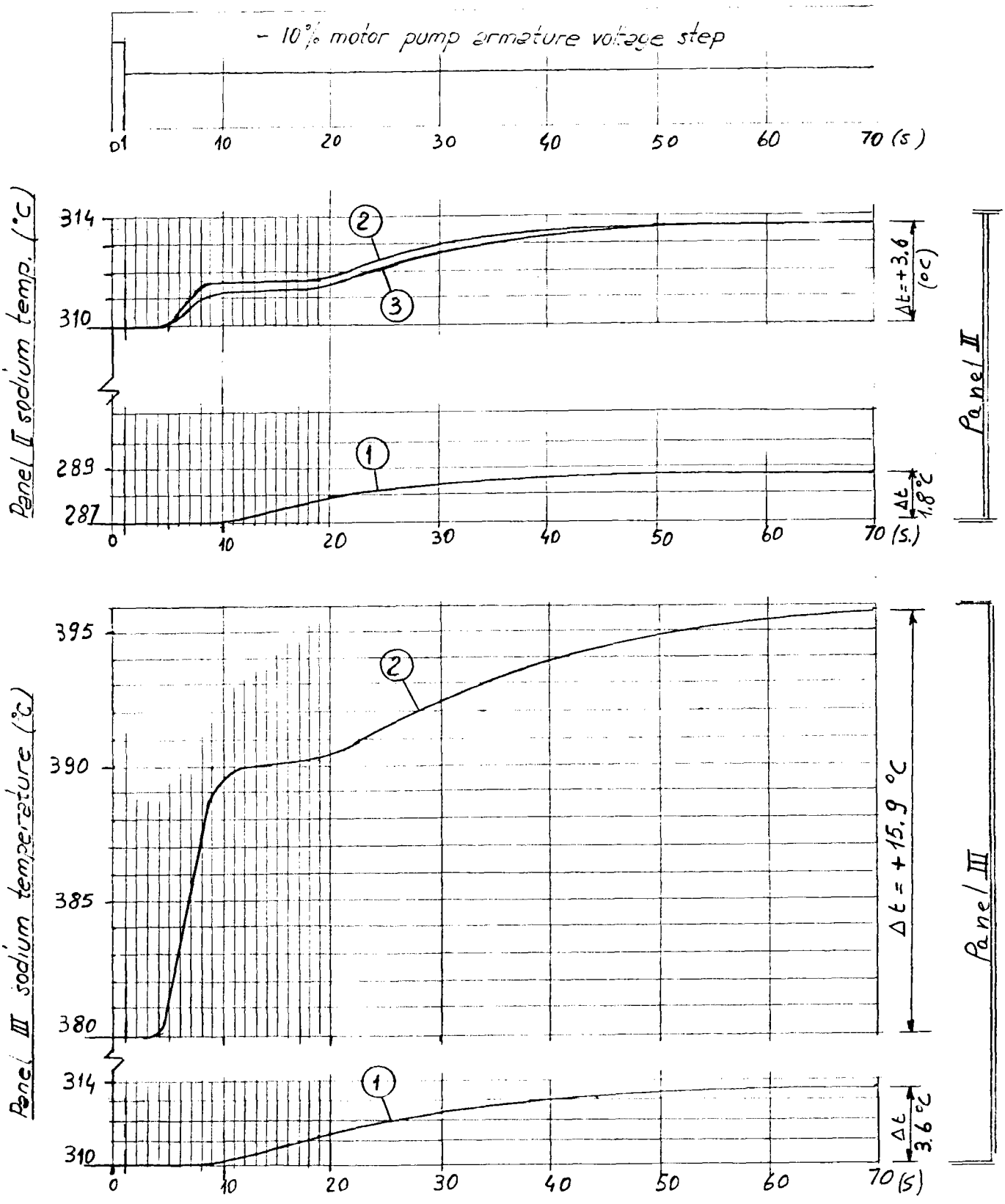

Fig. 9.3 - 10% M.P. armature voltage step
Receiver flow transient panels IV - V sodium
temperature transient

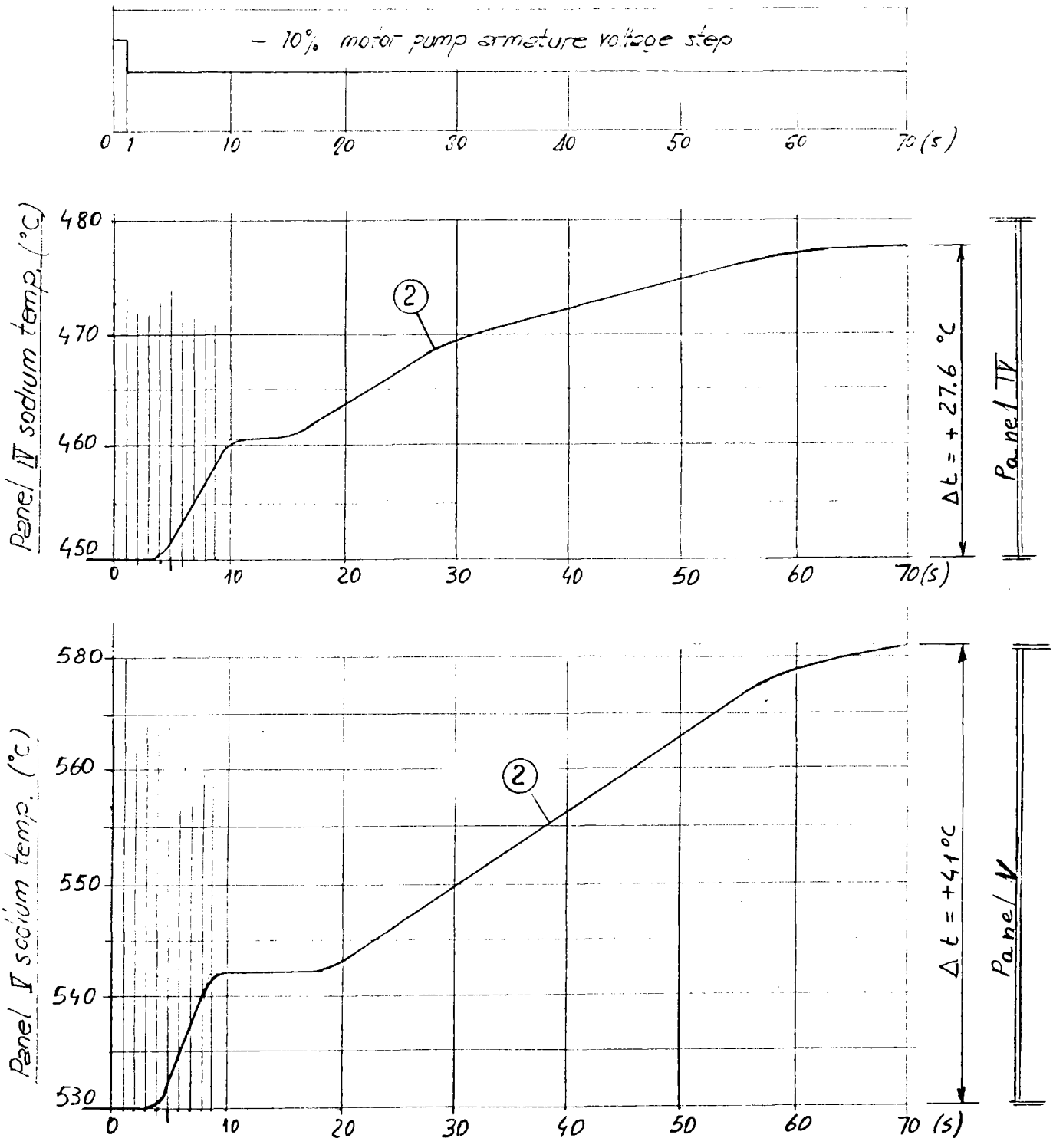

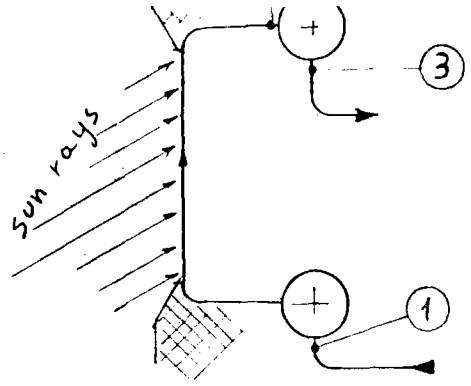

OPEN LOOP TRANSIENT

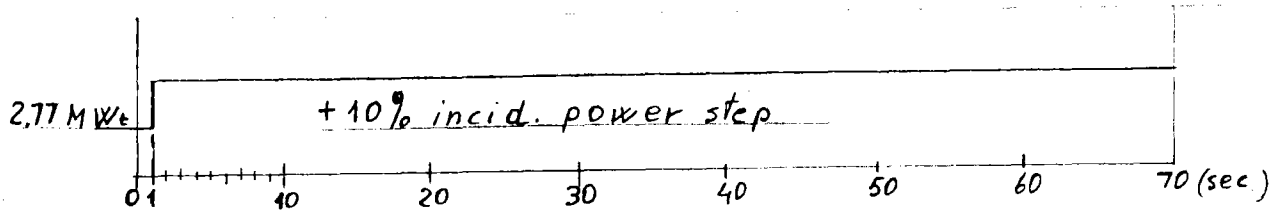

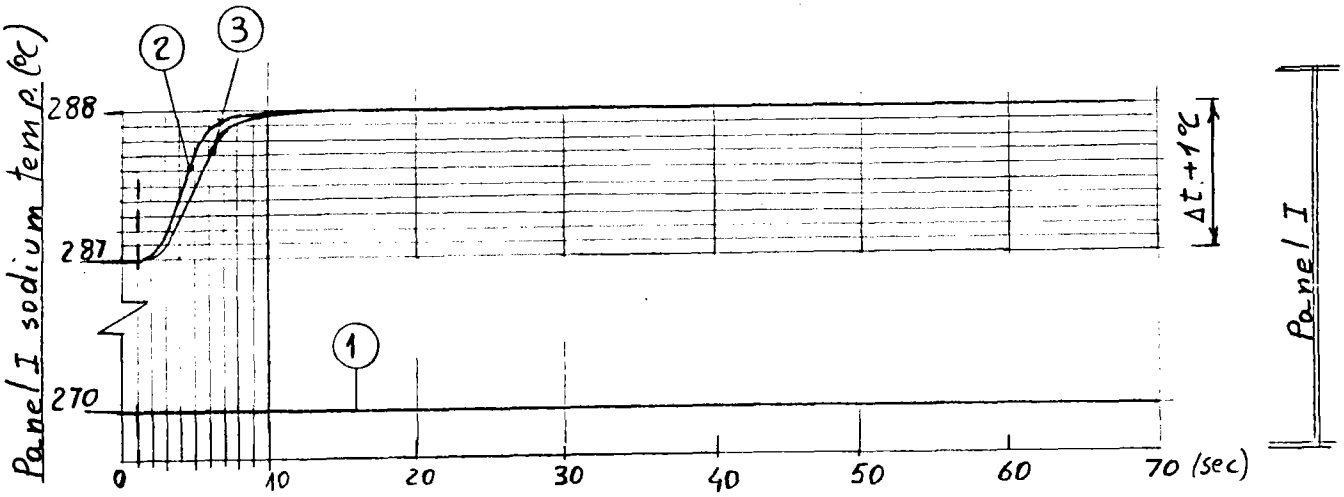

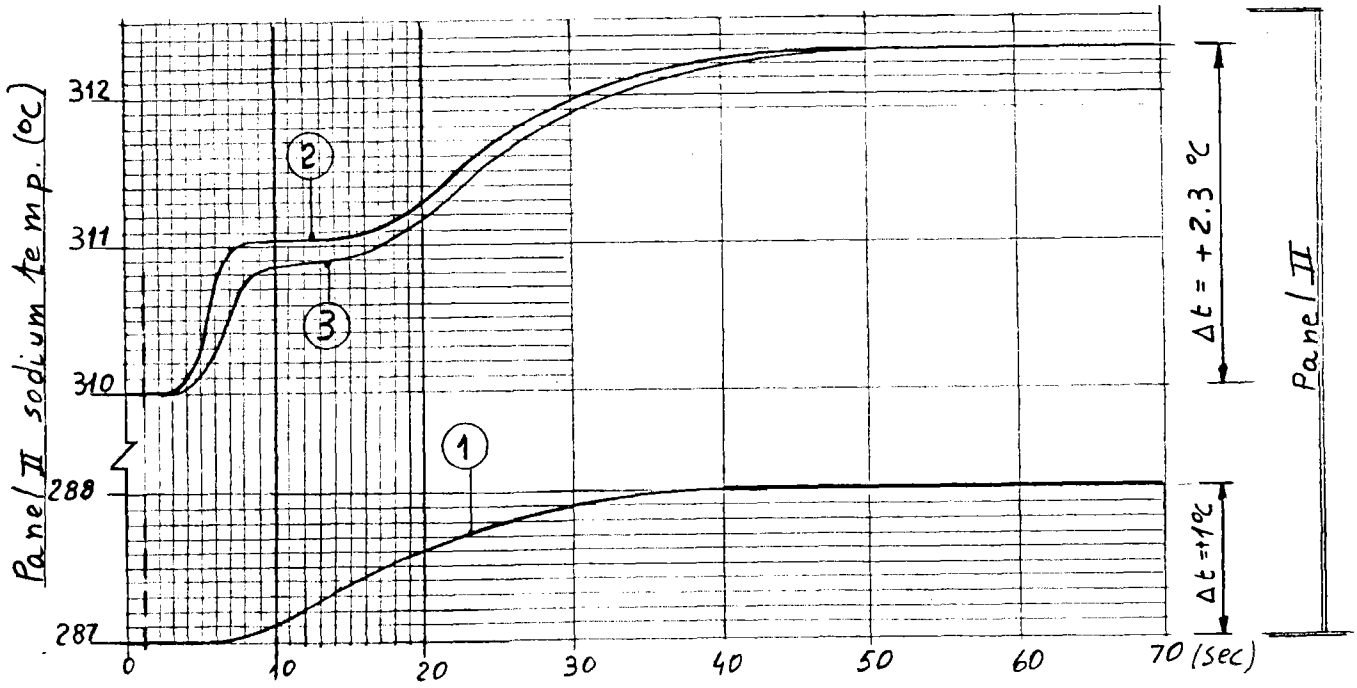

FIG. 9.4 + 10% incid. power step / Panels I & II sodium transient

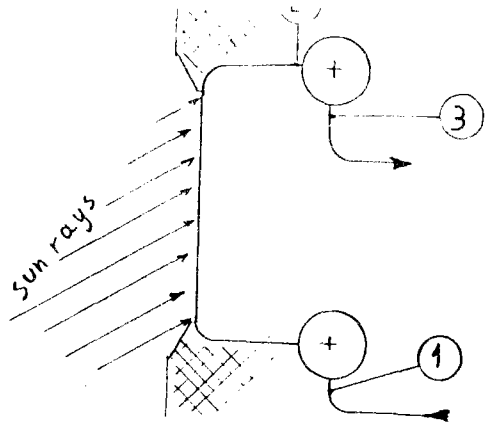

OPEN LOOP TRANSIENT

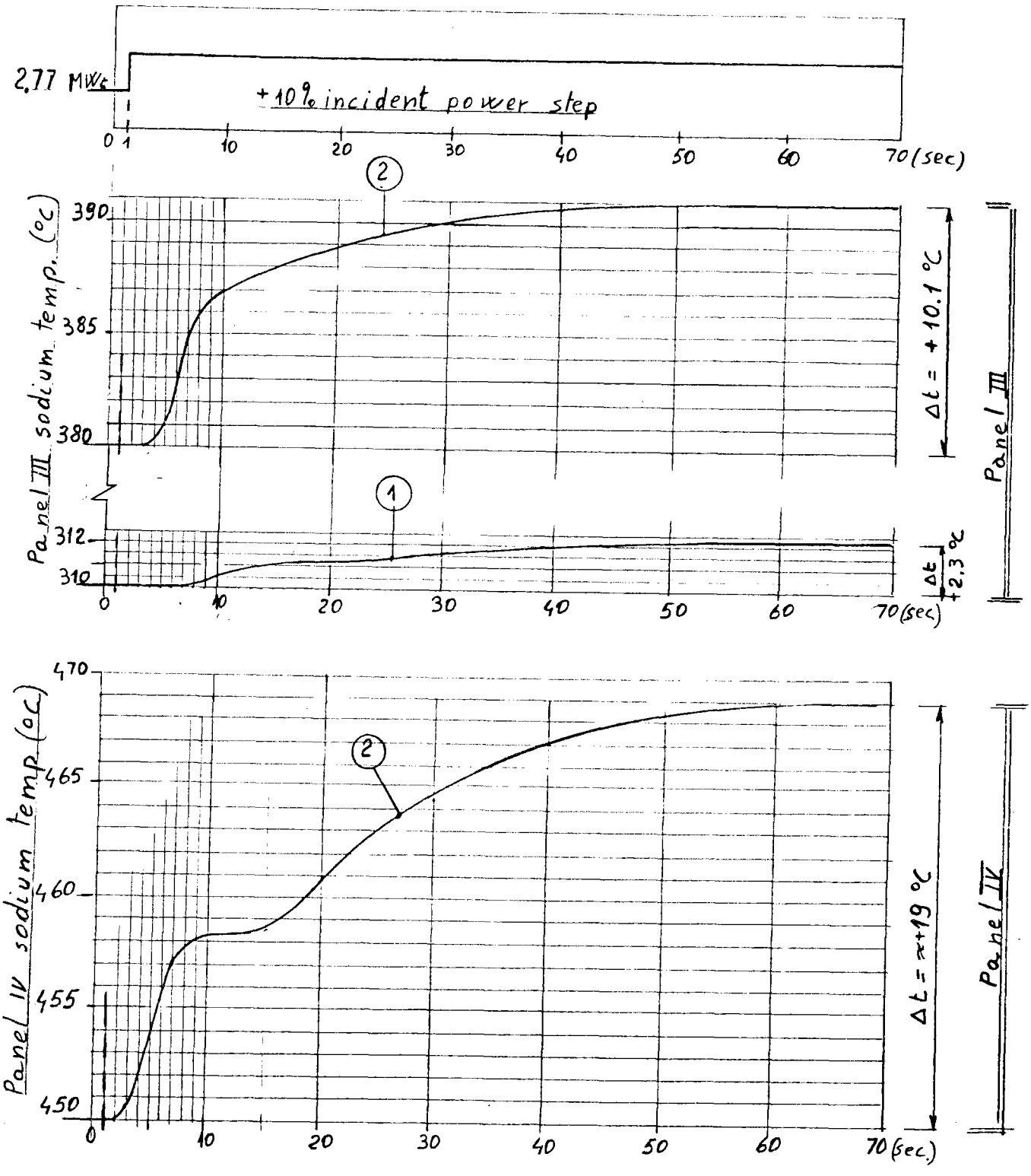

FIG. 9.5 Panels III & IV sodium temper. transient following a +10% incid. power step

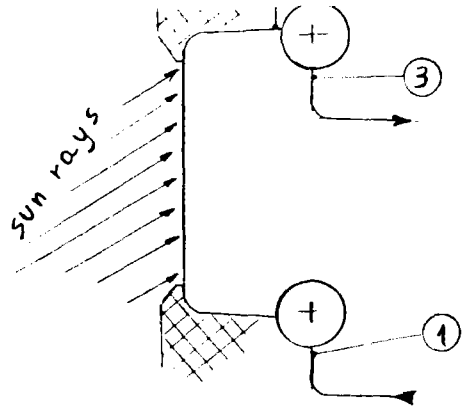

OPEN LOOP TRANSIENT

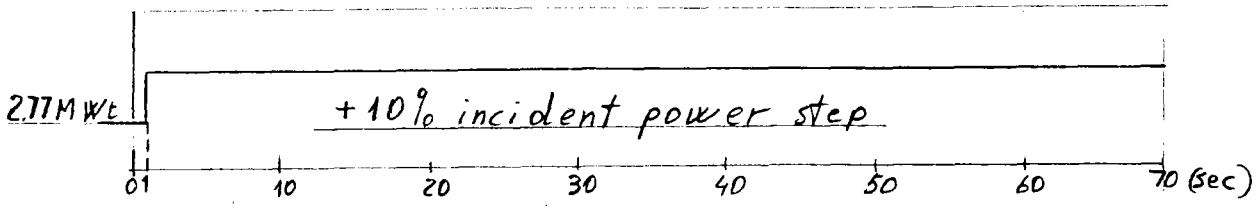

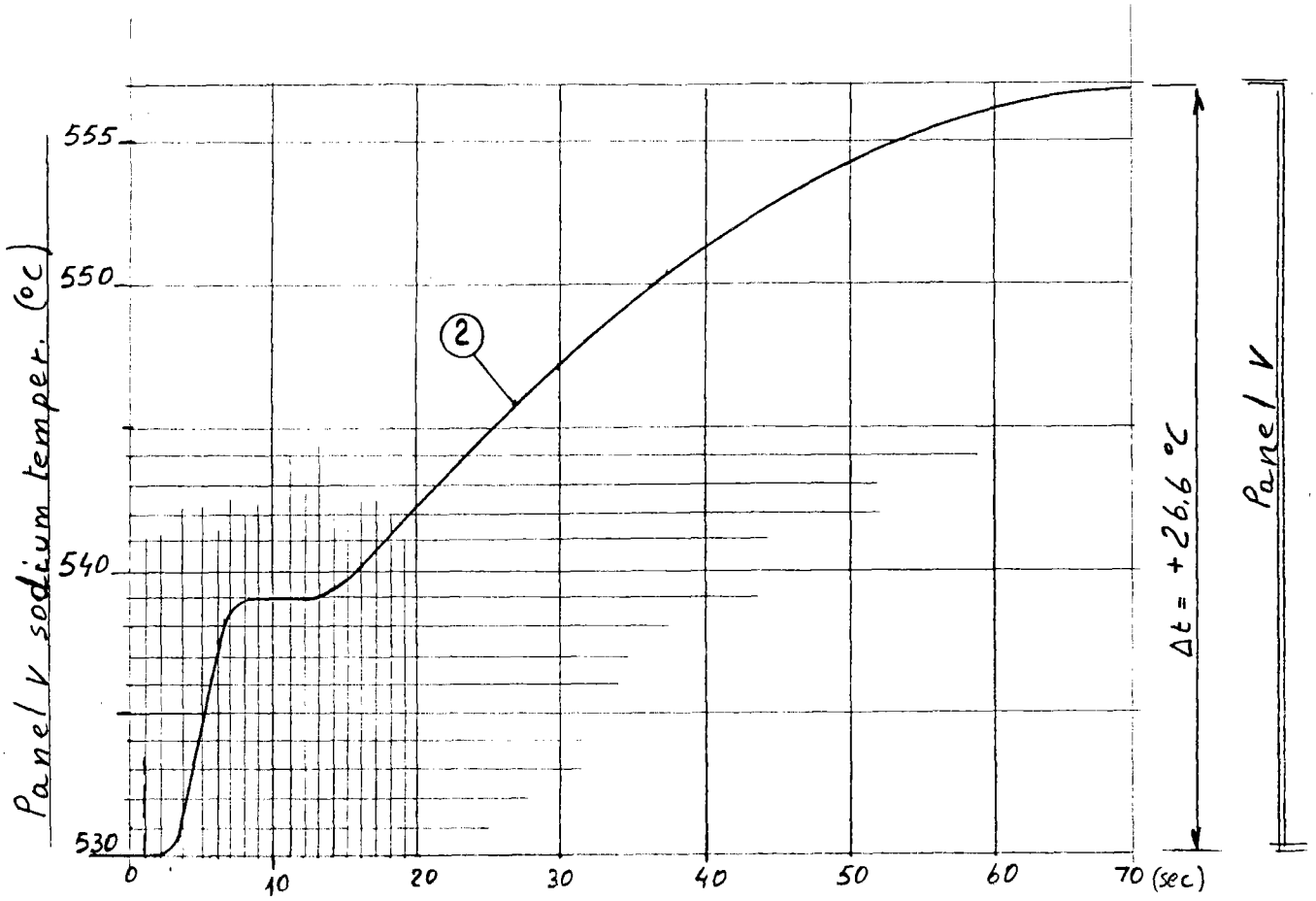

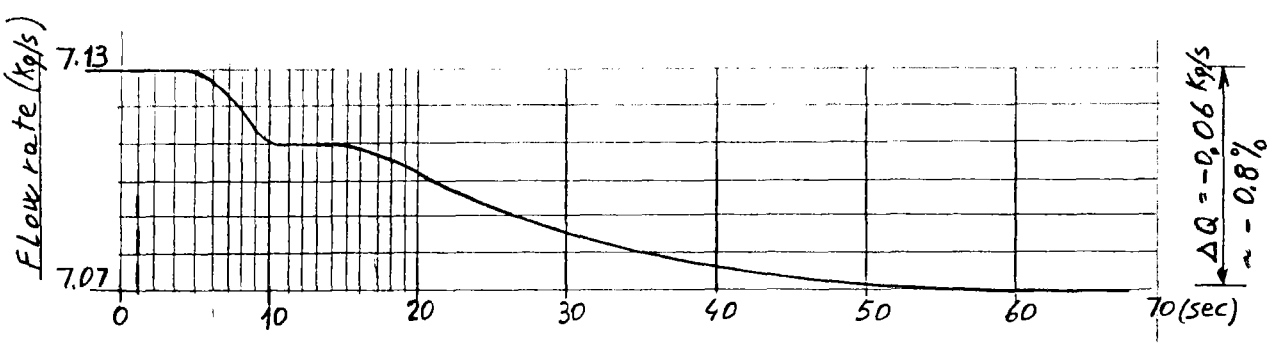

FIG. 9.6 +10% incid. power step / Panel V sodium transient / Receiver flow rate transient

ADVANCED SODIUM RECEIVER

(ASR)

Final design of ASR temperature control system.

Topic Report n. 5

Rev. 0

Date: 25 February, 1982

Prepared by: ENEL

FRANCO TOSI

SNAMPROGETTI

SUMMARY

In this report the final design results for Almeria ASR receiver control system are presented.

First, the basic design goals and the most important system constraints are briefly stated. The main dynamic and static features of the process are then discussed, since they have deeply influenced the choice of the control system structure; the criteria and the operating methods employed in carrying out the project are shown too.

Finally, the functional control scheme for ASR temperature regulation in shown, together with a series of transients which are significant to understand and to quantitatively evoluate the dynamic behaviour of the controlled system under the effect of the most typical disturbances.

INTRODUCTION

The receiver function is that of collecting the radiant energy coming from the heliostat field and to deliver it to the heat trasfer medium.

The operating conditions are quite particular owing to the intermittency of the radiant energy available on the mirror field and to the high level of the thermal fluxes on the receiver. These two effects have to be carefully taken into account in the mechanical design of the receiver, since they heavily influence its lifetime.

Thus, in order to reach the basic goal of maximizing the energy collected during the year, it is necessary to avoid too high transient temperature peaks during cloud passages, which cause quick variations of incident thermal flux. This is the main task of the receiver control system, which has to limit the transient temperature variations into an acceptable range.

The receiver temperature regulation is a very critical problem for many reasons:

- The thermal incident energy cannot be continuously varied for control purposes, since heliostats movement requires too long time as compared with the time constants of receiver dynamics; furtherly, as stated before, to collect at any instant the maximum available energy all the heliostats have to be focused on the receiver at any time.
- The transfer function of the controlled variable vs. the

control variable (sodium flow rate) and vs. the main disturbance has strong non-minimum phase effects owing to non negligible transport delays.

- The required control range, which spans from 10% to 100% of maximum load, is very wide; owing to process nonlinearity, this implies variations of the order of ten for what concerns the receiver dynamic parameters. Not only the amount but also the shape of the absorbed heat flux varies considerably during the day, the year or during a cloud passage. Therefore a detailed study has been necessary to compare different kinds of solutions, in which not only the above mentioned constraints have been taken into account, but also other factors such as practical difficulty of temperature measurements on the radiated tubes and ease of implementation and operation. The analyzed regulation structures are derived from a basic feedback scheme which satisfies the static specifications and in which suitable feedforward actions and further feedback signals are added. We have obtained in this way a final control structure which has been found very satisfactory for what concerns the compensation of the disturbances, with favourable effects on reduction of receiver lifetime consumption.

CHAPTER 1

CONTROL PROBLEM STATEMENT

The temperature control problem, in the foreseen operating conditions, that is with solar flux ranging from 10% to 100% of its nominal value, can be stated in the following terms:

- Controlled variable: sodium temperature at receivar outlet. This temperature must be maintained at a set point value of 530°C, according to plant design specifications. Due to the presence of the hot storage tank, a filtering effect is achieved for slight oscillations of receiver outlet temperature about its set point value; it is required, however, that the regulation be integral at low frequency. It is nevertheless necessary that the speed of response of the control system be very high to limit temperature variations which give rise to relevant thermal stresses on the receiver.
- Control variable: pump motor voltage, which is used to vary pump speed to obtain the required sodium flow rate.
- Disturbances: absorbed heat flux and sodium temperature at receiver inlet. The absorbed heat flux has to be considered as the most important disturbance because of its possible high amplitude and its high frequency compo-

nents. The presence of a cold storage tank limits the possible oscillations of receiver inlet sodium temperature, which can be considered constant for what concerns control system synthesis.

CHAPTER 2

BASIC DYNAMIC PROPERTIES OF THE PROCESS

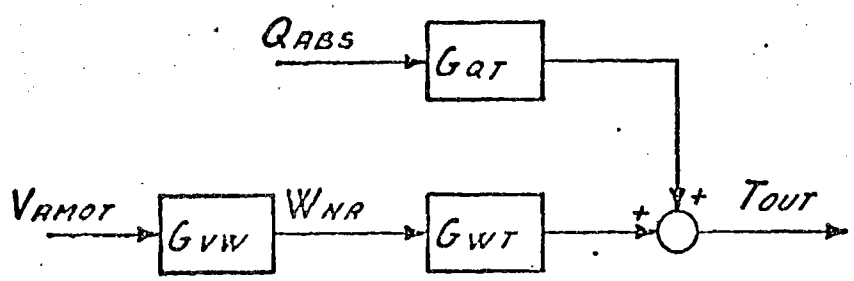

FIG. 1 - PROCESS BLOCK DIAGRAM

The most significant dynamic properties of the process are here briefly summarized (see [1] and [2] for a more detailed description) because they have had a deep influence on control system design.

A very synthetic block diagram of the process is shown in Fig. 1. The transfer fuctions represented are described below.

2.1 Transfer function between motor voltage and sodium flow rate [Gvw].

It has been obtained linearizing the fluid dynamic equations about several equilibrium points and then L-transforming. It consists of two real poles, the first of which is dominant and is due to the large inertance of the fluid in the ducts; the second one is due to pump and motor inertia. The poles and the static gains are strongly load dependent (see table 1).

LOAD (C)	g. [kg/s]	T1 [s]	T2 [s]
10	.07	6.36	.169
20	.046	3.79	.169
40	0.033	2.09	.168
80	0.0275	1.09	.167
100	0.0265	.88	.166

TABLE 1 - Transfer function parameters Vs. load

2.2 Transfer function between sodium flow rate and receiver outlet temperature [Gwt].

In order to evaluate this transfer function the receiver has been considered as a series connection of radiated pipes (one average pipe for every panel), headers and conecting pipes between the panels.

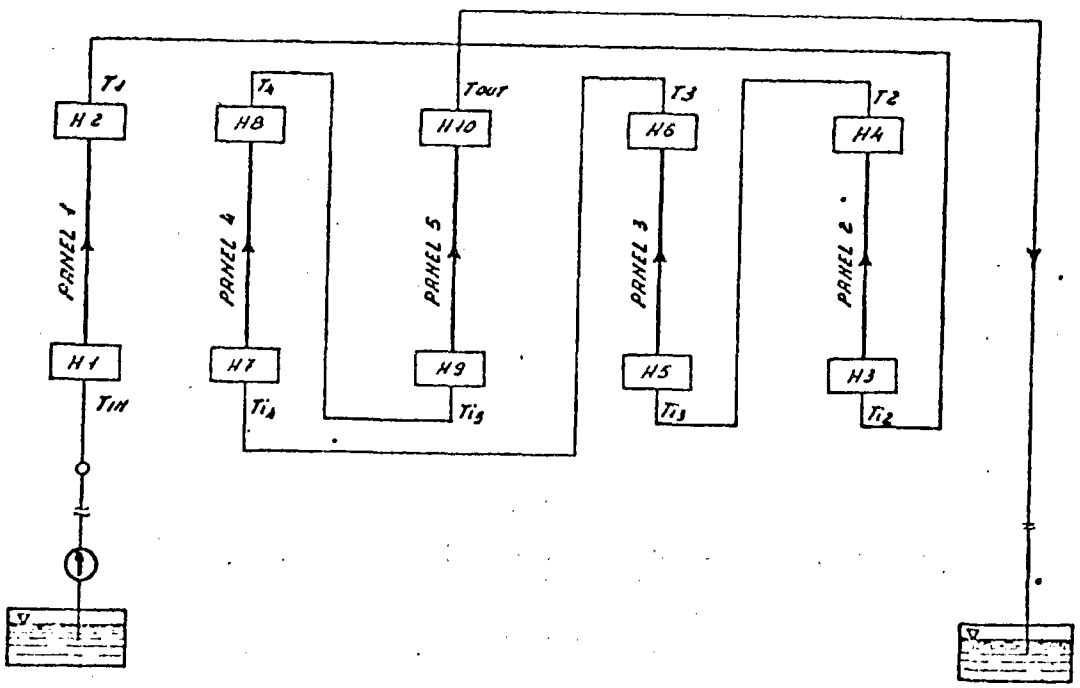

The main physical phenomenon involved is that of sodium transport. A sodium flow rate variation in the circuit acts on the outlet temperature of the k-th tube both directly and indirectly owing to the effects on the temperatures of the tubes upstream.

For small variations about an equilibrium point we have:

$$(1)\quad \delta T_{\sigma k}(s) = Gwtk(s)\,\delta W(s) + Gttkir(s)\,\delta Tik(s)$$

Where $\delta T_{\sigma k}(s)$ and $\delta Tik(s)$ represent the Laplace transform of sodium temperature variations at the outlet and at the inlet and δw represents flow rate variation. The function Gwtk takes into account the immediate effect of flow rate variation on outlet temperature and the function Gttkir takes into account the sodium transport phenomenon along the k-th tube.

We have:

$$(2)\quad \delta Tik(s) = Gttkcon\ \delta T\ k-1$$

Where Gttkcon takes into account the sodium transport from the outlet of tube k-1 to the inlet of tube k along the connecting pipe.

Recursively applying equation (1) to all the tubes in cascade the transfer function for the whole receiver can be obtained.

This function can be represented by the following block diagram:

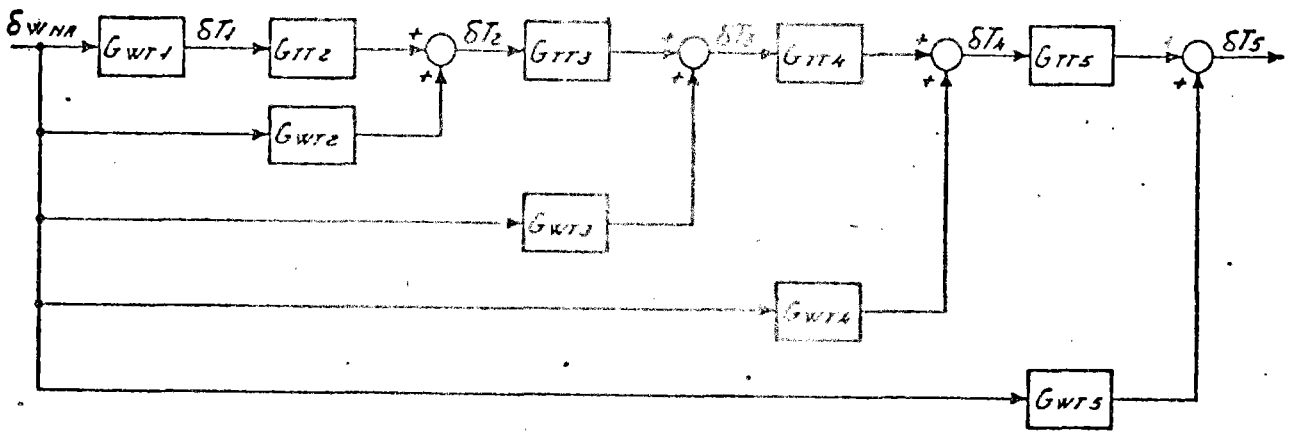

FIG. 3

Where the δTk (k=1,5) represent the outlet temperatures of the k-th panel and GTTK =Gttir•Gttkcon.

The dynamic features of the transfer functions which appear in the block diagram have been discussed in previous reports [(1), (2)]; however, to emphasize some important dynamic characteristics which affect control system definition we include also in this report the

transient time responses of sodium temperature to a step variation of sodium flow rate (Fig. 4).

In all the responses (except for T1) it is evident the presence of a fast component (due to Gwt_K) and of a delayed one.

In the fast components, the short initial delay is due to the last part of the tubes, which are non radiated; they all exhibit similar dynamic characteristics: only the static gain is dependent on the heat flux absorbed by the considered panel.

The delayed components exhibit dynamic characteristics which become slower for the downstream panels owing to the increase in transport delay from the first panel to the considered panel.

The ratio between the static gains of the fast part of the responses and that of the slower one in equal to the ratio between the power absorbed by the considered panel and the power absorbed by the panels located upstream. For this reason the dynamic characteristics of temperature responses are heavily dependent on flux distribution.

It can be noticed that the process is quite non linear, since the static gains, the time delays and the time constants vary, at a first approximation, inversely with flow. This can be seen from Figg. 5,6 in which are shown the process responses at 50% and 10% load, res-

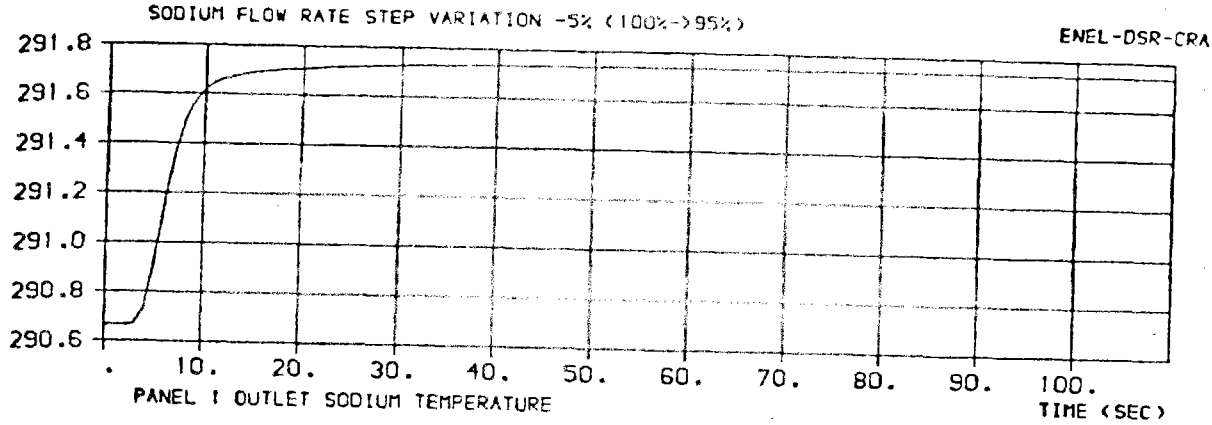
SODIUM FLOW RATE STEP VARIATION -5% (100%->95%)
ENEL-DSR-CRA
291.8
291.6
291.4
291.2
291.0
290.8
290.6
10. 20. 30. 40. 50. 60. 70. 80. 90. 100.
PANEL 1 OUTLET SODIUM TEMPERATURE
TIME (SEC)

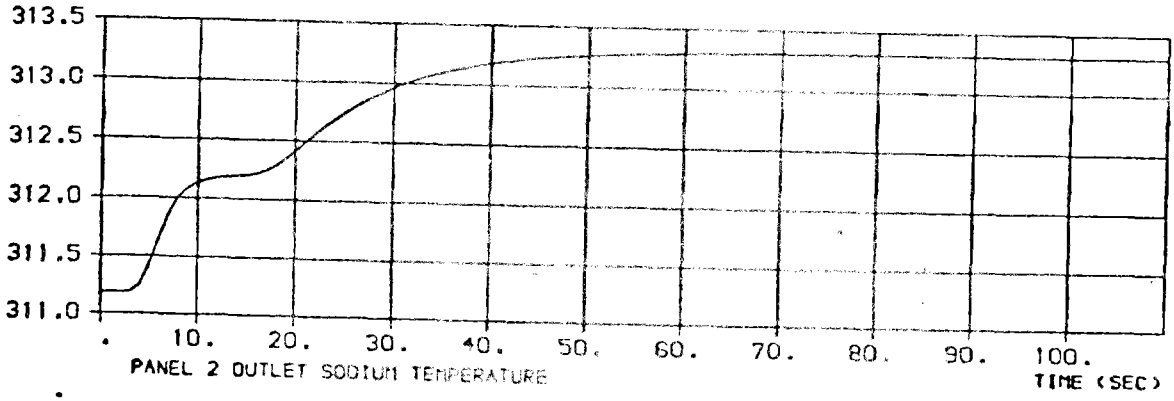
313.5
313.0
312.5
312.0
311.5
311.0
10. 20. 30. 40. 50. 60. 70. 80. 90. 100.
PANEL 2 OUTLET SODIUM TEMPERATURE
TIME (SEC)

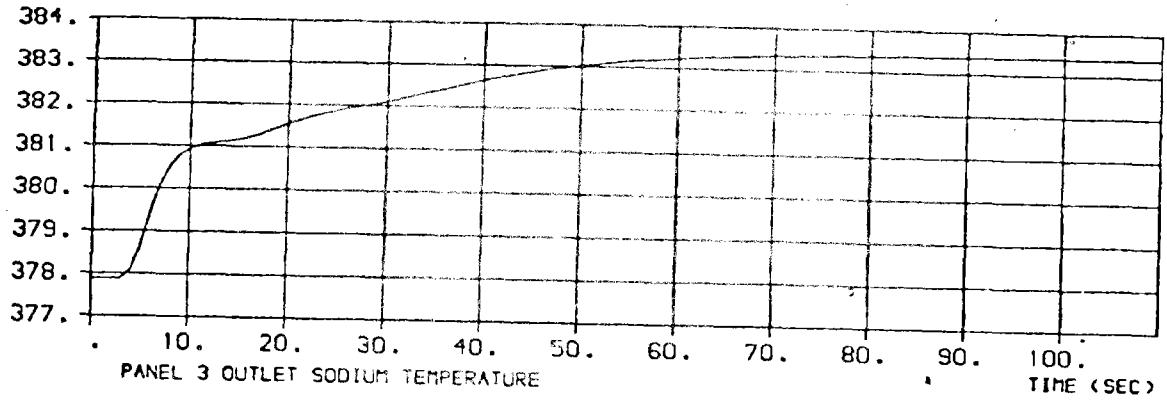
384.
383.
382.
381.
380.
379.
378.
377.
10. 20. 30. 40. 50. 60. 70. 80. 90. 100.
PANEL 3 OUTLET SODIUM TEMPERATURE
TIME (SEC)

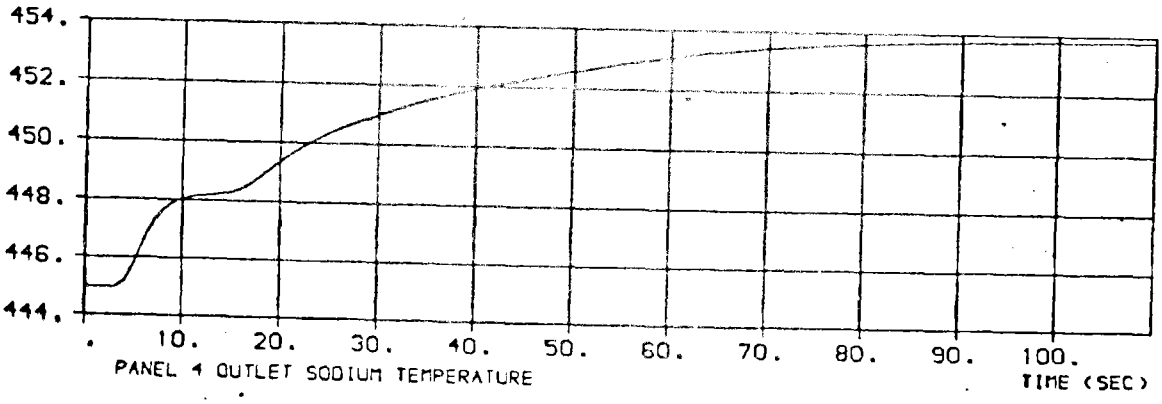
454.
452.
450.
448.
446.
444.
10. 20. 30. 40. 50. 60. 70. 80. 90. 100.
PANEL 4 OUTLET SODIUM TEMPERATURE
TIME (SEC)

Fig. 4a

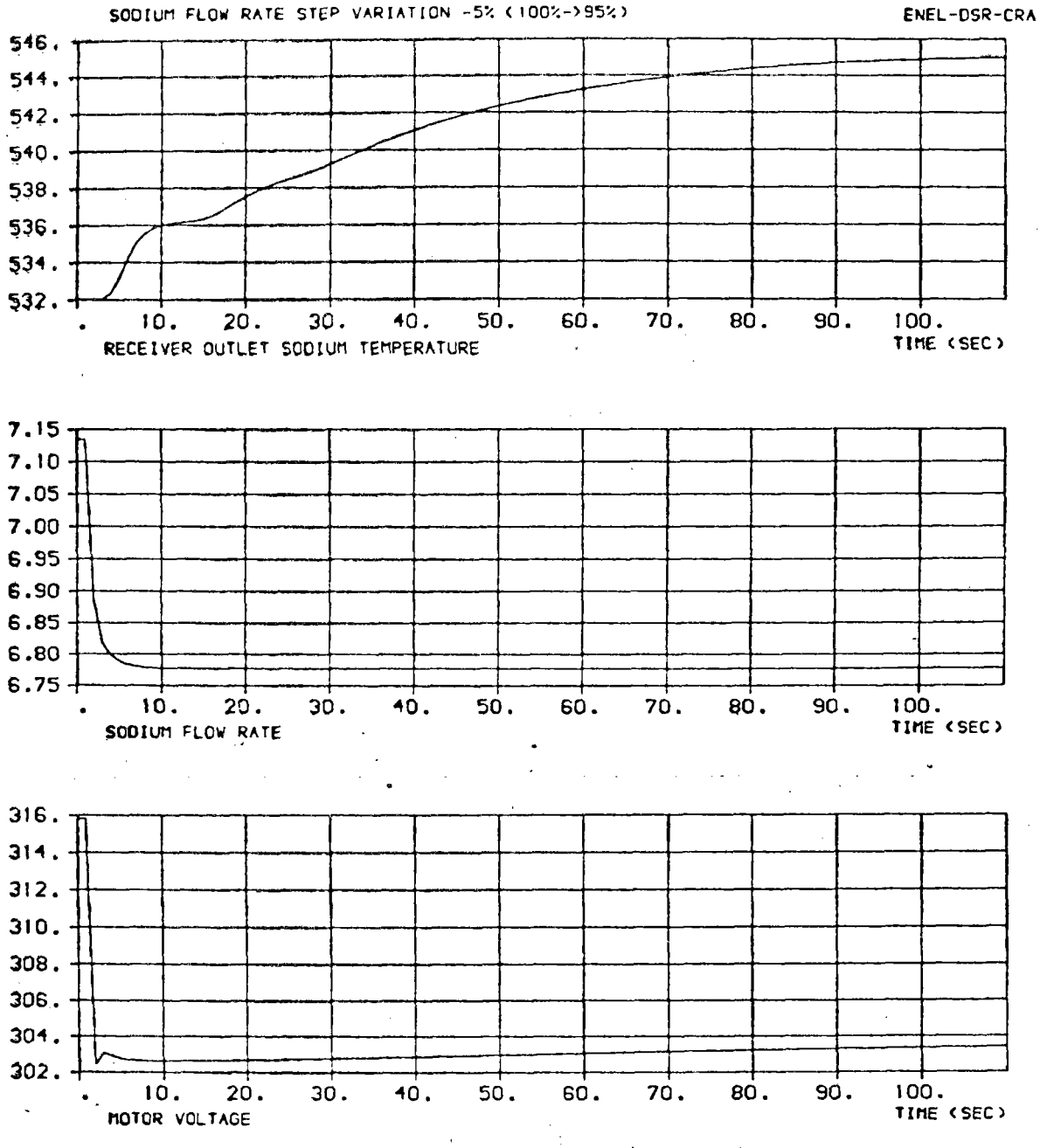
SODIUM FLOW RATE STEP VARIATION -5% (100%->95%)
ENEL-DSR-CRA
546.
544.
542.
540.
538.
536.
534.
532.
10. 20. 30. 40. 50. 60. 70. 80. 90. 100.
RECEIVER OUTLET SODIUM TEMPERATURE
TIME (SEC)
7.15
7.10
7.05
7.00
6.95
6.90
6.85
6.80
6.75
10. 20. 30. 40. 50. 60. 70. 80. 90. 100.
SODIUM FLOW RATE
TIME (SEC)
316.
314.
312.
310.
308.
306.
304.
302.
10. 20. 30. 40. 50. 60. 70. 80. 90. 100.
MOTOR VOLTAGE
TIME (SEC)

Fig. 4b

pectively.

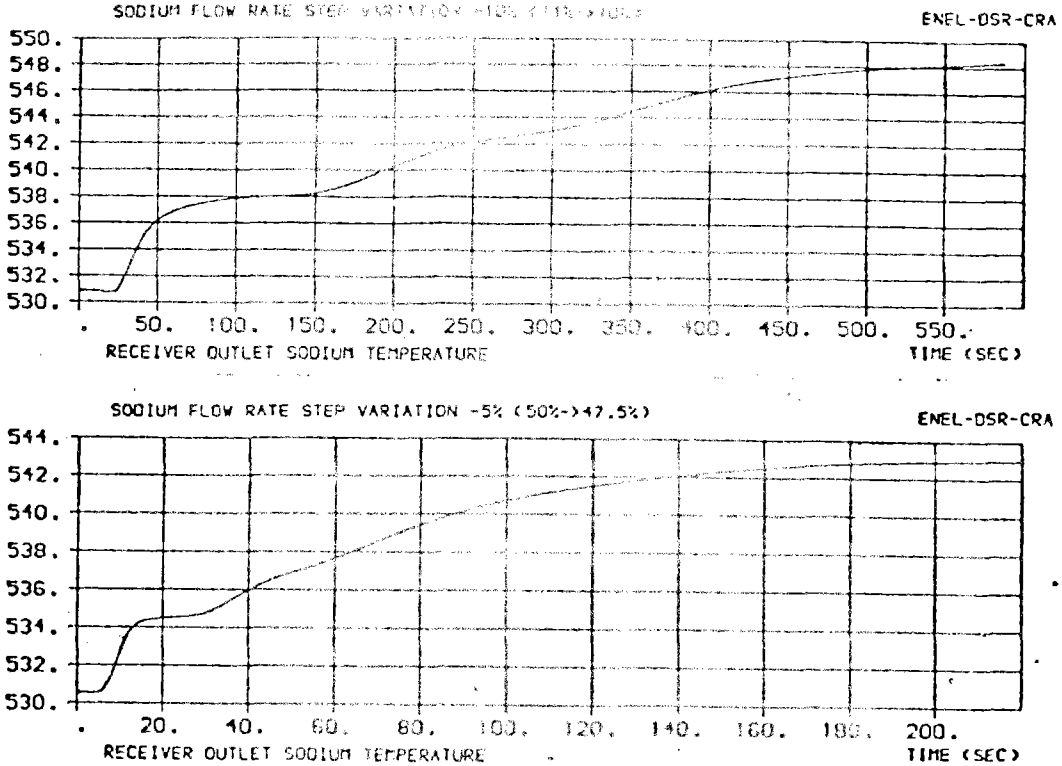

FIG.S.6

2.3 Transfer function between absorbed heat flux and receiver outlet temperature (GQT).

We define this transfer function by considering a percentually uniform variation of absorbed heat flux, so that the shape of the flux distribution is left unchanged:

$$\delta Qirr\ (x,\ t) = Qirr\ (x,\ 0)\ \delta K\ (t)$$

It is interesting to compare the functions GQT, with

the Gwt.

For a radiated tube, with any flux distribution shape, linearizing the energy equation about an equilibrium point, L-transforming respect to time and integrating along the curvilinear coordinate we obtain:

$$\Delta T(\ell,s) = e^{-B(s)\ell}\Delta T(0,s) + e^{-B(s)\ell}\overline{\Gamma}(s)\frac{Q_T}{(1+s\tau_m)CW_0}\Delta K(s) - e^{-B(s)\ell}\overline{\Gamma}(s)\frac{Q_T}{CW_0^2}\Delta W(s)$$

Where s is the complex Laplace variable and

$$Q_T = \int_0^\ell Q_{irr}(x,0)\,dx$$

$$\overline{\Gamma}(s) = \int_0^\ell e^{B(s)x} Q_{irr}(x,0)\,dx$$

$$B(s) = \frac{\tau s}{\ell}\left(1 + \frac{\tau_m/\tau_f}{1+s\tau_m}\right)$$

Then we have:

$$G_{QT}(s) = \frac{\Delta T(\ell,s)}{\Delta K(s)} = e^{-B(s)\ell}\overline{\Gamma}(s)\frac{Q_T}{(1+s\tau_m)CW_0}$$

$$G_{WT}(s) = \frac{\Delta T(\ell,s)}{\frac{\Delta W(s)}{W_0}} = e^{-B(s)\ell}\overline{\Gamma}(s)\frac{Q_T}{CW_0}$$

$$\frac{G_{QT}}{G_{WT}} = \frac{1}{1+s\tau_m}$$

From the last equation, having in mind the meaning of δK (s), it can be deduced that equal relative variations of heat flux and of sodium flow rate have the same static effect on temperature variations; the dynamic effect are approximately equal too, since the time constant τ_m is quite negligible in comparison with the other dynamic phenomena involved in the process.

CHAPTER 3

CONTROL SYSTEM DESIGN METHODS AND TOOLS

As it has been remarked in the preceeding chapters, the process is non linear, with distributed parameters.

The synthesis of regulation loops has been performed linearizing the model equations about various equilibrium points and then performing an interpolation among the obtained results.

The global stability has been verified by simulation, using the numerical code set up for process modelling, in which suitable routines for control system simulation have been included.

For regulator synthesis about an equilibrium point the classic frequency domain techinques for one input one output systems have been used; the final control structure, as it will be seen later consists of three cascaded loops, but since they are frequency decoupled, it has been possible to synthetize every loop separately.

For this purpose a numerical program has ben developped which, starting from the transfer functions of temperature vs. sodium flow rate obtained from the linearized phisical equations, provides Bode and Nyquist diagrams needed for

control system design [see (1) and (2)].

The results obtained in this way have been checked, in particular cases, against the results obtained using a parametric identification code [(3)], which provides the process transfer functions on the basis of model time responses.

The regulator design has been carried out on the basis of the classic dynamic specifications (maximum allowable bandwidth consistent with reasonable phase and gain margin).

The choice of regulator parameters has been ckecked by simulation, for small variations of temperature set point and incident thermal flux about the considered equilibrium point.

This procedure has been applied to different control structures, from the simplest one up to the more complex schemes, in which further temperature feedbacks have been added.

In this way a final control configuration has been found which has proved to be much better then the others, owing to a suitable feedback signal obtained from inlet and outlet temperature measurements at every panel. As it will be shown later this control philosophy allows to obtain very good dynamic performances and a high insensitivity to receiver flux distribution shape variation.

CHAPTER 4

CONTROL CONFIGURATION

According to design specifications the receiver must be normally operating with an outlet temperature held at 530°C; for this reason the receiver outlet temperature regulator must be at least of type 1 (integral).

To avoid flow instability in the receiver pipes, sodium flow rate must be always kept above 10% of its maximum value.

The main disturbances affecting sodium flow rate are the buoyancy forces due to density differences in the riser and downcomer pipes and the level differences between cold and hot tank.

According to these specifications it is necessary to include an inner loop for sodium flow rate control, which moreover allows to compensate motor nonlinearity.

These specifications are satisfied using the following very simple control structure:

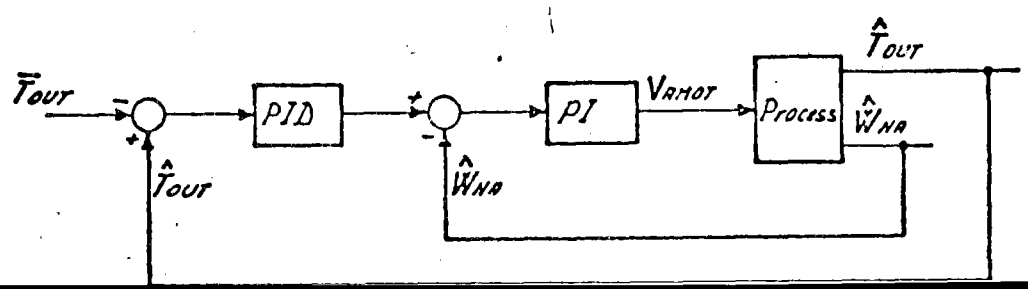

However, this structure cannot satisfactorily compensate the foreseen solar flux variations, owing to the long time delays present in outlet temperature responses vs. heat flux and flow rate variations.

Furthermore, the frequency response of temperature vs. flow rate is strongly dependent on flux distribution map; this fact heavily affects the stability of the controlled system.

A good compensation of incident heat flux transients could be obtained if it were possible to rely on an adequately accurate measure of the disturbance itself, to be utilized as a feedforward signal. Nevertheless, owing to the practical difficulty of obtaining a very accurate measure of the absorbed heat flux, it is necessary to improve the effectiveness of the feedback compensation. This aim has been reached, adopting a configuration based on a particular signal (ΔT) obtained from the inlet and outlet temperatures of every panel, as described below.

As it has been shown in chapter 2, the temperature variation at the outlet of a panel k is the sum of a fast and a delayed term. This is expressed by relation (1) which, setting:

$$\delta(\Delta T_k) = \delta T_{ok} - \delta T_{ik} \; Gttkir\,(s)$$

can be rewritten in the following way:

$$\delta \Delta T_k = \delta W \cdot Gttkir\,(s)$$

Thus, with reference to a sodium flow rate variation δw, the

temperature variation ΔTk contains only the fast term, related to the transfer function Gttir (s). To obtain this signal, the difference has to be done between the outlet temperature of a panel and the temperature at the inlet header of the panel, the last multiplied by the transfer function Gttkir (s). In Fig. 7, for instance, is represented the time behaviour of the signal $\Delta T=\sum_{k=1}^{5}\Delta Tk$ (total sum for the five panels) to a sodium flow rate variation, obtained with the above explained procedure.

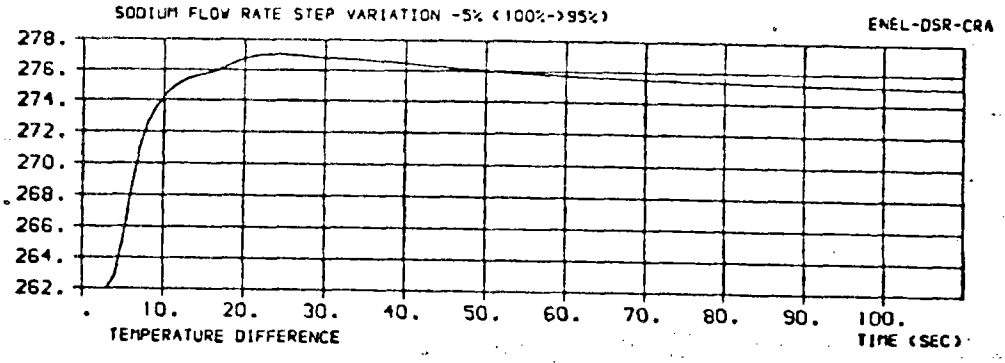

FIG. 7

So this signal provides a very rapid estimation of the transient energy unbalance on the receiver and can be very effectively utilized for temperature control. Furtherly, the use of this signal allows to obtain a good insensitivity of control system performance to variations of flux map shape. Suppose, for instance, that a transient occurs, which does not affect the total power absorbed, but has the only effect of increasing the heat flux on some panels and decreasing it on some others; in this case the value of the terms ΔTk varies but their sum remains unchanged.

CHAPTER 5

COMPLETE FEEDBACK CONFIGURATION

The block diagram of the control system becomes the one represented in Fig. 8 in which a new intermediate loop has been included, which controls the signal $\Delta T = \sum_{k=1}^{5} \Delta Tk$.

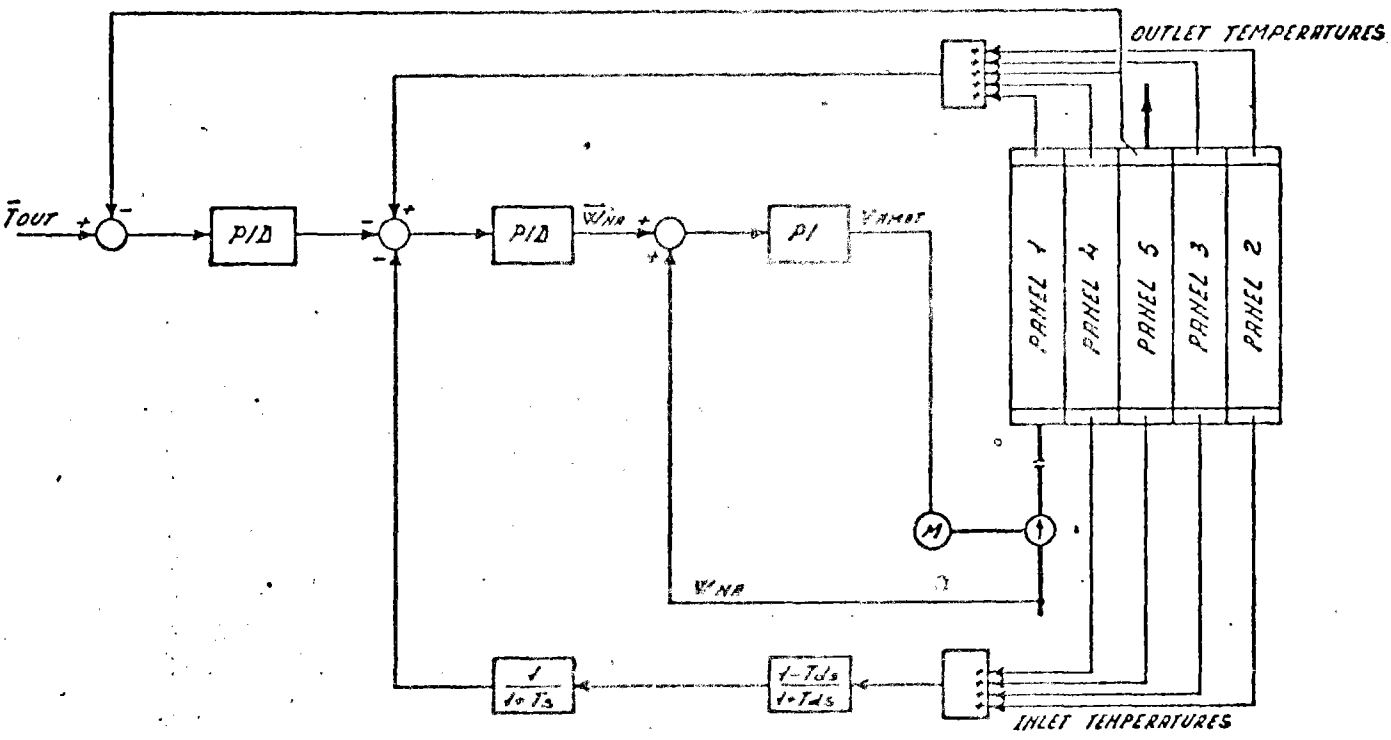

FIG. 8

The transfer function Gttir (s), needed to build up the signal ΔT, has been evaluated in a simplified way by a first order lag and a first order Pade' approximation.

The output of the intermediate loop acts as a set point for the inner loop, which controls the flow rate; the set point for the intermediate loop is given by the external regulator, which is driven by the difference between receiver outlet temperature and its reference value.

As it will be shown later, the intermediate loop is much faster than the external loop, thus allowing to considerably improve system dynamic performances.

In case of large disturbances due to incident heat flux variation, the intermediate loop acts immediately on flow rate set point, so as to maintain the required value for ΔT; at lower frequencies, the set point for ΔT is changed by the external, slower regulator so as to maintain the receiver outlet temperature at its desired value.

As it has been pointed out previously, the dynamic and static characteristics of the process are approximately a linear function of the inverse of sodium flow rate. For this reason, and owing to the wide operating range of the receiver it is necessary to adapt control system parameters to the process, making them vary as a function of sodium flow rate.

CHAPTER 6

SYNTHESIS OF REGULATOR PARAMETERS

6.1 Flow rate regulator

The characteristics and the Bode diagrams of this regulator have been already described in [2].

A proportional + integral regulator with fixed parameters has allowed to obtain a high speed of response with good stability margins for all the operating conditions.

Let Gpi the regulator transfer function, we have

$$G_{pi} = \frac{Ki}{s}(1 + Ts)$$

with $Ki = 37{,}17$ [V/kg]

$T = 1.2$ [s]

6.2 Intermediate regulator (temperature difference regulator)

As shown before, the signal to be controlled is:

$$\Delta T = \sum \Delta Tk = \sum [\ Tok - Tik\ Gttkir\ (s)]$$

Since all the radiated panels are geometrically equal, the transfer functions Gttkir (k = 1,5) are identical and calling Gttir their common expression, we have:

$$\Delta T = \sum T_{ok} - G_{ttir}(s) \sum T_{ik}$$

The Bode diagrams of the transfer function Gttir between the inlet and outlet temperature of a panel are shown in Fig. 9, for loads 10%, and 100%, respectively. From the diagrams it can be seen that the function Gttir (s) can be approximated as follows (with sufficient accuracy in a frequency range broad enough for control design purposes):

$$Gttir(s) = \frac{1}{1 + T_a s} \cdot \frac{1 - T_d s}{1 + T_d s}$$

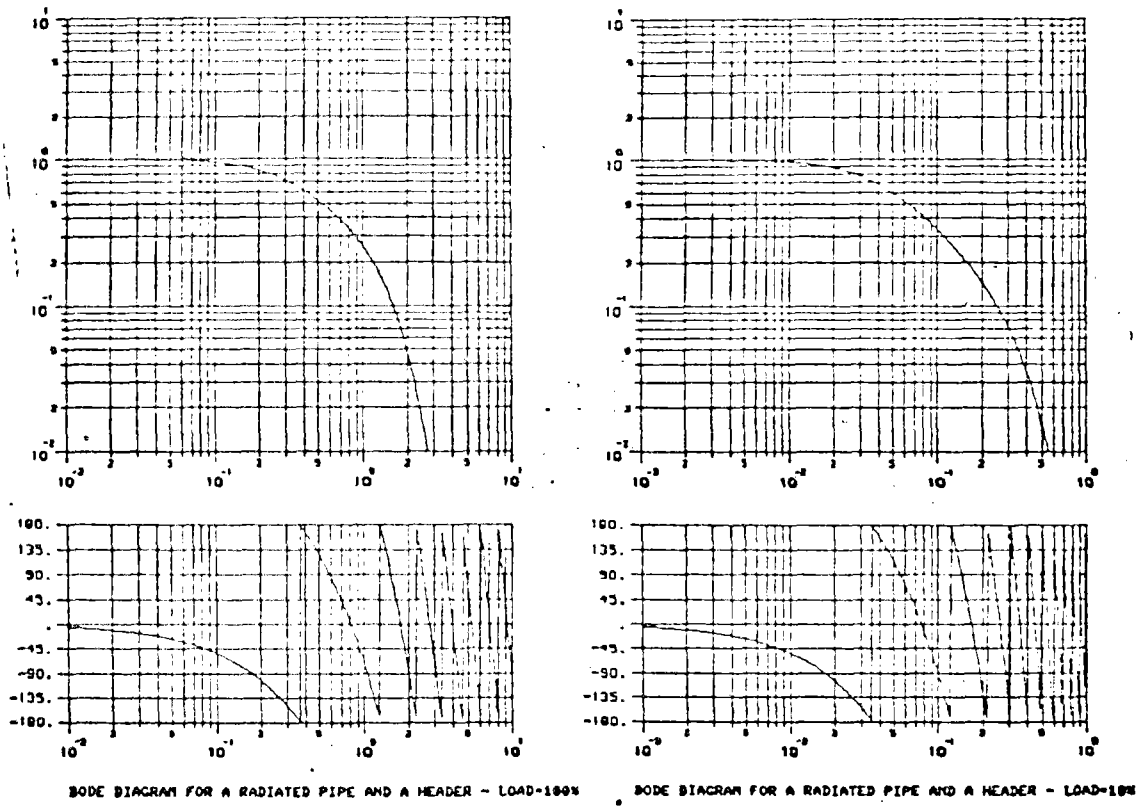

FIG. 9 Bode diagrams of the transfer function between the inlet and the outlet temperature of a panel.

The time constants T and Td are respectively a linear and a quadratic function of sodium flow rate as it can be seen from the following table:

LOAD (%)	Td [s]	T_a [s]
10	137.8	25
50	26.8	5.
100	7.94	2.5

TABLE 2

Once obtained the signal ΔT, to evaluate the regulator parameters it is necessary to calculate the transfer function between the manipulated variable $\delta \bar{W}$ (flow rate set point) and the controlled variable ΔT.

Since the inner loop is faster than the intermediate one it can be supposed $\delta \bar{W} = \delta W$. Therefore, the transfer function needed is:

(3) $$Gd(s) = \frac{\delta(\Delta T(s))}{\delta W(s)}$$

In Fig. 10 the Bode diagram of (3) is represented, evaluated at load 100%.

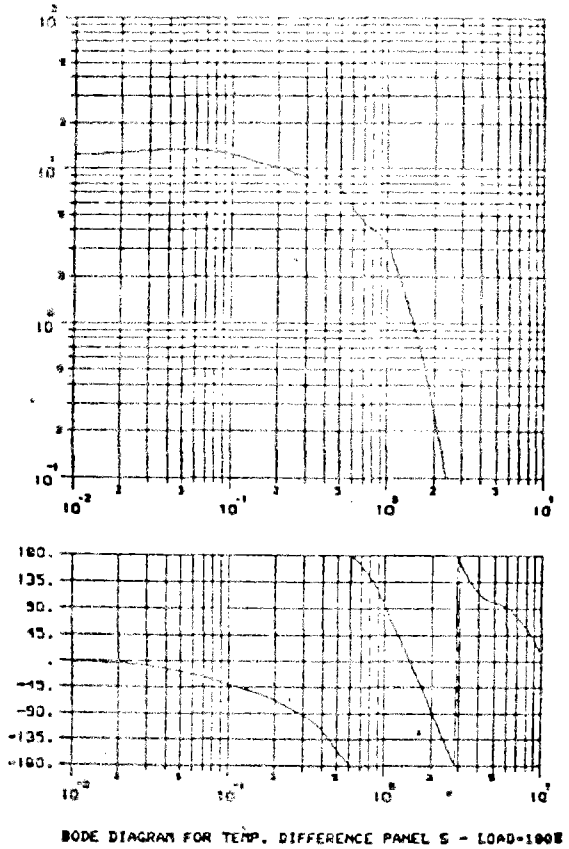

BODE DIAGRAM FOR TEMP. DIFFERENCE PANEL 5 - LOAD=100%

FIG. 10

At different loads the diagrams have the same shape but

are frequency translated (the 3db bandwidth is proportional to load); the static gain is proportional to the inverse of load. Using a regulator with load varying parameters (functions of flow rate)a large bandwidth for the controlled system can be obtained at every working condition.

In Fig. 11 the loop transfer functions are shown.

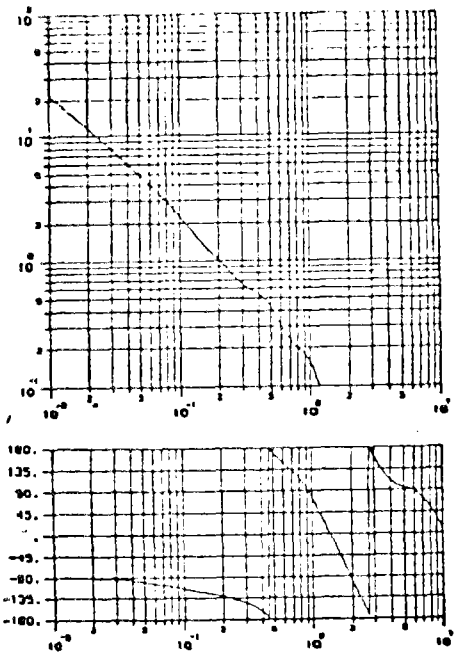

The regulator transfer function is:

$Gr2(s) = (1 + T1s)(1 + T2s).Ki/s$

The second zero (T2) is used to compensate the phase lag of the thermocouple.

For the other parameters we have:

LOAD (%)	Ki [kg/ CS2]	T1 [s]
10	.051510·10^{3}	25
50	1.5610 ·10^{3}	5
100	5.9510 ·10^{3}	2.5

TABLE 3

6.3 External loop (outlet temperature regulator)

Owing to the presence of the intermediate loop, it is not necessary that the external loop be particularly fast, since its main task is to maintain at steady state the outlet temperature at its nominal value.

To evaluate external regulator parameters, it is necessary to compute the transfer function between the control variable (set point T) and the controlled variable (receiver outlet temperature).

With reference to Fig. 12, it is necessary to evaluate the function:

$$GL1 = \delta T_{out} / \delta(\Delta T)$$

Let Lw be the closed loop transfer function of the flow rate loop, that is:

$$Lw = \frac{\delta w}{\delta w} = \frac{GR_3 G_{vw}}{1 + GR_3 G_{vw}}$$

Therefore we have:

$$GL1 = Gwt\ Lw$$

in particular at low frequencies we can suppose Lw = 1 and GR2LwGd>>1 and thus we have:

$$(4) \qquad GL1 = \frac{G_{wT}}{G_d} \ .$$

From (4) it can be noticed that the static gain of GL1 is independent from load, since the static gains of GwT and of Gd both vary with load with the same law.

The Bode diagrams of GL1 have been plotted about different equilibrium points (Fig. 13 shows the diagrams at 100% load). On their basis a PID regulator has been de-

signed with an integral gain linearly dependent from load and with a zero proportional to the inverse of load, as it is shown in the following table:

LOAD (%)	Ki [i/s]	T1 [s]
10	.0048	100.
50	. 024	20.
100	. 048	10.

TABLE 4

6.4 Feedforward action

The feedforward action obtained from the measure of the heat flux is particularly effective for disturbance compensation in processes affected by relevant non minimum phase shifts. An accurate measure of heat flux is nevertheless difficult to be obtained, and so the disturbance compensation is achieved in large amount by the feedback. However the feedforward action, even though imprecise, is necessary to limit temperature peaks during rapid and large rises of the solar flux, when it starts from very low values. In fact in this situation, the temperature variation at the outlet of the panels is very delayed respect to the rise speed of the flux, owing to the very slow speed of the fluid at low flow rates. For this reason the final control scheme includes a feedforward action, as shown in Fig. 14. It is worth noticing that considerable improvements in the feedback action during the transient described above

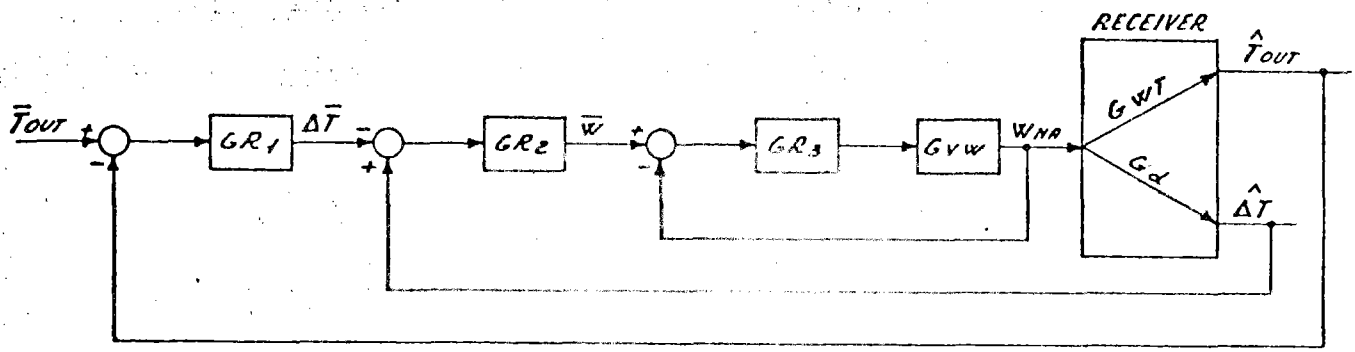
RECEIVER
$\bar{T}_{OUT}$
GR_1
$\Delta\bar{T}$
GR_2
$\bar{w}$
GR_3
G_{VW}
W_{HR}
G_{WT}
G_{α}
$\hat{T}_{OUT}$
$\Delta\hat{T}$

Fig. 12

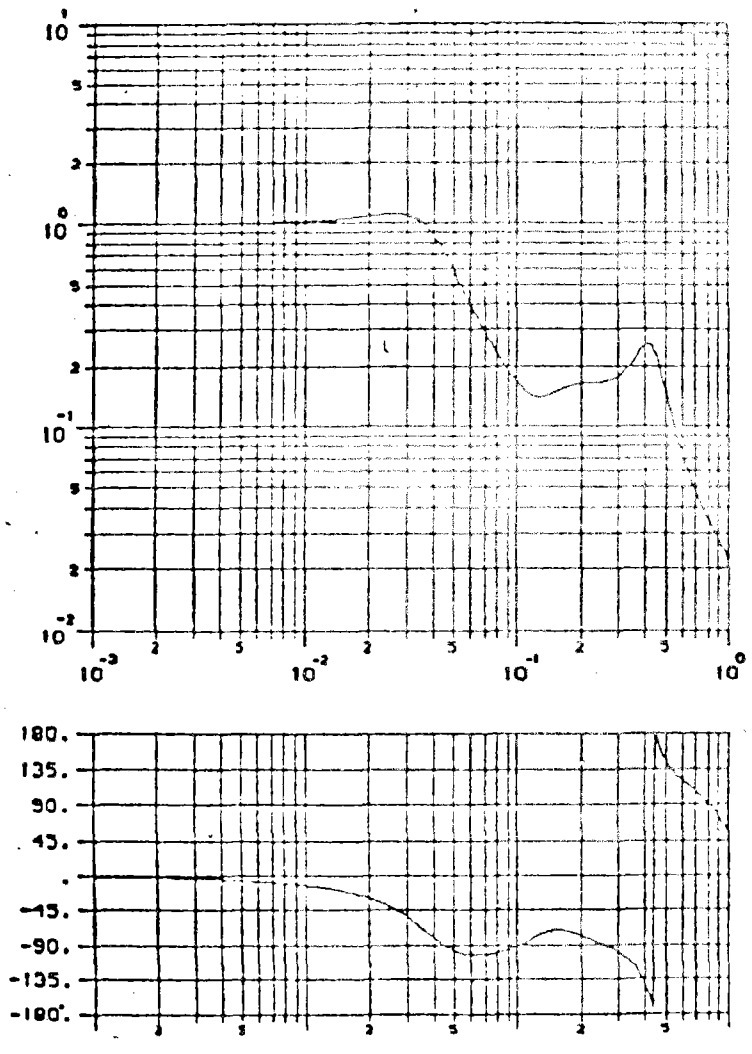
10^{1}
10^{0}
10^{-1}
10^{-2}
10^{-3}
10^{-2}
10^{-1}
10^{0}
180.
135.
90.
45.
-45.
-90.
-135.
-180.

Fig. 13

could be obtained using temperature measurements in radiated sections, with the sensing element located on the back wall of the tubes. Such temperature are not affected by any transportation delay at any working condition.

The results that can be obtained in this way are presented in Appendix A.

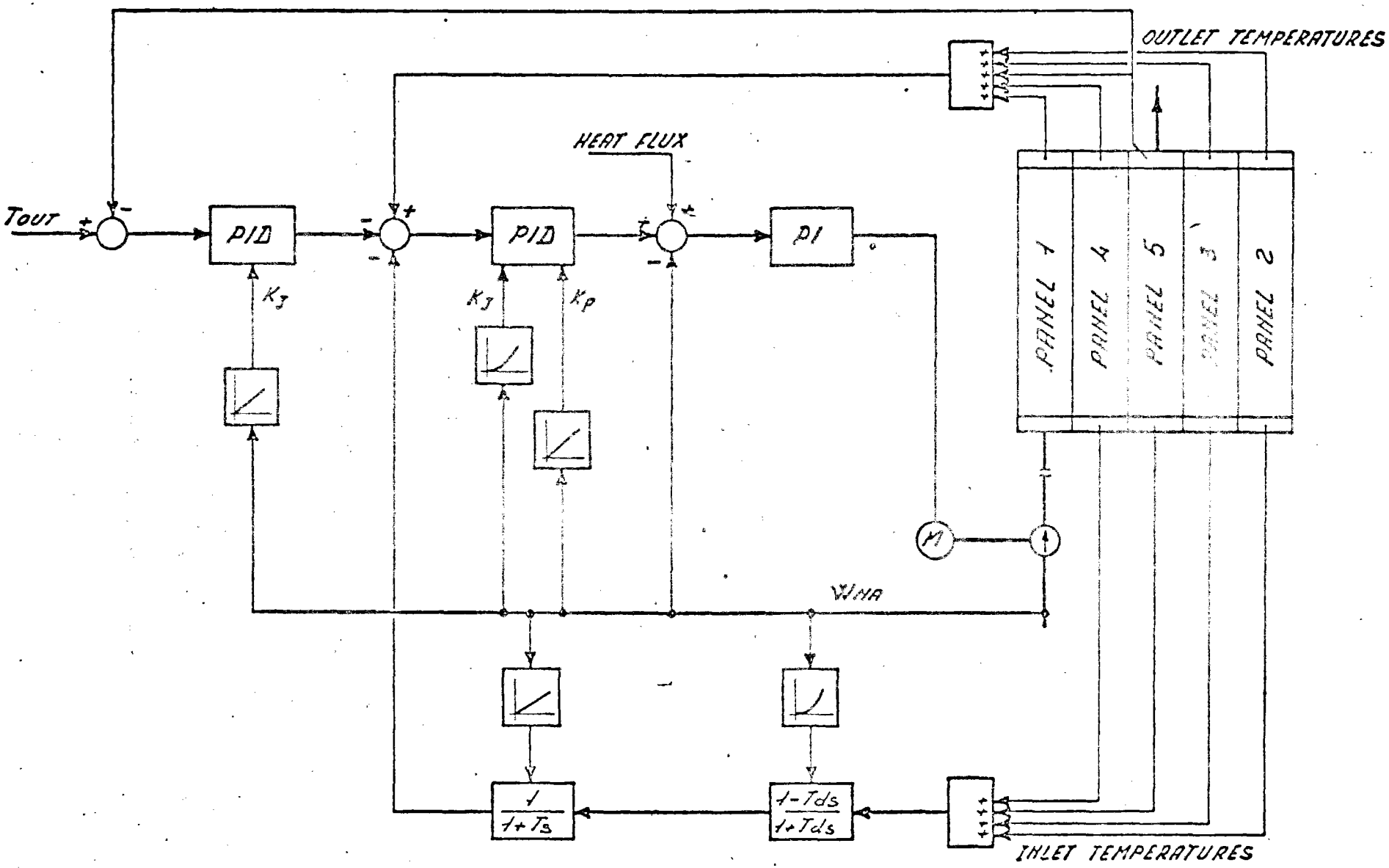

FIG. 14 Functional block diagram for ASR temperture control

ENEL - DSR - CRA

APPENDIX 1

SYMBOL LIST

Qabs	=	Absorbed heat flux
Qirr	=	Incident heat flux
W	=	Sodium flow rate
Vamot	=	Pump motor driving voltage
Tout	=	Receiver outlet temperature
Tk	=	Temperatures at the outlet of panel k
Tik	=	Temperatures at the inlet of panel k
Gqt (s)	=	Transfer function between absorbed heat flux and receiver outlet temperature
Gwt (s)	=	Transfer function between sodium flow rate and receiver outlet temperature
Gwtk (s)	=	Transfer functions between sodium flow rate and temperature at the outlet of panel k (k = 1, 2, 3, 4 and 5)

Gttk (s) = Transfer function between temperature at the outlet of panel k-1 and temperature at the outlet of panel k

Gttkir (s) = Transfer function between temperature at the inlet and the outlet of a radiated tube

Gttkcon (s) = Transfer function between temperature at the inlet and the outlet of a connecting tube.

APPENDIX A

Here some transients are shown which are significant to evaluate the controlled system performances. The transients have been produced using different control structures, in order to put in evidence the improvements that can be obtained adding to the simple structure shown at page 4.1 the feedback signal ΔT as proposed for the final control configuration.

Note - All the transients shown have been obtained without using the feed-forward action based on incident thermal flux measurement.

APPENDIX A1

Comparison between time responses obtained using two different control structures. The first (fig. A1-1) refers to the simple structure shown at page 4.1. The second (fig. A1-2) refers to the control structure shown in fig. 14.

Transient presented: Incident heat flux step variation (-10% at maximum load).

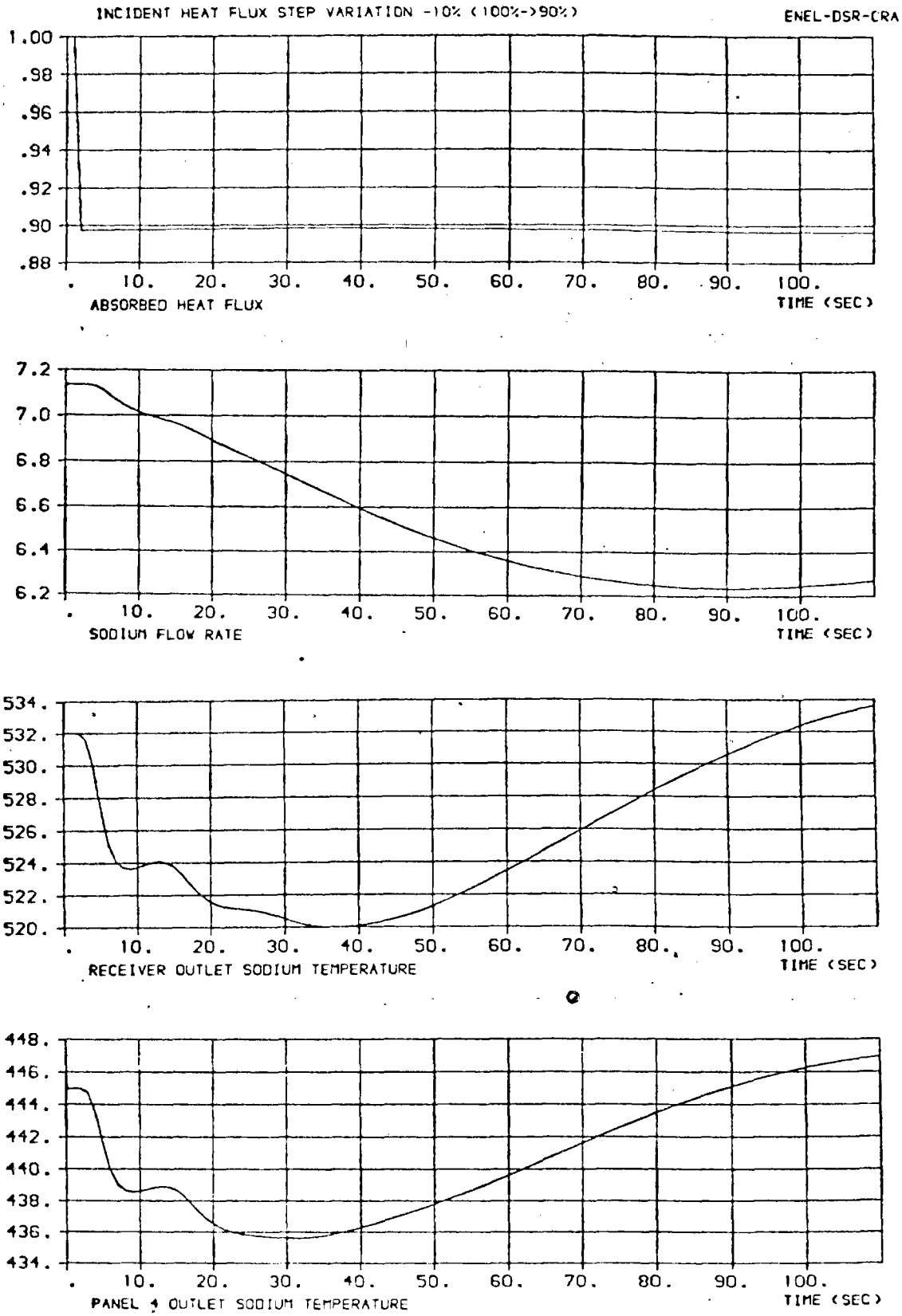
INCIDENT HEAT FLUX STEP VARIATION -10% (100%->90%)
ENEL-DSR-CRA
1.00
.98
.96
.94
.92
.90
.88
10. 20. 30. 40. 50. 60. 70. 80. 90. 100.
ABSORBED HEAT FLUX
TIME (SEC)
7.2
7.0
6.8
6.6
6.4
6.2
10. 20. 30. 40. 50. 60. 70. 80. 90. 100.
SODIUM FLOW RATE
TIME (SEC)
534.
532.
530.
528.
526.
524.
522.
520.
10. 20. 30. 40. 50. 60. 70. 80. 90. 100.
RECEIVER OUTLET SODIUM TEMPERATURE
TIME (SEC)
448.
446.
444.
442.
440.
438.
436.
434.
10. 20. 30. 40. 50. 60. 70. 80. 90. 100.
PANEL 4 OUTLET SODIUM TEMPERATURE
TIME (SEC)

Fig. A1-1

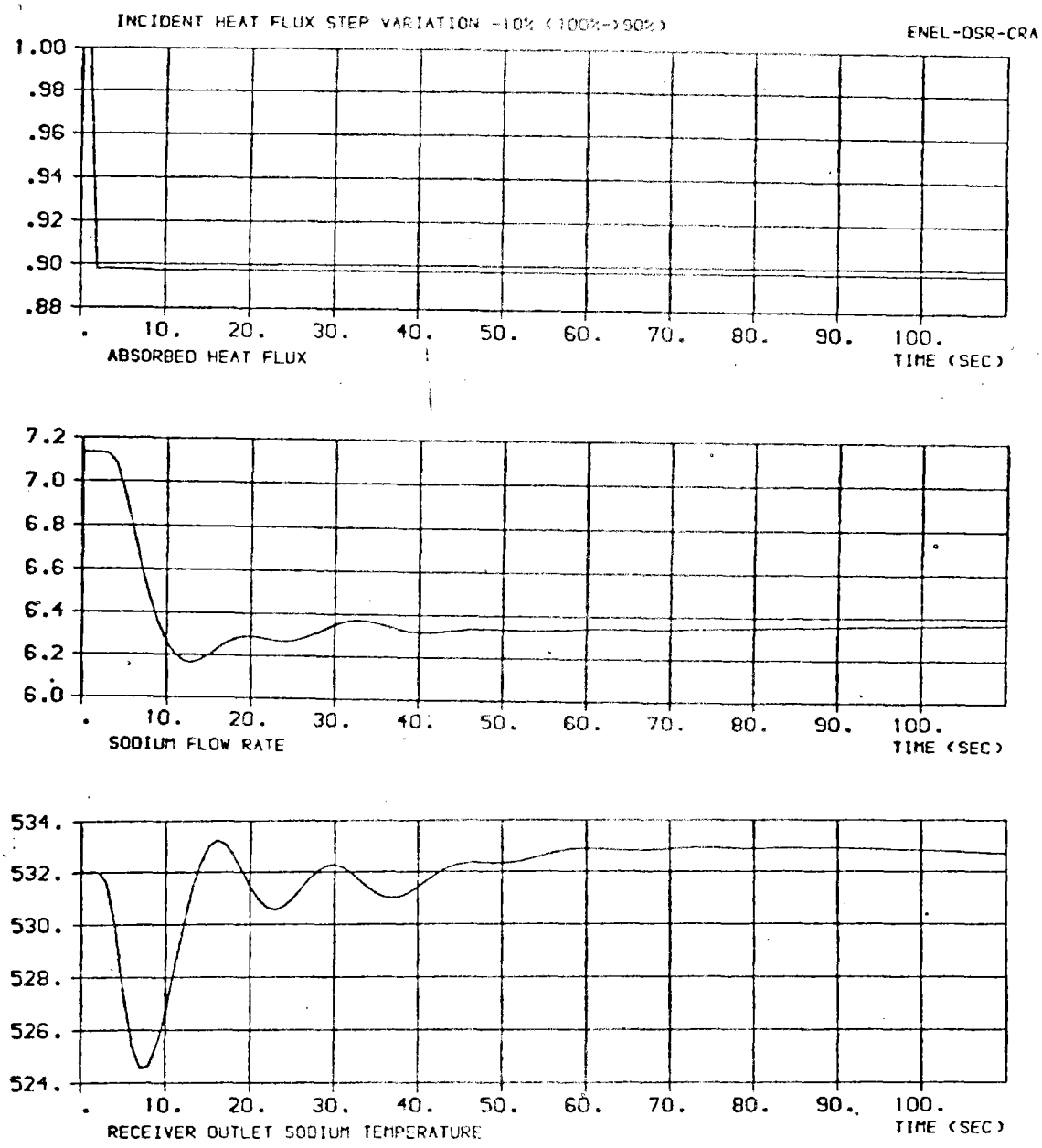
INCIDENT HEAT FLUX STEP VARIATION -10% (100%->90%)
ENEL-DSR-CRA
1.00
.98
.96
.94
.92
.90
.88
10.
20.
30.
40.
50.
60.
70.
80.
90.
100.
ABSORBED HEAT FLUX
TIME (SEC)
7.2
7.0
6.8
6.6
6.4
6.2
6.0
SODIUM FLOW RATE
534.
532.
530.
528.
526.
524.
RECEIVER OUTLET SODIUM TEMPERATURE

Fig. A1-2

APPENDIX A2

Time responses are obtained using the control structure shown in fig. 14.

Transients presented: A2-1) Outlet temperature set point step variation (5% at maximum load).

A2-2) Incident heat flux ramp variation (from 100% to 20% of maximum load).

A2-3) Incident heat flux ramp variation (from 30% to 100% of maximum load).

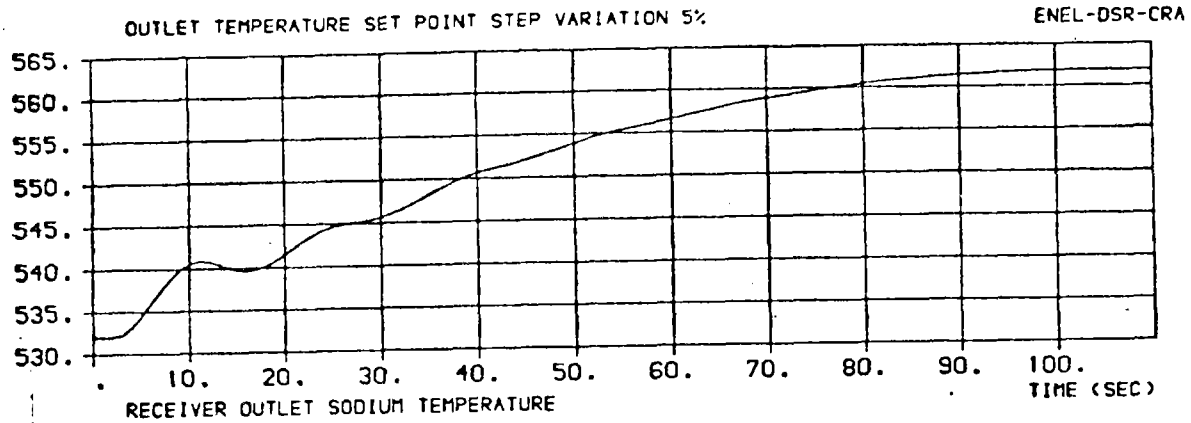
OUTLET TEMPERATURE SET POINT STEP VARIATION 5%
ENEL-DSR-CRA
565.
560.
555.
550.
545.
540.
535.
530.
10. 20. 30. 40. 50. 60. 70. 80. 90. 100.
TIME (SEC)
RECEIVER OUTLET SODIUM TEMPERATURE

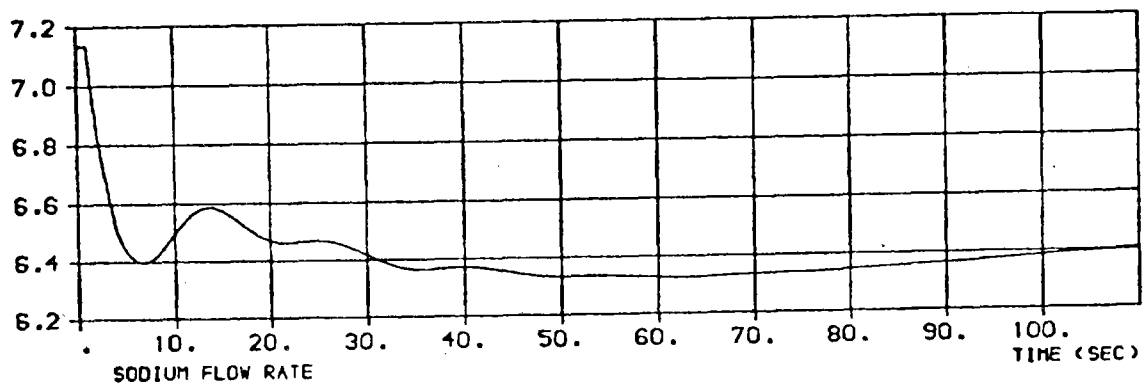
7.2
7.0
6.8
6.6
6.4
6.2
10. 20. 30. 40. 50. 60. 70. 80. 90. 100.
TIME (SEC)
SODIUM FLOW RATE

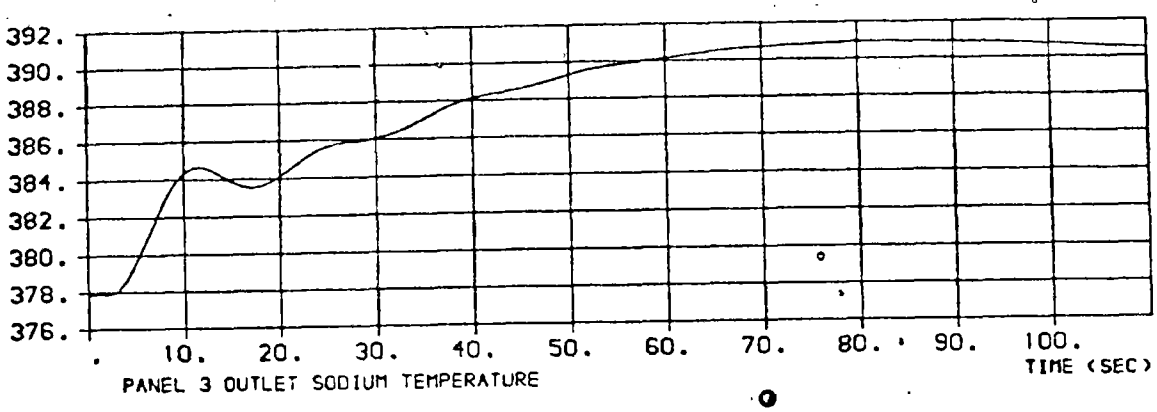
392.
390.
388.
386.
384.
382.
380.
378.
376.
10. 20. 30. 40. 50. 60. 70. 80. 90. 100.
TIME (SEC)
PANEL 3 OUTLET SODIUM TEMPERATURE

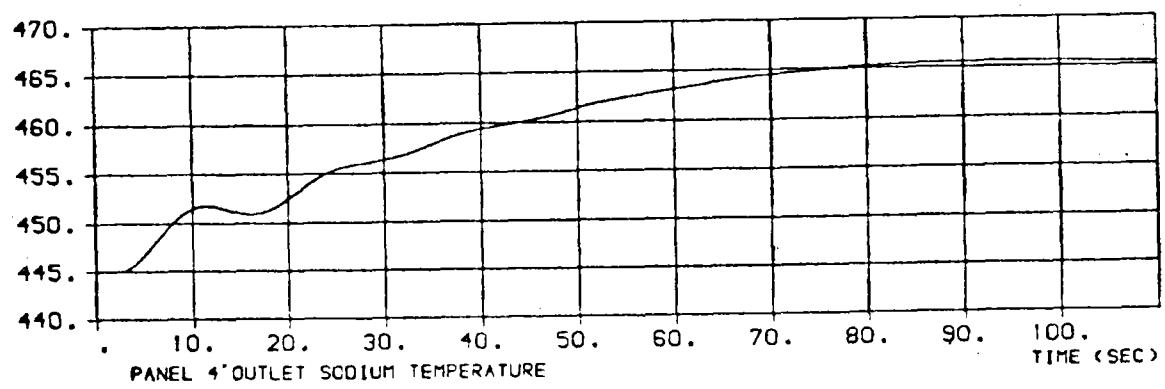
470.
465.
460.
455.
450.
445.
440.
10. 20. 30. 40. 50. 60. 70. 80. 90. 100.
TIME (SEC)
PANEL 4 OUTLET SODIUM TEMPERATURE

Fig. A2-1

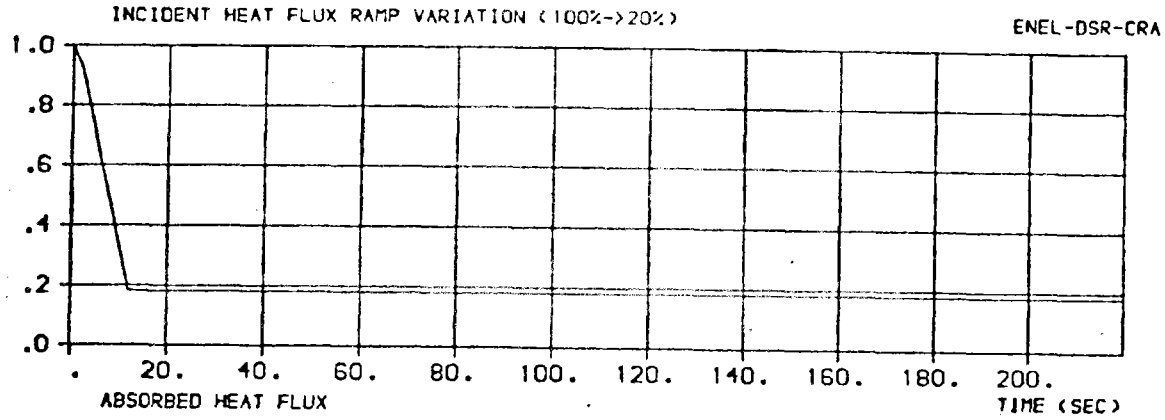
INCIDENT HEAT FLUX RAMP VARIATION (100%->20%)
ENEL-DSR-CRA
1.0
.8
.6
.4
.2
.0
20. 40. 60. 80. 100. 120. 140. 160. 180. 200.
ABSORBED HEAT FLUX
TIME (SEC)

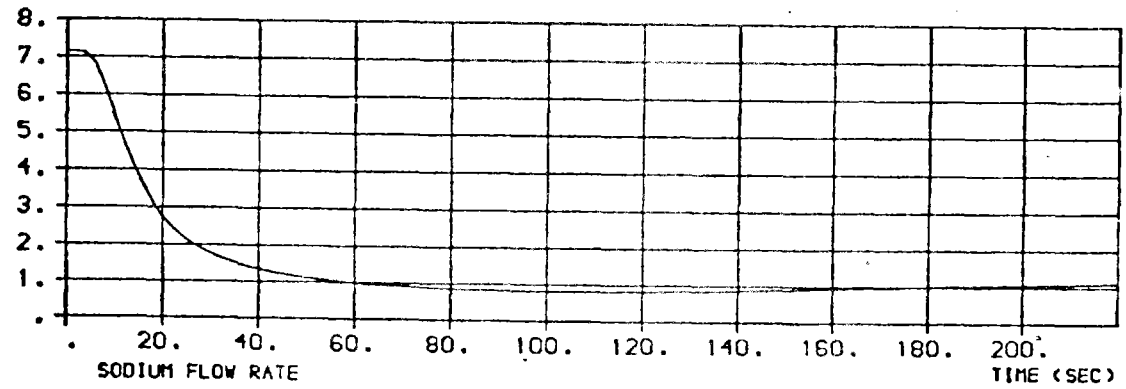
8.
7.
6.
5.
4.
3.
2.
1.
20. 40. 60. 80. 100. 120. 140. 160. 180. 200.
SODIUM FLOW RATE
TIME (SEC)

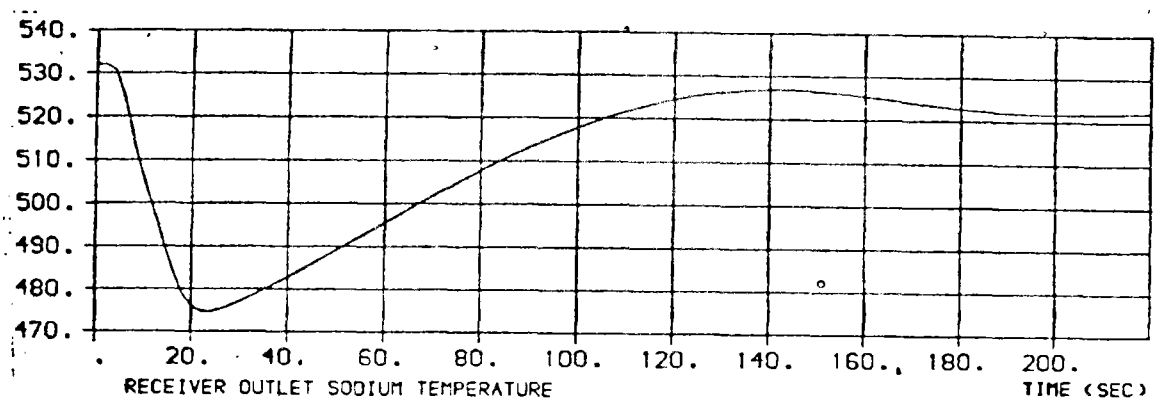
540.
530.
520.
510.
500.
490.
480.
470.
20. 40. 60. 80. 100. 120. 140. 160. 180. 200.
RECEIVER OUTLET SODIUM TEMPERATURE
TIME (SEC)

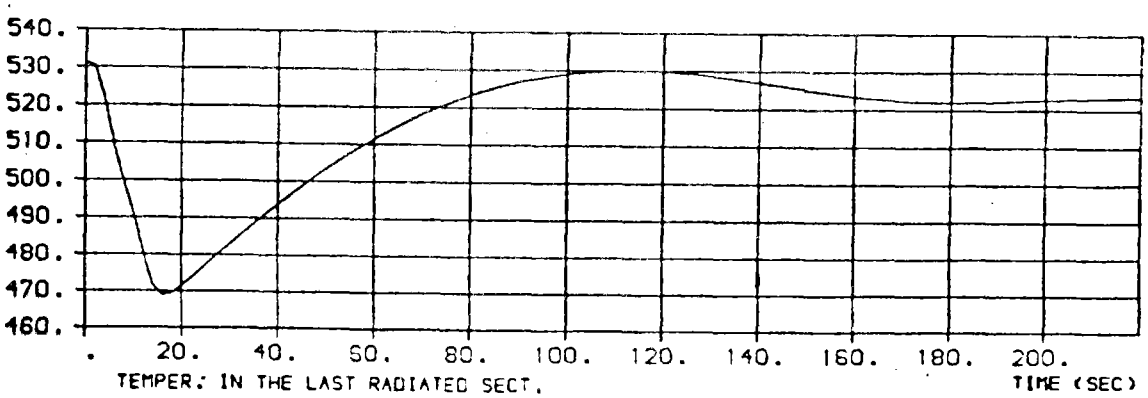
540.
530.
520.
510.
500.
490.
480.
470.
460.
20. 40. 60. 80. 100. 120. 140. 160. 180. 200.
TEMPER. IN THE LAST RADIATED SECT.
TIME (SEC)

Fig. A2-2

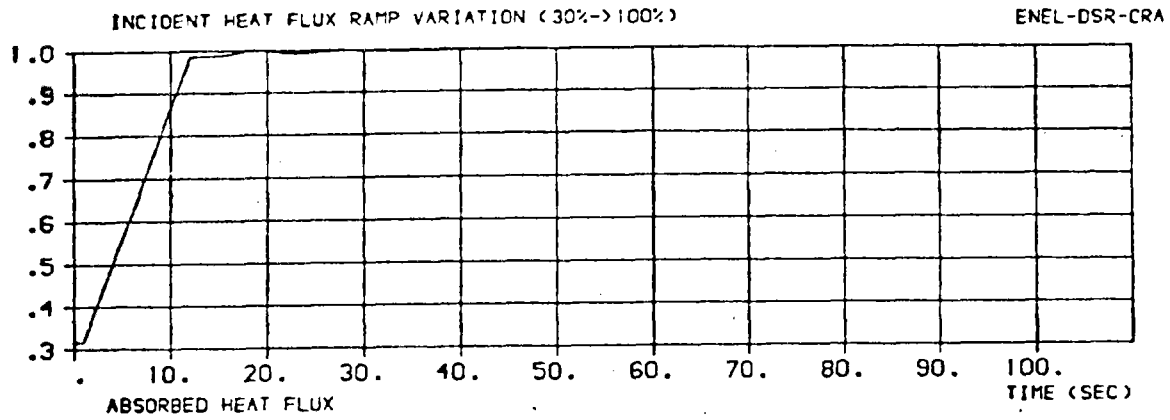
INCIDENT HEAT FLUX RAMP VARIATION (30%->100%)
ENEL-DSR-CRA
1.0
.9
.8
.7
.6
.5
.4
.3
10. 20. 30. 40. 50. 60. 70. 80. 90. 100.
TIME (SEC)
ABSORBED HEAT FLUX

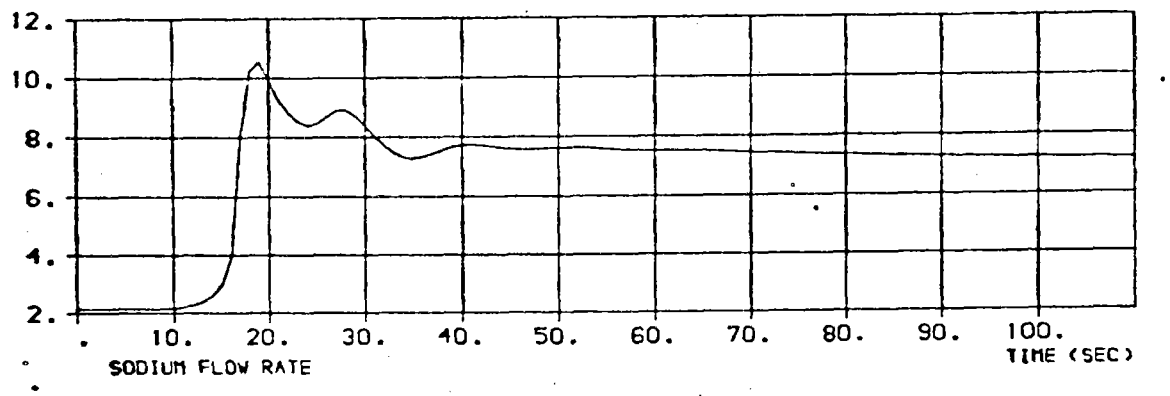
12.
10.
8.
6.
4.
2.
10. 20. 30. 40. 50. 60. 70. 80. 90. 100.
TIME (SEC)
SODIUM FLOW RATE

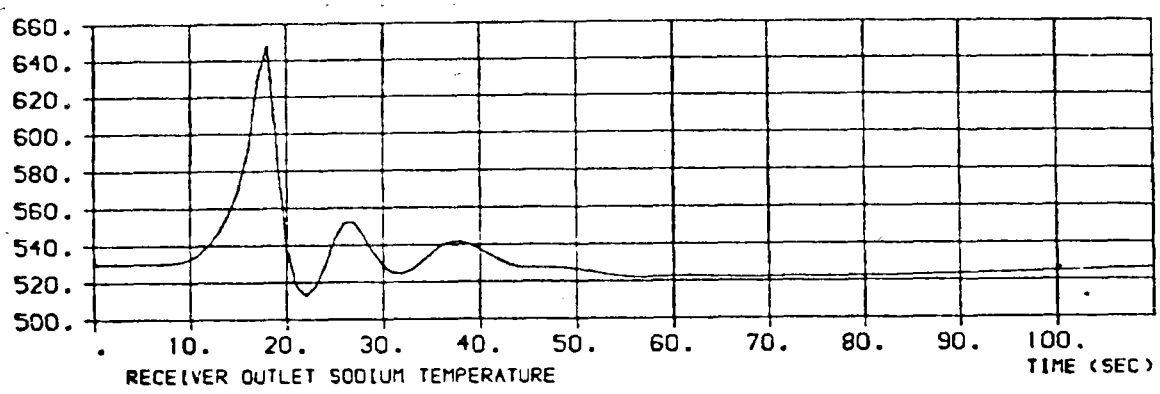
660.
640.
620.
600.
580.
560.
540.
520.
500.
10. 20. 30. 40. 50. 60. 70. 80. 90. 100.
TIME (SEC)
RECEIVER OUTLET SODIUM TEMPERATURE

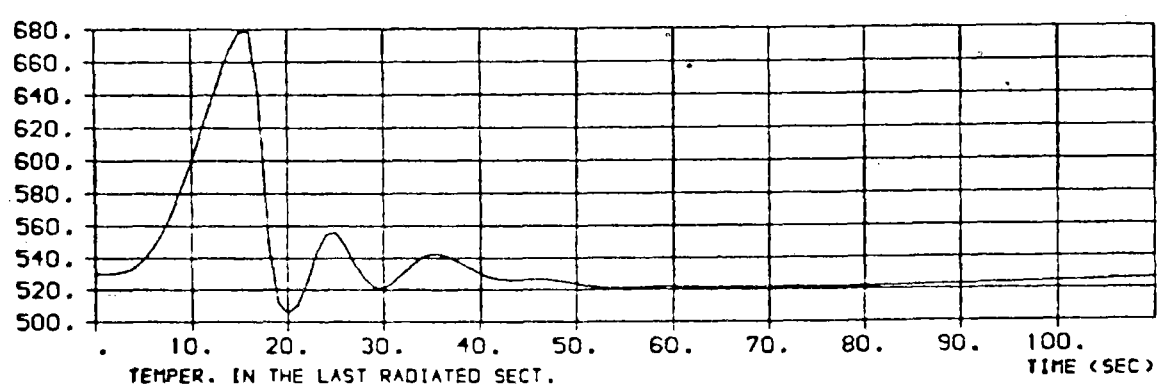
680.
660.
640.
620.
600.
580.
560.
540.
520.
500.
10. 20. 30. 40. 50. 60. 70. 80. 90. 100.
TIME (SEC)
TEMPER. IN THE LAST RADIATED SECT.

Fig. A2-3

APPENDIX A3

Time responses obtained using the control structure shown in fig. 14, but with the outlet temperatures measured on radiated tubes. Only the receiver outlet temperature is measured on the outlet header, this measure is used by the external regulator.

Transients presented: A3-1) Incident heat flux ramp variation (from 30% to 100% of maximum load).

NOTE - Compare with the some transient presented in fig. A2-3.

A3-2) Incident heat flux ramp variation (from 100% to 0 and then back to 100% of maximum load).

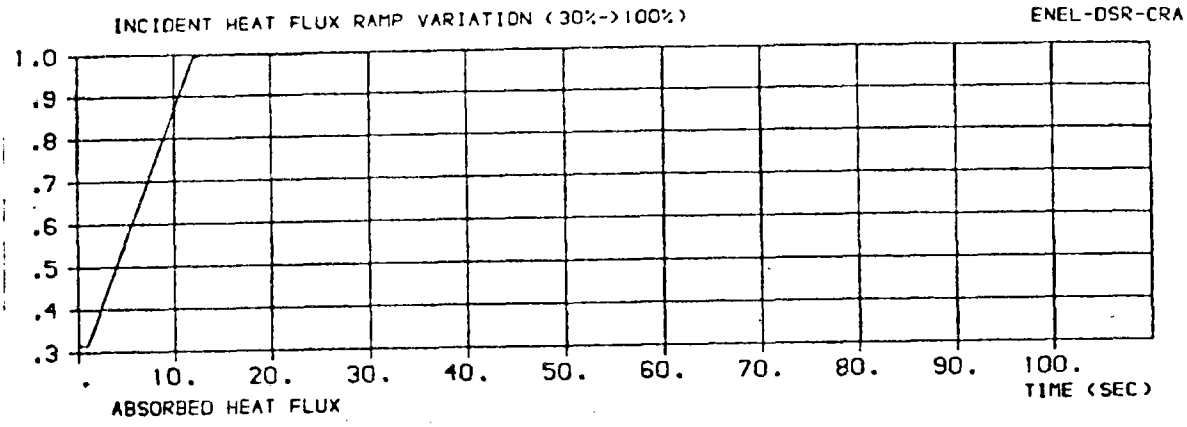
INCIDENT HEAT FLUX RAMP VARIATION (30%->100%)
ENEL-DSR-CRA
1.0
.9
.8
.7
.6
.5
.4
.3
10.
20.
30.
40.
50.
60.
70.
80.
90.
100.
TIME (SEC)
ABSORBED HEAT FLUX

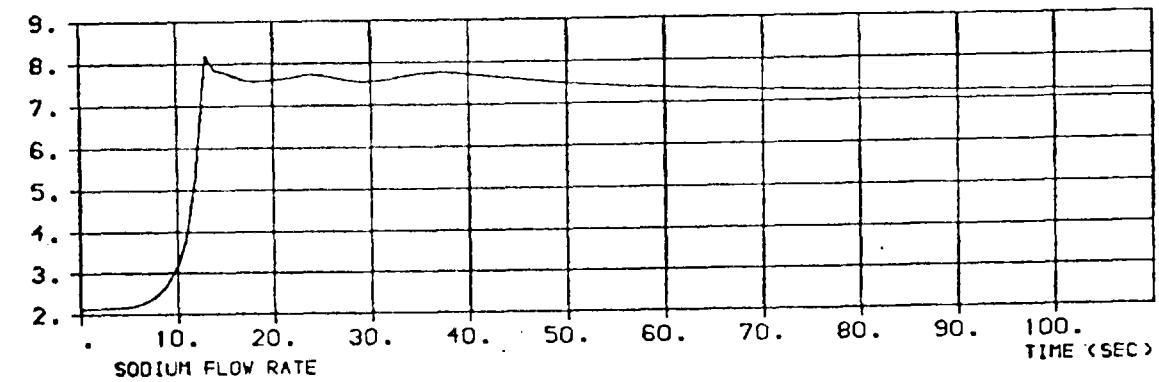
9.
8.
7.
6.
5.
4.
3.
2.
10.
20.
30.
40.
50.
60.
70.
80.
90.
100.
TIME (SEC)
SODIUM FLOW RATE

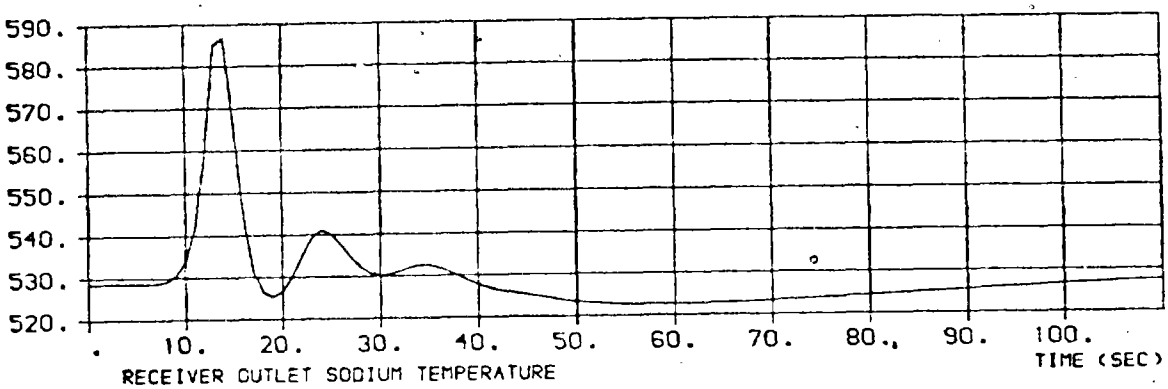
590.
580.
570.
560.
550.
540.
530.
520.
10.
20.
30.
40.
50.
60.
70.
80.
90.
100.
TIME (SEC)
RECEIVER OUTLET SODIUM TEMPERATURE

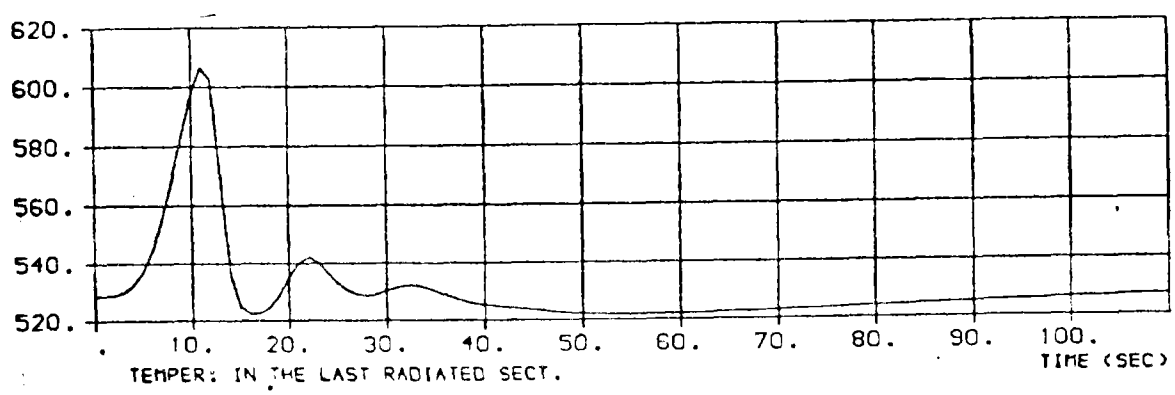
620.
600.
580.
560.
540.
520.
10.
20.
30.
40.
50.
60.
70.
80.
90.
100.
TIME (SEC)
TEMPER: IN THE LAST RADIATED SECT.

Fig. A3-1

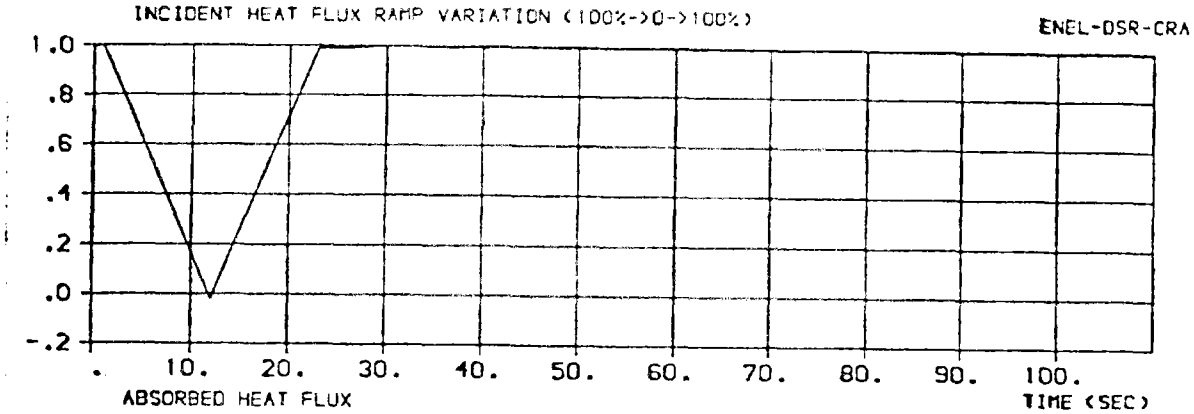
INCIDENT HEAT FLUX RAMP VARIATION (100%->0->100%)
ENEL-DSR-CRA
1.0
.8
.6
.4
.2
.0
-.2
10.
20.
30.
40.
50.
60.
70.
80.
90.
100.
ABSORBED HEAT FLUX
TIME (SEC)

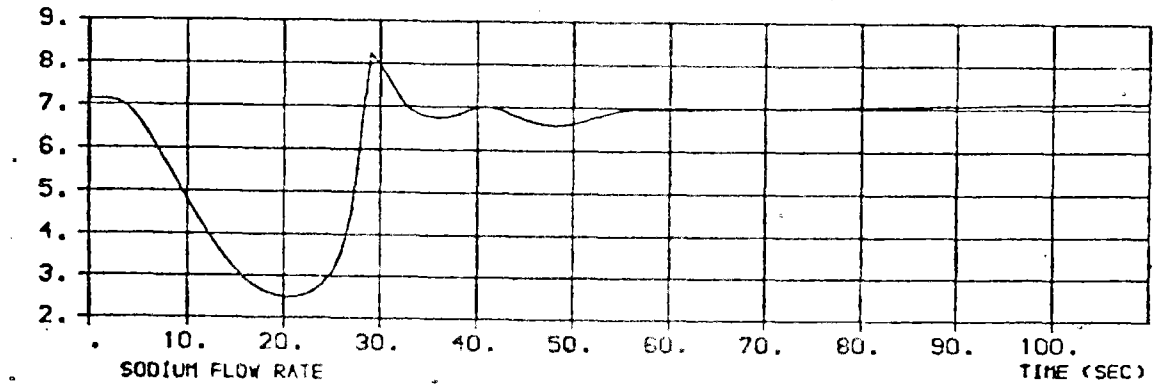
9.
8.
7.
6.
5.
4.
3.
2.
10.
20.
30.
40.
50.
60.
70.
80.
90.
100.
SODIUM FLOW RATE
TIME (SEC)

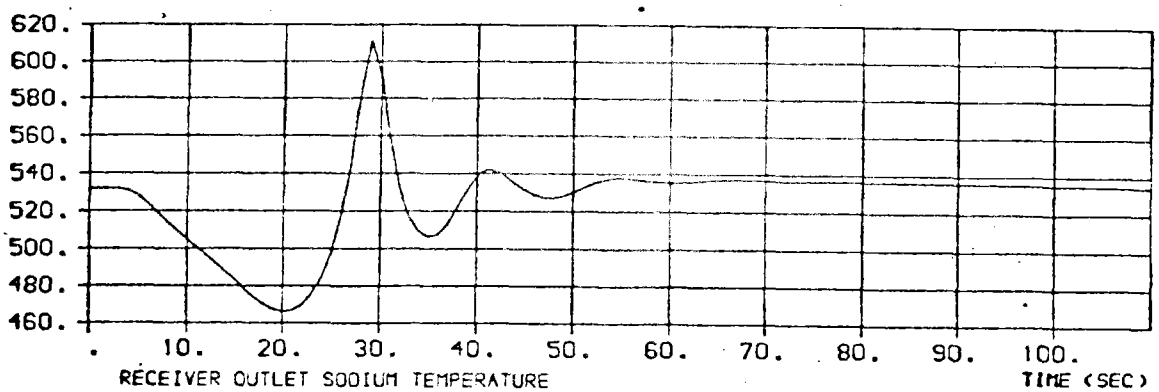
620.
600.
580.
560.
540.
520.
500.
480.
460.
10.
20.
30.
40.
50.
60.
70.
80.
90.
100.
RECEIVER OUTLET SODIUM TEMPERATURE
TIME (SEC)

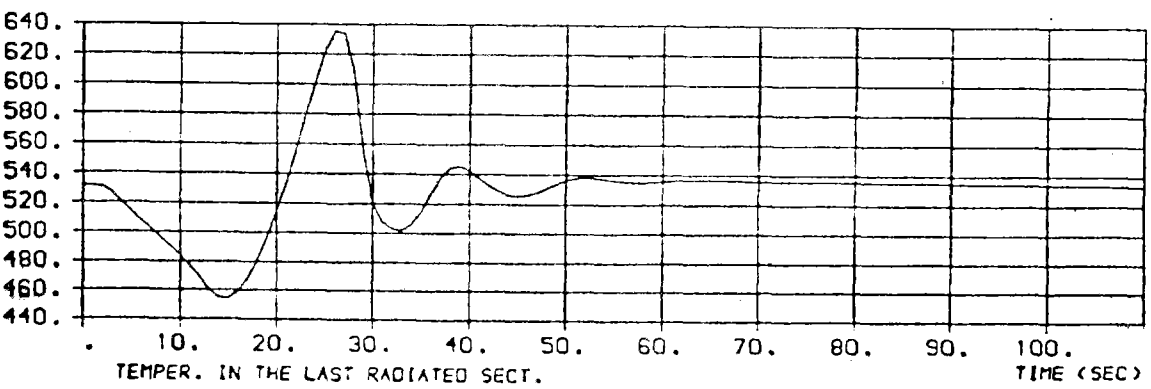
640.
620.
600.
580.
560.
540.
520.
500.
480.
460.
440.
10.
20.
30.
40.
50.
60.
70.
80.
90.
100.
TEMPER. IN THE LAST RADIATED SECT.
TIME (SEC)

Fig. A3-2

REFERENCES

(1) IEA Almeria Project - ASR Topic Report n. 4 - June 1981.

(2) IEA Almeria Project - ASR Progress Report n. 11 - November 1981.

(3) RIGHETTI-RAGNI/Metodi di identificazione e riduzione dell'ordine per sistemi dinamici lineari, invarianti nel tempo - Thesis, Politecnico di Milano, 1980-81.

(4) IEA Almeria Project - ASR Progress Report n. 6 - December 1980.

(5) L.GOULD/Chemical process control theory and application - Addison Wesley, Mass., 1969.

SSPS TECHNICAL REPORTS

1/79	HELIOSTAT FIELD AND DATA ACQUISITION SUBSYSTEM FOR CRS (BY MARTIN MARIETTA)	DECEMBER 1979
2/79	CRS-HELIOSTAT FIELD, INTERFACE CONTROL AND DATA ACQUISITION SYSTEM (BY MCDONNELL DOUGLAS)	DECEMBER 1979
1/80	COLLECTOR QUALIFICATION TESTS FOR THE IEA 500 KWE DISTRIBUTED COLLECTOR SYSTEM (BY SANDIA AND DFVLR)	JULY 1980
2/80	ANALYSIS OF SPECIAL HYDRAULICAL EFFECTS IN THE SHTS PIPING SYSTEM (BY BELGONUCLEAIRE)	NOVEMBER 1980
3/80	REDESIGN OF THE CRS - ALMERIA RECEIVER APERTURE AND COMPARISON OF INTERATOM AND MMC REFERENCE HELIOSTAT FIELD PERFORMANCE CALCULATIONS (BY INTERATOM)	NOVEMBER 1980
1/81	TABERNAS METEO DATA ANALYSIS BASED ON EVALUATED DATA PREPARED BY THE SSPS-O.A. (BY BELGONUCLEAIRE)	JUNE 1981
2/81	DCS INSTRUMENTATION REVIEW (BY BELGONUCLEAIRE)	JUNE 1981
3/81	CRS INSTRUMENTATION REVIEW (BY BELGONUCLEAIRE)	JUNE 1981
4/81	INTERNATIONAL ENERGY AGENCY SMALL SOLAR POWER SYSTEMS (SSPS) PROJECT REVIEW (JANUARY 1981) (BY A.F.BAKER, SANDIA)	JULY 1981
5/81	DEVICE FOR THE MEASUREMENT OF HEAT FLUX DISTRIBUTIONS (HFD) NEAR THE RECEIVER APERTURE PLANE OF THE ALMERIA CRS SOLAR POWER STATION (BY DFVLR)	NOVEMBER 1981
6/81	DETERMINATION OF THE SPECTRAL REFLECTIVITY AND THE BIDERECTIONAL REFLECTANCE CHARACTERISTICS OF SOME WHITE SURFACES (BY DFVLR)	DECEMBER 1981

SSPS TECHNICAL REPORTS CONTD.

1/82	SSPS WORKSHOP ON FUNCTIONAL AND PERFORMANCE CHARACTERISTICS OF SOLAR THERMAL PILOT PLANTS. PART I. RESULTS OF THE DCS-PLANT SESSION. (BY A. KALT, DFVLR)	APRIL 1982
	PART II. RESULTS OF THE TOWER FACILITIES SESSION (BY M. BECKER, DFVLR)	JULY 1982
2/82	CONCENTRATED SOLAR FLUX MEASUREMENTS AT THE IEA SSPS SOLAR CENTRAL RECEIVER POWER PLANT TABERNAS - ALMERIA (SPAIN) (BY G. VON TOBEL, CH. SCHELDERS, M. REAL, EIR)	APRIL 1982
3/82	EFFECT OF SUNSHAPE ON FLUX DISTRIBUTION AND INTERCEPT FACTOR OF THE SOLAR TOWER POWER PLANT AT ALMERIA (BY G. LEMPERLE, DFVLR)	SEPTEMBER 1982
1/83	DCS-MIDTERM-WORKSHOP PROCEEDINGS (EDITED BY A. KALT, J. MARTIN)	FEBRUARY 1983
2/83	FH-PTL WEDEL REFLECTOMETER, TYPE 02-1 NO.3 FINAL REPORT AND REPORT ON THE TEST PROGRAM (BY G. LENSCH, K. BRUDI, P. LIPPERT, FACHHOCHSCHULE WEDEL)	MARCH 1983
3/83	THE ADVANCED SODIUM RECEIVER (ASR) - TOPIC REPORTS - (AGIP NUCLEARE AND FRANCO TOSI)	MAY 1983

DISTRIBUTION LIST

1)	SSPS-MEMBER COUNTRY REPRESENTATIVES (EXECUTIVE COMMITTEE AND T+O ADVISORY BOARD)	L. REY	(EC CHAIRMAN)
		G. FANINGER	(A)
		H. KLEINRATH	(A)
		J. DELCROIX	(B)
		A. MICHEL	(B)
		P. KESSELRING	(CH)
		C.J. WINTER	(D)
		M. FISCHER	(D)
		W. HOFMANN	(D)
		A. MUNOZ TORRALBO	(E)
		C. ORTIZ	(E)
		E. CARABATEAS	(GR)
		F. REALE	(I)
		G. BEER	(I)
		L. BRANDELS	(S)
		J. HOLMBERG	(S)
		L. GUTIERREZ	(USA)
2)	IEA - SECRETERIAT	L. BOXER	
3)	B M F T	H. KLEIN	
4)	C E E	I. MARTIN	
5)	SANDIA LABORATORIES	A. BAKER	(3 X)
6)	D F V L R	R. KÖHNE	(3 X)
7)	OPERATING AGENT	M. BECKER	
		W. BUCHER	
		H. ELLGERING	
		W. GRASSE	
		P. HEINTZELMANN	
		A. KALT	
		W. VON KRIES	
8)	INTERNATIONAL TEST & EVALUATION TEAM	C. SELVAGE	(20 X)
9)	SEVILLANA	F. RUIZ	(3 X)
10)	ACUREX CORP.	A.F. SCHRAUB	
11)	BELGONUCLEAIRE	G. DEBIER	
12)	INTERATOM	B. FLOSS	
13)	MAN - NEUE TECHNOLOGIE	J. FEUSTEL	
14)	MARTIN MARIETTA CORP.	C. WROTON	
15)	SAIT	B. LORENT	
16)	AGIP NUCLEARE	G.C. SCARPI	
17)	FRANCO TOSI	V. BEDOGNI	